Engineering of redox metallocenic nanomaterials

Amalia Rapakousiou

université de BORDEAUX

THÈSE PRÉSENTÉE

POUR OBTENIR LE GRADE DE

DOCTEUR DE

L'UNIVERSITÉ DE BORDEAUX

ÉCOLE DOCTORALE DES SCIENCES CHIMIQUES DE BORDEAUX

SPÉCIALITÉ: Chimie Organique

Par Amalia RAPAKOUSIOU

Ingéniérie des nanomatériaux redox métallocèniques

Sous la direction de : Didier, ASTRUC

ISM, Groupe Nanosciences et Catalyse, Université Bordeaux

Soutenue le 19 décembre 2014 devant la commission d'examen

Membres du jury :

M. HAMON, Jean-René	Directeur de Recherche au CNRS (Rennes 1)	Rapporteur
M. BOUSSEKSOU Azzedine	Directeur de Recherche au CNRS (Toulouse)	Rapporteur
M. FRITSCH Alain	Professeur, Université de Bordeaux	Examinateur
M. SAILLARD, Jean-Yves	Professeur, Université de Rennes (IUF)	Examinateur
M. SAUVAGE Jean-Pierre	Directeur de Recherche au CNRS (ISIS, Strasbourg)	Examinateur
M. SALMON Lionel	Chargé de Recherche au CNRS (Toulouse)	Examinateur
Mme CSIBA-DALKO Maria	Directeur de Recherche à L'OREAL	Examinateur
M. RUIZ Jaime	Ingénieur contractuel, Université de Bordeaux	Membre invité
M. ASTRUC Didier	Professeur à l'Université de Bordeaux (IUF)	Directeur de thèse

Je dédie cette thèse à ma famille

Apostolos, Eleni, Giorgos and Alexandros

Merci beaucoup pour votre amour et support inconditionnel

Σας αγαπώ πολύ!

Research is to see what everybody else has seen, and to think what nobody else has thought.

Albert Szent-Gyorgyi

Remerciements

Ce travail a été effectué dans la Groupe Nanosciences et catalyse, ISM, Université de Bordeaux 1 (CNRS UMR 5255), sous la direction scientifique du Professeur Didier Astruc.

****

Je remercie le Professeur Didier Astruc pour m'avoir accueilli dans son groupe de recherche et pour m'avoir donné l'opportunité et la confiance de réaliser ma thèse sur des sujets passionnants. Je le remercie pour son souci permanent de me faire progresser tout le temps et me montrer que la chimie n'a pas des limites. C'était un vrai honneur pour moi de pouvoir travailler avec lui au sein de son laboratoire. Je lui exprime toute ma gratitude pour son soutien depuis le début jusqu'à la fin. Son enthousiasme et sa personnalité marquante resteront toujours dans mon cœur.

****

J'exprime toute ma gratitude à M. Jaime RUIZ, ingénieur de Recherche. Son encadrement au début de cette thèse m'a vraiment renforcé pour continuer jusqu'à la fin. Je le remercie vivement pour son écoute et ses encouragements aux moments difficiles, nos discussions scientifiques et sa joie de vivre qui faisaient ma vie au sein de laboratoire plus jolie. Je suis profondément reconnaissante Jaime! Un millón de gracias!

****

J'adresse mes sincères remerciements à M. Jean-René Hamon, Directeur de Recherche au CNRS (Rennes) et M. Azzedine Bousseksou, Directeur de Recherche (Toulouse) pour avoir accepté de juger ce manuscrit. J'exprime toute ma reconnaissance à M. Jean-Yves Saillard, Professeur à l' Université de Rennes, M. Jean-Pierre Sauvage, Directeur de Recherche au CNRS (Strasbourg), M. Fritsch Alain, Professeur à l' Université de Bordeaux, M. Lionel Salmon, Chargé de Recherche au CNRS (Toulouse) et Mme Maria Csiba-Dalko, Directeur de Recherche à L'Oréal, qui m'ont fait l'honneur de bien vouloir participer à mon jury de thèse.

****

Je remercie particulièrement mon copain Juan-Luis Hernandez-Navarro. On a partagé ensemble ce trajet de trois ans de thèse. Je te remercie pour ta patience durant les moments difficiles. Ton enthousiasme et admiration de ma recherche, ton écoute quand j'étais triste et/ou contente, tes conseils toujours intelligents et ta disponibilité toujours quand j'avais besoin. Tu étais la source de ma force. Je suis très fière et heureuse de partager ma vie avec toi ! Merci!

****

Je remercie du fond du cœur toutes les personnes qui ont participé à ce travail de recherche de près ou de loin. Je remercie la formidable équipe CESAMO, entre autres: Mme Claire Mouche, pour la spectroscopie de masse, M. Jean-Michel et M. Noel Pinaud pour les études RMN. Merci pour votre soutiens et aide quotidien. Je tiens aussi à remercier Mme Colette

Belin pour son amitié et les analyses AFM. J'ai beaucoup aimé les moments que nous avons travaillés ensemble. Je remercie beaucoup Lionel Salmon pour la microscopie TEM qui était très utile pour mon travail de recherche. Je remercie tout le personnel de l'ISM qui était toujours à mes côtés, entre autres: Bernadette, Vicky, Abdel, Sophie, Annie, Karine, Pascale Godard, Fred, Georges, Fabrice, Pascale, Kalinet (Thierry) et la doctorante Elise. Vous avez fait ma vie dans l'institut agréable!

****

Je remercie du fond du cœur mes amis et collaborateurs de notre groupe Christophe, mon 'frère d'arme'! Sa présence dans ma vie 24h/24h va spécialement me manquer. Egalement Frida, Lucia, Pengxiang, Rodrigue, Liyuan, Maxime, Roberto, Virginie, Martin et Sylvain. Votre amitié était très importante pour moi au niveau professionnel et personnelle. Je tiens à remercier mes amis du groupe 'Landais' Benjamin, Clément, Jonathan, Thomas pour ces trois ans qu'on a partagé dedans et dehors de l'ISM. Je suis très heureuse de vous avoir dans ma vie. Je remercie aussi Jessica, Paul, Alex, Hugo pour tous les moments agréables. Je remercie mes stagiaires Sabrina et spécialement Georgia qui m'ont offert une expérience très enrichissante! Je remercie tous les personnes de mon groupe: Lina, Dong, Changlong, Haibin, Xiang, Yanlan, Abdou. Je suis très heureuse de travailler avec tous vous, vos amitiés sont très précieuses. Je vous souhaite toutes de bonnes choses dans le futur.

****

Enfin je remercie aussi tous mes amis qui m'ont donné la force pour arriver jusqu'à la fin, entre eux, Efoula qui était toujours là.

Ingéniérie des nanomatériaux redox métallocéniques

Partie 3:

Dendrimères polycationiques de cobalticénium et de FeCp(mésitylène)

Partie 4:

Synthèse et activité rédox de polyélectrolytes de cobalticénium

Partie 5:

Les réservoirs dendritiques d’hydrures (RDH)

I) **Introduction générale**

Le groupe 'Nanosciences et Catalyse' dirigé par le Professeur Didier Astruc s'intéresse notamment à l'incorporation de complexes organométalliques dans les nanosystèmes afin de mettre en œuvre leurs propriétés rédox en vue d'applications en reconnaissance moléculaire, batteries moléculaires, catalyse et polyélectrolytes (1). Parmi les métaux les plus courants, le fer et le cobalt sont connus en tant que biométaux, ce qui leur confère des possibilités d'applications diverses en nanomédicine, catalyse et matériaux pour l'électronique et l'énergie (2). C'est dans cet esprit que s'inscrit cette thèse avec l'élaboration de macromolécules contenant des métallocènes, complexes de structure sandwich aux propriétés redox bien connues.

Tout d'abord, en première partie, nous décrivons la construction des assemblages supramoléculaires dendritiques.

La plupart des dendrimères sont construits de manière covalente, mais la liaison ionique a récemment attiré l'attention pour une meilleure encapsulation des médicaments et propriétés physico-chimiques spécifiques liés à l'énergie. L'objectif était d'étudier la possibilité de liaisons ioniques comme une méthode viable pour la conception de capteurs rédox et matériaux en relation avec des problèmes énergétiques.

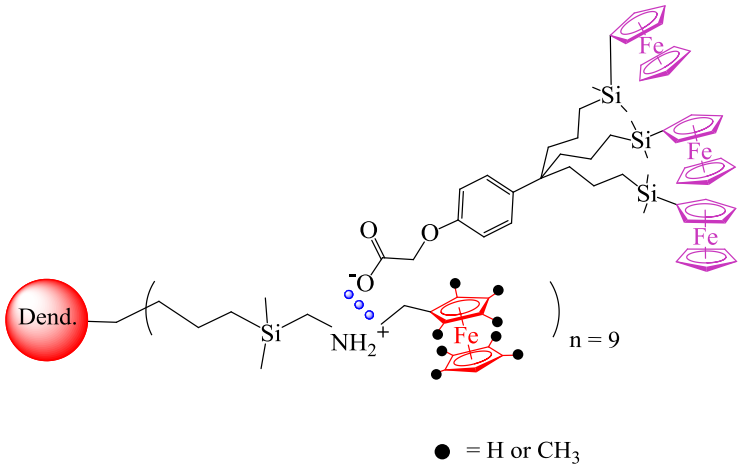

Schéma 1. Motifs de la 1ère partie de thèse (chapitre 1.1).

Intéressés par l'introduction de fonctions rédox dans les assemblages dendritiques, nous avons choisi d'une part les dérivés ferrocéniques pour la richesse de leurs applications rédox, comme par exemple la reconnaissance moléculaire (3), et d'autre part le cobalticénium et le rhodicénium qui sont des candidats excellents pour l'électronique moléculaire et la fabrication de polyélectrolytes.

Ces constructions ont été conçues afin d'examiner leurs conséquences physico-chimiques, en particulier les propriétés électrochimiques et rédox. Cette stratégie a été étendue à la conception d' électrodes dérivées de dendrimères ferrocèniques ioniques (G_1 et G_2) contenant des couches de ferrocène *intra* dendritiques et/ou périphériques ainsi que des polyélectrolytes

solubles dans l'eau, en particulier des sels de cobalticénium et rhodicénium macromoléculaires dendritiques.

En deuxième partie de cette thèse nous aborderons la synthèse de macromolécules contenant plusieurs groupements biferrocényles. Le biferrocène présente une chimie rédox riche comme le ferrocène, mais il a l'avantage notable de posséder trois différents états d'oxydation ($Fe^{II}Fe^{II}$/ $Fe^{II}Fe^{III}$/ $Fe^{III}Fe^{III}$) au lieu de seulement deux états facilement accessibles pour le ferrocène. Le cation de biferrocénium est plus robuste que le ferricenium car son groupe cationique ferricenium substitué est stabilisé par le groupe ferrocényle neutre qui est électro-donneur. Avant le début de cette thèse, un stage de six mois dans groupe du Prof. Didier Astruc a été effectué au cours duquel nous avons réussi à synthétiser et séparer les isomères de l'acétylbiferrocène, ce qui nous a conduits à synthétiser l'éthynylbiferrocène. Celui-ci est un composé-cléf car il nous a permis d'incorporer facilement le groupement biferrocènyle aux macromolécules grâce à la réaction 'click' CuAAC. En effet, plusieurs générations de dendrimères ont été synthétisés (jusqu'à la génération 4 (G_4) contenant 729 triazole-biferrocènes à la périphérie), et leurs dérivés à valence mixte ont été isolés.

Dans ce travail pré-thèse effectué en collaboration avec Dr. Djeda Rodrigue, nous avons également mis en évidence la reconnaissance de l'anion ATP^{2-} par les ferrocènes extérieurs des dendrimères alors que les ferrocènes intérieurs reconnaissent les cations des métaux de transition. Cette propriété de reconnaissance moléculaire redox confère à ces métallodendrimères une fonction particulièrement remarquable (4).

Ce concept a alors été étendu aux polymères et nanoparticules d'or pendant la thèse. Des polymères triazolyl-biferrocène ont été préparés par ROMP (5) et polymérisation radicalaire pour la première fois. Nous avons souhaité utiliser ces polymères comme réducteurs de l'or Au^{III} afin d'obtenir des nanoparticules d'or stabilisées par le polymère contenant des unités à valence-mixte triazolylbiferrocénium. L'incubation pendant une semaine, dans des conditions concrètes, a donné des nanoserpents encapsulant et stabilisant des nanoparticules d'or. Cette stratégie qui a été accompagnée par l'utilisation de plusieurs techniques analyses est décrite au chapitre 2.1.

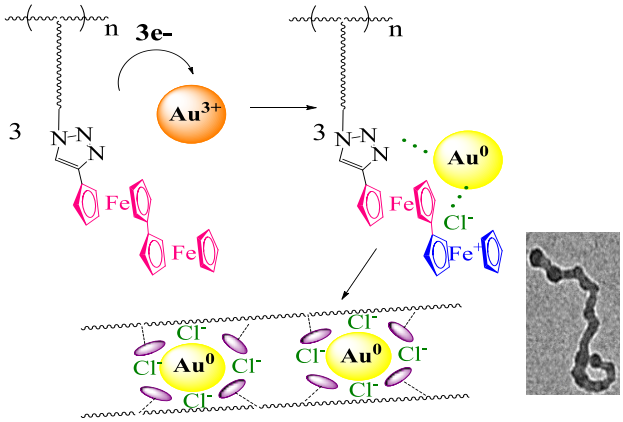

Schéma 2. Motifs de la 2ème partie de thèse (chapitre 2.1).

Des copolymères bistriazole(biferrocène)(PEG) ont aussi été synthétisés par Christophe Deraedt (chapitre 2.2). Ces polymères ont été utilisés dans notre groupe en collaboration avec Christophe Deraedt et Wang Yanlan pour des applications diverses. Les études rédox, la reconnaissance moléculaire de cations Pd^{2+} ainsi que la fabrication d'électrodes modifiées constituent une contribution dans le cadre de cette thèse. Parallèlement, nous les avons testés comme réducteurs d'Au^{III} donnant des réseaux polymériques de différentes formes de nanoserpents qui encapsulent également des nanoparticules d'or. Cette étude est décrite aussi dans le chapitre 2.1.

En troisième et quatrième parties est abordée l'incorporation de complexes cationiques comme par exemple le cobalticénium aux macromolécules par réaction 'click' afin d'accéder aux polyélectrolytes dendritiques et polymériques organométalliques aux multiples propriétés.

Les sel de cobalticénium possèdent trois degrés d'oxydation dont deux sont assez facilement accessibles et les complexes de Co^{III} présentent une grande stabilité et deux réductions monoélectroniques successives souvent réversibles. L'incorporation de ces complexes aux nanosystèmes permet d'obtenir des matériaux pouvant subir un transfert réversible d'un grand nombre d'électrons à peu près au même potentiel (au facteur électrostatique près, celui-ci étant extrêmement faible), du moins dans une vague électrochimique unique. Dans le chapitre 3.1 nous présentons la synthèse de trois générations de métallodendrimères contenant à la périphérie des groupements triazolylcobalticénium. Les études rédox effectuées démontrent la grande stabilité des nanosystèmes ayant des terminaisons triazolylcobalticénium, ce qui en fait de bons candidats pour les batteries moléculaires. Leur potentiel comme capteurs rédox ainsi que l'effet dendritique positif en reconnaissance moléculaire redox ont été également démontrés dans ce chapitre. La présence du groupement 'triazole' comme fonction de greffage confère au système des propriétés spécifiques qui permettent d'envisager des applications en nanosciences.

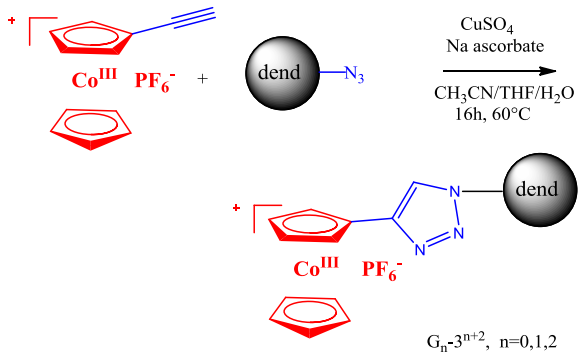

Schéma 3. Motifs de la 3ème partie de thèse (chapitre 3.1).

Des dendrimères cobalticénium ont été aussi préparés par une réaction 'click' différente, celle d'hydroamination. Cette chimie a été développée par Yanlan Wang au sein de notre laboratoire. Néanmoins, cette stratégie n'a pas été efficace pour l'incorporation de complexes FeCp(mésitylene) (6). En revanche, la réaction "click" CuAAC a donné accès à des

dendrimères stables contenant jusqu'à 27 complexes [FeCp(mésitylene)] à la périphérie, et ces résultats sont rapportés au chapitre 3.3.

En quatrième partie, des polyélectrolytes de cobalticénium de type polymères sont aussi préparés avec les mêmes méthodes que les dendrimères décrits en partie 3 et leurs propriétés physicochimiques sont discutées aux chapitres 4.1 et 4.2.

En cinquième et dernière partie sont introduits les réservoirs dendritiques d'hydrures (RDH) basés sur des terminaisons dendritiques à base de cobalticénium (7), leur fonction de réducteurs de cations de métaux nobles en nanoparticules métalliques (NPMs) stabilisées par les métallodendrimères et leur comparaison avec les réservoirs dendritiques d'électrons (RDE) à terminaisons ferrocéniques. Les études concernant des monomères triazolyl-cobalticénium sont décrites au chapitre 5.1 et les études concernant les RDH et RDE sont décrites au chapitre 5.2.

A la fin de cette thèse, divers projets effectués en collaboration sont rapportés (annexes). Ils ne sont pas connectés de façon centrale à la thèse, mais ces projets ont apporté des expériences enrichissantes supplémentaires concernant différents sujets de recherche de notre laboratoire.

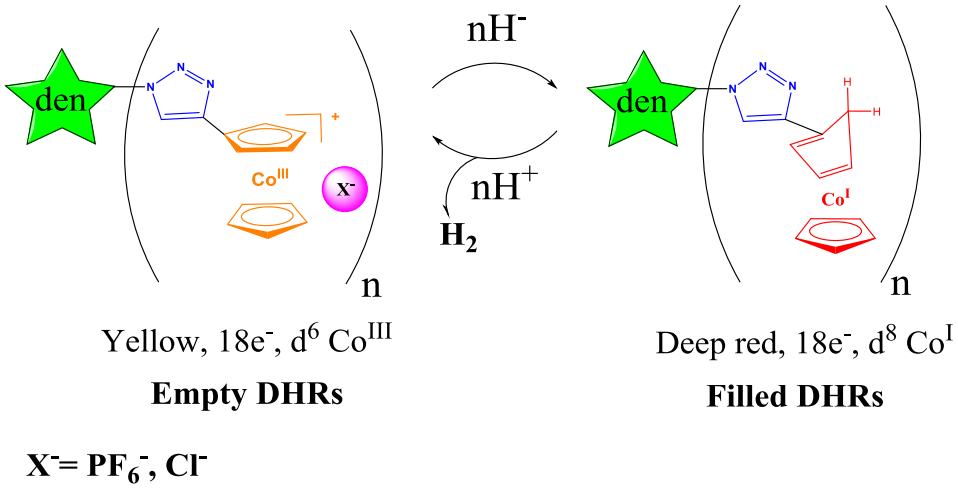

Schéma 4. Motifs de la 5ème partie de thèse (chapitre 5.2).

Références

(1) ‘Macromolecular Engineering: Precise Synthesis, Materials Properties, Applications.’ K. Matyjaszewski, Y. Gnanou, L. Leibers Eds., Wiley-VCH, Weinheim, 2007.

(2) D. Astruc. ‘Electron-Transfer Processes in Dendrimers, and their Implication in Biology, Catalysis, Sensing and Nanotehnology.’ *Nature Chem.* **2012**, *4*, 255-267.

(3) C. Ornelas, J. Ruiz, E. Cloutet, S. Alves, D. Astruc.‘Click Assembly of 1,2,3-Triazole-Linked Dendrimers, Including Ferrocenyl Dendrimers, Which Sense Both Oxo Anions and Metal Cations.’ *Angew Chem., Int. Ed.* **2007**, *46*, 872-877.

(4) R. Djeda, A. Rapakousiou, L. Liang, N. Guidolin, J. Ruiz, D. Astruc. ‘Click Syntheses of 1,2,3-Triazolylbiferrocenyl Dendrimers and the Selective Roles of the Inner and Outer Ferrocenyl Groups in the Redox Recognition of ATP^{2-} and Pd^{2+}.’ *Angew. Chem., Int. Ed.* **2010**, *49*, 8152-8156.

(5) G. C. Vougioukalakis, R. H. Grubbs. ‘Ruthenium-Based Heterocyclic Carbene-Coordinated Olefin Metathesis Catalysts.’ *Chem. Rev.* **2010**, *110*, 1746-1787.

(6) J. R. Hamon, D. Astruc, P. Michaud. ‘Syntheses, Characterization and Stereoelectronic Stabilization of Organometallic Electron-Reservoirs: the 19-Electron d^7 Redox Catalysts η^5-$C_5R_5Fe^I$ η^6-$C_6R'_6$.’ *J. Am. Chem. Soc.* **1981**, *103*, 758-766.

(7) M. L. H. Green, L. Pratt, G. Wilkinson. A New Type of Transition Metal-Cyclopentadiene Compound. *J. Chem. Soc.* **1959**, 3753–3767.

II) Parties de thèse

Partie 1

Macromolécules supramoléculaires métallocèniques.

Partie 1

Macromolécules supramoléculaires métallocèniques.

Introduction

Cette première partie est consacrée à la construction de dendrimères ou polymères ioniques liées de façon électrostatique des métallocènes cationiques. Au premier chapitre, nous avons reporté la synthèse de deux séries de dendrimères polyamines secondaires contenant du ferrocène ou octaméthylferrocène par condensation de dendrimères de polyamines, (obtenues par réduction des dendrimères polyazotures par $LiAlH_4$ ou $NaBH_4$) avec un aldéhyde ferrocényle ou octaméthylferrocényle, suivie par la réduction des dendrimères poly-imine. Des sels primaires et secondaires de dendrimères polyammonium ferrocényle ont été synthétisés par quaternisation des amines dendritiques dont polyamines ferrocényle secondaires, par réaction avec un dendron triferrocényle contenant un acide carboxylique comme point focal.

La formation des dendrimères, par liaison ammonium carboxylate, de génération plus élevées, a été démontrée par spectroscopie IR et RMN ainsi que la voltammétrie cyclique qui montre l'effet électrostatique des groupements ammonium secondaires *intra* dendritiques et la distinction entre les groupes ferrocényles *intra* dendritiques et périphériques.

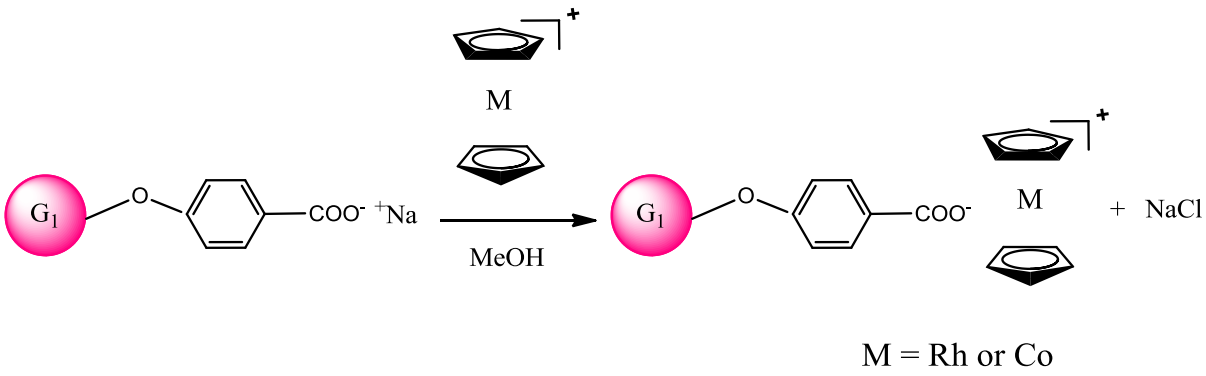

Schéma. Motifs du chapitre 1.2.

D'autre part, au chapitre 1.2, nous décrivons deux nouvelles synthèses, celle du chlorure de rhodicénium et celle du rhodicénium tetra (aryl) borate. Ce dernier présentant une solubilité dans des solvants apolaires ouvre la voie au développement de la chimie des organorhodium. Enfin, l'accès aux sels de rhodicénium (et cobalticénium) macromoléculaires contenant des anions polymèriques et dendritiques soluble dans l'eau a été démontré.

ORGANOMETALLICS

Article

pubs.acs.org/Organometallics

Ferrocenyl Dendrimers with Ionic Tethers and Dendrons

Amalia Rapakousiou, Yanlan Wang, Frida Nzulu, Rodrigue Djeda, Noël Pinaud, Jaime Ruiz, and Didier Astruc*

ISM, UMR CNRS No. 5255, University of Bordeaux, 33405 Talence Cedex, France

Supporting Information

ABSTRACT: Whereas covalently constructed dendrimers are very numerous, there are only a few examples of dendrimers based on ionic bonds with tethers or dendrons. Here such constructions were designed in order to examine their physicochemical consequences: in particular, the electrochemical and redox properties. Two series of *secondary* polyamine dendrimers containing ferrocenyl and octamethylferrocenyl were synthesized by condensation of polyamine dendrimers, obtained by reduction of the polyazide dendrimers by $LiAlH_4$ or $NaBH_4$ with ferrocenyl aldehyde or octamethylferrocenyl aldehyde, followed by reduction of the resulting polyimine dendrimers. Primary and secondary ferrocenyl polyammonium dendrimer salts have been synthesized by quaternization of the dendritic amines including ferrocenyl secondary polyamines by reaction with a triferrocenyl dendron containing a carboxylic acid as the focal point. Cyclic voltammetry data show the electrostatic effect of the intradendritic secondary ammonium groups and the distinction between intradendritic and peripheral ferrocenyl groups.

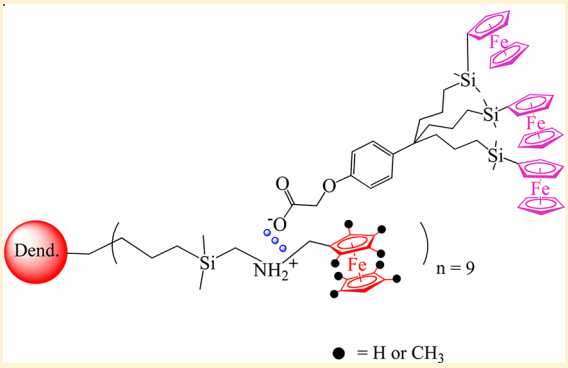

INTRODUCTION

Dendrimers now constitute a well-developed field[1] that has applications in biomedicine,[2] materials science,[3] and catalysis.[4] Most dendrimers are constructed covalently, but ionic bonding has recently attracted attention for enhanced drug encapsulation and specific physicochemical properties, including mesogens and energy-related aspects.[5,6] Here we report arene-centered polyamine dendrimers with ferrocenyl termini and a triferrocenyl dendron with a carboxylic group at the focal point and their ionic assemblies, i.e. dendrimers containing ammonium carboxylate linkers, some of which contain two kinds of functional ferrocenyl termini. The goal was to investigate the possibility of ionic linkages as a viable method for the design of redox sensors and energy-related materials. Among redox-active dendrimers, ferrocenyl derivatives[7] are the most practical ones, given the richness and applications of ferrocene chemistry[8] that is well illustrated inter alia in this issue and the robustness of the ferrocenyl derivatives.

RESULTS AND DISCUSSION

Synthesis of New Ferrocenyl Dendrimers Containing Secondary Amine Groups. We begin with the synthesis of arene-centered dendrimers according to our classic $CpFe^+$-induced nonaallylation of mesitylene in $[FeCp(\eta^6\text{-}1,3,5\text{-}C_6H_3(CH_3)_3)][PF_6]$[9] according to a 1→3 connectivity[10] providing the nonaallyl core[11] followed by hydrosilylation with chloromethyldimethylsilane, substitution of the terminal chloro group in **1** by reaction with sodium azide to give the nonaazide **2**,[11] and reduction of the azido groups in **2** to primary amine termini.[12] This sequence of reactions provides the dendritic zeroth-generation nonaamine core **3** that is protonated using aqueous HPF_6 to give the nonaammonium salt **4** (Scheme 1). The following generation is obtained upon Williamson reaction of the nonachloro core **1** with the phenol triallyl dendron **9** according to a known procedure followed by substitution of the terminal chloride by the azido group[11] that is subsequently reduced to the primary amine.[12] This gives the first-generation dendrimer **5** containing 27 NH_2 termini, and the 27-ammonium species **8** is obtained upon protonation of **5** with aqueous HPF_6 or aqueous HCl[12] (Scheme 2). These 9-NH_2- and 27-NH_2-terminated dendrimers are used to introduce the ferrocenyl groups upon reaction with either ferrocenyl aldehyde or octamethylferrocenyl aldehyde, although **5** slowly polymerizes in the condensed phase and should be used as freshly prepared. Both ferrocenyl[13] and octamethylferrocenyl[14] derivatives have already been condensed with polyimine DAB dendrimers by the groups of Jutzi and Casado, respectively, and have also been successfully used here to synthesize new ferrocenyl-terminated dendrimers. The imino-ferrocenyl dendrimers obtained using these reactions are reduced to the secondary aminomethylferrocenyl dendrimers **6** and **7** (Scheme 1). The new ferrocenyl-functionalized secondary polyamine dendrimer **6** (Scheme 1) is soluble in toluene, diethyl ether, dichloromethane, and tetrahydrofuran. This amino metallocene was insoluble in acetonitrile, but the ferrocenyl alcohol derived from the reduction of the excess of

Special Issue: Ferrocene - Beauty and Function

Received: July 2, 2013
Published: July 30, 2013

Scheme 1

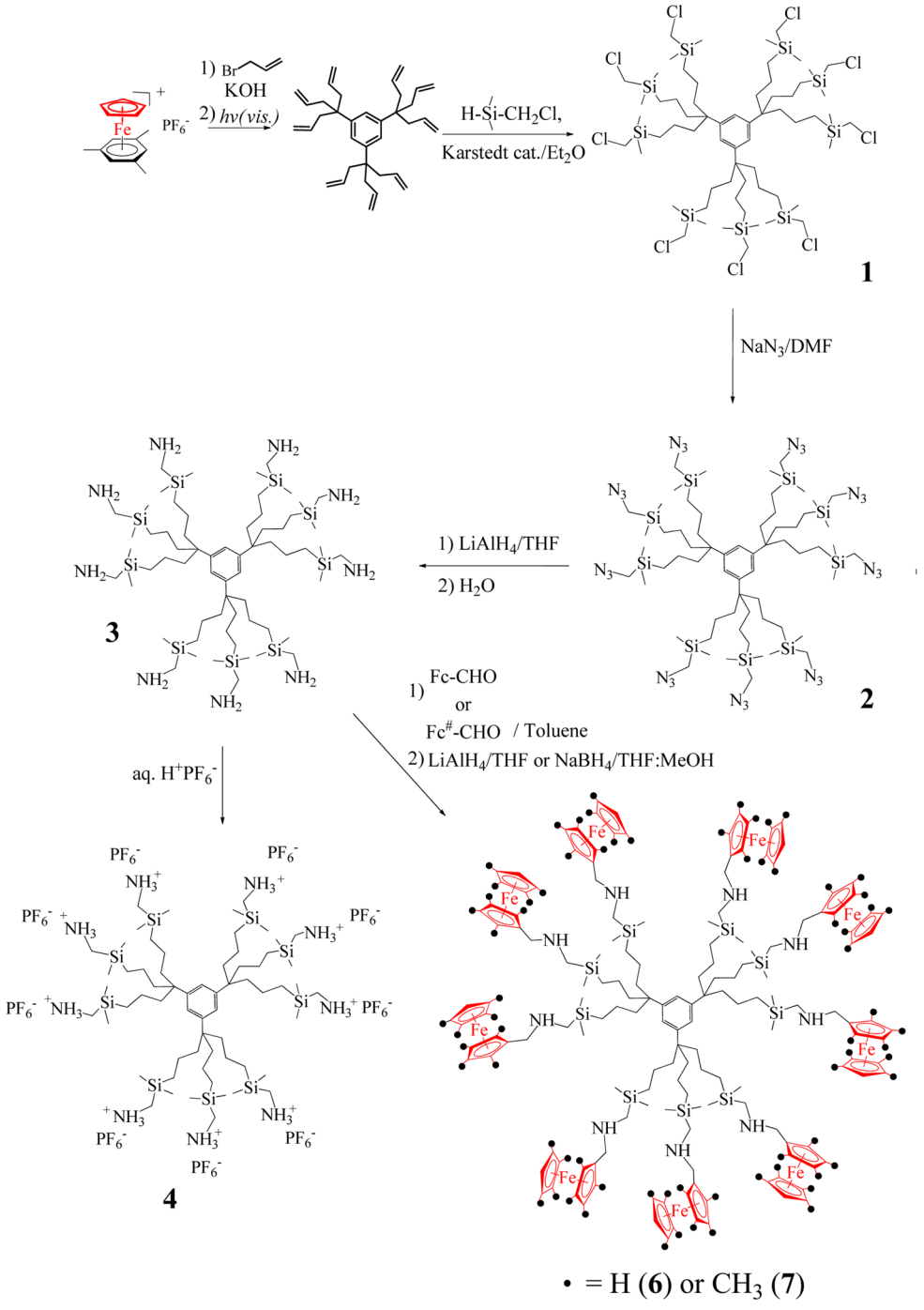

ferrocenyl aldehyde in the reaction solution is soluble in acetonitrile. We acted on this solubility difference to purify the products by precipitation of the crude reaction from acetonitrile with a small amount of dichloromethane. For the synthesis of the octamethylferrocenyl-functionalized dendrimer **7**, instead of ferrocenyl aldehyde, octamethylferrocenyl aldehyde[15] was used with the same route as the synthesis of the dendrimer ferrocenyl moieties, except for the process of reduction from imine to amine, which was achieved in this case by using $NaBH_4$ in a MeOH/THF mixture as solvent. The functionalized secondary polyamine dendrimer **7** with attached octamethylferrocenyl termini is soluble in toluene, diethyl ether, dichloromethane, and tetrahydrofuran. The polyamine ferrocenyl dendrimer is more aerobically stable than those containing octamethylferrocenyl termini in solution, because the eight methyl ferrocene substituents facilitate oxidation to ferrocenium derivatives by oxygen. These two secondary polyamine dendrimers **6** and **7** were characterized by ^{1}H NMR and ^{13}C NMR, IR, DOSY NMR, cyclic voltammetry, and elemental analyses.

Synthesis of the New Triferrocenyl Dendrons. A triferrocenyl dendron containing a carboxylic acid group at the focal point, **13**, used for the quaternization reaction, was synthesized according to Scheme 3. The synthesis of this dendron starts by the known $CpFe^+$-induced triallylation and exocyclic C−O cleavage in *p*-methylethoxytoluene obtained by

dx.doi.org/10.1021/om400650s | *Organometallics* 2013, 32, 6079−6090

Scheme 2

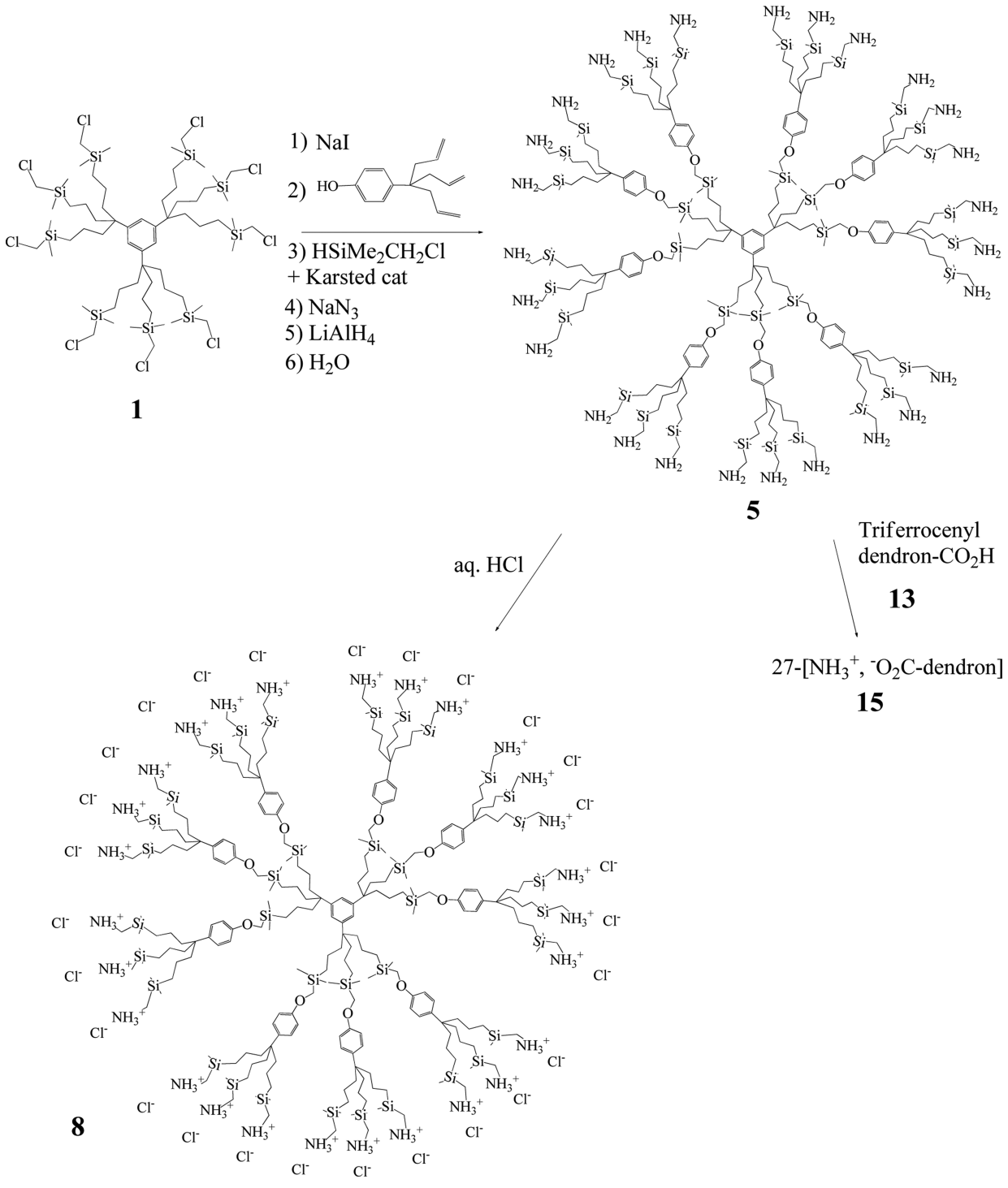

reaction of ethanol and sodium carbonate with [FeCp(η^6-*p*-$CH_3C_6H_4Cl$)][PF_6]. The phenol triallyl dendron **9** obtained in this way was hydrosilylated with dimethylsilylferrocene to give the known complex **10**.[9c] Then an S_N2 reaction of $BrCH_2COOMe$ with the phenol derivative **10** in the presence of K_2CO_3 provided the new ester **11**. Saponification[15] of the ester group was conducted with NaOH in H_2O/dioxane. The sodium carboxylate dendron product was obtained as a red oil in 90% yield, and acidification was carried out upon addition of aqueous HCl to give the ether-soluble carboxylic acid dendron **13** (Scheme 3). These new triferrocenyl dendrons were characterized by ^{1}H NMR and ^{13}C NMR, IR, mass spectrometry, cyclic voltammetry, and elemental analyses.

Synthesis of the Primary Polyammonium Dendrimers. The nonaammonium hexafluorophosphate dendrimer **4** was synthesized from the primary polyamine nona dendrimer **3** in dichloromethane by dropwise addition of aqueous HPF_6. The turbid solution was stirred for an additional 30 min. The same procedure was used for the synthesis of the ionic dendrimer **8** from the polyamine precursor **5** with aqueous HCl. These dendrimers were soluble only in very polar solvents such as water, DMF, and DMSO. In ^{1}H NMR and ^{13}C

Scheme 3

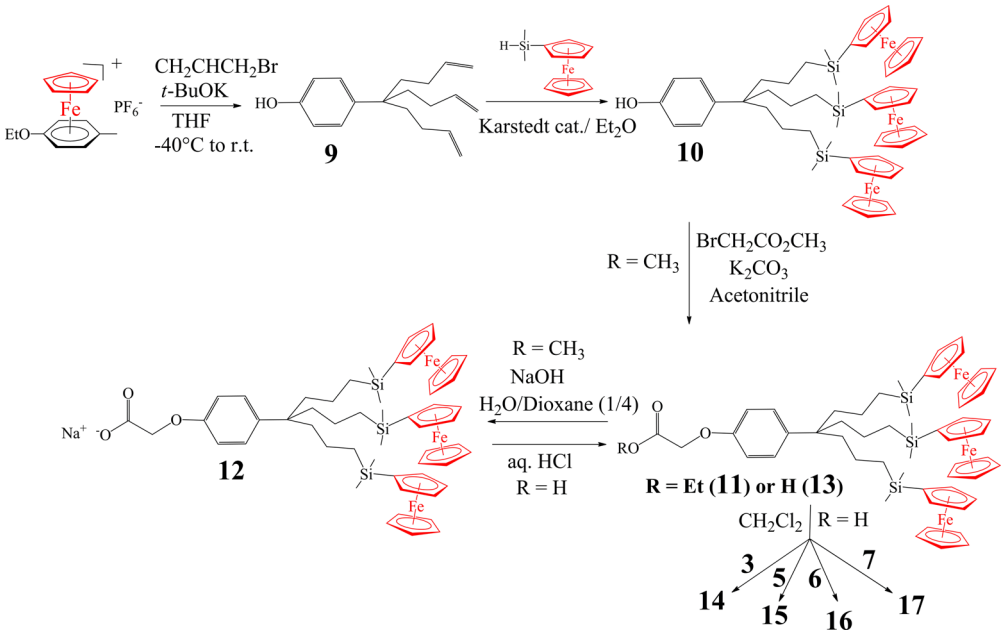

Chart 1

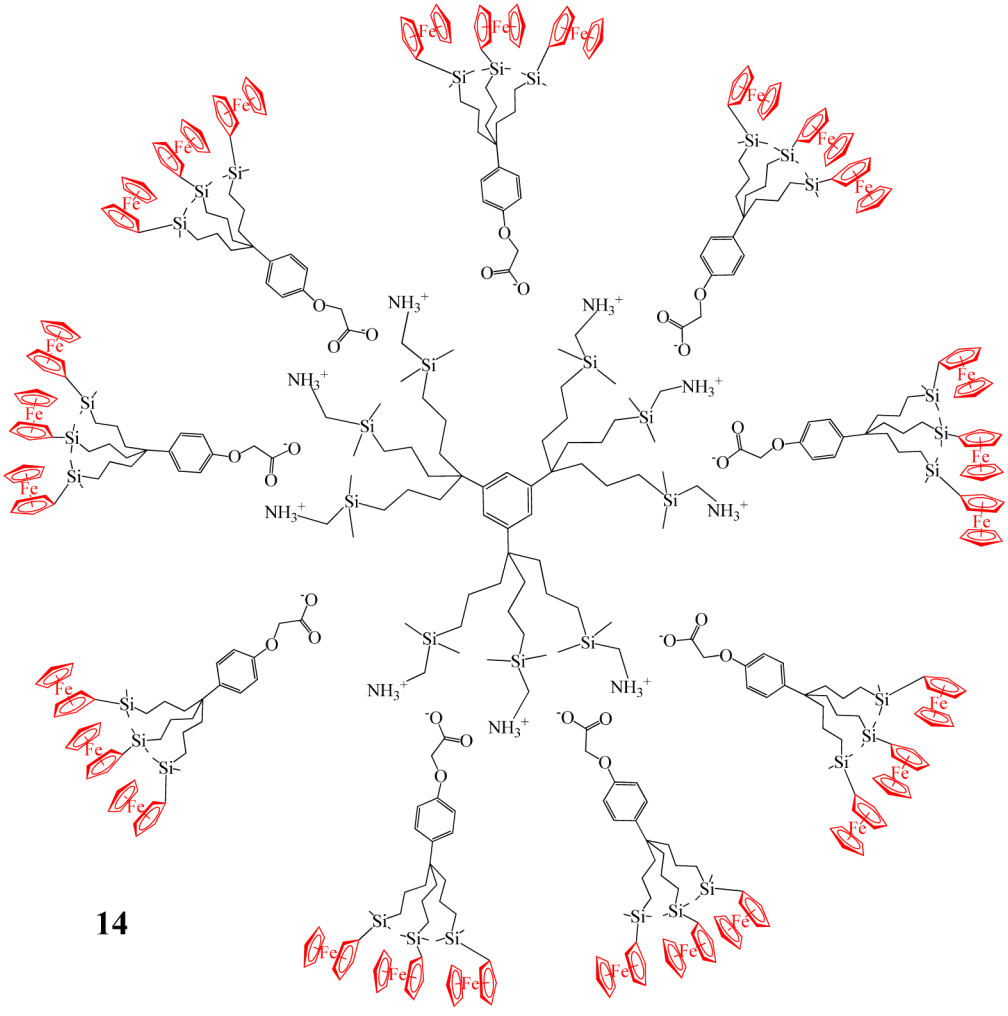

dx.doi.org/10.1021/om400650s | Organometallics 2013, 32, 6079−6090

Chart 2

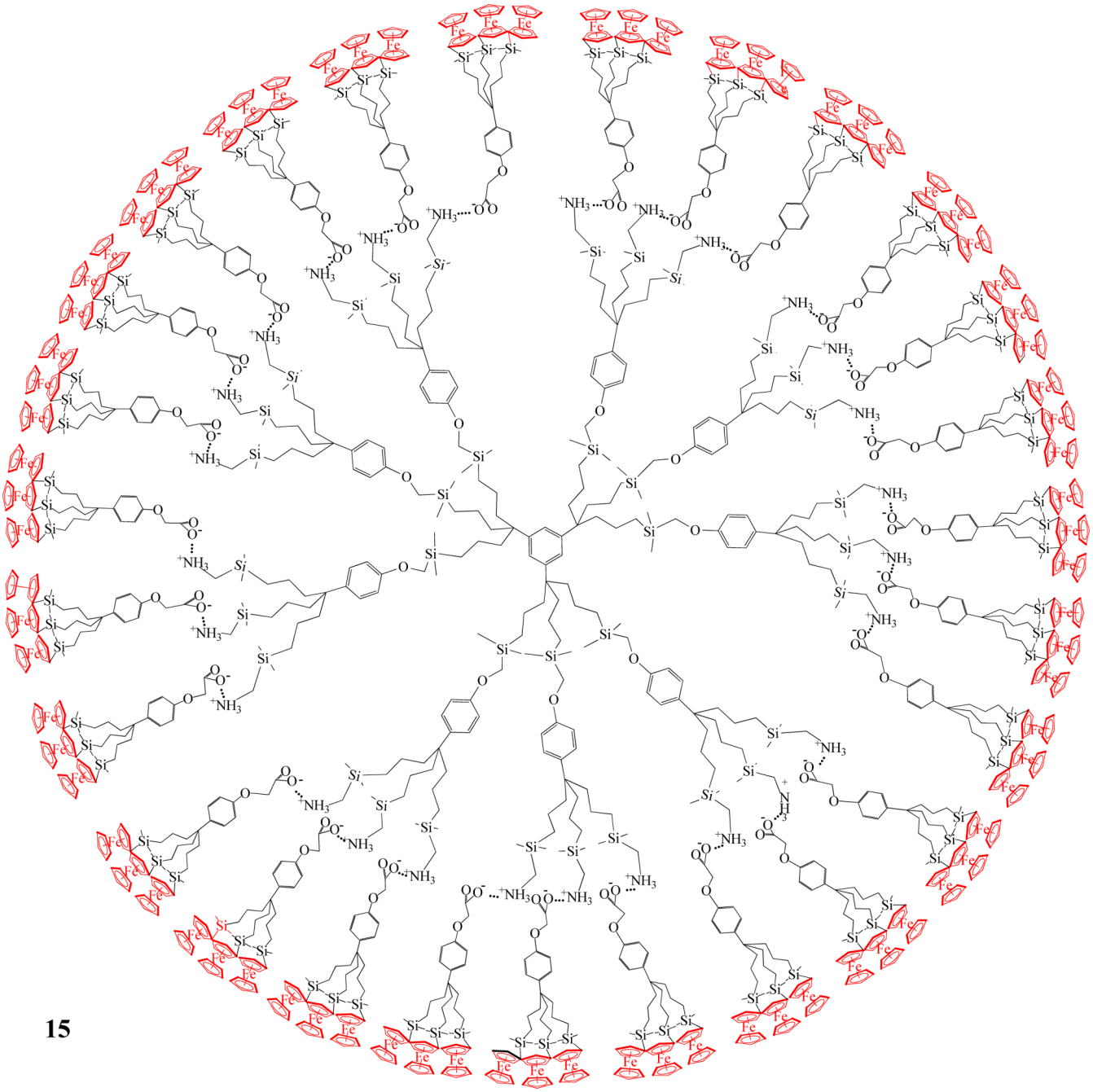

15

NMR in D_2O, all of the characteristic peaks of the dendrimers are observed. Products **4** and **8** were also analyzed by IR and elemental analysis.

Synthesis of the Supramolecular Ionic Ferrocenyl Dendrimers. The construction of higher generations of ferrocenyl dendrimers, generations 1 (products **14**, **16**, and **17**) and 2 (product **15**), were achieved in a facile and clean acid−base reaction (Charts 1−3). One equivalent of the primary and secondary polyamine dendrimer precursors, generations 0 and 1, were mixed with 9 and 27 equiv of the dendron **13** in dichloromethane at room temperature, yielding orange sticky oils. The solubility of the final supramolecular products is influenced as expected by the periphery of the dendrimers that contains 27 (products **14**, **16**, and **17**) and 81 (product **15**) ferrocenyl moieties, and these final dendrimers were soluble in dichloromethane, toluene, and THF. The dendron **13** with carboxylic acid at the focal point was ether soluble, as well as the secondary polyamine ferrocenyl and octamethylferrocenyl dendrimers **6** and **7**. On the other hand, the sodium carboxylate dendron **12** was insoluble in ether. The same phenomenon is noticed in the polyammonium carboxylate dendrimers that are not ether soluble. Finally, as the ammonium carboxylate functions are located at the interior of the dendrimers, the ionic groups are shielded, and they cause these ionic dendrimers to be insoluble in polar solvents such as water, acetone, and acetonitrile. Products **14**−**17** were characterized by ^{1}H NMR and ^{13}C NMR, IR, DOSY NMR, cyclic voltammetry, and elemental analyses.

NMR Spectroscopy. NMR spectroscopy proved to be a key tool for this study, confirming the proposed structures.

dx.doi.org/10.1021/om400650s | *Organometallics* 2013, 32, 6079−6090

Chart 3

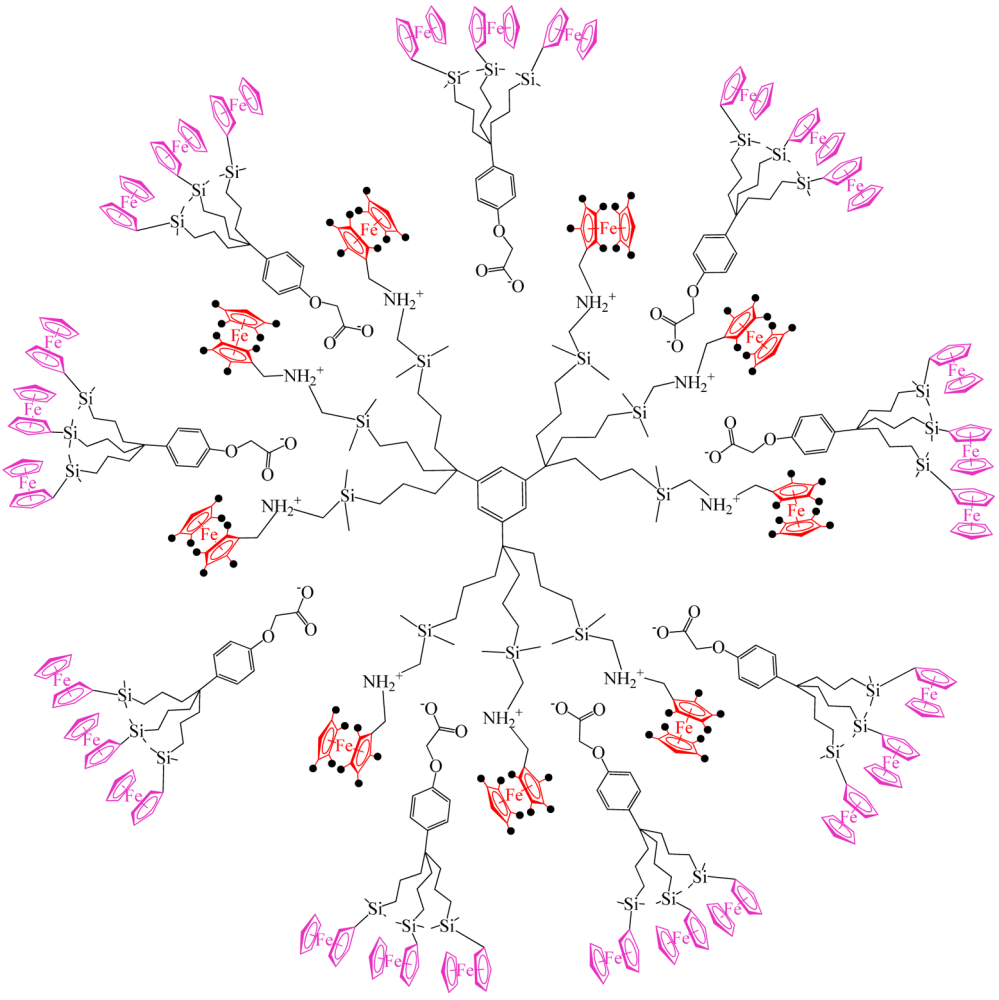

Table 1. ^{1}H NMR, ^{13}C NMR, and IR Data of Dendrons 11−13 and Dendrimers 3−8 and 14−17

compd	CH_2COOR $^{1}H/^{13}C$ (ppm)	$SiCH_2NH_x$ $^{1}H/^{13}C$ (ppm)	H_xNCH_2Cp $^{1}H/^{13}C$ (ppm)	IR KBr (cm^{-1})
dend-COOMe **11**[a]	4.66/65.10			1765; 1607
dend-COONa **12**[a]	4.29/64.00			1633
dend-COOH **13**[a]	4.56/66.29			1722; 1607
G0-NH_2 **3**[a]		2.04/29.90		3365; 1570
G1-NH_2 **5**[a]		2.06/30.00		3350; 1581
G0-NH_3PF_6 **4**[b]		2.34/27.76		3431; 830
G1-NH_3Cl **8**[b]		2.43/27.86		3425
G1-NH_3-Fc_{27} **14**[a]	4.38/67.98	2.27/25.58		3445; 1636
G2-NH_3-Fc_{81} **15**[a]	4.41/66.51	2.30/27.96		3452; 1643
G0-NH-Fc **6**[a]		2.10/29.70	3.54/53.15	3448; 1592
G0-NH-Fc[#] **7**[a]		2.04/29.72	3.48/50.20	3456; 1593
G1-NH_2-Fc_{36} **16**[a]	4.42/65.99	2.20/30.00	3.89/50.38	3452; 1641
G1-NH_2-$Fc^{\#}_{9}Fc_{27}$ **17**[a]	4.42/67.85	2.22/29.70	3.97/51.19	3461; 1630

[a]NMR in $CDCl_3$ at 25 °C. [b]NMR in D_2O at 25 °C.

Table 1 shows the comparative NMR (and IR) data for the dendronic carboxylic acid **13**, the corresponding carboxylate sodium salt **12**, the dendritic primary and secondary polyamines (**3** and **5**−**7**), and the dendritic primary and secondary polyammonium carboxylates (**4**, **8**, and **14**−**17**). For the dendron **11**, the ^{1}H NMR signals at 4.66 ppm of the CH_2COOMe group and the methyl group at 3.86 ppm appeared, integrating for two and three protons, respectively. After the saponification reaction, the dendron **12** showed the CH_2COONa signal at lower field as expected around 4.29 ppm, whereas the signal of the methyl group disappeared. The acidification reaction that turned the focal point into a

dx.doi.org/10.1021/om400650s | *Organometallics* 2013, 32, 6079−6090

carboxylic acid group was checked by the downfield shift of the CH_2COOH signal at 4.56 ppm. ^{13}C NMR spectroscopy also confirms the above structures (see the Supporting Information). The syntheses of the dendrimers **6** and **7** were also monitored by ^1H NMR. The resulting imine dendrimers resulting from the condensation reactions between **3** and the ferrocenyl and octamethylferrocenyl aldehydes showed the appearance of the −N=C*H*− signal at 8.1−8.2 ppm. After reduction to the corresponding secondary amines, this signal completely disappeared, and the $-NHCH_2-Cp$ signal appeared at 3.54 and 3.48 ppm, respectively. The corresponding signals of the ferrocene and octamethylferrocene moieties also confirmed the structures of the dendrimers **6** and **7**. The ionic dendrimers **4** and **8** were dissolved in D_2O, but their solubility in $CDCl_3$ (for the sake of comparison) was not determined. Nevertheless, the $-CH_2NH_3^+$ signals showed an important downfield shift. In the case of the primary polyammonium ferrocenyl dendrimers **14** and **15**, by comparison with the primary polyamine precursors **3** and **5** and dendron **13**, the $-CH_2NH_3^+$ proton signal was deshielded by about 0.25 ppm due to the presence of a nearby positive charge, and the signal of the $-CH_2COO^-$ protons was found to be shielded by about 0.17 ppm due to the presence of a nearby negative charge. These shifts in comparison to the neutral termini are in agreement with the formation of the ionic ammonium carboxylate linker. In the case of the secondary polyammonium dendrimers **16** and **17**, in comparison to the precursors **6** and **7** and dendron **13**, the differences are slightly smaller, as $-CH_2NH_2^+$ protons are deshielded by about 0.10 and 0.18 ppm, respectively and the $-CH_2COO^-$ protons are shielded by 0.14 ppm. This decrease of the charge effect is taken into account by the fact that the secondary ammonium groups are larger than the primary groups, resulting in a dilution of the positive charge and weaker (longer) ionic bond with the carboxylate. On the other hand, the $-NH_2^+CH_2-Cp$ signal of the secondary polyammonium dendrimers **16** and **17** are much more shifted (0.3 and 0.5 ppm) toward lower field than the signals of the other protons. Interestingly, the ^{13}C NMR spectra show the opposite effect for the $-CH_2NH_3^+$ (shielded compared to $-CH_2NH_2$) and $-CH_2COO^-$ carbons (deshielded in comparison to $-CH_2COOH$) in comparison to proton signals in dendrimers **14** and **15** (see Table 1). Finally, for the ionic dendrimers, the corresponding proton signals of the carboxylates are found at an intermediate region between those of the dendronic acid **13** and those of the dendronic sodium carboxylate salt **12**, probably because of the hydrogen bonding between the primary or secondary ammonium group with the carboxylate group.

Infrared Spectroscopy. The infrared spectra also provided valuable information on the new series of dendrons and dendrimers. Dendron **11** has the characteristic absorption of the ester group at 1765 cm^{-1}, and in dendron **13** the presence of a focal point consisting of the carboxylic acid was checked by the frequencies related to the carbonyl group at 1722 and 1607 cm^{-1} (and a broad band due to the O−H stretching at 3400 cm^{-1}). For the dendron **12** the single carbonyl band was shifted to the region between the two, at 1633 cm^{-1} due to the carboxylate absorption (both resonance forms equally contribute to the ground state of the molecule). Similarly, for the dendritic polyammonium carboxylates **14**−**17**, a strong band due to $-COO^-$ stretching was found in the region 1630−1643 cm^{-1}.

For the primary polyamines **3** and **5** two broad bands were observed in the region 3400−3300 cm^{-1} ($-NH_2$ stretching), whereas for the secondary polyamines **6** and **7** one broad band was observed in this region (−NH− stretching). For the primary and secondary polyammonium dendrimers (products **5**, **8**, and **14**−**17**), one broad absorption was observed in the region 3420−3460 cm^{-1} due to $-NH_3^+$ or $-NH_2^+-$ stretching (see Table 1).

DOSY NMR. DOSY (diffusion-ordered spectroscopy) experiments were conducted for the dendrimers **6**, **7**, **14**, **16**, and **17**. The main goal of these experiments was to measure the diffusion coefficient D and determine the size of the dendrimer in solution. The latter also reflects the purity of the products. The D value allows calculation of the hydrodynamic diameter of a molecule. Dendrimers are regarded as spherical molecular objects and characterized by an apparent diffusion coefficient. The Stokes−Einstein law, $D = k_BT/6\pi\eta r_H$, gives an estimate for the diameter of the molecule, where D is the diffusion coefficient, k_B the Boltzmann constant, T the absolute temperature, η the solvent viscosity, and r_H the hydrodynamic radius of the species (Table 2). The diameter values that are obtained include peripheral solvation of the products by solvent molecules in solution. This method was very useful for a clear comparison between the generations of the dendrimers and provided evidence for the formation of distinct ionic assemblies. For the nonionic dendrimers **6** and **7** (generation 0), the calculated r_H values are 2.08 and 2.29 nm, respectively, which shows the effect of the presence of methyl groups in **7** and provides a hydrodynamic radius that is 0.21 nm larger herewith. When the latter products were allowed to react with the dendron **13**, giving the next generation (generation 1) dendrimers **16** and **17**, it was found that the sizes of the obtained dendritic ionic assemblies represented by r_H are 3.21 and 3.33 nm, respectively. This finding that **17** has a larger r_H value than **16** is in agreement with the relative sizes of their precursors, respectively **6** and **7**. Finally, DOSY NMR, apart from providing valuable data such as the diffusion coefficients of the new dendrimers, also gives clear evidence of the size progression upon an increase of the dendrimer generation. It also allows comparing the sizes of the dendrimers (ionic and nonionic) that contain different metallocenes and distinguishing between the assemblies of primary and secondary polyammonium dendrimers of the same generation.

Table 2. Calculated Diffusion Coefficients and Hydrodynamic Radii Obtained by DOSY NMR

compd	D^a (±0.1), 10^{-10} m^2/s	$r_H{}^b$ (±0.1), nm
G0-NH-Fc **6**	1.947	2.08
G0-NH-Fc$^{\#}$ **7**	1.768	2.29
G1-NH_3-Fc_{27} **14**	1.044	3.87
G1-NH_2-Fc_{36} **16**	1.261	3.21
G1-NH_2-$Fc^{\#}{}_9Fc_{27}$ **17**	1.216	3.33

^aD is the diffusion coefficient, measured in $CDCl_3$ at 25 °C, ^br_H is the hydrodynamic radius, calculated using the Stokes−Einstein equation.

Cyclic Voltammetry.[16] The new dendron **13** and the series of polyamine and polyammonium ferrocenyl dendrimers were studied by cyclic voltammetry using decamethylferrocene ($FeCp^*_2$) as the internal reference,[17] although ferrocene was used in the cases of the octamethylferrocenyl dendrimers **7** and **17**. The cyclic voltammograms were recorded in dichloromethane, and the $E_{1/2}$ data (measured vs $FeCp^*_2$) are gathered

Table 3. Redox Potentials and Chemical (i_a/i_c) and Electrochemical ($E_{pa} - E_{pc} = \Delta E$) Reversibilities for Compounds 6, 7, and 13−17[α]

	$Fe^{III/II}$ dendron			$Fe^{III/II}$ dendrimer			$Fe^{\#III/II}$ dendrimer		
compd	$E_{1/2}$, V	ΔE, V	i_a/i_c	$E_{1/2}$, V	ΔE, V	i_a/i_c	$E_{1/2}$, V	ΔE, V	i_a/i_c
13	0.54	0.068	0.76						
6				0.55	0.065	1			
7							0.10	0.040	1
14	0.52	0.015	0.57						
15	0.53	0.012	0.42						
16	0.54	0.065	1	0.62	0.060	1			
17	0.52	0.025	1				0.27	0.030	0.9

[α]Conditions: supporting electrolyte, $[n\text{-}Bu_4N][PF_6]$ 0.1 M; solvent, CH_2Cl_2; reference electrode, Ag; working and counter electrodes, Pt; scan rate, 0.2 V/s; internal reference, $FeCp^*_2$.

in Table 3. For all of the dendrons and dendrimers, a single oxidation wave is observed for all the ferrocenyl groups, which appear seemingly equivalent, due to the weakness of the electrostatic factor between the redox sites of the dendron and metallodendrimers, as their redox sites are far away from one another, being separated by several bonds.[18] This single wave for all these three products is chemically and electrochemically reversible, although this reversibility is sometimes more or less perturbed by adsorption of these macromolecules onto the electrode. The electrochemical reversibility involving all the redox groups and signifying fast heterogeneous electron transfer is due to two factors that probably simultaneously occur: (i) fast rotation of the metallodendrimer within the electrochemical time scale, whereby all redox groups come in turn close to the electrode,[19] and (ii) electron hopping among the redox sites borne by flexible tethers, allowing hopping at an optimal distance and mutual orientation.[20] For dendron **13** and dendrimer **6**, the $Fe^{III/II}$ oxidation potentials of the ferrocenyl redox centers are about 0.54 V, whereas for dendrimer **7** this potential is 0.1 V. This cathodic shift is accounted for by both the electron-releasing property of the eight methyl substituents of the ferrocenyl groups that facilitate oxidation to ferrocenium. For primary polyammonium dendrimers **14** and **15**, the oxidation potentials are about the same as that of the dendron (only 20 mV less positive). The ferrocenyl centers at the periphery of the dendrimers are not influenced by the ammonium carboxylate linkages that are located in the dendritic interior. In the case of secondary polyammonium dendrimers with two kinds of ferrocenyl centers (product **16**) and the mixed ferrocenyl−octamethylferrocenyl dendrimer **17**, two waves are observed corresponding to each type of ferrocenyl redox center. For products **16** and **17**, oxidation of the peripheral ferrocenes also is recorded at 0.54 V, because they are not influenced by the remote interior ammonium carboxylate linkages. Oxidation of the interior ferrocenyl groups that are close to the ammonium groups now takes place at much more positive potentials, which is due to the interaction with and proximity of the ammonium cation. This trend is more marked for **17**, because the ammonium cation stabilizes the electron-rich octamethylferrocenyl group, which is oxidized at a potential 170 mV more positive (Figure 1).

The adsorption phenomenon during cyclic voltammetry of cationic dendrimers is much more marked for ionic dendritic assemblies than for neutral species. Indeed, for the dendron **13** and the generation-0 dendrimers **6** and **7**, adsorption is not observed, but in the case of the ionic compounds **14**−**17** adsorption is strong. Especially for compounds **14** and **15** adsorption onto the electrode is observed by scanning around

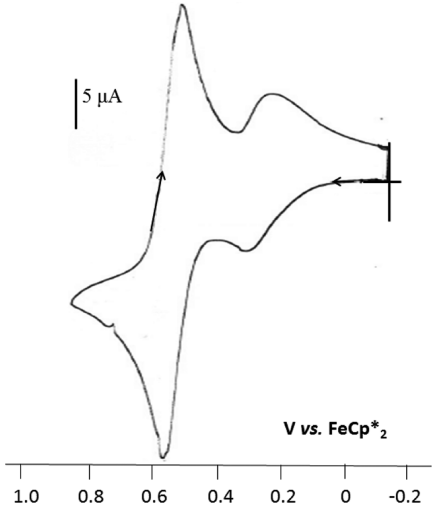

Figure 1. CV of **17** in CH_2Cl_2 solution. Conditions: reference electrode, Ag; working and counter electrodes, Pt; scan rate, 0.2 V/s; supporting electrolyte, $[n\text{-}Bu_4N][PF_6]$.

the oxidation potentials of the peripheral ferrocenyl groups, which confirms the formation of ionic generation-1 and -2 dendrimers and the existence of electrostatic forces. For the ionic compounds **16** and **17** adsorption is also highly marked. On the other hand, the dendron **13** and dendrimers **6** and **7** do not adsorb and cannot modify the Pt electrodes. This is not the case for dendrimers **14** and **16**, which deposit onto the electrode surfaces upon scanning toward potentials that are positive to ferrocenyl oxidation. Modification of electrodes with films of dendrimers containing reversible redox systems has been successful, resulting in detectable electroactive material. This electrochemical behavior of modified electrodes was studied in dichloromethane containing only the supporting electrolyte (Figures 2 and 3). A well-defined, symmetrical redox wave is observed, which is characteristic of a surface-confined redox couple, with the expected linear relationship of peak current with potential sweep rate v.[21] Repeated scanning does not change the voltammograms, demonstrating that the modified electrodes are stable to electrochemical recycling. However, splitting between oxidation and reduction peaks is observed (ΔE = 40 mV), which suggests that a structural reorganization takes place within the electrochemical redox process within these ionic dendritic assemblies. Values of the full width at half-maximum for compounds **14** and **16** were measured at a scan rate of 100 mV/s and found to be ΔE_{fwhm} = 150 and 140 mV, respectively, suggesting the existence of

dx.doi.org/10.1021/om400650s | Organometallics 2013, 32, 6079−6090

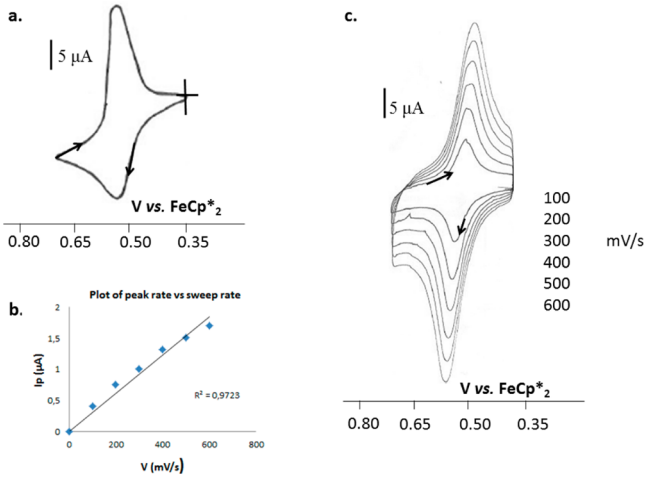

Figure 2. Cyclic voltammograms of **14** in CH_2Cl_2 solution containing 0.1 M [*n*-Bu_4N][PF_6]: (a) in solution; (b) intensity as a function of scan rate (linearity shows the expected behavior of an absorbed dendrimer); (c) modified Pt electrode at various scan rates in a CH_2Cl_2 solution (containing only the supporting electrolyte).

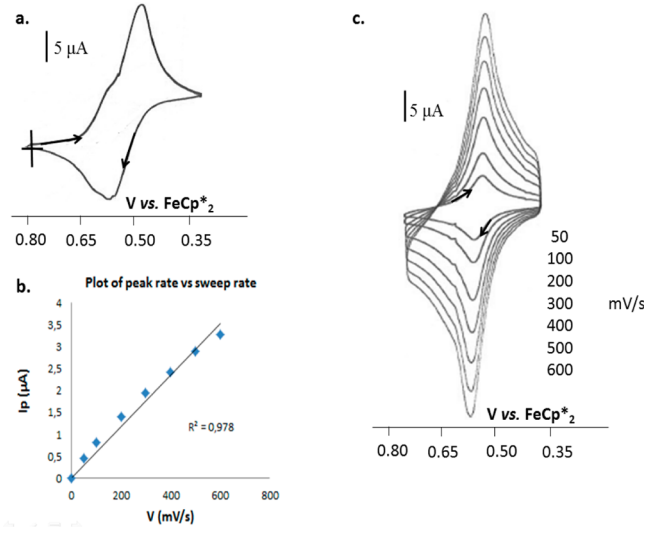

Figure 3. Cyclic voltammograms of **16** in CH_2Cl_2 solution containing 0.1 M [*n*-Bu_4N][PF_6]: (a) in solution; (b) intensity as a function of scan rate (linearity shows the expected behavior of an absorbed dendrimer); (c) modified Pt electrode at various scan rates in CH_2Cl_2 (solution containing only the supporting electrolyte).

repulsive forces between the ferrocenyl sites attached onto the electrode surface.[22] These Pt electrodes that are modified with dendrimers **14** and **16** are durable and reproducible, as no loss of electroactivity is observed after scanning several times or after standing in air for several days. The surface coverages of the electroactive ferrocenyl sites of the modified electrodes of metallodendrimers **14** and **16** are $\Gamma = 1 \times 10^{-11}$ and 1.7×10^{-11} mol cm^{-2}, respectively.

Concluding Remarks. The assembly of ionic dendrons and dendrimers represents a convenient way to synthesize large dendrimers with defect-free periphery insofar as the dendrimer purity solely depends on the purities of the dendrons and dendritic cores. The ionic linkers at the dendritic interiors are shielded so that the properties of these dendrimers essentially depend on the periphery. Of specific interest are ionic ferrocenyl dendrimers containing both intradendritic and peripheral ferrocenyl layers such as those synthesized here. The effect of the intradendritic positive charges of the ammonium groups clearly appears on the NMR chemical shifts and electrochemical potentials ($E_{1/2}$ values) of the inner ferrocenylmethyl groups. Interestingly, this electrostatic effect is more pronounced on the octamethylferrocenyl layer than on the parent ferrocenyl layer, probably because of the electron-rich methyl substituents in comparison to parent ferrocenyl sites. The $E_{1/2}$ value of the inner ferrocenyl layer is sufficiently shifted anodically to show a CV wave (shoulder) that is slightly distinct from that of the outer ferrocenyl layer. When the ferrocenyl substituents are different (H vs CH_3), the two separate CV waves clearly appear with relative intensities corresponding to their ratio (3/1). Finally, a characteristic of all the ionic ferrocenyl dendrimers is their strong ability to adsorb on electrodes and form derivatized electrodes that is considerably more marked than that of their neutral constituents. Potential applications are, for instance, the dendritic encapsulation of ionic or polar biomedical molecules in hydrophobic media and recyclable redox sensors.

EXPERIMENTAL SECTION

General Data. For general data including solvents, apparatuses, compounds, reactions, spectroscopy, and CV, see the Supporting Information . G_n indicates the generation number *n*.

G_0-9-dend-$NHCH_2$-Fc (6). To a solution of ferrocenyl aldehyde (0.077 g, 0.358 mmol, 1.02 equiv/branch) in 30 mL of dry toluene was added dropwise at 70 °C a solution of polyamine dendrimer **3** (0.050 g, 0.033 mmol) in 20 mL of dry toluene under nitrogen. The reaction mixture was heated at 75 °C for 12 h. The red solution was then evaporated to dryness under reduced pressure, the resulting reddish solid containing G_n-3*n*+2-dend-N═CH-Fc was dissolved in 20 mL of THF, and a suspension of $LiAlH_4$ (2 equiv/branch) in 20 mL of THF was added slowly at 0 °C. After the addition, the mixture was stirred for 16 h at 50 °C under nitrogen. To the reaction solution at 0 °C was added dropwise H_2O (6 equiv/branch), and the mixture was stirred for 20 min. After drying under vacuum, the crude product was washed with acetonitrile in order to remove the excess of ferrocene aldehyde/methanol. Further purification was achieved from precipitation in acetonitrile, and the product was obtained as an orange sticky oil. Yield: 70%.

^{1}H NMR ($CDCl_3$, 300 MHz): δ (ppm) 7.01 (3H, C*H* core), 4.22 (18H, Cp sub), 4.15 (45H, Cp free), 4.15 (18H, Cp sub), 3.54 (18H, $CpCH_2NH$), 2.10 (18H, $SiCH_2NH$), 1.63 (18H, $C_qCH_2CH_2CH_2Si$), 1.11 (18H, $C_qCH_2CH_2CH_2Si$) 0.54 (18H, $C_qCH_2CH_2CH_2Si$), 0.03 (s, 54H, $Si(CH_3)_2$). ^{13}C NMR ($CDCl_3$, 75 MHz): δ (ppm) 145.7 (C_q of arom core), 128.7 (CH of arom core), 86.3, 68.6, 68.4, 67.7 (Cp-C), 53.2 (CH_2-Cp), 43.1 ($C_qCH_2CH_2CH_2Si$), 42.1 ($C_qH_2CH_2CH_2Si$), 29.7 ($Si(CH_3)_2CH_2NH$), 17.7 ($C_qCH_2CH_2CH_2Si$), 15.1 ($C_qCH_2CH_2CH_2Si$), −3.8 ($Si(CH_3)_2$). Anal. Calcd for $C_{162}H_{237}Si_9N_9Fe_9$: C, 63.46; H, 7.79.. Found: C, 63.33; H, 7.80.

G_0-9-dend-$NHCH_2$-Fc# (7). To a solution of octamethylferrocene (54.8 mg, 0.16 mmol, 1.2 equiv/branch) in 30 mL of dry toluene was added dropwise at 70 °C a solution of nonaamine dendrimer (19.2 mg, 0.015 mmol) in 20 mL of dry toluene under nitrogen. The reaction mixture was heated to 75 °C for 16 h. The red solution was then evaporated to dryness under reduced pressure, and the resulting reddish solid containing G_0-dend-N═CH-Fc$^{\#}$ was washed with 20 mL of CH_3CN three times to remove the excess octamethylferrocene aldehyde/methanol. The resulting reddish solid was dried under reduced pressure and dissolved in a mixture of THF (10 mL) and CH_3OH (10 mL), and then $NaBH_4$ (3 equiv/branch) was slowly added at 0 °C. After the addition, the mixture was stirred for 30 min at 0 °C under nitrogen. The solvent was removed under reduced pressure. To the remaining solid was added dropwise H_2O (30 mL), and the compound was extracted three times with distilled diethyl ether. The combined organic phase was dried under anhydrous

dx.doi.org/10.1021/om400650s | *Organometallics* 2013, 32, 6079−6090

Na_2SO_4. After evaporation, the compound was obtained as a yellow solid without further purification. Yield: 77%.

^{1}H NMR ($CDCl_3$, 300 MHz): δ (ppm) 6.92 (3H, C*H* core), 3.48 (18H, NHCH_2C$_5$(CH$_3$)$_4$), 3.28 (9H, C$_5$(CH$_3$)$_4$*H*), 2.04 (18H, SiCH_2NH), 1.83, 1.79, 1.77, 1.71 (216H, C$_5$(CH_3)$_4$), 1.58 (18H, C$_q$CH_2CH$_2$CH$_2$Si), 1.04 (18H, C$_q$CH$_2$CH_2CH$_2$Si), 0.47 (18H, C$_q$CH$_2$CH$_2$CH_2Si), 0.05 (54H, Si(CH_3)$_2$). ^{13}C NMR ($CDCl_3$, 75 MHz): δ (ppm) 145.7 (C$_q$ of arom core), 128.7 (CH of arom core), 80.5, 80.0, 79.8, 79.7, 79.4, and 70.5 (Cp-C), 50.2 (Cp-CH_2NH), 43.8 (C$_q$CH_2CH$_2$CH$_2$Si), 42.0 (C$_q$CH$_2$CH$_2$CH$_2$Si), 29.7 (Si-(CH$_3$)$_2$CH_2NH), 17.8 (C$_q$CH$_2$CH$_2$CH$_2$Si), 15.1 (C$_q$CH$_2$CH$_2$CH$_2$Si), 11.0, 10.0, 9.9, 9.4 (C$_5$(CH_3)$_4$), −4.0 (Si(CH$_3$)═). Anal. Calcd for $C_{234}H_{381}Si_9Fe_9N_9$: C, 68.95; H, 9.43. Found: C, 68.71; H, 9.14.

G0-NH$_3^+$PF$_6^-$ (4). To a stirred solution of **3** (100 mg, 0.078 mmol) in 20 mL of distilled dichloromethane was added dropwise aqueous HPF_6 (1.1 equiv/branch) diluted in 3 mL of dichloromethane. Then a white precipitate started to form, but the product was stirred for an additional 30 min. The solution was evaporated, and the white solid was washed with acetone. The water-soluble white product **4** was obtained quantitatively.

^{1}H NMR (D_2O, 300 MHz): δ (ppm) 6.92 (3H, C*H* core), 2.26 (18H, SiCH_2NH$_3^+$), 1.55 (18H, C$_q$CH_2CH$_2$CH$_2$Si), 0.99 (18H, C$_q$CH$_2$CH_2CH$_2$Si) 0.50 (18H, C$_q$CH$_2$CH$_2$CH_2Si), 0.03 (s, 54H, Si(CH_3)$_2$). ^{13}C NMR (D_2O, 75 MHz): δ (ppm) 145.72 (C$_q$ arom), 121.65 (CH arom), 43.66 (C$_q$CH$_2$CH$_2$CH$_2$Si), 41.11 (C$_q$CH$_2$CH$_2$CH$_2$Si), 27.76 (Si(CH$_3$)$_2$CH$_2$NH$_2^+$), 17.41 (C$_q$CH$_2$CH$_2$CH$_2$Si), 13.60 (C$_q$CH$_2$CH$_2$CH$_2$Si), −4.95 (Si(CH_3)). Anal. Calcd for $C_{63}H_{156}Si_9N_9P_9F_{54}\cdot 2H_2O$: C, 28.73; H, 6.13. Found: C, 28.82; H, 6.17.

G1-NH$_3^+$Cl$^-$ (8). To a stirred solution of **5** (50 mg, 0.009 mmol) in 20 mL of distilled dichloromethane was added dropwise aqueous HCl (1.2 equiv/branch) diluted in 5 mL of dichloromethane. Then a white precipitate started to form, but the product was stirred for an additional 30 min. The solution was evaporated, and the white solid was washed with acetone. The water-soluble white waxy product **8** was obtained quantitatively.

^{1}H NMR (D_2O, 300 MHz): δ (ppm) 7.15, 6.72 (39H, C*H* core), 3.73 (18H, CH_2OAr), 2.43 (54H, SiCH_2NH$_3^+$), 1.88 (72H, C$_q$CH_2CH$_2$CH$_2$Si), 1.16 (72H, C$_q$CH$_2$CH_2CH$_2$Si), 0.63 (72H, C$_q$CH_2CH$_2$CH_2Si), 0.13 (216H, Si(CH_3)$_2$). ^{13}C NMR (D_2O, 75 MHz): δ (ppm) 158.72 (OC$_q$ arom of dendron), 139.56 (C$_q$ arom), 127.23, 113.77 (CH arom), 43.16 (C$_q$CH$_2$CH$_2$CH$_2$Si), 41.69 (C$_q$CH$_2$CH$_2$CH$_2$Si), 27.86 (Si(CH$_3$)$_2$CH$_2$NH$_3^+$), 17.60 (C$_q$CH$_2$CH$_2$CH$_2$Si), 14.56 (C$_q$CH$_2$CH$_2$CH$_2$Si), −4.19 (Si(CH$_3$)$_2$). Anal. Calcd for $C_{288}H_{624}Si_{36}N_{27}O_9Cl_{27}\cdot 5H_2O$: C, 51.88; H, 9.59. Found: C, 51.60; H, 9.57.

Triferrocenyl Carboxylic Acid (13). To a solution of **10** (0.351 g, 0.365 mmol) in 40 mL of acetonitrile were added K_2CO_3 (0.101 g, 0.731 mmol) and methyl bromoethanoate (0.084 g, 0.548 mmol), and the resulting solution was heated at 90 °C for 16 h under a nitrogen atmosphere. After the solvent and excess methyl bromethanoate were removed, the crude product was dissolved in 100 mL of dichloromethane and the solution filtered through Celite. The solvent was removed under vacuum, and the product was obtained as an orange oil. Then product **11** (0.360 g, 0.35 mmol) was dissolved in 18 mL of dioxane, and a solution of NaOH (56 mg, 1.39 mmol) in 5 mL of H_2O was added dropwise. The solution was stirred for 16h at room temperature. Then, the solution was evaporated, and the product was washed in water and extracted from dichloromethane. Acidification of **12** in dichloromethane/water with aqueous HCl gave product **13** as an orange shiny oil. Yield: 90%.

*Dendron **11**.* ^{1}H NMR ($CDCl_3$, 300 MHz): δ (ppm) 7.20, 6.90 (4H, arom), 4.66 (2H, CH_2COOMe), 4.35 (6H, Cp sub) 4.13 (15H, Cp free), 4.06 (6H, Cp sub), 3.86 (3H, CH$_2$COO$^-$CH_3), 1.65 (6H, C$_q$CH_2CH$_2$CH$_2$Si), 1.15 (6H, C$_q$CH$_2$CH_2CH$_2$Si), 0.65 (6H, C$_q$CH_2CH$_2$CH_2Si), 0.21 (18H, Si(CH_3)$_2$). ^{13}C NMR ($CDCl_3$, 75 MHz): δ (ppm) 168.48 (COOMe), 155.08 (OC$_q$ arom), 141.20 (C$_q$ arom), 127.32, 113.91 (CH arom), 72.75, 70.36 (CH of Cp sub), 71.16 (Cq of Cp sub), 67.81 (Cp free), 65.10 (CH$_2$COOMe), 52.17 (COOCH$_3$), 43.24 (C$_q$CH$_2$CH$_2$CH$_2$Si), 41.80 (C$_q$CH$_2$CH$_2$CH$_2$Si), 17.87 (C$_q$CH$_2$CH$_2$CH$_2$Si), 17.39 (C$_q$CH$_2$CH$_2$CH$_2$Si), −2.08 (Si-(CH$_3$)). MS (m/z): calcd for $C_{55}H_{72}O_3Si_3Fe_3$ 1032.2832, found 1032.7785.

*Dendron **12**.* ^{1}H NMR ($CDCl_3$, 300 MHz): δ (ppm) 7.15, 6.81 (4H, arom), 4.34 (6H, Cp sub), 4.29 (2H, CH_2COONa), 4.12 (15H, Cp free), 4.08 (6H, Cp sub), 3.86 (3H, CH$_2$COO$^-$CH_3), 1.62 (6H, C$_q$CH_2CH$_2$CH$_2$Si), 1.12 (6H, C$_q$CH$_2$CH_2CH$_2$Si), 0.64 (6H, C$_q$CH_2CH$_2$CH_2Si), 0.19 (18H, Si(CH_3)$_2$). ^{13}C NMR ($CDCl_3$, 75 MHz): δ (ppm) 167.16 (COONa), 154.07 (OC$_q$ arom), 140.17 (C$_q$ arom), 127.61, 113.71 (CH arom), 73.00, 70.72 (CH of Cp sub), 70.98 (Cq of Cp sub), 68.17 (Cp free), 64.00 (CH$_2$COONa), 42.89 (C$_q$CH$_2$CH$_2$CH$_2$Si), 41.82 (C$_q$CH$_2$CH$_2$CH$_2$Si), 17.76 (C$_q$CH$_2$CH$_2$CH$_2$Si), 17.23 (C$_q$CH$_2$CH$_2$CH$_2$Si), −1.79 (Si(CH_3)).

*Dendron **13**.* ^{1}H NMR ($CDCl_3$, 300 MHz): δ (ppm) 7.22, 6.90 (4H, arom), 4.56 (2H, CH_2COOH), 4.35 (6H, Cp sub), 4.13 (15H, Cp free), 4.06 (6H, Cp sub), 1.65 (6H, C$_q$CH_2CH$_2$CH$_2$Si), 1.17 (6H, C$_q$CH$_2$CH_2CH$_2$Si), 0.65 (6H, C$_q$CH_2CH$_2$CH_2Si), 0.21 (18H, Si-(CH_3)$_2$). ^{13}C NMR ($CDCl_3$, 75 MHz): δ (ppm) 174.41 (COOH), 155.11 (OC$_q$ arom), 141.32 (C$_q$ arom), 127.63, 114.42 (CH arom), 73.19, 70.90 (CH of Cp sub), 71.51 (Cq of Cp sub), 68.43 (Cp free), 66.29 (CH$_2$COOH), 43.33 (C$_q$CH$_2$CH$_2$CH$_2$Si), 42.04 (C$_q$CH$_2$CH$_2$CH$_2$Si), 18.26 (C$_q$CH$_2$CH$_2$CH$_2$Si), 17.74 (C$_q$CH$_2$CH$_2$CH$_2$Si), −1.87 (Si(CH$_3$)$_2$). MS (m/z): calcd for $C_{54}H_{70}O_3Si_3Fe_3$ 1018.2681, found 1018.2715. Anal. Calcd for $C_{54}H_{70}O_3Si_3Fe_3$: C, 63.65; H, 6.92. Found: C, 63.32; H, 7.07.

General Synthesis of Ionic Polyammonium Carboxylate Dendrimers. To a stirred solution of secondary or primary polyamine dendrimer in 10 mL of distilled dichloromethane was added dropwise a solution of triferrocenyl carboxylic acid (1 equiv/branch) in 10 mL of dichloromethane, and the mixture was stirred for 20 min. The solvent was removed under vacuum, and the compound was obtained as an orange-yellow sticky oil in quantitative yield.

*Dendrimer **14**.* The ionic dendrimer **14** was synthesized from **3** (10 mg, 0.008 mmol, 1 equiv) and **13** (71.5 mg, 0.070 mmol, 9 equiv) using the general synthesis of ionic polyammonium carboxylate dendrimers.

^{1}H NMR ($CDCl_3$, 300 MHz): δ (ppm) 7.17 (18H, arom), 7.02 (3H, arom core), 6.86 (18H, arom), 4.38 (18H, CH_2COO$^-$), 4.33 (54H, Cp sub), 4.12 (135H, Cp free), 4.05 (54H, Cp sub), 2.27 (18H, SiCH_2NH$_3^+$), 1.63 (72H, C$_q$CH_2CH$_2$CH$_2$Si), 1.15 (72H, C$_q$CH$_2$CH_2CH$_2$Si), 0.64 (72H, C$_q$CH_2CH$_2$CH_2Si), 0.20, 0.10 (216H, Si(CH_3)$_2$). ^{13}C NMR ($CDCl_3$, 75 MHz): δ (ppm) 174.88 (COO$^-$), 155.62 (OC$_q$ arom of dendron), 140.46 (C$_q$ arom), 127.48, 114.35 (CH arom), 72.91, 71.29, 70.75, 68.25 (Cp−C), 67.98 (CH$_2$COO$^-$), 43.24 (C$_q$CH$_2$CH$_2$CH$_2$Si), 42.19 (C$_q$CH$_2$CH$_2$CH$_2$Si), 25.58 (Si(CH$_3$)$_2$CH$_2$NH$_3^+$), 18.14 (C$_q$CH$_2$CH$_2$CH$_2$Si), 17.66 (C$_q$CH$_2$CH$_2$CH$_2$Si), −1.85, −3.99 (Si(CH$_3$)$_2$). Anal. Calcd for $C_{540}H_{777}Si_{36}Fe_{27}N_9O_{27}$: C, 62.69; H, 7.58. Found: C, 63.02; H, 7.73.

*Dendrimer **15**.* The ionic dendrimer **15** was synthesized from **5** (10 mg, 0.002 mmol, 1 equiv) and **13** (49.5 mg, 0.049 mmol, 27 equiv) using the general synthesis of ionic polyammonium carboxylate dendrimers.

^{1}H NMR ($CDCl_3$, 300 MHz): δ (ppm) 7.17 (72H, arom), 6.95 (3H, arom core), 6.85 (72H, arom), 4.41 (54H, CH_2COO$^-$), 4.33 (162H, Cp sub), 4.12 (405H, Cp free), 4.05 (162H, Cp sub), 3.55 (CH_2OAr), 2.30 (54H, SiCH_2NH$_3^+$), 1.64 (234H, C$_q$CH_2CH$_2$CH$_2$Si), 1.13 (234H, C$_q$CH$_2$CH_2CH$_2$Si), 0.65 (72H, C$_q$CH_2CH$_2$CH_2Si), 0.21, 0.05 (216H, Si(CH_3)$_2$). ^{13}C NMR ($CDCl_3$, 75 MHz): δ (ppm) 174.10 (COO$^-$), 154.87 (OC$_q$ arom of dendron), 141.22 (C$_q$ arom), 127.54, 114.34 (CH arom), 72.92, 71.28, 70.62, 68.09 (Cp-C), 66.51 (CH$_2$COO$^-$), 43.27 (C$_q$CH$_2$CH$_2$CH$_2$Si), 42.09 (C$_q$CH$_2$CH$_2$CH$_2$Si), 27.96 (Si(CH$_3$)$_2$CH$_2$NH$_3^+$), 18.07 (C$_q$CH$_2$CH$_2$CH$_2$Si), 17.60 (C$_q$CH$_2$CH$_2$CH$_2$Si), −1.91, −3.40 (Si(CH$_3$)$_2$). Anal. Calcd for $C_{1719}H_{2487}Si_{117}Fe_{81}N_{27}O_{90}\cdot 2CH_2Cl_2$: C, 62.74; H, 7.63. Found: C, 62.64; H, 7.89.

*Dendrimer **16**.* The ionic dendrimer **16** was synthesized from **6** (10 mg, 0.003 mmol, 1 equiv) and **13** (29.9 mg, 0.029 mmol, 9 equiv) using the general synthesis of ionic polyammonium carboxylate dendrimers.

^{1}H NMR ($CDCl_3$, 300 MHz): δ (ppm) 7.21, 6.89 (39H, arom), 4.41 (18H, CH_2COO^-), 4.35, 4.14, 4.07 (324H, Cp), 3.89 (18H, $^+NH_2CH_2Cp$), 2.20 (18H, $SiCH_2NH_2^+$), 1.65 (72H, $C_qCH_2CH_2CH_2Si$), 1.17 (72H, $C_qCH_2CH_2CH_2Si$) 0.66 (72H, $C_qCH_2CH_2CH_2Si$), 0.22, 0.07 (216H, $Si(CH_3)_2$). ^{13}C NMR ($CDCl_3$, 75 MHz): δ (ppm) 174.18 (COO^-), 155.70 (OC_q arom of dendron), 140.79 (C_q arom), 127.67, 114.56 (CH arom), 73.10, 71.50, 71.19, 70.81, 69.31, 68.99, 68.28 (Cp-C), 65.99 ($CH_2NH_2^+CH_2Cp$), 50.38 ($CH_2NH_2^+CH_2Cp$), 43.42 ($C_qCH_2CH_2CH_2Si$), 42.32 ($C_qCH_2CH_2CH_2Si$), 30.00 ($Si(CH_3)_2CH_2NH_2^+$), 18.26 ($C_qCH_2CH_2CH_2Si$), 17.76 ($C_qCH_2CH_2CH_2Si$), −1.73, −3.40 (Si-(CH_3)). Anal. Calcd for $C_{639}H_{867}Si_{36}Fe_{36}N_9O_{27}$: C, 63.28; H, 7.21. Found: C, 62.95; H, 7.12.

Dendrimer 17. The ionic dendrimer **17** was synthesized from **7** (10 mg, 0.002 mmol, 1 equiv) and **13** (22.5 mg, 0.022 mmol, 9 equiv) using the general synthesis of ionic polyammonium carboxylate dendrimers.

^{1}H NMR ($CDCl_3$, 300 MHz): δ (ppm) 7.16, 6.95, 6.82 (39H, arom), 4.42 (18H, CH_2COO^-), 4.34, 4.13, 4.06 (324H, Cp of Fc), 3.93 (18H, $^+NH_2CH_2Cp$ of Fc$^{\#}$), 3.28 (9H, $C_5(CH_3)_4H$ of Fc$^{\#}$), 2.23 (18H, $SiCH_2NH_2^+$), 1.83−1.68 (216H, $C_5(CH_3)_4$), 1.66 (72H, $C_qCH_2CH_2CH_2Si$), 1.22 (72H, $C_qCH_2CH_2CH_2Si$), 0.65 (72H, $C_qCH_2CH_2CH_2Si$), 0.21, 0.07 (216H, $Si(CH_3)_2$). ^{13}C NMR ($CDCl_3$, 75 MHz): δ (ppm) 174.18 (COO^-), 155.70 (OC_q arom of dendron), 140.79 (C_q arom), 127.55, 114.53 (CH arom), 86.31, 83.14, 81.88, 72.94, 71.19, 70.63, 68.11 (Cp-C), 67.85 (CH_2COO^-), 51.19 ($CH_2NH_2^+CH_2Cp$), 43.27 ($C_qCH_2CH_2CH_2Si$), 42.15 ($C_qCH_2CH_2CH_2Si$), 29.70 ($Si(CH_3)_2CH_2NH_2^+$), 18.09 ($C_qCH_2CH_2CH_2Si$), 17.76 ($C_qCH_2CH_2CH_2Si$), −1.02, −3.20 (Si-(CH_3)$_2$). Anal. Calcd for $C_{711}H_{1002}Si_{36}Fe_{36}N_9O_{27}\cdot 2CH_2Cl_2$: C, 64.39; H, 7.63. Found: C, 64.22; H, 7.85.

■ ASSOCIATED CONTENT

Supporting Information

Text and figures giving general data, spectroscopic data for compounds, NMR and mass spectra, IR and DOSY NMR spectra, and cyclic voltammograms. This material is available free of charge via the Internet at http://pubs.acs.org.

■ AUTHOR INFORMATION

Corresponding Author

*E-mail for D.A.: d.astruc@ism.u-bordeaux1.fr.

Notes

The authors declare no competing financial interest.

■ ACKNOWLEDGMENTS

Helpful assistance and discussion with Christophe Deraedt (synthesis), Claire Mouche (mass spectrometry), and Jean-Michel Lanier (NMR) from the CESAMO, Université Bordeaux 1, and financial support from the Université Bordeaux 1, the Centre National de la Recherche Scientifique (CNRS), the Agence Nationale de la Recherche (ANR), the Ministère de l'Enseignement Supérieur et de la Recherche Scientifique de Côte d'Ivoire (Ph.D. grant to R.D.), and the China Scholarship Council (Ph.D. grant to Y.W.) is gratefully acknowledged.

■ REFERENCES

(1) (a) Newkome, G. R.; Moorefield, C. N.; Vögtle, F. *Dendrons and Dendrimers. Concepts, Synthesis and Applications*; Wiley-VCH: Weinheim, Germany, 2001. (b) *Dendrimers and other Dendritic Polymers*; Tomalia, D., Fréchet, J. M. J., Eds.; Wiley-VCH: New York, 2002. (c) Vögtle, F.; Richardt, G.; Werner, N. *Dendrimer Chemistry. Concepts, Syntheses, Properties, Applications*; Wiley-VCH: Weinheim, Germany, 2009. (d) Astruc, D.; Boisselier, E.; Ornelas, C. *Chem. Rev.* **2010**, *110*, 1857−1959. (e) Caminade, A.-M.; Turin, C.-O.; Laurent, R.; Ouali, A.; Delavaux-Nicot, B. *Dendrimers. Towards Catalytic, Material and Biomedical Use*; Wiley: Chichester, U.K., 2011. (f) *Designing Dendrimers*; Campagna, S., Ceroni, P., Puntoriero, F., Eds.; Wiley: Hoboken, NJ, 2012.

(2) (a) Svenson, S.; Tomalia, D. A. *Adv. Drug. Deliv. Rev.* **2005**, *57*, 2106−2129. (b) Boas, U.; Heegard, P. M. H. *Chem. Soc. Rev.* **2004**, *33*, 43−63. (c) Gillies, E. R.; Fréchet, J. M. *J. Drug Deliv. Today* **2005**, *10*, 35−43. (d) Wolinsky, J. B.; Grinstaff, M. W. *Adv. Drug. Deliv. Rev.* **2008**, *60*, 1037−1055. (e) Tekade, R.; Kumar, P. V.; Jain, N. K. *Chem. Rev.* **2009**, *109*, 49−87. (f) Sevenson, S.; Tomalia, D. A. *Adv. Drug Delivery Rev.* **2012**, *64*, 102−115.

(3) (a) Moore, J. S. *Acc. Chem. Res.* **1997**, *30*, 402−413. (b) Newkome, G. R. *Pure Appl. Chem.* **1998**, *70*, 2337−2343. (c) Adronov, A.; Fréchet, J. M. J. *Chem. Commun.* **2000**, 1701−1710. (d) Nirengarten, J.-F. *Top. Curr. Chem.* **2003**, *228*, 87−110. (e) Scott, R.W. J.; Wilson, O. M.; Crooks, R. M. *J. Phys. Chem. B* **2005**, *109*, 692−704. (f) Lo, S.-C.; Burn, P.-L. *Chem. Rev.* **2007**, *107*, 1097−1116. (g) Balzani, V.; Bergamini, G.; Ceroni, P.; Vögtle, F. *Coord. Chem. Rev.* **2007**, *251*, 525−535. (h) Astruc, D. *Nat. Chem.* **2012**, *4*, 255−267.

(4) (a) Newkome, G. R.; He, E.; Moorefield, C. N. *Chem. Rev.* **1999**, *99*, 1689−1746. (b) Oosterom, G. E.; Reek, J. N. H.; Kamer, P. C. J.; van Leeuwen, P.W. N. M. *Angew. Chem., Int. Ed.* **2001**, *40*, 1828−1849. (c) Astruc, D.; Chardac, F. *Chem. Rev.* **2001**, *101*, 2991−3024. (d) Kreiter, R.; Kleij, A. W.; Gebbink, R. J. M. K.; van Koten, G. Dendrimers IV: Metal Coordination, Self Assembly, Catalysis. In *Topics in Current Chemistry*; Vögtle, F., Schalley, C. A., Eds.; Springer-Verlag: Berlin, 2001; Vol. *217*, pp 163−199. (e) van Heerbeeck, R.; Kamer, P. C. J.; van Leeuwen, P. W. N. M.; Reek, J. N. H. *Chem. Rev.* **2002**, *102*, 3717−3756. (f) Heuze, K.; Méry, D.; Gauss, D.; Blais, J.-C.; Astruc, D. *Chem. Eur. J.* **2004**, *10*, 3936−3944. (g) Liang, C.; Fréchet, J. M. *J. Prog. Polym. Sci.* **2005**, *30*, 385−402. (h) de Jesus, E.; Flores, J. C. *Ind. Eng. Chem. Res.* **2008**, *47*, 7968−7981. (i) Astruc, D. *Tetrahedron: Asymmetry* **2010**, *21*, 1041−1054. (j) Zaera, F. *Chem. Soc. Rev.* **2013**, *42*, 2746−2762.

(5) (a) Gonzales, L.; Skov, A. L.; Hvilstead, S. *J. Polym. Sci. Part A, Polym. Chem.* **2013**, *51*, 1359−1371. (b) Tanaka, K.; Chujo, Y. *Polym. J.* **2013**, *45*, 247−254. (c) Eleftheriou, E.; Karatass, K. J. *Chem. Phys.* **2012**, *137* (14), N°144905. (d) Pavan, G. M.; Monteagudo, S.; Guerra, J.; Carrion, B.; Ocana, V.; Rodriguez-Lopez, J.; Danani, A.; Perez-Martinez, F. C.; Cena, V. *Curr. Med. Chem.* **2012**, *19*, 4929−4941. (e) Prevette, L. E.; Nikoleva, E. N.; Al-Hashimi, H. M.; Holl, M. M. B. *Mol. Pharm.* **2012**, *9*, 2743−2749. (f) Das, S.; Sresh, B. R.; Jataraman, N.; Bhattacharyya, A. J. *J. Polym. Res.* **2012**, *19* (8), N° 9924. (g) Jeong, Y. H.; Yoon, H. J.; Jang, W. D. *Polym. J.* **2012**, *44*, 512−521. (h) Garzoni, M.; Cheval, N.; Fahmi, A.; Danani, A.; Pavan, G. M. *J. Am. Chem. Soc.* **2012**, *134*, 3349−3357. (i) Vergara, J.; Gimeno, N.; Cano, M.; Barbera, J.; Romero, P.; Serrano, J. L.; Ros, M. B. *Chem. Mater.* **2011**, *23*, 4931−4940. (j) Cgu, F. Q.; Lin, B. C.; Yan, F.; Qiu, L. H.; Lu, J. M. *J. Power Sources* **2011**, *196*, 7979−7984. (k) Choi, J. W.; Cho, B.-K. *Soft Matter* **2011**, *7*, 4045−4049. (l) Willerich, I.; Li, Y.; Franziska, G. *J. Phys. Chem. B* **2010**, *114*, 15466−15476.

(6) Reviews: (a) Tang, M. X.; Szka, F. C. *Gene Ther.* **1997**, *4*, 823−832. (b) Kojima, C.; Kono, K.; Maruyama, K.; Takagishi, T. *Bioconjugate Chem.* **2000**, *11*, 910−917. (c) Kohlhe, P.; Misra, E.; Kannan, R. M. *Int. J. Pharm.* **2003**, *259*, 143−160. (d) Gupta, U.; Agashe, H. B.; Asthana, A.; Jain, N. K. *Biomacromolecules* **2006**, *7*, 649−658.

(7) (a) Casado, C. M.; Cuadrado, I.; Moran, M.; Alonso, B.; Garcia, B.; Gonzales, B.; Losada, J. *Coord. Chem. Rev.* **1999**, *185−186*, 53−79. (b) Hwang, S. H.; Shreiner, C. D.; Moorefield, C. N.; Newkome, G. R. *New J. Chem.* **2007**, *31*, 1192−1217. (c) Astruc, D.; Liang, L.; Rapakousiou, A.; Ruiz, J. *Acc. Chem. Res.* **2012**, *45*, 630−640. (d) Casado, C. M.; Alonso, B.; Losada, J.; Garcia-Armada, M. P. In *Designing Dendrimers*; Campagna, S., Ceroni, P., Puntoriero, F., Eds.; Wiley: Hoboken, NJ, 2012; pp 219−262.

(8) (a) Togni, A.; Hayashi, T. *Ferrocenes*; Wiley-VCH: Weinheim, Germany, 1995. (b) Adams, R. D. *J. Organomet. Chem.* **2001**, *1*, 637−639. (c) *Ferrocenes*; Stepnicka, P., Ed.; Wiley: Weinheim, Germany,

2008. (d) For a recent overview of ferrocenes in nanomedicine, see: Ornelas, C. *New J. Chem.* **2011**, *35*, 1973−1985.
(9) (a) Valério, C.; Fillaut, J. L.; Ruiz, J.; Guittard, J.; Blais, J. C.; Astruc, D. *J. Am. Chem. Soc.* **1997**, *119*, 2588−2589. (b) Sartor, V.; Djakovitch, L.; Fillaut, J. L.; Moulines, F.; Neveu, F.; Marvaud, V.; Guittard, J.; Blais, J. C.; Astruc, D. *J. Am. Chem. Soc.* **1999**, *121*, 2929−2930. (c) Astruc, D.; Ruiz, J. *Tetrahedron* **2010**, *66*, 1769−1785.
(10) (a) Newkome, G. R.; Yao, Z.; Baker, G. R.; Gupta, V. K. *J. Org. Chem.* **1985**, *50*, 2003−2004. (b) Newkome, G. R.; Shreiner, C. *Chem. Rev.* **2010**, *110*, 6338−6442.
(11) (a) Ruiz, J.; Lafuentes, G.; Marcen, S.; Ornelas, C.; Lazare, S.; Cloutet, E.; Blais, J.-C.; Astruc, D. *J. Am. Chem. Soc.* **2003**, *125*, 7250−7257. (b) Ornelas, C.; Ruiz, J.; Belin, C.; Astruc, D. *J. Am. Chem. Soc.* **2009**, *131*, 590−601. (c) Boisselier, E.; Diallo, A. K.; Salmon, L.; Ornelas, C.; Ruiz, J.; Astruc, D. *J. Am. Chem. Soc.* **2010**, *132*, 2729−2742.
(12) Djeda, R.; Ornelas, C.; Ruiz, J.; Astruc, D. *Inorg. Chem.* **2010**, *49*, 6085−6101.
(13) Salmon, A.; Jutzi, P. *J. Organomet. Chem.* **2001**, *637*−*639*, 595−608.
(14) Zamora, M.; Herrero, S.; Losada, J.; Cuadrado, I.; Casado, C. M.; Alonso, B. *Organometallics* **2007**, *26*, 2688−2693.
(15) (a) Tezuka, Y.; Tanaka, S.; Imai, K. *Polymer* **1986**, *27*, 123−128. (b) Anderluh, M.; Cesar, J.; Stefanic, P.; Kikelj, D.; Janes, D.; Murn, J.; Nadrah, K.; Tominc, M.; Addicks, E.; Giannis, A.; Stegnar, M.; Dolenc, M. *Eur. J. Med. Chem.* **2005**, *40*, 25−49.
(16) (a) Geiger, W. E. *J. Am. Chem. Soc.* **1974**, *96*, 2632−2634. (b) Connelly, N. G.; Geiger, W. E. *Adv. Organomet. Chem.* **1984**, *23*, 1−93. (c) Geiger, W. E.; Connelly, N. G. *Adv. Organomet. Chem.* **1985**, *24*, 87−130. (d) Geiger, W. E. *J. Organomet. Chem. Libr.* **1990**, *23*, 142−172. (e) Connelly, N. G.; Geiger, W. E. *Chem. Rev.* **1996**, *96*, 877−910. (f) For a historical review, see: Geiger, W. E. *Organometallics* **2007**, *26*, 5738−5765. (g) For a perspective review, see: Geiger, W. E. *Organometallics* **2011**, *30*, 28−31.
(17) Ruiz, J.; Astruc, D. *C. R. Acad. Sci., Ser. IIc: Chim.* **1998**, *1*, 21−27.
(18) (a) Flanagan, J. B.; Margel, S.; Bard, A. *J. Am. Chem. Soc.* **1978**, *100*, 4248−4253. (b) Sutton, J. E.; Sutton, P. M.; Taube, H. *Inorg. Chem.* **1979**, *18*, 1017−1024. (c) Richardson, D. E.; Taube, H. *Coord. Chem. Rev.* **1984**, *60*, 107−129. (d) Barrière, F.; Geiger, W. E. *Acc. Chem. Res.* **2010**, *43*, 1030−1039.
(19) Gorman, C. B.; Smith, B. L.; Parkhurst, H.; Sierputowska-Gracz, H.; Haney, C. A. *J. Am. Chem. Soc.* **1999**, *121*, 9958−9966.
(20) Amatore, C.; Bouret, Y.; Maisonhaute, E.; Goldsmith, J. I.; Abruña, H. D. *Chem. Eur. J.* **2001**, *7*, 2206−2226.
(21) (a) Abruña, H. D. In *Electroresponsive Molecular and Polymeric Systems*; Skotheim, T. A., Ed.; Dekker: New York, 1988; Vol. *1*, p 97. (b) Murray, R. W. In *Molecular Design of Electrode Surfaces*; Murray, R. W., Ed.; Wiley: New York, 1992; Techniques of Chemistry *XXII*, p 1.
(22) (a) Peerce, P. J.; Bard, A. J. *J. Electroanal. Chem.* **1980**, *114*, 89−111. (b) Lenhard, J. R.; Murray, R. W. *J. Am. Chem. Soc.* **1978**, *100*, 7870−7875. (c) Brown, A. P.; Anson, F. C. *Anal. Chem.* **1977**, *49*, 1589−1595. (d) Laviron, E. *J. Electroanal. Chem.* **1981**, *122*, 37−44.

ORGANOMETALLICS

Article

pubs.acs.org/Organometallics

Rhodicenium Salts: From Basic Chemistry to Polyelectrolyte and Dendritic Macromolecules

Amalia Rapakousiou, Lucia Herrer Jimenez, Yanlan Wang, Claire Mouche, and Didier Astruc*

ISM, UMR CNRS No. 5255, Univ. Bordeaux, 33405 Talence Cedex, France

Supporting Information

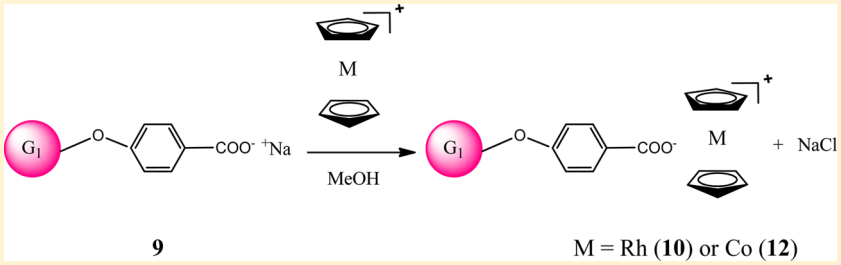

9 M = Rh (**10**) or Co (**12**)

ABSTRACT: A new, facile synthesis of rhodicenium chloride is described, leading to the synthesis of rhodicenium tetraarylborate, the first rhodicenium salt that is soluble in less polar solvents. This opens the route to further chemistry that was prevented by the insolubility of the formerly available rhodicenium salts. This strategy has been extended to the synthesis of water-soluble polyelectrolyte and dendritic macromolecular cobaltocenium and rhodicenium salts.

INTRODUCTION

After 60 years of metallocene chemistry, it is remarkable that rhodicenium chemistry has been so little developed. Following Wilkinson's seminal synthesis in 1953 from a cyclopentadienyl salt and tris(acetylacetonato)rhodium(III),[1] the generation of rhodicenium cations was reported in the gas phase by a metal switching reaction[2] and by the gas-phase photoinduced reaction of $RhC_5H_6^+$ with cyclopentane[3] before the use of modern microwave techniques.[4] Rhodicenium cations share with their first-row analogues cobaltocenium cations similar robustness owing to their 18-electron nature. Their salts with mineral acids are all very soluble in water; however, even with very large counteranions they are difficult to precipitate from water. A polarographic study by Wilkinson's group of $[RhCp_2][Cl]$ showed a cathodic wave at −1.53 V vs SCE representing a one-electron reduction; however, the neutral $RhCp_2$ could not be isolated from aqueous solutions. The reaction of anhydrous rhodium chloride with sodium cyclopentadiene produced the diamagnetic compound $RhC_{10}H_{11}$, which was formulated as the Rh^I cyclopentadiene complex $[Rh(\eta^4\text{-}C_5H_6)Cp]$ (Cp = η^5-C_5H_5), and the same compound was formed from reduction of $[RhCp_2][Cl]$ in aqueous ethanol by $NaBH_4$.[5] The suggested mechanism involved attack by a hydride either on the Cp ring or intermediately on the metal atom. Oxidation of $RhC_{10}H_{11}$ with HCl gave 50% of the initial rhodicenium cation. A gas also evolved consisting of hydrogen together with C_5 olefinic hydrocarbons. Rhodocene was reported upon reduction of rhodicenium cation with molten sodium and could be trapped only on a liquid-nitrogen-cooled ESR probe,[6] but it decomposed at room temperature with formation of the dimer $[RhCp(\eta^4\text{-}C_5H_5{-})]_2$, isolated in 8% yield, in which the η^8,μ_2-dicyclopentadiene ligand bridges the two Rh^I centers.[7] Geiger's group reported the electrochemical reduction of the rhodicenium ion in nonaqueous solvents (CH_3CN and DMF) in two one-electron-reduction processes, and the dimer $[RhCp(\eta^4\text{-}C_5H_5{-})]_2$ was isolated by electrolysis of rhodicenium solutions in good yield.[8] This material was quantitatively oxidized back to $[Cp_2Rh][BF_4]$ by $[(C_6H_5)_3C][BF_4]$ in dichloromethane. Rhodocene has been also observed in mass spectral studies of rhodicenium.[9] The instability of this odd-electron rhodocene in comparison to its thermally stable analogue cobaltocene is due to the fact that, in contrast to the first-row 19-electron transition-metal sandwich complexes, for which the orbital of the 19th valence electron is mostly metal based,[10] second- and third-row transition-metal sandwich complexes with one electron in excess vs the 18-electron configuration are ligand-based radicals. The first isolated polysubstituted rhodocene was $[Rh(C_5HPh_4)_2]$, obtained from the reduction of $[Rh(C_5HPh_4)_2]^+$ due to the very large tetraphenylcyclopentadienyl ligands, which inhibited dimerization.[11]

Various rhodicenium complexes with substituted cyclopentadienyl ligands have been reported,[12] including monophosphorylated rhodicenium analogues[13] and functionalized rhodicenium salts containing two acyl and/or imidoyl substituents.[14] Polymethyl rhodicenium complexes have been also reported,[15] including decamethylrhodicenium[16] and nonamethylrhodicenium,[17] imparting greater stability and solubility. Heteronuclear compounds such as rhodocenylferrocene, 1,1′-dirhodocenylferrocene, and 1-cobaltocenyl-1′-rhodocenylferrocene have also been prepared by the statistical nucleophilic

Received: January 13, 2014
Published: February 18, 2014

attack of 1,1′-dilithioferrocene on $[CoCp_2][PF_6]$ and $[RhCp_2][PF_6]$, followed by subsequent hydride abstraction with tritylium hexafluorophosphate, yielding the respective termetallocene dications.[18]

Altogether, rhodicenium chemistry is rather limited, and applications are scarce with only some mentions of biomedical usage.[19] Indeed, a major problem is the insolubility of the tetrafluoroborate and hexafluorophosphate salts in common solvents. Therefore, we have reinvestigated the basic rhodicenium chemistry, including an alternative synthesis of rhodicenium chloride from rhodium(III) chloride hydrate, in a two-step reaction which parallels that known for the synthesis of decamethylrhodicenium,[16] and we have disclosed the access to rhodicenium salts, including rhodicenium salts containing polymeric and dendritic macromolecular anions. Finally, the new family of ionic metallocenium dendrimers has been extended to the analogous and comparable cobaltocenium dendrimers.

RESULTS AND DISCUSSION

Synthesis of Rhodicenium Chloride. The new synthesis of rhodicenium chloride started from the reaction of (trimethylsilyl)cyclopentadiene[20] with rhodium(III) chloride hydrate in 2-propanol at room temperature, forming the cyclopentadiene rhodium dichloride oligomer[20] that is soluble only in water, DMF, and DMSO. Then, the synthesis of rhodicenium chloride[1] was achieved from the reaction of this oligomer with sodium cyclopentadiene in THF. The product was extracted with hot water, and washing with diethyl ether several times permitted the removal of unreacted organic species. Extraction with nitromethane (in which the other reaction product, NaCl, is insoluble) gave rhodicenium chloride as a yellowish oil (Scheme 1).

Scheme 1. New Synthesis of Rhodicenium Chloride (4)

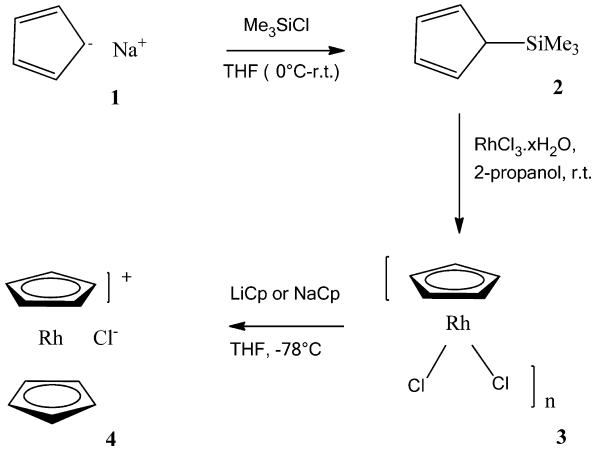

Access to the rhodicenium hexafluorophosphate **5** was also easily achieved by adding HPF_6 into the aqueous solution of rhodicenium chloride. ^{1}H NMR is a practical tool allowing comparison among the three rhodium complexes **3**–**5** (Figure 1).

The protons of the Cp ring of rhodicenium chloride are deshielded by ~0.1 ppm in comparison to rhodicenium hexafluorophosphate. The complexes **3**–**5** are soluble only in very polar solvents such as water, DMF, and DMSO, which is a drawback for further reactions of a rhodicenium salt. Therefore,

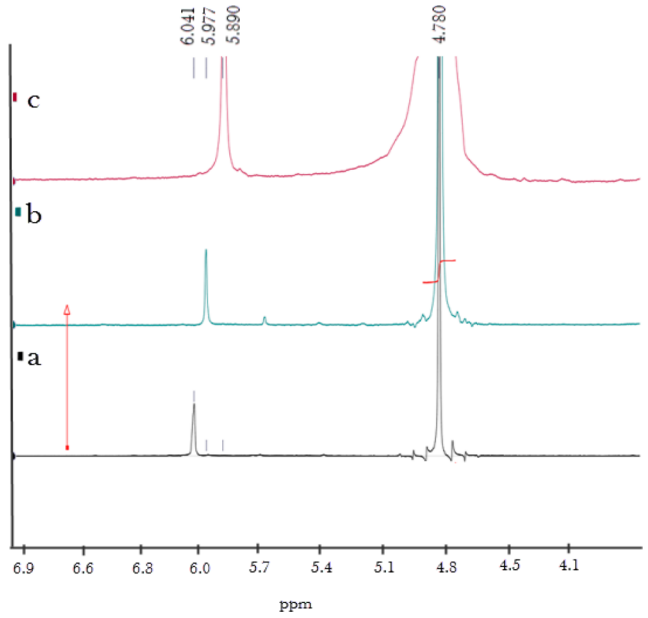

Figure 1. Comparative ^{1}H NMR spectra in D_2O of $[RhCp(Cl)_2]_n$ (**3**), $[RhCp_2][Cl]$ (**4**), and $[RhCp_2][PF_6]$ (**5**): (a) **3**, δ 6.04 ppm (10H, Cp); (b) **4**, δ 5.98 ppm (10H, Cp); (c) **5**, δ 5.89 ppm (10H, Cp).

the synthesis of rhodicenium salts with adequate counteranions for a better solubility in less polar solvents was envisaged.

Synthesis of a Rhodicenium Tetraarylborate. $Na[BAr^F_4]$ (Ar^F = 3,5-bis(trifuoromethyl)phenyl) was used as a starting material to react with rhodicenium chloride in order to form the salt $[RhCp_2][BAr^F_4]$ (**6**), in addition to easily removable NaCl (Scheme 2). Extraction of the product in

Scheme 2. Synthesis of a Rhodicenium Tetraarylborate

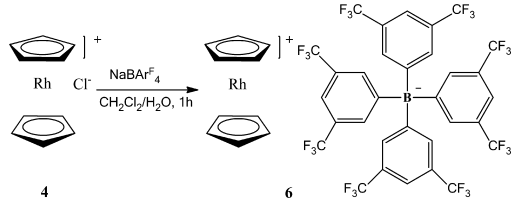

dichloromethane and evaporation of the solvent gave a red-violet powder. ^{1}H NMR in $CDCl_3$ showed the two typical signals of the aryl groups with the expected 4 and 8 protons and the 10 protons of the two Cp rings, whose signal is now found at 5.63 ppm. This new rhodicenium salt **6** is soluble in lower-polarity solvents such as diethyl ether, dichloromethane, and THF (Table 1). Further reactions of **6** can thus be conveniently achieved in less polar solvents, including hydride addition to rhodicenium salts. For instance, the reaction of **3** with $NaBH_4$ occurs in aqueous ethanol in 30 min,[5] whereas that of **6** proceeds in THF in 5 min followed by extraction with pentane, giving $[Rh(\eta^4\text{-}C_5H_6)Cp]$ (see the Supporting Information). It is likely that **6** will be an appropriate starting material for various nucleophilic reactions with rhodicenium that are impossible with **4** and **5** due to their insolubility in less polar solvents such as THF and dichloromethane, in which **6** is readily soluble.

A sample of the complex **6** in diethyl ether solution was analyzed by FD mass spectrometry, showing the mass peak of

dx.doi.org/10.1021/om500028e | Organometallics 2014, 33, 1259–1265

Table 1. Solubilities of the Cyclopentadienylrhodium Dichloride Oligomer 3 and Rhodicenium Complexes 4−6, 8, 10, and 12 as a Function of Their Counteranion, at 25 °C[a]

compd	counteranion	$(C_2H_5)_2O$	CH_2Cl_2	THF	CH_3CN	H_2O	DMSO
3		−	−	−	−	+	+
4	Cl^-	−	−	−	−	+	+
5	PF_6^-	−	−	−	+	+	+
6	$BAr^F{}_4^-$	+	+	+	+	−	−
8	Poly-SO_3^-	−	−	−	−	+	+
10	Dend-COO^-	−	−	−	−	+	+
12	Dend-COO^-	−	−	−	−	+	+

[a]Legend: +, very soluble; −, insoluble.

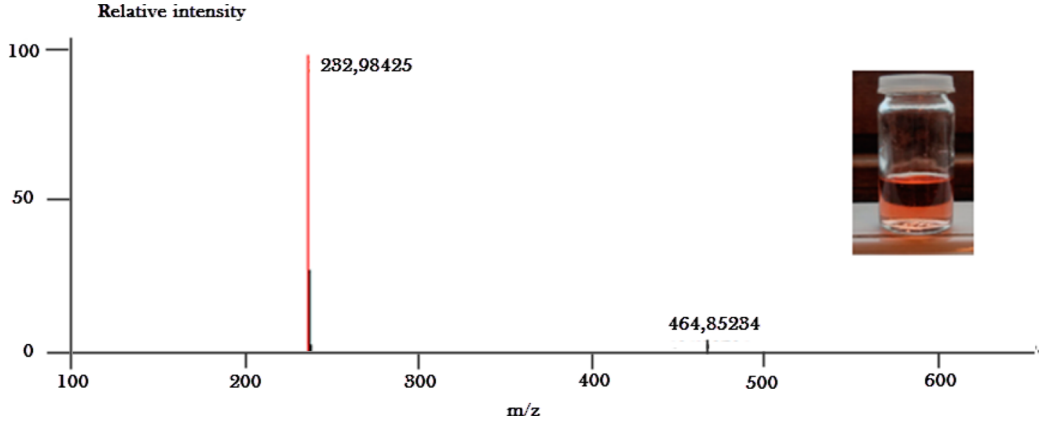

Figure 2. FD MS of $[RhCp_2][BAr^F{}_4]$ (**6**) and photo of the FD MS sample of **6** in diethyl ether.

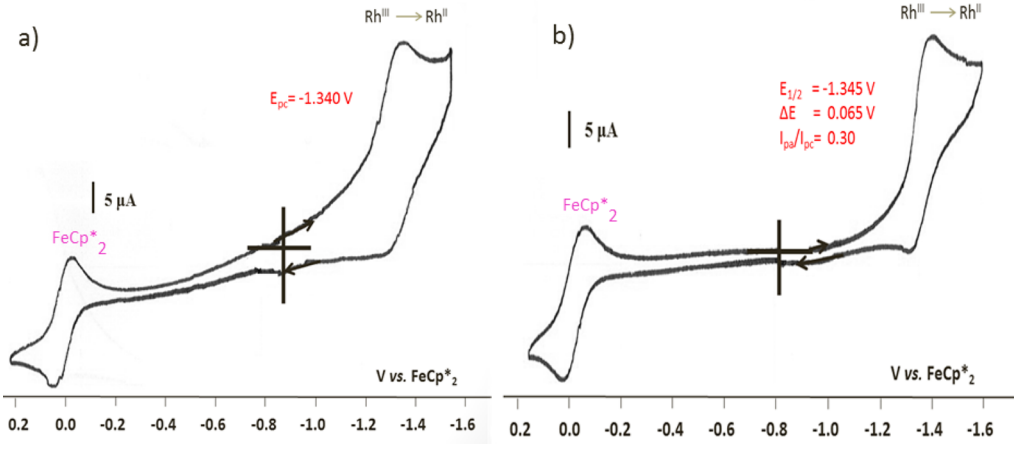

Figure 3. Cyclic voltammetry of $[RhCp_2][BAr^F{}_4]$ (**6**) in THF at (a) 22 °C and (b) −50 °C. The wave at 0.0 V corresponds to the internal reference $[FeCp^*{}_2]$.[22] Conditions: reference electrode, Ag; working and counter electrodes, Pt; scan rate, 0.05 V/s; supporting electrolyte, $[n\text{-}Bu_4N][BAr^F{}_4]$.

the ionized rhodicenium cation at m/z 232.98 that confirmed the $[RhCp_2][BAr^F{}_4]$ structure (Figure 2).

Product **6** was also characterized by cyclic voltammetry using decamethylferrocene as the internal reference.[22] The cyclic voltammograms were recorded in THF, a very good solubility being accessible with this solvent, at two different temperatures: 22 and −50 °C (Figure 3). At 22 °C an irreversible wave is observed at E_{pc} = −1.340 V, due to a one-electron reduction of compound **6** ($Rh^{III/II}$). However, under the same conditions, lowering the temperature to −50 °C allowed the observation of a partial chemical reversibility of the same wave at $E_{1/2}$ = −1.345 V. This wave is electrochemically reversible (ΔE = 65 mV) but only partially chemically reversible, as the intensity of the anodic peak is much smaller than that of the cathodic peak (i_{pa}/i_{pc} = 0.30). This confirms the results by Geiger et al. including the great instability of the single-electron-transfer product rhodocene, even at −50 °C in THF, and the absence of significant structural rearrangement along the single-electron transfer to the rhodicenium salt **6**.[8]

Synthesis of Water-Soluble Rhodicenium Polystyrene Sulfonate Polymer. Ionic macromolecules such as polymers and dendrimers have been mentioned previously, even though this field of chemistry has not been extensively explored. We envisaged synthesizing ionic rhodicenium polymers and dendrimers in order to study the properties of these new kinds of ionic metallomacromolecules. The starting polymer material sodium polystyrene sulfonate reacted with compound

dx.doi.org/10.1021/om500028e | Organometallics 2014, 33, 1259−1265

4 to give the rhodicenium polystyrene sulfonate polymer **8** and NaCl (Scheme 3).

Scheme 3. Synthesis of a Polystyrene Sulfonate Rhodicenium Polymer

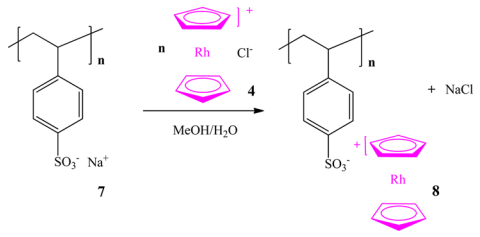

The sodium polystyrene sulfonate polymer has an average molecular weight of m/z 70.000; thus, the number of rhodicenium units in polymer **8** is 330 ± 30. The solubility of this new polymer **8** in water is good, being similar to that of its precursor compounds **4** and **7**. The ^{1}H NMR spectrum in water shows the correct ratio between the rhodicenium and polymer protons. The downfield shift of 0.175 ppm for the 10H of Cp of the rhodicenium cation also shows the formation of ionic bonds between the sulfonate anion and the rhodicenium cation (Table 2). Infrared spectroscopy is also a remarkable

Table 2. ^{1}H NMR and IR Data for the Metallocenium Complexes 3, 8, and 10−12

complex/ counteranion	Cp (ppm)	Δδ (ppm)	IR in KBr (cm^{-1})
3[a]/Cl^-	5.977		3104
3[b]/Cl^-	5.969		3104
8[a]/Poly-SO_3^-	5.802	0.175[d]	1698; 1216; 1129; 1042; 1010
10[b]/Dend-COO^-	5.957	0.012[e]	3107; 1603
11[c]/Cl^-	5.907		3100
12[c]/Dend-COO^-	5.823	0.084[f]	3099; 1690

[a]NMR in D_2O at 25 °C. [b]NMR in methanol-d_4 (1). [c]NMR in methanol-d_4 (5). [d]$\Delta\delta_{ppm} = \delta$(Cp of **3**) − δ(Cp of **8**). [e]$\Delta\delta_{ppm} = \delta$(Cp of **3**) − δ(Cp of **10**). [f]$\Delta\delta_{ppm} = \delta$(Cp of **11**) − δ(Cp of **12**).

tool to study the differences in the sulfonate anions between polymers **7** and **8** (Figure 4). The bands at 1191, 1129, and 1042 cm^{-1} of polymer **7** are assignable to sulfonate anions. The change of the band from 1191 to 1216 cm^{-1} in polymer **8** is due to the change of the ionic bond that is now formed between the sulfonate anion and the rhodicenium cation. Another difference is the aromatic C=C bending band that appears at 1633 cm^{-1} in polymer **7** and in polymer **8** changes to 1698 cm^{-1} (Table 2). Finally, DOSY NMR provided the diffusion coefficient of the polymer: $D = [1.38(\pm0.1)] \times 10^{-10}$ m^2/s. The spectrum is in agreement with rhodicenium being bound to the polymer **7**, providing polymer **8** (Supporting Information).

Synthesis of Water-Soluble G_1-Carboxylate Rhodicenium and Cobaltocenium Dendrimers. The supramolecular aspects of dendrimers[23] have been largely considered for various uses such as molecular boxes,[24] exoreceptors,[25] sensors,[25] electron-transfer nanodevices,[26] molecular micelles,[27] nanoreactors,[28] and catalysts.[29] Ionic interactions of dendrimers have been studied previously for different applications such as drug vectors,[30] molecular batteries, and modified electrodes. Polyanionic dendrimers usually display acceptable biocompatibility.[30,31] Therefore, we have synthesized the polybenzoate-

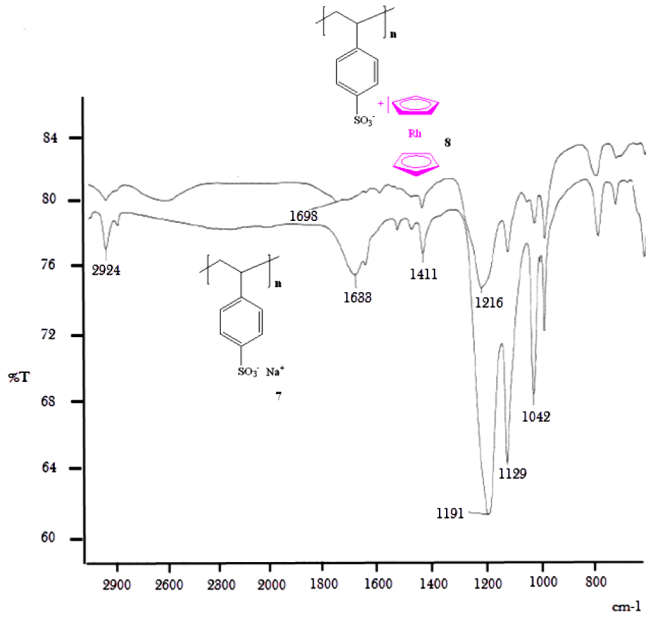

Figure 4. Comparative IR spectra of polymers **7** and **8**.

terminated dendrimer **9** from a polyiodomethylsilyl precursor.[32] This dendrimer reacted as a sodium salt with complex **4** according to a metathesis ion exchange among the two reacting ion pairs to form a polybenzoate rhodicenium-terminated dendrimer (Scheme 4). Dendrimer **10** (Chart 1) presents a good solubility in methanol and water. Its ^{1}H NMR spectrum discloses the corresponding ratio for the dendritic/peripheral protons (Cp), showing a downfield shift of 0.012 for the 10H of Cp of the rhodicenium cation. The ^{13}C NMR spectrum also confirms the structure of the dendrimeric salt **10**. The nature of the carboxylate anion has changed between dendrimers **9** and **10**, and this is clearly shown by the IR spectrum, in which the absorption due to the carboxylate anion (area 1600−1690 cm^{-1}) in dendrimers **9** and **10** undergoes significant changes (Table 2). Additionally, the DOSY NMR spectrum of **10** provided the diffusion coefficient $D = [4.8(\pm0.2)] \times 10^{-11}$ m^2/s (Supporting Information).

The expected similar properties of rhodicenium cations and cobaltocenium cations suggest that analogous structures and properties can be obtained for related cobaltocenium salts. Thus, the dendrimer **12** containing cobaltocenium cations in the periphery was also synthesized (Chart 1). Cobaltocenium chloride **11** reacted with the polybenzoate sodium dendrimer **9**, giving the polybenzoate cobaltocenium dendrimer **12** (Scheme 4). The ^{1}H NMR spectrum shows a downfield shift of 0.084 ppm for the 10H of the Cp of the cobaltocenium cation, and the IR spectrum showed a change in the band of the carboxylate anion (Table 2). Finally, the DOSY NMR spectrum of **12** provided the diffusion coefficient $D = [5.5(\pm0.2)] \times 10^{-11}$ m^2/s (Supporting Information).

■ CONCLUDING REMARKS

The insolubility of classic rhodicenium salts contrasted with the good solubility of rhodium analogues, possibly because the larger inter-ring distance led to more exposed positive charge in rhodicenium than in cobaltocenium, which prevented extension of the organorhodium chemistry. An alternative synthesis of rhodicenium chloride and the preparation of new rhodicenium salts that are soluble in less-polar solvents open the possibilities

Scheme 4. Synthesis of the Rhodicenium and Cobaltocenium Dendrimers[a]

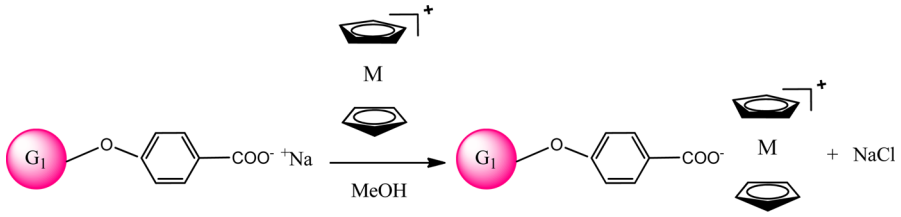

9 M = Rh (**10**) or Co (**12**)

[a] G_1 stands for a first-generation dendrimer; see the structures in Chart 1.

Chart 1

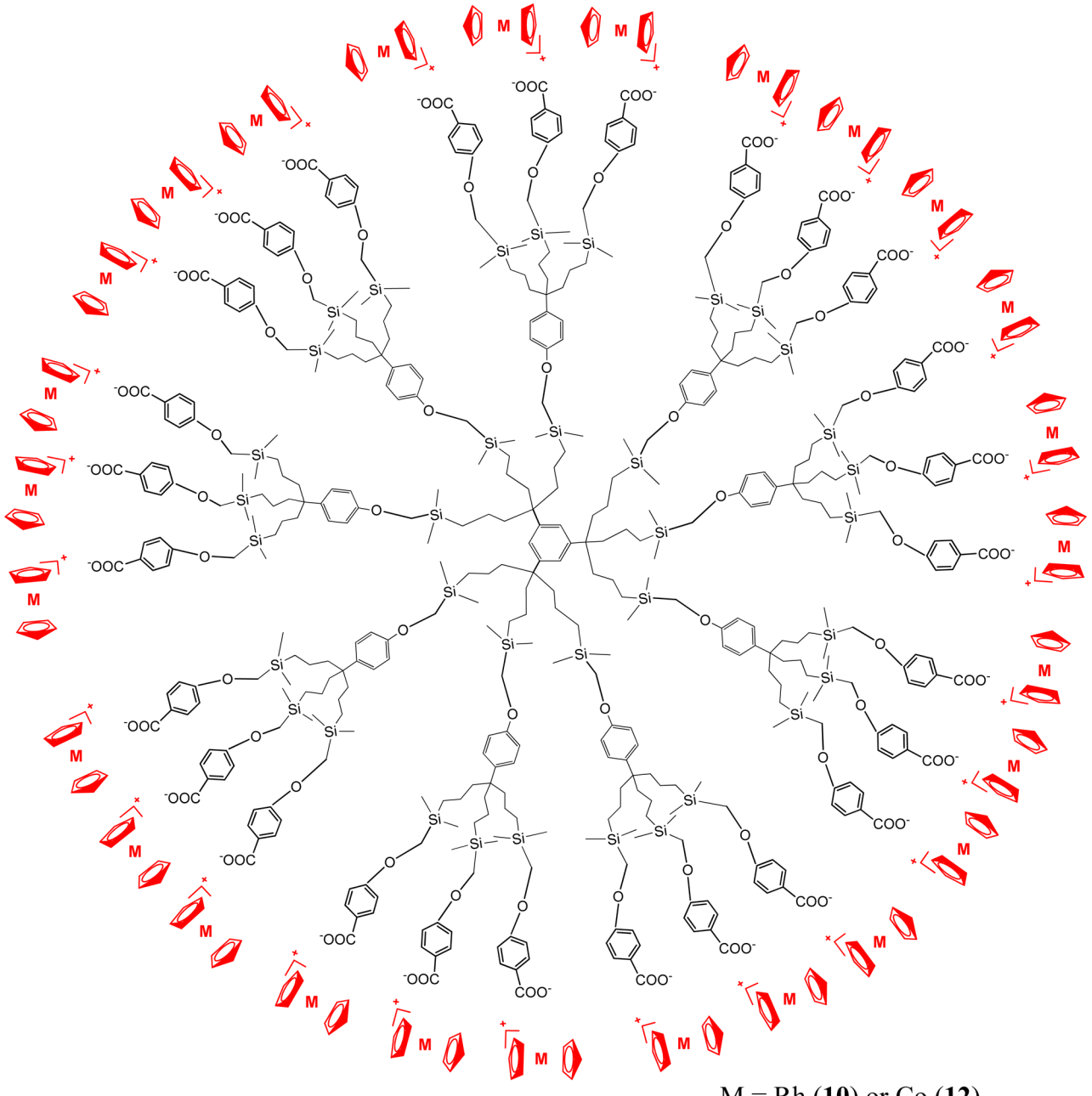

of further carrying on organorhodium chemistry. In parallel, ionic water-soluble cobaltocenium and rhodicenium polyelectrolytes and dendrimers with unusual properties have now been made available.

dx.doi.org/10.1021/om500028e | *Organometallics* 2014, 33, 1259−1265

EXPERIMENTAL SECTION

General Data. Reagent-grade diethyl ether and tetrahydrofuran (THF) were predried over Na foil and distilled from sodium benzophenone anion under argon immediately prior to use. Dichloromethane (DCM) was distilled over CaH_2 under argon prior to use. All other solvents and chemicals were used as received. The ^{1}H NMR spectra were recorded at 25 °C with a 300 MHz spectrometer. The ^{13}C NMR spectra were obtained in the pulsed FT mode at 75.0 MHz with a 300 MHz spectrometer. All chemical shifts are reported in parts per million (δ, ppm) with reference to Me_4Si (TMS). The infrared (IR) spectra were recorded on a FT-IR spectrophotometer. All electrochemical measurements were recorded under a nitrogen atmosphere. Conditions: dried solvent; temperature, 22 °C; supporting electrolyte, $[n\mathrm{Bu_4N}][\mathrm{BAr^F_4}]$ 0.1 M; working and counter electrodes, Pt; reference electrode, Ag; internal reference, $\mathrm{FeCp^*_2}$ ($\mathrm{Cp^*} = \eta^5\text{-}\mathrm{C_5Me_5}$); scan rate, 0.200 V/s. Diffusion measurements were performed at 25 °C with a 400 MHz spectrometer. They were performed using a ^{1}H NMR pulsed-gradient experiment: the simulated spin−echo sequence leads to the measurement of the diffusion coefficient D, where D is the slope of the straight line obtained when ln I is displayed against the square of the gradient-pulse power according to the equation $\ln I = -\gamma^2G^2D\delta^2(\Delta - \delta/3)$, where I is the relative intensity of a chosen resonance, γ is the proton gyromagnetic ratio, Δ is the intergradient delay (150 ms), δ is the gradient pulse duration (5 ms), and G is the gradient intensity. The diffusion constant of water (2.3×10^{-9} m^2/s) was used to calibrate the instrument. The mass spectra were measured by the CESAMO (University of Bordeaux 1, France) on a AccuTOF-GcV instrument which is a GC-TOF. The instrument was equipped with an FD (field desorption) sample introduction system. The elemental analyses were performed by the CESAMO (University of Bordeaux 1, France). The results were obtained with a Thermo Flash 2000 EA instrument. The sample was introduced in a tin container for NCHS analysis.

(Trimethylsilyl)cyclopentadiene.[20] To a solution of sodium cyclopentadienide (1.76 g, 0.02 mol) in 10 mL of THF was added dropwise a solution of trimethylsilyl chloride (2.17 g, 0.02 mol) in 10 mL of THF at 0 °C. The reaction mixture was stirred at 0 °C for 3 h and an additional 2 h at room temperature. Then, the reaction mixture was cautiously treated with cold water and extracted with ether. The organic phase was dried over Na_2SO_4. Further purification was achieved by column chromatography (pentane), and the product was obtained as a colorless liquid (1.8 g, yield 65%).

$[\mathrm{CpRhCl_2}]_n$ (3).[20] To solution of (trimethylsilyl)cyclopentadiene in 7 mL of 2-propanol (0.250 g, 1.81 mmol) was added a solution of hydrated rhodium trichloride (0.161 g, 0.77 mmol) in 7 mL of 2-propanol. The mixture was stirred at room temperature overnight. Pentane was added to the mixture (60 mL), and the precipitate was filtered. The solid was washed several times with dichloromethane. The oligomeric product $[\mathrm{CpRhCl_2}]_n$ was obtained as an orange powder (178.3 mg, yield 97%).

Rhodicenium Chloride (4). The oligomer $[\mathrm{CpRhCl_2}]_n$ (152 mg, 0.64 mmol) was cooled to −78 °C, and then solid CpLi (92 mg, 1.28 mmol) was added slowly. The reaction mixture was stirred for 3 h at −78 °C and then slowly warmed to room temperature and stirred overnight. The solvent was removed under reduced pressure. The solid was extracted with hot water, and the aqueous phase was washed several times with diethyl ether to remove organic impurities. Extraction overnight with nitromethane and filtration gave 106 mg of a yellowish orange powder. Yield: 62%. (Addition of aqueous HPF_6 to product **4** in water and extraction in nitromethane gave 140 mg of rhodicenium hexafluorophosphate (**5**).)

Complex 6. To a solution of rhodicenium chloride (**4**) in 3 mL of water (100 mg, 0.37 mmol) was added $\mathrm{NaBAr^F_4}$ (330 mg, 0.37 mmol) as a solid. The solution was stirred for 1 h. NaCl was added to the water solution until saturation. Product **6** was extracted in dichloromethane. Evaporation of the solvent gave **6** as a reddish violet powder (397 mg, 0.36 mmol). Yield: 98%. ^{1}H NMR of **6** ($CDCl_3$, 300 MHz): δ 7.68 (8H, CF_3CH), 7.52 (4H, CF_3CHCF_3), 5.63 (10H, Cp). ^{13}C NMR of **6** (CD_2Cl_2, 75 MHz): δ 134.9 (CCF_3), 129.0, 128.9, 127.6 (BCCH, $CF_3CCHCCF_3$), 122.1 ($BCCHCCF_3$), 117.5 (CF_3), 87.1 (Cp). FD MS (m/z): calcd for $C_{10}H_{10}Rh^+$ 232.984, found 232.984. Anal. Calcd for $C_{42}H_{22}BF_{24}Rh$: C, 46.01; H, 2.02. Found: C, 45.93; H, 2.08.

Complex 8. To a stirred solution of polymer **7** (20 mg, 0.00028 mmol) in 2 mL of H_2O was added a solution of 2 mL of compound **4** (25.6 mg, 0.096 mmol) in MeOH. The mixture was stirred for $^1/_2$ h. The solvent was removed under vacuum, and the product was extracted twice in nitromethane and filtered. Evaporation of the solvent provided product **8** as a yellowish gel in quantitative yield. ^{1}H NMR of **8** (D_2O, 300 MHz): δ 7.56, 6.62 (4H, C*H* of Ar of styrenyl), 5.80 (10H of Cp), 1.70 (C*H* and CH_2 of polymer chain). ^{13}C NMR of **8** (D_2O, 75 MHz): δ 141.6 (*Cq* of Ar), 128.3 (*Cq*-CH_2 of Ar), 126.4 and 126.0 (CH of Ar), 86.66 (Cp of rhodicenium), 40.1 (CH and CH_2 of polymeric chain). DOSY NMR: $D = [1.38(\pm0.1)] \times 10^{-10}$ m^2/s.

Complex 10. To a stirred solution of dendrimer **9** (20 mg, 0.002 mmol) in 2 mL of MeOH was added 2 mL of a solution of compound **4** (15.2 mg, 0.056 mmol) in MeOH. The mixture was stirred for 0.5 h. The solvent was removed under vacuum; the product was extracted twice in nitromethane and filtered. Evaporation of the solvent gave product **10** as a yellow-orange gel in quantitative yield. ^{1}H NMR (CD_3OD, 300 MHz): δ 7.84 and 6.78 (144H, C*H* arom), 5.96 (270H, Cp), 3.42 (54H, $SiCH_2$-trz), 1.56 (72H, $CH_2CH_2CH_2Si$), 1.10 (72H, $CH_2CH_2CH_2Si$), 0.49 (72H, $CH_2CH_2CH_2Si$), −0.07 (216H, $Si(CH_3)_2$). ^{13}C NMR (MeOD, 75 MHz): δ 169.3 (C═O), 163.6 (arom O*Cq*), 131.0 (*Cq* of arom core), 128.0 and 114.3 (arom *C*H), 86.9 (Cp), 60.1 (CH_2OAr), 44.0 ($CqCH_2CH_2CH_2Si$), 42.8 ($CqCH_2CH_2CH_2Si$), 17.9 ($CqCH_2CH_2CH_2Si$), 14.4 ($CqCH_2CH_2CH_2Si$), −5.3 ($Si(CH_3)_2$). DOSY NMR: $D = [4.8(\pm0.2)] \times 10^{-11}$ m^2/s.

Complex 12. To a stirred solution of the dendrimer **9** (20 mg, 0.002 mmol) in 2 mL of MeOH was added a solution of **11** (12.6 mg, 0.056 mmol) in 2 mL of MeOH. The mixture was stirred for $^1/_2$ h. The solvent was removed under vacuum, and the product was extracted twice with nitromethane and filtered. Evaporation of the solvent gave **12** as a yellow gel in quantitative yield. ^{1}H NMR (CD_3OD, 300 MHz): δ 7.88 and 6.86 (144H, C*H* arom), 5.82 (270H, Cp), 3.46 (54H, $SiCH_2$-trz), 1.56 (72H, $CH_2CH_2CH_2Si$), 1.12 (72H, $CH_2CH_2CH_2Si$), 0.49 (72H, $CH_2CH_2CH_2Si$), −0.05 (216H, $Si(CH_3)_2$). ^{13}C NMR (MeOD, 75 MHz): δ 165.3 (C═O), 163.6 (arom O*Cq*), 131.5 (*Cq* of arom core), 122.3 and 115.5 (arom *C*H), 84.8 (Cp), 60.4 (CH_2OAr), 42.9 ($CqCH_2CH_2CH_2Si$), 41.7 ($CqCH_2CH_2CH_2Si$), 17.5 ($CqCH_2CH_2CH_2Si$), 14.3 ($CqCH_2CH_2CH_2Si$), −5.5 ($Si(CH_3)_2$). DOSY NMR: $D = [5.5(\pm0.2)] \times 10^{-11}$ m^2/s.

ASSOCIATED CONTENT

Supporting Information

Text giving additional experimental details and figures giving spectroscopic data for all of the new complexes and NMR, IR, and DOSY NMR spectra. This material is available free of charge via the Internet at http://pubs.acs.org.

AUTHOR INFORMATION

Corresponding Author

*E-mail for D.A.: d.astruc@ism.u-bordeaux1.fr.

Notes

The authors declare no competing financial interest.

ACKNOWLEDGMENTS

Helpful assistance and discussion with Drs. Jaime Ruiz, Noël Pinaud (DOSY NMR), and Jean-Michel Lanier (NMR) from the CESAMO, Univ. Bordeaux, and financial support from the Univ. Bordeaux, the Centre National de la Recherche Scientifique (CNRS), the Chinese Research Council (CRC), and the Agence Nationale de la Recherche (ANR) are gratefully

acknowledged. Dedicated to Prof. Helmut Werner, a distinguished pioneer of organometallic chemistry.

REFERENCES

(1) Cotton, F. A.; Whipple, R. O.; Wilkinson, G. *J. Am. Chem. Soc.* **1953**, *75*, 3586−3587.
(2) Jacobson, D. B.; Byrd, G. D.; Freiser, B. S. *J. Am. Chem. Soc.* **1982**, *104*, 2320−2321.
(3) Gord, J. R.; Buckner, S. W.; Freiser, B. S. *J. Am. Chem. Soc.* **1989**, *111*, 3753−3754.
(4) Baghurst, D. R.; Mingos, D. M. P.; Watson, M. J. *J. Organomet. Chem.* **1989**, *368*, C43−C45.
(5) Green, M. L. H.; Pratt, L.; Wilkinson, G. *J. Chem. Soc.* **1959**, *0*, 3753−3766.
(6) Keller, H. J.; Wawersik, H. *J. Organomet. Chem.* **1967**, *8*, 185−188.
(7) Fischer, E. O.; Wawersik, H. *J. Organomet. Chem.* **1966**, *5*, 559−567.
(8) (a) El Murr, N.; Sheats, J. E.; Geiger, W. E.; Holloway, J. D.L. *Inorg. Chem.* **1979**, *18*, 1443−1446. (b) For reviews and detailed discussions of the electrochemistry of the transition-metal metallocenes, see: (c) Connelly, N. G.; Geiger, W. E. *Chem. Rev.* **1996**, *96*, 877−910. (d) Geiger, W. E. *Organometallics* **2007**, *26*, 5738−5765. (e) Geiger, W. E. *Organometallics* **2011**, *30*, 28−31. (f) For discussions of ion-pairing effects, see: Barrière, F.; Geiger, W. E. *Acc. Chem. Res.* **2010**, *43*, 1030−1039.
(9) Zagorevskii, D. V.; Holmes, J. L. *Organometallics* **1992**, *11*, 3224−3227.
(10) (a) Hamon, J.-R.; Astruc, D.; Michaud, P. *J. Am. Chem. Soc.* **1981**, *103*, 758−766. (b) Astruc, D. *Organometallic Chemistry and Catalysis*; Springer: Heidelberg, Germany, 2007; Chapter 10.
(11) Collins, J. E.; Castellani, M. P.; Rheingold, A. L.; Miller, E. J.; Geiger, W. E.; Rieger, A. L.; Rieger, P. H. *Organometallics* **1995**, *14*, 1232−1238.
(12) (a) Donovan-Merkert, B. T.; Tjiong, H. I.; Rhinehart, L. M.; Russell, R. A.; Malik, J. *Organomettalics* **1997**, *16*, 819−821. (b) Philippopoulos, A. I.; Hadjiliadis, N. *Inorg. Chem.* **1997**, *36*, 1842−1849. (c) Han, W. S.; Lee, S. W. *Organometallics* **2005**, *24*, 997−1003.
(13) Forissier, K.; Ricard, L.; Carmichael, D.; Mathey, F. *Organometallics* **2000**, *19*, 954−956.
(14) Eisenstecken, D.; Enk, B.; Kopacka, H.; Wurst, K.; Muller, T.; Penvy, F.; Winter, R. F.; Bildstein, B. *Eur. J. Inorg. Chem.* **2011**, 2958−2966.
(15) (a) Moseley, K.; Kang, J. W.; Maitlis, P. M. *J. Chem. Soc. A* **1970**, 2875−2883. (b) Buchholz, D.; Gloaguen, B.; Fillaut, J.-L.; Cotrait, M.; Astruc, D. *Chem. Eur. J.* **1995**, *1*, 374−381. (c) Donovan-Merkert, B. T.; Clontz, C. R.; Rhinehart, L. M.; Tjiong, H. I.; Carlin, C. M. *Organometallics* **1998**, *17*, 1716−1724. (d) Gusev, O. V.; Morozova, L. N.; Peganova, T. A.; Petrovskii, P. V.; Ustynyuk, N. A.; Maitlis, P. M. *J. Organomet. Chem.* **1994**, *472*, 359−363.
(16) (a) Koelle, U.; Klaui, W. *Z. Naturforsch.* **1991**, *46b*, 75−83. (b) Buchholz, D.; Zsolnai, L.; Huttner, G.; Astruc, D. *J. Organomet. Chem.* **2000**, *593*−*594*, 494−496.
(17) Mohapatra, S. K.; Romanov, A.; Angles, G.; Timofeeva, T. V.; Barlow, S.; Marder, S. R. *J. Organomet. Chem.* **2012**, *706*−*707*, 140−143.
(18) Andre, M.; Schottenberger, H.; Tessadri, R.; Ingram, G.; Jaitner, P.; Schwarzhans, K. E. *Chromatographia* **1990**, *30*, 543−545.
(19) (a) Wenzel, M.; Wu, Y. *Appl. Radiat. Isot.* **1988**, *39*, 1237−1241. (b) Wenzel, M.; Wu, Y. *Appl. Radiat. Isot.* **1987**, *38*, 67−69.
(20) Kraihauzel, C. A.; Losee, M. L. *J. Am. Chem. Soc.* **1968**, *90*, 4701−4705.
(21) Winter, C. H.; Pirzard, S.; Graf, D. D.; Cao, D. H.; Heeg, M. J. *Inorg. Chem.* **1993**, *32*, 3654−3659.
(22) (a) Bashkin, J. K.; Kinlen, P. J. *Inorg. Chem.* **1990**, *29*, 4507−4509. (b) Ruiz, J.; Astruc, D. *C. R. Acad. Sci., Ser. IIc: Chim.* **1998**, 21−27. (c) Noviandri, I.; Brown, K. N.; Fleming, D. S.; Gulyas, P. T.; Lay, P. A.; Masters, A. F.; Philllips, L. J. *J. Phys. Chem. B* **1999**, *103*, 6713−6722.
(23) (a) Percec, V.; Johansson, G.; Ungar, G.; Zhou, J. P. *J. Am. Chem. Soc.* **1996**, *118*, 9855−9866. (b) Zeng, F.; Zimmermann, S. C. *Chem. Rev.* **1997**, *97*, 1681−1712. (c) Balzani, V.; Campana, S.; Denti, G.; Juris, A.; Serroni, S.; Venturi, M. *Acc. Chem. Res.* **1998**, *31*, 26−34. (d) Newkome, G. R.; He, E.; Moorefield, C. N. *Chem. Rev.* **1999**, *99*, 1689−1746. (e) Astruc, D.; Boisselier, E.; Ornelas, C. *Chem. Rev.* **2010**, *110*, 1857−1959. (f) Rapakousiou, A.; Wang, Y.; Nzulu, F.; Djeda, R.; Pinaud, N.; Ruiz, J.; Astruc, D. *Organometallics.* **2013**, *32*, 6079−6090.
(24) (a) Jansen, J. F. G. A.; de Brabander-van den Berg, E. M. M.; Meijer, E. W. *Science* **1994**, *266*, 1226−1229. (b) Bosman, A. W.; Jensen, E. W.; Meijer, E. W. *Chem. Rev.* **1999**, *99*, 1665−1688. (c) Newkome, G. *Pure Appl. Chem.* **2000**, *70*, 2337−2343.
(25) (a) Valerio, C.; Fillaut, J.-L.; Ruiz, J.; Guittard, J.; Blais, J.-C.; Astruc, D. *J. Am. Chem. Soc.* **1997**, *119*, 2588−2589. (b) Albrecht, M.; Hovestad, N. J.; Boersma, J.; Van Koten, G. *Chem. Eur. J.* **2001**, *7*, 1289−1294. (c) Kleij, A. W.; Ford, A.; Jastrzebski, J. T. B. H.; van Koten, G. In *Dendrimers and Other Dendritic Polymers*; Fréchet, J. M. J., Tomalia, D. A., Eds.; Wiley: New York, 2002; p 185. (d) Newkome, G. R.; Shreiner, C. *Chem. Rev.* **2010**, *110*, 6338−6442. (e) Casado, C.-M. ; Alonso, B. ; Losada, J. ; Garcia-Armada, M. P. In *Designing Dendrimers*; Campagna, S., Ceroni, P., Puntoriero, F., Eds.; Wiley: Hoboken, NJ, 2012; pp 219−262.
(26) (a) Casado, C.-M.; Cuadrado, I.; Moran, M.; Alonso, B.; Garcia, B.; Gonzales, B.; Losada, J. *Coord. Chem. Rev.* **1999**, *185*−*186*, 53−79. (b) Smith, J. C.; Gorman, C. B. *Acc. Chem. Res.* **2001**, *34*, 60−71. (c) Kaifer, A. E. *Eur. J. Inorg. Chem.* **2007**, *9*, 5015−5027. (d) Ornelas, C.; Ruiz, J.; Belin, C.; Astruc, D. *J. Am. Chem. Soc.* **2009**, *131*, 590−601. (e) Astruc, D. *Nat. Chem.* **2012**, *4*, 255−267.
(27) (a) Newkome, G. R.; Yao, Z.; Baker, G. R.; Gupta, V. K. *J. Org. Chem.* **1985**, *50*, 2003−2004. (b) Boisselier, E.; Diallo, A. K.; Salmon, L.; Ornelas, C.; Ruiz, J.; Astruc, D. *J. Am. Chem. Soc.* **2010**, *132*, 2729−2742. (c) Bergamini, G.; Marchi, E.; Ceroni, P.; Balzani, V. In *Designing Dendrimers*; Campagna, S., Ceroni, P., Puntoriero, F., Eds.; Wiley: Hoboken, NJ, 2012; pp 341−366.
(28) (a) Crooks, R. M.; Zhao, M.; Sun, L.; Chechik, V.; Yeung, L. K. *Acc. Chem. Res.* **2001**, *34*, 181−190. (b) Imaoka, T.; Yamamoto, K. In *Designing Dendrimers*; Campagna, S., Ceroni, P., Puntoriero, F., Eds.; Wiley: Hoboken, NJ, 2012; pp 303−340. (c) Deraedt, C.; Astruc, D. *Acc. Chem. Res.* **2013**, DOI: 10.1021/ar400168s.
(29) (a) Oosterom, G. E.; Reek, J. N. H.; Kamer, P. C. J.; van Leeuwen, P. W. N. M. *Angew. Chem., Int. Ed.* **2001**, *40*, 1828−1849. (b) Astruc, D.; Heuze, K.; Gatard, S.; Méry, D.; Nlate, S.; Plault, L. *Adv. Synth. Catal.* **2005**, *347*, 329−338. (c) Hwang, S. H.; Shreiner, C. D.; Moorefield, C. N.; Newkome, G. R. *New J. Chem.* **2007**, *31*, 1192. (d) Martinez-Olid, F.; Benito, J. M.; Flores, J. C.; de Jesus, E. *Isr. J. Chem.* **2009**, *49*, 99. (e) Wang, D.; Astruc, D. *Coord. Chem. Rev.* **2013**, *257*, 2317−2334.
(30) (a) Astruc, D. *C. R. Acad. Sci., Ser. IIb: Mec., Phys., Chim., Astron.* **1996**, *322*, 757−766. (b) Grinstaff, M. W. *Chem. Eur. J.* **2002**, *8*, 2838−2846. (c) Boas, U.; Heegarard, P. M. H. *Chem. Soc. Rev.* **2004**, *33*, 43−63. (d) Lee, C. C.; Mac Kay, J. A.; Fréchet, J. M. J.; Szoka, F. *Nat. Biotechnol.* **2005**, *23*, 1517−1526.
(31) (a) Malik, N.; Wiwattanapatapee, R.; Klopsch, R.; Lorenz, K.; Frey, H.; Weener, J. W.; Meijer, E. W.; Paulus, W.; Duncan, R. *J. Controlled Release* **2000**, *65*, 133−148. (b) Jevprasesphant, R.; Penny, J.; Jalal, R.; Attwood, D.; McKown, N. B.; Emmanuele, A. D. *Int. J. Pharm.* **2003**, *252*, 263−266. (c) Llevot, A.; Astruc, D. *Chem. Soc. Rev.* **2012**, *41*, 242−257.
(32) Ornelas, C.; Boisselier, E.; Martinez, V.; Pianet, I.; Ruiz, J.; Astruc, D. *Chem. Commun.* **2007**, 5093−5095.

Partie 2

Polymères biferrocéniques à valence mixte pour l'ingénierie de matériaux à base de nanoparticules d'or

Partie 2

Polymères biferrocéniques à valence mixte pour l'ingénierie de matériaux à base de nanoparticules d'or

Introduction

Dans cette partie, nous décrivons trois types de polymères différents contenant des groupements triazolylbiferrocène, d'une part des polynorbornènes et un polystyrène contenant le triazolylbiferrocène (trz-BiFc) sur la chaine latérale et d'autre part des copolymères contenant le trz-BiFc sur la chaine principale. Au chapitre 2.1 on démontre les réactions de ces polymères avec $HAuCl_4$ conduisant à la formation de nanoparticules d'or de 12-15 nm stabilisées par les polymères de valence mixte triazolylbiferrocénium. L'incubation en solution pendant une semaine a donné naissance aux nanoréseaux polymériques encapsulant ces nanoparticules d'or. Quand le trz-BiFc est sur la chaine latérale la formation des nanoserpents a été observée par TEM et AFM (contrairement aux polymères contenant le trz-BiFc en chaine principale). Cette architecture est observée quelques soit le nombre d'unités polymères-trz-BiFc sur la chaine latérale. Quand les biferrocènes sont remplacé par les ferrocènes simples, les nanoserpents ne sont pas observés et les nanoparticules d'or formées présentent un diamètre de 6 nm. En outre, la réduction par $NaBH_4$ du polymère à valence-mixte, stabilisant les nanoparticules d'or, en polymère neutre, provoque la destruction de ces nanostructures et la floculation des nanoparticules. Ceci est dû à l'absence de stabilisation électrostatique. Ces paramètres permettent de conclure que le triazole et le cation biferrocénium sont co-responsables de la formation des réseaux polymériques contenant des nanoparticules d'or. Cependant, la formation de nanoserpents par des polymères entrelacés est spécifique des métallopolymères électrolytiques contenant le triazolylbiferrocénium sur la chaîne latérale.

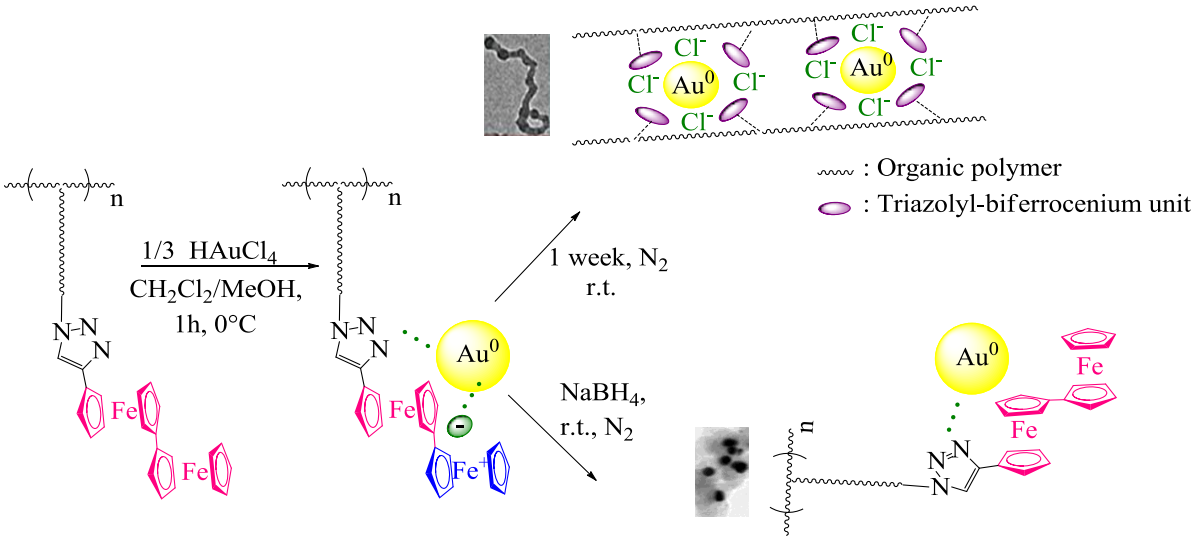

Schéma. Motifs du chapitre 2.1.

Au chapitre 2.2 nous décrivons la synthèse de copolymères par la méthode de polycondensation de bis-azoture (PEG) et bis-éthynylbiferrocène. Dans ce travail effectué en collaboration avec Christophe Deraedt et Yanlan Wang, nous avons étudié différentes applications comme la catalyse dans l'eau, la reconnaissance rédox, les électrodes modifiées et les propriétés électrochromiques et polyélectrolytiques.

Aux chapitres 2.3 et 2.4 nous décrivons le greffage des groupements trz-BiFc aux polymères et nanoparticules d'or avec des ligands thiolates, leurs propriétés redox et leurs applications en reconnaissance moléculaire.

JACS
JOURNAL OF THE AMERICAN CHEMICAL SOCIETY
Communication
pubs.acs.org/JACS

Mixed-Valent Click Intertwined Polymer Units Containing Biferrocenium Chloride Side Chains Form Nanosnakes that Encapsulate Gold Nanoparticles

Amalia Rapakousiou,[†] Christophe Deraedt,[†] Haibin Gu,[†] Lionel Salmon,[‡] Colette Belin,[†] Jaime Ruiz,[†] and Didier Astruc*[,†]

[†]ISM, UMR CNRS 5255, Univ. Bordeaux, 351 Cours de la Libération, 33405 Talence Cedex, France
[‡]Laboratoire de Chimie de Coordination, UPR CNRS 8241, 205 Route de Narbonne, 31077 Toulouse Cedex 04, France

Supporting Information

ABSTRACT: Polymers containing triazolylbiferrocene are synthesized by ROMP or radical chain reactions and react with $HAuCl_4$ to provide class-2 mixed-valent triazolylbiferrocenium polyelectrolyte networks (observed *inter alia* by TEM and AFM) that encapsulate gold nanoparticles (AuNPs). With triazolylbiferrocenium in the side polymer chain, the intertwined polymer networks form nanosnakes, unlike with triazolylbiferrocenium in the main polymer chain. By contrast, simple ferrocene-containing polymers do not form such a ferricenium network upon reaction with Au^{III}, but only small AuNPs, showing that the triazolyl ligand, the cationic charge, and the biferrocenium structure are coresponsible for such network formations.

Gold nanoparticles (AuNPs) have attracted considerable interest because of their applications in optics, nanoelectronics, nanomedicine, and catalysis depending on their size, shape and stabilizer.[1] Therefore, the way into which specific macromolecules direct such NP formation and assembly including size, shape, and organized network is of paramount importance toward nanoscience applications.[2] Ferrocene-containing macromolecules[3] may be biocompatible candidates for AuNP stabilization owing to the suitably matching redox potentials of ferrocenes and Au^{III} precursors[4] and the antitumoral properties of various ferrocene derivatives,[5] although such a strategy has not yet been envisaged. An engineered approach to biferrocene polymer-mediated stabilization and encapsulation of AuNPs is presented here together with the intriguing properties of these new nanomaterials.

A simple way to construct ferrocene polymers is to branch ferrocene to polymerizable monomers by click Cu(I)-catalyzed Azide Alkyne Cycloaddition (CuAAC) reaction using commercial ethynylferrocene **1**.[6] A ferrocenyl-containing poly(norbornene) polymer **4** was synthesized using the ring-opening metathesis polymerization (ROMP) of monomer **2** using the third-generation Grubbs catalyst **3**.[7] The reaction of **4** with $HAuCl_4$ leads to a triazolylferricenium polymer, but this product rapidly decomposes due to the instability of the ferricenium group under these conditions. Therefore, we subsequently addressed the possibility of using biferrocene, because the mixed-valent biferrocenium cation[8] is much more robust than ferricenium (Scheme 1). Thus, low-dispersity biferrocene analogues **7** and **8** of **6** were synthesized identically with 30 and 60 triazolylbiferrocene units, respectively. These polymers were characterized by ^1H and ^{13}C NMR including HSQC 2D, HMBC 2D, and NOESY 2D NMR (Supporting Information (SI)) and cyclic voltammetry showing only the two chemically and electrochemically reversible waves of the biferocenyl units at 0.42 and 0.75 V[8] due to the absence of intramolecular electronic interaction among the multiple biferrocenyl units.

Scheme 1. Synthesis of Biferrocene Polymers 7 and 8 Involving ROMP Initiated by the Ru Metathesis Catalyst "Grubbs III"

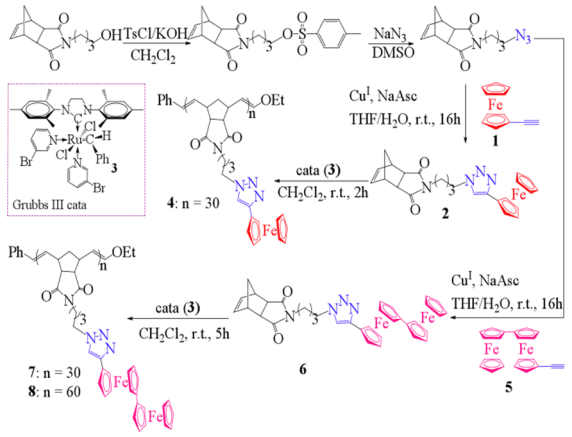

The reactions of these biferrocene polymers with $HAuCl_4$ in dichloromethane–methanol provided the formation of Au^0NP-containing nanostructures **7a** and **8a** that were stabilized by the green mixed-valent triazolylbiferrocenium polymer $\mathbf{7}^+,Cl^-$ or $\mathbf{8}^+,Cl^-$ (Scheme 2) according to the stoichiometry of eq 1:

$$3Fe^{II}Fe^{II} + H^+Au^{III}Cl_4^- \rightarrow 3[Fe^{II}Fe^{III}]^+Cl^-, Au^0, H^+Cl^- \quad (1)$$

IR spectroscopy of **7a** and **8a** shows the presence of both Fe^{II} (ferrocene C–H bending, 813 cm^{-1}) and Fe^{III} (ferricenium C–

Received: August 2, 2014
Published: September 25, 2014

Scheme 2. Formation of Biferrocenium Chloride Polymer-Encapsulated AuNPs upon Reaction of 7, 8, or 9 with $HAuCl_4$

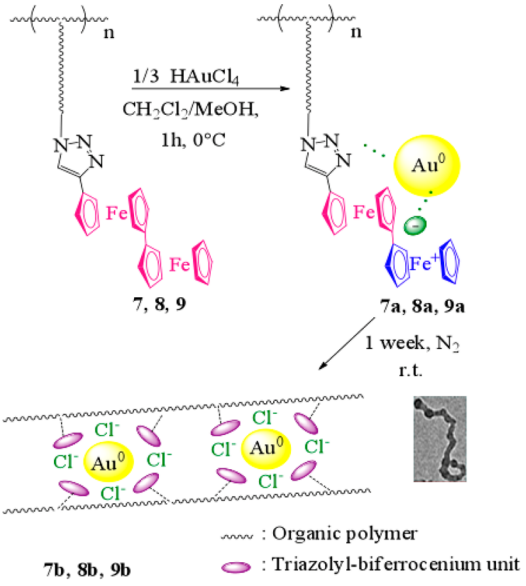

H bending, 834 cm^{-1}), near-infrared spectroscopy shows the presence of the intervalent charge-transfer band at λ_{max} = 1558 nm, characteristic of class-II mixed valency,[9] and CV shows the same waves as the precursor polymers **7** and **8** (SI).

Incubation for 1 week progressively led to the formation of polymer nanosnakes **7b** and **8b** (Scheme 2). After only 3 days, the nanosnakes are not yet formed, but their nanostructuration appears in progress by TEM (SI, p S74). Finally, the isolated nanosnakes shown in Figure 2a presents a thickness of 8.7 nm ±1.5 nm, a length of 210 ± 15 nm, and encapsulated 11 spherical AuNPs of 13.5 ± 1.5 nm size observed by transmission electron microscopy (TEM) with inter-AuNP distances of 5.2 ± 3 nm. The formation of polymer nanosnakes is taken into account by the electrostatic repulsion between the cationic biferrocenium units that is characteristic of polyelectrolytes.[10]

At this point, it was necessary to investigate the relationship between the polymer structure and the morphology of the AuNPs that are formed upon reaction with $HAuCl_4$. Lengthening the polymer by increasing the number of biferrocene units from 30 in **7** to 60 units in **8** did not provoke a significant morphology change.

The polymer framework was modified otherwise by designing another monosubstituted polymer **9** containing biferrocenyl units in the side chain. The CuAAC "click" reaction with ethynylbiferrocene **5** and a polystyrene core with an azido terminus catalyzed by $[Cu^{I}tren(benzyl)_6]$, **10**,[11] provided the triazolylbiferrocene polymer **9** (Figure 1).

Upon treatment of **9** (containing approximately 30 biferrocene units; see SI, pp S48, S53, and S56) with $HAuCl_4$ followed by incubation for 1 week under the same conditions as those with **7** and **8**, the isolated biferrocenium-containing

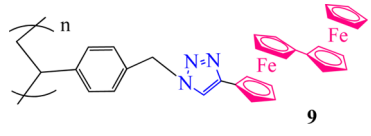

Figure 1. Polystyrene-derived polymer containing the biferrocene units in the side chain synthesized by "click" CuAAC reaction.

polymer nanosnake **9b** presented in TEM a length of 269 ± 10 nm, a thickness of 8.5 ± 2 nm and contained 14 AuNPs of 14.5 ± 1.5 nm size with inter-AuNP distances of 13.5 ± 1.5 nm (Figure 2b). Thus, the similarity of nanosnakes **7b**, **8b**, and **9b** that

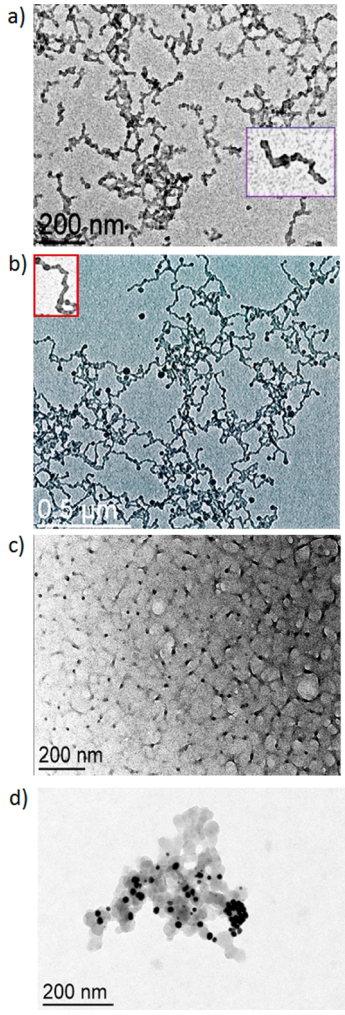

Figure 2. TEM of (a) **8b**, (b) **9b**, (c) **13b**, and (d) **9c**.

encapsulate spherical AuNPs obtained with the two very distinct types of polymerization and distinct polymer length showed that the nanosnake formation does not significantly depend on these parameters. Reduction of **9b** by $NaBH_4$ to its neutral biferrocenyl form **9c** leads to flocculation, and TEM (Figure 2d) shows AuNPs of the same size as in the case of **9b**, but the network is destroyed due to the absence of electrostatic contribution to the AuNPs stabilization.

Another drastic structural modification is the incorporation of the biferrocenyl unit in the main polymer chain instead of the side chain. Thus, such a disubstituted biferrocene-diyl polymer **13** was prepared by CuAAC polycondensation of bis(azido) triethylene glycol **11** with bis(ethynyl)biferrocene **12** (Scheme 3).[4b]

Reactions of these polymers with $HAuCl_4$ were carried out analogously and also provided AuNPs that are stabilized and encapsulated by mixed-valent biferrocenium chloride polymers **13a** (Scheme 4). Incubation showed that the polymer containing bis(triazolylferrocenium) in the main chain led to a well-organized non-nanosnake network **13b** (TEM, Figure 2c). It can be concluded that the nanomaterial containing biferrocenium

dx.doi.org/10.1021/ja5079267 | J. Am. Chem. Soc. 2014, 136, 13995−13998

Scheme 3. "Click" CuAAC Synthesis of Biferrocene Polymers Containing the Biferrocene Units in the Main Chain[4b]

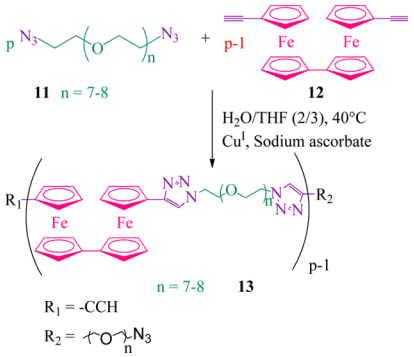

Scheme 4. Reaction of the Biferrocene Polymer 13 with $HAuCl_4$ Giving Biferrocenium Chloride Polymer-Encapsulated AuNPs in the Polymer Network 13b after Incubation

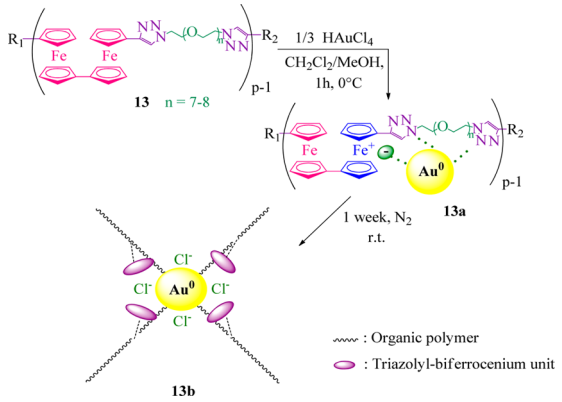

chloride in the main chain lacks the driving force for nanosnake formation. The much larger distance between the biferrocenium units than in the nanomaterials containing biferrocenium choride in the side chain considerably weakens the electrostatic repulsion between the cationic charges of all biferrocenium units that is a key parameter for the nanosnake formation.

The large thickness of the nanosnakes in **7b**, **8b**, and **9b** indicates that more than a single polymer unit is involved in each nanosnake and that a group of several biferrocenium chloride polymer units are intertwined. Likewise, the length of the nanosnakes is much larger than that of a single polymer unit, which confirms the requirement of intertwining several polymer units in order to reach the nanosnake length.

Although trz-ferrocene polymers decompose upon oxidation by $HAuCl_4$, comparison of these nanosnakes with a related ferricenium polymer can be done upon using an amidoferrocene polymer **14** (Figure 3). Indeed, oxidation of **14** by $HAuCl_4$ yields a stable ferricenium nanostructure **14b** in which only small

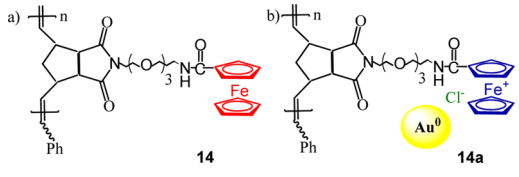

Figure 3. (a) Homopolymer **14** synthesized by ROMP and (b) its oxidation product **14a** by reaction with $HAuCl_4$.

AuNPs are observed by TEM without an apparent network (SI, p S81). This points out the importance of the triazole in the AuNP network formation that originates from the complexation of precursor Au^{III} ions by the triazole moiety.

Atomic force microscopy studies of AuNPs **8** and **8b** were performed on a graphite surface by peak force tapping mode where adhesion is mapped simultaneously with topography. The topography images of **8** showed the polymer with an average height of 7 ± 1.5 nm that did not form nanosnakes (SI, p S43). In the case of **8b** however very long nanosnakes on the order of 200−300 nm were observed with a height of 18−35 nm. Adhesion of **8b** was mapped providing qualitative mechanical information on the sample. Figure 4a shows an adhesion image of

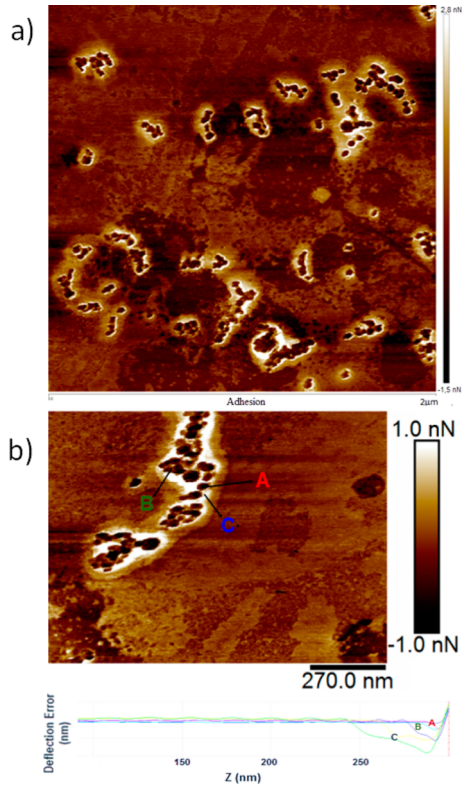

Figure 4. AFM adhesion images of biferrocenium chloride polymer-encapsulated AuNPs **8b**: (a) at 2 μm scale, (b) at 270 nm scale at which the force curves of A, B, and C were recorded.

8b, and Figure 4b shows a zoom of one of the nanosnakes. The force curves were obtained while the two images were recorded which allowed examining the nature of the nanomaterial. In all cases three different regions A, B, and C were observed corresponding to three different force curves (Figure 4b).

The force curves of region A show that the round black zones belong to a less elastic and stiffer part of material that would belong to the AuNPs. On the other hand the force curves of region C show a larger adhesion of the white zones presenting a softer and more flexible nanomaterial that would correspond to the organic part of polymer **8b**. At last brown zones B (surrounding regions A) show intermediate force curves with a different adhesion from regions A and C, presumably due to the electrostatic forces of the biferrocenium chloride units that are stabilizing the AuNPs. These three different kinds of force curves A, B, and C are similar in all recorded adhesion images of the sample of **8b**.

dx.doi.org/10.1021/ja5079267 | J. Am. Chem. Soc. 2014, 136, 13995−13998

In conclusion, it has been shown that the first metallopolymers containing biferrocene in the side chain synthesized with various structures by ROMP with the Grubbs-III metathesis catalyst or radical chain form, upon oxidation with $HAuCl_4$ in dichloromethane−methanol followed by one-week incubation, class-II mixed-valent biferrocenium chloride nanosnake polymers that encapsulate AuNPs. With biferrocene in the main polymer chain, a non-nanosnake network that encapsulates AuNPs also forms, but only small AuNPs without a polymer network are observed by TEM when polyferrocene without a triazolyl substituent synthesized by ROMP is oxidized by $HAuCl_4$. This shows that the combination of the triazole ligand and the positive charge of the biferrocenium polymer are responsible for the AuNP encapsulation. The nanosnake formation by intertwining polymers is specific to electrolyte metallopolymers with triazolylbiferrocenium in the side chain. This nanoengineering strategy involving structural and electrostatic parameter variations shows that AuNP wrapping and encapsulation by metallopolymers can control networks eventually forming nanosnakes. Applications are forecasted for the control and visualization of polymers and nanostructures.

■ ASSOCIATED CONTENT

Supporting Information

Experimental methods, 1D and 2D (^{1}H) and (^{13}C) NMR spectroscopy, infrared, UV−vis, and mass spectra, SEC, DLS, cyclic voltammograms, TEM and AFM data. This material is available free of charge via the Internet at http://pubs.acs.org.

■ AUTHOR INFORMATION

Corresponding Author

didier.astruc@u-bordeaux.fr

Notes

The authors declare no competing financial interest.

■ ACKNOWLEDGMENTS

Helpful assistance and discussions with Claire Mouche (mass spectrometry, CESAMO) and Noël Pinaud (2D NMR spectroscopy, CESAMO, University of Bordeaux) and financial support from the University of Bordeaux, the Centre National de la Recherche Scientifique (CNRS), and L'Oréal are gratefully acknowledged.

■ REFERENCES

(1) (a) Haruta, M.; Date, M. *Appl. Catal., A* **2001**, *222*, 227. (b) Cao, Y. W. C.; Jin, R.; Mirkin, C. A. *Science* **2002**, *297*, 1536−1540. (c) Daniel, M.-C.; Astruc, D. *Chem. Rev.* **2004**, *104*, 293−346. (d) Myroshnychenko, V.; Rodriguez-Fernandez, J.; Pastoriza-Santos, I.; Funston, A. M.; Novo, C.; Mulvaney, P.; Liz-Marzan, L. M.; de Abajo, F. J. G. *Chem. Soc. Rev.* **2008**, 1792−1805. (e) Xia, Y.; Xiong, B.; Lim; Skrabalak, S. E. *Angew. Chem., Int. Ed.* **2009**, *48*, 60−103. (f) Lal, S.; Clare, S. E.; Halas, N. J. *Acc. Chem. Res.* **2008**, *41*, 1842−1851. (g) Corma, A.; Leyva-Perez, A.; Maria Sabater, J. *Chem. Rev.* **2011**, *111*, 1657. (h) Dimitratos, N.; Lopez-Sanchez, J. A.; Hutchings, G. J. *Chem. Sci.* **2012**, *3*, 20−44. (i) Herves, P.; Perez-Lorenzo, M.; Liz-Marzan, L. M.; Dzubiella, J.; Lu, Y.; Ballauff, M. *Chem. Soc. Rev.* **2012**, *41*, 5577−5587. (j) Li, N.; Zhao, P.; Astruc, D. *Angew. Chem., Int. Ed.* **2014**, *52*, 1756−1789.

(2) (a) Sau, T. K.; Murphy, C. J. *Langmuir* **2005**, *21*, 2923−2929. (b) DeVries, G. A.; Brunnbauer, M.; Hu, Y.; Jackson, A. M.; Long, B.; Neltner, B. T.; Yzun, O.; Wunsch, B. H.; Stellaci, F. *Science* **2007**, *315*, 358−361. (c) Wang, X. J.; Li, G. P.; Chen, T.; Yang, M. X.; Zhang, Z.; Wu, T.; Chen, H. Y. *Nano Lett.* **2008**, *8*, 2643−2647. (d) Chen, G.; Wang, Y.; Tan, L. H.; Yang, M.; Tan, L. S.; Chen, Y.; Chen, H. *J. Am. Chem. Soc.* **2009**, *131*, 4218−4219. (e) Shen, X.; Chen, L.; Li, D.; Zhu, L.; Wang, H.; Liu, C.; Wang, Y.; Xiong, Q.; Chen, H. *ACS Nano* **2011**, *5*, 8426−8433. (f) Buck, M. R.; Bondi, J. F.; Schaak, R. E. *Nat. Chem.* **2012**, *4*, 37−44. (g) Buck, M. R.; Schaak, R. E. *Angew. Chem., Int. Ed.* **2013**, *52*, 6154−6178. (h) Wang, Y.; Salmon, L.; Ruiz, J.; Astruc, D. *Nat. Commun.* **2014**, *5*, number 3489. (i) Wang, H.; Song, X.; Liu, C.; He, J.; Chong, W. H.; Chen, H. *ACS Nano* **2014**, *8*, 8063−8073.

(3) (a) Manners, I. *Science* **2001**, *294*, 1664−1666. (b) Hudson, R. D. A. *J. Organomet. Chem.* **2001**, *637*−*639*, 47−69. (c) Wang, X.; Guérin, G.; Wang, H.; Wang, Y.; Manners, I.; Winnik, M. A. *Science* **2007**, *317*, 644−647. (d) Boisselier, E.; Diallo, A. K.; Salmon, L.; Ornelas, C.; Ruiz, J.; Astruc, D. *J. Am. Chem. Soc.* **2010**, *132*, 2729−2742. (e) Astruc, D. *Nat. Chem.* **2012**, *4*, 255−267. (f) Abd-El-Aziz, A. S.; Agatemor, C.; Etkin, N. *Macromol Rapid Commun.* **2014**, *35*, 513−559. (g) Deraedt, C.; Rapakousiou, A.; Wang, Y.; Salmon, L.; Bousquet, M.; Astruc, D. *Angew. Chem., Int. Ed.* **2014**, *53*, 8445−8449.

(4) Ag nanoparticles have been encapsulated inside block copolymers: (a) Wang, X. S.; Wang, H.; Coombs, N.; Winnik, M. A.; Manners, I. *J. Am. Chem. Soc.* **2005**, *127*, 8924−8925. (b) Wang, H.; Wang, X.; Winnik, M. A.; Manners, I. *J. Am. Chem. Soc.* **2008**, *130*, 12921−12930.

(5) (a) Ornelas, C. *New J. Chem.* **2011**, *35*, 1973−1985. (b) Graga, S. S.; Silva, A. M. S. *Organometallics* **2013**, *32*, 5626−5639. (c) Jaouen, G.; Top, S. In *Advanced in Organometallic Chemistry and Catalysis*; Pombeiro, A. J. L., Ed.; Wiley: Hoboken, NJ, USA, 2014; pp 563−580.

(6) (a) Ornelas, C.; Ruiz, J.; Cloutet, E.; Alves, S.; Astruc, D. *Angew. Chem., Int. Ed.* **2007**, *46*, 872−877. (b) Astruc, D.; Liang, L.; Rapakousiou, A.; Ruiz, J. *Acc. Chem. Res.* **2012**, *45*, 630−640.

(7) (a) Vougioukalakis, G. C.; Georgios, C.; Grubbs, R. H. *Chem. Rev.* **2010**, *110*, 1746−1787. (b) Gu, H.; Rapakousiou, A.; Ruiz, J.; Astruc, D. *Organometallics* **2014**, *33*, 4323−4335.

(8) (a) Levanda, C.; Cowan, D. O.; Bechgaard, K. *J. Am. Chem. Soc.* **1975**, *97*, 1980−1981. (b) Dong, T. Y.; Lee, T. Y.; Lee, S. H.; Lee, G. H.; Peng, S. M. *Organometallics* **1994**, *13*, 2337−2348. (c) Yamada, M.; Nishihara, H. *Chem. Phys. Chem.* **2004**, *5*, 555−559. (d) Nijhuis, C. A.; Dolatowska, K. A.; Jan Ravoo, B.; Huskens, J.; Reinhoudt, D. N. *Chem.—Eur. J.* **2007**, *13*, 69−80. (e) Djeda, R.; Rapakousiou, A.; Liang, L.; Guidolin, N.; Ruiz, J.; Astruc, D. *Angew. Chem., Int. Ed.* **2010**, *49*, 8152−8156.

(9) (a) Robin, M. B.; Melvin, B.; Day, P. *Adv. Inorg. Chem. Radiochem.* **1967**, *10*, 247−422. (b) Allen, G. C.; Hush, N. S. *Prog. Inorg. Chem.* **1967**, *8*, 357−389. (c) Richardson, D. E.; Taube, H. *Coord. Chem. Rev.* **1984**, *60*, 107−129.

(10) (a) Decher, G. *Science* **1997**, *277*, 1232−1237. (b) Paul, C. F. J.; Antonietti, M. *Adv. Mater.* **2003**, *15*, 673−683. (c) Jiang, H.; Taranekar, P.; Reynolds, J. R.; Shanze, K. S. *Angew. Chem., Int. Ed.* **2009**, *48*, 4300−4316. (d) Lu, J.; Yan, F.; Texter, J. *Prog. Polym. Sci.* **2009**, *34*, 431−448. (e) Couture, G.; Alaaeddine, A.; Boschet, F.; Ameduri, B. *Prog. Polym. Sci.* **2011**, *36*, 1521−1557.

(11) Liang, L.; Ruiz, J.; Astruc, D. *Adv. Synth. Catal.* **2011**, *353*, 3434−3450.

DOI: 10.1002/anie.201403062

Biferrocene Polymers

Multifunctional Redox Polymers: Electrochrome, Polyelectrolyte, Sensor, Electrode Modifier, Nanoparticle Stabilizer, and Catalyst Template**

*Christophe Deraedt, Amalia Rapakousiou, Yanlan Wang, Lionel Salmon, Melanie Bousquet, and Didier Astruc**

Dedicated to Alan H. Cowley on the occasion of his 80th birthday

Abstract: *Simple "click" polycondensation metallopolymers of redox-robust bis(ethynyl)biferrocene (biFc) and di(azido) poly(ethylene glycol) (PEG400 and PEG1000) were designed for multiple functions including improvement of water solubility and biocompatibility, the introduction of mixed valency and sensing capabilities, and as nanoparticle stabilizers for catalysis.*

The development of sustainable and biocompatible nanomaterials that have a variety of functions is highly desirable.[1] Here we propose a significant step toward this goal by using biferrocene units to construct water-soluble polymers, which can be used for a variety of applications including sensing and catalysis. Nowadays, a variety of ferrocene-based polymers are known, which exhibit very useful electrochromic properties. For example, orange ferrocene polymers that turn blue upon oxidation to ferricenium were synthesized by ring-opening polymerization of ferrocenophanes by Manners and co-workers.[2] To strengthen the electron-deficient ferricenium groups in polymers, we have now synthesized biferrocene[3,4] polymers in which the electron-releasing ferrocene units stabilize the adjacent ferricenium units to produce robust blue-green mixed-valence biferrocenium polymers. In addition to the electrochromic properties, these new metallopolymers have been constructed with poly(ethylene glycol) (PEG) chains that not only introduce water solubility and biocompatibility to the nanomaterials but also provide reasonable dimesions to make use of the enhanced permeability and retention (EPR) effect to achieve accumulation in cancer cells.[5] The PEG chains and biferrocene (BiFc) units have been assembled by the copper-catalyzed alkyne–azide 1,3-cycloaddition (CuAAC) reaction ("click" chemistry),[6,7] generating 1,2,3-triazole (trz) linkages. Indeed, these heterocyclic nitrogen ligands are known to sense and stabilize transition-metal ions such as Pd^{II} and Au^{III}, which in turn are precursors for useful metal nanoparticles (NPs) if the polymer can protectively encapsulate and stabilize them.[8] Small Pd NPs and Au NPs are efficient catalysts for a variety of reactions, and their stabilization through the triazole-containing polymer would be a fast and efficient way to provide templated catalysts. Depending on the Au^{III} to Au^0 reduction mode, the size of the Au NPs might be tuned for various applications in catalysis or biomedicine, in which the PEG coating provides additional benefits. Another interesting property of the biferrocene polymers is that the parent unit itself reduces Au^{III} to the polymer-stabilized Au NPs.

The synthesis of the copolymers PEG-trz-biFc **4** [poly-(PEG_{400}-biFc)] and **5** [poly(PEG_{1000}-biFc)] was achieved by the simple CuAAC "click" reaction between bis-azido-poly(ethylene glycol) with molecular weights of 400 or 1000 $g\,mol^{-1}$ (PEG_{400} and PEG_{1000}; **1** and **2**, respectively)[9] and 1,1′-biethynyl-biFc **3**.[10] The biferrocene unit provides the electrochemical properties (recognition ability, polyelectrolytic and polyelectrochromic features) while the PEG chains of variable length introduce tunable solubility into the polymer. The 1,2,3-triazole ring constructed by "click" chemistry stabilizes active palladium nanoparticles for catalysis of the Suzuki–Miyaura[11] reaction, which was performed with as little as 2 to 20 ppm of Pd. Additionally, gold nanoparticles were used to efficiently catalyze the reduction of 4-nitrophenol.

The "click" polymerization (polycondensation) between **1** or **2** and diethyne **3** is carried out at 40 °C over 2 days in THF/H_2O (3:2) using the Sharpless–Fokin catalyst consisting of $CuSO_4$, H_2O (5 equiv), and sodium ascorbate (NaAsc; Scheme 1). After removal of the copper ions the polymers are precipitated from Et_2O providing **4** as a red-orange air-stable film and **5** as a paste in 78 % and 58 % yield, respectively (see the Supporting Information, SI).

These neutral metallopolymers have been fully characterized by NMR, UV/Vis, and IR spectroscopy, matrix-assisted laser desorption/ionization time-of-flight (MALDI-TOF) mass spectrometry, elemental analysis (EA), cyclic

[*] C. Deraedt, A. Rapakousiou, Y. Wang, Prof. D. Astruc
ISM, UMR CNRS N°5255, Univ. Bordeaux
33405 Talence, cedex (France)
E-mail: d.astruc@ism.u-bordeaux.fr
Homepage: http://astruc.didier.free.fr
M. Bousquet
Laboratoire de Chimie des Polymères Organiques
UMR CNRS N° 5629, Univ. Bordeaux
33607 Pessac, cedex (France)
Dr. L. Salmon
Laboratoire de Chimie de Coordination UPR CNRS N°8241
31077 Toulouse cedex (France)

[**] Helpful discussions with Dr. J. Ruiz (Univ. Bordeaux) and financial support from the Univ. Bordeaux and Toulouse III, the CNRS, and the Ministère de l'Enseignement Supérieur et de la Recherche (Ph.D. grant to C.D.) are gratefully acknowledged.

Supporting information for this article is available on the WWW under http://dx.doi.org/10.1002/anie.201403062.

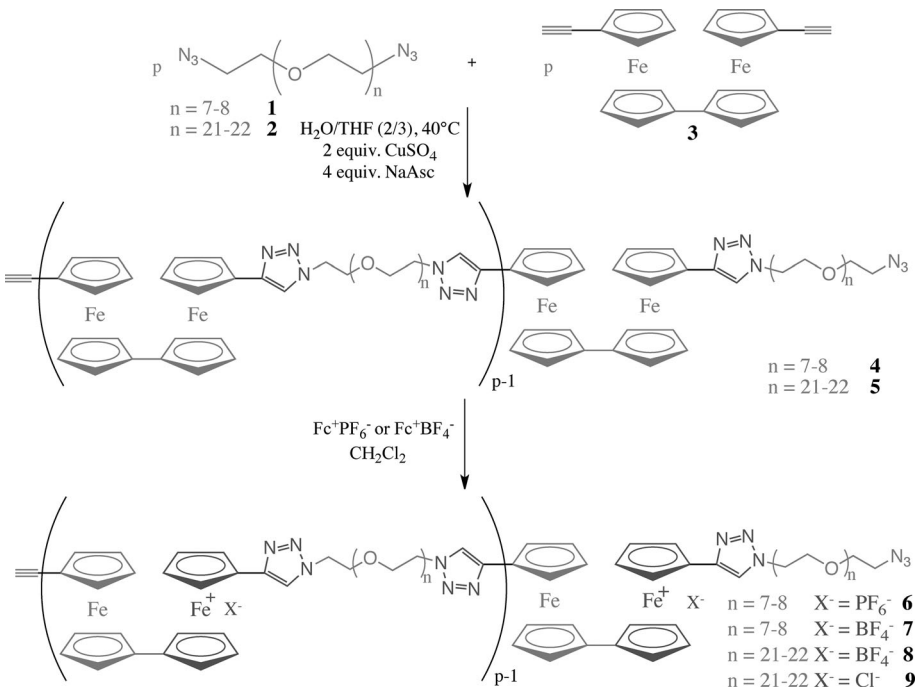

Scheme 1. Synthesis of the PEG-biFc polymers **4** and **5** and the mixed-valence polymers **6**–**9**).

voltammetry (CV), and size-exclusion chromatography (SEC) (SI). Mass spectrometry shows that **4** is composed of at least eight co-units, which corresponds to 15 trz rings. No higher polymer has been observed by mass spectrometry presumably due to saturation of the detector with small oligomers. The polydispersity of PEG_{1000} prevents the observation of **5** by mass spectrometry. No chain terminus (CH_2-N_3 or -C≡CH) has been observed in the NMR spectra of either polymer. The polymeric nature of **4** and **5** was also confirmed by IR spectroscopy (no vibrations corresponding to azide and alkyne groups were found) and by CV measurements (estimation for **4**: 62 ± 12 co-units; **5**: 131 ± 20 co-units; SI). The dispersity of the polymers was measured by SEC analyses (**4**: $D = 1.24$ and **5**: $D = 1.27$) and is particularly low for a polycondensation process, which makes it possible to exclude the formation of macrocyles. If any macrocycles would be formed in small quantities, they would be removed during the precipitation from ether.[12]

The polymers exhibit a variety of interesting features. First of all, the synthesis is very simple, because only one step is needed from known products, and the CuAAC reaction conveniently yields products, which are easy to purify. Secondly, the use of PEG units introduces biocompatibility, while at the same time the easy availability and simple synthesis from the starting materials **1** and **2** is maintained. Additionally, the use of linear PEG minimizes steric bulk around the trz-biFc-trz units. Thirdly, the "click" chemistry provides triazolyl groups, which are important for the binding of metals and the stabilization of metal NPs. The crucial role of the trz rings in the catalysis by metal NPs is exemplified below.[13] Finally, the presence of biFc units results in multiple stable redox states, which is the most interesting feature of polymers **4** and **5**. These polymers have multifaceted supramolecular properties: because of their redox properties and as stable and isolable mixed-valence compounds, they can act as molecular electron storage systems. Cyclic voltammetry involving the bis(trz-Fc) units has been applied to sense ions with potential applications such as the fabrication of modified electrodes. The solubilization properties of the two polymers with distinct PEG lengths are complementary; indeed **4** is soluble only in CH_2Cl_2, $CHCl_3$, DMF, whereas due to the long PEG chain, **5** is soluble in many more solvents including THF, MeOH, EtOH, and H_2O.

The cyclic voltammograms of **4** and **5** measured with a Pt electrode in CH_2Cl_2 using 0.1 M $[nBu_4N][PF_6]$ as the supporting electrolyte and decamethylferrocene, $[Cp^*_2Fe]$ ($Cp^* = \eta^5$-C_5Me_5), as the internal reference show two reversible waves at 0.440 and 0.785 V vs. $[Cp^*_2Fe]^{+/0}$ (Figure 1a) and 0.420 and 0.800 V vs. $[Cp^*_2Fe]^{+/0}$ (SI), respectively. The presence of only two reversible waves, like in biferrocene itself, implies that the two Fc moieties of one biFc unit are dependent on each other, whereas each biFc unit is independent of other biFc units. One interesting

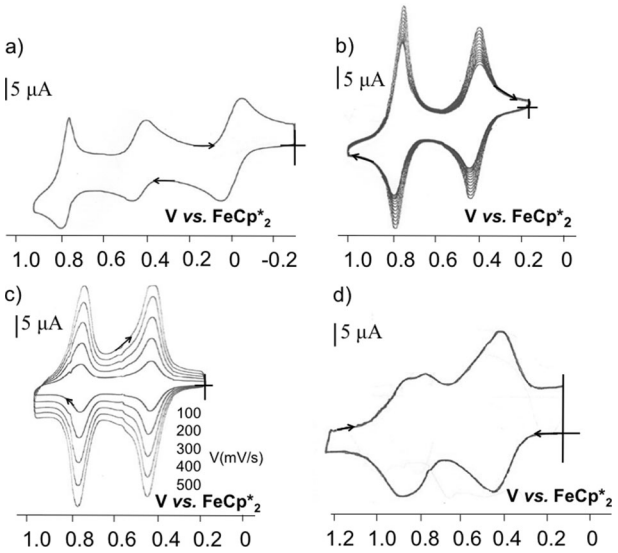

Figure 1. a) Cylic voltammogram of **4** in CH_2Cl_2; reference electrode: Ag; working and counter electrodes: Pt; scan rate: 0.2 $V s^{-1}$; supporting electrolyte: $[nBu_4N][PF_6]$. Two reversible waves are present, one at 0.440 V and a second at 0.785 V. b) Progressive adsorption of **4** upon scanning around the biFc area. c) The modified Pt electrode at various scan rates in a CH_2Cl_2 solution, which only contains the supporting electrolyte). d) Splitting of the second oxidation wave upon addition of $Pd(OAc)_2$ to **4** (1 equiv of Pd^{II} per BiFc unit).

feature of **4** is its progressive adsorption on the electrode, as can be seen from the cyclic voltammogram (Figure 1b). This allows the facile formation of robust metallopolymer-modified electrodes upon scanning back and forth around the biFc potential zone (Figure 1c). Variation of the intensity with the scan rate during the electrode modification provides a linear function as it would be expected for a correctly modified electrode (SI). The adsorption of **5** on the electrode is weaker than that of **4** owing to the better solubility of **5** and its ferricenium form. The CV behavior of **4** allows its use and that of the corresponding modified electrode for ion recognition. After addition of $Pd(OAc)_2$ to a solution of **4**, a splitting of 70 mV of the second biFc oxidation wave is observed, reflecting the coordination of Pd^{II} to the nitrogen atoms of the trz ligand. This modifies the electron density of the Fc centers (Figure 1d). The complexation of $Pd(OAc)_2$ by trz can also be monitored by ^1H NMR spectroscopy in $CDCl_3$/MeOH (this solvent mixture was also used in the Pd NP catalysis, see below). The ^1H NMR signal of the acetate is shifted upon addition of **4**. This shift is observed until 1 equiv $Pd(OAc)_2$ per triazolyl ring has been added (SI). The 1:1 stoichiometry of Pd^{II}/trz ligand proves to be important in catalysis (see below), when Pd NPs resulting from the reduction of trz-coordinated Pd^{II} species are used.

The proximity of the Fc moieties in the BiFc units implies another application, which is the synthesis of stable mixed-valence polymers affording electrochromic and polyelectrolyte materials. The mixed-valence polymers **6** and **7** were quantitatively synthesized by stoichiometric exergonic reactions of **4** in CH_2Cl_2 with $[Cp_2Fe][PF_6]$ and $[Cp_2Fe][BF_4]$, respectively, because the redox potential of $[Cp_2Fe]^{+/0}$ is higher than the first oxidation potential of the $biFc^{+/0}$ units. An additional driving force for these reactions is the precipitation of the mixed-valence polymers **6** and **7** from CH_2Cl_2. The acetonitrile-soluble polymers **6** and **7** are blue-green, whereas the starting material **4** is orange. Likewise, the mixed-valence polymer **8** was synthesized from **5** in the presence of 1 equiv $[Cp_2Fe][BF_4]$ per biFc unit and fully characterized (SI). The mixed-valence polyelectrolytes **6** and **7** are insoluble in water, whereas **8** is water-soluble. The three polymers were characterized by UV/Vis, FTIR, near-IR, and Mössbauer spectroscopy. The FTIR spectrum of **6** conveniently contains a band of PF_6^- at 841 cm^{-1}, but both the ferrocenyl and the ferricinium groups of the BF_4^- polymeric salts **7** and **8** are detected at 818 cm^{-1} (ν_{Fc}) (compare to 819 cm^{-1} in **4**) and 832 cm^{-1} (ν_{Fc^*}), respectively (SI), indicating a localized mixed valency even at high IR frequency (10^{13} s^{-1}), which was already observed for the parent biferrocenium. Further proof of this class II mixed valency is the presence of absorption bands in the near-infrared range corresponding to a transition from the ground state to the intervalence charge-transfer (IVCT) state (SI). The recorded Mössbauer spectrum of **6** (Figure 2) at zero field and 78 K further confirms the localized class II mixed valency with the presence of both the ferrocenyl and the ferricinium groups, which was expected since this spectroscopic method covers lower frequencies (10^7 s^{-1}) than IR. Finally in the UV/Vis spectra the λ_{max} of **6**–**8** (ca. 600 nm) was strongly shifted relative to the λ_{max} of **4** and **5** (ca. 456 nm) (SI).

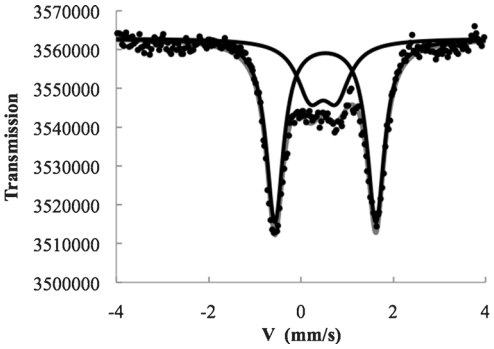

Figure 2. Mössbauer spectrum of **6** at zero field and 78 K showing the localized class II mixed valency at 10^7 s^{-1} with both ferrocenyl (doublet I.S. = 0.536 mm s^{-1} vs. Fe; Q.S. = 2.192 mm s^{-1}) and ferricinium groups (doublet I.S. = 0.490 mm s^{-1} vs. Fe; Q.S. = 0.571 mm s^{-1}).

The presence of triazole units in the polymer chains allows the coordination of 1 equiv Pd^{II} or Au^{III} ions per heterocycle ligand (see above and SI) and further reduction leads to the formation of polymer-stabilized Pd NPs and Au NPs, respectively. These nanomaterials were shown to be active catalysts for various reactions. In addition, it was shown that the longer PEG chains in **5** (PEG_{1000}) result in the solubilization of these stabilized NPs in water.

The Suzuki–Miyaura reaction has been conducted in the presence of Pd NPs stabilized by **4** and **5**. Polymer **4** is mixed with $Pd(OAc)_2$ (1 equiv per triazole unit) in $CHCl_3$/MeOH (2/1) and stirred for 5 min. Then $NaBH_4$ (10 equiv per Pd^{II}) is added to the solution, leading to the formation of black Pd NPs. These stable Pd NPs at a loading of 0.25 mol% Pd are efficient in the Suzuki–Miyaura cross-coupling reaction of various bromoarenes with phenylboronic acid (Table 1) in $CHCl_3$/MeOH (2:1) at 90 °C for 16 h. The water-soluble Pd NPs stabilized by **5** are prepared by mixing aqueous solutions of **5** and K_2PdCl_4 at 20 °C and stirring for 5 min (1/1 Pd/triazole stoichiometry) followed by the quick addition of a $NaBH_4$ solution (10 equiv per Pd^{II}). The yellow solution of Pd^{II}-**5** instantaneously turned orange-brown (SI), confirming the formation of Pd NPs. Transmission electron microscopy (TEM) reveals that the size of Pd NPs stabilized by **5** is (2.3 ± 0.6) nm after they had been stored for one month, which is ideal for efficient catalysis (Figure 3).

The Suzuki–Miyaura reaction has also been performed with this catalyst system, using the "greener" solvent mixture EtOH/H_2O (1:1) at 80 °C for 24 h with only 20 ppm of Pd (Pd NPs). The results are summarized in Table 1 and demonstrate the high activity of **5**-Pd NPs. A loading of only 20 ppm Pd is sufficient to obtain good yields using both activated as well as deactivated bromoarenes. Moreover, the amount of Pd can be further reduced. In the case of the coupling of 4-bromoacetophenone and phenylboronic acid at 80 °C only 2 ppm of Pd was necessary to achieve a reaction yield of 82% after 36 h (TON = 410000, TOF = 11400 h^{-1}). The use of such a low amount of catalyst is very rare in the Suzuki–Miyaura reaction, further underlining the interesting properties of the nanomaterial described here. A comparative table (SI) positions **5**-Pd NPs as one of the best catalysts known for the Suzuki–Miyaura reaction.

Table 1: Results of the Suzuki–Miyaura reaction of bromoarenes in the presence of Pd NPs stabilized by **4** and **5**.

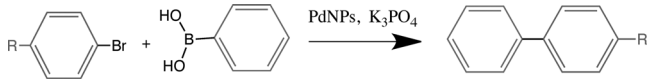

Bromoarene R =	Conditions[a]	Conv. [%][b]	Yield [%][c]	TON [h^{-1}]	TOF [h^{-1}]
H	A (PdNP-**4**)	100	99	396	24.8
CH_3	A (PdNP-**4**)	100	97	388	24.3
OCH_3	A (PdNP-**4**)	98	97	388	24.3
NO_2	A (PdNP-**4**)	100	99	396	24.8
CHO	A (PdNP-**4**)	100	99	396	24.8
$COCH_3$	A (PdNP-**4**)	100	99	396	24.8
H	B (PdNP-**5**)	100	90	45 000	1875
CH_3	B (PdNP-**5**)	100	80	40 000	1667
OCH_3	B (PdNP-**5**)	100	78	39 000	1625
NO_2	B (PdNP-**5**)	100	91	45 500	1896
CHO	B (PdNP-**5**)	100	91	45 500	1896
$COCH_3$	B (PdNP-**5**)	100	99	49 500	2062

[a] Conditions A: the reactions were carried out with 1 mmol of bromoarene, 1.5 mmol of phenylboronic acid, 2 mmol of K_3PO_4, and 0.25 mol% of Pd NPs stabilized by **4** in 3 mL of $CHCl_3$/MeOH (2:1) for 16 h at 90°C. Conditions B: the reactions were carried out with 1 mmol of bromoarene, 1.5 mmol of phenylboronic acid, 2 mmol of K_3PO_4, and 0.002 mol% of Pd NPs stabilized by **5** in 6 mL of EtOH/H_2O (1:1) for 24 h at 80°C. [b] The conversion was determined by ^1H NMR analysis. [c] Yield of isolated product.

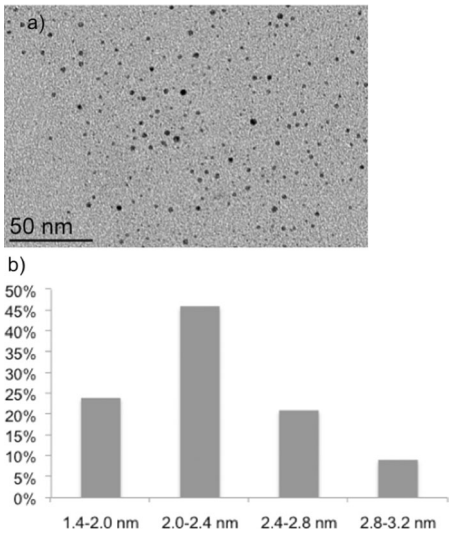

Figure 3. a) TEM image of Pd NPs stabilized by **5**. b) Size distribution of the Pd NPs present in the TEM picture (average size of 103 Pd NPs: (2.3 ± 0.6) nm).

Polymer **5** is oxidized to the mixed-valence water-soluble polyelectrolyte **9** when 1 equiv $HAuCl_4$ is added per 3 equiv biferrocene unit according to the redox stoichiometry, thereby forming Au^0 atoms that give polymer-stabilized Au NPs. Due to the plasmon absorption, which is detected by UV/Vis spectroscopy at 534 nm (SI) the Au NPs solution presents a purple coloration. TEM analysis shows that these Au NPs have an average size of around (12 ± 2) nm

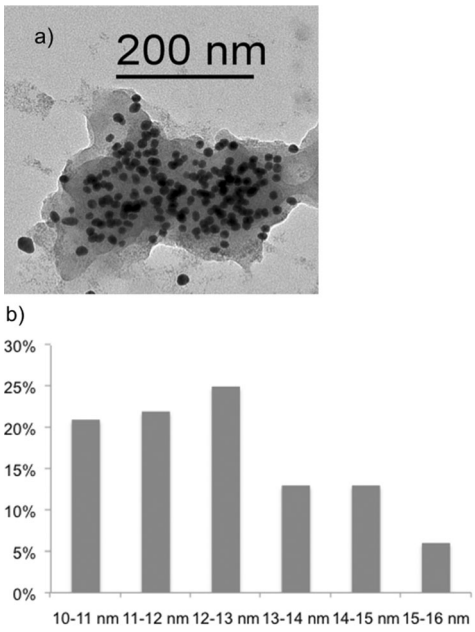

Figure 4. a) TEM image of Au NPs synthesized by reduction of Au^{III} with **5**. b) Size distribution of the Au NPs present in the TEM picture (average size of 98 Au NPs: (12 ± 2) nm).

(Figure 4). Scheme 2 shows the reduction and stabilization of both **5**-Pd NPs and **5**-Au NPs. The Au NPs (0.6–1.2 mol%) were used to catalyze the reduction of 4-nitrophenol to 4-aminophenol by an excess of $NaBH_4$; 4-aminophenol is a potential industrial intermediate in the production of many analgesic and antipyretic drugs, anticorrosion lubricants, and hair dyeing agents.[14] When 1.2 mol% of Au NPs is used, the reaction is complete within 350 seconds, which corresponds to a k_{app} value of 6.0×10^{-3} s^{-1}. The reaction rate constant k_{app} is calculated using the rate equation $-\ln(C_t/C_0) = k_{app}t$ (the catalyst exhibits pseudo-first-order kinetics; SI).

In conclusion, the two copolymers **4** and **5** synthesized by "click" polycondensation show multifunctional properties as polyelectrolytes and electrochromes, redox sensors for transition-metal cations, electrode modifiers, and excellent templates for the synthesis of efficient Pd and Au nanoparticle catalysts. The biferrocene unit provides a more stable ferricenium form than the parent ferricenium, which makes the polymers ideal as class II mixed-valence polyelectrolytes and electrochromes. The proximity of the triazole ring to the biFc units facilitates redox sensing as well as the understanding of the stoichiometry of metal cation complexation. The stabilization and solubilization of Pd NPs and Au NPs by easily available polymers yield extremely efficient catalysts for current organic reactions.

Received: March 6, 2014
Published online: May 28, 2014

Keywords: biferrocenes · click chemistry · heterogeneous catalysis · nanoparticles · polymers

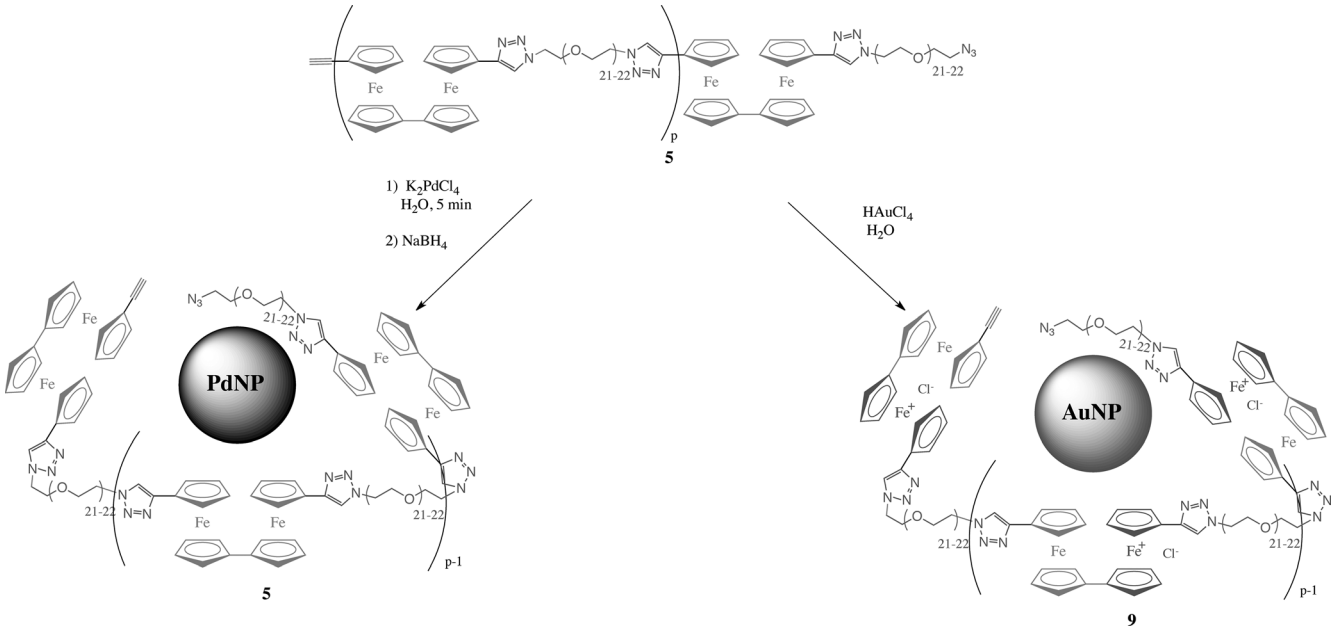

Scheme 2. Synthesis of Pd NPs (left) and Au NPs (right).

[1] a) J.-M. Lehn, *Science* **2002**, *295*, 2400 – 2403; b) J. C. Love, L. A. Estroff, J. K. Kriebel, R. G. Nuzzo, G. M. Whitesides, *Chem. Rev.* **2005**, *105*, 1103 – 1169; c) M. R. Langille, M. L. Personick, C. A. Mirkin, *Angew. Chem.* **2013**, *125*, 14158 – 14189; *Angew. Chem. Int. Ed.* **2013**, *52*, 13910 – 13930; d) D. Astruc, *Nat. Chem.* **2012**, *4*, 255 – 267.

[2] a) E. M. Leitao, T. Jurca, I. Manners, *Nat. Chem.* **2013**, *5*, 817 – 829; b) R. Rulkens, A.-J. Lough, I. Manners, S. R. Lovelace, C. Grant, W. E. Geiger, *J. Am. Chem. Soc.* **1996**, *118*, 12683 – 12695.

[3] a) D. O. Cowan, F. Kaufman, *J. Am. Chem. Soc.* **1970**, *92*, 219 – 220; b) T. Yamamoto, T. Morikita, T. Maruyama, *Macromolecules* **1997**, *30*, 5390 – 5396.

[4] a) Y. Men, K. Kubo, M. Kurihara, H. Nishihara, *Phys. Chem. Chem. Phys.* **2001**, *3*, 3427 – 3430; b) M. Yamada, H. Nishihara, *Chem. Commun.* **2002**, 2578 – 2579; c) M. Yamada, H. Nishihara, *Eur. Phys. J. D* **2003**, *24*, 257 – 260; d) C. A. Nijhuis, K. A. Dolatowska, B. Jan Ravoo, J. Huskens, D. N. Reinhoudt, *Chem. Eur. J.* **2007**, *13*, 69 – 80; e) R. Djeda, A. Rapakousiou, L. Liang, N. Guidolin, J. Ruiz, D. Astruc, *Angew. Chem.* **2010**, *122*, 8328 – 8332; *Angew. Chem. Int. Ed.* **2010**, *49*, 8152 – 8156.

[5] a) I. Brigger, C. Dubernet, P. Couvreur, *Adv. Drug Delivery Rev.* **2002**, *54*, 631 – 651; b) A. Llevot, D. Astruc, *Chem. Soc. Rev.* **2012**, *41*, 242 – 257.

[6] a) V. V. Rostovtsev, L. G. Green, V. V. Fokin, K. B. Sharpless, *Angew. Chem.* **2002**, *114*, 2708 – 2711; *Angew. Chem. Int. Ed.* **2002**, *41*, 2596 – 2599; b) C. W. Tornøe, C. Christensen, M. Meldal, *J. Org. Chem.* **2002**, *67*, 3057 – 3064.

[7] a) For CuAAC "click" polymer assemblies, see: G. W. Goodall, W. Hayes, *Chem. Soc. Rev.* **2006**, *35*, 280 – 312; b) M. Malkoch, R. Vestberg, N. Gupta, L. Mespouille, P. Dubois, A. F. Mason, J. L. Hedrick, Q. Liao, C. W. Frank, K. Kingsbury, C. J. Hawker, *Chem. Commun.* **2006**, 2774 – 2776; c) J. E. Moses, A. D. Moorhouse, *Chem. Soc. Rev.* **2007**, *36*, 1249 – 1262; d) P. L. Golas, K. Matyjaszewski, *Chem. Soc. Rev.* **2010**, *39*, 1338 – 1354; e) L. Liang, D. Astruc, *Coord. Chem. Rev.* **2011**, *255*, 2933 – 2945; f) F. Herbst, S. Seiffert, W. H. Binder, *Polym. Chem.* **2012**, *3*, 3084 – 3092; g) M. H. Samiullah, D. Reichert, T. Zinkevich, J. Kressler, *Macromolecules* **2013**, *46*, 6922 – 6935.

[8] a) C. Ornelas, J. Ruiz, E. Cloutet, S. Alves, D. Astruc, *Angew. Chem.* **2007**, *119*, 890 – 895; *Angew. Chem. Int. Ed.* **2007**, *46*, 872 – 877; b) A. K. Diallo, C. Ornelas, L. Salmon, J. Ruiz, D. Astruc, *Angew. Chem.* **2007**, *119*, 8798 – 8802; *Angew. Chem. Int. Ed.* **2007**, *46*, 8644 – 8648; c) E. Boisselier, A. K. Diallo, L. Salmon, C. Ornelas, J. Ruiz, D. Astruc, *J. Am. Chem. Soc.* **2010**, *132*, 2729 – 2742.

[9] PEG derivatives **1** and **2** were synthesized from PEG_{400} and PEG_{1000}: L. A. Canalle, S. S. van Berkel, L. T. de Haan, J. C. M. van Hest, *Adv. Funct. Mater.* **2009**, *19*, 3464 – 3470.

[10] Diethynyl biFc **3** was synthesized from ferrocene: T.-Y. Dong, S.-W. Chang, S.-F. Lin, M.-C. Lin, Y.-S. Wen, L. Lee, *Organometallics* **2006**, *25*, 2018 – 2024.

[11] a) N. Miyaura, A. Suzuki, *Chem. Rev.* **1995**, *95*, 2457 – 2483; b) J. Hassan, M. Sévignon, C. Gozzi, E. Schulz, M. Lemaire, *Chem. Rev.* **2002**, *102*, 1359 – 1469; c) F. Bellina, A. Carpita, R. Rossi, *Synthesis* **2004**, 2419 – 2440; d) I. Beletskaya, A. V. Cheprakov, *J. Organomet. Chem.* **2004**, *689*, 4055 – 4082; e) D. Astruc, F. Lu, J. Ruiz, *Angew. Chem.* **2005**, *117*, 8062 – 8083; *Angew. Chem. Int. Ed.* **2005**, *44*, 7852 – 7872; f) D. Astruc, K. Heuzé, S. Gatard, D. Méry, S. Nlate, L. Plault, *Adv. Synth. Catal.* **2005**, *347*, 329 – 338; g) I. Favier, D. Madec, E. Teuma, M. Gomez, *Curr. Org. Chem.* **2011**, *15*, 3127 – 3174; h) *Nanomaterials in Catalysis* (Eds.: P. Serp, K. Philippot), Wiley-VCH, Weinheim, **2013**.

[12] B. P. Mudraboyina, M. M. Obadia, R. Sood, A. Serghei, E. Drockenmüller, *Chem. Mater.* **2014**, *26*, 1720 – 1726.

[13] a) C. Deraedt, L. Salmon, J. Ruiz, D. Astruc, *Adv. Synth. Catal.* **2013**, *355*, 2992 – 3001; b) C. Deraedt, D. Astruc, *Acc. Chem. Res.* **2014**, *47*, 494 – 503.

[14] a) K. Kuroda, M. Haruta, *J. Mol. Catal. A* **2009**, *298*, 7 – 11; b) S. Wunder, Y. Lu, M. Albrecht, M. Ballauf, *ACS Catal.* **2011**, *1*, 908 – 916; c) J. P. Zhang, C. Shao, Z. Zhang, M. Zhang, J. Mu, Z. Guo, Y. Liu, *Nanoscale* **2011**, *3*, 3357 – 3363; d) P. Hervés, M. Pérez-Lorenzo, L. M. Liz-Marzán, J. Dzubiella, M. Ballauf, *Chem. Soc. Rev.* **2012**, *41*, 5577 – 5587; e) A. Shivhare, S. J. Ambrose, H. Zhang, R. W. Purves, R. W. Scott, *Chem. Commun.* **2013**, *49*, 276 – 278.

Synthesis and Redox Activity of "Clicked" Triazolylbiferrocenyl Polymers, Network Encapsulation of Gold and Silver Nanoparticles and Anion Sensing

Amalia Rapakousiou,[†] Christophe Deraedt,[†] Joseba Irigoyen,[‡] Yanlan Wang,[†] Noël Pinaud,[†] Lionel Salmon,[§] Jaime Ruiz,[†] Sergio Moya,[‡] Didier Astruc*,[†]

[†]ISM, UMR CNRS No. 5255, Univ. Bordeaux, 33405 Talence Cedex, France
[‡] CIC biomaGUNE, Unidad Biosuperficies, Paseo Miramón 182, Edif. "C", 20009 Donostia-San Sebastián, Spain
[§]Laboratoire de Chimie de Coordination UPR CNRS N°8241, 31077 Toulouse Cedex, France
e-mail: d.astruc@ism.u-bordeaux1.fr

Keywords: ethynylbiferrocene, triazole, biferrocene, polymers, mixed valence, gold nanoparticles, silver nanoparticles, nanosnakes, redox sensing, modified electrodes.

ABSTRACT

The design of redox-robust polymers is called for in view of interactions with nanoparticles and surfaces toward applications in nanonetwork design, sensing and catalysis. Redox-robust triazolybiferrocenyl (trzBiFc) polymers have been synthesized with the organometallic group in the side chain by ring-opening metathesis polymerization using Grubbs-III catalyst or radical polymerization and with the organometallic group in the main chain by Cu(I) azide alkyne cycloaddition (CuAAC) catalyzed by [Cu(I)(hexabenzyltren)]Br. Oxidation of the trzBiFc polymers with ferricenium hexafluorophoshate yields the stable 35-electron class-II mixed-valent biferrocenium polymer. Oxidation of these polymers with Au^{III} or Ag^{I} gives nanosnake-shaped networks (observed by TEM and AFM) of this mixed-valent $Fe^{II}Fe^{III}$ polymer with encapsulated metal nanoparticles (NPs) when the organoiron group is located on the side chain. The factors that are suggested to be synergistically responsible for the NP stabilization and network formation are the polymer bulk, the trz coordination, the nearby cationic charge of trzBiFc and the inter-BiFc distance. For instance reduction of such an oxidized trzBiFc-AuNP polymer to the neutral trzBiFc-AuNP polymer with $NaBH_4$ destroys the network, and the product flocculates. The polymers easily provide modified electrodes that sense, via the oxidized $Fe^{II}Fe^{III}$ and $Fe^{III}Fe^{III}$ polymer states, respectively ATP^{2-} via the outer ferrocenyl (Fc) units of the polymer and Pd^{II} via the inner Fc units; this recognition works well in dichloromethane (DCM), but also to a lesser extent in water with NaCl as the electrolyte.

INTRODUCTION

Ferrocene[1] and related iron sandwich complexes[2] have long been shown to disclose excellent redox stabilities[3] that have allowed the development of properties and applications in electrochemistry,[4] catalysis,[5] nanomedicine,[6] and sensing.[7] Consequently, metallocene-containing polymers have attracted considerable related attention in materials science.[8] Most of these nanomaterials involve the ferrocene (Fc) prototype; in particular ring-opening of ferrocenophane monomers directly leads to the synthesis of Fc polymers and herewith to the controlled design of mono- and bidimentional nanomaterials.[9] Despite the well-known stability of the d^5 17-electron ferricenium cation,[1] many ferricenium compounds are fragile and air-sensitive in organic solutions.[10] Therefore we have investigated the synthesis of metallopolymers based on the biferrocene (BiFc) unit,[11] because the stereoelectronic stabilization of the mixed valency in cationic biferrocenium derivatives leads to much more robust nanomaterials than with single ferricenium groups. BiFc redox chemistry includes three easily accessible oxidation states, and biferrocenium cation belongs to class II of the Robin and Day classification with valence localization at the infrared time scale.[12] BiFc has been incorporated into nanosystems such as gold nanoparticles (AuNPs) for electrodeposition[13] and dendrimers for "molecular printboards",[14] fabrication of molecular junctions[15] and further studies of their redox properties.[16] However, the multi-electron properties of BiFc polymers[17] have not yet been much studied, and the remarkable availability and stability of biferrocenium polymers allows to design useful redox reactions starting from BiFc polymers and leading to original nanomaterials and their networks.

A breakthrough in the mono-functionalization of BiFc was the synthesis of ethynylbiferrocene allowing the easy incorporation of BiFc moieties into dendrimers and gold nanoparticles by Sonogashira, homocoupling or "click" reactions[18] The latter reaction introduces the 1,2,3-triazolyl (trz) group that is very useful for various applications including redox recognition, coordination to transition-metal cations and stabilization of AuNPs and PdNPs for catalysis,[19] and is biocompatible.[20] Indeed, triazolylbiferrocenyl (trzBiFc) dendrimers proved to be excellent selective exo-receptors in homogeneous phase, as the outer Fc moiety could recognize oxo-anions, whereas the inner Fc recognized transition-metal cations.[18b,c] However, these molecular tools should be immobilized onto solid surfaces in order to be incorporated in electrochemical sensing devices. Following this strategy we envisaged to extend the "click" BiFc functionalization to polymers by preparing easily-accessible trzBiFc polymers and co-polymers with polyethylene glycol chains as co-units using ring-opening metathesis polymerization (ROMP), copper-catalyzed azide alkyne cycloaddition (CuAAC, "click") polycondensation and free-radical polymerization.[21] The full characterization of these metallopolymers by ^{1}H, ^{13}C, HSQC, HMBC, COSY and NOESY, DOSY NMR spectroscopy is shown here including infrared, UV-vis., Dynamic Light Scattering (DLS), Size Exclusion Chromatography (SEC), MALDI-TOF mass spectrometry and Cyclic Voltammetry (CV). Oxidation of the metallopolymers using $HAuCl_4$ leads to mixed-valent trz-biferrocenium polymers that encapsulate AuNPs and AgNPs in snake-shape networks, as shown by Transmission Electron Microscopy (TEM), Atomic Force Microscopy (AFM), UV-Vis., DLS,

IR, near-IR and CV. The new trzBiFc-terminated metallopolymers were used to derivatize Pt electrodes for redox recognition of ATP^{2-} and Pd^{2+} in organic and aqueous media.

Results and discussion

1. Synthesis and characterization of triazolylBiFc polymers 9, 10, 14, 18 and 19

*Synthesis of ethynylbiferrocene **3***

Ethynylbiferrocene **3** was synthesized in two steps from BiFc,[22] **1**. (Scheme 1) The first step is the synthesis of acetylbiferrocene **2** that consists in a Friedel-Crafts acetylation of BiFc and is based on the work by Doisneau *et al* that was reported in 1992.[23] Ethynylbiferrocene[18e] **3** was subsequently prepared in a reaction similar to that used for the synthesis of ethynylferrocene[24] between acetylbiferrocene and lithiumdiisopropylamide (LDA)/diethylchlorophosphate followed by column chromatography with pentane as eluent. This provided **3** as an orange crystalline powder in a 50% overall yield from BiFc.

Scheme 1: Synthesis of ethynylbiferrocene **3**.

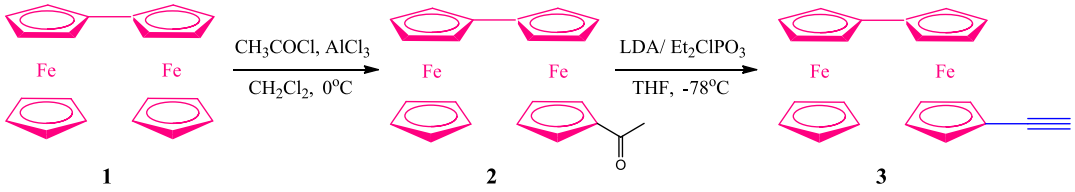

*Synthesis of the trzBiFc-functionalized norbornene monomer **7***

Commercial *cis*-5-norbornene-*exo*-2,3-dicarboxylic anhydride reacts at 110°C with 4-aminobutanol to give the 4-hydroxylbutyl-cis-5-norbornene-exo-2,3-dicarboximide in quantitative yield.[25] Then under basic conditions the nucleophilic substitution of **4** by TsCl (Ts = tosyl) gives **5**, and nucleophilic substitution of tosyl by azide yields the azidonorbornene monomer **6**. Then CuAAC reaction between ethynylbiferrocene and monomer **6** catalyzed by Cu(I) leads to the trz-BiFc-functionalized norbornene monomer **7** in 97% yield (Scheme 2). After purification, compounds **5**, **6** and **7** are identified and characterized by ^{1}H and ^{13}C NMR and IR spectroscopy, ESI mass spectrometry, UV-vis., elemental analysis and cyclic voltammetry (CV). The ^{1}H NMR spectra of **5** shows the appearance of the four tosylate protons at 7.74 and 7.31 ppm and the $-CH_2OTs$ protons at 3.97 ppm, whereas in compound **6** the four protons of the tosylate groups are no longer observed, and the new $-CH_2N_3$ peak appears at 3.47 ppm. The appearance of a strong absorption band at 2097 cm^{-1} is observed in the IR spectrum corresponding to the $-N_3$ group. After the "click" reaction, the triazolyl proton appears at 7.03 ppm, and the $-CH_2$trz peak is deshielded at 4.50 ppm because of the electron-withdrawing property of the trz group. The $-N_3$ absorption band in the IR is no longer observed, indicating the disappearance of the starting material **6**. The UV-vis. spectrum recorded in DCM shows a strong absorption at λ_{max}

= 450 nm (SI, S20) due to the d-d* transitions of BiFc. Finally, ESI MS and elemental analysis confirm the molecular structure of **7**.

Scheme 2: Synthesis of the trz-BiFc-functionalized norbornene monomer **7**.

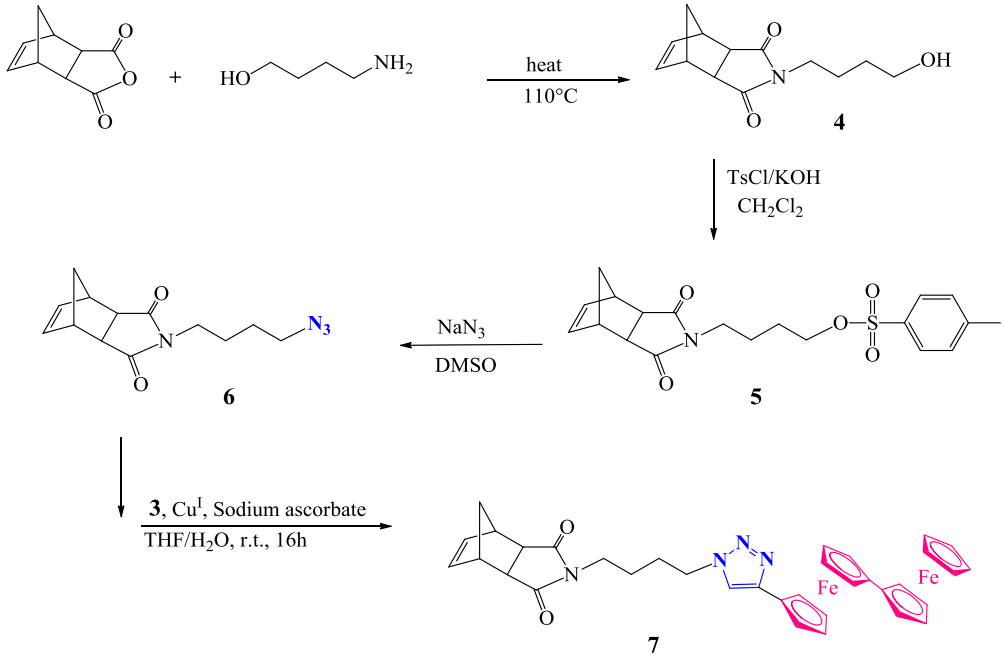

Ring-opening-metathesis polymerization of the norbornene functionalized with a trzBiFc group

The polymerization of the trzBiFc-substituted norbornene monomer **7** (Scheme 3) proceeds in distilled DCM in the presence of the 3rd-generation of Grubbs' Ru metathesis catalyst (called Grubbs III, **8**[26], Figure 1) at r.t. in 5h.

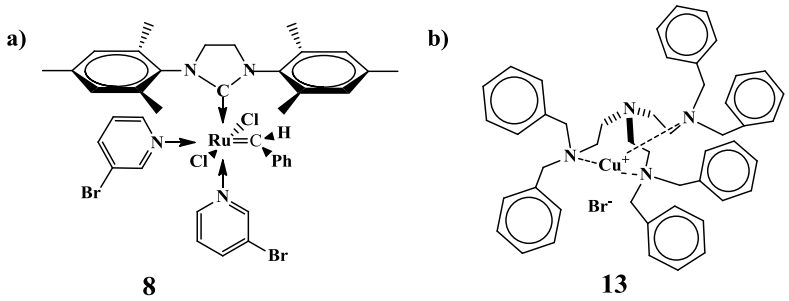

Figure 1: a) 3rd generation Ru metathesis catalyst, Grubs III (**8**) b) CuACC catalyst copper [Cu^{I}tren($CH_2Ph)_6$][Br] (**13**).

Then excess ethyl vinyl ether is added to quench the reaction. The use of monomer/catalyst ratios of 30 and 60 respectively gives polymers **9** and **10** in 98% and 99% yield, as bright orange crystalline solids (Scheme 3). Various concentrations of the monomer are examined for the ROMP polymerization of monomer **7** and the optimal conditions (highest conversion in a shorter time) are achieved when the concentration of monomer **7** is ≥ 0.25 M.

Scheme 3: ROMP reaction of the trzBiFc norbornene monomer **7**.

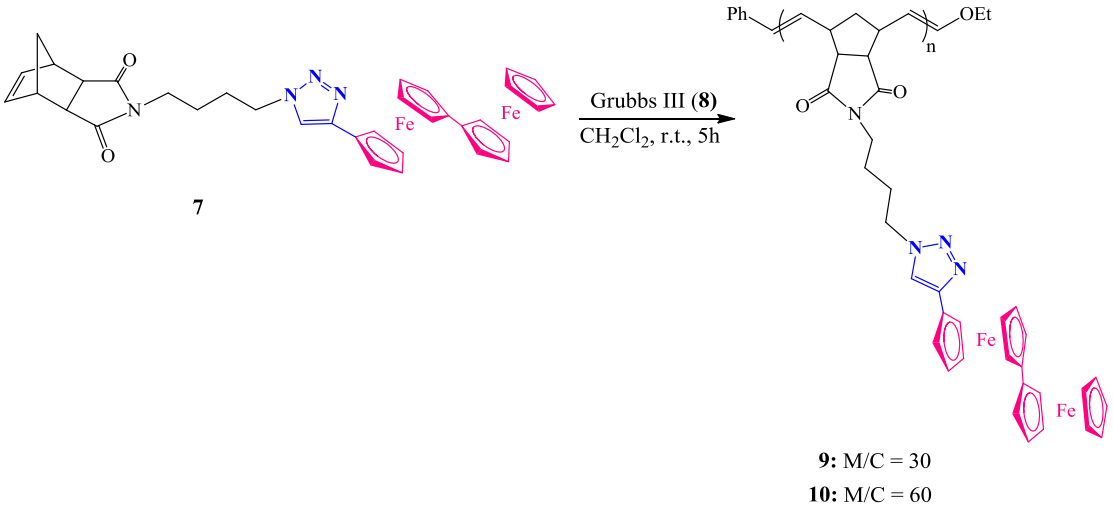

^{1}H NMR is a key tool to check whether the polymerization is finished. Indeed the olefinic protons that are found at 6.3 ppm in monomer **7** are now displaced to the region of 5.5-5.8 ppm after polymerization. The bulky nature of the trzBiFc group is also shown by ^{1}H NMR for polymers **9** and **10**. The trz proton that is represented by a single peak in monomer **7** is split into a doublet due to two distinct sterically hindered conformations of the BiFc units composing polymers **9** and **10**. For instance in HSQC 2D NMR for polymer **9** both trz proton peaks correspond to the single –*C*H carbon peak of trz at 119.85 ppm, and in HMBC 2D NMR they both correspond to the –*Cq* of trz at 145.31 ppm. Interestingly, NOESY 2D NMR shows that only one of the two peaks representing the trz proton is correlated to the substituted protons of the BiFc group. The protons of the alkyl chain and the –C*H*$_2$CH of the NBR part indicate that some trz units are spatially close to the polymeric chain, whereas others are not spatially constrained. Last, the phenyl group of the catalyst is located at the end of the polymer chain after polymerization. This phenyl group is found in the area of 7.20-7.40 ppm that is merged with that of the trz proton. However, extracting the assignment of this area

(7.1-7.4 ppm) allows the rough estimation of the number of units of polymers **9** and **10** by end-group analysis that is in accordance with the theoretical values (30 and 60 units respectively) (SI, S22 and S35). The IR spectrum shows the characteristic band of the C=O stretching that is found at 1698 cm^{-1}. Additionally, a strong absorption band is found at 816 cm^{-1} that is a characteristic frequency of the C-H out-of-plane bending vibration of ferrocene. Finally, the absorption due to the =C-H stretching of the trz and the Cp groups of the trzBiFc units is found at around 3090 cm^{-1}.

*Synthesis of the trzBiFc polystyrene **14***

Poly(biferrocenylmethylstyrene) **14** is synthesized in an easy three-step reaction (Scheme 4). First, poly(chloromethylstyrene) polymer **11** is prepared by free-radical polymerization of commercial chloromethylstyrene using 0.5% of AIBN as the initiator (Scheme 4), a reaction that takes place in toluene at 80°C. Nucleophilic substitution of the chloro groups using sodium azide yields 85 % of the azido-polymer **12**.[27]

Scheme 4: Synthesis of the poly(biferrocenylmethylstyrene) **14**

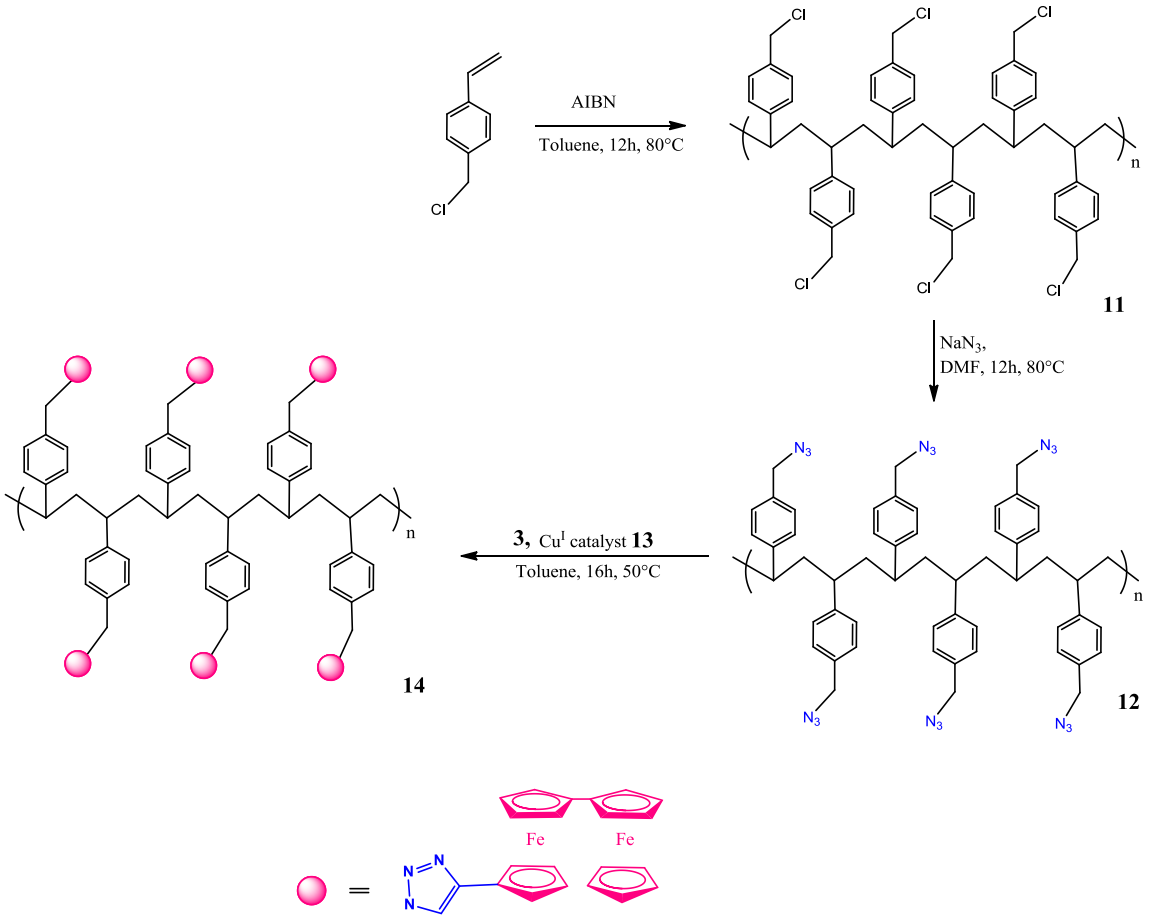

The two polymer precursors **11** and **12** are analyzed by SEC that shows the molecular weight distribution curve of **11** with a polydispersity index PDI = 1.40 and **12** with PDI = 1.25. The polydispersity is easily improved from **11** to **12** after the azidation reaction by precipitation of **12** in MeOH twice. Molecular weight data using polystyrene as the standard reference show

that polymer **12** consists of 31 units. The IR spectrum (KBr) shows a strong band at 2097 cm^{-1} attributed to the $-N_3$ absorption of **12**.

The third step of the synthesis of polymer **14** is the CuAAC functionalization of the poly(azidomethylstyrene) polymer with multiple trzBiFc units. The most common Cu^{I} catalyst used for this reaction is copper sulfate that is reduced *in situ* by sodium ascorbate from Cu^{II} to Cu^{I}.[28] However, its use for macromolecules with multiple azide groups such as dendrimers, polymers or nanoparticles is not adequate, leading to lower reaction rates and low yields, and other catalysts are envisaged.[29] Additionally stoichiometric amounts of the "catalyst" $CuSO_4.5H_2O$ are required, with difficulties for the separation of the remaining catalyst that remains trapped inside the macromolecule at the multiple trz units.[30] Recently the CuAAC catalyst [Cu(I)(hexabenzyl)tren]Br **13** (Figure 1b) was reported with excellent efficiency, including for synthesis of dendrimers[31] and gold nanoparticles.[32]

Consequently, polymer **14** is successfully synthesized by CuAAC reaction between ethynylbiferrocene **3** and the azido polymer **12** using 15% of catalyst **13**. The reaction occurs at 60°C under nitrogen in toluene in which the precursors **3** and **12** as well as the catalyst **13** are very soluble. After 16h, the polymer **14** is formed in 97% yield as an orange precipitate allowing its easy separation from the catalyst **13** that remains in toluene solution. The IR characteristic absorption of the azido groups in the region of 2094 cm^{-1} of poly-azido precursor **12** disappears completely at the end of the reaction, confirming that all the azido groups are replaced by trz groups. NMR spectroscopy confirms the structure of the poly-trzBiFc polymer **14**. Specifically, the formation of the trz unit is shown in the ^{1}H NMR spectrum by the appearance of the proton peaks at 7.68 ppm corresponding to the proton of the trz unit. The CH_2-N_3 protons for precursor **12** at 4.25 ppm are replaced by the CH_2-trz at 5.41 ppm. The other characteristic peaks of the polymer **14** are also observed, and the correct ratio between polymer/BiFc protons finally confirms the structure of compound **14**. Last, ^{13}C NMR shows the characteristic peaks of *Cq*, *C*H of trz and *C*H_2-trz of the polymer **14**.

*Synthesis of triazolyl-biferrocenyl-PEG copolymers **18** and **19***[17c]

The copolymers containing both biferrocene and PEG units are synthesized by "click" CuAAC polycondensation reactions (Scheme 5).

Scheme 5: Synthesis of the poly-trzBiFc-PEG polymers **18** and **19**

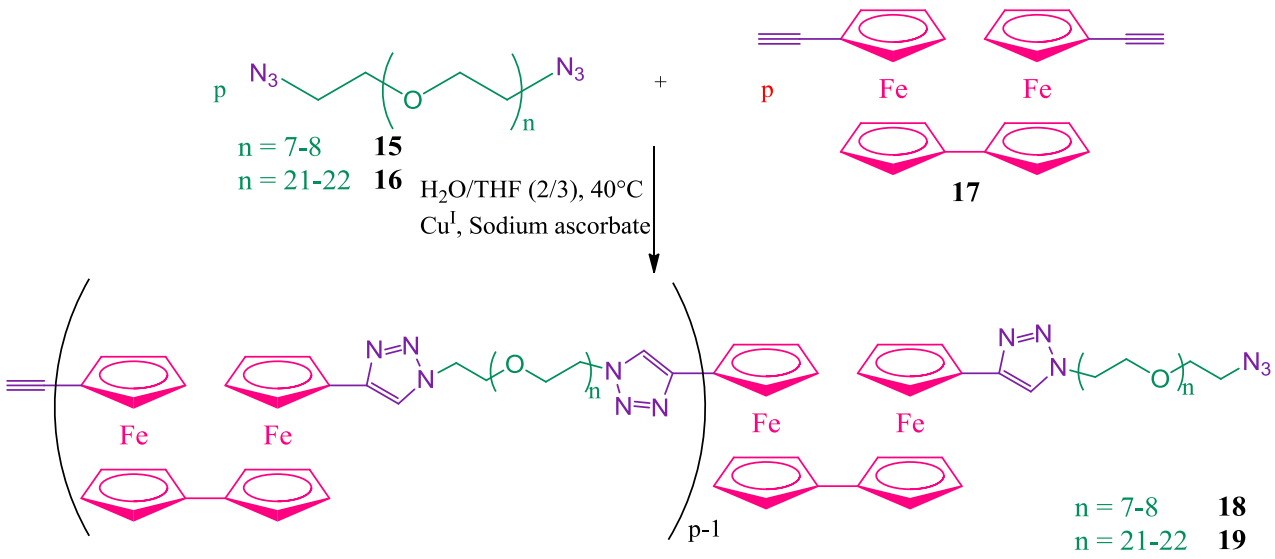

The CuAAC reactions take place between the bis-azido-PEG derivatives **15** and **16** that contain 7-8 and 21-22 ethyleneglycol units respectively and bis-ethynyl-BiFc[33] in a mixture of THF/H_2O, at 40°C for 2 days. The use of the Sharpless-Fokin catalyst $CuSO_4.5H_2O$ + Na ascorbate leads to the polymers **18** and **19** in 78% and 58% yield, respectively. Both polymers were purified by precipitation in diethyl ether twice. The introduction of several PEG units in polymeric materials is of interest for biocompatibility, water-solubility and enhanced permeation and retention (EPR).[34] Polymer **18** containing PEG units of molecular weight 400 Da presents solubility properties that are similar to those of the homo-polymers **9**, **10** and **14**, whereas polymer **19** containing PEG units of molecular weight 1000 is also soluble in very polar solvents including water. The ^{1}H NMR and ^{13}C NMR spectra confirm the structures of the co-polymers **18** and **19**, whereas IR spectroscopy indicates the absence of trace of azide or alkyne groups, suggesting that these polymers consist in several units without possibility to observe the end groups.

The HSQC, HMBC and COSY NMR spectra helped to make the correct assignments of proton and carbon signals for all the series of trzBiFc polymers **9**, **10**, **14**, **18** and **19**. The objective of DOSY NMR is double: measure the hydrodynamic diameter of the polymers in solution and obtain a DOSY spectrum that reflects the purity of the polymers. The DOSY NMR spectra of the polymers **9**, **10**, **14**, **18** and **19** are obtained as well as their diffusion coefficient (SI). The higher the molecular weight of the polymer, the smaller the diffusion coefficient and the larger the hydrodynamic diameter; the latter is calculated using the Stokes-Einstein equation $D = K_BT/6\pi\eta r_H$. The largest r_H value, 13.1 ±1.0 nm, is calculated for the co-polymer **19**, whereas the smallest r_H value, 1.5 ± 0.5 nm, is calculated for the polymer **9**.

Finally, DLS also gives access to the hydrodynamic diameter of the polymers **9**, **10** and **14** that are $d_1 = 14.3 \pm 3$ nm, $d_2 = 36.9 \pm 7$ nm and $d_3 = 11.9 \pm 2$ nm respectively.

The MALDI-TOF mass spectra of the polymers **9** and **14** show well-defined individual peaks for polymers fragments that are separated by 654 ± 1 Da (polymer **9**) and 553 ± 2 Da (polymer **14**) corresponding to the mass of a single unit of the corresponding polymers. The highest molecular peak, 13990.1 Da, obtained for polymer **14**, corresponds to a polymer fraction of 25 trzBiFc units. The intensities of the peaks, separated by 654 ± 1 Da (polymer **9**) or 553 ± 2 DA (polymer **14**), progressively decrease and vanish towards higher molecular masses. The same phenomenon is observed for the co-polymer **18**, where the repetition of peaks for polymer fragments are separated by approximately 800 ± 50 Da, as it is known that PEG400 (part of precursor **15**) is an average number of several lengths of PEG fragments. These MALDI TOF mass spectra clearly show the structure and motifs of polymers **9**, **14** and **18**.

All the polymers were also characterized by UV-vis. spectra in which a strong absorption band is observed in the visible region peaking at 450-451 nm due to the d-d* transitions of BiFc and is typical of BiFc compounds.[35] The molar extinction coefficients ε of all polymers are calculated from Lambert's-Beer law $A = \varepsilon bc$ (Table 2).

SEC of the trzBiFc polymers **9**, **10**, **14**, **18** and **19** provides PDI = 1.21-1.27, the smallest PDI value being observed for the ROMP polymers **9** and **10** as expected. The Mw values that are obtained from SEC in all cases indicate polymers that are not in accord with the expected molecular weights, having less trzBiFc units. It is possible that these polymers interact with the column phase inducing a longer retention time and a smaller molecular weight. The calculated molecular weights are discussed below and gathered in Table 2.

CV usually provides information on the ligand electronic effect;[36] here it is used for polymers **9**, **10**, **14**, **18** and **19** with decamethylferrocene, $FeCp^*_2$ ($Cp^* = \eta^5$-C_5Me_5), as the internal reference[37] in order to examine the thermodynamics and kinetics of the heterogeneous electron-transfer processes, the stability of the oxidized states and finally estimate the number of monomer units in the polymers. The CVs are recorded in CH_2Cl_2 -a good solubility being accessible with this solvent for all polymers-, on a Pt electrode, using 0.1 M [nBu$_4$N][PF_6] as the supporting electrolyte. All polymers show two reversible waves vs. $FeCp^*_2$. The first oxidation wave of polymers **9**, **10**, **14**, **18** and **19** corresponds to the oxidation of the first Fc center to the mixed-valent 35-electron complex $Fe^{II}Fe^{III}$ biferrocenium, and the second wave corresponds to the oxidation of the second Fc center to the 34-electron $Fe^{III}Fe^{III}$ biferricenium species.

The BiFc groups of the trz-BiFc polymers give two single waves, which indicates that these BiFc groups are independent from one another; this is explained by the weakness of the electrostatic factor between the redox sites of the trzBiFc polymers due to the fact that these redox centers being far from one another, being separated by many bonds.[38]

The electrochemical reversibility of the CV waves of all the redox groups signifying fast electron transfer between these redox groups and the electrode is due to very fast access of

these groups to the electrode within the electrochemical time scale, all the redox groups coming in turn close to the electrode,[39] and/or the electron-hopping mechanism.[40]

Table 1. Redox potentials and chemical (i_a/i_c) and electrochemical (Ep_a-Ep_c = ΔE) reversibility data for monomers **3**, **7** and **17** and for polymers **9**, **10**, **14**, **18** and **19** [a].

Compound	$E_{1/2}$ (V)[b]	ΔE (mV)[b]	i_c/i_a[b]	$E_{1/2}$ (V)[c]	ΔE (mV)[c]	i_c/i_a[c]
3	0.48	59	1.0	0.93	56	1
7	0.43	50	1.1	0.79	40	0.8
9	0.42	15	1.1	0.76	20	1.4
10	0.42	30	1.8	0.74	20	1.3
14	0.41	10	1.7	0.72	15	1.5
17	0.58	60	1.1	0.93	55	1.0
18	0.44	55	1.4	0.79	40	1.5
19	0.42	35	1.3	0.80	45	1.0

[a]Supporting electrolyte: [*n*-Bu_4N][PF_6] 0.1M; solvent: dry CH_2Cl_2; working and counter electrodes: Pt; reference electrode: Ag; internal reference: $FeCp^*_2$; scan rate: 0.200 $V.s^{-1}$. [b]Data obtained for the first wave ($Fe^{II/III}$). [c]Data obtained for the second wave ($Fe^{II/III}$).

For polymers **9**, **10** and **14** containing side BiFc chains the first oxidation wave is assigned to the outer Fc groups that are easier to oxidize than the inner ones, as they bear only the electron-releasing inner Fc groups, whereas the second oxidation wave is assigned to the inner Fc groups that bear the electron-withdrawing trz substituents (Table 1).

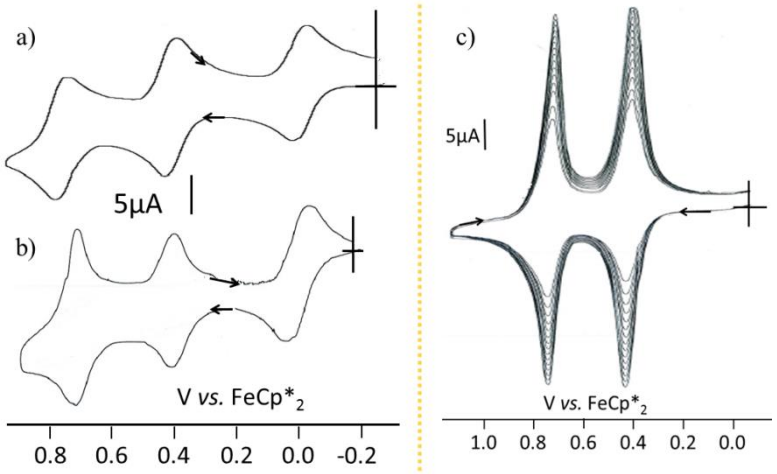

Figure 2. CVs of a) monomer **7**, b) polymer **9** and c) progressive adsorption of polymer **9** onto a Pt electrode upon 20 scans around the BiFc potentials. Solvent: DCM ; reference electrode : Ag ; working and counter electrodes: Pt ; scan rate: 0.2 V/s; supporting electrolyte: 0.1 M [*n*-Bu_4N][PF_6]. The wave at 0.0V belongs to the internal reference $FeCp^*_2$.

Adsorption during CV that is common for redox-active macromolecules[41] is observed for all polymers studied here. The $\Delta(E_{pc}-E_{pa})$ value is < 59 mV, signifying partial adsorption on the electrode surface. In Figure 2a and 2b the CVs of monomer **7** and polymer **9** are shown where the adsorption is clear in polymer **9** even from the first scan, whereas as expected it is not observed for monomer **7**. This facile adsorption favors the easy fabrication of metallopolymer-modified electrodes. In Figure 2c, progressive adsorption on the Pt-electrode of polymer **9** is demonstrated after approx. 20 scans around the potential region of the BiFc CV waves. The same phenomenon is observed for all polymers, except for polymer **19** probably due to the long PEG units that increase the solubility. This adsorption phenomenon for polymers **9**, **10** and **18** progresses until 27 ± 4 scans, then a decay of the CV waves progressively takes place presumably due to a structural rearrangement of the polymers on the electrode surface. Surprisingly this is not the case for polymer **14** where the adsorption phenomenon continues until at least 60 scans without any structural rearrangement on the surface of the electrode, which makes polymer **14** an ideal candidate for the fabrication of modified electrodes.

2. Molecular weights of polymers 9, 10, 14, 18 and 19

Different techniques are used for the calculation of the molecular weights of the trzBiFc polymers. For the polymers **9** and **10** that are synthesized by ROMP the end-group (^{1}H NMR) analysis allows the approximate determination of the number of units in these polymers and consequently their molecular weight (Table 2). For polymer **9** the molecular weight determined by this method is M_n = 22000 g/mol, whereas for the larger polymer **10** the calculated molecular weight is M_n = 36000 g/mol. For both polymers the calculated molecular weights are close to the theoretical ones determined by the monomer/catalyst molar ratio. SEC analysis (*vs*. polystyrene reference) of the precursor polystyrene polymer **12** is a more viable method to determine the total number of units in the case of polymer **14**, giving a molecular weight of 4938 g/mol corresponding to **31** units. As the CuAAC reaction of precursor **12** with compound **3** is complete (no $-N_3$ absorption in the IR after the reaction) and the PDI of **12** and **14** are the same, the number of trzBiFc units in this case remains the same as the number of azido groups in polymer **12**.

CV also is a valuable tool for the estimation of the number of units in the trzBFc polymers **9**, **10**, **14**, **18** and **19**. The total number of electrons transferred in the oxidation wave for the polymer (n_e) can be estimated from the limiting currents and approximate relative values of the diffusion coefficients of the monomer (D_m) and the polymer (D_p):

$$D_p/D_m = (M_m/M_p)^{0.55} \quad (1)$$

Since the oxidation of each redox moiety is a one-electron reaction ($Fe^{II} \rightarrow Fe^{III}$), the value of n_e can be estimated by employing Bard's equation previously derived for conventional polarography:[41,42]

$$n_e = (i_{dp}/C_p)/(i_{dm}/C_m)\ (M_p/M_m)^{0.275} \quad (2)[42]$$

Consequently comparison with the internal reference $FeCp^*_2$ provides a good estimation of the number of electrons n_p involved in the $Fe^{II/III}$ redox process as a function of the monomer and polymer intensities (i), concentrations (c) and molecular weights (M). Measurement of the respective intensities for the reference $FeCp^*_2$ and the first anodic wave (See SI for the CVs with $FeCp^*_2$ as the reference) led to the data of n_e for the polymers **9**, **10**, **14**, **18** and **19.** The n_e values of polymers **9**, **10**, and **14** are slightly superior to the theoretical number of polymeric units, probably due to their slight adsorption on the Pt electrode starting even from the first scan around the BiFc potentials. For co-polymers **18** and **19** the molecular weight was calculated only by this electrochemical method by both equations 1 and 2 by using the diffusion coefficients of the monometallic reference $FeCp^*_2$ and polymers **18** and **19**.

UV-vis. spectroscopy was used to confirm the number of units in the polymers in all cases. The Lambert-Beer law $A = \varepsilon bc$ was used to determine the actual total number of metallocene (BiFc) groups in polymers **9**, **10**, and **14**. The UV-vis. spectra of the polymers present an absorption band at 450 nm due to the d-d* transitions of BiFc. The number of BiFc termini in each polymer is estimated by comparing the molar extinction coefficient (ε) of the polymers with that of the corresponding monomer (ε_0).[43] The mono-trzBiFc monomer **7** was used for this comparison. The number of metallocenes found in each polymer (**9**, **10**, **14**) confirms the molecular weights calculated with the other methods.

Table 2. Sizes of the polymers **9**, **10**, **14**, **18**, **19** (number of molecular units) obtained from end-group analysis, CV analyses and UV-vs. spectroscopy.

Compound	**Conversion**	$\mathbf{n_t}^{\mathbf{a}}$ / $\mathbf{n_p}^{\mathbf{c}}$	$\mathbf{n_e}^{\mathbf{d}}$	$\mathbf{n_m}^{\mathbf{f}}$
Mono **7**	-	1	-	-
Poly **9**	98%	30/ 33±4	32±3	33±4
Poly **10**	99%	60/ 55±7	66±6	53±7
Poly **14**	97%	31[b]/ -	36±4	29±3
Poly **18**	78%	-	151±23[e]	- [g]
Poly **19**	58%	-	62±12 [e]	- [g]

[a] Theoretical number of branches corresponding to [M]/[C] molar ratio. [b] Obtained from the SEC analysis of the organic precursor **12** (using polystyrene as standard). [c] Values obtained by ^{1}H NMR end-group analysis in CD_2Cl_2, at 25°C. [d] Number of electrons obtained by CV from equation 2. [e] Molecular weight of polymers **18** and **19** were calculated by equation 1 upon using the diffusion coefficients obtained from DOSY NMR analysis. [f] Number of metallocene units obtained by UV-vis. spectroscopy using equation: $n_{m=} \varepsilon/\varepsilon_o$. [g] The equation $n_{m=} \varepsilon/\varepsilon_o$ is not adequate for polymers **18** and **19** because of the existence of the PEG units.

3. Reaction of polymers with Au^{III}: formation of mixed-valent polymers and stabilization of encapsulated gold nanoparticles by snake-shaped nanonetworks

The BiFc polymers are stoichiometrically oxidized by one equiv. of ferricenium tetrafluoroborate *per* BiFc unit to robust cationic mixed-valent biferrocenium[43] polymers **18a** and **19a** that are characterized by UV-vis., FT-IR, near-IR and Mössbauer spectroscopy. The

IR spectra of **18a** and **19a** show both ν_{Fc} and ν_{Fc}^{+} at 818 cm^{-1} and 833 cm^{-1} indicating that the mixed-valent polymers **18a** and **19a** are localized on the time scale of the molecular vibrations. These two mixed-valent polymers present a band in the near-IR region (at λ_{max} = 1954 and λ_{max} = 1921) indicating that they belong to class II of mixed-valent compounds in the Robin-Day classification. Mössbauer spectroscopy finally confirms that these two polyelectrolytes **18a** and **19a** are localized class-II mixed-valent complexes.[17c]

The reducing power of the BiFc polymers and the stability of cationic biferrocenium polymers **9**, **10**, and **14** are attractive in view of Au^{III} reduction to Au^{0} nanoparticles (AuNPs)[45] that are stabilized in the biferrocenium polymer frameworks.[21,44] Consequently, $HAuCl_4$ is chosen as the oxidant of the outer Fc groups of the trz-BiFc polymers, the reaction being described by eq. 3 with the successful stabilization of AuNPs:

$$3Fe^{II}Fe^{II} + H^{+}Au^{III}Cl_4^{-} \rightarrow 3[Fe^{II}Fe^{III}]^{+}Cl^{-}, Au^{0}, H^{+}Cl^{-} \qquad (3)$$

The reactions proceed in a DCM/ methanol medium (Scheme 6). The polymer reductant is added dropwise into the $HAuCl_4$ methanol solution, and the color immediately turns from orange-yellow to green suggesting the formation of the mixed-valent polymers **9a**, **10a**, **14a**. The factors that provide AuNP stabilization are mild ligands (trz) at the AuNP surface, electrostatic (chloride counter-anions and biferrocenium cations), and steric (bulky biferrocenium units and the polymer frameworks). Surprisingly, a one-week incubation time of the AuNPs stabilized by the mixed-valent biferrocenium polymers progressively leads to the formation of polymer nanosnakes that encapsulate AuNPs in **9b**, **10b** and **14b** (Scheme 6).

Scheme 6: Synthesis of gold nanosnakes AuNSs from polymers **9**, **10** and **14**: photograph: isolated nanosnake from the TEM analysis of AuNSs-**14b**.

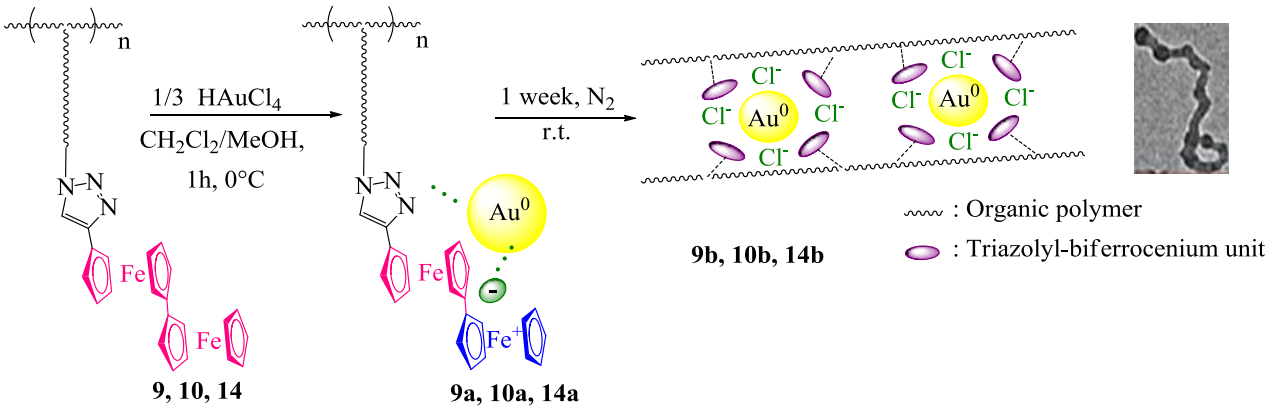

These peculiar AuNP-encapsulating nanosnake networks are clearly seen by TEM analysis (Figure 10, polymer **14**). The average diameter of these AuNSs-**14b** is d = 14.5 ± 1.5 nm and the calculated distribution of the sizes is shown in Figure 10c. The inter-nanoparticle distance stabilized in the several nanosnakes is r = 13.5 ± 1.5 nm (for statistical distribution see SI). In the red caption of Figure 10a (zoom), an isolated nanosnake (AuNS) is shown (length: 269 ±

10 nm; thickness: 8.5 ± 2 nm containing 14 AuNPs). UV-vis. spectroscopy characterizes the AuNPs with the classic plasmon band absorption at 531 nm.

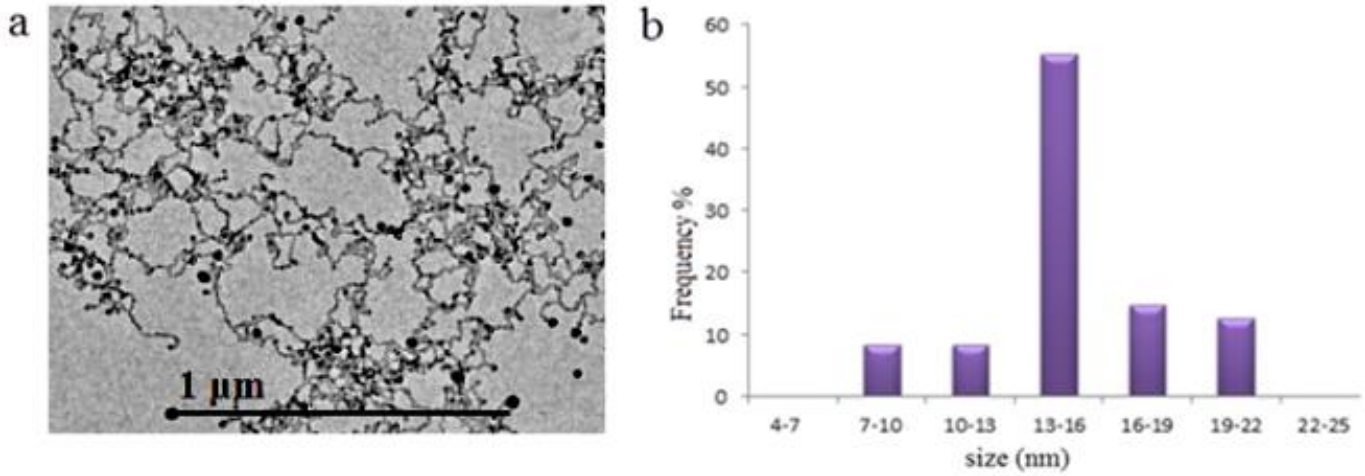

Figure 10: a) TEM analysis of mixed-valent biferrocenium polymer-stabilized AuNSs-**14b** at 0.5 µm; b) size distribution of AuNSs.

Incubation for one week of AuNPs-**9a** and AuNPs-**10a** also leads to AuNSs-**9b** and AuNSs-**10b**. TEM analysis of AuNSs-**9b** shows AuNPs of 10.5 ± 1.5 nm (SI) and TEM analysis of AuNSs-**10b** shows AuNPs of 13.5 ± 1.5 nm (SI). An isolated nanosnake of AuNSs-**10b** presents a thickness of 8.7 ± 1.5 nm, a length of 210 ± 15 nm and encapsulates 11 spherical AuNPs with an inter-nanoparticle distance of 5.2 ± 1.5 nm.

Atomic Force Microscopy (AFM) studies are performed on a graphite surface upon Peak Force Tapping. The topography images of polymer **10** show that polymer **10** has an average height of 7 ± 1.5 nm on the graphite surface (Figure 11a). However, the situation changes in the case of AuNSs-**10b.** Long nanosnakes assemblies are observed of the order of 200-300 nm, with a height between 18 nm and 35 nm (Figure 11b). Peak Force Tapping mode also permits to extract qualitative nanomechanical properties. Adhesion of **10b** is mapped and the force curves are recorded. Adhesion images recorded at 2µm and a zoom at one of the nanosnakes at 270 nm respectively, provide information on the nature of the nanomaterials. Under the same experimental conditions, in all cases three different force curves are observed corresponding to three different regions. For instance, regions A, B and C (SI) are giving different force curves. Larger adhesion forces are observed in region C (white color) corresponding to an elastic and flexible material that is the organic polymer part. Then, zone A, with the smaller adhesion forces (black color), belongs to a stiffer part of the nanomaterial that corresponds to the AuNPs and last zone B (brown color) surrounding regions A presents intermediate force curves due to the electrostatic forces of the trz-BiFc^{+}Cl^{-} units surrounding the AuNPs.

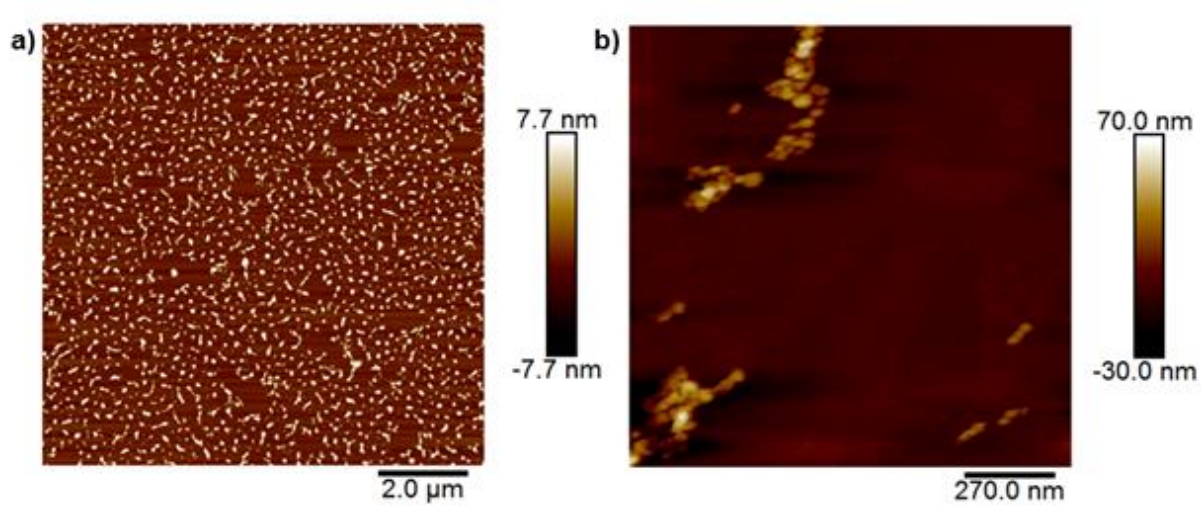

Figure 11. a) AFM topography image (2 µm scale) of **10**, b) AFM topography image (270 nm scale) of AuNSs-**10b**.

Even if the polymer structure and length differ, the type of AuNSs is similar in all cases where the trzBiFc units are in the side polymer chain. The role of the incubation time is then examined. TEM analyses of AuNSs-**10b** after 1 and 3 days confirm the need of one week-incubation time for the completed formation of these nanostructures. After 1 day round AuNPs of the same size (13.5 ± 1.5 nm) are formed, whereas after 3 days the rapprochement of these nanoparticles is observed even though the nanosnake structure is not yet formed. However, after one week incubation time, the rapprochement of the polymer-stabilized AuNPs is completed, forming nanosnakes as observed by TEM and AFM microscopies.

Additionally, as expected the role of the polymer/$HAuCl_4$ stoichiometry is crucial. Indeed, for instance upon adding one more equivalent of polymer **10** to $HAuCl_4$ under the same conditions, stable AuNPs of the same size are observed, but after one week the formation of nanosnakes does not occur.

In an effort to further confirm the crucial role of the electrostatic interactions of the $BiFc^+$ cations in the formation of the snake-shaped networks and stabilization of AuNPs **AuNS's-14b** was reduced by $NaBH_4$ in DCM/methanol solution. The result is that neutral trzBiFc-stabilized **AuNPs-14c** presents a flocculation phenomenon after 10 min. that is taken into account by the absence of electrostatic stabilization. Shaking of the solution re-dissolves the **AuNPs-14c**, however, and the flocculation phenomenon is fully reversible. The UV-vis. spectrum shows the presence of a small shoulder at 450 nm belonging to the trzBiFc and the plasmon band at 539 nm. TEM clearly shows the destruction of the snake-shape network, whereas the AuNPs remain of the same size (d = 13.5 ± 1.5 nm) (Figure 12).

Besides TEM and UV-vis. analysis the AuNSs-**9b,** AuNSs-**10b** and AuNSs-**14b** are also characterized by IR, near-IR and CV. IR spectroscopy is an excellent tool to determine whether a mixed-valent complex is electron delocalized or not in the time scale of molecular vibrations. More particularly, the difference of the perpendicular C-H bending vibration is around 815 cm^{-1} for ferrocene, whereas for ferricenium salts it is found around 852 cm^{-1}. For

all the AuNSs the IR analysis gives two distinct bands corresponding to the existence of Fe^{II}/Fe^{III}. For example in the case of polymer **14b**, two distinct bands are observed: one at 844 cm^{-1} (corresponding to Fe^{III}) and one at 824 cm^{-1} (corresponding to Fe^{II}) showing localized Fe^{II} and Fe^{III} moieties on the IR time scale. The presence of the Fc^{+} center close to the Fc group increases the frequency of the Fc side by 9 cm^{-1}, compared to the neutral analogue, polymer **14**. This shift results from the presence of the electron-withdrawing Fc^{+} substituent (Figure 13).

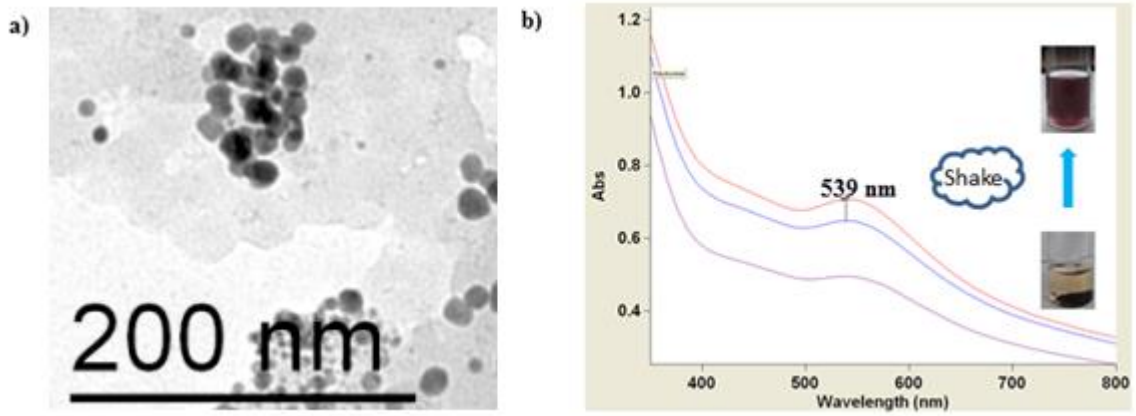

Figure 12. a) TEM **ofAuNPs-14c** and b) UV-vis. spectrum of **14c** (blue line). The violet line corresponds to the UV-vis. spectrum after 5 min and the red line is recorded after shaking of the sample. The photograph shows the flocculated AuNPs and their redissolution by shaking.

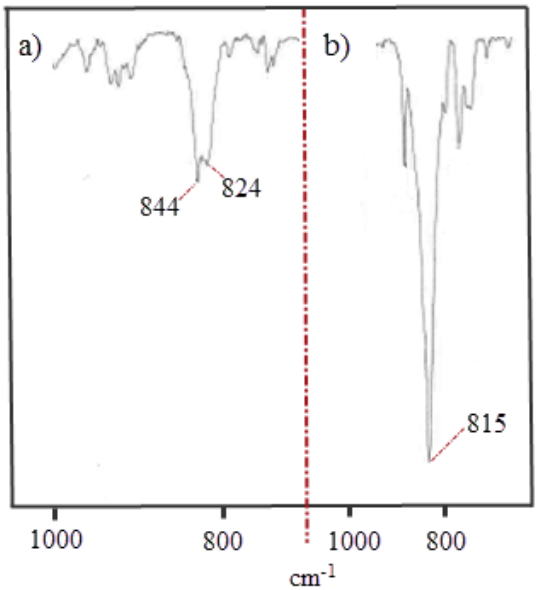

Figure 13. FT-IR (KBr) of a) mixed-valent biferrocenium-stabilized AuNSs **14b**, 844 cm^{-1} (ν_{Fc}+) and 824 cm^{-1} (ν_{Fc}), b) polymer **14**, 815 cm^{-1} (ν_{Fc}).

In order to distinguish between class-I and class-II electron localized mixed valency, the use of near-IR spectroscopy is necessary in order to search the intervalent charge-transfer band that characterizes the optical transition from the ground state to the intervalence charge-transfer state of the class-II mixed-valent compounds. Indeed, the near-IR spectra of all the AuNSs provide the intervalence band (SI) indicating that the mixed-valent polymers stabilizing the AuNPs belong to class II of mixed-valent compounds.

CV of these AuNSs show both reversible redox waves of the BiFc units, confirming the stability of these nanostructures that also present a strong adsorption phenomenon onto the electrode surface (SI). However, when the same reaction is conducted with polymer **18** in which the trzBiFc^{+}Cl^{-} units are in main polymer chain, the situation is different (Scheme 7). AuNPs are formed with 12 ± 1 nm size for which surprisingly incubation leads to a well-organized non-nanosnake network (AuNN, Figure 14). This is taken into account by the fact that the larger distance between trz-BiFc^{+} units induces much reduced electrostatic repulsion among the cationic centers that are a key parameter for the nanosnake formation.

Scheme 7: Synthesis of gold nano-networks AuNNs-**18b**.

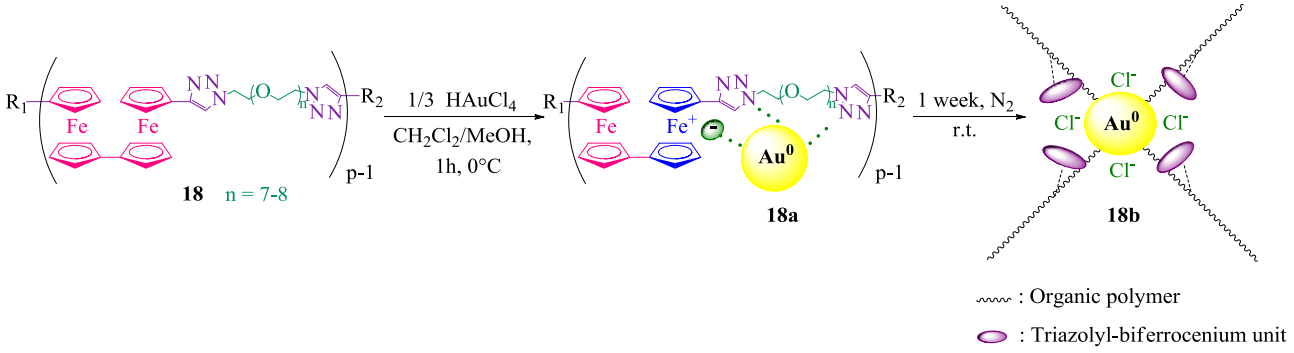

A key comparison concerns the possibility of AuNP network formation in the trz-Fc polymers and the non-trz Fc polymers. The reaction of a trz-Fc-containing poly(norbornene) polymer synthesized by ROMP with $HAuCl_4$ leads to a trz-Fc^{+} polymer-AuNP species that immediately decomposes owing to the instability of the trz-Fc^{+} moiety. However, when an amido-Fc ROMP polymer **20**[45] reacts with $HAuCl_4$, small AuNPs-**20a** of 6 ± 1 nm size form, but after one week incubation time the remained the TEM picture does not show the formation of a network (Figure 15).

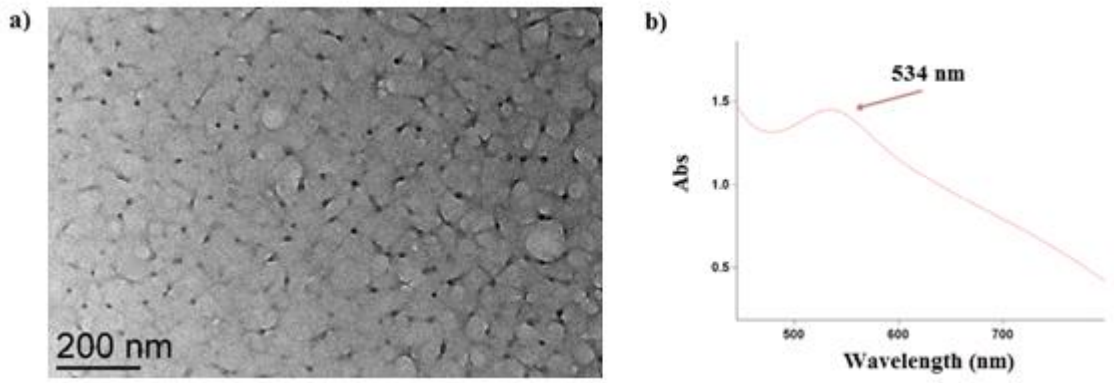

Figure 14. a) TEM analysis of AuNNs-**18b** at 200 nm, b) UV-vis. spectrum of AuNNs-**18b** peaking at 534 nm (plasmon band).

The trz together with biferrocenium cations are co-responsible for the organization of the nanomaterials in nanosnakes (when trzBiFc$^+$ are in the side chain) or nanonetworks (when trzBiFc$^+$ are in the main chain).

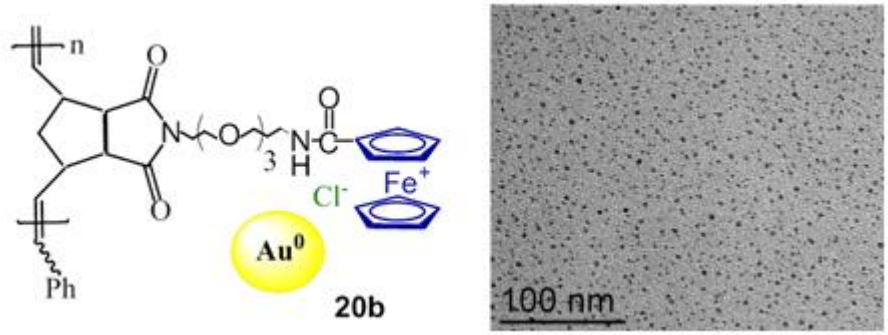

Figure 15: TEM analysis of **20b** at 100 nm.

The method was extended in order to obtain structured silver nanoparticles (AgNPs). Manners et al have shown the reduction of Ag^I to AgNPs by macromolecules resulting from ferrocenophane ring-opening polymerization.[46] Therefore we tested the formation of AgNP networks using trzBiFc polymers as reductant under the same conditions as **AuNSs-14b**. Polymer **14** was used to reduce Ag^I stoichiometrically (1:1, trz-BiFc/$AgBF_4$) yielding **AgNPs-21b** in a one-pot reaction. The reduction was immediate as witnessed by the color change from colorless to grey-purple. **AgNPs-21b** are very stable, and after a 4-day incubation time TEM analysis revealed the polymeric nanosnake-network formation with a thickness of 36 ± 4 nm in which AgNPs of size d = 4 ± 1 nm are encapsulated (Figure 16). The plasmon band of **AgNSs-21b** was found at λ = 450 nm indicating the formation of the AgNPs, and the ferricenium band was recorded at λ = 600 nm.

The smaller size of the AgNPs found into the polymeric snake-shaped network is possibly due to the faster one-electron reduction of Ag^I compared to the three-electron reduction of Au^{III} under the same conditions. The snake-shaped network is formed in both cases **AuNSs-14b** and **AgNSs-21b** confirming that the synergy between the biferrocenium cation, trz ligand coordination, the inter BiFc distance and the polymer bulk is responsible for this snake-shaped network that encapsulates NPs of metals such as gold and silver.

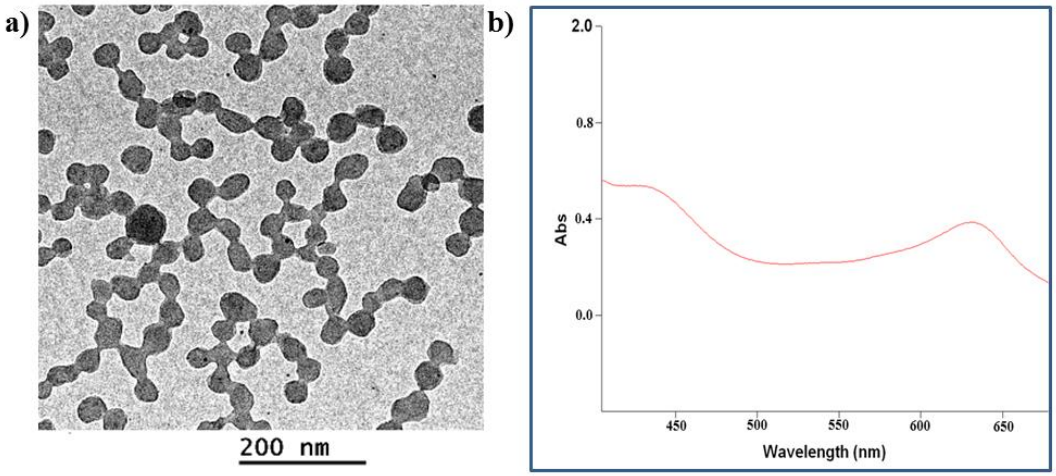

Figure 16. a) TEM analysis of **AgNSs-21b**, b) UV-vis. spectrum of **AgNSs-21b** showing the plasmon band of AgNPs at λ= 434 nm and the biferrocenium band at λ = 630 nm.

4. Modified electrodes and redox recognition

Modification of electrodes with polymer films containing reversible redox systems has been successful resulting in detectable electroactive materials.[47] Modified electrodes of polymers **9**, **10**, **14** and **18** are prepared via absorption by scanning around the BiFc potentials. The electrochemical behavior of these Pt-modified electrodes is first studied in DCM containing only the supporting electrolyte. Two well-defined, symmetrical redox waves are observed in all cases, which is characteristic of surface-confined redox couples, with the expected linear relationship of peak current with potential sweep rate υ (Figure 17b). Repeated scanning does not change the CVs demonstrating that the modified electrodes are stable to electrochemical cycling. However the stability differs depending on the polymer. The value of the full width at half-maximum (fwhm) for polymers **9**, **10**, **14** and **18** is measured at a scan rate of 100 mV/s (Table 3). For polymers **9**, **10** and **14** the ΔE_{fwhm} are $< 99/n$ mV, suggesting the existence of attractive interactions between the BiFc sites attached onto the electrode surface.[48] On the other hand for polymer **18** the ΔE_{fwhm} is 115 mV showing that the biferrocenyl sites have repulsive interactions on the electrode surface (Table 3).

Table 3: Compared modified electrodes with polymers **9**, **10**, **14** and **18** after 20 ± 5 scans.

Compound	ΔE_{fwhm} [a]	Γ (mol cm^{-2}) [b]	n_d [c]
Poly **9**	75 mV	2.1 x 10^{-10}	3
Poly **10**	72 mV	2.9 x 10^{-10}	4
Poly **14**	80 mV	3.1 x 10^{-10}	14
Poly **18**	115 mV	10.4 x 10^{-10}	1

[a]Values of the full width at half-maximum. [b]Surface coverage of the electroactive BiFc sites of the polymers. [c]Number of days for which the modified electrodes show no loss of electroactivity.

The Pt electrodes that are modified with polymer **14** are the most durable and reproducible ones, as no loss of electroactivity is observed after scanning several times or after standing in air for several days. In Figure 17a the modified electrode is shown with polymer **14** (prepared upon adsorption after 35 cycles around the BiFc potentials) at various scan rates. The intensity as a function of scan rate in Figure 17b shows the expected behavior of an absorbed polymer. The surface coverage of the electroactive biferrocenyl sites of the modified electrode is $\Gamma = 5.3 \times 10^{-10}$ mol cm^{-2}. Consequently, polymer **14** shows the best stability and electroactivity for fabrication of Pt-modified electrodes, and it is further used for redox-recognition studies.

The fabrication of stable modified electrodes in purely aqueous solutions is a step towards redox recognition in water of substrates of biological importance or of water pollutants. Due to its strong polarity, however, water is responsible for the decrease of electrostatic interactions and the unfavorable hydrogen bonding between host and guest molecules. This makes recognition in water much more difficult than in organic solvent. The Pt-modified electrodes that are modified with polymer **14** successfully provide both redox waves of the BiFc units in water. The electrode is first checked in water containing KNO_3 as supporting electrolyte, and both redox waves are observed herewith. The electrochemical reactions of the adjacent BiFc moieties give rise to broad oxidation and reduction CV waves giving a ΔE value for the first wave of 200 mV and the second one of 260 mV, suggesting a very slow heterogeneous electron-transfer process with the electrode surface. However, when NaCl is used as a supporting electrolyte the situation changes. Both waves appear as well defined, well separated and chemically and electrochemically reversible under these conditions. The difference between anodic and cathodic peak potentials is superior to 0.0 V, as in such polar media as water the electron transfer becomes slower. Last, the electrode does not lose its electroactivity until at least six successive scans (Figure 18).

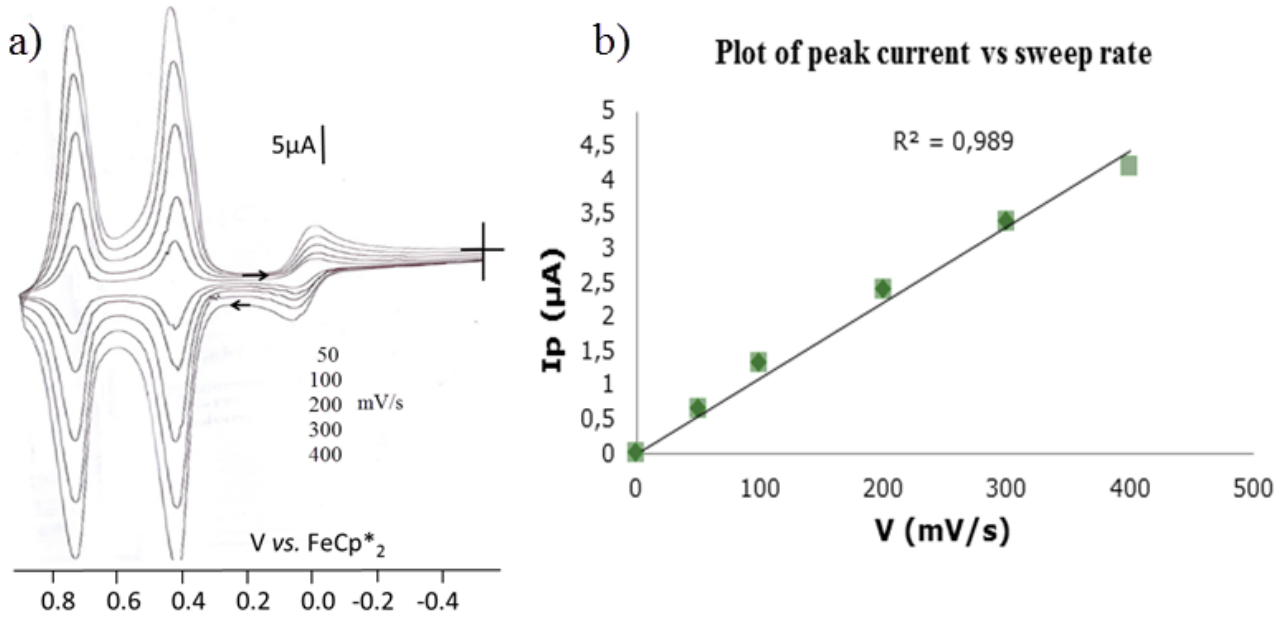

Figure 17: a) Modified Pt electrode of polymer **14** at various scan rates in a DCM solution containing only 0.1 M [*n*-Bu_4N][PF_6] as the supporting electrolyte; b) intensity as a function of scan rate; linearity shows the expected behavior of an adsorbed polymer.

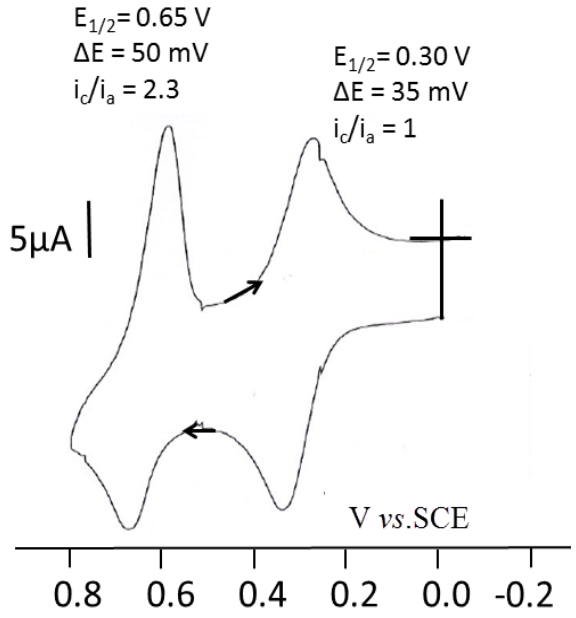

Figure 18. Voltammetric response of a platinum electrode modified with polymer **14**, measured in H_2O/ 0.1 M NaCl; scan rate: 50 mV s^{-1}.

*Redox sensing using Pt electrodes modified with polymer **14** in organic media.* Adenosine triphosphate (ATP) is an essential coenzyme that transports chemical energy within cells for the metabolism. A Pt electrode modified with polymer **14** was used for the recognition of ATP in DCM solution containing only [*n*-Bu_4N][PF_6] as the supporting electrolyte. Indeed, addition of the adenosyl triphosphate salt [*n*-Bu_4N]$_2$[ATP] provokes a splitting of the outer Fc CV wave at 0.41 V. During titration the new wave is shifted at 120 mV less positive potentials, signifying a rather strong interaction of the outer Fc^+ group with the ATP^{2-} anion, which now makes the oxidation of this Fc group easier than in the absence of ATP. When excess of [*n*-Bu_4N]$_2$[ATP] is added the initial cathodic wave disapears and is replaced by the new wave (Figure 19). However, electrochemical irreversibility is observed, which is the sign of a strong structural rearrangement involving supramolecular interactions (hydrogen bonding and electrostatic interactions) in the course of the heterogeneous electron transfer.

The most remarkable feature found with trzBiFc-terminated dendrimers[18b] synthesized by CuAAC reaction is the selective recognition in solution of anions by the outer Fc/Fc^+ groups and the recognition of transition-metal cations by the inner Fc/Fc^+ groups. Indeed, in this case, using the Pt electrode modified with polymer **14**, addition of the salt $Pd(OAc)_2$ also provokes the splitting of the wave of the inner Fc group, the new wave appearing at 70 mV more positive potentials. This is due to the coordination of the Pd^{2+} cation to the trz group attached to the inner Fc group and the larger perturbation of this dicationic BiFc- group in the presence of another cation such as Pd^{2+} in the electrochemical cell (see SI, S79).

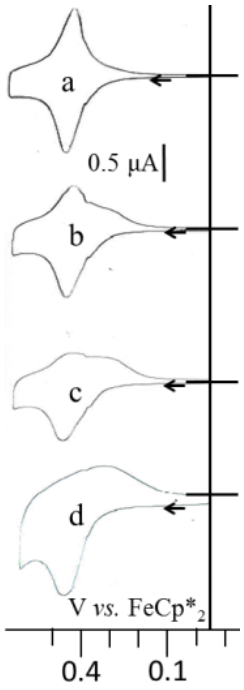

Figure 19. Recognition of ATP^{2-} with a Pt modified electrode with polymer **14**. a) Modified electrode alone; b) and c) in the course of titration (the second wave is not represented as scanning until more positive potentials upon addition of ATP anions provokes instability of the electrode); d) with an excess of [*n*-Bu_4N]$_2$[ATP]. Solvent: DCM; reference electrode: Ag; working and counter electrodes: Pt ; scan rate: 0.3 V/s ; supporting electrolyte: 0.1 M [*n*Bu_4N][PF_6].

Remarkably, modified Pt electrodes made with polymer **14** recognize both cations and anions in a selective way. The outer Fc center recognizes the ATP anion in both DCM and water solutions, and the inner Fc center recognizes the Pd cation.

Redox sensing using Pt electrodes modified with polymer **14** *in aqueous media:* Recognition of the ATP anion using a Pt-modified electrode with polymer **14** was also attempted in an aqueous medium containing only NaCl as the supporting electrolyte. Upon addition of $[Na]_2[ATP]$ the $E_{1/2}$ of the outer Fc/Fc^+ wave shifts to 30 mV less positive potentials (SI), a change that is less significant than in organic media, as expected. The ΔE value between the anodic and cathodic potentials for both waves (inner and outer Fc/Fc^+ groups) now becomes much larger (250 mV and 280 mV respectively). This is due to the binding of the ATP anions to the polymer film provoking a strong structural reorganization of the polymer that is attached to the electrode surface and slows down the heterogeneous electron transfer. Last, the intensity of the anodic peak of the second (inner Fc/Fc^+ group) wave decreases in the presence of the ATP anions, indicating strong electrostatic interactions between the cationic biferrocenium groups and the trapped anions. The high electron density around the ferrocenium centers caused by immobilized inserted ATP anions may inhibit the reversible electrochemical response of a fraction of the redox-active groups.

CONCLUDING REMARKS

The various syntheses of BiFc-containing polymers (ROMP, radical type, polycondensation), their rich redox activity and the robustness of the cationic triazolybiferrocenium moiety contrasting with the instability of triazolylferricenium opens multiple applications. Au^{III} and Ag^{I} are reduced to Au^0 and Ag^0 respectively by the BiFc units to mixed-valent biferrocenium polymer-stabilized AuNPs resp. AgNPs in which the remarkable network formation and AuNP encapsulation is controlled by the polymer design, in particular by the location in the polymer branches or in the polymer main chain of the BiFc units. For instance, with BiFc groups in the side polymer chains, rare interwining snake-shaped polymer networks encapsulating AuNPs are characterized by TEM and AFM. The roles of the trz ligand, electrostatic interactions and inter-BiFc group distance are crucial in network formation and AuNP and AgNP stabilization. With BiFc groups in the polymer side chains, the outer Fc groups are oxidized at less positive potentials than the inner trzBiFc groups, which allows selective anion (ATP^{2-}) and cation (Pd^{II}) redox recognition in organic solvents using Pt electrodes modified with the polymers, and even to a lesser extent in water in spite of the strong competition with the supramolecular interactions involving this strongly polar solvent.

EXERIMENTAL SECTION

Genearl Data. See SI.

Compound 5. *N*-[4-hydroxybutyl]-cis-5-norbornene-exo-2,3-dicarboximide (425 mg, 1.8 mmol) and TsCl (343.6 mg, 1.8 mmol) were dissolved in 30 mL of DCM. Then at 0°C KOH (403.9 mg, 7.2 mmol) was added in small portions. The mixture was left stirring for 1h at 0°C and 10h at r.t. Then 30 mL of distilled water was added, and the organic phase was separated. The water phase was washed three times with 15 mL of DCM, and the combined organic phases were washed 3 times with 15 mL of water. The organic phase was dried with Na_2SO_4 and filtered. The solvent was evaporated giving product **5** in 90% yield (668 mg). ^{1}H NMR ($CDCl_3$, 300 MHz), δ_{ppm}: 7.74 and 7.31 (C*H*, 4H of Tos. group), 6.23 (C*H*=C*H*, 2H), 3.97 (CH_2-Tos, 2H), 3.37 (CONCH_2, 2H), 3.20 (C*H*CON, 2H), 2.61 (CH_2C*H*, 2H), 2.37 (CH_3 of Tos group, 3H), 1.55 ($CH_2CH_2CH_2CH_2$-Tos, 4H), 1.42 and 1.14 (CH_2CH, 2H). ^{13}C NMR ($CDCl_3$, 75 MHz), δ_{ppm}: 177.98 (*C*=O), 144.80 (O*Cq* of Tos. group), 137.87 (*C*H=*C*H), 132.99 (CH_3*Cq* of Tos. group), 129.91 and 127.96 (*C*H of Tos. group), 69.70 (*C*H_2-Tos), 47.86 (*C*H_2CH), 45.25 (CON*C*H_2), 42.74 (CH_2*C*H), 37.81 (*C*HCON), 26.38 (CH_2CH_2*C*H_2CH_2-Tos), 23.96 (CH_2*C*$H_2CH_2CH_2$-Tos), 21.55 (*C*H_3 of Tos. group). ESI MS: Calcd: 412.45, found: 412.12. IR (KBr): 3065 cm^{-1} (=C-H stretching), 1694 cm^{-1} (*C*=O).

Compound 7. *N*-[4-tosylatebutyl]-*cis*-5-norbornene-*exo*-2,3-dicarboximide **5** (650 mg, 1.6 mmol) was dissolved in 5 mL of DMSO in which NaN_3 (312 mg, 4.8 mmol) was added in small portions. The mixture was left under vigorous stirring at r.t. for 2d. Then 10 mL of water and 5 mL of DCM were added in the solution. The organic phase was separated, and the water phase was washed 3 times with DCM. The combined organic phase was washed 10 times with 5 mL of water in order to remove all the traces of DMSO. ^{1}H NMR of *N*-[4-azidobutyl]-*cis*-5-norbornene-*exo*-2,3-dicarboximide **6** ($CDCl_3$, 300 MHz), δ_{ppm}: 6.28 (C*H*=C*H*, 2H), 3.47 (CH_2-N_3, 2H), 3.25 (4H, CONCH_2 and C*H*CON), 2.66 (CH_2C*H*, 2H), 1.59 ($CH_2CH_2CH_2CH_2$- N_3, 4H), 1.48 and 1.16 (CH_2CH, 2H). IR of *N*-[4-azidobutyl]-*cis*-5-norbornene-*exo*-2,3-dicarboximide (KBr): 3065 cm^{-1} (=C-H stretching), 2097 cm^{-1} (-N_3), 1698 cm^{-1} (*C*=O). *N*-[4-azidobutyl]-*cis*-5-norbornene-*exo*-2,3-dicarboximide **6** (200 mg, 0.76 mmol) and compound **3**[2] (359.4 mg, 0.91 mmol) were dissolved in 20 mL of distilled THF. Then 3 mL of degassed water was added into the solution, and the reaction mixture was cooled to 0°C. Then, an aqueous solution of $CuSO_4$ 1M (1.1 eq.) was added dropwise, followed by the dropwise addition of a freshly prepared solution of sodium ascorbate (2.2 eq.). The color of the solution changed from orange to dark red upon addition of sodium ascorbate. The reaction mixture was allowed to stir for 16h at r.t. under nitrogen atmosphere. Then, the mixture of solvents was evaporated *in vacuo*, and 100 mL of DCM was added, followed by the addition of an aqueous solution of ammonia. The mixture was allowed to stir for 15 min. in order to remove the copper salt. The organic phase was washed twice with water, dried over sodium sulfate, filtered and the solvent was removed *in vacuo*. Then the product was precipitated twice from a DCM solution in pentane. Product **7** was obtained as an orange crystalline powder. Yield: 97% (488 mg). ^{1}H NMR ($CDCl_3$, 300 MHz), δ_{ppm}: 7.03 (trz, 1H), 6.26 (C*H*=C*H*, 2H), 4.50 (CH_2-trz, 2H), 4.21, 4.14, 4.10, 4.06, (Cp sub., 12H), 3.90 (Cp free, 5H), 3.49 (2H, CONCH_2), 3.25 (2H, C*H*CON), 2.66 (CH_2C*H*, 2H), 1.53

($CH_2CH_2CH_2CH_2$-trz, 4H), 1.47 and 1.18 (CH_2CH, 2H). ^{13}C NMR ($CDCl_3$, 75 MHz), δ_{ppm}: 177.96 (*C*=O), 145.33 (*Cq* of trz), 137.75 (*C*H=*C*H), 119.36 (*C*H of trz), 85.39, 83.46 and 72.92 (*Cq* of BiFc), 69.38, 69.19, 68.94, 67.51, 67.09, 66.10 (*C*H of BiFc) 47.85 (CH_2CH), 45.13 ($CONCH_2$), 42.74 (CH_2CH), 37.61 (*C*HCON), 27.43 ($CH_2CH_2CH_2CH_2$-trz), 24.81 ($CH_2CH_2CH_2CH_2$-trz). IR (KBr): 3090 cm^{-1} (=C-H stretching), 1698 cm^{-1} (*C*=O), 815 cm^{-1} (Fe^{II}). ESI MS: Calcd: 654.35, found: 654.14. UV-Vis: λ_{max} = 450 nm, ε_o = 500.4 L.cm^{-1}mol^{-1}. Anal. Calcd. for $C_{35}H_{34}N_4O_2Fe_2$: C, 64.25; H, 5.24. Found: C, 64.12; H, 4.98.

Polymer 9. Compound **7** (60 mg, 0.09 mmol) was added into a small Schlenk flask that was flushed with nitrogen and dissolved in 0.2 mL of dry DCM. Then, catalyst **8** (2.6 mg, 0.003 mmol) in 0.1 ml of dry DCM was quickly added into the monomer solution under nitrogen atmosphere with vigorous stirring. The reaction mixture was vigorously stirred for 5 h, and then quenched with 0.2 mL ethyl vinyl ether (EVE). The orange solid polymer **9** was purified by precipitation in methanol twice and dried *in vacuo* (57 mg, yield 98%). ^{1}H NMR (CD_2Cl_2, 400 MHz), δ_{ppm}: 7.22 and 7.16 (C*H* of trz), 5.75 and 5.55 (C*H*=C*H*, 2H), 4.60 (CH_2-trz, 2H), 4.30, 4.28, 4.19 (Cp sub. of BiFc), 3.98 (Cp free of BiFc), 3.49 ($CONCH_2$, 2H), 3.04 (C*H*CON, 2H), 2.69 and 2.09 (CH_2CH, 2H), 1.86 and 1.61 ($CH_2CH_2CH_2CH_2$-trz, 4H) and (CH_2CH, 2H). ^{13}C NMR (CD_2Cl_2, 75 MHz), δ_{ppm}: 178.39 (*C*=O), 145.31 (*Cq* of trz), 133.50 and 132.07 (*C*H=*C*H), 119.85 (*C*H of trz), 85.73, 83.02, 77.06, 70.98 (*Cq* of Cp of BiFc), 70.98, 69.57 (*C*H of Cp free of BiFc) 69.35, 67.84, 67.47, 66.53 (*C*H of Cp sub. of BiFc), 49.59 (CH_2CH), 46.39 ($CONCH_2$), 42.97 (CH_2CH), 37.90 (*C*HCON), 26.33 ($CH_2CH_2CH_2CH_2$-trz), 26.29 (CH_2-trz), 25.11 ($CH_2CH_2CH_2CH_2$-trz). IR (KBr): 3090 cm^{-1} (=C-H stretching), 1698 cm^{-1} (*C*=O), 816 cm^{-1} (Fe^{II}). UV-Vis: λ_{max} = 450 nm, ε = 15673,7 L.cm^{-1}mol^{-1}. Maldi-Tof MS for $C_6H_6(C_{37}H_{36}N_4O_2Fe_2)_3C_2H_2Na$: Calcd: 2168.3, Found: 2168.5. SEC: PDI =1.23. Dynamic Light Scattering (DLS): d = 14.3 ± 3 nm.

Polymer 10. Compound **7** (60 mg, 0.09 mmol) was added into a small Schlenk flask that was flushed with nitrogen and dissolved in 0.2 mL of dry DCM. Then, catalyst **8** (1.3 mg, 0.002 mmol) in 0.1 mL of dry DCM was quickly added into the monomer solution under nitrogen atmosphere with vigorous stirring that was continued for 5 h. The catalyst was quenched with 0.2 mL ethyl vinyl ether (EVE), and the orange solid polymer **10** was purified by precipitation in methanol twice and dried *in vacuo* (58 mg, 99% yield). ^{1}H NMR (CD_2Cl_2, 400 MHz), δ_{ppm}: 7.21 and 7.13 (C*H* of trz), 5.72 and 5.53 (C*H*=C*H*, 2H), 4.55 (CH_2-trz, 2H), 4.28, 4.27, 4.16 (Cp sub. of BiFc), 3.94 (Cp free of BiFc), 3.45 ($CONCH_2$, 2H), 3.00 (C*H*CON, 2H), 2.67 and 2.06 (CH_2CH, 2H), 1.82 and 1.56 ($CH_2CH_2CH_2CH_2$-trz, 4H) and (CH_2CH, 2H). ^{13}C NMR (CD_2Cl_2, 75 MHz), δ_{ppm}: 178.22 (*C*=O), 145.14 (*Cq* of trz), 133.38 and 131.94 (*C*H=*C*H), 119.58 (*C*H of trz), 85.08, 82.99, 76.72, 70.00 (*Cq* of Cp of BiFc), 69.39, 69.20 (*C*H of Cp free of BiFc) 68.99, 67.57, 67.34, 66.37 (*C*H of Cp sub. of BiFc), 49.32 (CH_2CH), 46.03 ($CONCH_2$), 45.87 (CH_2CH), 37.59 (*C*HCON), 29.69 ($CH_2CH_2CH_2CH_2$-trz), 27.42 (CH_2-trz), 24.71 ($CH_2CH_2CH_2CH_2$-trz). IR (KBr): 3091 cm^{-1} (=C-H stretching), 1698 cm^{-1} (*C*=O), 816 cm^{-1} (Fe^{II}). . UV-vis: λ_{max} = 450 nm, ε = 26470 L.cm^{-1}mol^{-1}. SEC: PDI = 1.21. DLS: d = 36.9 ± 7 nm;

Polymer 14. Azidomethylpolystyrene (13.4 mg, 0.084 mmol, 1 eq.) and ethynylbiferrocene **3** (36.0 mg, 0.091 mmol, 1.1 eq.) were dissolved in distilled toluene under nitrogen. Then, 15%

of the catalyst **13**, [Cu^{I}tren($CH_2Ph)_6$][Br], (11 mg, 0.013 mmol, 0.15 eq.) was added. The mixture was left for 16h at 50°C. The orange precipitate that was formed was washed twice with hot toluene and solubilized in DCM. Evaporation of the solvent *in vacuo* gave the polytriazolyl(biferrocenyl) methylstyrene **14** as an orange waxy product (45 mg, 97% yield). ^{1}H NMR (THF-d_8, 300 MHz) δ_{ppm}: 6.92 (C*H* of trz), 6.82, 6.32 (4H, C*H* of Ar of styrenyl), 5.41 (2H, CH_2-triazole), 4.71, 4.32, 4.16 (12H of Cp sub. BiFc), 3.92 (5H of Cp BiFc), 1.62, 1.16 (C*H* and CH_2 of polymer chain). ^{13}C NMR (THF-d_8, 75 MHz) $\delta_{ppm:}$ 145.00 (*Cq* of trz), 144.40 (*Cq* of Ar), 133.68 (*Cq*-CH_2 of Ar), 127.82 and 127.39 (*C*H of Ar), 120.76 (*C*H of trz) 85.36, 82.55, 77.57 (*Cq* of Cp sub. of BiFc), 69.77, 69.20, 68.96 and 67.57 (*C*H of BiFc), 52.92 (*C*H_2-trz), 40.21 (*C*H and *C*H_2 of polymeric chain). SEC: PDI = 1.25. DLS: d = 11.9 ± 2 nm. IR (KBr): 3092 cm^{-1} (=C-H vibration of Cp and trz) and 815 cm^{-1} (Fe^{II}). UV-vis: λ_{max} = 455 nm, ε = 14896,6 $L.cm^{-1}mol^{-1}$.

Polymer 18. 1.665 x 10^{-4} mol of **15** (74.9 mg, Mw = 450 $g.mol^{-1}$) and the same molar quantity of **17** (69.9 mg, Mw = 418 $g.mol^{-1}$) were introduced into a Schlenk flask with 2.8 mL of THF under nitrogen. Then 3.33 x10^{-4} mol of $CuSO_4$, $5H_2O$ (53.24 mg) were solubilized in 1.8 mL of water and added in the reaction medium, and 6.66 x10^{-4} mol of NaAsc (131.84 mg) was solubilized in 1 mL of water and added dropwise to the reaction medium. The reaction was stirred at 40°C during 2 days, and an orange precipitate was observed on the wall of the Schlenk flask. Then 1 mL of an ammonia solution (37% mol) was added together with 5 mL of H_2O and 5 mL of DCM. The solution was stirred for 5 min., the organic phase was recovered, and the aqueous phase was washed twice with 5 mL of DCM. The combined organic phase was gathered, washed with H_2O (3 x 5 mL) and dried with Na_2SO_4. After concentration of the organic phase (1 mL), the polymer was precipitated twice in 60 mL of Et_2O. Then 113 mg of **18** were obtained (78% yield) as an orange solid film polymer. ^{1}H NMR ($CDCl_3$, 400 MHz) δ_{ppm}: 7.23 (2H, C*H* of trz), 4.48 (4H, Cp sub.), 4.43 (4H, -CH_2trz), 4.09 (4H, Cp sub.), 4.04 (8H, Cp sub.), 3.83 (4H, -OCH_2CH_2trz), 3.57-3.60 (-OCH_2CH_2O of PEG_{400}). ^{13}C NMR ($CDCl_3$, 100 MHz), δ_{ppm}: 145.2 (*Cq* of trz), 120.6 (*C*H of trz), 83.9 and 77.0 (*Cq* of Cp sub.), 70.7 (-OCH_2CH_2O of PEG_{400}), 69.7 and 69.6 (*C*H of Cp sub.), 68.9 (-OCH_2CH_2trz), 67.7 and 67.4 (*C*H of Cp sub.), 50.2 (-OCH_2CH_2trz). IR (KBr): 3121 cm^{-1} (=C-H vibration of Cp and trz) 1110 (C-O) and 819 cm^{-1} (Fe^{II}).

Polymer 19. 1.196 x10^{-4} mol of **2** (125.8 mg, Mw = 1052 $g.mol^{-1}$) and the same molar quantity of **3** (50 mg, Mw = 418 $g.mol^{-1}$) were introduced under nitrogen into a Schlenk flask together with 3 mL of THF. Then 1.53 x10^{-4} mol of $CuSO_4$, $5H_2O$ (38 mg) were solubilized in 1 mL of water and added in the reaction medium, and 4.75 x10^{-4} mol of NaAsc (94 mg) was solubilized in 1 mL of water and added dropwise to the reaction medium. The reaction was stirred at 40°C during 2 days, and an orange precipitate was observed on the wall of the Schlenk flask. Then 1 mL of an ammonia solution (37% mol) was added together with 5 mL of H_2O and 5 mL of DCM. The solution was stirred during 5 min, then the organic phase was recovered, and the aqueous phase was washed twice with 5 mL of DCM. The organic phases were gathered, washed with H_2O (3 x 5 mL) and dried with Na_2SO_4. After concentration of the organic phase (1 mL), the polymer was precipitated in 60 mL of Et_2O, and 62.5 mg were obtained as an orange-red paste (58% yield). ^{1}H NMR ($CDCl_3$, 200 MHz) δ_{ppm}: 7.25 (2H, C*H*

of trz), 4.54 (4H, Cp sub.), 4.44 (4H, -C*H*$_2$trz), 4.11 (8H, Cp sub.), 4.08 (4H, Cp sub.), 3.84 (4H, OC*H*$_2$CH$_2$trz), 3.61-3.65 (-OC*H*$_2$C*H*$_2$O of PEG$_{400}$). ^{13}C NMR ($CDCl_3$, 100 MHz), δ_{ppm}: 145.1 (*Cq* of trz), 120.5 (*C*H of trz), 83.9 and 76.3 (*Cq* of Cp sub.), 70.5 (-O*C*H$_2$*C*H$_2$O of PEG$_{400}$), 69.4 and 69.3(*C*H of Cp sub.), 68.7 (-O*C*H$_2$CH$_2$trz), 67.4 and 67.2 (*C*H of Cp sub.), 50.2. IR (KBr): 3092 cm^{-1} (=C-H vibration of Cp and trz), 1109 (C-O) and 819 cm^{-1} (Fe^{II}).

AuNSs-9b. Polymer **9** [10 mg, 0.015 mmol (Mw monomer: 654 g.mol^{-1}), 1 equiv.] was dissolved in 1 ml DCM and added dropwise at 0°C into a stirring solution of $HAuCl_4.3H_2O$ (2.0 mg, 0.005 mmol, 1/3 equiv.) in 4 mL of methanol/ DCM 3:1. The color immediately changed from orange to deep green, stirring continued for another 30 min., then the mixture was concentrated *in vacuo* to 3 mL and kept in a closed Schlenk tube for one week (incubation time) giving compound **9b**. IR (KBr): 3098 cm^{-1} (=C-H vibration of Cp and trz), 834 cm^{-1} (Fe^{III}) and 813 cm^{-1} (Fe^{II}). UV-vis.: λ_{max} = 535 nm. TEM: 10.5 ± 1.5 nm.

AuNSs-10b. Polymer **10** [10 mg, 0.015 mmol (MW monomer: 654 g.mol^{-1}), 1 equiv.] was dissolved in 1 mL DCM and was added dropwise at 0°C in a stirring solution of $HAuCl_4$ (2.0 mg, 0.005 mmol, 1/3 equiv.) in 4 mL of methanol/ DCM 3:1. The color instantaneously changed from orange to deep green, and stirring was continued for another 30 min. The mixture was concentrated *in vacuo* to 3 mL and kept in a closed Schlenk tube for one week (incubation time) giving compound **10b**. IR (KBr): 3087 cm^{-1} (=C-H vibration of Cp and trz), 834 cm^{-1} (Fe^{III}) and 815 cm^{-1} (Fe^{II}). UV-vis.: λ_{max} = 537 nm. TEM: 13.5 ± 1.5 nm.

AuNSs-14b. Polymer **14** [10 mg, 0.018 mmol (monomer Mw: 553 g.mol^{-1}), 1 equiv.] was dissolved in 1 mL DCM and was added dropwise, at 0°C in a stirring solution of $HAuCl_4$ (2.4 mg, 0.006 mmol, 1/3 equiv.) in 4 mL of methanol/ DCM 3:1. The color changed instantaneously from orange to deep green, and stirring was continued for another 30 min. The mixture was concentrated *in vacuo* to 3 mL and kept in a closed Schlenk tube for one week (incubation time) giving compound **14b**. IR (KBr): 3093 cm^{-1} (=C-H vibration of Cp and trz), 844 cm^{-1} (Fe^{III}) and 824 cm^{-1} (Fe^{II}). UV-vis.: λ_{max} = 531 nm. TEM: 13.5 ± 1.5 nm.

AuNPs-14c. To the above solution of **14b** was added 3 mL of CH_2Cl_2. Then under N_2 and vigorous stirring a solution of $NaBH_4$ (1 mg, 0.027 mmol) in 2 mL of methanol was added dropwise. The color immediately changed from green to deep red. The solution was stirred for an additional 5 min., then the product was immediately filtered. The compound **14c** precipitated (flocculation) in 10 min., but it is again re-dissolved upon shaking, and this process is reversible. UV-vis.: λ_{max} = 539 nm. TEM: 13.5 ± 1.5 nm.

AuNNs-18b. Polymer **18** [10 mg, 0.012 mmol (monomer Mw: 868 g.mol^{-1}), 1 equiv.] was dissolved in 1 mL DCM and added dropwise at 0°C into a stirring solution of $HAuCl_4$ (1.5 mg, 0.004 mmol, 1/3 equiv.) in 4 mL of methanol/ DCM 3:1. The color instantaneously changed from orange to deep green, and stirring continued for another 30 min. The mixture was concentrated *in vacuo* to 3 mL and kept in a closed Schlenk tube for one week (incubation time) giving compound **18b**. IR (KBr): 3087 cm^{-1} (=C-H vibration of Cp and trz), 834 cm^{-1} (Fe^{III}) and 815 cm^{-1} (Fe^{II}). UV-vis.: λ_{max} = 534 nm. TEM: 12.0 ± 1 nm.

AuNPs-20b. Polymer **20** [10 mg, 0.018 mmol (monomer Mw: 550 $g.mol^{-1}$), 1 equiv.] was dissolved in 1 mL DCM was added dropwise at 0°C into a stirring solution of $HAuCl_4$ (2.4 mg, 0.006 mmol, 1/3 equiv.) in 4 mL of methanol/ DCM 3:1. The color changed silmutaneously from orange to deep green, and stirring continued for another 30 min. The mixture was concentrated by vacuum to 3 mL and kept in a closed Schlenk tube for one week (incubation time) giving compound **20b**. UV-vis.: λ_{max} = 528 nm. TEM: 6 ± 1 nm.

AuNSs-21b. Polymer **14** [10 mg, 0.018 mmol (monomer Mw: 553 $g.mol^{-1}$), 1 equiv.] was dissolved in 1 mL DCM and added dropwise at 0°C in a stirring solution of $AgBF_4$ (3.5 mg, 0.018 mmol, 1 equiv.) in 4 mL of methanol/ DCM 3:1. The color instantaneously changed from orange to grey-purple, and stirring was continued for another 30 min. The mixture was concentrated *in vacuo* to 3 mL and kept in a closed Schlenk tube for one week (incubation time) giving compound **21b**. IR (KBr): 818 cm^{-1} (Fe^{III}) and 808 cm^{-1} (Fe^{II}). UV-vis.: λ_{max} = 434 nm. TEM: 4 ± 1 nm.

CV measurements. All electrochemical measurements were recorded under nitrogen atmosphere. Solvent: dry DCM; temperature: 20ºC; supporting electrolyte: [*n*-Bu_4N][PF_6] 0.1M; working and counter electrodes: Pt; reference electrode: Ag; internal reference: $FeCp^*_2$; scan rate: 0.200 $V.s^{-1}$. The number of electrons involved in the oxidation wave of the BiFc polymers was calculated using Bard's equation: $n_p = (i_{dp}/C_p)/(i_{dm}/C_m)\ (M_p/M_m)^{0.275}$ (see text).[42] The experiments were conducted by adding a known amount of each polymer in 3 mL of dry DCM and a known amount of $FeCp^*_2$ in 2 mL of DCM. After recording the CVs, the intensities of the oxidation waves of the polymers and of the internal reference ($FeCp^*_2$) were measured. The values were introduced in the above equation giving the final number of electrons (n_e). The compared modified electrodes were prepared by approx. 20 adsorption cycles around the BiFc potentials on Pt electrodes. Their electrochemical behavior was checked in 5 mL DCM solution containing only [*n*-Bu_4N][PF_6] 0.1M at various scan rates: 25, 50, 100, 200, 300, 400, 500 and 600 mV/s. The modified electrodes used for redox recognition were prepared using approx. 35 adsorption cycles around the BiFc potentials on Pt electrodes. Their electrochemical behavior was checked in 5 mL DCM solution containing only [*n*-Bu_4N][PF_6] 0.1M at various scan rates: 25, 50, 100, 200, 300, 400, 500 and 600 mV/s and in 5mL H_2O solution containing only [NaCl] 0.1M. Redox recognition was conducted in two different ways: a) the CVs were recorded upon addition of [*n*-Bu_4N]$_2$[ATP] or $Pd(OAc)_2$ to an electrochemical cell containing a Pt modified electrode in DCM and b) the CVs were recorded upon addition of [Na]$_2$[ATP] to an electrochemical cell containing a Pt modified electrode in water.

ASSOCIATED CONTENT

Supporting Information

Spectroscopic data for all the complexes and NMR, IR, near-IR, UV-vis. spectra and CVs. This material is available free of charge via the Internet at http: / / pubs.acs.org.

AUTHOR INFORMATION

Corresponding Author

*E-mail: d.astruc@ism.u-bordeaux1.fr

Notes

The authors declare no competing financial interest.

ACKNOWLEDGMENTS

Helpful assistance and discussion with Jean-Michel Lanier (NMR) and Claire Mouche (MALDI-TOFF MS) from the CESAMO and Dr Roberto Ciganda (Université de Bordeaux), and financial support from the Université de Bordeaux, the Centre National de la Recherche Scientifique (CNRS), the Agence Nationale pour la Recherche (ANR) and L'Oréal are gratefully acknowledged.

REFERENCES

(1) (a) Page, J. A. Wilkinson, G. *J. Am. Chem. Soc*. **1952**, *74*, 6149-6150. (b) Nishihara, H. *Adv. Inorg. Chem.* **2002**, *53*, 41-86 ; (c) Geiger, W. E. *Organometallics* **2007**, *26*, 5738-5765. (d) Geiger, W. E. *Orgnanometallics* **2011**, *30*, 28-31.

(2) (a) Connelly, N. G.; Geiger, W. E. *Adv. Organomet. Chem*. **1984**, *23*, 1-93. (b) Connelly, N. G.; Geiger, W. E. *Chem. Rev*. **1996**, *96*, 877-910. (e) Madonik, A. M.; Astruc, D. *J. Am. Chem. Soc.* **1984**, *106*, 2437-2439. (f) Lacoste, M.; Varret, F.; Toupet, L.; Astruc, D. *J. Am. Chem. Soc.* **1987**, *109*, 6504-6506. (g) Desbois, M.-H.; Astruc, D.; Guillin, J.; Varret, F.; Trautwein, A. X.; Villeneuve, G. *J. Am. Chem. Soc.* **1989**, *111*, 5800-5809.

(3) (a) Hamon, J.-R. ; Astruc, D. ; Michaud, P. *J. Am. Chem. Soc*. **1981**, *103*, 758-766. (b) Green, J. C.; Kelly, M. R.; Pane, M. P.; Seddon, E. A. ; Astruc, D. ; Hamon, J.-R. *Organometallics* **1983**, *2*, 211-218.

(4) (a) Gagne, R. R.; Koval, C. A.; Licensky, G. C. *Inorg. Chem*. **1980**, *19*, 2854-2855. (c) Krejic, M.; Danek, M.; Hartl, F. *J. Electroanal. Chem*. **1991**, *317*, 179-187. (d) Menon, V. P.; Martin, C. R. *Anal. Chem*. **1995**, *67*, 1920-1928. (e) Losada, J.; Cuadrado, I. ; Moran, M. ; Casado, C. M. ; Alonso, B. ; Barranco, M. *Anal. Chim. Acta* **1997**, *338*, 191-198. (f) Daeneke, T.; Kwon, T. H.; Holmes, A. B.; Duffy, N. W.; Bach, U.; Spiccia, L. *Nat. Chem*. **2011**, *3*, 211-215.

(5) (a) Wakatsuki, Y.; Yamazaki, H. *Synthesis* **1976**, *1*, 26-28. (b) Astruc, D. *Nat. Chem.* **2012**, *4*, 255-267. (c) Foo, C.; Sella, E.; Thomé, I.; Eastgate, M. D.; Baran, P. S. *J. Am. Chem. Soc.* **2014**, *136*, 5279-5282.

(6) (a) Top, S.; Dauer, B.; Vaissermann, J. ; Jaouen, G. *J. Organomet. Chem*. **1997**, *541*, 355-361. (b) Van Staveren, D. R.; Metzler-Nolte, N. *Chem. Rev*. **2004**, *104*, 5931-

5985. (c) Ornelas, C. *New J. Chem*. **2011**, *35*, 1973-1985. (d) Gasser, G.; Ott, I.; Metzler-Nolte, N. *J. Med. Chem*. **2011**, *54*, 3-25. (e) Pigeon, P.; Gormen, M.; Kowalski, K.; Muller-Bunz, H.; McGlinchey, M. J.; Top, S.; Jaouen, G. *Molecules* **2014**, *19*, 10350-10369. (f) Matschke, M.; Alborzinia, A.; Lieb, M.; Metzler-Nolte, N. *ChemMedChem* **2014**, *9*, 1188-1194.

(7) (a) Cass, A. E. G, Davis, G.; Francis, G. D. ; Hill, H. A. O. ; Aston, W. J. ; Giggins, I. J. ; Plotkin, E. V. ; Scott, L. D. L. ; Turner, A. P. F. *Anal. Chem*. **1984**, *56*, 667-671. (b) Beer, P. D. *Acc. Chem. Res*. **1998**, *31*, 71-80. (c) Casado, C. M.; Cuadrado, I.; Moran, M.; Alonso, B. ; Garcia, B. ; Gonzales, B. ; Losada, J. *Coord. Chem. Rev*. **1999**, *185-6*, 53-79. (d) Beer, P. D.; Gale, P. A. *Angew Chem., Int. Ed*. **2001**, *40*, 486-516. (d) Casado, C. M.; Alonso, B.; Losada, J. ; Garcia-Armada, M. P. in *Designing Dendrimers*, Campagna, S. ; Ceroni, P. ; Punteriero, F., Wiley, Hobojen, NJ, U. S. A. 2012, pp. 219-262. (e) Jimenez, A.; Armada, M. P. G.; Losada, L. ; Villena, C. ; Alonso, B. ; Casado, M. *Sensors Actuators B-Chem*. **2014**, **190**, 111-119.

(8) (a) Nguyen, P.; Gomez-Elipe, P.; Manners, I. *Chem. Rev*. **1999**, *99*, 1515-1548. (b) Abd-El-Aziz, A.S.; Bernardin, S. *Coord. Chem. Rev.* **2000**, *203*, 219–267. Abd-El-Aziz, A. S.; Todd, E. K. *Coord. Chem. Rev.* **2003**, 246, 3-52. (c) *Macromolecules Containing Metal and Metal-Like Elements, Organoiron Polymers*, Vol 2 , Eds: Abd-El-Aziz, A. S.; Carraher Jr., C. E.; Pittman Jr., C. U.; Sheats, J. E.; Zeldin, M.; Wiley-Interscience, New Jersey 2003. (d) Abd-El-Aziz, A. S.; Manners, I. *J. Inorg. Organomet. Polym.* **2005**, 15, 157-195. (e) *Frontiers in Transition-Metal Containing Polymers*, A.S. Abd-El-Aziz, I. Manners, ed.; Wiley, New York, 2007.(f) F. J. Martinez, B. Gonzalez, B. Alonso, J. Losada, M. P. Garcia-Armada, C. M. Casado, *J. Inorg. Organomet. Polym. Mater*. **2008**, *18*, 51-58.

(9) (a) Manners, I. *Science* **2001**, *294*, 1664-1666. (b) Whittel, G. R.; Manners, I. *Adv. Mater*. **2007**, *19*, 3439-3468. (c) Hudson, Z.; Boot, C. E.; Robinson, M. E.; Rupar, P. A. Winnink, M. A. ; Manners, I. *Nat. Chem*. **2014**, *6*, 893-898.

(10) (a) Abakumova, L. G.; Abakumov, G. A.; Razuvaev, G. A. *Dokl. Akad. Nauk SSSR* **1975**, *220*, 1317-1320. (b) Huang, W. H.; Jwo, J. J. *J. Chin, Chem. Soc.* **1991**, *38*, 343-350. (c) Zotti, G.; Schiavon, G.; Zecchin, S.; Berlin, A.; Pagani, G. *Langmuir* **1998**, *14*, 1728-1733; (d) Hurvois, J.; Moinet, C. *J. Organomet. Chem.* **2005**, *690*, 1829-1839.

(11) Cowan, D. O.; Kaufman, F. *J. Am. Chem. Soc.* **1970**, *92*, 219-220; Cowan, D. O.; Kaufman, F. *J. Am. Chem. Soc.* **1971**, *93*, 3889-3893; Levanda, C.; Cowan, D. O.; Bechgaard, K. *J. Am. Chem. Soc.***1975**, *97*, 1980-1981; Power, M. J.; Meyer, T. J. *J. Am. Chem. Soc.* **1978**, *100*, 4393-4398.

(12) (a) Robin, M. B.; Melvin, B.; Day, P. *Adv. Inorg. Chem. Radiochem*. **1967**, *10*, 247. (b) Allen, G.C.; Hush, N.S. *Prog. Inorg. Chem*. **1967**, *8*, 357. (c) Richardson, D. E.; Taube, H. *Coord. Chem. Rev*. **1984**, *60*, 107.

(13) (a) Horikoshi, T.; Itoh, M.; Kurihara, M.; Kubo, K.; Nishihara, H. J. *Electroanal. Chem*. **1999**, *473*, 113-116. (b) Nishihara, H. *Bull. Soc. Chem. Jpn*. **2001**, *74*, 19-29. (c) Yamada, M.; Nishihara, H. *Chem. Commun*. **2002**, 2578-2579. (d) Yamada, M.; Nishihara, H. *Eur. Phys. J.* **2003**, *24*, 257-260. (e) Yamada, M.; Nishihara, H. *Langmuir* **2003**, *19*, 8050-8056. (f) Yamada, M.; Nishihara H.

ChemPhysChem **2004**, *5*, 555-559. (g) Yamada, M.; Tadera, T.; Kubo, K.; Nishihara, H. *J. Phys. Chem. B* **2003**, *107*, 3703-3711. (h) Muraa, M.; Nishihara, H. *J. Inorg. Organomet. Polym*. **2005**, *15*, 147-156.

(14) Nijhuis, C. A.; Dolatowska, K. A.; Ravoo, B. J.; Huskens, J.; Reinhoudt, D. N. *Chem. Eur. J.* **2007**, *13*, 69-80.

(15) Wimbush, K. S.; Reus, W. F.; van der Wiel, W. G.; Reinhoudt, D. N.; Whitesides, G. M.; Nijhuis, C. A.; Velders, A. H. *Angew. Chem., Int. Ed*. **2010**, *49*, 10176-10180.

(16) (a) Ochi, Y.; Suzuki, M.; Imaoka, T.; Murata, M.; Nishihara, H.; Einaga, Y.; Yamamoto, K. *J. Am. Chem. Soc*. **2010**, *132*, 5061-5069. (b) Cuadrado, I., Casado, C. M. Alonso, B., Moran, M., Losada, J., Belsky, V *J. Am. Chem. Soc.* **1997**, *119*, 7613-7614. (c) Villena, C.; Losada, J.; Garcia-Armada, P.; Casado, C. M.; Alonso, B. *Organometallics* **2012**, *31*, 3284-3291.

(17) (a) Yamamoto, T.; Morikita, T.; Maruyama, T. ; Kubota, K. ; Katada, M. *Macromolecules* **1997**, *30*, 5390-5396. (b) Yan, S. G.; Hupp, J. T. ; *J. Electroanal. Chem.* **1995**, *397*, 119-26. (c) Deraedt, C.; Rapakousiou, A.; Wang, Y.; Salmon, L.; Bousquet, M.; Astruc, D. *Angew. Chem., Int. Ed.* **2014**, *53*, 8445-8449.

(18) (a) Wang, Y.; Rapakousiou, A.; Chastanet, G.; Salmon, L.; Ruiz, J.; Astruc, D., *Organometallics* **2013**, *32*, 6136-6146. (b) Djeda, R.; Rapakousiou, A.; Liang, L.; Guidolin, N.; Ruiz, J.; Astruc, D. *Angew. Chem., Int. Ed*. **2010**, *49*, 8152-8156. (c) Astruc, D.; Liang, L.; Rapakousiou, A.; Ruiz, J. *Acc. Chem. Res*. **2012**, *45*, 630-640. (d) Poppitz, E. A.; Hildebrandt, A.; Korb, N.; Lang, H. *J. Organomet. Chem.* **2014**, *752*, 133-140. (e) Rapakousiou, A.; Djeda, R.; Grillaud, M.; Li, N.; Ruiz, J.; Astruc, D.; *Organometallics* **2014**, dx.doi.org/10.1021/om501031u.

(19) (a) Deraedt, C.; Pinaud, N.; Astruc, D. *J. Am. Chem. Soc*. **2014**, *136*, 12092-12098. (b) Deraedt, C.; Astruc, D. *Acc. Chem. Res*. **2014**, *47*, 494-503.

(20) (a) Myachina, G. F.; Konkova, T. V.; Korzhova, S. A.; Ermakova, T. G.; Pozdnyakov, A. S.; Sukhov, B. G.; Arsentev, K. Yu.; Likhoshvai, E. V.; Trofimov, B. A., *Dokl. Chem*. **2010**, *431*, 63-64. (b) Oldham, E. D.; Seelam, S.; Lema, C.; Agulera, R. J.; Fiegel, J.; Rankin, S. E.; Knutson, B. L.; Lehmler, H. Carbohydrate Res. **2013**, *379*, 68-77. (c) Dallmann, A.; El-Sagheer, A. H.; Dehmel, L.; Mügge, C.; Griesinger, C.; Ernsting, N. P.; Brown, T. *Chem. Eur. J*. **2011**, *17*, 14714-14717.

(21) Rapakousiou, A.; Deraedt, C.; Gu, H.; Salmon, L.; Belin, C. Ruiz, J. Astruc, D. *J. Am. Chem. Soc*. **2014**, *136*, 13995-13998.

(22) Rosenberg, N.; Neuse, E. W. *J. Organomet. Chem.* **1966**, *6*, 76-85.

(23) Doisneau, G.; Balavoine, G.; Fillebeen-Khan, T. *J. Organomet. Chem.* **1992**, *425*, 113–117.

(24) Polin, J.; Schottenberger, H. *Org. Synth.* **1996**, *73*, 262-269.

(25) Zhang, K.; Tew, G. N. *ACS Macro Lett.* **2012**, *1*, 574-579.

(26) Vougioukalakis, G. C.; Georgios, C.; Grubbs, R. H. *Chem. Rev.* **2010**, *110*, 1746-1787.

(27) Liang, L.; Rapakousiou, A.; Salmon, L.; Ruiz, J.; Astruc, D.; Dash, P.; Satapathy, R.; Hosmane, N. S. *Eur. J. Inorg. Chem*. **2011**, *20*, 3043-3049.

(28) (a) Rostovtsev, V. V. ; Green, L. G. ; Fokin, V. V. ; Sharpless, K. B. *Angew.*

Chem. Int. Ed. **2002**, *41*, 2596–2599. (b) Meldal, M. ; Tornoe, C. W. *Chem. Rev.* **2008**, *108,* 2952-3015.

(29) Binder, W. H. ; Sachsenhofer, R. *Macromol. Rapid Commun.* **2008**, *29*, 952-981.

(30) (a) Ornelas, C. ; Ruiz, J. ; Cloutet, E. ; Alves, S. ; Astruc, D. *Angew. Chem., Int. Ed.* **2007**, *46*, 872–877.

(31) Liang, L.; Ruiz, J. ; Astruc, D. *Adv. Synth. Catal.* **2011**, *353*, 3434–3450.

(32) Zhao, P. ; Grillaud, M. ; Salmon, L. ; Ruiz, J. ; Astruc, D. *Adv. Synth. Catal.* **2012**, *354*, 1001-1011.

(33) Dong, T. Y. ; Chang, S. W. ; Lin, S. F. ; Lin, M. C. ; Wen, Y. S. ; Lee, L. *Organometallics* **2006,** *25,* 2018-2024.

(34) Brigger, I. ; Dubernet, C. ; Couvreur, P. *Adv. Drug Delivery Rev.* **2002**, *54*, 631-651.

(35) Lohan, M. ; Ecorchard, P. ; Rüffer, T. ; Justaud, F. ; Lapinte, C. ; Lang, H. *Organometallics* **2009,** *28,* 1878-1890.

(36) Powers, M. J.; Meyer, T. J. *J. Am. Chem. Soc.* **1980**, *102*, 1289–1297.

(37) Ruiz, J.; Astruc, D. *C.R. Acad. Sci. t. 1*, *Ser IIc* **1998**, *32*, 21.

(38) (a) J. E. Sutton, P. M. Sutton, H. Taube *Inorg. Chem*. **1979**, *18*, 1017-1024. (b) Richardson, D. E.; Taube, H. *Coord. Chem. Rev.* **1984**, *60*, 107-129. (c) Barrière, F.; Geiger, W. E. *Acc. Chem. Res*. **2010**, *43*, 1030-1039.

(39) Gorman, C. B.; Smith, B. L.; Parkhurst, H.; Sierputowska-Gracz, H.; Haney, C. A. *J. Am. Chem. Soc.* **1999**, *121*, 9958-9966.

(40) Amatore, C.; Bouret, Y.; Maisonhaute, E.; Goldsmith, J. I.; Abruña, H. D. *Chem.-Eur. J.* **2001**, *7*, 2206-2226.

(41) Bard, A. J.; Faulkner, L. R. *Electrochemical Methods: Fundamentals and Applications*. 2nd edn. , Wiley, New York, 2001.

(42) Flanagan, J. B.; Margel, S.; Bard, A. *J. Am. Chem. Soc.* **1978**, *100*, 4248-4253.

(43) (a) Cheon, K. S. ; Kazmaier, P. M. ; Keum, S. R. ; Park, K. T. ; Buncel, E. *Can. J. Chem.* **2004**, 82, 551–556 ; (b) Liu, D. ; De Feyter, S. ; Cotlet, M. ; Stefan, A. ; Wiesler, U. M. ; Herrman, A. ; Grebel-Koehler, D. ; Qu, J. ; Müllen, K. ; De Schryver, F. C. *Macromolecules* **2003**, *16*, 5918–5928.

(44) (a) Morrison, W. H. ; Krogsrud, S. ; Hendrickson, D. N. *Inorg. Chem.* **1973**, *12*, 1998-2004. (b) Levanda, C. ; Cowan, D. O. ; Beechgaard, *J. Am. Chem. Soc.* **1975**, *97*, 1980-1981. (c) Dong, T. Y. ; Hendrickson, D. N. ; Iwai, K. ; Cohn, M. J. ; Geib, S. J. ; Rheingold, A. L. ; Sano, H. ; Motoyama, I. ; Nakashima, S. *J. Am. Chem. Soc.* **1985**, *107*, 7996. (d) McManis, G. E. ; Gochev, A. ; Nielson, R. M. ; Weaver, M. J. *J. Phys. Chem.* **1989**, *93*, 7733-7739. (e) Nakashima, S. ; Sano, H. *Hyperfine Interact.* **1990**, *53*, 367-372. (f) Gu, H.; Rapakousiou, A.; Ruiz, J.; Astruc, D. *Organometallics* **2014**, *33*, 4323-4335.

(45) (a) Haruta, M.; Date, M. *Appl. Catal. A* **2001**, *222*, 227. (b) Cao, Y. W. C. ; Jin, R. ; Mirkin, C. A. *Science* **2002**, *297*, 1536–1540. (c) Daniel, M.-C.; Astruc, D. *Chem. Rev*. **2004**, *104*, 293-346. (d) Myroshnychenko, V.; Rodriguez-Fernandez, J.; Pastoriza-Santos, I.; Funston, A. M.; Novo, C.; Mulvaney, P.; Liz-Marzan, L. M.; de Abajo, F. J. G. *Chem. Soc. Rev.* **2008**, 1792-1805. (e) Xia, Y. Xiong, B. Lim and S. E. Skrabalak, *Angew. Chem., Int. Ed.*

2009, *48*, 60-103. (f) Lal, S.; Clare, S. E.; Halas, N. J. *Acc. Chem. Res*. **2008**, *41*, 1842-1851. (g) Corma, A.; Leyva-Perez, A.; Maria Sabater, J. *Chem. Rev*. **2011**, *111*, 1657. (h) Dimitratos, N.; Lopez- Sanchez, J. A.; Hutchings, G. J. *Chem. Sci*. **2012**, *3*, 20-44. (i) Herves, P.; Perez-Lorenzo, M.; Liz-Marzan, L. M.; Dzubiella, J .; Lu, Y.; Ballauff, M. *Chem. Soc. Rev*. **2012**, *41*, 5577-5587. (j) Buck, M. R.; Schaak, R. E. *Angew. Chem., Int. Ed*. **2013**, *52*, 6154-6178. (k) Li, N.; Zhao, P.; Astruc, D. *Angew. Chem., Int. Ed*. **2014**, *52*, 1756–1789. (l) Wang, H.; Song, X.; Liu, C.; He, J.; Chong, W. H.; Chen, H. *ACS Nano* **2014**, *8*, 8063-8073.

(46) (a) Wang, X. S.; Wang, H.; Coombs, N.; Winnik, M. A.; Manners, I. *J. Am. Chem. Soc.* **2005**, *127*, 8924-8925. (b) Wang, H.; Wang, X.; Winnik, M. A.; Manners, I. *J. Am. Chem. Soc.* **2008**, *130*, 12921-12930.

(47) (a) Huo, J.; Wang, L.; Yu, H.; Deng, L.; Ding, J.; Tan, Q.; Liu, Q.; Xiao, A.; Ren, G. *J. Phys. Chem. B* **2008**, *112*, 11490-11497; (b) Takahashi, S.; Anzai, J. I. *Materials* **2013**, *6*, 5742-5762; (c) Abruña, H. D. In *Electroresponsive Molecular and Polymeric Systems*: Skotheim, T. A., Ed.; Dekker: New York, 1988; Vol. 1, p. 97. (d) Murray, R. W. In *Molecular Design of Electrode Surfaces*; Murray, R.W., Ed.; *Techniques of Chemistry XXII*; Wiley: New York, NY, 1992; p 1.

(48) (a) Peerce, P. J.; Bard, A. J. *J. Electroanal. Chem.* **1980**, *114*, 89-111. (b) Lenhard, J. R.; Murray, R. W. *J. Am. Chem. Soc*. **1978**, *100*, 7870-7875. (c) Brown, A. P.; Anson, F. C. *Anal. Chem.* **1977**, *49*, 1589-1595; (d) Laviron, E. *J. Electroanal. Chem*. **1981**, *122*, 37-44.

TOC:

Polymers containing triazolylbiferrocenyl groups in the side chain or the main chain are synthesized by ROMP, radical or click CuAAC polycondensation and oxidized by $[FeCp_2][PF_6]$, $H[AuCl_4]$ or $Ag[BF_4]$ to stable class-II mixed-valent biferrocenium salts. Various Au and Ag nanoparticle networks stabilized by triazolylbiferrocenium salts and modified electrodes are obtained, and ATP^{2-} and Pd^{II} are recognized both in dichloromethane and in water.

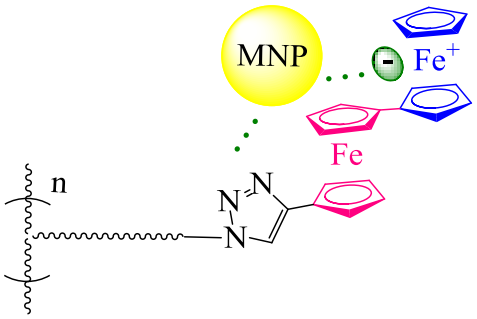

MNP = Au or Ag nanoparticle

ORGANOMETALLICS

Article

pubs.acs.org/Organometallics

"Click" Assemblies and Redox Properties of Arene- and Gold-Nanoparticle-Cored Triazolylbiferrocene-Terminated Dendrimers

Amalia Rapakousiou, Rodrigue Djeda, Maxime Grillaud, Na Li, Jaime Ruiz, and Didier Astruc*

ISM, UMR CNRS No. 5255, Univ. Bordeaux, 33405 Talence Cedex, France

Supporting Information

ABSTRACT: Large dendritic assemblies terminated by organometallic groups that possess a rich redox chemistry and stability in two or more oxidation states are highly desired as electron-reservoir systems, sensors, and redox catalysts. Here the synthesis and click (CuAAC) chemistry of ethynyl biferrocene including branching onto dendrons, arene-cored dendrimers, and gold nanoparticles are developed, and the role of the 1,2,3-triazole linkers and redox chemistry of these assemblies are discussed including the properties and stabilities of the redox states.

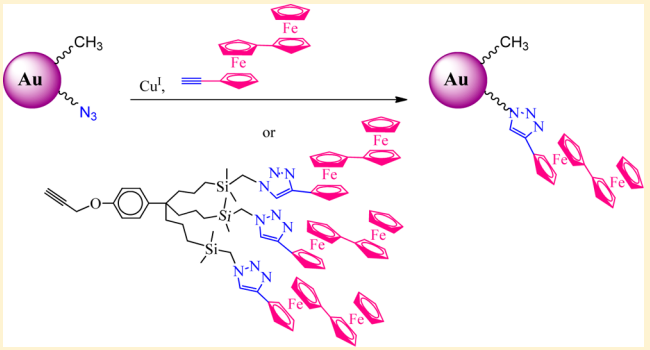

INTRODUCTION

Macromolecules containing redox-active units have recently been largely developed due in particular to their electrochromic and polyelectrolyte properties.[1] Among the various transition-metal sandwich complexes that display remarkable redox properties,[2] ferrocenyl derivatives are the most frequently studied, because of the richness of ferrocene chemistry and its easy oxidation to ferricenium.[3] In the ferrocene family, biferrocene[4] derivatives present a great interest, as they include three easily accessible oxidation states, a characteristic that makes their redox properties much richer than those of the parent ferrocene compounds. In addition, the biferrocenium cation is extremely robust because the electron-releasing ferrocenyl group stabilizes the neighboring ferricenium cation. Indeed, it is well known that biferrocenium belongs to the class 2 of the mixed-valent compounds according to Robin and Day's classification following the localization of the valence at the infrared time scale.[5] Therefore, biferrocenyl units have often been incorporated in various nanostructures such as dendrimers and nanoparticles.[6] Ferrocenyl-terminated dendrimers[7] and nanoparticle-cored ferrocenyl-terminated branched assemblies[8] represent a class of metallodendrimers[9] that have proved useful especially for redox sensing,[10] although ferricenium or related Fe(III) analogues were rarely isolated and studied.[11]

Biferrocenyl dendrimers have been constructed with up to eight electronically communicated silicon-bridged biferrocenyl groups in the periphery where stable modified electrodes were prepared with interacting ferrocenes.[5a] Water-soluble poly(propyleneimine) biferrocenyl dendrimers complexed with β-CD were studied as well as their adsorption at self-assembled monolayers on gold for molecular printboards.[5b] Redox-active biferrocenes entrapped in polyphenylazomethine dendrimers were studied with an impressive control of reversible encapsulation/release due to the stability of the biferrocenium cation,[5c] whereas molecular junctions were also prepared from biferrocenyl-terminated dendrimers.[5d] Biferrocenyl-terminated diaminobutane poly(propyleneimine) dendrimers were also synthesized by Casado's group, who demonstrated electrochemical anion sensing and successful immobilization onto electrode surfaces.[5e] Finally, dendritic tris- and tetra-biferrocenes linked by rigid ethynylaryl spacers were synthesized through Sonogashira coupling and homocoupling reactions displaying an electron-rich chemistry.[5f]

Gold nanoparticles (AuNPs) are a prolific field with applications in optics, sensing, nanomedicine, and catalysis,[12] and Nishihara's group has extensively studied AuNPs with biferrocene-terminated thiolate ligands forming thin redox-active films by electrodeposition.[7] Additionally, biferrocene-functionalized terpyridine octanethiols and the studies of their self-organization chemisorbed on AuNPs were reported.[13]

Click methodology,[14] in particular the copper-catalyzed azide−alkyne cycloaddition (CuAAC) forming 1,2,3-triazoles (trz),[14b−g] has recently appeared as one of the most powerful and practical means to form metallocene-terminated nanoassemblies. The triazolyl linkage is significant for redox recognition and subsequent stabilization of gold and palladium nanoparticles for catalysis,[15] and in many cases it shows remarkable biocompatibility.[16] Triazolyl-metallocenyl dendrimers have been successfully synthesized by a CuAAC-type click reaction using the Sharpless catalyst and showed various applications in redox recognition and catalysis.[17]

Herein, we report the detailed synthesis of ethynylbiferrocene and its CuAAC-type click reactions providing access to triazolylbiferrocenyl nanosystems.[18] Therefore, three generations

Received: October 9, 2014

Scheme 1. Synthesis of Ethynylbiferrocene, 3

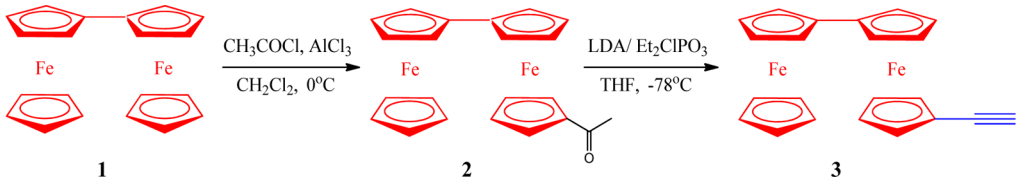

Scheme 2. Construction of G_1, G_2, and G_3 Allyl Dendrimers

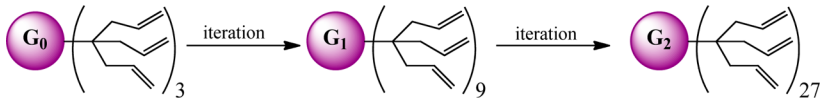

Scheme 3. Click Synthesis of G_0, G_1, and G_2 trz-BiFc-Terminated Dendrimers

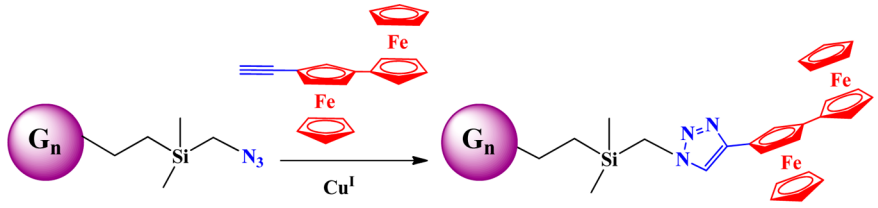

n = 0: 9 N_3 (**4**)
1: 27 N_3 (**5**)
2: 81 N_3 (**6**)

n = 0: 9 trz-BiFc (**7**)
1: 27 trz-BiFc (**8**)
2: 81 trz-BiFc (**9**)

of triazolylbiferrocenyl dendrimers together with a new tris-trz-BiFc dendron containing a propargyl group at the focal point are reported and detailed in this article. Additionally, the construction of dendritic AuNPs with triazolylbiferrocenyl termini at the periphery was achieved, allowing the study of their properties and redox behavior.

RESULTS AND DISCUSSION

Synthesis of Ethynylbiferrocene, 3. Ethynylbiferrocene, **3**, was synthesized in two steps from biferrocene,[19] **1** (Scheme 1). The first step is the synthesis of acetylbiferrocene, **2**, consisting in a Friedel–Crafts acetylation of biferrocene; this reaction is based on the work by Doisneau et al. in 1992.[20] The acetylation of biferrocene yields four acetylbiferrocene isomers. The isomer in which the acetyl group is attached to the cyclopentadienyl opposite the two rings joining the two ferrocenyl moieties was isolated following column purification using dichloromethane (DCM) as eluent and recrystallization from cold pentane (0 °C). Ethynylbiferrocene,[18] **3**, was subsequently prepared in a reaction similar to that carried out for the synthesis of ethynylferrocene.[21] The reaction was conducted between acetylbiferrocene and LDA/diethylchlorophosphate under nitrogen at −78 °C. Purification by column chromatography using pentane as eluent provided an orange crystalline powder in 50% overall yield from biferrocene, **1**.

Synthesis and Characterization of G_0, G_1, and G_2 Triazolylbiferrocenyl (trz-BiFc) Dendrimers. The syntheses of the G_0, G_1, and G_2 chloromethyl(dimethyl)silyl dendrimers with 1→3 connectivity[22] were carried out as described previously upon $CpFe^+$-induced polyallylation of mesitylene and *p*-methoxytoluene. This was followed, after decomplexation, by hydrosilylation of the polyallyl dendritic cores and dendron using chloromethyldimethylsilane and iteration using a Williamson reaction with the tribranched phenol triallyl dendron (Scheme 2).[23] The terminal chloro groups were then substituted by azido groups upon reaction with sodium azide, providing the azido-terminated dendrimers **4**, **5**, and **6** (Scheme 2).[24]

Subsequently, the CuAAC reaction was conducted between the G_0, G_1, and G_2 azido-terminated dendrimers and the terminal alkyne **3**, catalyzed by Cu^I obtained from $CuSO_4$/sodium ascorbate. The solvent chosen for these reactions is THF/H_2O (1:1), in which the polyazido precursors **4**, **5**, **6**, and **3** are soluble. Upon addition of sodium ascorbate, which reduces Cu^{II} to Cu^I, the color immediately changed from brown to light orange, and the mixture was stirred under N_2 for 24 h. The G_0–G_1–G_2 trz-BiFc dendrimers **7**, **8**, and **9** were purified by precipitation in methanol and pentane and obtained as yellow solids showing excellent solubility in DCM, THF, and chloroform (Scheme 3).

The three dendrimers were characterized by IR, ^1H and ^{13}C NMR spectra, MALDI-TOF MS, SEC, DLS, elemental analyses, and CV.

The ^1H NMR spectra of dendrimers **7**, **8**, and **9** show the disappearance of the ethynyl proton at 2.7 ppm and CH_2N_3 protons of the polyazido-terminated dendrimers at 2.8 ppm and the appearance of the proton of triazole (7.0–7.1 ppm) formed upon click reaction as well as the CH_2trz signal at 3.7 ppm. The presence of triazoles is also confirmed by the appearance of the characteristic peaks of *Cq* and CH of trz as well as the CH_2trz in the ^{13}C NMR spectra. Finally, the assignments of the number of protons in ^1H NMR show the expected ratio between the dendritic frame part and the trz-BiFc peripheral groups.

IR was a useful tool to follow the reaction using the distinct absorption band of N_3 at 2094 cm^{-1}, which disappeared at the end of the click reactions, confirming the complete formation of 1,2,3-triazoles. The absorptions due to the =C–H stretching of the triazoles and Cp groups of BiFc units are found in the range 3091–3096 cm^{-1}.

dx.doi.org/10.1021/om501031u | *Organometallics* XXXX, XXX, XXX–XXX

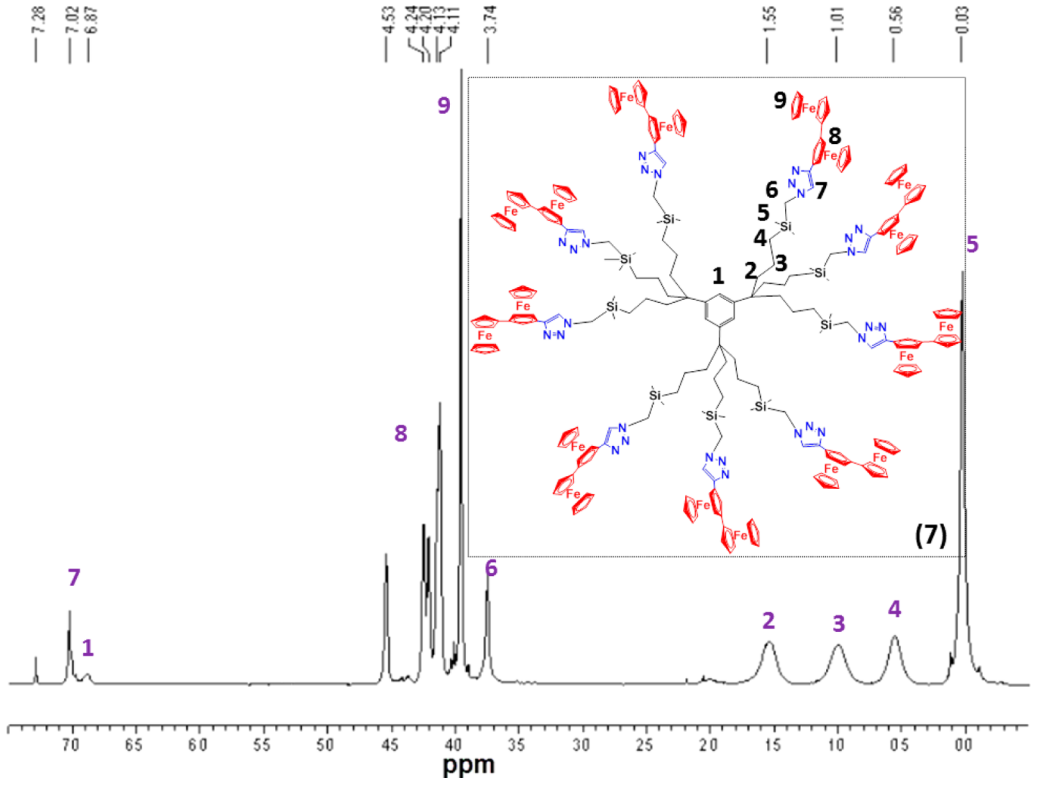

Figure 1. ^{1}H NMR spectrum and assignments of the signals of dendrimer **7**.

MALDI-TOF mass spectrometry of the dendrimer **7** (M^+) showed the molecular ion peak at 5087.11 Da, whereas the calculated mass is 5086.98 Da. SEC analyses gave the polydispersity index of the dendrimers **7**, **8**, and **9** and most importantly showed the progressive size evolution between the generations of dendrimers.[18a] The PDIs of **7**, **8**, and **9** are 1.01, 1.02, and 1.15, respectively. The DLS analyses show the size progression, disclosing an increase of the hydrodynamic diameter among G_1 and G_2. Finally, elemental analysis confirmed the structure of all the dendrimers.

The three generations of trz-BiFc dendrimers (compounds **7**, **8**, and **9**) were studied by cyclic voltammetry using decamethylferrocene as the internal reference.[25] The cyclic voltammograms (CVs) were recorded in DCM, a good solubility being accessible with this solvent. The first oxidation wave of all the products corresponds to the oxidation of the outer ferrocene that is only bearing as substituent the electron-rich inner ferrocene, whereas the second wave corresponds to the oxidation of the inner ferrocene bearing also the electron-withdrawing triazole. Both waves are single in DCM, which can be explained by the weakness of the electrostatic factor among the redox sites of the metallodendrimers, these redox centers being far from one another and separated by long tethers.[26]

Both waves in DCM appear to be chemically and electrochemically reversible. The electrochemical reversibility involving equally all the redox groups is due to very fast rotation within the electrochemical time scale, where all the redox groups come close to the electrode, provoking fast electron transfer between all the redox groups and the electrode[27] and/or the electron-hopping mechanism.[28]

Adsorption during cyclic voltammetry recording of dendrimers is common, and it is marked for the high dendrimer generations. This large adsorption phenomenon for the large dendrimers is due to the low solubility of the oxidized dendrimers in DCM. Adsorption begins with the nona-trz-BiFc dendrimer **7** (i_c/i_a = 1.25) and gradually increases as the generation number of dendrimer increases. In particular, the i_c/i_a value for dendrimers **8** and **9** is 1.6 and 1.8, respectively, concerning the first oxidation wave ($Fe^{II}Fe^{II} \rightarrow Fe^{II}Fe^{III}$). Adsorption is much more intense for the second oxidation wave ($Fe^{II}Fe^{III} \rightarrow Fe^{III}Fe^{III}$) in the case of dendrimers **7** (i_c/i_a = 3.0) and **8** (i_c/i_a = 3.2). However, in the case of dendrimer **9** the phenomenon is less intense (i_c/i_a = 1.3) presumably due to partial degradation of the dendritic products during oxidation of all the biferrocenyl termini to $Fe^{III}Fe^{III}$ dicationic compounds.

Synthesis and Characterization of a trz-BiFc Phenol Dendron. A tris-trz-biferrocenyl dendron containing a propargyl group at the focal point, **14**, was synthesized according to Scheme 4. The synthesis of this dendron starts by the known $CpFe^+$-induced benzylic triallylation of the methyl substituent of the *p*-methoxytoluene iron complex [FeCp(η^6-*p*-$CH_3C_6H_4OCH_3$)]-[PF_6] obtained by reaction of ethanol and sodium carbonate with [FeCp(η^6-*p*-$CH_3C_6H_4Cl$)][PF_6] and subsequent exocyclic C–O cleavage in the methoxy group.[23] The triallylated phenol dendron **10** obtained in this way is hydrosilylated with chloromethyldimethylsilane to give complex **11**. The terminal chloro groups were then substituted by azido groups upon reactions with sodium azide, providing the azido-terminated phenoltriallyl dendron **12**.[29] Subsequently, a click reaction was carried out between **12** and complex **3** using $CuSO_4$/sodium ascorbate in a mixture of THF/H_2O at rt during 24 h. The new dendron **13** was purified by precipitation in pentane twice and characterized by ^{1}H and ^{13}C NMR, IR, and Maldi-TOF spectroscopies. ^{1}H NMR (in CD_3COCD_3) showed the presence of the trz-proton at 7.44 ppm and the CH_2trz protons at 3.90 ppm together with the other proton signals of the dendron. ^{13}C NMR spectroscopy confirmed the structure of **13**; IR showed the replacement of the azido termini by 1,2,3-triazoles, and finally Maldi-TOF MS of dendron

dx.doi.org/10.1021/om501031u | *Organometallics* XXXX, XXX, XXX–XXX

Chart 1. Generations 1 and 2 of trz-BiFc-Terminated Dendrimers 8 and 9

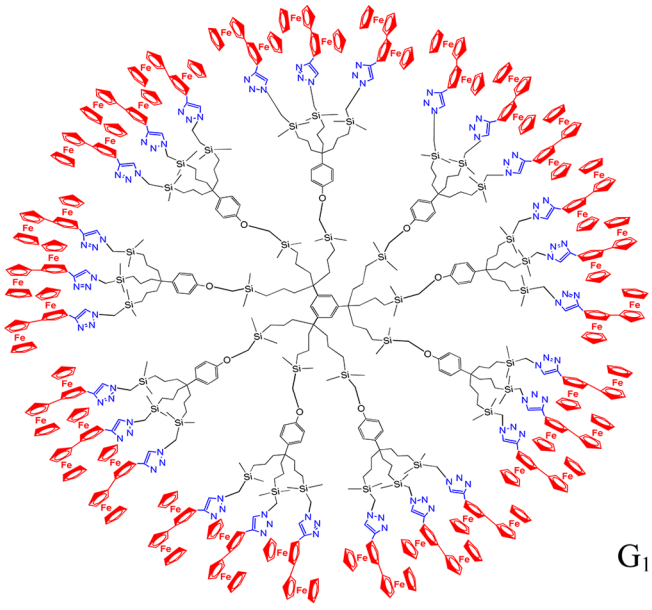

G_1 **(8)**

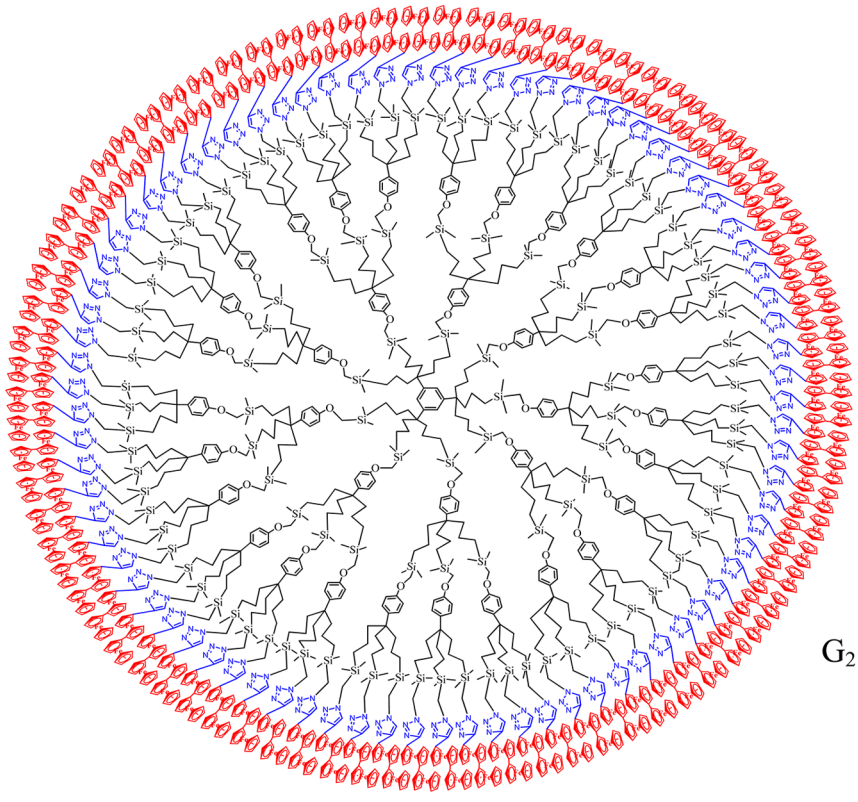

G_2 **(9)**

13 was found at 1755.7 Da, whereas the calculated mass was 1755.3 Da.

The next step was the functionalization of **13** with a propargyl group at the focal point that would allow attaching to azido-terminated assemblies. The propargylation reaction occurred in acetone solvent, at 60 °C for 24 h, using propargyl bromide and Cs_2CO_3 as a base. At the end of the reaction, the excess of propargyl bromide was removed under vacuum, and extraction with diethyl ether/H_2O gave dendron **14** in 90% yield. By ^1H NMR spectroscopy, the CC*H* proton is observed at 2.75 ppm and the CH_2O signal at 4.73 ppm, whereas the OCH_2C signal in ^{13}C NMR appears at 55.8 ppm. In IR spectroscopy, a weak absorption is observed at 2.100 cm^{-1}; this absorption is due to the alkyne group of the focal point of dendron **14**. Mass spectrometry confirmed the structure of **14** (SI).

Synthesis of trz-BiFc-Terminated Gold Nanoparticles. Click modification of AuNPs has been a challenge in the past years because of serious aggregation problems that consequently induced low product yields.[30] However, the efficient Cu^I catalyst[31] $[Cu^I(CH_2Ph)_6tren][Br]$ was recently reported for the efficient click functionalization of AuNPs.[32] Therefore, grafting of biferrocene on the AuNPs was attempted using this efficient catalyst. Dodecanethiolate AuNPs, **15**, were synthesized by the well-known Brust–Schiffrin method.[33] A ligand-exchange

dx.doi.org/10.1021/om501031u | *Organometallics* XXXX, XXX, XXX–XXX

Scheme 4. Overall Synthesis of the tris-trz-BiFc Dendron with a Propargyl Group at the Focal Point

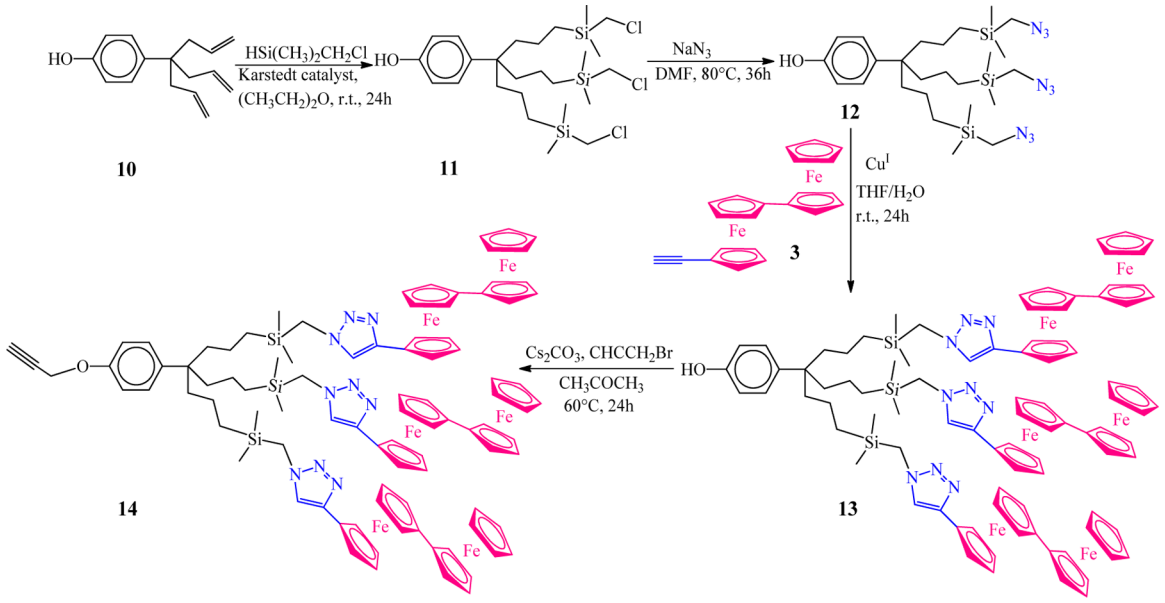

Scheme 5. Overall Synthesis of trz-BiFc-Terminated AuNPs 17 and 18

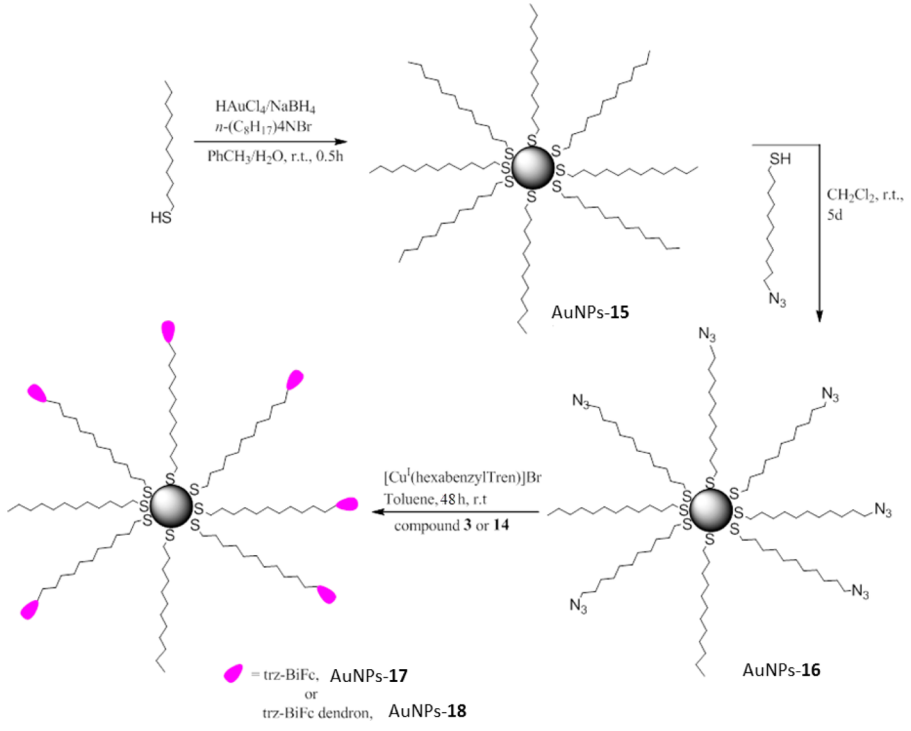

reaction was then conducted in DCM for 7 days in the presence of azidoundecanethiol ligands to finally provide AuNPs **16** in 90% yield. ^{1}H NMR spectroscopy allowed estimating the ratio of azido-terminated ligands versus nonazido ligands by comparing the integration of the $-CH_3$ methyl signal (0.84 ppm) with that of the CH_2N_3 signal (see SI, ^{1}H NMR of the AuNPs **16**, S03). Thus, 70% of the ligands on the surface of the AuNPs were replaced by azido-terminated ligands (Scheme 5). TEM revealed the size of the AuNPs, which was 2.2 ± 0.2 nm, where the area of a AuNP **16** was calculated to be 15.2 nm^2. With the help of theoretical studies of Leff et al.[34] the number (n_{Au}) of gold atoms of a AuNP **2** was estimated: n_{Au} = 328. Considering that the alkanethiol footprint occupies a surface of 0.21 nm^2,[35] the approximate number of ligands on a AuNP **16** is ∼72 thiolate ligands. With the proportion of azido/nonazido ligands being determined by ^{1}H NMR (70/30), ∼50 azido ligands per gold nanoparticle is deduced.

The click functionalization of AuNPs was carried out between azido-terminated AuNPs **16** and either ethynylbiferrocene (**3**) or dendron **14** to finally give the dendritic AuNPs **17** and **18**, respectively. The reactions occurred in toluene using [Cu^I(CH$_2$Ph)$_6$tren][Br], **19**, as a catalyst (20%). An excess of ethynyl derivative **3** or **14** was employed (1.5 equiv per azido-terminated ligand), and the reactions lasted for 2 and 1 d,

dx.doi.org/10.1021/om501031u | *Organometallics* XXXX, XXX, XXX−XXX

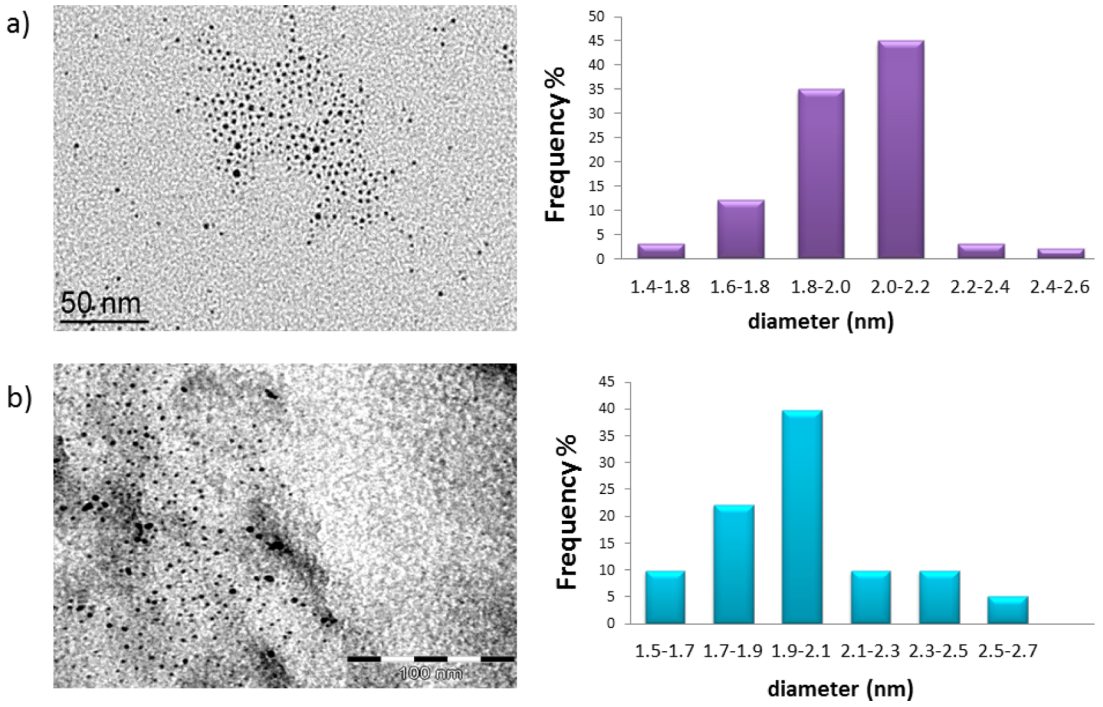

Figure 2. (a) TEM and size distribution of AuNPs **17**; (b) TEM and size distribution of AuNPs **18** (bar scale: 100 nm).

Table 1. Core Size, Number of Gold Atoms (n_{Au}), Number of Ligands (n_L), Number of trz-BiFc Ligands (n_{BiFc}), and Approximative Molecular Weight (MW)

compound	TEM (nm)	n_{Au}	n_L	n_{BiFc}	MW
AuNPs **16**	2.2 ± 0.2	328 ± 90	72 ± 13		80 500
AuNPs **17**	2.1 ± 0.1	285 ± 41	66 ± 06	40 (±06)	86 000
AuNPs **18**	2.0 ± 0.1	246 ± 38	60 ± 06	108 (±18)	126 000

respectively. At the end of the reaction, the catalyst and excess of alkyne were removed by washing the AuNPs with ethanol/pentane in the case of AuNPs **17** (yield: 65%) and ethanol/diethyl ether in case of AuNPs **18** (yield: 77%). Presumably, the click reaction with dendron **14** was faster and provided a better yield than with **3**, due to its less encumbered alkyne group at the focal point in **14** compared to the more encumbered ethynyl group of compound **3**. The AuNPs **17** and AuNPs **18** were characterized by ^{1}H NMR, IR, and UV−visible spectroscopy, TEM, DLS, and cyclic voltammetry.

Characterization of AuNPs 17. First, IR spectroscopy confirmed that all the azido groups were replaced by 1,2,3-trz-BiFc groups at the periphery of the AuNPs, as indicated by the disappearance of the typical absorption of the N_3 groups.[1] H NMR spectroscopy showed all the corresponding peaks of the AuNPs **17**: the BiFc protons, ligands, and a weak peak of the triazole proton. The $-CH_2N_3$ at 3.22 ppm of AuNPs **16** and the −CC*H* proton at 2.70 ppm of **3** were not observed, indicating that all the azido groups were replaced by trz-BiFc groups and that no excess of **3** remained after purification. In Figure 2 the TEM of AuNPs **17** shows that their diameter is $d = 2.1 \pm 0.1$ nm, a value slightly smaller than that observed for AuNPs **16**. The calculated number of ligands of AuNPs **17** is ∼66; thus it can be concluded that there are 40 ± 6 trz-BiFc moieties in each AuNP **17** (Table 1). This indicates that a rearrangement of the AuNPs takes place during the click reaction with a loss of trz-BiFc-terminated ligands occurring to produce the more stable AuNPs **17**. Finally, DLS revealed that the overall hydrodynamic diameter of AuNPs **17** was $d = 20 \pm 3$ nm.

Characterization of AuNPs 18. As for the AuNPs **17**, the reaction of AuNPs **18** was followed by IR spectroscopy, which confirmed that the click reaction was completed; this was monitored by the disappearance of the N_3 absorption.

TEM analysis showed that the size (diameter) of the dendronized AuNPs **18** is $d = 2.0 \pm 0.1$ nm (Figure 2), whereas the hydrodynamic diameter (by DLS) was found to be $d = 23 \pm 4$ nm.

Consequently, in this case the calculated number of trz-BiFc groups at the periphery of AuNPs **4** is 108 ± 18 (Table 1). Similarly, the UV−vis spectrum shows a very weak and broad absorption shoulder corresponding to the surface plasmon band of the AuNPs **18**, which can be explained by the small size of these nanoparticles. The ^{1}H NMR spectrum of the AuNPs **18** shows the corresponding peaks of the BiFc dendron, alkyl chains, and triazole peaks, confirming the structure of these AuNPs. At the same time, the disappearance of the CH_2N_3 signal of the AuNPs **16** at 3.22 ppm confirms that the reaction is finished and that the CC*H* peak of the dendron **14** at 2.75 ppm shows that the excess of **14** was successfully removed. The click reaction of the AuNPs **16** with the dendron **14** allowed the introduction of a considerably larger number of trz-BiFc ligands.

Cyclic Voltammetry of AuNPs 17 and 18. Both AuNPs **17** and **18** were also studied by cyclic voltammetry in DCM, in which they were soluble. The recorded CV of the AuNPs (see SI, S18) **17** showed two redox waves of the trz-BiFc peripheral moieties. Both waves are chemically and electrochemically reversible. However, this heterogeneous electron transfer is observed with adsorption on the electrode, as characterized by

dx.doi.org/10.1021/om501031u | *Organometallics* XXXX, XXX, XXX−XXX

Chart 2. Triazolylbiferrocenyl-Terminated AuNPs 17

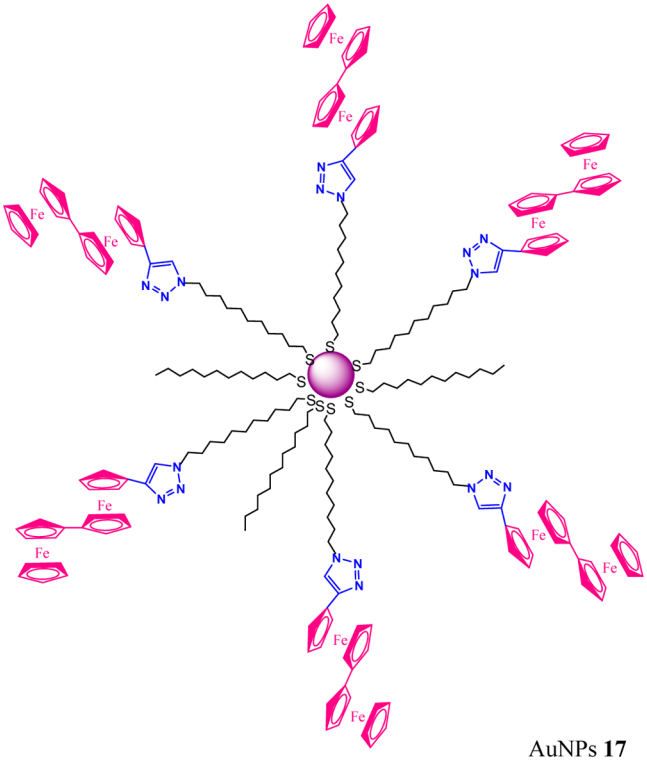

Chart 3. Triazolylbiferrocenyl-Terminated AuNPs 18

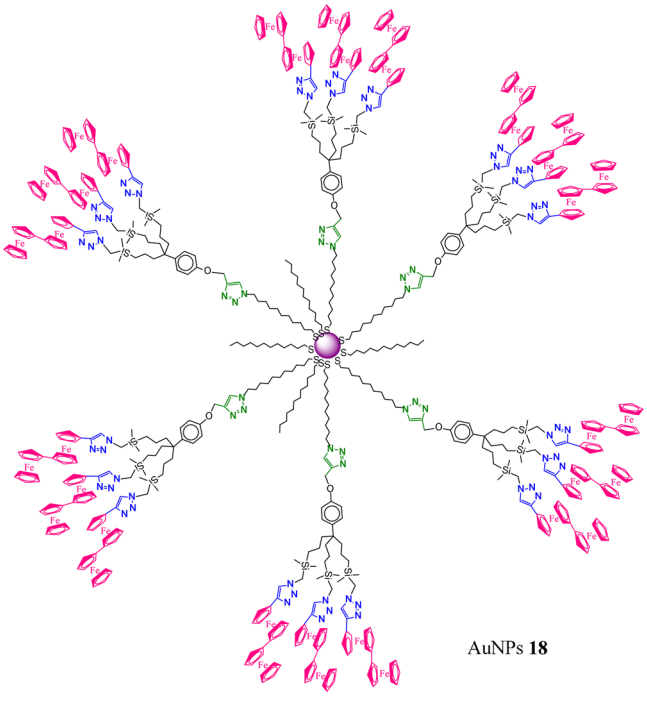

separation values between the forward and return peak potentials ΔE that are significantly lower than the Nerstian value of 59 mV at 25 °C (ΔE = 20 mV for the first redox wave and ΔE = 30 mV for the second redox wave). Continuous scanning around the BiFc potentials leads to full adsorption on the Pt electrode (ΔE = 0 mV). The case of the AuNPs **18** is different, however. The first oxidation wave that corresponds to the more easily oxidized outer ferrocenyl groups of the biferrocenes also appears to be chemically and electrochemically reversible. The second oxidation wave of the AuNPs **18** that corresponds to the less easily oxidized inner (internal) ferrocenyl groups appears at 60 mV more positive potentials than that of the AuNPs **17**. Presumably, the electrostatic factor is more important in the AuNPs **18** after the oxidation of the first (outer) ferrocenyl groups than in AuNPs **17**, which means that more energy is required for the second oxidation, that of the inner ferrocenyl groups (Figure 3).

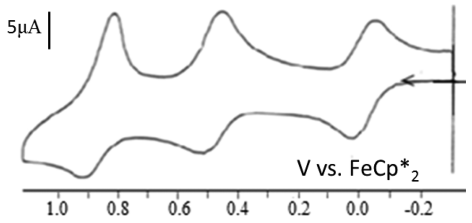

Figure 3. CV of the AuNPs **18**. Solvent: CH_2Cl_2; internal reference: $FeCp^*_2$ ($Cp^* = \eta^5$-C_5Me_5); reference electrode: Ag; working and counter electrodes: Pt; scan rate: 0.2 V/s; supporting electrolyte: [n-Bu_4N][PF_6]. The wave at 0.0 V corresponds to decamethylferrocene (reference).[25]

Presumably this is due to the proximity of the trz-BiFc moieties inside each dendron in the dendronized AuNPs **18** unlike in the AuNPs **17**. Additionally, this wave (internal Fc) of the AuNPs **18** appears to be quasi-reversible (ΔE_p = 85 mV), indicating that some structural reorganization (that may be decomplexation) somewhat slows down the heterogeneous electron transfer. Adsorption is also observed on the electrode, but continuous scanning leads to degradation of the product on the surface of the Pt-electrode (probably decomplexation) so that a fine modified electrode is not accessible, unlike in the case of the AuNPs **17** described above.

CONCLUSION

The synthesis and purification of ethynylbiferrocene was a key step for the click assembly of dendrons, dendrimers, and gold nanoparticles containing biferrocenyl termini. These organometallic nanomaterials show very useful redox properties involving the three distinct oxidation states of biferrocene. In particular the biferrocenyl termini are all equivalent, and cyclic voltammograms of the metallodendrimers show only two waves that are not broadened by the nanostructure due to the weakness of the electrostatic effect. This equivalence is essential for sensing applications with these metallodendrimers. In nanoparticle-cored dendrimers, however, the second biferrocene oxidation wave is found at slightly more positive potential value than in nondendronized nanoparticles with quasi-reversibility, presumably due to some electrostatic effect within the three biferrocenium units of the dendrons. The result is that modified electrodes with the nanoparticles can be formed only with nanoparticles containing nondendronized biferrocenyl tethers. The electron-withdrawing triazolyl groups linked to the biferrocenyl termini plays a key role in differentiating the inner and outer ferrocenyl groups of the dendrimers, which is most useful for sensing both anionic and cationic substrates and stabilizing well-defined nanoparticles.

EXPERIMENTAL SECTION

Synthesis of 2.[20] In a flask were placed 10.24 g of zinc powder and a solution of biferrocene **1** (4.0 g, 10.8 mmol) in 100 mL of anhydrous DCM under nitrogen. In another flask, also under nitrogen, acetyl

dx.doi.org/10.1021/om501031u | *Organometallics* XXXX, XXX, XXX−XXX

chloride (0.76 mL, 10.7 mmol) was dissolved in 100 mL of anhydrous DCM. To this was slowly added anhydrous aluminum chloride (1.4 g, 10.8 mmol). The second solution was added to the first dropwise at 0 °C, forming a rich purple color. The mixture was stirred for 20 h at 0 °C and hydrolyzed cautiously with water at 0 °C. The product was extracted with DCM and washed several times with water. After drying over Na_2SO_4 the solvent was removed *in vacuo*. The crude product was purified by column chromatography on silica gel. Elution with pentane removed unreacted species. Then elution with DCM removed acetylbiferrocene (red band). Recrystallization in 10 mL DCM/500 mL cold pentane at 0 °C gave product **2** (800 mg, yield: 17%). ^{1}H NMR ($CDCl_3$, 300 MHz) δ_{ppm}: 4.600 (t, 2H, sub. Cp), 4.387 (m, 4H, sub. Cp), 4.344 (t, 2H, sub. Cp), 4.243 (d, 4H, sub. Cp), 4.000 (5H, Cp free), 2.179 (s, 3H, CH_3COBiFc).

Synthesis of 3.[18] Compound **2** (0.800 g, 1.94 mmol) was dissolved in 50 mL of THF and cooled to −78 °C, and a 1.1 equiv solution of freshly prepared lithium diisopropylamide [100 mL of THF, diisopropylamine (1.1 equiv, 2.13 mmol, 0.3 mL), *n*-butyllithium (1.21 equiv, 2.35 mmol)] was added dropwise. The reaction mixture was stirred for 1 h at −78 °C; then diethylchlorophosphate (1.05 equiv, 2.04 mmol, 0.29 mL) was added, and the reaction mixture was maintained at −78 °C for 1 h. Then the reaction mixture was warmed to room temperature (rt) before cooling again to −78 °C and adding again dropwise a 2.3 equiv solution of freshly prepared lithium diisopropylamine [100 mL of THF, diisopropylamine (2.3 equiv, 4.46 mmol, 0.62 mL), *n*-butyllithium (2.53 equiv, 4.91 mmol)]. After raising the temperature again to rt the reaction was hydrolyzed at 0 °C. After extraction with DCM, drying on sodium sulfate, and evaporation of the solvent the crude product was purified by column chromatography on silica gel with pentane/DCM (9:1) as eluent. The product was isolated as a red solid (0.368 g, 48%). ^{1}H NMR ($CDCl_3$, 300 MHz), δ_{ppm}: 4.43−4.38 (m, 4H, CH of sub. Cp), 4.27−4.22 (m, 6H, CH of sub. Cp), 4.05−4.03 (m, 7H, CH of Cp free and sub. Cp), 2.71 (s, 1H, C≡*CH*).

Synthesis of 7. Ethynylbiferrocene (**3**; 0.178 g, 0.454 mmol) and G_0-9-N_3 (0.050 g, 0.033 mmol) were dissolved in oxygen-free THF (50 mL), and oxygen-free water (50 mL) was added. A solution of 1 M $CuSO_4$ (1 equiv per branch) was added at 0 °C, with subsequent dropwise addition of a freshly prepared solution of 1 M sodium ascorbate (2 equiv per branch). The brown solution immediately changed to orange. The reaction mixture was allowed to stir for 24 h under N_2 at rt. Then DCM (100 mL) was added followed by the addition of an aqueous solution of ammonia. The mixture was allowed to stir for 10 min in order to remove all the copper salts trapped inside the dendrimer. The organic phase was washed twice with water, dried over sodium sulfate, and filtered, and the solvent was removed *in vacuo*. The product was then washed with methanol to remove the excess alkyne and precipitated from DCM with methanol and then with pentane, giving a yellow powder (0.134 g, yield 80%).

^{1}H NMR ($CDCl_3$, 200 MHz), δ_{ppm}: 7.02 (s, 9H of triazole), 4.53, 4.24, 4.20, and 4.11 (s, 108H, Cp sub.), 3.94 (s, 45H, Cp), 3.74 (s, 18H, SiCH_2-triazole), 1.55 (s, 18H, $CH_2CH_2CH_2Si$), 1.01 (s, 18H, $CH_2CH_2CH_2Si$), 0.56 (s, 18H, $CH_2CH_2CH_2Si$), 0.03 (s, 54H, $Si(CH_3)_2$). ^{13}C NMR ($CDCl_3$, 50 MHz), δ_{ppm}: 145.6 (*Cq* core), 144.9 (*Cq* of triazole), 121.3 (*CH* of arom. core), 120.4 (*CH* of triazole), 84.9, 82.6, and 70.7 (*Cq* of Cp sub.), 69.4, 67.9, 67.4, 67.2, 66.1 (*CH* of Cp sub.), 69.1 (*CH* of Cp), 43.8 ($CqCH_2CH_2CH_2Si$), 41.7 ($CqCH_2CH_2CH_2Si$), 40.6 (triazole-CH_2Si), 17.5 ($CqCH_2CH_2CH_2Si$), 14.8 ($CqCH_2CH_2CH_2Si$), −3.7 ($Si(CH_3)_2$). MALDI-TOF-MS (*m*/*z*): calcd 5086.98; found 5087.11 (M+, 100%). Anal. Calcd for $C_{261}H_{291}Fe_{18}N_{27}Si_9$: C 61.56, H 5.72. Found: C 60.58, H 7.91.

Synthesis of 8. Ethynylbiferrocene (**3**; 0.127 g, 0.324 mmol) and G_1-27-N_3 (0.050 g, 0.008 mmol) were dissolved in oxygen-free THF (50 mL), and oxygen-free water (50 mL) was added. A solution of 1 M $CuSO_4$ (1 equiv per branch) was added at 0 °C, with subsequent dropwise addition of a freshly prepared solution of 1 M sodium ascorbate (2 equiv per branch). The color of the brown solution immediately changed to orange. The reaction mixture was allowed to stir for 24 h under N_2 at rt. Then DCM (100 mL) was added followed by the addition of an aqueous solution of ammonia. The mixture was allowed to stir for 10 min in order to remove all the copper salts trapped inside the dendrimer. The organic phase was washed twice with water, dried over sodium sulfate, and filtered, and the solvent was removed *in vacuo*. The product was then washed with methanol to remove the excess alkyne and precipitated from DCM with methanol and then with pentane, giving a yellow powder (0.114 g, yield 85%).

^{1}H NMR ($CDCl_3$, 200 MHz), δ_{ppm}: 7.12 (d, 18H, arom.), 6.95 (s, 27H of triazole), 6.88 (d, 18H, arom.), 4.52, 4.23, 4.18, and 4.10 (s, 324H, Cp sub.), 3.94 (s, 135H, Cp), 3.74 (s, 54H, SiCH_2-triazole), 3.48 (s, 18H, CH_2OAr), 1.55 (s, 72H, $CH_2CH_2CH_2Si$), 1.04 (s, 72H, $CH_2CH_2CH_2Si$), 0.55 (s, 72H, $CH_2CH_2CH_2Si$), 0.05 (s, 216H, $Si(CH_3)_2$). ^{13}C NMR ($CDCl_3$, 50 MHz), δ_{ppm}: 158.9 (arom. OCq), 144.9 (*Cq*-triazole), 138.6 (arom. *Cq*), 127.9 and 113.4 (arom. *CH* of dendron), 120.1 (*CH* of triazole), 84.8, 82.4, and 70.7 (*Cq* of Cp sub.), 69.4, 69.0, 67.4, 67.2, and 66.1 (*CH* of Cp sub.), 69.1 (*CH* of Cp), 60.3 (CH_2OAr), 42.8 ($CqCH_2CH_2CH_2Si$), 41.8 ($CqCH_2CH_2CH_2Si$), 40.6 (triazole-CH_2Si), 17.3 ($CqCH_2CH_2CH_2Si$), 14.7 ($CqCH_2CH_2CH_2Si$), −3.8 ($Si(CH_3)_2$). Anal. Calcd for $C_{882}H_{1029}Fe_{54}N_{81}O_9Si_{36}$: C 62.55, H 6.12. Found: C 62.20, H 6.46.

Synthesis of 9. Ethynylbiferrocene (**3**; 0.116 g, 0.294 mmol) and G_2-81-N_3 (0.050 g, 0.003 mmol) were dissolved in oxygen-free THF (50 mL), and oxygen-free water (50 mL) was added. A solution of 1 M $CuSO_4$ (1 equiv per branch) was added at 0 °C, with subsequent dropwise addition of a freshly prepared solution of 1 M sodium ascorbate (2 equiv per branch). The color of the brown solution immediately changed to orange. The reaction mixture was allowed to stir for 24 h under N_2 at rt. Then DCM (100 mL) was added followed by the addition of an aqueous solution of ammonia. The mixture was allowed to stir for 10 min in order to remove all the copper salts trapped inside the dendrimer. The organic phase was washed twice with water, dried over sodium sulfate, and filtered, and the solvent was removed *in vacuo*. The product was then washed with methanol to remove the excess alkyne and precipitated from DCM with methanol and then with pentane, giving a yellow powder (0.103 g, yield 81%).

^{1}H NMR ($CDCl_3$, 200 MHz), δ_{ppm}: 7.13 (d, 72H, arom.), 6.96 (s, 81H of triazole), 6.88 (d, 72H, arom.), 4.53, 4.23, 4.20, and 4.11 (s, 972H, Cp sub.), 3.94 (s, 405H, Cp), 3.74 (s, 162H, SiCH_2-triazole), 3.53 (s, 72H, CH_2OAr), 1.57 (s, 234H, $CH_2CH_2CH_2Si$), 1.04 (s, 234H, $CH_2CH_2CH_2Si$), 0.57 (s, 234H, $CH_2CH_2CH_2Si$), 0.08 (s, 702H, $Si(CH_3)_2$). ^{13}C NMR ($CDCl_3$, 50 MHz), δ_{ppm}: 159.1 (arom. OCq), 144.9 (*Cq*-triazole), 138.7 (arom. *Cq*), 127.1 and 113.6 (arom. *CH* of dendron), 120.1 (*CH* of triazole), 85.1, 82.7, and 70.8 (*Cq* of Cp sub.), 69.4, 69.0, 67.9, 67.4, 67.2, and 66.2 (*CH* of Cp sub.), 69.1 (*CH* of Cp), 60.2 (CH2OAr), 43.0 ($CqCH_2CH_2CH_2Si$), 41.8 ($CqCH_2CH_2CH_2Si$), 40.6 (triazole-CH_2Si), 17.4 ($CqCH_2CH_2CH_2Si$), 14.9 ($CqCH_2CH_2CH_2Si$), −3.7 ($Si(CH_3)_2$). Anal. Calcd for $C_{2745}H_{3243}Fe_{162}N_{243}O_{36}Si_{117}$: C 62.74, H 6.22. Found: C 62.48, H 6.43.

Synthesis of 13. The tris-azido phenol dendron **12** (124.6 mg, 0.217 mmol, 1 equiv) and ethynylbiferrocene (**3**; 257 mg, 0.652 mmol, 3 equiv) were dissolved in 50 mL of THF, and 50 mL of water was added (1:1 THF/water). At 0 °C, $CuSO_4$ was added (162.7 mg, 0.652 mmol; 3 equiv; 1 M aqueous solution), followed by the dropwise addition of a freshly prepared solution of sodium ascorbate (258.3 mg, 1.304 mmol; 6 equiv; 1 M aqueous solution). The solution was allowed to stir for 24 h at rt. An aqueous solution of ammonia was added, and the mixture was allowed to stir for 10 min. The organic phase was washed twice with water, dried over sodium sulfate, and filtered, and the solvent was removed *in vacuo*. The product was washed with pentane in order to remove the excess of **3**; then it was precipitated in pentane twice. The product was obtained as an orange powder (0.305 g, yield: 80%).

^{1}H NMR ($CDCl_3$, 300 MHz), δ_{ppm}: 7.05 (3H, *CH* trz), 6.85 and 6.74 (4H, *CH* arom.), 4.61, 4.23, 4.17, and 4.80 (51H, Cp of BiFc), 3.74 (6H, SiCH_2trz), 1.65 (6H, $CH_2CH_2CH_2Si$), 1.01 (6H, $CH_2CH_2CH_2Si$), 0.53 (6H, $CH_2CH_2CH_2Si$), 0.05 (18H, $Si(CH_3)_2$). ^{13}C NMR ($CDCl_3$, 75 MHz) δ_{ppm}: 154.3 (*Cq*OH), 145.0 (*Cq* of trz), 127.2 and 115,2 (*CH* arom.), 120.2 (*CH* of trz), 85.0, 82.6, 70.8 (*Cq* of Cp sub.), 69.5, 69.1, 67.5, 67.3, 66.2 (*CH* of Cp sub.), 69.2 (*CH* of Cp), 43.0 ($CqCH_2CH_2CH_2Si$), 41.7 (*Cq*$CH_2CH_2CH_2Si$), 40.8 (trz-CH_2Si), 17.4 ($CqCH_2CH_2CH_2Si$), 14.8 ($CqCH_2CH_2CH_2Si$), −3.8 ($Si(CH_3)_2$). IR (KBr): 3400 cm^{-1} (O−H), 3083 cm^{-1} (=C−H of trz and Cp), 818 cm^{-1} (C−H out-of-plane

dx.doi.org/10.1021/om501031u | *Organometallics* XXXX, XXX, XXX−XXX

bending of Fc). Maldi-TOF mass spectrum: calcd for $C_{91}H_{100}Si_3N_9Fe_6O$ 1755.3 Da, found 1755.7 Da.

Synthesis of 14. Dendron **13** (248 mg, 0.14 mmol, 1 equiv) was dissolved in 60 mL of acetone. Then 5.6 mg of Cs_2CO_3 (0.42 mmol, 3 equiv) and 0.0015 mL of propargyl bromide (0.21 mmol, 1.5 equiv) were added. The reaction mixture was heated under nitrogen at 60 °C for 24 h. The excess of propargyl bromide was removed *in vacuo*. After extraction of the product in diethyl ether/water, the organic phase was washed twice with water. The organic phase was evaporated, and the product was an orange-brown powder (0.225 g, yield: 90%). ^{1}H NMR (CD_3COCD_3, 300 MHz) δ_{ppm}: 7.50 (*CH* of trz), 7.26 and 6.96 (4H, C*H*, arom.), 4.74 (2H, CH_2O), 4.55, 4.31, 4.28, 4.13, 3.93 (51H, Cp of BiFc), 3.91 (6H, $SiCH_2N$), 3.07 (1H, OCH_2CCH), 1.68 (6H, $CH_2CH_2CH_2Si$), 1.21 (6H, $CH_2CH_2CH_2Si$), 0.62 (6H, $CH_2CH_2CH_2Si$), 0.10 (18H, $Si(CH_3)_2$). ^{13}C NMR (CD_3COCD_3, 75 MHz) δ_{ppm}: 155.2 (*Cq*O), 144.41 (*Cq* of trz), 127.48 and 114,53 (CH arom.), 121.12 (CH of trz), 85.11, 82.91, 71.98 (*Cq* of Cp sub.), 79.04 ($CqOCH_2CCH$), 77.38 ($CqOCH_2CCH$), 69.42, 69.25, 67.56, 67.00, 66.50 (CH of Cp sub.), 69.24 (CH of Cp), 55.79 ($CqOCH_2CCH$) 42.93 ($CqCH_2CH_2CH_2Si$), 41.48 ($CqCH_2CH_2CH_2Si$), 40.28 (trz-CH_2Si), 17.41 ($CqCH_2CH_2CH_2Si$), 14.76 ($CqCH_2CH_2CH_2Si$), −4.18 (Si-$(CH_3)_2$). IR (KBr): 3091 cm^{-1} (=C−H of trz and Cp), 2117 cm^{-1} (CCH), 823 cm^{-1} (C−H out-of-plane bending of Fc). Maldi-TOF mass spectrum: calcd for $C_{94}H_{102}Si_3N_9Fe_6O$ 1793.4 and for $C_{94}H_{102}Si_3N_9Fe_6OK$ 1832.3, found 1793.9 and 1832.9, respectively. Anal. Calcd for $C_{94}H_{103}Si_3N_9Fe_6O$: C 62.94, H 5.79. Found: C 62.63, H 5.81.

Synthesis of AuNPs 17. The azido-terminated AuNPS **16** (50 mg, 6×10^{-4} mmol, 1 equiv) and ethynylbiferrocene (**3**; 18 mg, 0.045 mmol, 75 equiv) were dissolved in 40 mL of distilled toluene. At rt, 20% of the catalyst **19** was added. The solution was allowed to stir for 48 h at rt. The solvent was distilled, and the black solid was washed with ethanol and subsequently with pentane to remove the catalyst and the excess of **3**. The product was solubilized again in DCM and filtered. The product was obtained as a black/brown oil (0.036 g, yield: 65%).

^{1}H NMR ($CDCl_3$, 300 MHz), δ_{ppm}: 6.97 (1H, trz), 4.53, 4.38, 4.34, 4.22, 4.16, 3.97, 3.91 (19H, Cp sub., Cp free and $-CH_2$trz), 1.54 (22H, $-CH_2$ of ligands with BiFc termini), 1.23 (22H, $-CH_2$ of ligands with methyl termini), 0.86 (3H, $-CH_3$). DLS: hydrodynamic diameter, $d = 20 \pm 3$ nm. IR (KBr): disappearance of the N_3 band at 2097 cm^{-1}, 801 cm^{-1} (C−H out-of-plane bending of Fc). TEM: $d = 2.1 \pm 0.1$ nm. CV: $E_{1/2} = 0.48$ V, $\Delta E = 20$ mV, $i_a/i_c = 1$ and $E_{1/2} = 0.80$ V, $\Delta E = 30$ mV, $i_a/i_c = 0.9$.

Synthesis of AuNPs 18. The azido-terminated AuNPS **16** (50 mg, 6×10^{-4} mmol, 1 equiv) and dendron **14** (81 mg, 0.045 mmol, 75 equiv) were dissolved in 50 mL of distilled toluene. At rt, 20% of catalyst **19** was added, and the solution was allowed to stir for 24 h at rt. The solvent was distilled, and the black solid was washed with ethanol and subsequently with pentane to remove the catalyst and the excess of **3**. The product was solubilized again in DCM and filtered. The product was obtained as black-brown oil (0.060 g, yield: 77%).

^{1}H NMR ($CDCl_3$, 300 MHz), δ_{ppm}: 7.13−7.21 (4H, *CH* of triazoles and 4H, C*H* of Ar), 4.82 (2H, CH_2O of each dendron), 4.40, 4.23, 4.03, 3.74 (51H, Cp of BiFc-dendron), 3.48 (6H, $SiCH_2N$ of BiFc-dendron), 1.60 (6H, $CH_2CH_2CH_2Si$ of BiFc-dendron and 22H, $-CH_2$ of the alkyl BiFc-terminated chain), 1.27 (6H, $CH_2CH_2CH_2Si$ of BiFc-dendron and 22H, $-CH_2$ of the alkyl chain), 0.88 (3H, $-CH_3$), 0.54 (6H, $CH_2CH_2CH_2Si$ of each dendron), 0.05 (18H, $Si(CH_3)_2$ of BiFc-dendron). IR (KBr): disappearance of the N_3 band at 2097 cm^{-1}, 802 cm^{-1} (C−H out-of-plane bending of Fc). DLS: hydrodynamic diameter, $d = 23 \pm 4$ nm. TEM: $d = 2.0 \pm 0.1$ nm. CV: $E_{1/2} = 0.48$ V, $\Delta E = 50$ mV, $i_a/i_c = 0.7$ and $E_{1/2} = 0.86$ V, $\Delta E = 85$ mV, $i_a/i_c = 0.6$.

■ ASSOCIATED CONTENT

Supporting Information

General data, spectroscopic data (NMR, UV−visible, IR), MALDI-TOF mass spectra, and cyclic voltammograms. This material is available free of charge via the Internet at http://pubs.acs.org.

■ AUTHOR INFORMATION

Corresponding Author

*E-mail: d.astruc@ism.u-bordeaux1.fr.

Notes

The authors declare no competing financial interest.

■ ACKNOWLEDGMENTS

Helpful assistance and discussion with Claire Mouche (mass spectrometry) from the CESAMO, Université de Bordeaux, and financial support from the Université de Bordeaux, the Centre National de la Recherche Scientifique (CNRS), and the Agence Nationale de la Recherche (ANR PNANO-026) are gratefully acknowledged.

■ REFERENCES

(1) (a) Nguyen, P.; Gomez-Elipe, P.; Manners, I. *Chem. Rev.* **1999**, *99*, 1515−1548. (b) Abd-El-Aziz, A. S.; Bernardin, S. *Coord. Chem. Rev.* **2000**, *203*, 219−267. (c) Abd-El-Aziz, A. S.; Todd, E. K. *Coord. Chem. Rev.* **2003**, *246*, 3−52. (d) *Macromolecules Containing Metal and Metal-Like Elements, Organoiron Polymers*, Vol. 2; Abd-El-Aziz, A. S.; Carraher, C. E., Jr.; Pittman, C. U., Jr.; Sheats, J. E.; Zeldin, M., Eds.; Wiley-Interscience: NJ, 2003. (e) Abd-El-Aziz, A. S.; Manners, I. *J. Inorg. Organomet. Polym.* **2005**, *15*, 157−195. (f) *Frontiers in Transition-Metal Containing Polymers*; Abd-El-Aziz, A. S., Manners, I., Eds.; Wiley: New York, 2007.

(2) (a) Sheats, J. E.; Rausch, M. D. *J. Org. Chem.* **1970**, *35*, 3245−3248. (b) Madonik, A. M.; Astruc, D. *J. Am. Chem. Soc.* **1984**, *106*, 2437−2439. (c) Lacoste, M.; Varret, F.; Toupet, L.; Astruc, D. *J. Am. Chem. Soc.* **1987**, *109*, 6504−6506. (d) Desbois, M.-H.; Astruc, D.; Guillin, J.; Varret, F.; Trautwein, A. X.; Villeneuve, G. *J. Am. Chem. Soc.* **1989**, *111*, 5800−5809.

(3) (a) Manners, I. *Science* **2001**, *294*, 1664−1666. (b) Hudson, R. D. A. *J. Organomet. Chem.* **2001**, *637*−*639*, 47−69. (c) Wang, X.; Guérin, G.; Wang, H.; Wang, Y.; Manners, I.; Winnik, M. A. *Science* **2007**, *317*, 644−647. (d) Astruc, D. *Nat. Chem.* **2012**, *4*, 255−267. (e) Abd-El-Aziz, A. S.; Agatemor, C.; Etkin, N. *Macromol. Rapid Commun.* **2014**, *35*, 513−559. (f) Deraedt, C.; Rapakousiou, A.; Wang, Y.; Salmon, L.; Bousquet, M.; Astruc, D. *Angew. Chem., Int. Ed.* **2014**, *53*, 8445−8449. (g) Rapakousiou, A.; Deraedt, C.; Gu, H.; Belin, C.; Salmon, L.; Ruiz, J.; Astruc, D. *J. Am. Chem. Soc.* **2014**, *126*, 13995−13998.

(4) (a) Cowan, D. O.; Kaufman, F. *J. Am. Chem. Soc.* **1970**, *92*, 219−220. (b) Cowan, D. O.; Kaufman, F. *J. Am. Chem. Soc.* **1971**, *93*, 3889−3893. (c) Levanda, C.; Cowan, D. O.; Bechgaard, K. *J. Am. Chem. Soc.* **1975**, *97*, 1980−1981.

(5) (a) Cuadrado, I.; Casado, C. M.; Alonso, B.; Moran, M. L.; Jose, B. V. *J. Am. Chem. Soc.* **1997**, *119*, 7613−7614. (b) Nijhuis, C. A.; Dolatowska, K. A.; Ravoo, B. J.; Huskens, J.; Reinhoudt, D. N. *Chem.—Eur. J.* **2007**, *13*, 69−80. (c) Ochi, Y.; Suzuki, M.; Imaoka, T.; Murata, M.; Nishihara, H.; Einaga, Y.; Yamamoto, K. *J. Am. Chem. Soc.* **2010**, *132*, 5061−5069. (d) Wimbush, K. S.; Reus, W. F.; van der Wiel, W. G.; Reinhoudt, D. N.; Whitesides, G. M.; Nijhuis, C. A.; Velders, A. H. *Angew. Chem., Int. Ed.* **2010**, *49*, 10176−10180. (e) Villena, C.; Losada, J.; Garcia-Armada, P.; Casado, C. M.; Alonso, B. *Organometallics* **2012**, *31*, 3284−3291. (f) Wang, Y.; Rapakousiou, A.; Chastanet, G.; Salmon, L.; Ruiz, J.; Astruc, D. *Organometallics* **2013**, *32*, 6136−6146.

(6) (a) Yamada, M.; Nishihara, H. *Chem. Commun.* **2002**, 2578−2579. (b) Yamada, M.; Tadera, T.; Kubo, K.; Nishihara, H. *J. Phys. Chem. B* **2003**, *107*, 3703−3711. (c) Yamada, M.; Nishihara, H. *Langmuir* **2003**, *19*, 8050−8056. (d) Yamada, M.; Nishihara, H. *Eur. Phys. J. D* **2003**, *24*, 257−260. (e) Yamada, M.; Nishihara, H. *C. R. Chim.* **2003**, *6*, 919−934.

(7) (a) Casado, C. M.; Cuadrado, I.; Moran, M.; Alonso, B.; Garcia, B.; Gonzales, B.; Losada, J. *Coord. Chem. Rev.* **1999**, *185*−*6*, 53−79. (b) Casado, C. M.; Alonso, B.; Losada, J.; Garcia-Armada, M. P. In *Designing Dendrimers*; Campagna, S.; Ceroni, P.; Puntoriero, F., Eds.; Wiley: Hoboken, NJ, 2012; pp 219−262. (c) Astruc, D.; Liang, L.; Rapakousiou, A.; Ruiz, J. *Acc. Chem. Res.* **2011**, *45*, 630−640.

(8) Daniel, M. C.; Ruiz, J.; Nlate, S.; Blais, J.-C.; Astruc, D. *J. Am. Chem. Soc.* **2003**, *125*, 2617−2628.
(9) (a) Newkome, G. R.; Moorefield, C. N. *Chem. Rev.* **1999**, *99*, 1689−1746. (b) Hwang, S. H.; Shreiner, C. D.; Moorefield, C. N.; Newcome, G. R. *New J. Chem.* **2007**, *31*, 1192−1217. (c) de Jesus, E.; de Flores, J. C. *Ind. Eng. Chem. Res.* **2008**, *47*, 7968−7981. (d) Astruc, D.; Boisselier, E.; Ornelas, C. *Chem. Rev.* **2010**, *110*, 1857−1959. (e) Wang, D.; Astruc, D. *Coord. Chem. Rev.* **2013**, *257*, 2317−2334.
(10) (a) Valério, C.; Fillaut, J. L.; Ruiz, J.; Guittard, J.; Blais, J. C.; Astruc, D. *J. Am. Chem. Soc.* **1997**, *119*, 2588−2589. (b) Casado, C. M.; Cuadrado, I.; Alonso, B.; Moran, M.; Losada, J. *J. Electroanal. Chem.* **1999**, *463*, 87−92. (c) Alonso, B.; Garcia-Armada, P.; Losada, J.; Cuadrado, I.; Gonzales, B.; Cuadrado, C. M. *Biosens. Bioelectron.* **2004**, *19*, 1617−1625. (d) Losada, J.; Zamora, M.; Garcia-Armada, P.; Cuadrado, I.; Alonso, B.; Casado, C. M. *Anal. Bioanal. Chem.* **2006**, *385*, 1209−1217. (e) Garcia-Armada, P.; Losada, J.; Zamora, M.; Alonso, B.; Cuadrado, I.; Casado, C. M. *Bioelectrochemistry* **2006**, *69*, 65−73. (f) Villoslada, R.; Alonso, B.; Casado, C. M.; Garcia-Armada, P.; Losada, J. *Organometallics* **2009**, *28*, 727−733. (g) Martinez, M. G.; Alonso, B.; Casado, C. M.; Losada, J.; Armanda, M. P. G. *Electroanalysis* **2011**, *23*, 2888−2897. (h) Jimenez, A.; Armanda, M. P. G.; Losada, J.; VIllena, C.; Alonso, B.; Casado, C. M. *Sensors Actuat. B: Chem.* **2014**, *190*, 111−119.
(11) (a) Daniel, M. C.; Ruiz, J.; Blais, J. C.; Daro, N.; Astruc, D. *Chem.—Eur. J.* **2003**, *9*, 4371−4379. (b) Wang, Y.; Salmon, L.; Ruiz, J.; Astruc, D. *Nat. Commun.* **2014**, *5*, doi: 10.1038/ncomms4489.
(12) (a) Daniel, M. C.; Astruc, D. *Chem. Rev.* **2004**, *104*, 293−346. (b) Xia, Y.; Xiong, Y.; Lim, B.; Skabalak, S. E. *Angew. Chem., Int. Ed.* **2009**, *48*, 60−103. (c) Giljohann, D. A.; Seferos, D. S.; Daniel, W. L.; Massich, M. D.; Patel, P. C.; Mirkin, C. A. *Angew. Chem., Int. Ed.* **2010**, *49*, 3280−3294. (d) *Gold Nanoparticles for Physics, Chemistry, Biology*; Louis, C., Pluchery, O., Eds.; Imperial College Press: London, U.K., 2012.
(13) Shih, H. W.; Dong, T. Y. *Inorg. Chem.* **2004**, *43*, 645−649.
(14) (a) Kolb, H. C.; Finn, M. G.; Sharpless, K. B. *Angew. Chem., Int. Ed.* **2001**, *40*, 2004−2021. (b) Rostovtsev, V. V.; Green, L. G.; Fokin, V. V.; Sharpless, K. B. *Angew. Chem., Int. Ed.* **2002**, *41*, 2596−2599. (c) Tornøe, C. W.; Christensen, C.; Meldal, M. *J. Org. Chem.* **2002**, *67*, 3057−3064. (d) Franc, G.; Kakkar, A. *Chem. Commun.* **2008**, 5267−5276. (e) Meldal, M.; Tornøe, C. W. *Chem. Rev.* **2008**, *108*, 2952−3015. (f) Hein, J. E.; Fokin, V. V. *Chem. Soc. Rev.* **2010**, *39*, 1302−1315.
(15) (a) Crooks, R. M.; Zhao, M.; Sun, L.; Chechik, V.; Yeung, L. K. *Acc. Chem. Res.* **2001**, *34*, 181−190. (b) Scott, R. W. J.; Wilson, O. M.; Crooks, R. M. *J. Phys. Chem. B* **2005**, *109*, 692−718. (c) Deraedt, C.; Astruc, D. *Acc. Chem. Res.* **2014**, *47*, 494−503.
(16) Diallo, A. K.; Ornelas, C.; Salmon, L.; Ruiz, J.; Astruc, D. *Angew. Chem., Int. Ed.* **2007**, *46*, 8644−8648.
(17) (a) Myachina, G. F.; Konkova, T. V.; Korzhova, S. A.; Ermakova, T. G.; Pozdnyakov, A. S.; Sukhov, B. G.; Arsentev, K. Yu.; Likhoshvai, E. V.; Trofimov, B. A. *Dokl. Chem.* **2010**, *431*, 63−64. (b) Oldham, E. D.; Seelam, S.; Lema, C.; Aguilera, R. J.; Fiegel, J.; Rankin, S. E.; Knutson, B. L.; Lehmler, H. J. *Carbohydr. Res.* **2013**, *379*, 68−77. (c) Dallmann, A.; El-Sagheer, A. H.; Dehmel, L.; Mügge, C.; Griesinger, C.; Ernsting, N. P.; Brown, T. *Chem.—Eur. J.* **2011**, *17*, 14714−14717.
(18) (a) Djeda, R.; Rapakousiou, A.; Liang, L.; Guidolin, N.; Ruiz, J.; Astruc, D. *Angew. Chem., Int. Ed.* **2010**, *49*, 8152−8156. (b) Poppitz, E. A.; Hildebrandt, A.; Korb, N.; Lang, H. *J. Organomet. Chem.* **2014**, *752*, 133−140.
(19) Rosenberg, N.; Neuse, E. W. *J. Organomet. Chem.* **1966**, *6*, 76−85.
(20) Doisneau, G.; Balavoine, G.; Fillebeen-Khan, T. *J. Organomet. Chem.* **1992**, *425*, 113−117.
(21) Polin, J.; Schottenberger, H. *Org. Synth.* **1996**, *73*, 262−269.
(22) (a) Newkome, G. R.; Yao, Z.; Baker, G. R.; Gupta, V. K. *J. Org. Chem.* **1985**, *50*, 2003−2004. (b) Newkome, G. R. *Pure Appl. Chem.* **1998**, *70*, 2337−2343. (c) Narayanan, V. V.; Newkome, G. R. *Top. Curr. Chem.* **1998**, *197*, 19−33.
(23) (a) Moulines, F.; Astruc, D. *Angew. Chem., Int. Ed. Engl.* **1988**, *27*, 1347−1349. (b) Ruiz, J.; Lafuente, G.; Marcen, S.; Ornelas, C.; Lazare, S.; Cloutet, E.; Blais, J.-C.; Astruc, D. *J. Am. Chem. Soc.* **2003**, *125*, 7250−7257.
(24) Ornelas, C.; Cloutet, E.; Alves, S.; Astruc, D. *Angew. Chem., Int. Ed.* **2007**, *46*, 872−877.
(25) Ruiz, J.; Astruc, D. *C. R. Acad. Sci.* **1998**, *t. 1, Sér. IIc*, 21−27.
(26) (a) Flanagan, J. B.; Margel, S.; Bard, A. *J. Am. Chem. Soc.* **1978**, *100*, 4248−4253. (b) Sutton, J. E.; Sutton, P. M.; Taube, H. *Inorg. Chem.* **1979**, *18*, 1017−1024. (c) Richardson, D. E.; Taube, H. *Coord. Chem. Rev.* **1984**, *60*, 107−129. (d) Barrière, F.; Geiger, W. E. *Acc. Chem. Res.* **2010**, *43*, 1030−1039.
(27) Gorman, C. B.; Smith, B. L.; Parkhurst, H.; Sierputowska-Gracz, H.; Haney, C. A. *J. Am. Chem. Soc.* **1999**, *121*, 9958−9966.
(28) Amatore, C.; Bouret, Y.; Maisonhaute, E.; Goldsmith, J. I.; Abruna, H. D. *Chem.—Eur. J.* **2001**, *7*, 2206−2226.
(29) Sartor, V.; Djakovitch, L.; Fillaut, J.-L.; Moulines, F.; Neveu, F.; Marvaud, V.; Guittard, J.; Blais, J.-C.; Astruc, D. *J. Am. Chem. Soc.* **1999**, *121*, 2929−2930.
(30) (a) Fleming, D. A.; Thode, C. J.; Williams, M. E. *Chem. Mater.* **2006**, *18*, 2327−2334. (b) Thode, C. J.; Williams, M. E. *J. Colloid Interface Sci.* **2008**, *320*, 346−352.
(31) Liang, L.; Ruiz, J.; Astruc, D. *Adv. Synth. Catal.* **2011**, *353*, 3434−3450.
(32) Zhao, P.; Grillaud, M.; Salmon, L.; Ruiz, J.; Astruc, D. *Adv. Synth. Catal.* **2012**, *354*, 1001−1011.
(33) Brust, M.; Walker, M.; Bethell, D.; Sciffrin, D. J.; Whyman, R. *J. Chem. Soc., Chem. Commun.* **1994**, *7*, 801−802.
(34) Leff, D. V.; Ohara, P. C.; Heath, J. R.; Gelbart, W. M. *J. Phys. Chem.* **1995**, *99*, 7036−7041.
(35) Wuelfing, W. P.; Gross, S. M.; Miles, D. T.; Murray, R. W. *J. Am. Chem. Soc.* **1998**, *120*, 12696−12697.

Partie 3

Conception de dendrimères polycationiques de cobalticénium et de FeCp(mésitylène)

Partie 3

Conception de dendrimères polycationiques de cobalticénium et de FeCp(mésitylène)

Introduction

Cette partie concerne la synthèse par la méthode “click” CuAAC de dendrimères contenant plusieurs cations triazolylmétallocényles en terminaison développant des nanomatériaux à propriétés polyélectroniques, c’est-à-dire permettant de transférer plusieurs électrons au même potentiel (approximativement) avec des valeurs de potentiels redox variant en fonction du biométal (Fe, Co) et des ligands (Cp, arène) utilisés. En même temps, la présence du groupement triazolyle confère aux systèmes des propriétés spécifiques sur le plan de la reconnaissance redox et de l’influence électronique sur le centre redox voisin.

Dans un premier chapitre, les réactions click catalysées au Cu^{I} de l’éthynyl-cobalticénium avec un dendron tris-azoture et trois générations de dendrimères polyazoture sont développées. La montée en génération, c'est-à-dire l’augmentation du nombre de trz-Cob^{+} du dendron (n = 3) au plus grand dendrimère G_2 (n = 81) étudiée par plusieurs techniques, procure à ces molécules des propriétés différentes (comme par exemple la solubilité). La spectroscopie UV-visible montre la croissance de nombres d’unités qui est analogue à la croissance du coefficient d’extinction molaire, ainsi que les études statistiques d’AFM qui ont fourni une preuve claire de la progression de la taille lors de la progression en génération du dendrimère. Par voltammètrie cyclique (VC), il est démontré que le solvant joue un rôle notable concernant la réversibilité de la vague $Co^{III/II}$. En outre la VC indique que la réversibilité de la deuxième vague $Co^{II/I}$ dépend de la génération du dendrimère. La possibilité de reconnaissance de l’anion H_2PO_4 qui est un fragment du *co*-enzyme ATP^{2-} par le dendrimère G_2 est également mis en évidence.

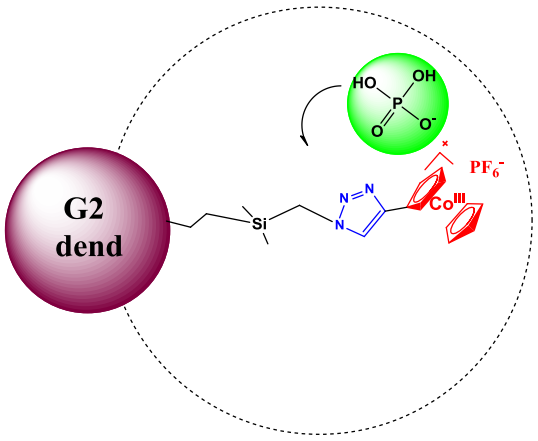

Schéma. Motifs du chapitre 3.1.

Les dendrimères de FeCp(mésitylène) ont aussi été synthétisés par réaction click CuAAC malgré leur sensibilité à la lumière visible et aux solvants coordinants (Chapitre 3.2) et les études rédox de ces dendrimères sont détaillées ici.

Au chapitre 3.3 nous présentons la synthèse de poly-cobalticénium dendritiques par une différente méthode, celle de la réaction de hydroamination. Ces études sont réalisées dans le cadre d'une collaboration avec Dr.Wang Yanlan et sont présentées en cette partie.

Inorganic Chemistry

Article

pubs.acs.org/IC

'Click' Synthesis and Redox Properties of Triazolyl Cobalticinium Dendrimers

Amalia Rapakousiou, Yanlan Wang, Colette Belin, Noël Pinaud, Jaime Ruiz, and Didier Astruc*

ISM, UMR CNRS N° 5255, Univ. Bordeaux 1, 33405 Talence Cedex, France

Supporting Information

ABSTRACT: The derivatization of macromolecules with redox-stable groups is a challenge for molecular electronics applications. The large majority of redox-derivatized macromolecules involve ferrocenes, and there are only a few reports with cobalticinium. We report here the first click derivatization of macromolecules with the cobalticinium redox group using ethynylcobalticinium hexafluorophosphate, **1**. Cu^{I} catalysis was used for these selective click metallodendrimer syntheses starting from **1** and providing the tripodal dendron **3** that contains three 1,2,3-triazolylcobalticinium termini and a phenol focal point and the dendrimers of generations 0, 1, and 2 containing 9, 27, and 81 triazolylcobalticinium units for the dendrimers **4**, **5**, and **6**, respectively. Atomic force microscopy (AFM) statistical studies provided the progression of height upon increase of dendrimer generation. Cyclic voltammetry studies in MeCN and dimethylformamide (DMF) show the solvent-dependent reversibility of the $Co^{III/II}$ wave (18e/19e) and generation dependent reversibility of the $Co^{II/I}$ (19e/20e) wave in DMF. The $H_2PO_4^-$ anion is only recognized by the largest metallodendrimer **6** by a significant cathodic shift of the $Co^{III/II}$ wave.

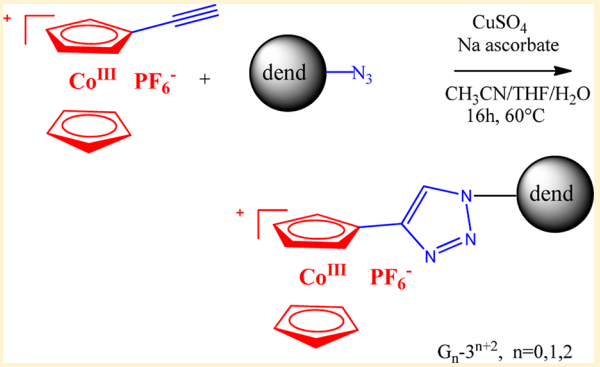

INTRODUCTION

Cobalticinium salts[1] have been the subject of attention for their useful electrochemistry and electron-transfer chemistry. They present a relative stability of three oxidation states, including the 19-electron neutral cobaltocene[1,2] and the very electron rich 20-electron cobaltocene anion.[3] When redox-reversible transition-metal complexes are linked to nanosystems, they undergo chemically and electrochemically reversible transfer of a large number of electrons, and these multiple redox processes are useful for nanodevices behaving as nanobatteries,[4] redox sensing,[5] and biosensing,[6] modified electrode surfaces[7] and redox catalysis.[8] Poly cobalticinium receptors were extensively studied by Beer et al. for anion recognition,[5] and various cobalticinium polymers obtained either by ring-opening cobaltocenophane[9] or from cobalticinium carboxylic acid as a side group[10] have been reported.

Metallodendrimers have a rich chemistry that has been extensively reviewed.[11] The dendritic structures offer the opportunity of introduction of many redox centers at the periphery of the molecular frame, allowing multiple possibilities of functionalization.[12] This concept has been widely studied with ferrocene dendrimers.[13] However, cobalticinium dendrimers are much less developed even though they have been already reported by several groups.[14] These metallodendritic syntheses have systematically used cobalticinium carboxylic acid. Click methodology,[15] in particular the copper catalyzed azide−alkyne cycloaddition (CuAAC) forming 1,2,3 triazoles (trz),[16] however, has recently appeared as one of the most powerful and practical means to form such nanoassemblies.[17] Ferrocenyl dendrimers have been synthesized in this way,[18] and advantage of the introduction of trz ligands on the dendritic tethers has appeared as a powerful means to stabilize palladium[19] and gold[20] nanoparticles with remarkable catalytic[19] and sensor properties.[18]

Recently, complexes containing a single trz-cobalticinium unit have been synthesized from ethynylcobalticinium, verifying the possibility to link cobalticinium to other groups in this way by CuAAC click chemistry.[21] Herein we now report the use of the click CuAAC strategy using ethynyl cobalticinium to synthesize a metallodendron with 1→3 connectivity[22] and three generations (G0, G1, and G2) of cobalticinium dendrimers **4**, **5**, and **6** (Chart 1) with the same connectivity containing respectively 9, 27, and 81 cobalticinium termini. Cyclic voltammetry studies of these new redox-active metallodendrimers including redox recognition of the $H_2PO_4^-$ anion with positive dendritic effects[23] are also reported here.

RESULTS AND DISCUSSION

1. Synthesis of the Dendrimers Series and Phenol-triallyl Dendron. The construction for the G0, G1, and G2 chloromethyl(dimethyl)silyl dendrimers with 1→3 connectivity[22] were synthesized as described previously upon $CpFe^+$-induced triallylation of mesitylene and *p*.methoxytoluene followed, after decomplexation, by hydrosilylation of the polyallyl dendritic cores and dendron using chloromethyldimethylsilane and iteration using a Williamson reaction with the

Received: March 26, 2013
Published: May 21, 2013

Chart 1

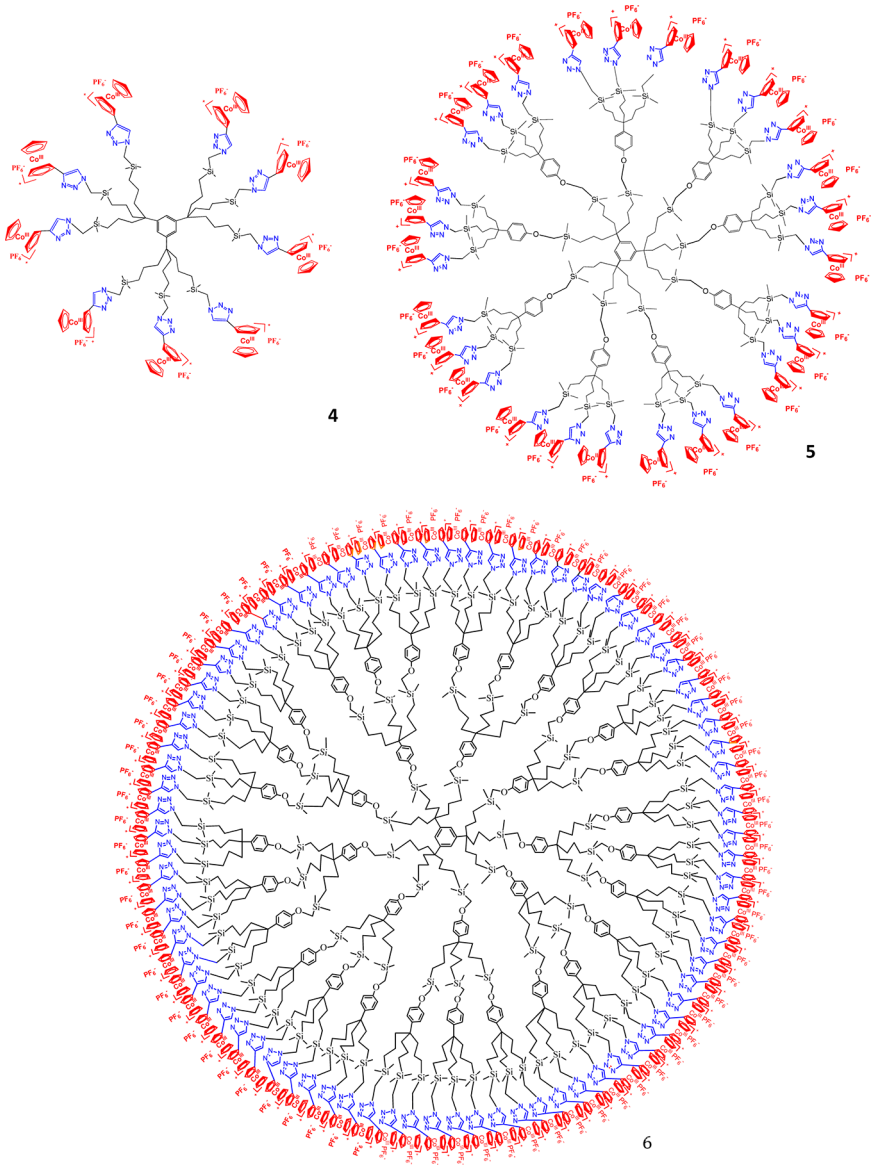

Scheme 1. Click Synthesis of the tris-trz-Cobalticinium Phenoltriallyl Dendron 3

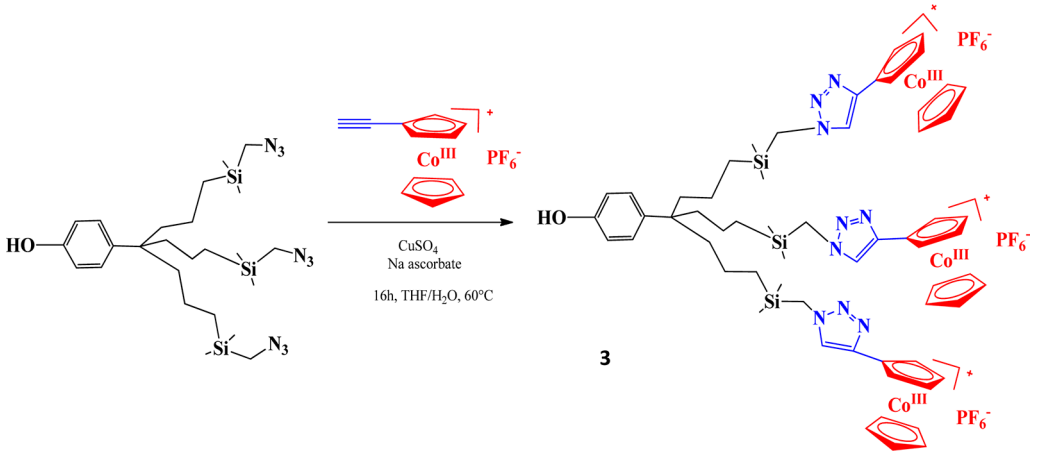

tribranched phenol dendron (phenol triallyl).[24] The terminal chloro groups were then substituted by azido groups by reaction with sodium azide providing azido-terminated dendrimers and dendron.[18]

dx.doi.org/10.1021/ic400747y | Inorg. Chem. 2013, 52, 6685−6693

2. Click Synthesis of the Dendron and Dendrimers. Ethynylcobalticinium **1** was synthesized as previously described in 60% overall yield from cobalticinium hexafluorophosphate.[25] The uncatalyzed Huisgen reaction[26] between **1** and benzyl azide conducted in the absence of copper catalyst in 1,2 dimethoxyethane at 80 °C was completed in 2 days giving 92% of the 1−4 disubstituted triazole **2 (a)** and only 8% of the 1−5 disubstituted triazole **2 (b)** (see Supporting Information). The selectivity for the 1−4 isomer is remarkable under these conditions; it is likely due to steric reasons favoring the 1−4 substitution.[23] The mixture of isomers was characterized by ^{1}H, ^{13}C, and ^{31}P NMR, IR, UV−vis, and ESI mass spectrometry. Comparing to the CuAAC click reaction with the use of copper catalyst ($CuSO_4$ + ascorbic acid), however, the latter does not give isomerization at all, but only the 1−4 disubstituted trz product, and the reaction is much more rapid. Consequently, the catalyzed CuAAC reaction of **1** with the azido-terminated dendron and dendrimers was appropriate for the metallodendrimer assembly. Thus the syntheses of the trz-cobalticinium dendron **3** and dendrimers **4**, **5**, **6** were carried out using $CuSO_4$/sodium ascorbate between the terminal alkyne **1** and the tris-azido phenoltriallyl dendron (Scheme 1) and three generations G0, G1, and G2 of dendrimers dend-N_3 containing 3, 9, 27, 81 azido termini respectively (Scheme 2). The solvents in each reaction were chosen to

Scheme 2. Click Synthesis of the Dendrimers 4, 5, and 6 with 9, 27, and 81 trz-Cobalticinium Termini, Respectively

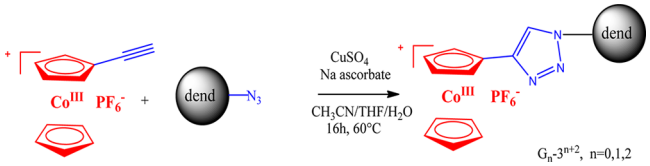

achieve the solubility of the final product, because the polycationic cobalticinium dendrimers were soluble only in high polarity solvents, the reaction of the dendron was carried out in THF/H_2O, that of **4** in CH_3CN/H_2O and those of **5** and **6** in a mixture of THF/CH_3CN/H_2O, because the azido-terminated precursors were not soluble in CH_3CN. The temperature of the reaction was 60 °C, and the reactions were left stirring during 16 h. The reactions needed stoichiometric rather than catalytic amounts of Cu^{I} because of encapsulation of Cu^{I} by coordinating to the resulting trz ligand, as previously encountered with ferrocenyl analogues.[18,27] The copper salt was finally removed as $[Cu(NH_3)_2(H_2O)_2]$ $[SO_4]$ by adding an aqueous solution of NH_3 that was left stirring for 15 min. The resulting tris-trz-cobalticinium terminated dendron and trz-cobalticinium dendrimers were purified, after workup, by precipitation in diethyl ether as orange powder. They were isolated as orange-red products in high yields. They were characterized by ^{1}H, ^{13}C, and ^{29}Si NMR, IR, UV−vis., DOSY NMR, MALDI-TOF mass spectrometry, AFM measurements, cyclic voltammetry, and elemental analysis.

3. Characterizations. The characterization of the dendritic cobalticinium salts depends on their solubility that varies with the number of cobalticinium moieties in the molecule. The trz-cobalticinium group is very hydrophilic, and it is soluble only in polar solvents. As the number of trz-cobalticinium groups increases in a molecule, the polarity of the solvent in which it can be solubilized also increases. Indeed the monomers **2 (a)**, **2 (b)** can be dissolved in dichloromethane, tetrahydrofuran (THF), acetone, acetonitrile, and DMF, whereas the dendrimer **6** can be solubilized only in very polar solvents such as CH_3CN, DMF, and DMSO. The solubility of the products is summarized in Table 1.

Table 1. Solubilities of the trz-Cobalticinium Hexafluorophosphate Derivatives 2 (a), 3, 4, 5, and 6 as a Function of the Number of trz-Cobalticinium Termini, at 25°C[a]

product	CH_2Cl_2	THF	acetone	CH_3CN/DMF
2 (a)	+	+	+	+
3	−	+	+	+
4	−	−	+	+
5	−	−	+	+
6	−	−	−	+

[a] +: very soluble; −: insoluble.

The infrared spectra are a very useful tool to monitor the click reactions, because the characteristic peak of the azido groups at about 2094 cm^{-1} disappears at the end of the reactions confirming that the azido groups are replaced by the 1,2,3-triazole groups. The characteristic absorption of the PF_6 anion of these trz-cobalticinium products shows a strong band in the range 836−838 cm^{-1}. The absorptions due to the =C−H stretching of the triazole and Cp groups of the trz-cobalticinium unit are found in the range 3118−3127 cm^{-1} (Figure 1).

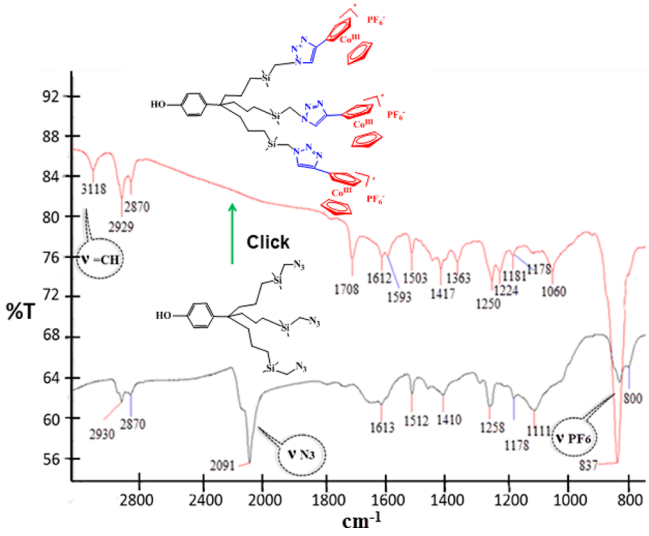

Figure 1. IR spectra of the tris-azido phenoltriallyl precursor and product **3** after the CuAAC click reaction.

NMR spectroscopy confirms the structure of the trz-cobalticinium products. Particularly, in ^{1}H NMR the formation of the trz ring is clearly shown by the appearance of the peaks around 8.4 ppm (in CD_3COCD_3) for the products **3**, **4**, and **5**, and around 8.0 (in CD_3CN) for the product **6**. In all the cases, the peak of $SiCH_2$-N_3 at 2.7−2.8 ppm has disappeared, whereas the appearance of the new peak of $SiCH_2$-trz takes place at about 4.1 ppm. The presence of the trz group is also confirmed by the appearance of the characteristic peaks of *Cq* and CH of trz as well as $SiCH_2$-trz in the ^{13}C NMR spectra. The ^{29}Si NMR spectra of the dendrimers are very simple, showing one peak at 3.41 ppm (compounds **4** and **5**) and 3.50 ppm (compound **6**) for $SiCH_2$-trz and another smaller peak at 0.46 ppm that corresponds to $SiCH_2O$ for compounds **5** and **6**. Finally, the

dx.doi.org/10.1021/ic400747y | Inorg. Chem. 2013, 52, 6685−6693

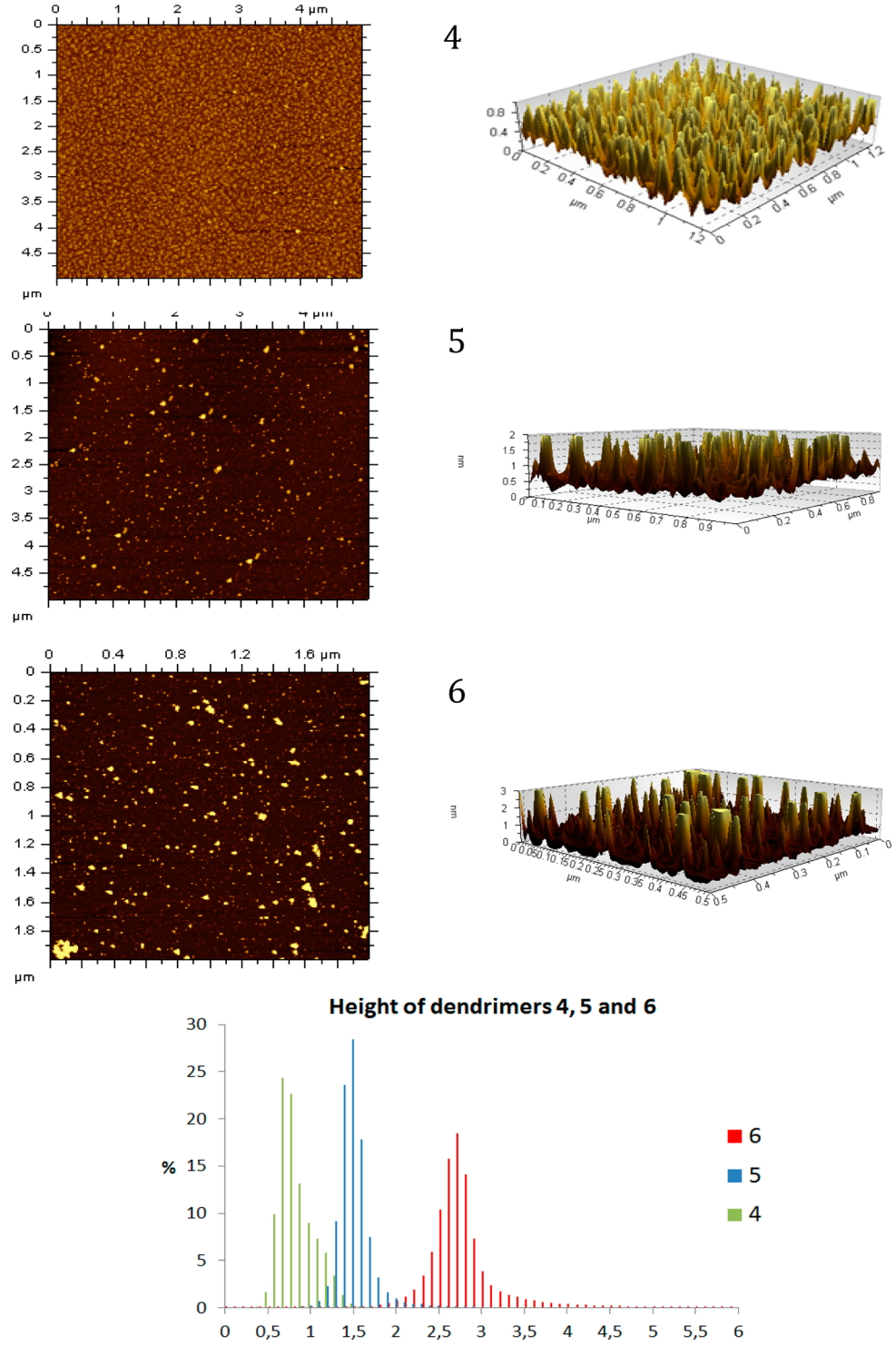

Figure 2. AFM images and statistical height distribution of dendrimers **4**, **5**, and **6**.

assignments of the number of protons in ^{1}H NMR show the expected ratio between the dendritic frame part and the cobalticinium part, including for the large dendrimer **6**.

Maldi-TOF mass spectrometry confirms the structure of the positively monocharged trz-cobalticinium dendron **3** (showing two PF_6 anions) and trz-cobalticinium dendrimer **4** (see Supporting Information). *Elemental analysis* also confirms the structures of **3**, **4**, **5**, and **6**.

UV−visible Spectroscopy. A strong absorption band is observed for all the dendrimers in the ultraviolet region peaking at 354.8 nm, whereas a less intense absorption shoulder is observed in the visible region peaking at about 427 nm. From the Lambert−Beer's law, we calculated the molar extinction coefficient ε for the compounds **3**, **4**, **5**, and **6**. Its value increases upon increase of dendrimer generation, which also confirms the progressivity of the trz-cobalticinium generations (**3**, **4**, **5**, and **6**). (For ε values: see the Supporting Information)

DOSY (diffusion-ordered spectroscopy) experiments were carried out for the dendrimers **4**, **5**, and **6**. The main goal of these experiments was to measure the diffusion coefficient D that was

dx.doi.org/10.1021/ic400747y | *Inorg. Chem.* 2013, 52, 6685−6693

extracted from the DOSY ^{1}H NMR spectra. The latter also reflect the purity of the products. For compound **4**, the average diffusion coefficient value obtained is $D = 2.85\ (\pm 0.1) \times 10^{-6}$ cm^2/s. In the case of the dendrimer **5** (27 branches), the calculated diffusion coefficient is $D = 2.58\ (\pm 0.1) \times 10^{-6}$ cm^2/s, whereas in the case of the dendrimer **6** (81 branches), the calculated diffusion coefficient is $D = 6.46\ (\pm 0.1) \times 10^{-7}$ cm^2/s.

In an effort to better characterize the three polycobalticinium dendrimers and their interaction with surfaces, and obtain a clearer evidence of the size progression, atomic force microscopy (AFM) studies have been conducted. Freshly cleaved mica surfaces (that have a negative surface charge density) have been used as clean imaging substrates. A diluted acetonitrile solution of each dendrimer was deposited on a mica surface by spin-coating (800−1000 rpm for one minute, 0.1% w/w). In their condensed phase, the dendrimers collapse onto the mica surface. The height of the dendrimer layer usually represents a monolayer, and the dendrimers agglomerate in large packages of variable sizes on the surface.[13] In our studies, the heights of the dendrimers were quite uniform. Therefore, statistical study of the height of each dendrimer by AFM analysis was obtained and provided a clear evidence of the size progression upon increase of dendrimer generation. (Figure 2).

Although both the DOSY ^{1}H NMR and AFM experiments yield dendrimer sizes, the two methods are not comparable, because the former provides a diameter that includes peripheral solvation or/and even eventually dendritic agglomerates in solution, whereas the latter gives the height (thicknesses) of a collapsed dendrimer in the condensed phase. The reproducible DOSY measuments indicated above leads to diameters of 4.8 nm for **4**, 5.6 nm for **5**, and 19.6 nm for **6** that are much larger than the AFM thicknesses indicated in the condensed phase for the reasons indicated above. In the present case, it is highly probable that interdendrimer ion-pairing intervenes for the formation of agglomerates in solution given the charged branch termini of the dendrimers, which increases the observed DOSY sizes in solution.

4. Cyclic Voltammetry Studies. The tris-triazolyl cobalticinium dendron **3** and the three generations of triazolyl-cobalticinium dendrimers (compounds **4**, **5**, and **6**) were studied by cyclic voltammetry using decamethylferrocene as the internal reference.[28] The cyclic voltammograms (CVs) were recorded in acetonitrile and DMF, a good solubility being accessible with both solvents, and the results are gathered in Table 2. The first reduction wave of all the products corresponds to the reduction of cobalticinium to the 19-electron complex cobaltocene ($Co^{III/II}$), and the second wave corresponds to the reduction of cobaltocene to the 20-electron cobaltocenyl anion ($Co^{II/I}$). Both waves are single in acetonitrile and DMF, which can be explained by the weakness of the electrostatic factor between the redox sites of the metallodendrimers, these redox centers being far from one another and separated by long tethers.[29]

The first wave in both acetonitrile and DMF appears chemically and electrochemically reversible, a result similar to that obtained with the monomeric complex **2** (**a**).[21] The electrochemical reversibility involving equally all the redox groups is due to very fast rotation within the electrochemical time scale, where all the redox groups come close to the electrode provoking fast electron transfer between all the redox groups and the electrode,[30] and/or the electron-hopping mechanism.[31]

Adsorption during the cyclic voltammetry recording of dendrimer is common, and it is more marked with cationic dendrimers than with neutral ones. It is observed for the first wave only in acetonitrile, and it is marked for the high dendrimer

Table 2. Redox Potentials and Chemical (i_a/i_c) and Electrochemical ($E_{pa} - E_{pc} = \Delta E$) Reversibility Data for Compounds 2(a)−6[a]

		$Co^{III/II}$ [V]			$Co^{II/I}$ [V]		
	solvent	$E_{1/2}$	ΔE	i_a/i_c	E	ΔE	i_a/i_c
2 (a)[21]	MeCN	−0.75	0.060	1.0	$E_p = -1.76$	0	0
3	MeCN	−0.78	0.040	0.6	$E_p = -1.72$	0	0
3[b]	MeCN	−0.78	0.060	1.0			
3	DMF	−0.81	0.060	0.3	$E_p = -1.81$	0	0
4	MeCN	−0.74	0.030	0.5	$E_{1/2} = -1.65$	0.050	0.2
4[b]	MeCN	−0.74	0.065	1.1			
4	DMF	−0.81	0.060	0.7	$E_{1/2} = -1.79$	0.070	0.8
5	MeCN	−0.75	0.015	0.3	$E_{1/2} = -1.80$	0.010	0.3
5[b]	MeCN	−0.75	0.010	2.0			
5	DMF	−0.82	0.060	0.9	$E_{1/2} = -1.77$	0.060	1
6[b]	MeCN	−0.72	0.030	2.7			
6	DMF	−0.82	0.040	0.9	$E_{1/2} = -1.78$	0.050	0.7
6[b]	DMF	−0.82	0.040	1.0			

[a]Supporting electrolyte: [*n*-Bu_4N][PF_6] 0.1M; working and counter electrodes: Pt; reference electrode: Ag; internal reference: $FeCp^*_2$ ($Cp^* = \eta^5$-C_5Me_5); scan rate: 0.200 V s^{-1}. [b]Scanning until −1.0 V.

generations. This large adsorption phenomenon for the large dendrimers is due to the low solubility of the reduced neutral dendrimer in acetonitrile. The monomer and dendron compounds **2** (**a**) and **3** do not adsorb on the electrode. Adsorption begins with the nona-cobalticinium dendrimer **4** (i_a/i_c =1.1) and gradually increases as the generation number of dendrimer increases. In particular, the i_a/i_c value for dendrimers **5** (Figure 3) and **6** is 2.0 and 2.7 respectively (Table 2).

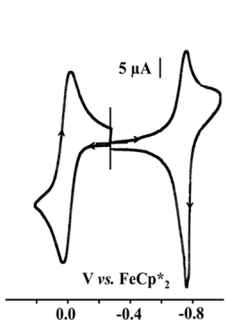

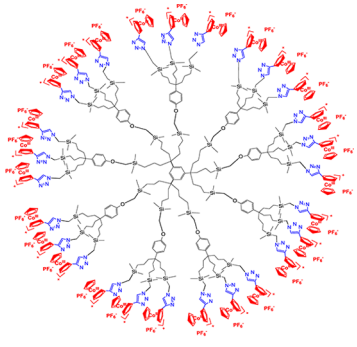

5

Figure 3. CV of **5** in CH_3CN. The wave at 0.0 V corresponds to the internal reference $FeCp^*_2$. Solvent: CH_3CN; reference electrode: Ag; working and counter electrodes: Pt; scan rate: 0.2 V/s; supporting electrolyte: [*n*-Bu_4N][PF_6].

The second wave for compound **3** is completely irreversible just like for the monomer **2** (**a**), whereas in dendrimers (**4**, **5**, and **6**) the situation changes. In acetonitrile, this second wave is reversible at the electrochemical time scale but chemically irreversible. This is due to partial degradation of the dendritic products during reduction ($Co^{II/I}$), caused by population of antibonding e^*_1 orbitals, which destabilizes the cobalt-ligand bonds in synergy with the solvent interaction.[32] This thermodynamic destabilization is indeed combined with kinetic destabilization when the solvent is a ligand that can easily displace the Cp ring, which is especially the case with MeCN. This chemical irreversibility is responsible for the appearance of a shoulder at the anode of the first wave during

dx.doi.org/10.1021/ic400747y | Inorg. Chem. 2013, 52, 6685−6693

oxidation. Upon scanning until less negative potentials in the same solvent, the first $Co^{III/II}$ wave is completely reversible, and no splitting is observed (Figure 4), showing that decomposition of the

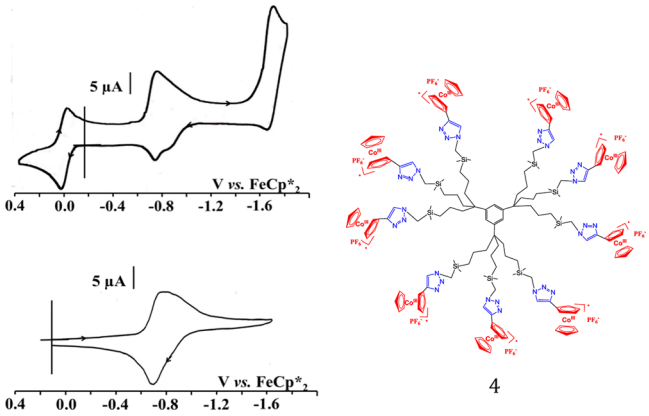

Figure 4. CV of **4** in CH_3CN. The wave at 0.0 V corresponds to the internal reference $FeCp^*_2$. Solvent: CH_3CN; reference electrode: Ag; working and counter electrodes: Pt; scan rate: 0.2 V/s; supporting electrolyte: $[n\text{-}Bu_4N][PF_6]$.

Co complex does not occur at the 19-electron level, but only upon scanning the 20-electron state. However, in DMF such degradation does not take place as the second wave appears both chemically and electrochemically reversible (Figure 5). Another observation is

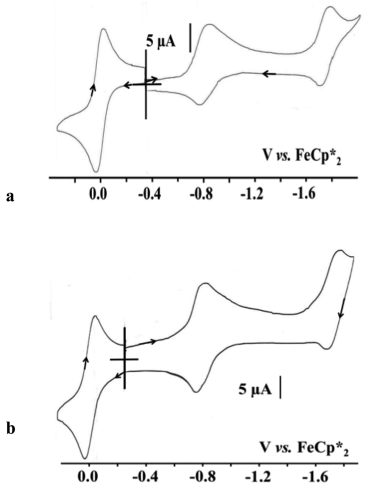

Figure 5. (a) CV of **4** in DMF. (b) CV of **5** in DMF. The wave at 0.0 V corresponds to the internal reference $FeCp^*_2$. Solvent: DMF; reference electrode: Ag; working and counter electrodes: Pt; scan rate: 0.2 V/s; supporting electrolyte: $[n\text{-}Bu_4N][PF_6]$.

that the envelope of the first redox wave is broad, whereas in the $Co^{II/I}$ wave that does not contain cationic species this phenomenon does not appear. Thus the broad first wave could be due to electrostatic interactions differentiating the various single electron-transfer steps, that is, the electrostatic interaction for the first electron transfer involves all the cationic charges, whereas that for the last electron transfer involves only one positive charge for the whole dendrimer. Interactions between the cationic centers and the counteranions and the solvent molecules are responsible for the variation of the energy engaged in the heterogeneous electron transfers.

Redox recognition of anions by cyclic voltammetry is possible with the triazolylcobalticinium dendrimers. Recognition and sensing of anions are of importance in many fields, ranging from environmental monitoring, biology, and industrial applications to clinical diagnostics. To investigate this property, the recognition of the H_2PO_4 anion as its $n\text{-}Bu_4N^+$ salt was probed. Such redox recognition has been first studied by Beer's group with polycobalticinium endoreceptors,[4] and extended by our group to dendritic exoreceptors.[23] Indeed, its addition to the electrochemical cell containing compound **6** provokes a splitting of the $Co^{III/II}$ CV wave for which the new part resulting from the addition of $[n\text{-}Bu_4N][H_2PO_4]$ is found at a potential 0.15 V more negative than the original one (Figure 6). The electrostatic

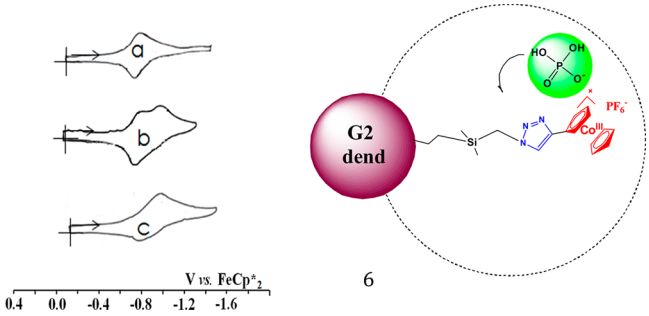

Figure 6. CVs of compound **6**: (a) In DMF, $[n\text{-}Bu_4N][PF_6]$ 0.1M; see Table 2 for data and conditions; (b) splitting of the reduction CV wave upon addition of $Bu_4NH_2PO_4$; (c) complete disappearance of the first wave upon addition of $Bu_4NH_2PO_4$.

binding of the anionic guest partly masks the positive charge, rendering the positively charged cobalticinium moiety more difficult to reduce to its neutral 19-electron form. Overall, the reasons for redox recognition combine the electrostatic and supramolecular interaction with dendritic (exoreceptor) effect. The supramolecular interactions are those of the hydrogen bonding between the OH groups of the $H_2PO_4^-$ anion and the nitrogen atoms of the trz group and eventually the interaction of oxygen atoms of the anion with the positively charged cobalt center (or eventually a chelating interaction involving both the trz and the Co center). The combined electrostatic and supramolecular interactions are not sufficient, however, to induce redox recognition in the present case (as in others involving monomers and small dendrimers), as demonstrated by the lack of redox recognition here with the trz-cobalticinium **2** (**a**), **3**, **4**, and **5**. A significant topological effect is required in synergy with the electrostatic and supramolecular effect to recognize the oxo-anions. This strong dendritic effect (i.e., the effect increases as the dendrimer generation increases) is only obtained here with the second-generation metallodendrimer **6**, whereas interestingly it is insufficient with the zeroth and first-generation dendrimers **4** and **5**. This confirms the positive dendritic effect in redox recognition, that is, the recognition improves as the dendrimer generation increases (note that we believe that in homogeneous catalysis, the dendritic effect with dendrimers terminated with catalysts is negative for steric reasons[33]). These trz-cobaticinium dendrimers are not adequate for $H_2PO_4^-$ anion titration, however, because the exact number of equivalents of the anion could not be calculated because of some precipitation occurring during addition of $[n\text{-}Bu_4N][H_2PO_4]$.

■ CONCLUDING REMARKS

The paucity of cobalticinium chemistry has largely favored the development of ferrocene-containing dendrimers and polymers.

dx.doi.org/10.1021/ic400747y | Inorg. Chem. 2013, 52, 6685−6693

The great interest in polycationic dendrimers and polymers has recently led to research on cobalticinium polymers especially favored by the cobaltocenophane ring-opening polymerization and the use of cobalticinium-carboxylic acid. Click chemistry introduced a decade ago was ideal for the synthesis of cobaltocenyl dendrimer and polymers, which has been achieved for dendrimers in this article. The redox-active click cobalticinium dendrimers also benefit from the location of a 1,2,3-triazolyl (trz) ring attached to the cobalticinium group. Previous work has shown the interest of the trz ring as a ligand that was very useful for the stabilization of catalytically active nanoparticles[19] in metallodendrimers and for sensing.[17] Thus the present click metallodendrimers that are the first cobalticinium dendrimers benefit from both the trz unit attached to the cobalticinium redox group allowing facile redox recognition of substrates interacting with this heterocycle and the positive charge on each dendrimer termini that should enable further supramolecular anion design and ion-pair interaction. These systems will thus serve as a basis for further research in these directions as well as the development of soft materials of interest. Reduction studies of the trz-cobalticinium monomers involving 19-electron species[34] should also be extended to trz-cobalticinium dendrimers and polymers to search for molecular battery materials. Such studies are currently underway in our laboratory.

EXPERIMENTAL SECTION

General Data. For general data including solvents, apparatuses, compounds, reactions, spectroscopies, and CV, see the Supporting Information. G*n* indicates the generation number *n*. The mononuclear compound **1** was synthesized according to ref 25.

General Procedure for the Click Synthesis of Polycobalticinium Dendron and Dendrimers. The compound **1** (1.5 equiv per branch) and the azido-terminated dendron or dendrimers (**3**, **4**, **5**, or **6**) were dissolved in degassed THF, CH_3CN or both, then degassed water was added and the reaction mixture was cooled to 0 °C. Then, an aqueous solution of $CuSO_4$ 1 M (1.1 equiv per branch) was added dropwise, followed by the dropwise addition of a freshly prepared solution of sodium ascorbate (2.2 equiv per branch) The color of the solution changed from orange to dark red upon addition of sodium ascorbate. The reaction mixture was allowed to stir for 16 h at 60 °C under nitrogen atmosphere. Then, the mixture of solvents was removed under vacuum, and 100 mL of nitromethane was added followed by the addition of an aqueous solution of ammonia. The mixture was allowed to stir for 15 min to remove all the copper salt trapped inside the dendron or dendrimer. The organic phase was washed twice with water, dried over sodium sulfate, filtered, and the solvent was removed under vacuum. Then the product was washed with THF to remove the excess of alkyne and precipitated from an acetone or acetonitrile solution in diethyl ether.

Tris-triazolylcobalticinium Dendron 3. The synthesis was carried out from ethynylcobalticinium **1** (406 mg, 1.134 mmol) and tris-azido phenoltriallyl dendron (144.6 mg, 0.252 mmol) using the above general procedure for click synthesis. The reaction was carried out in 60 mL of THF−40 mL of H_2O. The product **3** was obtained as an orange-red powder (400 mg). Yield: 96% ^{1}H NMR (1D 1H), (CD_3COCD_3, 400 MHz): δ_{ppm}: 8.39 (3H, C*H* of trz), 7.15 and 6.78 (4H, C*H* arom.), 6.42 (6H, C*H* of Cp sub.), 6.03 (6H, C*H* of Cp sub.), 5.73 (15H, C*H* of Cp), 4.12 (6H, SiCH_2-trz), 1.67 (6H, CH_2CH$_2$CH$_2$Si), 1.18 (6H, CH$_2$CH_2CH$_2$Si), 0.67 (6H, 18H, CH$_2$ CH$_2$ CH_2 Si), 0.11 (18H, Si(CH_3)$_2$). ^{13}C NMR (1D 1H), (CD_3COCD_3, 75 MHz): δ_{ppm}: 155.74 (*Cq*OH), 138.34 (*Cq*-trz), 128.14 and 115,63 (CH arom.), 125.77 (CH of trz), 97.02 (*Cq* of Cp sub.), 86.69 (CH of Cp), 85.29 (CH of Cp sub.), 81.52 (CH of Cp sub.), 43.74 (CqCH$_2$CH$_2$CH$_2$Si), 42.50 *Cq*CH$_2$CH$_2$CH$_2$Si), 41.67 (trz-CH$_2$Si), 18.14 (CqCH$_2$CH$_2$CH$_2$Si), 15.20 (CqCH$_2$CH$_2$CH$_2$Si), −3.82 (Si(CH$_3$)$_2$). MALDI-TOF-MS (*m*/*z*) of $C_{61}H_{77}Si_3N_9Co_3(PF_6)_2$: calc. 1503.29; found 1503.35. Anal. Calc. for $C_{61}H_{77}Si_3N_9Co_3(PF_6)_3(C_4H_8O)$: C 45.81, H 5.03; found: C 46.05 H 4.93.

Dendrimer 4. The synthesis was carried out from ethynylcobalticinium **1** (252 mg, 0.705 mmol) and G0−9N$_3$ (79.1 mg, 0.052 mmol) using the general procedure for click synthesis above. The reaction was carried out into 20 mL of CH_3CN−5 mL of H_2O. Product **4** was obtained as an orange-red powder (239 mg). Yield: 97% ^{1}H NMR (1D 1H), (CD_3COCD_3, 400 MHz): δ_{ppm}: 8.39 (9H, C*H* of trz), 7.14 (3H, C*H* of arom.core), 6.39 (18H, C*H* of Cp sub.), 5.99 (18H, C*H* of Cp sub.), 5.70 (45H, C*H* of Cp), 4.12 (18H, SiCH_2-trz), 1.76 (18H, CH_2CH$_2$CH$_2$Si), 1.23 (18H, CH$_2$CH_2CH$_2$Si), 0.71 (18H, 18H, CH$_2$CH$_2$CH_2Si), 0.10 (54H, Si(CH_3)$_2$). ^{13}C NMR (1D 1H), (CD_3COCD_3, 75 MHz): δ_{ppm}: 146.72 (*Cq* of arom.core), 138.41 (*Cq* of trz), 125.92 (CH of trz), 122.58 (CH of arom.core), 97.21 (*Cq* of Cp sub.), 86.78 (CH of Cp), 85.39, 81.59 (CH of Cp sub.), 44.84 (CqCH$_2$CH$_2$CH$_2$Si), 42.63 (*Cq*CH$_2$CH$_2$CH$_2$Si), 41.87 (trz-CH$_2$Si), 18.53 (CqCH$_2$CH$_2$CH$_2$Si), 15.56 (CqCH$_2$CH$_2$CH$_2$Si), −3.51 (Si(CH$_3$)$_2$). ^{29}Si NMR (CD_3COCD_3, 79.5 MHz): δ_{ppm}: 3.41 (9Si, *Si*CH$_2$trz). MALDI-TOF-MS (*m*/*z*) of $C_{171}H_{225}Si_9N_{27}Co_9(PF_6)_2$: calc. 3729.0; found 3729.1. Anal. Calc. for $C_{171}H_{219}Si_9N_{27}Co_9(PF_6)_9$: C 43.32, H 4.66; found: C 43.59 H 4.82.

Dendrimer 5. The synthesis was carried out from ethynylcobalticinium 1 (232 mg, 0.648 mmol) and G1-27N$_3$ (100.0 mg, 0.016 mmol) using the general procedure for click synthesis above. The reaction was carried out into 15 mL of CH_3CN−20 mL of THF and 5 mL of H_2O. Product **5** was obtained as an orange powder (202 mg). Yield: 80% ^{1}H NMR (1D 1H), (CD_3COCD_3, 400 MHz): δ_{pmp}: 8.37 (27H, C*H* of trz), 7.23, 6.91 (39H, C*H* of arom.core), 6.38 (54H, C*H* of Cp sub.), 5.97 (54H, C*H* of Cp sub.), 5.67 (135H, C*H* of Cp), 4.10 (54H, SiCH_2-trz), 3.60 (18H, SiCH_2O), 1.66 (72H, CH_2CH$_2$CH$_2$Si), 1.20 (72H, CH$_2$CH_2CH$_2$Si), 0.66 (72H, 18H, CH$_2$CH$_2$CH_2Si), 0.08 (216H, Si(CH_3)$_2$). ^{13}C NMR (1D 1H), (CD_3COCD_3, 75 MHz): δ_{ppm}: 160.05 (arom. O*Cq*), 139.76 (*Cq* of trz), 138.40 (*Cq* of arom.core), 128.02 and 114.34 (arom. CH), 125.92 (CH of trz), 97.35 (*Cq* of Cp sub.), 86.66 (CH of Cp), 85.27, 81.44 (CH of Cp sub.), 60.81 (CH$_2$OAr), 43.97 (CqCH$_2$CH$_2$CH$_2$Si), 42.77 (*Cq*CH$_2$CH$_2$CH$_2$Si), 41.67 (trz-CH$_2$Si), 18.26 (CqCH$_2$CH$_2$CH$_2$Si), 15.33 (CqCH$_2$ CH$_2$ CH$_2$ Si), −3.78 (Si(CH$_3$)$_2$). ^{29}Si NMR (CD_3COCD_3, 79.5 MHz): δ_{ppm}: 0.46 (9 Si, *Si*CH$_2$O), 3.41 (27Si, *Si*CH$_2$trz). Anal. Calc. for $C_{612}H_{786}Si_{36}N_{81}Co_{27}O_9(PF_6)_{27}$: C 46.11, H 4.97; found: C 45.98 H 5.12.

Dendrimer 6. The synthesis was carried out from ethynylcobalticinium 1 (218 mg, 0.608 mmol) and G2-81N$_3$ (100.0 mg, 0.005 mmol) using the general procedure for click synthesis above. The reaction was carried out into 15 mL of CH_3CN−20 mL of THF and 5 mL of H_2O. Product **6** was obtained as an orange powder (175 mg). Yield: 73% ^{1}H NMR (1D 1H), (CD_3CN, 400 MHz): δ_{ppm}: 8.04 (81H, C*H* of trz), 7.15, 6.82 (147H, C*H* arom.), 6.16 (162H, C*H* of Cp sub.), 5.74 (162H, C*H* of Cp sub.), 5.48 (405H, C*H* of Cp), 3.98 (162H, SiCH_2-trz), 3.50 (72H, SiCH_2O), 1.57 (234H, CH_2CH$_2$CH$_2$Si), 1.08 (234H, CH$_2$ CH_2 CH$_2$ Si), 0.56 (234H, 18H, CH$_2$CH$_2$CH_2Si), 0.01 (702H, Si(CH_3)$_2$). ^{13}C NMR (1D 1H), (CD_3CN, 75 MHz): δ_{ppm}: 160.45 (arom. O*Cq*), 140.60 (*Cq* of arom.core), 138.77 (*Cq* of trz), 128.66 and 114.82 (arom. CH), 126.07 (CH of trz), 97.30 (*Cq* of Cp sub.), 87.10 (CH of Cp), 85.70, 81.89 (CH of Cp sub.), 61.67 (CH$_2$OAr), 44.31 (CqCH$_2$CH$_2$CH$_2$Si), 42.92 (*Cq*CH$_2$CH$_2$CH$_2$Si), 42.31 (trz-CH$_2$Si), 18.61 (CqCH$_2$CH$_2$CH$_2$Si), 15.74 (CqCH$_2$CH$_2$CH$_2$Si), −3.35 (Si(CH$_3$)$_2$). ^{29}Si NMR (CD_3CN, 79.5 MHz): δ_{ppm}: 0.46 (36 Si, *Si*CH$_2$O), 3.50 (81Si, *Si*CH$_2$trz). Anal. Calc. for $C_{1935}H_{2514}Si_{117}N_{243}Co_{81}O_{36}(PF_6)_{81}(H_2O)_5$: C 46.81, H 5.12; found: C 47.00 H 5.16.

ASSOCIATED CONTENT

Supporting Information

General data, detailed experimental procedures, spectroscopic data for compounds, NMR, and MALDI-TOF mass spectra, and CVs. This material is available free of charge via the Internet at http://pubs.acs.org.

AUTHOR INFORMATION

Corresponding Author

*E-mail: d.astruc@ism.u-bordeaux1.fr.

Notes

The authors declare no competing financial interest.

■ ACKNOWLEDGMENTS

Helpful assistance and discussion with Claire Mouche (mass spectrometry), Jean-Michel Lanier (^{29}Si NMR) from the CESAMO, Université Bordeaux 1, and financial support from the Université Bordeaux 1, the Centre National de la Recherche Scientifique (CNRS) and the Agence Nationale de la Recherche (ANR) are gratefully acknowledged.

■ REFERENCES

(1) (a) Wilkinson, G. *J. Am. Chem. Soc.* **1952**, *74*, 6148−6149. (b) Wilkinson, G.; Pauson, P. L.; Cotton, F. A. *J. Am. Chem. Soc.* **1954**, *76*, 1970−1974. (c) Sheats, J. E.; Rausch, M. D. *J. Org. Chem.* **1970**, *35*, 3245−3249. (d) Sheats, E. *J. Organomet. Chem. Libr.* **1979**, *7*, 461−521. (e) Kemmit, R. D. W.; Russell, D. R. In *Comprehensive Organometallic Chemistry*; Pergamon Press: Oxford, U.K., **1982**; Vol *5*, Chapter 34.4.5.1, pp 244−248.

(2) (a) Connelly, N. J.; Geiger, W. E. *Chem. Rev.* **1966**, *96*, 877−910. (b) Geiger, W. E. *Organometallics* **2007**, *26*, 5738−5765.

(3) (a) Geiger, W. E. *J. Am. Chem. Soc.* **1974**, *96*, 2632−2634. (b) Geiger, W. E.; Bowden, W. L.; El Murr, N. *Inorg. Chem.* **1979**, *18*, 2358−2361.

(4) Astruc, D. *Nat. Chem.* **2012**, *4*, 255−267.

(5) (a) Beer, D. P.; Hesek, D.; Hodacova, J.; Stokes, S. E. *J. Chem. Soc., Chem. Commun.* **1992**, 270−272. (b) Beer, D. P.; Chen, Z.; Goulden, A. J.; Graydon, A.; Stokes, S. E.; Wear, T. *J. Chem. Soc., Chem. Commun.* **1993**, 1834−1836. (c) Beer, D. P.; Drew, M. G. B.; Hesek, D.; Jagessar, R. *J. Chem. Soc., Chem. Commun.* **1995**, 1187−1188.

(6) Losada, J.; Armada, M. P. G.; Zamora, M.; Alonso, B.; Cuadrado, I.; Casado, C. M. *Bioelectrochemistry* **2006**, *69*, 65−73.

(7) (a) Abruña, H. D. *Coord. Chem. Rev.* **1988**, *86*, 135−189. (b) Nishihara, H.; Noguchi, M.; Aramaki, K. *Inorg. Chem.* **1987**, *26*, 2862−2869. (c) Nishihara, H.; Asai, H.; Aramaki, K. *J. Chem. Soc., Faraday Trans.* **1991**, *87*, 1771−1777.

(8) Astruc, D. *Electron-Transfer and Radical Processes in Transition-Metal Chemistry*; VCH: New York, 1995; Chapter 7.

(9) (a) Mayer, U. F. J.; Charmant, J. P. H.; Rae, J.; Manners, I. *Organometallics* **2008**, *27*, 1524−1533. (b) Mayer, U. F. J.; Gilroy, J. B.; O'Hare, D.; Manners, I. *J. Am. Chem. Soc.* **2009**, *131*, 10382−10383. (c) Qiu, H.; Gilry, J. B.; Manners, I. *Chem. Commun.* **2013**, *49*, 42−44.

(10) (a) Ito, T.; Kenjo, T. *Bull. Soc. Chem. Jpn.* **1968**, *41*, 614−619. (b) Pittman, C. U.; Ayers, O. E.; McManus, S. P.; Sheats, J. E.; Whitten, C. E. *Macromolecules* **1971**, *4*, 360−362. (c) Casado, C. M.; Lobete, F.; Alonso, B.; Gonzalez, B.; Losada, J.; Amadr, U. *Organometallics* **1999**, *18*, 4960−4969. (d) Masakazu, K.; Ikuyoshi, T. *Nippon Kagakkai Koen Yokoshu* **2003**, *83*, 805. (e) Kondo, M.; Hayakawa, Y.; Miyazawa, M.; Oyama, A.; Unoura, K.; Kawaguchi, H.; Naito, T.; Maeda, K.; Uchida, F. *Inorg. Chem.* **2004**, *43*, 5801−5803. (f) Ren, L. X.; Hardy, C. G.; Tang, C. B. *J. Am. Chem. Soc.* **2010**, *132* (26), 8874−8876. (g) Ren, L. X.; Hardy, C. G.; Tang, S. F.; Doxie, D. B.; Hamidi, N.; Tang, C. B. *Macromolecules* **2010**, *43*, 9304−9310. (h) Zhang, J. Y.; Ren, L. X.; Hardy, C. G.; Tang, C. *Macromolecules* **2012**, *45*, 6857−6863. (i) Ren, L. X.; Zhang, J. Y.; Hardy, C. G.; Ma, S. G.; C. B. Tang, C. B. *Macromol. Commun.* **2012**, *33*, 510−516. (j) Ren, L. X.; Zhang, J. Y.; Bai, X. L.; Hardy, C. G.; Shimizu, K. D.; Tang, C. B. *Chem. Sci.* **2012**, *3*, 580−583.

(11) (a) Newkome, G. R.; Moorefield, C. N.; Vogtle, F. *Dendrons and Dendrimers. Concepts, Synthesis and Applications*; Wiley-VCH: Weinheim, Germany, 2001. (b) Oosterom, G. E.; Reek, J. N. H.; Kamer, P. C. J.; van Leeuwen, P.W. N.M. *Angew. Chem., Int. Ed.* **2001**, *40*, 1828−1849. (c) Astruc, D.; Chardac, F. *Chem. Rev.* **2001**, *101*, 2991−3024. (d) Kreiter, R.; Kleij, A. W.; Klein Gebbink, R. J. M.; van Koten, G. Dendrimers IV: Metal Coordination, Self Assembly, Catalysis. In *Topics in Current Chemistry*; Springer-Verlag: Berlin, Germany. (e) Vögtle, F., Schalley, C. A., Eds.; *Dendrimers and other Dendritic Polymers*; Springer-Verlag: Berlin, Germany, 2001; Vol. *217*, p 163. (f) Tomalia, D., Frechet, J. M. J., Eds.;*Dendrimers and Nanosciences*; Wiley-VCH: New York, 2002. (g) Astruc, D., Ed.; Elsevier: Paris, *C. R. Chim.* 2003, *6*, 709−1208. (h) van Heerbeeck, R.; Kamer, P. C. J.; van Leeuwen, P. W. N. M.; Reek, J. N. H. *Chem. Rev.* **2002**, *102*, 3717−3756. (i) Astruc, D.; Heuze, K.; Gatard, S.; Méry, D.; Nlate, S. *Adv. Syn. Catal.* **2005**, *347*, 329−338. (j) Liang, C.; Fréchet, J. M. J. *Prog. Polym. Sci.* **2005**, *30*, 385−402. (k) Scott, R.W. J.; Wilson, O. M.; Crooks, R. M. *J. Phys.Chem. B* **2005**, *109*, 692−704. (l) Méry, D.; Astruc, D. *Coord. Chem. Rev.* **2006**, *250*, 1965−1979. (m) de Jesus, E.; Flores, J. C. *Ind. Eng. Chem. Res.* **2008**, *47*, 7968−7981. (n) Astruc, D.; Boisselier, E.; Ornelas, C. *Chem. Rev.* **2010**, *110*, 1857−1959. (o) Caminade, A.-M.; Turin, C.-O.; Laurent, R.; Ouali, A.; Delavaux-Nicot, B. *Dendrimers. Towards Catalytic, Material and Biomedical Uses*; Wiley: Weinheim, Germany, 2011. (p) Campana, S.; Ceroni, P.; Punteriero, F. *Designing Dendrimers*; Wiley: New York, 2012.

(12) (a) Newkome, G. R.; Moorefield, C. N.; Vogtle, F. *Dendrimers and Dendrons, Syntheses, Concepts, Applications*; Wiley-VCH: Weinheim, Germany, 2001. (b) Newkome, G. R.; Moorefield, C. N. *Chem. Rev.* **1999**, *99*, 1689−1746. (c) Newkome, G. R.; Shreiner, C. *Chem. Rev.* **2010**, *110*, 6338−6442. (d) Hwang, S. H.; Shreiner, C. D.; Moorefield, S. N.; Newkome, G. R. *New J. Chem.* **2007**, *31*, 1192−1217.

(13) (a) Casado, C. M.; Cuadrado, I.; Moran, M.; Alonso, B.; Garcia, B.; Gonzales, B.; Losada, J. *Coord. Chem. Rev.* **1999**, *185*−*6*, 53−79. (b) Ruiz, J.; Lafuente, G.; Marcen, S.; Ornelas, C.; Lazare, S.; Cloutet, E.; Blais, J.-C.; Astruc, D. *J. Am. Chem. Soc.* **2003**, *125*, 7250−7257. (c) Ornelas, C.; Ruiz, J.; Belin, C.; Astruc, D. *J. Am. Chem. Soc.* **2009**, *131*, 590−601.

(14) (a) Alonso, E.; Valerio, C.; Ruiz, J.; Astruc, D. *New. J. Chem.* **1997**, *21*, 1139−1141. (b) Valério, C.; Ruiz, J.; Fillaut, J.-L.; Astruc, D. *C. R. Acad. Sci.*, **1999**, *2*, *Sér. II c*, 79-83. (c) Takada, K.; Diaz, D. J.; Abruña, H. D.; Cuadrado, I.; Gonzalez, B.; Casado, C. M.; Alonso, B.; Moran, M.; Losada, J. *Chem.—Eur. J.* **2001**, *7*, 1109−1117. (d) Sobransingh, D.; Kaifer, A. E. *Langmuir* **2006**, *22*, 10540−10544. (e) Ornelas, C.; Ruiz, J.; Astruc, D. *Organometallics* **2009**, *28*, 2716−2723.

(15) Kolb, H. C.; Finn, M. G.; Sharpless, K. B. *Angew. Chem., Int. Ed.* **2001**, *40*, 2004−2021.

(16) (a) Rostovtsev, V. V.; Green, L. G.; Fokin, V. V.; Sharpless, K. B. *Angew. Chem., Int. Ed.* **2002**, *41*, 2596−2599. (b) Tornøe, C. W.; Christensen, C.; Meldal, M. *J. Org. Chem.* **2002**, *67*, 3057−3064. (c) Bock, V. D.; Hiemstra, H.; van Maarseveen, J. H. *Eur. J. Org. Chem.* **2005**, 51−68. (d) Franc, G.; Kakkar, A. *Chem. Commun.* **2008**, 5267−5276. (e) Meldal, M.; Tornøe, C. W. *Chem. Rev.* **2008**, *108*, 2952−3015. (f) Hein, J. E.; Fokin, V. V. *Chem. Soc. Rev.* **2010**, *39*, 1302−1315. (g) Liang, L.; Astruc, D. *Coord. Chem. Rev.* **2011**, *255*, 2933−2945.

(17) Astruc, D.; Liang, L.; Rapakousiou, A.; Ruiz, J. *Acc. Chem. Res.* **2011**, *45*, 630−640.

(18) (a) Ornelas, C.; Cloutet, E.; Alves, S.; Astruc, D. *Angew Chem., Int. Ed.* **2007**, *46*, 872−877. (b) Djeda, R.; Rapakousiou, A.; Liang, L.; Guidolin, N.; Ruiz, J.; Astruc, D. *Angew Chem., Int. Ed.* **2010**, *49*, 8152−8156.

(19) (a) Diallo, A. K.; Ornelas, C.; Salmon, L.; Ruiz, J.; Astruc, D. *Angew. Chem., Int. Ed.* **2007**, *46*, 8644−8648. (b) Ornelas, C.; Ruiz, J.; Salmon, L.; Astruc, D. *Adv. Syn. Catal.* **2008**, *350*, 837−845. Astruc, D. *Tetrahedron Asymmetry* **2010**, *21*, 1041−1054.

(20) Boisselier, E.; Diallo, A. K.; Salmon, L.; Ornelas, C.; Ruiz, J.; Astruc, D. *J. Am. Chem. Soc.* **2010**, *132*, 2729−2742.

(21) (a) Diallo, A. K.; Menuel, S.; Monflier, E.; Ruiz, J.; Astruc, D. *Tetrahedron Lett.* **2010**, *51*, 4617−4619. (b) Rapakousiou, A.; Mouche, C.; Duttine, M.; Ruiz, J.; Astruc, D. *Eur. J. Inorg. Chem.* **2012**, *31*, 5071−5077.

(22) (a) Newkome, G. R.; Yao, Z.; Baker, G. R.; Gupta, V. K. *J. Org. Chem.* **1985**, *50*, 2003−2004. (b) Newkome, G. R. *Pure Appl. Chem.* **1998**, *70*, 2337−2343. (c) Narayanan, V. V.; Newkome, G. R. *Top. Curr. Chem.* **1998**, *197*, 19−33. (d) Newkome, G. R.; Schreiner, C. D. *Chem. Rev.* **2010**, *110*, 6338−6442.

(23) (a) Valério, C.; Fillaut, J.-L.; Ruiz, J.; Guittard, J.; Blais, J.-C.; Astruc, D. *J. Am. Chem. Soc.* **1997**, *119*, 2588−2589. (b) Valério, C.; Alonso, E.; Ruiz, J.; Blais, J.-C.; Astruc, D. *Angew. Chem., Int. Ed. Engl.* **1999**, *38*, 1747−1751.

(24) (a) Sartor, V.; Djakovitch, L.; Fillaut, J.-L.; Moulines, F.; Neveu, F.; Marvaud, V.; Guittard, J.; Blais, J.-C.; Astruc, D. *J. Am. Chem. Soc.*

1999, *121*, 2929−2930. (b) Ruiz, J.; Lafuente, G.; Marcen, S.; Ornelas, C.; Lazare, S.; Cloutet, E.; Blais, J.-C.; Astruc, D. *J. Am. Chem. Soc.* **2003**, *125*, 7250−7257.
(25) Wildschek, M.; Rieker, C.; Jaitner, P.; Schottenberger, H.; Schwarzhans, K. E. *J. Organomet. Chem.* **1990**, *396*, 355−361.
(26) (a) Huisgen, R. *Angew. Chem., Int. Ed.* **1963**, *2*, 565−598. (b) Huisgen, R. In *1,3-Dipolar Cycloaddition Chemistry*; Padwa, A., Ed.; John Wiley: New York, 1984; pp 1−176. (c) Howell, S. J.; Spencer, N.; Philip, D. *Tetrahedron* **2001**, *57*, 4945−4954.
(27) Alternatively, the encapsulation of copper ions requiring a stoichiometric use of the catalyst can be avoided using the very efficient catalyst [Cu(hexabenzyltren)]Br in 5−10% mol amounts for large dendrimer and functional nanoparticle syntheses: (a) Liang, L.; Ruiz, J.; Astruc, D. *Adv. Syn. Catal* **2011**, *353*, 3434−3450. (b) Zhao, P.; Grillaud, M.; Salmon, L.; Ruiz, J.; Astruc, D. *Adv. Syn. Catal.* **2012**, *354*, 1001−1011.
(28) Ruiz, J.; Astruc, D. *C. R. Acad. Sci.* **1998**, *t. 1, Sér. IIc*, 21−27.
(29) (a) Flanagan, J. B.; Margel, S.; Bard, A. *J. Am. Chem. Soc.* **1978**, *100*, 4248−4253. (b) Sutton, J. E.; Sutton, P. M.; Taube, H. *Inorg. Chem.* **1979**, *18*, 1017−1024. (c) Richardson, D. E.; Taube, H. *Coord. Chem. Rev.* **1984**, *60*, 107−129. (d) Barrière, F.; Geiger, W. E. *Acc. Chem. Res.* **2010**, *43*, 1030−1039.
(30) Gorman, C. B.; Smith, B. L.; Parkhurst, H.; Sierputowska-Gracz, H.; Haney, C. A. *J. Am. Chem. Soc.* **1999**, *121*, 9958−9966.
(31) Amatore, C.; Bouret, Y.; Maisonhaute, E.; Goldsmith, J. I.; Abruna, H. D. *Chem.—Eur. J.* **2001**, *7*, 2206−2226.
(32) (a) Ammeter, J. H.; Ostwald, N.; Bucher, R. *Helv. Chim. Acta* **1975**, *58*, 671−682. (b) Ammeter, J. H. *J. Magn. Reson.* **1978**, *30*, 299−325.
(33) (a) Astruc, D.; Heuze, K.; Gatard, S.; Méry, D.; Nlate, S.; Plault, L. *Adv. Syn. Catal.* **2005**, *347*, 329−338. (b) Ornelas, C.; Ruiz, J.; Salmon, L.; Astruc, D. *Adv. Syn. Catal.* **2008**, *350*, 837−845.
(34) (a) Moinet, C.; Román, E.; Astruc, D. *J. Electroanal. Chem. Interfacial Electrochem.* **1981**, *121*, 241−246. (b) Green, J. C.; Kelly, M. R.; Payne, M. P.; Seddon, E. A.; Astruc, D.; Hamon, J.-R.; Michaud, P. *Organometallics* **1983**, *2*, 211−218.

ORGANOMETALLICS

Article

pubs.acs.org/Organometallics

Click Chemistry of an Ethynylarene Iron Complex: Syntheses, Properties, and Redox Chemistry of Cationic Bimetallic and Dendritic Iron-Sandwich Complexes

Amalia Rapakousiou, Yanlan Wang, Roberto Ciganda, Jean-Michel Lasnier, and Didier Astruc*

ISM, UMR CNRS 5255, University of Bordeaux, 33405 Talence Cedex, France

Supporting Information

ABSTRACT: The functionalization of dendrimers and other macromolecules with cationic redox-active organometallics remains a target toward metal-containing dendrimers and polymers that can serve in particular as polyelectrolytes and multielectron redox reagents. Along this line, we report the click functionalization of organometallics and dendrimers with a redox-active ethynylarene iron complex, [FeCp(η^6-ethynylmesitylene)][PF_6], **3**, easily available from [FeCp(η^6-mesitylene)][PF_6], **1**. Complex **3** reacts with azidomethylferrocene upon catalysis by copper sulfate and sodium ascorbate (CuAAC reaction) to give a bimetallic complex that is reduced on the mesitylene ligand to a mixture of isomeric cyclohexadienyl complexes. Complex **3** also reacts according to the same click reaction with zeroth- and first-generation metallodendrimers containing, respectively, 9 and 27 azido termini to provide new polar polycationic metallodendrimers that are reversibly reduced, on the electrochemical time scale, to 19-electron Fe^I species.

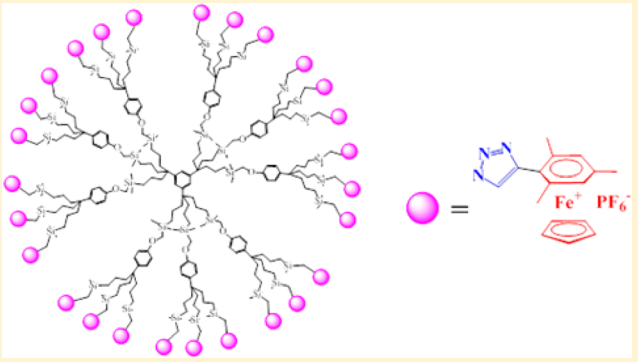

INTRODUCTION

Metallodendrimers are a rich chemistry[1] that finds applications in catalysis,[2] sensing,[3] molecular electronics,[4] and other molecular materials properties.[1] Metallocene-terminated dendrimers occupy a large part of this chemistry because of their rich redox properties that are especially developed and applied with ferrocene dendrimers.[5] Very few polycationic dendrimers are known, almost exclusively cobalticenium dendrimers,[6,7] however, despite their polyelectrolyte properties. The chemistry of the family of complexes [FeCp(η^6-arene)][PF_6][8] (Cp = η^5-C_5H_5) parallels that of cobalticenium[9] and is also quite rich. For instance, the basic properties of the readily available complex [FeCp(η^6-mesitylene)][PF_6], **1**,[10] are illustrated in Scheme 1. Further functionalization of **1** was thus a target in order to graft this cheap and easily available cationic and redox-active organoiron complex onto the periphery of dendrimers.

Recently, it has been possible to nearly quantitatively functionalize complex **1** by the introduction of an ethynyl group on the arene ligand upon addition of the ethynyl carbanion in the form of lithium acetylideethylenediamine in THF giving *exo*-cyclohexadienyl adduct **2**, followed by removal of the *endo* hydride using commercial trityl hexafluorophosphate providing the ethynyl-substituted arene complex [FeCp-(η^6-ethynylmesitylene)][PF_6], **3** (Scheme 2).[11]

This procedure is an extension of the very useful analogous functionalization of cobalticenium.[12] Complex **3** that is readily obtained in this way serves in further functionalization. For instance, the new facile hydroamination of this complex **2** leads

Scheme 1. Basic Chemistry of Complex 1

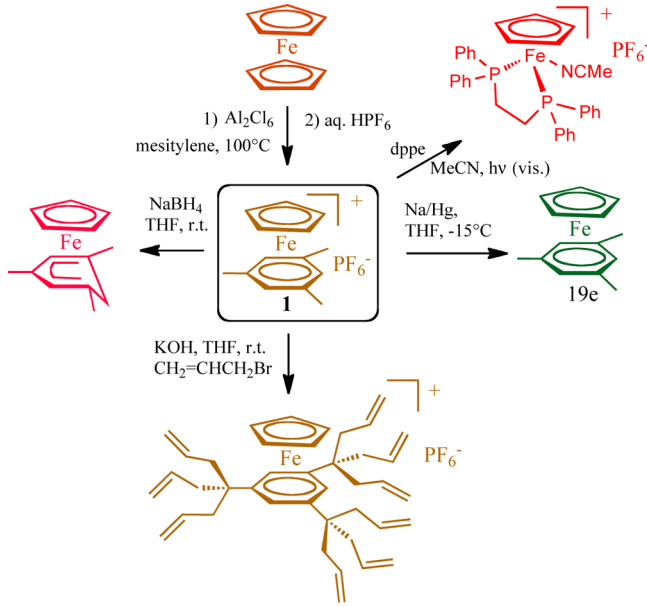

Received: May 9, 2014
Published: July 1, 2014

Scheme 2. Synthesis of Ethynyl Derivative 3

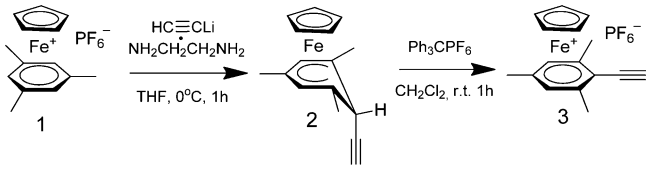

to the formation of conjugated *trans*-enamines,[11] but attempts to extend this functionalization to dendritic amines were unsuccessful, although such an extension worked well with ethynylcobalticenium.[13] However, we report here the successful and facile CuAAC click reaction[14] of **2** with azidomethylferrocene and dendritic azides yielding cationic bi- and polymetallic complexes of hexahapto-coordinated 1,2,3-triazolylmesitylene. The redox chemistry of these new cationic bimetallic and dendritic complexes is also detailed here.

RESULTS AND DISCUSSION

Click Reaction of Ethynylmesitylene Complex 3 with Azidomethylferrocene. The ethynyl derivative **3** of the complex $[FeCp(\eta^6\text{-}C_6H_3Me_3)]PF_6$, **1**, is synthesized according to the nucleophilic addition of lithium acetylideethylenediamine followed by hydride abstraction by $[Ph_3C][PF_6]$ (Scheme 2). (Azidomethyl)ferrocene **4** is then used in the CuAAC reaction with compound **3** to selectively produce 1,4-disubstituted triazolyl (trz) complex **5** in quantitative yield (Scheme 3).

The new dark-orange complex **5** is soluble in dichloromethane, THF, and chloroform and must be kept in the dark in the solid state in order to avoid its visible-light-induced photodecomplexation. The infrared spectroscopy shows the disappearance of the azido group at 2097 cm^{-1} and the appearance of the characteristic band of the PF_6^- anion at 839 cm^{-1}. The formation of the trz group is clearly shown in ^1H NMR spectroscopy by the appearance of the CH_2-trz and trz *CH* peaks at 5.55 and 8.41 ppm, respectively, and is also confirmed by the presence of the characteristic peaks of *Cq* and *CH* of trz in the ^{13}C NMR spectrum. Product **5** was additionally characterized by HMBC, HSQC, COSY, ^{31}P, and ^{19}F NMR spectroscopic techniques (Supporting Information). Finally, the structure of **5** was confirmed by the molecular peak at 506 Da in the mass spectrum corresponding to the positively charged complex **5** and by elemental analysis.

The cyclic voltammetry and redox chemistry of the iron-sandwich complexes including that of ferrocene[15] and of the family of $[FeCp(\eta^6\text{-arene})][PF_6]$ complexes[16] are well documented. The cyclic voltammograms (CVs) of complex **5** were recorded in DMF using decamethylferrocene as the internal reference[17] in order to investigate the redox properties of the triazolyl-$[Fe^{II}Cp(\eta^6\text{-}C_6H_2Me_3\text{-})]PF_6$ group. The oxidation wave at 0.55 V vs $[FeCp^*_2]^{+/0}$ ($Cp^* = \eta^5\text{-}C_5Me_5$) is due to the oxidation of the ferrocenyl fragment to the 17-electron ferricenium species, and the reduction wave at −1.36 V vs $[FeCp^*_2]^{+/0}$ is due to the reduction of the triazolyl-$[Fe^{II}Cp(\eta^6\text{-}C_6H_2Me_3\text{-})]PF_6$ fragment to its 19-electron Fe^I isostructural analogue.[8b] Both waves show electrochemical and chemical reversibility under N_2 indicating the robustness of compound **5** and the triazolyl group attached to the $[Fe^{II}Cp(\eta^6\text{-}C_6H_2Me_3\text{-})]\text{-}PF_6$ sandwich under these conditions. When the CV is recorded under air, the situation changes, however. The reduction wave of triazolyl-$[Fe^{II}Cp(\eta^6\text{-}C_6H_2Me_3\text{-})]PF_6$ is then irreversible with a potential Ep of −1.34 V vs $[FeCp^*_2]^{+/0}$, whereas remarkably a new irreversible oxidation wave appeared at −0.68 V vs $[FeCp^*_2]^{+/0}$. It is known that the 19-electron complex $[Fe^{II}(\eta^5\text{-}Cp)(\eta^6\text{-}C_6Me_6)]$ is extremely reactive toward O_2, reacting with an overall H atom abstraction from a benzylic methyl substituent according to a mechanism that comprises electron transfer from Fe^I to O_2 followed by deprotonation by superoxide O_2^- giving the 18-electron cyclohexadienylidene-methylene complex $[Fe^{II}(\eta^5\text{-}Cp)(\eta^5\text{-}C_6Me_5CH_2)]$.[18] It seems that the 19-electron species triazolyl-$[Fe^I(\eta^5\text{-}Cp)(\eta^6\text{-}C_6H_2Me_3\text{-})]$ generated at the cathode by single-electron reduction of **5** reacts analogously with O_2 from air giving triazolyl-$[Fe^{II}(\eta^5\text{-}Cp)(\eta^5\text{-}C_6H_2Me_2CH_2\text{-})]$, although this cyclohexadienylidene-methylene species has not been isolated in this case. This reaction appears here to be faster than the electrochemical time scale as expected; thus, it probably is this oxidized species that is then oxidized at −0.68 V (Figure 1).

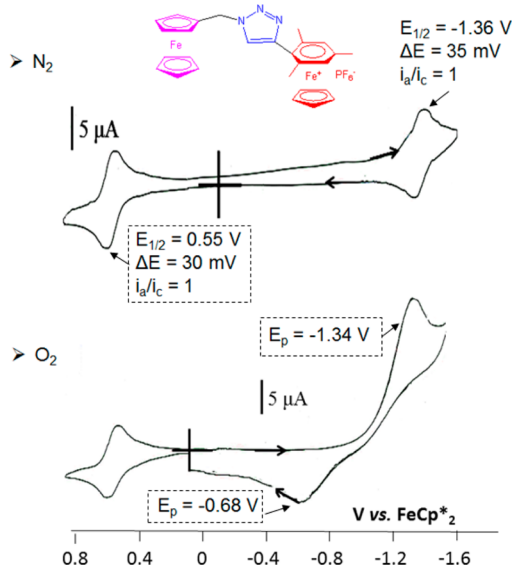

Figure 1. CVs of **5** under N_2 and under O_2 (air). Solvent, DMF; reference electrode, Ag; working and counter electrodes, Pt; scan rate, 0.2 V/s; and supporting electrolyte, $[n\text{-}Bu_4N][PF_6]$, 0.1M.

Scheme 3. "Click" Synthesis of Bimetallic Complex 5

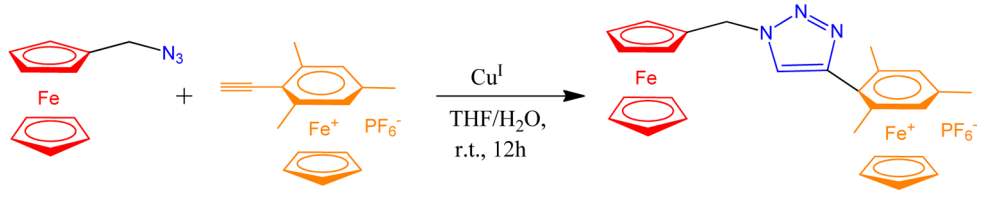

dx.doi.org/10.1021/om500495r | *Organometallics* 2014, 33, 3583−3590

Scheme 4. Reduction of the Complex Fc-CH_2-trz-$Fe^{II}(\eta^5$-Cp)$(\eta^6$-$C_6H_2Me_3$-)]PF_6, 5, (Fc = ferrocenyl) by $NaBH_4$ Giving Neutral Bimetallic Complex 6 and Isomers

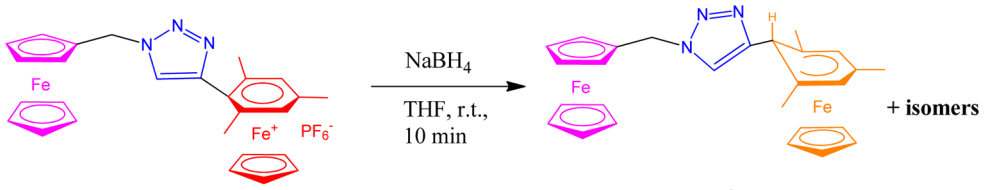

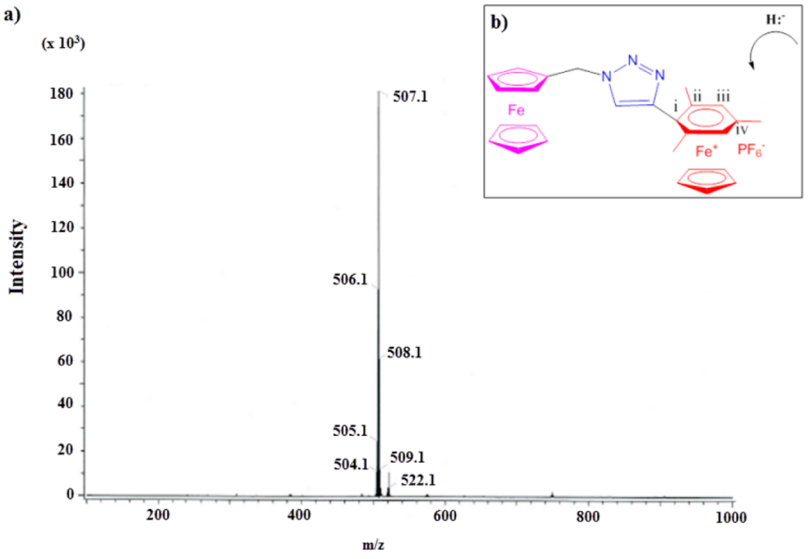

Figure 2. (a) FD-MS of neutral compound **6** and isomers and (b) possible hydride addition on four positions i, ii, iii, and iv of the mesitylene ligand (ii and iv are steroelectronically disfavored).

Reduction of Binuclear Triazole Complex 5 by $NaBH_4$. The complexes of the [FeCp(η^6-arene)][PF_6] family are known to be reducible by $NaBH_4$ on the arene ligand producing a decrease of hapticity to yield cyclohexadienyl complexes, and in the presence of methyl substituents on the arene ligand, the unsubstituted carbon atoms of the ligand are preferentially attacked.[19] In accord with this rule,[20] reduction of the dark-orange cationic complex **5** by $NaBH_4$ at 0 °C in THF produces the light-orange complex **6** that contains two iron-sandwich units with both pentahapto ligands. Complex **6** is soluble in less polar solvents such as diethyl ether, which allows its extraction under N_2 (Scheme 4). Compound **6** is air-sensitive but not light-sensitive, contrary to the complexes of the [$Fe^{II}(\eta^5$-Cp)$(\eta^6$-arene)]PF_6 family.[8b,21]

Compound **6** together with isomers have been isolated in 80% yield, and their structure is confirmed by the observation of the molecular peak in the FD-mass spectrum (Figure 2a). Compound and isomers **6** have been further characterized by ^{1}H NMR, ^{13}C NMR, and HSQC spectroscopy, which is rather complex, showing the formation of a mixture of isomers corresponding to different positions of the hydride addition. The same phenomenon has been observed for the reduction of triazolyl-cobalticenium complexes by $NaBH_4$.[22] Indeed the hydride reduction of compound **5** might occur on positions i, ii, iii, and iv of the mesitylene ligand (preferentially in i and iii due to sterically and electronically disfavored hydride attack on the methyl-substituted arene carbon atoms) as indicated in Figure 2b. In all cases, the hydride is located in *exo* position on the mesitylene ligand as a result of the *exo* hydride attack. No attempt was made to identify and separate the isomers.

The cyclic voltammogram in THF shows a totally irreversible oxidation wave at 0.20 V vs. $[FeCp_2^*]^{+/0}$. It is suggested that this wave corresponds to the oxidation of the compound **6** and its isomers (Supporting Information). This wave is very large, representing the subsequent irreversible oxidation of **6** and its isomers back to the starting material, complex **5**.

Grafting [FeCp(η^6-ethynylmesitylene)][PF_6] onto Dendrimers by Click Chemistry. Grafting [FeCp(η^6-ethynylmesitylene)][PF_6] on macromolecules was a challenge because of several factors. First, the visible-light sensitivity of the complexes of the [FeCp(η^6-arene)][PF_6] family and more particularly of the click reaction products because of the electron-withdrawing trz substituent[21] leads to a rapid decoordination of the mesitylene ligand. Then, an additional difficulty is the solubility problem that reduces the choice of solvent, while coordinating solvents are not permitted because of ligand displacement due to the cationic electron-poor arene ligand bond in **3**. Finally, the steric effect of the *ortho*-methyl groups that had most probably been responsible for the lack of success of the extension of the useful hydroamination to dendritic amines might also cause failure of the click reaction. Finally, however, click chemistry has proved to be an efficient way for the incorporation of **3** into dendrimers, and the CuAAC reaction has been successfully conducted between **3** and polyazido-terminated dendritic precursors for the synthesis of the cationic metallodendrimers.

The synthesis of the polyazido dendrimers begins with the synthesis of arene-centered dendrimers according to the classic $CpFe^+$-induced nona-allylation of mesitylene in [FeCp(η^6-1,3,5-$C_6H_3(CH_3)_3$)][PF_6][23] according to the 1 → 3 con-

dx.doi.org/10.1021/om500495r | *Organometallics* 2014, 33, 3583−3590

Scheme 5. Synthesis of the Dendrimer G_0-Nona-[$Fe^{II}(\eta^5$-Cp)$(\eta^6$-$C_6H_2Me_3$-)]PF_6, 9

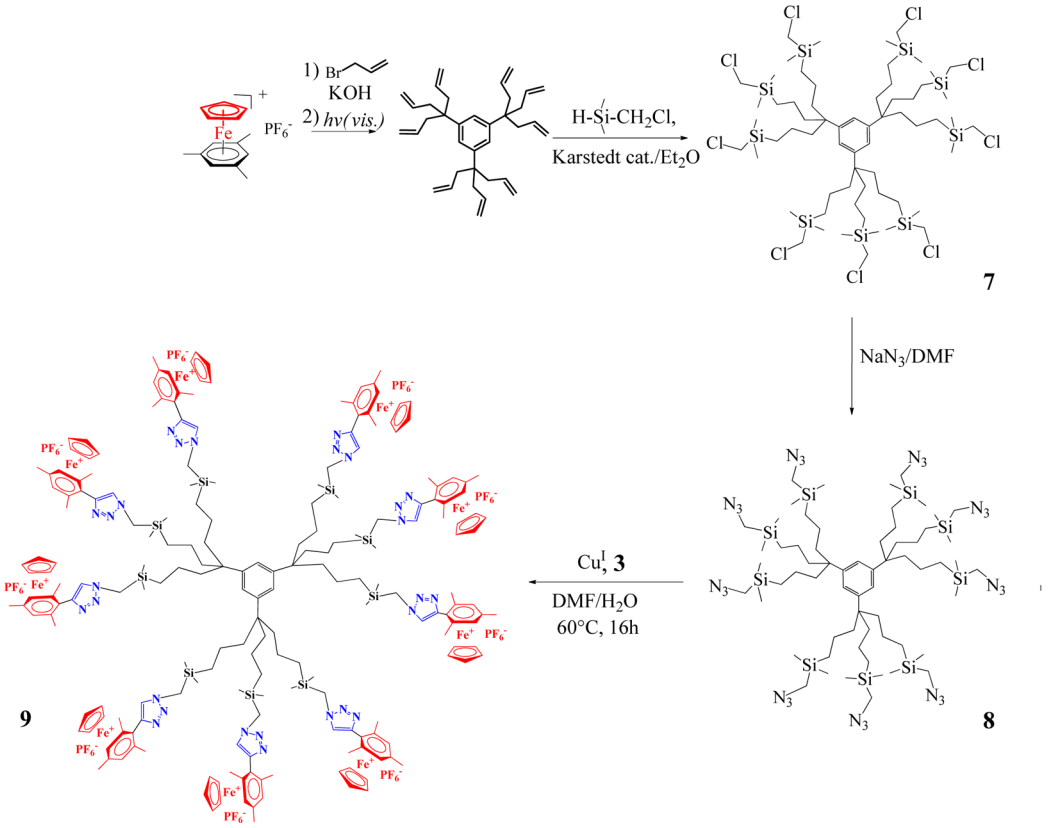

nectivity pioneered by Newkome.[24] This reaction provides the nonaallyl core and is followed by hydrosilylation with chloromethyldimethylsilane[25] and substitution of the terminal chloro group in **7** by reaction with sodium azide giving the zeroth-generation dendritic nonaazide **8**. The following dendrimer generation containing 27 terminal allyl groups is obtained by Williamson reaction of the nona-chloro core **7** with a phenol triallyl dendron[23] according to a known procedure.[23b] It is followed by substitution of the terminal chloride by the azido group by reaction with NaN_3. This sequence of reactions provides the known first-generation dendrimer **10** containing 27 N_3 termini.[26]

Click reactions follow between these dendritic azido precursors and alkyne **3**. The solvents in each reaction are chosen in order to achieve the solubility of the final product because the polycationic poly-[Fe^{II}Cp$(\eta^6$-$C_6H_2Me_3$-)]PF_6 dendrimers are soluble only in high polarity solvents. For the synthesis of the dendrimer, G_0-nona-[Fe^{II}Cp$(\eta^6$-$C_6H_2Me_3$-)]-PF_6, **9**, DMF/H_2O 4:1 is chosen as solvent, whereas for the dendrimer of higher generation G_1-27-[$Fe^{II}(\eta^5$-Cp$)(\eta^6$-$C_6H_2Me_3$-)]PF_6, **11**, a mixture of DMF/THF/H_2O is used because the azido-terminated precursor **10** is insoluble in DMF. The temperature of the reactions is maintained at 60 °C, and the reaction mixtures are left stirring during 16 h. The copper salt is finally removed as [$Cu(NH_3)_2(H_2O)_2$] [SO_4] by adding an aqueous solution of NH_3 that is left stirring with the mixture for 15 min. The resulting dendrimers **9** (Scheme 5) and **11** (Scheme 6) are purified, after workup in the dark, by precipitation in diethyl ether as yellowish powders. Washing with the less polar THF solvent in which they are insoluble permits one to separate the excess of starting material **3** and further impurities to finally give products **9** and **11** that are fully characterized by ^{1}H, ^{13}C, ^{19}F, ^{31} P, HMBC, HSQC, COSY NMR, IR, cyclic voltammetry, and elemental analysis. MALDI-TOF analysis is also attempted for the smaller dendrimer **9** for which the molecular peak is observed even though the mass spectrum is an ensemble of multiple fragments due to the high instability of the dendrimer under these conditions (see Supporting Information).

Indeed, dendrimers **9** and **11** are very polar because the fragment trz-[$Fe^{II}(\eta^5$-Cp$)(\eta^6$-$C_6H_2Me_3$-)]PF_6 is very hydrophilic and soluble only in very polar solvents. Particularly, dendrimers **9** and **11** can be dissolved in acetone, acetonitrile, methanol, and DMF. However, these dendrimers are not soluble in water despite the presence of several cationic organometallic fragments at their periphery. Another observation is that dendrimers **9** and **11** are not stable in acetonitrile solution because acetonitrile is a competing ligand with mesitylene for coordination to iron(II), and precipitation occurs after several hours. Furthermore, exposure of these dendrimers to ambient light in solution or in the solid state also leads to rapid decomplexation of the mesitylene ligand. When kept in the dark, however, dendrimers **9** and **11** are stable compounds.

Infrared spectroscopy is a very useful tool to monitor the click reactions with dendrimers because the characteristic peak of the azido groups at about 2094 cm^{-1} disappears at the end of the reactions confirming their replacement by the 1,2,3-triazole groups. The characteristic absorption of the PF_6^- anion of these PF_6^- salts shows a strong band in the range 836−842 cm^{-1}. The absorptions due to the =C−H stretching of the triazole and Cp groups of the trz-[$Fe^{II}(\eta^5$-Cp$)(\eta^6$-$C_6H_2Me_3$-)]PF_6 unit are found in the range 3095−3127 cm^{-1}.

dx.doi.org/10.1021/om500495r | *Organometallics* 2014, 33, 3583−3590

Scheme 6. Synthesis of G_1-27-$[Fe^{II}(\eta^5\text{-Cp})(\eta^6\text{-}C_6H_2Me_3\text{-})]PF_6$ Dendrimer 11

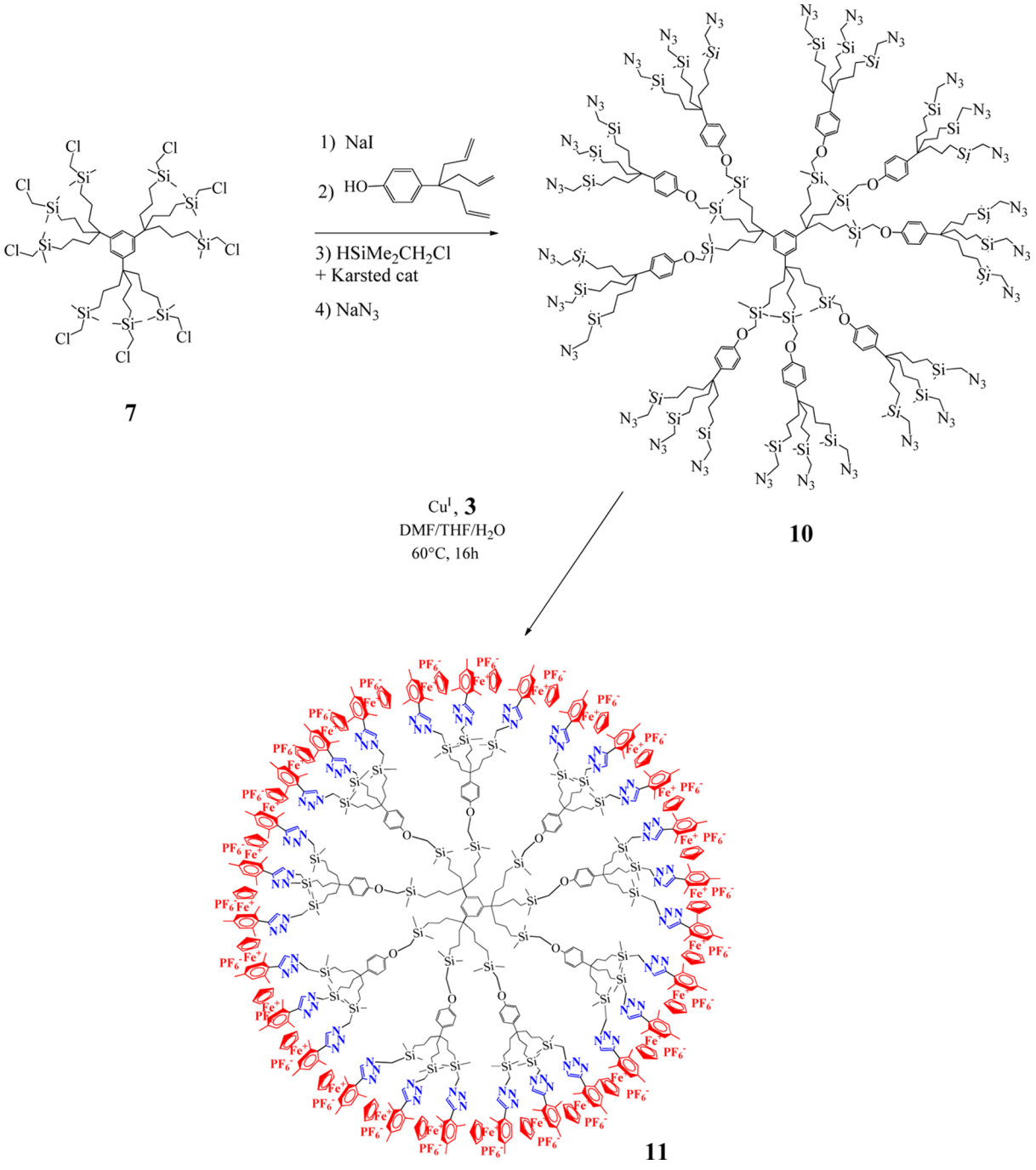

NMR spectroscopy confirms the structure of the trz-$[Fe^{II}(\eta^5\text{-Cp})(\eta^6\text{-}C_6H_2Me_3\text{-})]PF_6$ products. Particularly, in ^1H NMR the formation of the trz ring is clearly shown by the appearance of the peaks around 8.27 ppm (in CD_3OD or CD_3COCD_3) for the products **9** and **11**. In both cases, the peak of $SiCH_2\text{-}N_3$ at 2.7−2.8 ppm disappears, whereas the appearance of the new peak of $SiCH_2$-trz takes place at about 4.2 ppm. The presence of the trz group is also confirmed by the appearance of the characteristic peaks of *Cq* and CH of trz as well as $SiCH_2$-trz in the ^{13}C NMR spectra. Finally, the assignments of the number of protons in ^1H NMR show the expected ratio between the dendritic frame part and the trz-$[Fe^{II}(\eta^5\text{-Cp})(\eta^6\text{-}C_6H_2Me_3\text{-})]$-$PF_6$ groups. The ^{19}F and ^{31}P NMR spectra show the characteristic peaks of the PF_6^- counteranion. 2-D NMR data (HSQC, HMBC, and COSY) show the correct correlation between proton/proton and proton/carbon peaks. Finally, elemental analysis confirms the structure of the dendrimers **9** and **11**.

Cyclic Voltammetry of the Cationic Metallodendrimers 9 and 11. Both dendrimers **9** and **11** are also studied by cyclic voltammetry using decamethylferrocene as the internal reference,[17] in DMF, a good solubility being accessible with this solvent. Different conditions such as temperature and air $(O_2)/N_2$ atmosphere are examined. A cathodic CV wave in all the products is observed around −1.34 V vs $[FeCp^*_2]^{0/+}$ and corresponds to the reduction of $[Fe^{II}Cp(\eta^6\text{-}C_6H_2Me_3\text{-})]$-$PF_6$ to the 19-electron species $[Fe^{I}Cp(\eta^6\text{-}C_6H_2Me_3\text{-})]$. In all cases, this wave is single in DMF, which is explained by the

dx.doi.org/10.1021/om500495r | *Organometallics* 2014, 33, 3583−3590

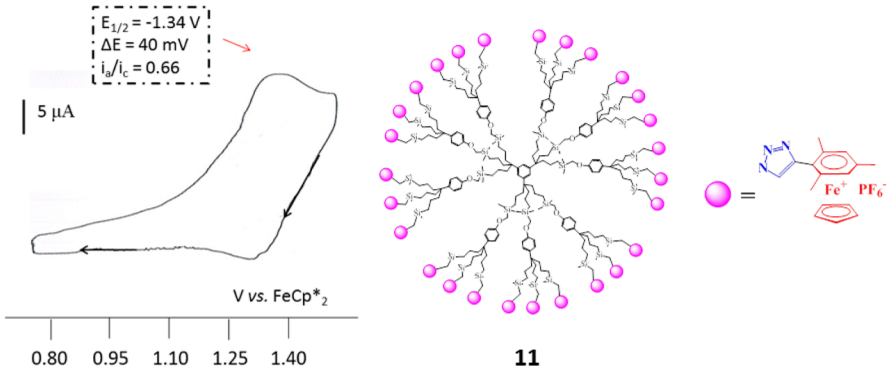

Figure 3. CV of dendrimer **11** in DMF under N_2. Internal reference, $FeCp^*_2$; reference electrode, Ag; working and counter electrodes, Pt; scan rate, 0.2 V/s; supporting electrolyte, $[n\text{-}Bu_4N][PF_6]$.

weakness of the electrostatic factor between the redox sites of the metallodendrimers, these redox centers being far from one another and separated by long tethers.[27] However, the envelope of the redox wave is broad, which is presumably due to electrostatic interactions differentiating the various single electron-transfer steps.

When recording the CVs of dendrimers **9** and **11** under aerobic (O_2) atmosphere, the same phenomenon as that for compound **5** is observed. The reduction wave of the fragments $[Fe^{II}Cp(\eta^6\text{-}C_6H_2Me_3\text{-})]PF_6$ is irreversible due to the fast reaction of the 19-electron species with O_2 (vide supra). However, when the electrochemical experiments are performed under nitrogen at room temperature, the cathodic wave ($Fe^{II/I}$) becomes chemically and electrochemically reversible. The peak-to-peak potential difference between the cathodic and anodic waves is 30−40 mV, significantly narrower compared with the Nernstian one-electron process, probably due to some adsorption onto the electrode. The electrochemical reversibility involving equally all of the redox groups is due to very fast rotation within the electrochemical time scale because all of the redox groups come close to the electrode, provoking fast electron transfer between these groups and the electrode,[28] and/or the electron-hopping mechanism.[29] The CV wave under N_2 of dendrimer **11** containing 27 $[Fe^{II}(\eta^5\text{-}Cp)(\eta^6\text{-}C_6H_2Me_3\text{-})]PF_6$ termini is shown in Figure 3.

CONCLUDING REMARKS

The currently used click reaction, i.e., the Huisgen-type CuAAC, proves to be most useful to graft organometallic complexes onto the periphery of dendrimers.[30] Here, the newly functionalized, easily available complex **3** is a remarkable illustration insofar as the hydroamination of **3** could not provide such iron-sandwich terminated dendrimers. In spite of their sensivity to visible light and coordinating solvents such as acetonitrile, the polycationic metallodendrimers were fully characterized. The electron-withdrawing 1,2,3-triazolyl linkage formed by the CuAAC reaction does not significantly perturb the chemical and electrochemical reversibility of the cathodic reduction to the Fe^I 19-electron species at least during the electrochemical time scale under an inert atmosphere. This chemistry adds to the versatility of the functionalization and redox properties of the family of $[FeCp(\eta^6\text{-arene})][PF_6]$ complexes that parallels the cobalticenium family and opens the route to new cationic metallodendrimers and metal-containing macromolecules and polyelectrolytes.

EXPERIMENTAL SECTION

General Data. Reagent-grade tetrahydrofuran (THF) was predried over Na foil and distilled from sodium-benzophenone anion under argon immediately prior to use. All other solvents and chemicals were used as received. The ^1H NMR spectra were recorded at 25 °C with a Bruker AVANCE II 400 MHz spectrometer. The ^{13}C NMR spectra were obtained in the pulsed FT mode at 100 MHz with a Bruker AVANCE 400 spectrometer. ^{19}F NMR spectra were recorded at 25 °C in a 376 MHz with a Bruker AVANCE II 400 MHz spectrometer. ^{31}P NMR was recorded at 25 °C at 162 MHz with a Bruker AVANCE II 400 MHz spectrometer. All chemical shifts are reported in parts per million (δ, ppm) with reference to Me_4Si (TMS). The infrared (IR) spectra were recorded on an ATI Mattson Genesis series FT-IR spectrophotometer. The results of elemental analysis were obtained by a Thermo Flash 2000 EA. The sample was introduced in a tin container for NCHS analysis and in a silver container for oxygen analysis. The mass spectra were performed by the CESAMO (Bordeaux, France) on a QStar Elite mass spectrometer (Applied Biosystems). The instrument is equipped with an ESI source, and spectra were recorded in the positive mode. The electrospray needle was maintained at 5000 V and operated at room temperature. Samples were introduced by injection through a 20 μL sample loop into a 4500 μL/min flow of methanol from the LC pump. The mass spectrum of compound **6** was obtained by the CESAMO on a AccuTOF-GcV (JEOL), which is a GC-TOF. The instrument is equipped with a sample introduction system named FD (Field Desorption). The MALDI-TOF mass spectra were obtained by the CESAMO (Bordeaux, France) on a PerSeptive Biosystems Voyager Elite (Framingham, MA) time-of-flight mass spectrometer. All electrochemical measurements (CV) were recorded under the following conditions: solvent, dry DMF; temperature, 20 °C; supporting electrolyte, $[nBu_4N][PF_6]$ 0.1M; working and counter electrodes, Pt; reference electrode, Ag; internal reference, $FeCp^*_2$; scan rate, 0.200 V·s^{-1}.

Complex 5. A mixture of 1 equiv of azidomethylferrocene (60 mg, 0.23 mmol) and 1 equiv of ethynyl compound **3** (94 mg, 0.23 mmol) were dissolved in 3/2 distilled THF/H_2O. At 0 °C, $CuSO_4$ was added (1 equiv; 1 M aqueous solution), followed by dropwise addition of a freshly prepared solution of sodium ascorbate (2 equiv; 1 M aqueous solution). The solution was allowed to stir for 12 h at r.t. under N_2. Then, an aqueous solution of ammonia was added, and the mixture was allowed to stir for 10 min. The organic phase was washed twice with water, dried with sodium sulfate, and filtered through paper, and the solvent was removed *in vacuo*. Complex **5** was purified by precipitation with diethyl ether and obtained as dark-orange powder in quantitative yield (154 mg). ^1H NMR of **5** (CD_3COCD_3, 400 MHz), δ_{ppm}: 8.41 (1H, C*H* of trz), 6.43 (2H, C*H* of mesitylene), 5.55 (2H of trz−CH_2), 5.17 (5H, C*H* of Cp of $[Fe^{II}Cp(\eta^6\text{-}C_6H_2Me_3\text{-})]PF_6$, 4.45 (2H, C*H* of Cp sub. of $FeCp_2$), 4.25 (2H, C*H* of Cp sub. and 5H, C*H* of Cp free of $FeCp_2$), 2.56 (3H, −CHCCH_3) and 2.35 (6H, trzCCCH_3). ^{13}C NMR of **5** (CD_3COCD_3, 100 MHz), δ_{ppm}: 139.88 (*Cq* of trz), 125.86 (CH of trz), 102.80 (trz-*Cq*), 102.75 (trz-C*Cq*),

94.44 (CHCq of mesitylene), 88.48 (CH of mesitylene), 82.50 (Cq of Cp sub. of $FeCp_2$), 78.78 (CH of Cp of -[$Fe^{II}Cp(\eta^6$-$C_6H_2Me_3$-)]PF_6, 69.01 (CH of Cp of $FeCp_2$), 68.93 and 68.88 (CH of Cp sub. of $FeCp_2$), 50.08 (trz-CH_2), 19.61 and 19.54 (−CH_3 of mesitylene). ^{19}F NMR of **5** (CD_3COCD_3, 376 MHz), δ_{ppm}: doublet centered at −73.3 ppm (J_{F-P} = 710 Hz). ^{31}P NMR of **5** (CD_3COCD_3, 162 MHz), δ_{ppm}: −144.1 ppm (hept., PF_6^-) (J_{P-F} = 710 Hz). ESI MS of **5** (*m*/*z*): Calcd for $C_{27}H_{28}N_3Fe_2^+$, 506.097 Da; found, 506.098 Da. Anal. Calcd for $C_{27}H_{28}N_3Fe_2PF_6$: C, 49.80; H, 4.33. Found C, 50.10; H, 4.51.

Complex 6. A mixture of 1 equiv of **5** (30 mg, 0.046 mmol) with 2 equiv of $NaBH_4$ (1.7 mg, 0.092 mmol) in 20 mL of distilled THF was stirred for 10 min under N_2. Then, the solvent was evaporated *in vacuo*, and distilled diethyl ether was added to solubilize the neutral product. After filtration under N_2 and evaporation of the solvent *in vacuo*, the product was obtained as a light-orange powder. Yield: 80% (19 mg). Complex **6** is not stable in air and was stored under N_2. ^1H NMR of **6** ($CDCl_3$, 400 MHz), δ_{ppm}: 7.88−7.11 (1H, CH of trz), 6.36−6.06 (CH of mesitylene), 5.42−5.25 (2H of trz−CH_2 and H of diene), 4.93−4.00 (5H, CH of Cp of [$Fe^{II}Cp(\eta^6$-$C_6H_2Me_3$-)]PF_6 and (9H, CH of Cp of $FeCp_2$), 2.46−2.20 and 1.40−1.17 (9H, −CH_3), 1.90−1.64 (H in exo position). ^{13}C NMR of **6** ($CDCl_3$, 100 MHz), δ_{ppm}: 137.65 (Cq of trz), 123.20 (CH of trz), 102.31 (trz-Cq), 98.71 (trz-CCq), 94.60 (CHCq of mesitylene), 88.33 (CH of mesitylene), 79.56 (Cq of Cp sub. of $FeCp_2$), 79.56−75.04 (CH of Cp of -[$Fe^{II}Cp(\eta^6$-$C_6H_2Me_3$-)]PF_6, 69.48−68.78 (CH of $FeCp_2$), 49.93 (trz-CH_2), 39.74, 39.00 and 30,02 (CH exo), 25.65−19.96 (−CH_3 of mesitylene). MS (*m*/*z*) of **6**: Calcd for $C_{27}H_{29}Fe_2N_3$, 507.1060; found, 507.1055.

Compound 9. Azido-terminated dendrimer **8** (1 equiv, 30 mg, 0.020 mmol) and complex **3** (13.5 equiv., 110.7 mg, 0.27 mmol) were dissolved in 20 mL of anhydrous and degassed DMF, then 3 mL of degassed water was added, and the reaction mixture was cooled to 0 °C. Then, an aqueous solution of 1 M $CuSO_4$ (1.1 equiv per branch) was added dropwise, followed by the dropwise addition of a freshly prepared solution of sodium ascorbate (2.2 equiv per branch). The color of the solution changed from yellow to dark orange upon addition of sodium ascorbate. The reaction mixture was allowed to stir for 16 h at 60 °C under nitrogen atmosphere. Then, the mixture of solvents was evaporated *in vacuo*, and 100 mL of nitromethane was added followed by the addition of an aqueous solution of ammonia. The mixture was allowed to stir for 15 min in order to remove all of the copper salt trapped inside the dendrimer. The organic phase was washed twice with water, dried over sodium sulfate, and filtered, and the solvent was removed *in vacuo*. Then, the product was precipitated from an acetone solution in diethyl ether and washed with THF to remove the excess of alkyne and further impurities. Product **9** was obtained as an orange-yellow powder. Yield: 65% (67 mg). ^1H NMR of **9** (CD_3OD, 400 MHz): δ_{ppm}: 8.23 (9H, CH of trz), 7.18 (3H, CH of arom.core), 6.33 (18H, CH of mesitylene), 5.03 (45H, CH of Cp of [$Fe^{II}Cp(\eta^6$-$C_6H_2Me_3$-)]PF_6, 4.16 (18H, SiCH_2-trz), 2.48 (27H, −CHCCH_3), 2.25 (54H, trzCCCH_3) 1.80 (18H, CH_2CH$_2$CH$_2$Si), 1.31 (18H, CH$_2$CH_2CH$_2$Si), 0.76 (18H, CH$_2$CH$_2$CH_2Si), 0.13 (54H, Si(CH_3)$_2$). ^{13}C NMR of **9** (CD_3OD, 100 MHz), δ_{ppm}: 145.09 (Cq of arom.core), 138.24 (Cq of trz), 127.12 (CH of trz), 124.41 (CH of arom.core), 102.46 (trz-Cq and trz-CCq), 94.05 (CHCq of mesitylene), 88.34 (CH of mesitylene), 78.37 (CH of Cp of [$Fe^{II}Cp(\eta^6$-$C_6H_2Me_3$-)]PF_6, 44.00 (CqCH$_2$CH$_2$CH$_2$Si), 42.01 (CqCH$_2$CH$_2$CH$_2$Si), 40.72 (trz-CH_2Si), 20.34 and 20.20 (−CH_3 of mesitylene), 17.91 (CqCH$_2$CH$_2$CH$_2$Si), 14.92 (CqCH$_2$CH$_2$CH$_2$Si), −4.61 (Si(CH_3)$_2$). ^{19}F NMR of **9** (CD_3OD, 376 MHz), δ_{ppm}: doublet centered at 75.3 ppm (J_{F-P} = 710 Hz). Anal. Calcd for $C_{207}H_{282}Si_9N_{27}Fe_9P_9F_{54}(H_2O)$: C 47.57, H 5.48; found, C 47.64 H 5.22.

Compound 11. Azido-terminated dendrimer **10** (1 equiv, 22.5 mg, 0.004 mmol) and complex **3** (40.0 equiv, 60 mg, 0.144 mmol) were dissolved in a mixture of 20 mL of anhydrous and degassed DMF and 15 mL of anhydrous and degassed THF, then 3 mL of degassed water was added, and the reaction mixture was cooled to 0 °C. Then, an aqueous solution of 1 M $CuSO_4$ (1.1 equiv per branch) was added dropwise, followed by the dropwise addition of a freshly prepared solution of sodium ascorbate (2.2 equiv per branch). The color of the solution changed from yellow to dark orange upon addition of sodium ascorbate. The reaction mixture was allowed to stir for 16 h at 60 °C under nitrogen atmosphere. Then, the mixture of solvents was evaporated *in vacuo*, and 100 mL of nitromethane was added followed by the addition of an aqueous solution of ammonia. The mixture was allowed to stir for 15 min in order to remove all the copper salt trapped inside the dendrimer. The organic phase was washed twice with water, dried over sodium sulfate, and filtered, and the solvent was removed *in vacuo*. Then, the product was precipitated from an acetone solution in diethyl ether and washed with THF to remove the excess of alkyne and further impurities. Product **11** was obtained as an orange-yelow powder. Yield: 56% (35 mg). ^1H NMR of **11** (CD_3COCD_3, 400 MHz), δ_{ppm}: 8.32 (27H, CH of trz), 7.30, 6.90 (39H, CH of arom.core), 6.42 (54H, CH of mesitylene), 5.12 (135H, CH of Cp of [$Fe^{II}Cp(\eta^6$-$C_6H_2Me_3$-)]PF_6, 4.20 (54H, SiCH_2-trz), 3.59 (18H, SiCH_2O), 2.51 (3H, −CHCCH_3) and 2.31 (6H, trzCCCH_3), 1.73 (72H, CH_2CH$_2$CH$_2$Si), 1.28 (72H, CH$_2$CH_2CH$_2$Si), 0.71 (72H, CH$_2$CH$_2$CH_2Si), 0.10 (216H, Si(CH_3)$_2$). ^{13}C NMR of **11** (CD_3COCD_3, 100 MHz), δ_{ppm}: 159.58 (arom. OCq), 139.66 (Cq of trz), 137.47 (Cq of arom.core), 127.51 and 113.81 (arom. CH), 125.59 (CH of trz), 102.76 (trz-Cq), 102.67 (trz-CCq), 94.58 (CHCq of mesitylene), 88.53 (CH of mesitylene), 78.78 (CH of Cp of [$Fe^{II}Cp(\eta^6$-$C_6H_2Me_3$-)]PF_6, 60.20 (CH_2OAr), 43.25 (CqCH$_2$CH$_2$CH$_2$Si), 42.21 (CqCH$_2$CH$_2$CH$_2$Si), 40.97 (trz-CH_2Si), 19.61 (−CH_3 of mesitylene), 17.70 (CqCH$_2$CH$_2$CH$_2$Si), 14.82 (CqCH$_2$CH$_2$CH$_2$Si), −4.16 (Si(CH_3)$_2$). ^{19}F NMR of **11** (CD_3COCD_3, 376 MHz), δ_{ppm}: doublet centered at 73.3 ppm (J_{F-P} = 710 Hz). ^{31}P NMR of **11** (CD_3COCD_3, 162 MHz), δ_{ppm}: −144.1 ppm (hept., PF_6^-) (J_{P-F} = 710 Hz). Anal. Calcd for $C_{720}H_{975}Si_{36}N_{81}Fe_{27}O_9(PF_6)_{27}(H_2O)_2$: C 49.76, H 5.68; found, C 49.48 H 5.81.

■ ASSOCIATED CONTENT

Supporting Information

Spectroscopic data for the bimetallic and metallodendritic complexes (IR, NMR, and mass spectra) and cyclic voltammograms. This material is available free of charge via the Internet at http://pubs.acs.org.

■ AUTHOR INFORMATION

Corresponding Author

*E-mail: d.astruc@ism.u-bordeaux1.fr.

Notes

The authors declare no competing financial interest.

■ ACKNOWLEDGMENTS

Helpful assistance and discussions with Claire Mouche (mass spectrometry, CESAMO), Noël Pinaud (NMR, CESAMO), and Jaime Ruiz (dendrimers, ISM) at the University of Bordeaux and financial support from L'Oréal, the University of Bordeaux, and the Centre National de la Recherche Scientifique (CNRS) are gratefully acknowledged.

■ REFERENCES

(1) (a) Newkome, G. R.; Moorefield, C. N. *Chem. Rev.* **1999**, *99*, 1689−1746. (b) Newkome, G. R.; Moorefield, C. N.; Vögtle, F. *Dendrimers and Dendrons, Syntheses, Concepts, Applications*; Wiley-VCH: Weinheim, Germany, 2001. (c) Hwang, S. H.; Shreiner, C. D.; Moorefield, C. N.; Newkome, G. R. *New J. Chem.* **2007**, *31*, 1192−1217. (d) Vögtle, F.; Richardt, G.; Werner, N. *Dendrimer Chemistry Concepts, Syntheses, Properties, Applications*; Wiley: Weinheim, Germany, 2009. (e) Astruc, D.; Boisselier, E.; Ornelas, C. *Chem. Rev.* **2010**, *110*, 1857−1959. (f) Caminade, A.-M.; Turin, C.-O.; Laurent, R.; Ouali, A.; Delavaux-Nicot, B. *Dendrimers. Towards Catalytic, Material and Biomedical Uses*; Wiley: Weinheim, Germany,

2011. (g) Campana, S.; Ceroni, P.; Punteriero, F. *Designing Dendrimers*; Wiley: Hoboken, NJ, 2012.
(2) (a) Knapen, J. W. J.; van Dermade, A. X.; Dewilde, J. C.; van Leuwen, P. W. N. M.; Wijkens, P.; Grove, D. M.; van Koten, G. *Nature* **1994**, 659−663. (b) Oosterom, G. E.; Reek, J. N. H.; Kamer, P. C. J.; van Leeuwen, P. W. N. M. *Angew. Chem., Int. Ed.* **2001**, *40*, 1828−1849. (c) Astruc, D.; Chardac, F. *Chem. Rev.* **2001**, *101*, 2991−3024. (d) van Heerbeeck, R.; Kamer, P. C. J.; van Leeuwen, P. W. N. M.; Reek, J. N. H. *Chem. Rev.* **2002**, *102*, 3717−3756. (e) Astruc, D.; Heuze, K.; Gatard, S.; Méry, D.; Nlate, S. *Adv. Synth. Catal.* **2005**, *347*, 329−338. (f) Liang, C.; Fréchet, J. M. J. *Prog. Polym. Sci.* **2005**, *30*, 385−402. (g) Scott, R.W. J.; Wilson, O. M.; Crooks, R. M. *J. Phys.Chem. B* **2005**, *109*, 692−704. (h) de Jesus, E.; Flores, J. C. *Ind. Eng. Chem. Res.* **2008**, *47*, 7968−7981. (i) Wang, D.; Astruc, D. *Coord. Chem. Rev.* **2013**, *257*, 2317−2334.
(3) (a) Percec, V.; Johansson, G.; Ungar, G.; Zhou, J. P. *J. Am. Chem. Soc.* **1996**, *118*, 9855−9866. (b) Zeng, F.; Zimmermann, S. C. *Chem. Rev.* **1997**, *97*, 1681−1712. (c) Balzani, V.; Campana, S.; Denti, G.; Juris, A.; Serroni, S.; Venturi, M. *Acc. Chem. Res.* **1998**, *31*, 26−34. (d) Matthews, O. A.; Shipway, A. N.; Stoddart, J. F. *Prog. Polym. Sci.* **1998**, *23*, 1−56. (e) Bosman, A. W.; Janssen, H. M.; Meijer, E. W. *Chem. Rev.* **1999**, *99*, 1665. (f) Armada, M. P. G.; Losada, J.; Zamora, M.; Alonso, B.; Cuadrado, I.; Casado, C. M. *Bioelectrochemistry* **2006**, *69*, 65−73. (g) Balzani, V.; Bergamini, G.; Ceroni, P.; Vögtle, F. *Coord. Chem. Rev.* **2007**, *251*, 525. (h) Martinez, F. J.; Gonzales, B.; Alonso, B.; Losada, J.; Garcia-Armada, M. P.; Casado, C. M. *J. Inorg. Organomet. Polym. Mater.* **2008**, *18*, 51−58.
(4) (a) Jiang, D.-L.; Aida, T. *J. Am. Chem. Soc.* **1999**, *121*, 10895−10901. (b) Andronov, A.; Fréchet, J. M. J. *Chem. Commun.* **2000**, 1701−1710. Astruc, D. *Nat. Chem.* **2012**, *4*, 255−267. Bergamini, G.; Marchi, E.; Ceroni, P.; Balzani, V. In *Designing Dendrimers*; Campagna, S., Ceroni, P., Puntoriero, F., Eds.; Wiley: Hoboken, NJ, 2012; pp 341−366.
(5) (a) Casado, C. M.; Morán, M.; Alonso, B.; Barranco, M.; Losada, J. *Appl. Organomet. Chem.* **1999**, *13*, 245−259. (b) Casado, C. M.; Cuadrado, I.; Morán, M.; Alonso, B.; Garcia, B.; Gonzales, B.; Losada, J. *Coord. Chem. Rev.* **1999**, *185*−*186*, 53. (c) Casado, C. M.; Alonso, B.; Losada, J.; Garcia-Armada, M. P. In *Designing Dendrimers*; Campagna, S., Ceroni, P., Puntoriero, F., Eds.; Wiley: Hoboken, NJ, 2012; pp 219−262.
(6) (a) Casado, C. M.; González, B.; Cuadrado, I.; Alonso, B.; Morán, M.; Losada, J. *Angew. Chem., Int. Ed.* **2000**, *39*, 2135−2138. (b) Takada, K.; Diaz, D.; Abruña, H. D.; Cuadrado, I.; Gonzales, B.; Casado, C. M.; Alonso, B.; Morán, M.; Losada, J. *Chem.—Eur. J.* **2001**, *7*, 1109−1117. (c) Yao, H.; Grimes, R. N.; Corsini, M.; Zanello, P. *Organometallics* **2003**, *22*, 4381−4383. (d) Rapakousiou, A.; Wang, Y.; Belin, C.; Pinaud, N.; Ruiz, J.; Astruc, D. *Inorg. Chem.* **2013**, *52*, 6685−6693.
(7) For dendrimers terminated by $[Fe(\eta^5\text{-}C_5H_4\text{-})(\eta^6\text{-}C_6Me_6)][PF_6]$ groups, see Djeda, R.; Ornelas, C.; Ruiz, J.; Astruc, D. *Inorg. Chem.* **2010**, *49*, 6085−6101.
(8) (a) Nesmeyanov, A. N. *Adv. Organomet. Chem.* **1972**, *10*, 1−16. (b) Hamon, J.-R.; Astruc, D.; Michaud, P. *J. Am. Chem. Soc.* **1981**, *103*, 758−766. (c) Green, J. C.; Kelly, M. R.; Payne, M. P.; Seddon, E. A.; Astruc, D.; Hamon, J.-R.; Michaud, P. *Organometallics* **1983**, *2*, 211−218. (d) Moulines, F.; Astruc, D. *Angew. Chem., Int. Ed. Engl.* **1988**, *27*, 1347−1349. (e) Abd-El-Aziz, A. S.; Bernardin, S. *Coord. Chem. Rev.* **2000**, *203*, 219−267. (f) Abd-El-Aziz, A. S.; Todd, E. K. *Coord. Chem. Rev.* **2003**, *246*, 3−52.
(9) (a) Sheats, J. E.; Rausch, M. D. *J. Org. Chem.* **1970**, *35*, 3245−3249. (b) Geiger, W. E. *J. Am. Chem. Soc.* **1974**, *96*, 2632−2634. (c) Sheats, E. *J. Organomet. Chem. Libr.* **1979**, *7*, 461−521. (d) Kemmit, R. D. W.; Russel, D. R. In *Comprehensive Organometallic Chemistry*; Pergamon Press: Oxford, U. K., 1982; Vol *5*, Chapter 34, 4.5.1, pp 244−248. (e) Gloaguen, B.; Astruc, D. *J. Am. Chem. Soc.* **1990**, *112*, 4607−4609.
(10) Astruc, D. *Organometallic Chemistry and Catalysis*; Springer: Heidelberg, Germany, 2008; Chapter 10, pp 275−286.
(11) (a) Wang, Y.; Latouche, C.; Rapakousiou, A.; Lopez, C.; Ledoux-Rak, I.; Ruiz, J.; Saillard, J.-Y.; Astruc, D. *Chem.—Eur. J.* **2014**, *20*, 8076−8088.
(12) Wildschek, M.; Rieker, C.; Jaitner, P.; Schottenberger, H.; Schwarzhans, K. E. *J. Organomet. Chem.* **1990**, *396*, 355−361.
(13) Wang, Y.; Rapakousiou, A.; Ruiz, J.; Astruc, D. *Chem.—Eur. J.* **2014**, DOI: 10.1002/chem.201403085.
(14) (a) Rostovtsev, V. V.; Green, L. G.; Fokin, V. V.; Sharpless, K. B. *Angew. Chem., Int. Ed.* **2002**, *41*, 2596−2599. (b) Tornøe, C. W.. (b1) Christensen, C.; Meldal, M. *J. Org. Chem.* **2002**, *67*, 3057−3064.
(15) (a) Flanagan, J. B.; Margel, S.; Bard, A. J.; Anson, F. C. *J. Am. Chem. Soc.* **1978**, *100*, 4248−4253. (b) Connelly, N. G.; Geiger, W. E. *Chem. Rev.* **1996**, *96*, 877−910. (c) Nishihara, H. *Adv. Inorg. Chem.* **2002**, *53*, 41−86. (d) Zatsepin, T. S.; Andreev, S. Y.; Hianik, T.; Oretskaya, T. S. *Russ. Chem. Rev.* **2003**, *72*, 537−554. (e) Zanello, P. *Inorganic Electrochemistry. Theory, Practice and Applications*; RSC: Cambridge, U.K., 2003. (f) Geiger, W. E. *Organometallics* **2007**, *26*, 5738−5765.
(16) (a) Dessy, R. E.; Stary, F. E.; King, R. B.; Waldrop, M. *J. Am. Chem. Soc.* **1966**, *88*, 471. (b) Moinet, C.; Román, E.; Astruc, D. *J. Electroanal. Chem.* **1981**, *121*, 241−253. (c) Lacoste, M.; Varret, F.; Toupet, L.; Astruc, D. *J. Am. Chem. Soc.* **1987**, *109*, 6504−6506. (d) Desbois, M.-H.; Astruc, D.; Guillin, J.; Varret, F.; Trautwein, A. X.; Villeneuve, G. *J. Am. Chem. Soc.* **1989**, *111*, 5800−5809. (e) Ruiz, J.; Lacoste, M.; Astruc, D. *J. Am. Chem. Soc.* **1990**, *112*, 5471−5483.
(17) Ruiz, J.; Astruc, D. *C. R. Acad. Sci.* **1998**, *t. 1, Sér. IIc*, 21−27.
(18) Astruc, D.; Hamon, J.-R.; Román, E.; Michaud, P. *J. Am. Chem. Soc.* **1981**, *103*, 7502−7514.
(19) Khand, U.; Pauson, P. L.; Watts, W. E. *J. Chem. Soc. C* **1968**, 2257−2259.
(20) (a) Davies, S. G.; Green, M. L. H.; Mingos, D. M. P. *Tetrahedron* **1978**, *34*, 20−50. (b) Astruc, D.; Michaud, P.; Madonik, A.; Saillard, J.-Y.; Hoffmann, R. *Nouv. J. Chim.* **1985**, *9*, 41−50.
(21) Gill, T. P.; Mann, K. R. *Inorg. Chem.* **1980**, *19*, 3007−3010. (b) Gill, T. P.; Mann, K. R. *J. Organomet. Chem.* **1981**, *216*, 65−71.
(22) Rapakousiou, A.; Mouche, C.; Duttine, M.; Ruiz, J.; Astruc, D. *Eur. J. Inorg. Chem.* **2012**, 5071−5077.
(23) (a) Moulines, F.; Djakovitch, L.; Boese, R.; Gloaguen, B.; Thiel, W.; Fillaut, J.-L.; Delville, M.-H.; Astruc, D. *Angew. Chem., Int. Ed.* **1993**, *32*, 1075−1077. (b) Valério, C.; Fillaut, J. L.; Ruiz, J.; Guittard, J.; Blais, J. C.; Astruc, D. *J. Am. Chem. Soc.* **1997**, *119*, 2588−2589.
(24) (a) Newkome, G. R.; Yao, Z.; Baker, G. R.; Gupta, V. K. *J. Org. Chem.* **1985**, *50*, 2003−2004. (b) Newkome, G. R.; Shreiner, C. *Chem. Rev.* **2010**, *110*, 6338−6442.
(25) (a) Sartor, V.; Djakovitch, L.; Fillaut, J.-L.; Moulines, F.; Neveu, F.; Marvaud, V.; Guittard, J.; Blais, J. C.; Astruc, D. *J. Am. Chem. Soc.* **1999**, *121*, 2929−2930. (b) Ruiz, J.; Lafuentes, G.; Marcen, S.; Ornelas, C.; Lazare, S.; Cloutet, E.; Blais, J.-C.; Astruc, D. *J. Am. Chem. Soc.* **2003**, *125*, 7250−7257.
(26) (a) Ornelas, C.; Ruiz, J.; Belin, C.; Astruc, D. *J. Am. Chem. Soc.* **2009**, *131*, 590−601. (b) Boisselier, E.; Diallo, A. K.; Salmon, L.; Ornelas, C.; Ruiz, J.; Astruc, D. *J. Am. Chem. Soc.* **2010**, *132*, 2729−2742. (c) Djeda, R.; Rapakousiou, A.; Liang, L.; Guidolin, N.; Ruiz, J.; Astruc, D. *Angew. Chem., Int. Ed.* **2010**, *49*, 8152−8156.
(27) (a) Sutton, J. E.; Sutton, P. M.; Taube, H. *Inorg. Chem.* **1979**, *18*, 1017−1024. (b) Richardson, D. E.; Taube, H. *Coord. Chem. Rev.* **1984**, *60*, 107−129. (c) Barrière, F.; Geiger, W. E. *Acc. Chem. Res.* **2010**, *43*, 1030−1039.
(28) Gorman, C. B.; Smith, B. L.; Parkhurst, H.; Sierputowska-Gracz, H.; Haney, C. A. *J. Am. Chem. Soc.* **1999**, *121*, 9958−9966.
(29) Amatore, C.; Bouret, Y.; Maisonhaute, E.; Goldsmith, J. I.; Abruña, H. D. *Chem.—Eur. J.* **2001**, *7*, 2206−2226.
(30) Wang, Y.; Salmon, L.; Ruiz, J.; Astruc, D. *Nat. Commun.* **2014**, DOI: 10.1038/ncomms4489.

ChemPubSoc Europe

DOI: 10.1002/chem.201403085

CHEMISTRY
A European Journal
Full Paper

Dendrimers

Metalation of Polyamine Dendrimers with Ethynylcobalticenium for the Construction of Mono- and Heterobimetallic Polycationic Metallodendrimers

Yanlan Wang, Amalia Rapakousiou, Jaime Ruiz, and Didier Astruc*[a]

Abstract: The introduction of robust redox groups at the periphery of common amine-terminated dendrimers is of interest in the design of dendritic nanobatteries, sensors, and redox catalysts. Here we are applying the recently discovered uncatalyzed hydroamination of ethynylcobalticenium, a mild "green" reaction that quantitatively yields *trans*-enamines without the formation of any byproduct, to functionalize dendrimers that are terminated with primary or secondary amino groups. Poly(amido amine) (PAMAM) dendrimers terminated by primary amino groups and arene-centered dendrimers terminated by secondary amino groups yield dendrimers that contain up to 81 *trans*-enamine-cobalticenium termini using this reaction. The hydroamination reaction was also conducted with dendrimers that contained ferrocenylmethylamino groups, which yielded dendrimers that contained both ferrocenyl and cobalticenium termini. The size of the dendrimers was investigated using both dynamic light scattering and diffusion-ordered spectroscopy (DOSY) ^{1}H NMR spectroscopy, and the number of electrons involved in heterogeneous multielectron transfers at electrodes was searched by cyclic voltammetry. The latter works well up to the 27-branch dendrimer, whereas the 81-dendrimer yielded a result in an excess amount (110 electrons) owing to adsorption onto the cathode that becomes all the more significant as the metallodendrimer size increases.

Introduction

Metallodendrimers[1] are a class of well-defined metal-containing macromolecules[2] that show applications in sensing, catalysis, and materials science[1,3] in which the metal fragments are located inside the dendrimers[4] or at the periphery.[5] Metallodendrimers that contain stable redox centers are by and large ferrocene-terminated dendrimers.[6] Cobalticenium dendrimers[7,8] are of interest because of the robustness of the $Co^{III/II}$ redox center[9,10] and their complementarity with ferrocene dendrimers and other iron complexes[11] for electrochemical investigations of anion recognition and sensing and as nanobatteries.

Although cobalticenium branching relied for a long time on tedious synthesis and the functionalization of cobalticenium carboxylic acid,[10] recently the functionalization of ethynylcobalticenium using either click chemistry[12] or uncatalyzed mild hydroamination[13] opened new avenues for the derivatization of cobalticenium on nanomaterials. This latter reaction of readily available ethynylcobalticenium hexafluorophosphate[14,15] with primary and secondary amines is facile, quantitative, and does not form byproducts. It yields air-stable, strongly colored push–pull conjugated cobalticenium *trans*-enamines and thus appears to be an ideal "green" reaction for the efficient and facile functionalization of a variety of aminated dendrimers. These dendrimer functionalizations are illustrated and developed in this article [Eq. (1)].

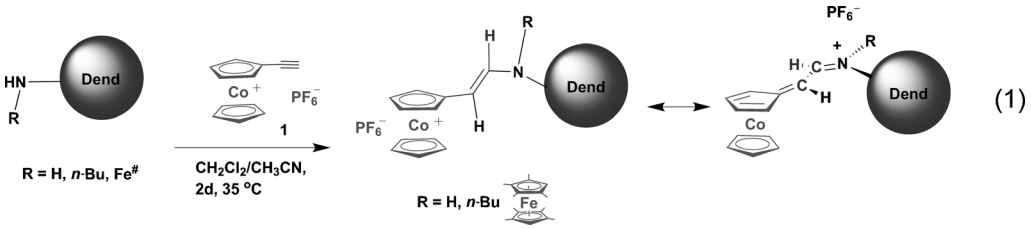

(1)

Results and Discussion

Hydroamination of ethynylcobalticenium 1 with a PAMAM dendrimer

Ethynylcobalticenium **1** was easily synthesized as previously described in 60% overall yield from cobalticenium hexafluorophosphate.[14] The reaction between **1** and the commercially available first-generation poly(amido amine) (PAMAM) dendri-

[a] Dr. Y. Wang, Dr. A. Rapakousiou, Dr. J. Ruiz, Prof. D. Astruc
ISM, UMR CNRS No. 5255, Université Bordeaux
33405 Talence Cedex (France)
E-mail: d.astruc@ism.u-bordeaux1.fr

Supporting information for this article is available on the WWW under http://dx.doi.org/10.1002/chem.201403085.

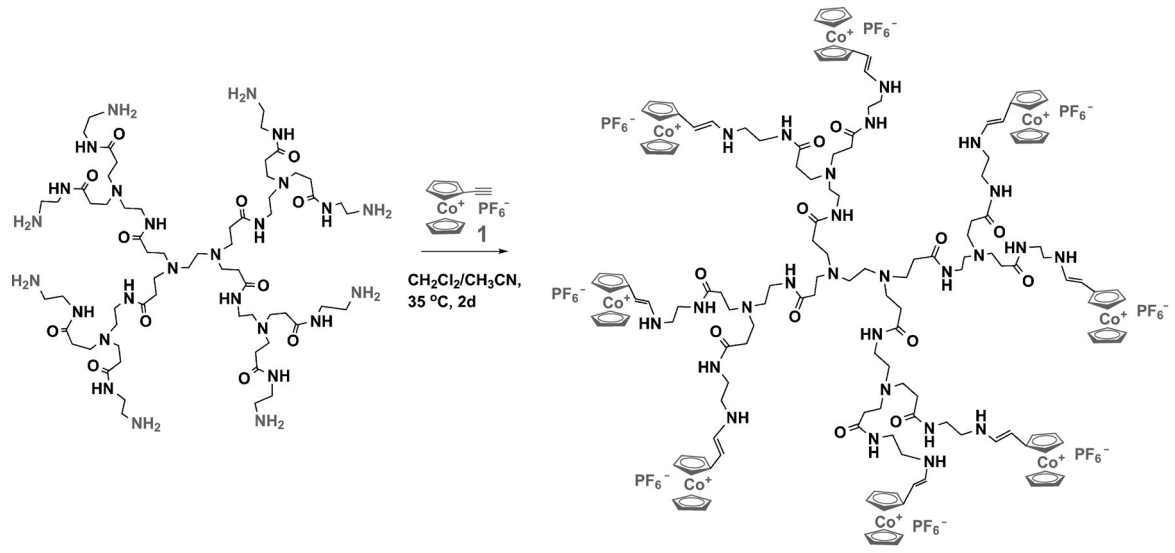

Scheme 1. Reaction of **1** with the first-generation PAMAM dendrimer yielding the all-*trans*-enamine-cobalticenium dendrimer **2**.

mer that contained eight terminal NH_2 groups (20 wt% solution in MeOH) in CH_3CN/CH_2Cl_2 (1:1) at 35 °C for two days yields the all-*trans*-enamine-cobalticenium dendrimer **2** (Scheme 1). The color of the mixture changed from yellow to deep red while stirring the reaction mixture, which indicates the formation of the enamine product. The workup gave a dark red solid that was washed with dry THF to remove the excess amount of complex **1** by using the solubility differences between dendrimer **2** and complex **1** in THF (yield 90%). Dendrimer **2** was fully characterized by ^{1}H (including diffusion-ordered spectroscopy (DOSY)), ^{13}C, ^{29}Si, and ^{31}P NMR spectroscopy; elemental analysis; IR and UV/Vis spectroscopy; and cyclic voltammetry in DMF.

Hydroamination of 1, with three generations of arene-centered dendrimers terminated with (9, 27, 81) secondary amine groups

The hydroamination reaction to construct cobalticenium-functionalized nanomaterials was analogously extended to dendrimers terminated with secondary amine groups. Construction of the generations G0, G1, and G2 chloromethyl(dimethyl)silyl dendrimers with 1→3 connectivity[16] proceeded as described previously upon $CpFe^+$-induced (Cp = cyclopentadienyl) triallylation of mesitylene and *p*-methoxytoluene followed, after decomplexation, by hydrosilylation of the polyallyl dendritic cores and dendron using chloromethyldimethylsilane and iteration using a Williamson reaction with the tri-branched phenol dendron (phenol triallyl).[17] The terminal chloro groups were then substituted by iodo groups by reaction with sodium iodide to provide iodo-terminated dendrimers. Thus, the arene-cored dendrimer with terminal −NH*n*Bu groups (easily available upon Williamson reaction between the benzaldehyde dendrimer and butylamine followed by imine reduction) reacts with **1** to give the three generations of all-*trans*-enamine-cobalticenium dendrimers (Schemes 2, 3, and 4), which were fully characterized by ^{1}H (including DOSY), ^{13}C, ^{29}Si NMR spectroscopy; IR and UV/Vis spectroscopy; elemental analysis; and cyclic voltammetry.

Hydroamination of 1 with a nona-NHFc$^{\#}$ dendrimer and synthesis of the bimetallic dendrimer 12

The convenience of the functionalization of nanomaterials with the ethynylcobalticenium PF_6 and the stability of the enamine-functionalized dendrimers encouraged the construction of heterobimetallic dendrimers **12** by this effective method (Scheme 5). The nona-NHFc$^{\#}$ dendrimer terminated with nine octamethylferrocenylmethyl secondary amines was reported previously.[18] Its synthesis involves the reaction of FcCHO with the dendritic amine, a method that was pioneered by Casado's group.[18b] The reaction of this nona-NHFc$^{\#}$ dendrimer with **1** leads to the heterobimetallic dendrimer **12** as a dark red solid (yield 90%) that was characterized by ^{1}H (including DOSY), ^{13}C, and ^{29}Si NMR spectroscopy; IR and UV/Vis spectroscopy; elemental analysis; and cyclic voltammetry.

Characterizations of the enamine cobalticenium dendrimers

In the course of the synthesis of **5**, the new intermediate dendrimer **3** obtained by Williamson reaction was characterized by ^{1}H, ^{13}C, and ^{29}Si NMR spectroscopy; IR spectroscopy; MALDI-MS; and elemental analysis. The ^{1}H NMR spectrum showed the typical chemical shift of the proton on the CHO group at $\delta =$ 9.88 ppm in $CDCl_3$, which corresponded to the peak at $\delta =$ 190.64 ppm in the ^{13}C NMR spectrum assigned to the CHO carbon. The IR (KBr) spectrum also confirmed the structure with the strong absorbance at 1690 cm^{-1} ($\nu_{C=O}$) and 2750 cm^{-1} (ν_{CHO}), and the molecular ion in MALDI-TOF spectroscopy for

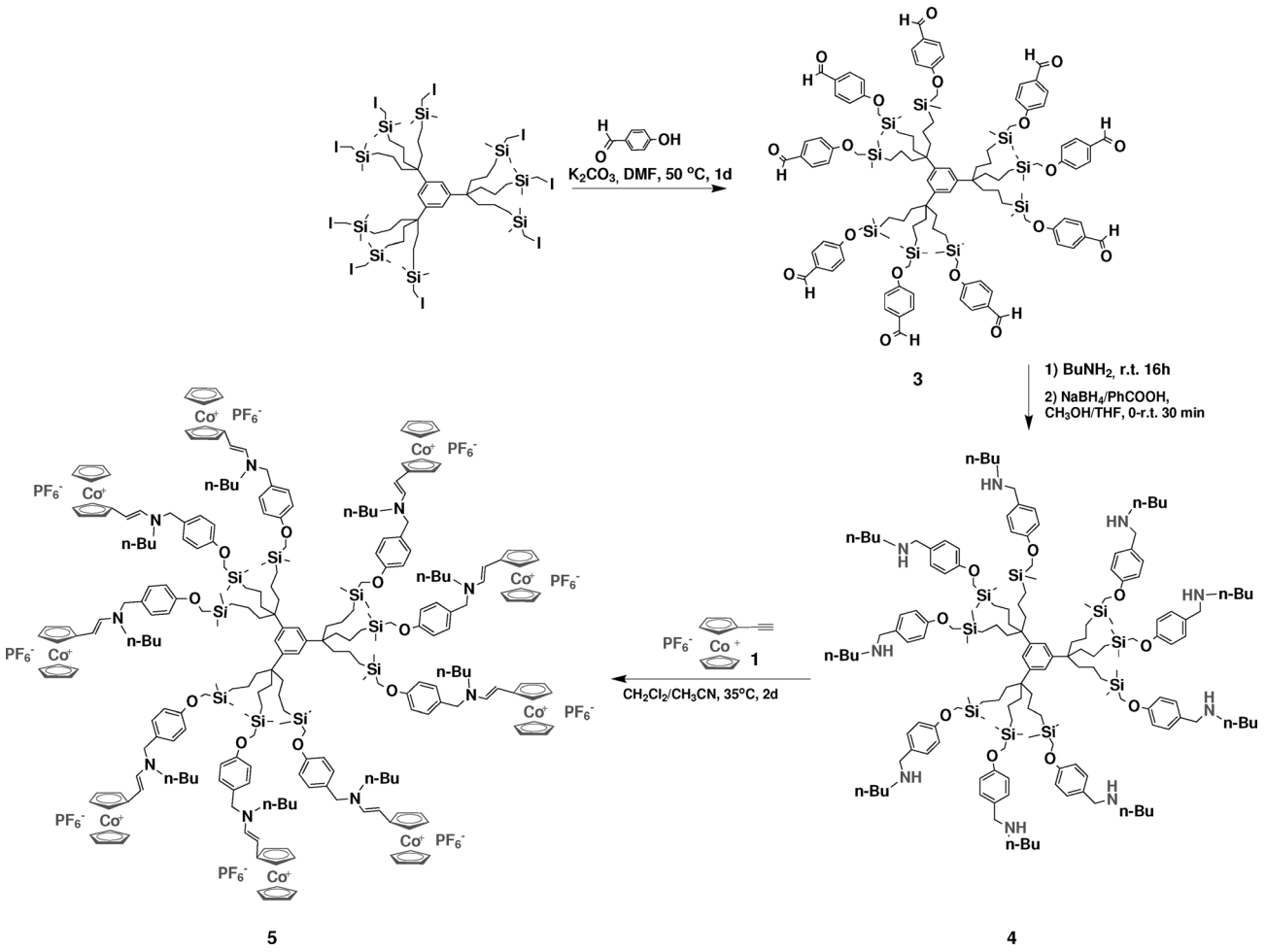

Scheme 2. Synthesis of the dendrimer G0-**3** by Williamson reaction between G0-CH_2I (nine branches) and 4-hydroxybenzaldehyde; synthesis of the G0 dendrimer **4** terminated with nine secondary amine groups and uncatalyzed hydroamination of **1** with dendrimer **4** to give the all-*trans*-enamine-cobaltocenium dendrimer **5**.

$(C_{126}H_{174}O_{18}Si_9)Na^+$ was found at 2251.7 (see the Supporting Information).

The reaction between the 9-benzaldehyde dendrimer **3** and an excess amount of neat *n*-butylamine at RT under N_2 gave a light yellow oil as the intermediate imine complex that was characterized by ^1H, ^{13}C, and ^{29}Si NMR spectroscopy; IR spectroscopy; MALDI-TOF MS; and elemental analysis. The ^1H NMR spectrum showed the disappearance of the CHO group at $\delta =$ 9.88 ppm (300 MHz, $CDCl_3$) and the appearance of the new chemical shift at $\delta = 8.12$ ppm for the –CH=N– proton, and the IR (KBr) showed the strong absorbance at 1645 cm^{-1} assigned to the C=N bond absorption. In the MALDI-TOF spectrum of the G0 nona-imine ($C_{162}H_{255}O_9Si_9N_9$), the molecular peak was found at 2725.4 (see Supporting Information). Then this G0-nona-imine was reduced by $NaBH_4$/PhCOOH at 0 °C in MeOH/THF (1:1),[19] thus giving the 9-NH*n*Bu dendrimer **4** as a light yellow oil (yield 90%), which was characterized by ^1H, ^{13}C, ^{29}Si NMR spectroscopy; IR spectroscopy; MALDI-TOF MS; and elemental analysis. The ^1H NMR spectrum showed the disappearance of the chemical shift at $\delta = 8.12$ ppm that belonged to the –CH=N– group and the appearance of the new peak at $\delta = 3.45$ ppm that was assigned to the two protons on the –$PhCH_2N$– groups. The IR spectrum (KBr) showed the absorbance at 3300 cm^{-1} (ν_{N-H}), and the molecular ion in MALDI-TOF for **4** ($(C_{116}H_{273}O_9Si_9N_9)Na^+$ was found at *m/z* 2765.4. Upon reaction between **1** and the 9-NH*n*Bu dendrimer **4** in CH_3CN/CH_2Cl_2 (1:1) at 35 °C, the color of the mixture changed from yellow to deep red, and after two days the reaction was completed, thus giving the quite air-stable all-*trans*-enamine-cobalticenium dendrimer **5** that was characterized by ^1H (including DOSY), ^{13}C, ^{29}Si, and ^{31}P NMR spectroscopy; elemental analysis; IR and UV/Vis spectroscopy; MALDI-TOF MS; and cyclic voltammetry. The two protons on the –CH=CH– groups appeared at $\delta = 4.87$ ppm (d, $J = 11.72$ Hz, 9H) and 7.60 ppm (d, $J =$ 11.72 Hz, 9H) of the ^1H NMR spectrum in $(CD_3)_2CO$ and showed the all *trans*-enamine cobalticenium structure, and the MALDI-TOF spectrum confirmed the structure of **5**: *m/z* calcd for $(C_{270}H_{363}O_9Si_9N_9Co_9)(PF_6)_9$: 5965.4; molecular ion found for $(C_{270}H_{363}O_9Si_9N_9Co_9)(PF_6)_8$ at *m/z* 5820.4, for $(C_{270}H_{363}O_9Si_9N_9Co_9)$-$(PF_6)_7$ at *m/z* 5675.5, and for $(C_{270}H_{363}O_9Si_9N_9Co_9)(PF_6)_6$ at *m/z* 5530.7 (Figure 1). All these characterizations indicated that the hydroamination that yielded **5** was quantitative.

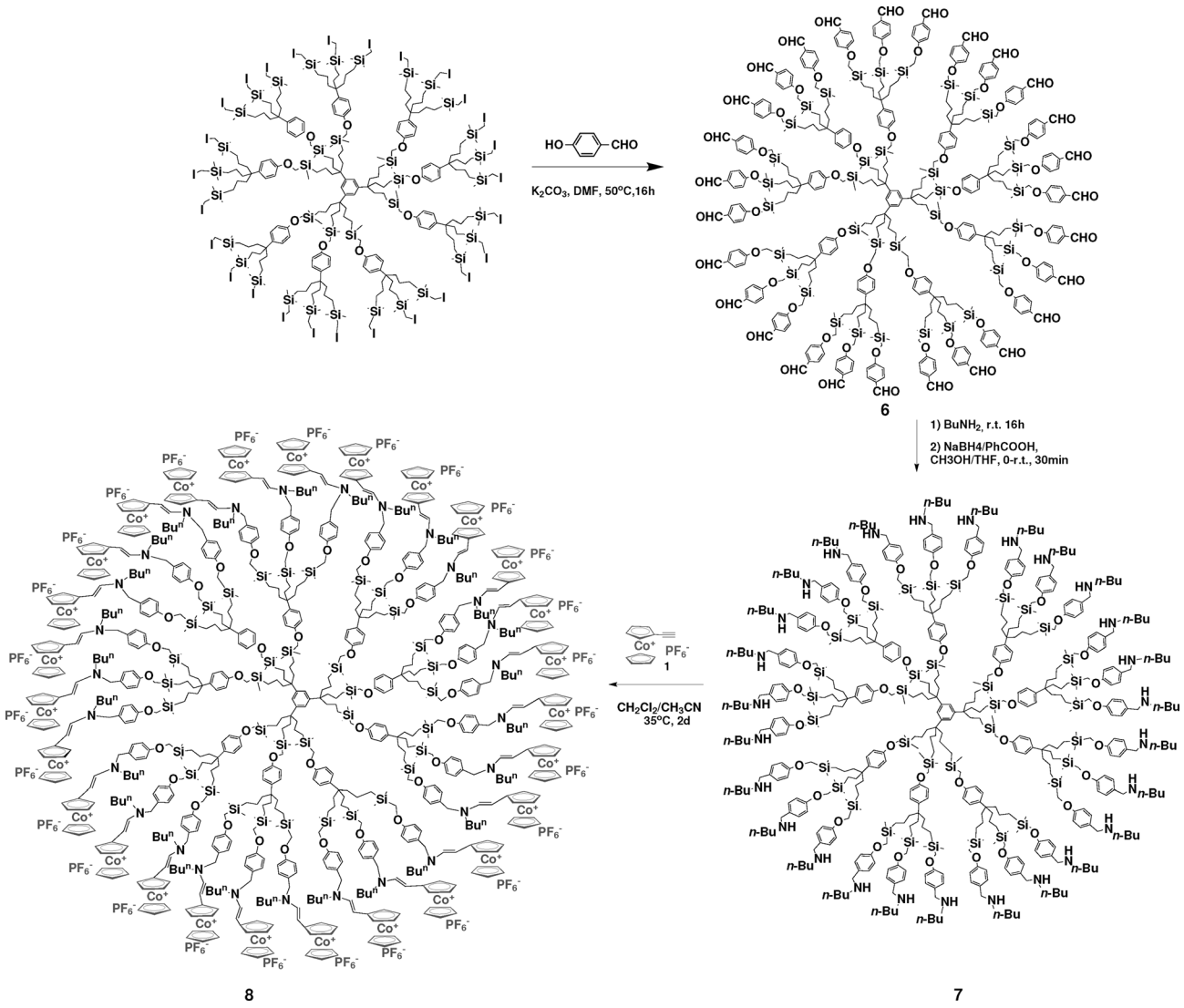

Scheme 3. Synthesis of dendrimer G1-**6** by Williamson reaction between G1-CH_2I (27 branches) and 4-hydroxybenzaldehyde; synthesis of the dendrimer **7** and hydroamination of **1** with dendrimer **7** giving the all-*trans*-enamine-cobalticenium dendrimer **8**.

Generations G1 and G2 of all-*trans*-enamine cobalticenium dendrimers that contained 27 and 81 cobalticenium PF_6 at the periphery were constructed, respectively, by the method described above for the synthesis of the G0 dendrimer; these reactions were completed in two days at 35 °C (Scheme 3 and 4). The intermediate dendrimers **6**, **7**, **9**, and **10** were fully characterized by ^1H, ^{13}C, ^{29}Si NMR spectroscopy; IR spectroscopy; and elemental analysis. These large-generation dark red all *trans*-enamine cobalticenium dendrimers **8** and **11** were fully characterized by ^1H (including DOSY), ^{13}C, ^{29}Si, ^{31}P NMR spectroscopy; IR and UV/Vis spectroscopy; elemental analysis; and cyclic voltammetry in DMF and showed properties that were similar in all these characterizations to those of dendrimer **5** (see the Supporting Information).

As the numbers of cobalticenium hexafluorophosphate groups in the dendrimers increased, the solubility in THF decreased regularly. The smaller dendrimers **2**, **5**, and **12** showed good solubility in THF. However, the solubility of dendrimer **8** in THF was very limited, and the largest dendrimer **11** was not soluble in THF but only DMF. The IR (KBr) for all the cobalticenium-enamine dendrimers showed a strong absorbance at 1614 cm^{-1} for the C=C bond and 836 cm^{-1} for the PF_6 group (Table 1). In the UV/Vis spectra, the weak adsorption in the region of 410–422 nm was assigned to the d–d* transition of cobalticenium,[20] and the transitions in the area of 483–514 nm for all the dendrimers seem to be due to d–d* mixed

Table 1. IR and UV/Vis absorptions for dendrimers **2**, **5**, **8**, **11**, and **12**.

Dendrimer	UV/Vis [nm]		IR [cm^{-1}]	
	λ_{max1}	λ_{max2}	$\nu_{C=C}$	ν_{PF6}
2 (8 Co)	410	483	1621	840
5 (9 Co)	415	495	1614	836
8 (27 Co)	415	495	1614	838
11 (81 Co)	415	495	1814	838
12 (9 Co + 9 Fe[#])	422	514	1607	838

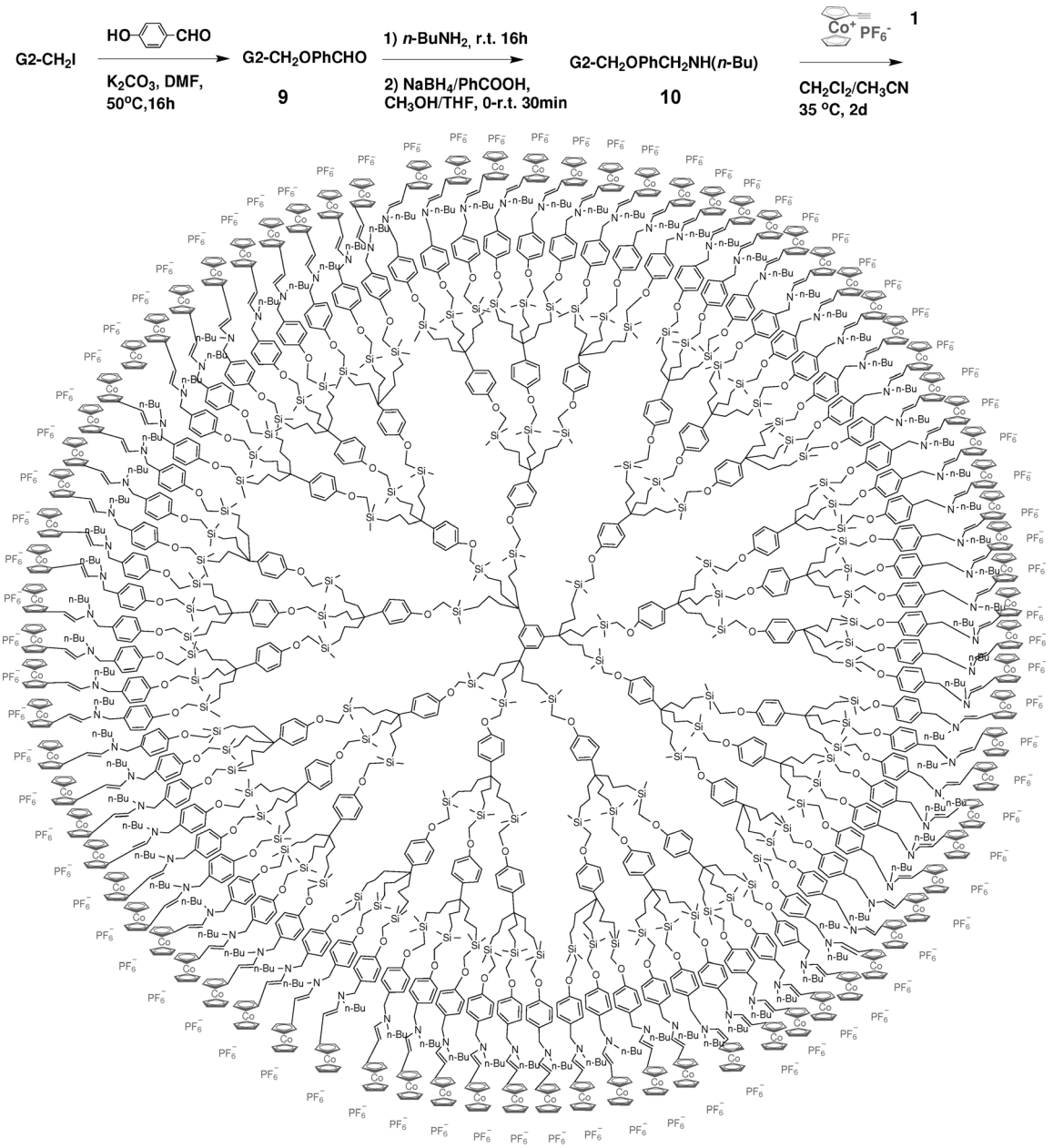

Scheme 4. Synthesis of dendrimer G2-**9** by Williamson reaction with G2-CH_2I (81 branches) and 4-hydroxybenzaldehyde; synthesis of the G2 dendrimer **10** terminated with 81 secondary amine groups and hydroamination of **1** with dendrimer **10** giving the all-*trans*-enamine-cobaltocenium dendrimer **11**.

with charge transfer from the ligand to the metal (Figure 2, Table 1). The variation of λ_{max} within the group of dendrimers **2**, **5**, and **12** is probably caused by the variation of functional group on the enamine (Figure 2).

DOSY experiments were carried out for dendrimers **2**, **5**, **8**, **11**, and **12** in $CO(CD_3)_2$ at 25 °C (Table 2). The main goal of these

Table 2. DOSY and DLS experiments for dendrimers **2**, **5**, **8**, **11**, and **12**.

Compound	D[a] (±0.1) [$m^2 s^{-1}$]	r_H[b] (±0.1) [nm]	r_H[c] (±5) [nm]
2 (8 Co)	1.65×10^{-10}	4.13	–
5 (9 Co)	1.65×10^{-10}	4.13	–
8 (27 Co)	1.03×10^{-10}	6.64	–
11 (81 Co)	0.87×10^{-10}	7.86	35
12 (9 Co + 9 Fe#)	2.22×10^{-10}	3.09	–

[a] Diffusion coefficient measured in $CO(CD_3)_2$ at 25 °C. [b] Hydrodynamic radius from DOSY calculated using the Stokes–Einstein equation. [c] Hydrodynamic diameter from DLS. The values were obtained in acetone. The results are not reliably available for small dendrimers in DLS.

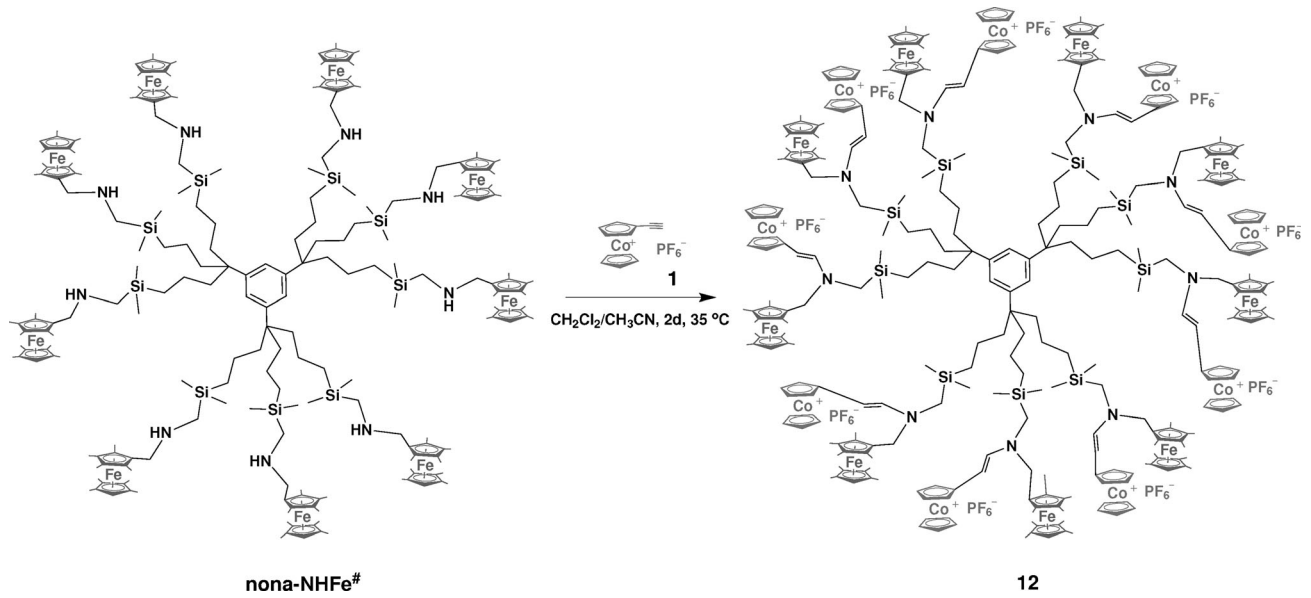

Scheme 5. Synthesis of the bimetallic dendrimer **12** by hydroamination reaction of **1** with nona-NHFc# (Fc# = octamethylferrocenyl).

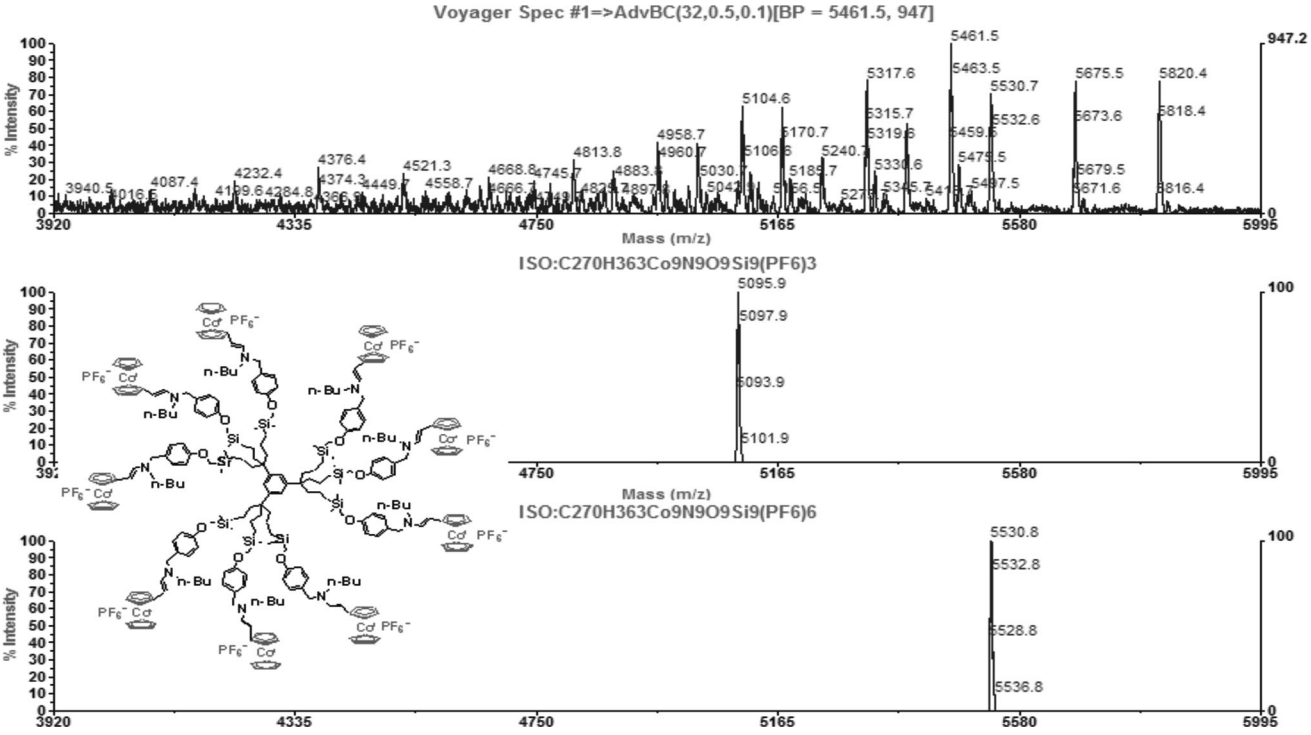

Figure 1. MALDI-TOF spectrum for dendrimer **5**.

experiments was to measure the diffusion coefficient D by ^{1}H NMR spectroscopy. In the ^{1}H NMR spectroscopic experiment, diffusion is mathematically treated as DOSY to obtain the equivalent of 'spectral' chromatography. The objective is thus double: to measure the diffusion coefficients of the molecules in solution and to obtain a DOSY spectrum that reflects the purity of the assembly (see the Supporting Information). For compound **2** (eight branches), the average diffusion coefficient value obtained was $D = (1.65 \pm 0.1) \times 10^{-10}$ m^2 s^{-1}. In the case of the G0 dendrimer **5** (nine branches), the calculated diffusion coefficient was $D = (1.65 \pm 0.1) \times 10^{-10}$ m^2 s^{-1}, and for the dimetallic G0 dendrimer **12** (nine branches) the calculated diffusion coefficient was $D = (2.22 \pm 0.1) \times 10^{-10}$ m^2 s^{-1}. These three small-sized dendrimers **2**, **5**, and **12** gave close hydrodynamic radii of 4.13, 4.13, and 3.09 nm, respectively, under identical conditions. In the case of G1 dendrimer **8** (27 branches), the calculated diffusion coefficient was $D = (1.03 \pm 0.1) \times 10^{-10}$ m^2 s^{-1}, and the hydrodynamic radius was 6.64 nm, whereas in the

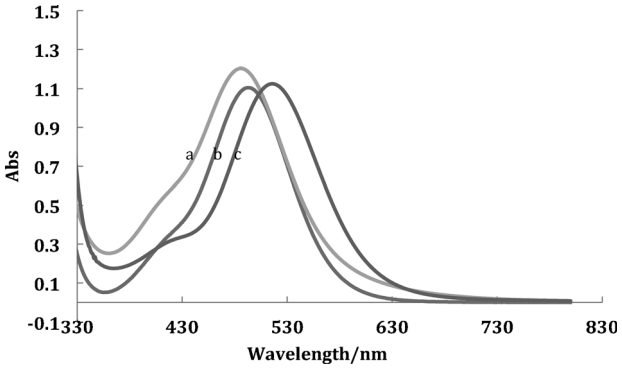

Figure 2. Compared UV/Vis absorptions for dendrimers a) **2**, b) **5**, and c) **12**.

case of the G2 dendrimer **11** (81 branches) the calculated diffusion coefficient was $D=(0.87\pm0.1)\times10^{-10}$ m^2s^{-1}, and the hydrodynamic radius was 7.86 nm. The DOSY experiment results give clear evidence of size progression as dendrimer generation increases. Otherwise, for the largest dendrimer **11**, the values obtained from dynamic light scattering (DLS) were larger than the sizes obtained from DOSY experiments, which is taken into account by the intermolecular associations. For dendrimers **2**, **5**, **8**, **12**, it was not possible to obtain reproducible sizes by DLS because of strong electrostatic intermolecular associations.[21]

Cyclic voltammograms of the dendrimers terminated with cobalticenium

Seminal electrochemical studies of cobalticenium and derivatives have been reported by Geiger, including a reversible $Co^{III/II}$ reduction that generated the neutral d^7 "19-electron" cobaltocene species and at much more negative potential another single-electron reduction to the d^8 "20-electron" Co^{I} anion.[9] Cobaltocenes are thermally stable, air-sensitive complexes, whereas the very-high-energy Co^{I} anion has never been isolated. In molecular nanomaterials such as large metallodendrimers, the second wave is marred by considerable adsorption and chemical irreversibility, therefore the attention here focuses on the first cyclic voltammetry wave that is very useful because its reversibility is still present. The cyclic voltammograms (CVs) of dendrimers **2**, **5**, **8**, **11**, and **12** were determined in DMF with $FeCp^*_2$ ($Cp^*=\eta^5$-C_5Me_5)$_2$)[22] as the reference. The $Co^{III/II}$ reduction wave was indeed found to be chemically and electrochemically reversible (Figure 2). The redox potential $E_{1/2}$ of this reversible $Co^{III/II}$ CV wave in dendrimers ranged from -1.03 to -1.07 V versus $FeCp^*_2$. For the comparatively small dendrimers **2**, **5**, **8**, and **12**, the CVs show an adsorption that is negligible for this reversible $Co^{III/II}$ wave ($i_a/i_c=1$), so that comparison with the internal reference $FeCp^*_2$ provides a good estimation, by using the Bard–Anson equation [Eq. (2)],[23] of the number of electrons n_d involved in the $Co^{III/II}$ redox process as a function of the monomer and dendrimer intensities (i), concentrations (c), and molecular weights (M).

$$n_d = (i_d c_m / i_m c_d)(M_m/M_d)^{0.275} \quad (2)$$

According to this equation, the number of electrons found to be transferred in the $Co^{III/II}$ wave are $n_d=(7.5\pm1)$, (8.2 ± 1), (28 ± 2), and (8.5 ± 1) when using this equation for dendrimers **2**, **5**, **8**, and **12**, respectively, which is in good agreement with the theoretical values of 8, 9, 27, and 9 redox groups in the dendrimers (Table 3). The CV of dendrimer **12** also showed the chemically and electrochemically reversible $Fe^{II/III}$ oxidation wave for the octamethylferrocenyl group. The redox potential $E_{1/2}$ of the $Fe^{II/III}$ wave was 0.20 V versus $FeCp^*_2$ and -0.27 V versus $FeCp_2$, respectively (Table 3, Figure 3C and D). However, for the largest dendrimer **11**, the adsorption during the electrochemistry measurements was more significant than with the smaller dendrimers (Figure 3B), and consequently a larger value $n_d=(110.5\pm5)$ than the theoretical number of redox groups was found.

Table 3. Compared $E_{1/2}$ values and numbers of electrons involved in the redox wave of the cyclic voltammogram for all the cobalticenium dendrimers.[a]

Compound	$E_{1/2}$ [V]	ΔE [mV]	n_d (number of electrons)
2 (8 Co)	−1.05	65	7.5 ± 1
5 (9 Co)	−1.04	60	8.2 ± 1
8 (27 Co)	−1.03	65	28.0 ± 2
11 (81 Co)	−1.03	50	110.5 ± 5
12 (9 Fe^{II} + 9 Co)[b]	−1.07	70	8.5 ± 1

[a] Cyclic voltammetry of cobalticenium-enamine-terminated dendrimers (2 mM) obtained at a Pt electrode at 25 °C in DMF; supporting electrolyte: [nBu$_4$N][PF_6], reversible $Co^{III/II}$ wave. Internal reference: $[FeCp^*_2]^{0/+}$. [b] The redox potential $E_{1/2}$ of the $Fe^{II/III}$ wave was 0.20 V versus $FeCp^*_2$ and −0.27 V versus $FeCp_2$, respectively.

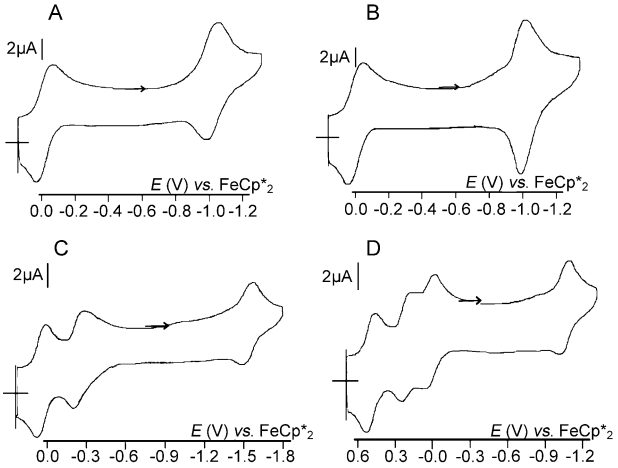

Figure 3. Cyclic voltammograms of A) **5**, B) **11**, and C, D) **12**.

Conclusion

With amine-terminated dendrimers, which are among the most common dendrimers (including the well-known PAMAM dendrimers), the addition of ethynylcobalticenium produces highly conjugated, deeply red-colored *trans*-enamine dendrimers and proceeds smoothly and quantitatively at 35 °C without the need of a catalyst (in contrast to the CuAAC "click" reaction) and without the formation of any byproduct. This uncatalyzed alkyne hydroamination is thus a "green" organometallic reaction that is very useful, because it is the most practical method of introducing the cobalticenium group onto dendrimers and thus also into a variety of other nanomaterials that are functionalized with a primary or secondary amine group. The ease and simplicity of the reaction allowed us to readily synthesize heterobimetallic dendrimers that contain both ferrocenyl and cobalticenium groups, which means that sophisticated nanomaterials become accessible using this method. The cobalticenium dendrimers are valuable since the $Co^{III/II}$ redox center is robust, as shown by the electrochemical studies reported in this article, and very complementary to the ferricenium/ferrocene redox couple. In spite of its robustness and utility, up to now it has been minimally employed owing to tedious synthetic methods, but the present modified procedure reported herein should greatly enhance its applications in the near future.

Experimental Section

General information

THF was dried over Na foil and distilled from the sodium benzophenone anion under nitrogen immediately prior to use. Dichloromethane (CH_2Cl_2) and CH_3CN were distilled from calcium hydride under nitrogen prior to use. All other solvents and chemicals were used as received. ^{1}H NMR spectra were recorded at 25 °C using a Bruker AC (200, 300, 400, 600 MHz) spectrometer. The ^{13}C NMR spectra were obtained in the pulsed FT mode at 75 MHz using a Bruker AC 300 spectrometer. All the chemical shifts (δ) are reported in parts per million with reference to Me_4Si for the ^{1}H and ^{13}C NMR spectra. All the ^{1}H, ^{13}C, ^{29}Si, and ^{31}P and DOSY NMR spectroscopic data and spectra are gathered in the Supporting Information. The mass spectra were recorded using an Applied Biosystems Voyager-DE STR-MALDI-TOF spectrometer (see the Supporting Information). The infrared spectra were recorded using an ATI Mattson Genesis series FTIR spectrophotometer. UV/Vis absorption spectra were measured using a Perkin–Elmer Lambda 19 UV/Vis spectrometer (see the Supporting Information). Electrochemical measurements (cyclic voltammetry) were recorded using a PAR 273 potentiostat under a nitrogen atmosphere at 293 K (see main text and the Supporting Information). The elemental analyses were performed at the Center of Microanalyses of CNRS at Lyon Solaize (France). DOSY NMR spectroscopic measurements were performed at 25 °C using a Bruker AVANCE II 600 MHz spectrometer. They were performed using ^{1}H NMR pulsed-gradient spectroscopic experiments, the simulated spin–echo sequence that leads to the measurement of the diffusion coefficient *D*, in which *D* is the slope of the straight line obtained when ln(*I*) is displayed against the square of the gradient-pulse power according to the following equation [Eq. (3)]:

$$\ln(I) = -\gamma^2 G^2 D \delta^2 (\Delta - \delta/3) \quad (3)$$

in which *I* is the relative intensity of a chosen resonance, γ is the proton gyromagnetic ratio, Δ is the intergradient delay (150 ms), δ is the gradient pulse duration (5 ms), and *G* is the gradient intensity. The diffusion constant of water (2.3×10^9 $m^2 s^{-1}$) was used to calibrate the instrument (see the Supporting Information).

Dendrimer 2

Complex **1** (43.0 mg, 1.2×10^{-4} mol, 1.5 equiv for each branch) and the PAMAM dendrimer G1 (87 μL, 1×10^{-5} mol, 20 wt% solution in MeOH) were dissolved in CH_3CN/CH_2Cl_2 (1:1, 10 mL), then the mixture was stirred for 2 d under N_2 at 35 °C. The color of the mixture changed from yellow to deep red during the stirring. The solvent was removed under vacuum, and the residual solid was washed with dry THF three times, then the residual solid was dried under vacuum to give the all-*trans*-enamine-cobalticenium dendrimer **2** as a dark red solid (42.3 mg, yield 90%). UV/Vis: $\lambda_{max1}=410$ nm, $\lambda_{max2}=483$ nm, $\varepsilon=1.00\times10^5$ $L mol^{-1}$; IR (KBr): $\tilde{\nu}=3430$ (ν_{N-H}), 1614 ($\nu_{CH=CH}$), 838 cm^{-1} (ν_{PF6}); CV = 2 mM, solvent: DMF, *T*: 20 °C, supporting electrolyte: $[nBu_4N][PF_6]$ (0.1 M), working and counter electrodes: Pt, reference electrode: Ag, scan rate: 0.200 $V s^{-1}$, internal reference: $FeCp^*_2$; $E_{1/2(rev)}=-1.05$ V, $\Delta E=65$ mV; elemental analysis calcd (%) for $C_{158}H_{208}N_{26}O_{12}Co_8(PF_6)_8$: C 44.19, H 4.88, N 8.48; found: C 44.36, H 4.59, N 8.57.

Dendrimer 3

The nona-CH_2I dendrimer (228.1 mg, 1×10^{-4} mol, 1 equiv), 4-hydroxybenzaldehyde (1.098 g, 9×10^{-3} mol, 10 equiv for each branch), and K_2CO_3 (2.484 g, 1.8×10^{-2} mol, 20 equiv for each branch) were mixed in one flask under N_2. DMF (10 mL) was added into the mixture with a syringe needle, the solution was stirred at 50 °C under N_2 for 24 h. The color of the solution changed from light yellow to light violet. Distilled H_2O (100 mL) was added to this mixture, a white precipitate formed, and the mixture was kept stirring for 10 min. After filtration, the filtrate was violet, and the residual white solid was on the surface of the Celite. This white solid was washed with H_2O (100 mL four times) to remove the DMF, 4-hydroxybenzaldehyde, and K_2CO_3. The white product was dissolved in CH_2Cl_2 to give a colorless solution. This solution was dried with anhydrous Na_2SO_4, the solvent was evaporated, and the dendrimer was obtained as a colorless gel (200 mg, yield 89%). IR (KBr): $\tilde{\nu}=$ 1690 ($\nu_{C=O}$), 2750 cm^{-1} (ν_{CHO}); MALDI-TOF: *m/z* calcd for $(C_{126}H_{174}O_{18}Si_9)Na^+$: 2252.0; found: 2251.7; elemental analysis calcd (%) for $C_{126}H_{174}O_{18}Si_9$: C 67.88, H, 7.87; found: C 67.93, H 7.77.

Dendrimer 4

The 9-benzaldehyde dendrimer (223 mg, 10^{-4} mol) was dissolved in dry *n*-butylamine (10 mL), and this mixture was stirred at RT under N_2 for 16 h. The excess amount of *n*-butylamine was removed under vacuum to give a light yellow oil as the intermediate imine. IR (KBr): $\tilde{\nu}=1645$ cm^{-1} ($\nu_{C=N}$); MALDI-TOF: *m/z* calcd for $(C_{162}H_{255}O_9Si_9N_9)$: 2725.6; found: 2725.4; elemental analysis calcd (%) for $C_{162}H_{255}O_9Si_9N_9$: C 71.39, H 9.43, N 4.63; found: C 71.50, H 9.55, N 4.67.

The G0-imine dendrimer (824 mg, 3×10^{-4} mol) was dissolved in MeOH/THF (1:1, 10 mL), then the mixed powder of $NaBH_4$ (306.4 mg, 8.1×10^{-3} mol, 3 equiv for each branch) and PhCOOH (998.5 mg, 8.1×10^{-3} mol, 3 equiv for each branch) was added to the solution slowly at 0 °C, and the mixture was left stirring under 0 °C for 30 min. The solvent was removed under vacuum, then dry

CH_2Cl_2 (30 mL) was added to the residual white solid. After separation, the organic solution was washed three times with a saturated $NaHCO_3$ solution and three times with distilled H_2O. The organic phase was dried with anhydrous Na_2SO_4, and the solvent was removed under vacuum to give the 9-NH*n*Bu dendrimer as a light yellow oil (746 mg, yield 90%). IR (KBr): $\tilde{\nu}=3300\ cm^{-1}$ (ν_{N-H}); MALDI-TOF: *m/z* calcd for $(C_{162}H_{273}O_9Si_9N_9)Na^+$: 2764.9; found: 2765.4; elemental analysis calcd (%) for $C_{162}H_{273}O_9Si_9N_9$: C 70.92, H 10.03, N 4.59; found: C 70.67, H 10.12, N 4.65.

Dendrimer 5

Complex **1** (87 mg, 0.23 mmol, 2.63 equiv for each branch) and the 9-NH*n*Bu dendrimer **4** (27.43 mg, 0.01 mmol) were dissolved in CH_3CN/CH_2Cl_2 (1:1, 10 mL), then the mixture was stirred for 2 d under N_2 at 35 °C, and the color of the mixture changed from yellow to deep red during the stirring. The solvent was removed under vacuum, the dark red solid was washed three times with dry THF, then the residual dark red solid was dried under vacuum to give **5** as a dark red solid (53.7 mg, yield 90%). IR (KBr): $\tilde{\nu}=1614$ ($\nu_{C=C}$), 836 cm^{-1} (ν_{PF6}); UV/Vis: $\lambda_{max1}=415$ nm, $\lambda_{max2}=495$ nm, $\varepsilon=1.12\times10^5\ L\,mol^{-1}\,cm$; CV = 2 mM, solvent: DMF, *T*: 20 °C, supporting electrolyte: $[nBu_4N][PF_6]$ (0.1 M), working and counter electrodes: Pt, reference electrode: Ag, scan rate: $0.200\ V\,s^{-1}$, internal reference: $FeCp^*_2$; $E_{1/2(rev)}=-1.03$ V, $\Delta E=65$ mV; MALDI-TOF: *m/z* calcd for $(C_{270}H_{363}O_9Si_9N_9Co_9)(PF_6)_9$: 5965.4; found $(C_{270}H_{363}O_9Si_9N_9Co_9)(PF_6)_8$: 5820.4; elemental analysis calcd for $(C_{270}H_{363}O_9Si_9N_9Co_9)(PF_6)_9$: C 54.35, H 6.13, N 2.11; found: C 53.40, H 6.18, N 2.23.

Dendrimer 6

The G1-CH_2I dendrimer (228.1 mg, 1×10^{-4} mol, 1 equiv), 4-hydroxybenzaldehyde (1.098 g, 9×10^{-3} mol, 10 equiv for each branch), and K_2CO_3 (2.484 g, 1.8×10^{-2} mol, 20 equiv for each branch) were mixed in a flask under N_2. DMF (10 mL) was added into the mixture with a syringe needle, and the solution was stirred at 50 °C under N_2 for 24 h. The color of the solution changed from light yellow to light violet. H_2O (100 mL) was added to this mixture, a white precipitate formed, and the mixture was kept stirring for 10 min. After filtration, the filtrate was violet, and the residual white solid was left on the surface of the Celite. The white solid was washed with H_2O (100 mL four times) to remove the DMF, 4-hydroxybenzaldehyde, and K_2CO_3. The white product was dissolved in CH_2Cl_2 to give a colorless solution. The solution was dried with anhydrous Na_2SO_4 and evaporated, and the compound was obtained as a colorless gel (200 mg, yield 89%). IR (KBr): $\tilde{\nu}=1691\ cm^{-1}$ ($\nu_{CH=O}$); MALDI-TOF: *m/z* calcd for $(C_{477}H_{678}O_{63}Si_{36}Na^+)$: 8454.5; found: 8454.3; elemental analysis calcd (%) for $C_{477}H_{678}O_{63}Si_{36}$: C 67.95 H 8.11; found: C 67.58, H 8.01.

Dendrimer 7

The 27-benzaldehyde dendrimer **6** (843.2 mg, 1×10^{-4} mol) was dissolved in dry *n*-butylamine (10 mL), and this mixture was stirred at RT under N_2 for 16 h. The excess amount of *n*-butylamine was removed under vacuum, which gave the G1-imine as a light yellow oil. This compound was dissolved in MeOH/THF (1:1, 10 mL), then the mixed powder of $NaBH_4$ (306.4 mg, 8.1×10^{-3} mol, 3 equiv for each branch) and PhCOOH (998.5 mg, 8.1×10^{-3} mol, 3 equiv for each branch) was slowly added to the solution at 0 °C, then the mixture was left stirring under 0 °C for one hour. The solvent was removed under vacuum, dry CH_2Cl_2 (30 mL) was added to the residual white solid, and after filtration the organic solution was washed three times with saturated $NaHCO_3$ and three times with distilled H_2O. The organic phase was dried with anhydrous Na_2SO_4, and the solvent was removed under vacuum to give the 27-NH*n*Bu dendrimer **7** as a light yellow oil (897 mg, yield 90%). For G1-imine: IR (KBr): $\tilde{\nu}=1645\ cm^{-1}$ ($\nu_{CH=N}$); elemental analysis calcd (%) for $C_{585}H_{921}N_{27}O_{36}Si_{36}$: C 70.83, H 9.36, N 3.81; found: C 70.65, H 9.46, N 3.67. For **7**: MALDI-TOF: *m/z* calcd for $(C_{585}H_{975}N_{27}O_{36}Si_{36}Na^+)$: 9997.2; found: 9998.2; elemental analysis calcd (%) for $C_{585}H_{975}N_{27}O_{36}Si_{36}$: C 70.44, H 9.85, N 3.79; found: C 70.61, H 9.62, N 3.68.

Dendrimer 8

Complex **1** (90 mg, 2.43×10^{-4} mmol, 1.5 equiv for each branch) and the 27-NH*n*Bu dendrimer **7** (60 mg, 6×10^{-6} mol) were dissolved in CH_3CN/CH_2Cl_2 (1:1, 10 mL), then the mixture was stirred for 2 d under N_2 at 35 °C; the color of the mixture changed from yellow to deep red during the stirring. The solvent was removed under vacuum, the dark red solid was washed with dry THF and filtered three times, and the residual dark red solid was dried under vacuum to give compound **8** as a dark red solid (108 mg, yield 90%). UV/Vis: $\lambda_{max1}=415$ nm, $\lambda_{max2}=495$ nm, $\varepsilon=3.38\times10^5\ L\,mol^{-1}$; IR (KBr): $\tilde{\nu}=1614$ ($\nu_{CH=CH}$), 838 cm^{-1} (ν_{PF6-}); CV = 2 mM, solvent: DMF, *T*: 20 °C; supporting electrolyte: $[nBu_4N][PF_6]$ (0.1 M), working and counter electrodes: Pt, reference electrode: Ag, scan rate: $0.200\ V\,s^{-1}$; internal reference: $FeCp^*_2$; $E_{1/2(rev)}=-1.03$ V, $\Delta E=65$ mV; elemental analysis calcd (%) for $C_{909}H_{1245}N_{27}O_{36}Si_{36}Co_{27}(PF_6)_{27}$: C 55.58, H 6.39, N 1.93; found: C 55.95, H 6.64, N 1.81.

Dendrimer 9

The G2-CH_2I dendrimer (145 mg, 5.27×10^{-3} mmol, 1 equiv), 4-hydroxybenzaldehyde (521 mg, 4.27×10^{-3} mmol, 10 equiv for each branch), and K_2CO_3 (1.178 g, 8.54×10^{-3} mmol, 20 equiv for each branch) were mixed in a flask under N_2. DMF (10 mL) was added into the mixture with a syringe needle, the solution was stirred at 50 °C under N_2 for 24 h and the color of the solution changed from light yellow to light violet. H_2O (100 mL) was added to this mixture, a white precipitate formed, and the mixture was kept stirring for 10 min. After filtration, the filtrate was violet and the residual white solid was on the surface of the Celite. The white solid was washed with H_2O (100 mL four times) to remove the DMF, the excess amount 4-hydroxybenzaldehyde, and K_2CO_3, and the white product was dissolved in CH_2Cl_2 to give a colorless solution. After drying with anhydrous Na_2SO_4, and under vacuum, compound **9** was obtained as a colorless gel (128 mg, yield 90%). IR (KBr): $\tilde{\nu}=1688\ cm^{-1}$ ($\nu_{CH=O}$); elemental analysis calcd (%) for $C_{1530}H_{2190}O_{198}Si_{117}$: C 67.97, H 8.16; found: C 67.65, H 8.32.

Dendrimer 10

The 81-benzaldehyde dendrimer **9** (142 mg, 5.27×10^{-3} mmol) was dissolved in dry *n*-butylamine (10 mL), this mixture was stirred at RT under N_2 for 16 h, the excess amount of *n*-butylamine was removed under vacuum, and the residual light yellow oil was dissolved in MeOH/THF (1:1, 10 mL). The mixed powder of $NaBH_4$ (80.8 mg, 2.135×10^{-3} mol, 5 equiv for each branch) and PhCOOH (260.5 mg, 2.135×10^{-3} mol, 5 equiv for each branch) was slowly added to the solution at 0 °C. The mixture was left stirring under 0 °C for 30 min, the solvent was removed under vacuum, and dry CH_2Cl_2 (30 mL) was added to the residual white solid. After filtration, the organic solution was washed three times with saturated $NaHCO_3$ solution and three times with distilled H_2O. The organic phase was dried with anhydrous Na_2SO_4, and the solvent was removed under vacuum to give the 81-NH*n*Bu dendrimer as light

yellow oil (137.5 mg, yield 90%). For G2-imine: IR (KBr): $\tilde{\nu}$ = 1645 cm^{-1} ($\nu_{CH=N}$); elemental analysis calcd (%) for $C_{1854}H_{2919}O_{117}Si_{117}N_{81}$: C 70.69, H 9.34, N 3.60; found: C 70.65, H 9.32, N 3.35. For **10**: elemental analysis calcd (%) for $C_{1854}H_{3081}O_{117}Si_{117}N_{81}$: C 70.32, H 9.81, N 3.58; found: C 70.60, H 9.64, N 3.69.

Dendrimer 11

Complex **1** (27.9 mg, 7.8×10^{-2} mmol, 1.5 equiv for each branch) and the 81-NH*n*Bu dendrimer **10** (20 mg, 6.4×10^{-4} mmol) were dissolved in CH_3CN/CH_2Cl_2 (1:1, 10 mL), the mixture was stirred for 2 d under N_2 at 35 °C, and the color of the mixture changed from yellow to deep red during the stirring. The solvent was removed under vacuum, the dark red solid was washed three times with dry THF, then the residual solid was dried under vacuum to give **11** as a dark red solid (34.7 mg, yield 90%). UV/Vis: λ_{max1} = 410 nm, λ_{max2} = 496 nm ($\varepsilon = 1.12\times10^6$ L mol^{-1} cm^{-1}); IR (KBr): $\tilde{\nu}$ = 1614 ($\nu_{CH=CH}$), 838 cm^{-1} (ν_{PF6}); CV = 2 mM, solvent: DMF, *T*: 20 °C, supporting electrolyte: [*n*Bu_4N][PF_6] (0.1 M), working and counter electrodes: Pt, reference electrode: Ag, scan rate: 0.200 V s^{-1}, internal reference: $FeCp^*_2$; $E_{1/2(rev)} = -1.03$ V, ΔE = 50 mV; elemental analysis calcd (%) for $C_{2826}H_{3891}O_{117}Si_{117}N_{81}Co_{81}(PF_6)_{81}$: C 55.94, H 6.46, N 1.87; found: C 56.30, H 6.64, N 1.69.

Dendrimer 12

Complex **1** (27.8 mg, 7.8×10^{-2} mmol, 1.5 equiv for each branch) and the nona-NHFc# dendrimer (25 mg, 5.75×10^{-3} mmol) were dissolved in a mixture of CH_3CN (10 mL) and CH_2Cl_2 (10 mL). This solution was stirred for 2 d under N_2 at 35 °C. The color of the mixture changed from yellow to deep red during the stirring, dibutylamine (5 mL) was added, and the mixture was stirred for 30 min at RT. The solvent was removed under vacuum, the residual dark red solid was washed with dry diethyl ether and filtered three times, and it was dried under vacuum to give **12** as a dark red solid (38.8 mg, yield 90%). UV/Vis: λ_{max1} = 322 nm, λ_{max2} = 422 nm, λ_{max3} = 514 nm ($\varepsilon = 1.15\times10^5$ L mol^{-1} cm^{-1}); IR (KBr): 1607 ($\nu_{C=C}$), 838 cm^{-1} (ν_{PF6}); CV 2 mM, solvent: DMF, *T*: 20 °C, supporting electrolyte: [*n*Bu_4N][PF_6] 0.1 M, working and counter electrodes: Pt, reference electrode: Ag, scan rate: 0.200 V s^{-1}, internal reference: $FeCp^*_2$; $E_{1/2(rev)} = 0.20$ V, ΔE = 70 mV; $E_{1/2(rev)} = -1.07$ V, ΔE = 70 mV; elemental analysis calcd (%) for $C_{360}H_{525}Si_9N_9Co_9Fe_9(PF_6)_9$: C 57.12, H 6.99, N 1.67; found: C 57.30, H 6.74, N 1.69.

Acknowledgements

Helpful assistance and discussions with Claire Mouche (mass spectrometry) and Jean-Michel Lanier (NMR spectroscopy) from the CESAMO, Université de Bordeaux, and financial support from the Université of Bordeaux, the Centre National de la Recherche Scientifique (CNRS), and the China Scholarship Council (PhD grant to Y.W.) is gratefully acknowledged.

Keywords: cyclic voltammetry · dendrimers · electron transfer · enamines · redox chemistry

[1] a) G. R. Newkome, E. He, C. N. Moorefield, *Chem. Rev.* **1999**, *99*, 1689–1746; b) S.-H. Hwang, C. D. Shreiner, C. N. Moorefield, C. N. Newkome, *New J. Chem.* **2007**, *31*, 1192–1217; c) M. Gingras, J. M. Raimondo, Y.-M. Chabre, *Angew. Chem.* **2007**, *119*, 1028–1035; *Angew. Chem. Int. Ed.* **2007**, *46*, 1010–1017; d) T. Imioka, K. Yamamoto, S. Campagna, P. Ceroni, F. Puntoriero, *Designing Dendrimers*, Wiley, **2012**, Hoboken, New Jersey, pp. 303–339.

[2] a) P. Nguyen, P. Gomez-Elipe, C. Manners, *Chem. Rev.* **1999**, *99*, 1515–1528; b) I. Manners, *Science* **2001**, *294*, 1664–1666; c) G. R. Whittell, I. Manners, *Adv. Mater.* **2007**, *19*, 3239–3468; d) *Frontiers in Transition-Metal-Containing Polymers* (Eds.: A. S. Abd-El-Aziz, I. Manners), Wiley, New York, **2007**; e) G. R. Whittell, M. D. Hager, U. S. Schubert, I. Manners, *Nat. Mater.* **2011**, *10*, 176–188.

[3] D. Astruc, E. Boisselier, C. Ornelas, *Chem. Rev.* **2010**, *110*, 1857–1959.

[4] a) V. Balzani, G. Bergamini, P. Ceroni, F. Vögtle, *Coord. Chem. Rev.* **2007**, *251*, 525–535; b) D. Astruc, *Nat. Chem.* **2012**, *4*, 255–267.

[5] a) G. R. Newkome, C. N. Moorefield, F. Vögtle, *Dendrimers and Dendrons. Concepts, Syntheses, Applications*, Wiley-VCH, Weinheim, **2001**; b) A.-M. Caminade, C.-O. Turrin, R. Laurent, A. Ouali, B. Delavaux-Nicot, *Dendrimers,* Wiley, Chichester, UK, **2011**.

[6] a) C. M. Casado, I. Cuadrado, M. Morán, B. Alonso, B. Garcia, B. Gonzales, J. Losada, *Coord. Chem. Rev.* **1999**, *185–186*, 53–79; b) C. Ornelas, J. Ruiz, C. Belin, D. Astruc, *J. Am. Chem. Soc.* **2009**, *131*, 590–601; c) C. M. Casado, B. Alonso, M. P. Garcia-Armanda, S. Campagna, P. Ceroni, F. Puntoriero, *Designing Dendrimers,* Wiley, **2012**, Hoboken, New Jersey, pp. 219–262.

[7] a) B. González, C. Casado, B. Alonso, I. Cuadrado, M. Moran, Y. Wang, A. E. Kaiker, *Chem. Commun.* **1998**, 2569–2570; b) C. M. Casado, B. González, I. Cuadrado, B. Alonso, M. Morán, J. Losada, *Angew. Chem.* **2000**, *112*, 2219–2222; *Angew Chem. Int. Ed. Engl.* **2001**, *40*, 224–227; c) K. Takada, D. J. Diaz, H. D. Abruña, I. Cuadrado, B. Gonzalez, C. M. Casado, B. Alonso, M. Morán, J. Losada, *Chem. Eur. J.* **2001**, *7*, 1109–1117; d) B. González, I. Cuadrado, B. Alonso, C. M. Casado, M. Morán, A. E. Kaifer, *Organometallics* **2002**, *21*, 3544–3551; e) H. Yao, R. N. Grimes, M. Corsini, P. Zanello, *Organometallics* **2003**, *22*, 4381–4383.

[8] B. Alonso, A. P. García, J. Losada, I. Cuadrado, B. González, C. M. Casado, *Biosens. Bioelectron.* **2004**, *19*, 1617–1625.

[9] a) W. E. Geiger, *J. Am. Chem. Soc.* **1974**, *96*, 2632–2634; b) W. E. Geiger, W. L. Bowden, N. El Murr, *Inorg. Chem.* **1979**, *18*, 2358–2361; c) N. G. Connelly, W. E. Geiger, *Chem. Rev.* **1996**, *96*, 877–910; d) W. E. Geiger, *Organometallics* **2007**, *26*, 5738–5765 (a historical review); e) W. E. Geiger, *Organometallics* **2011**, *30*, 28–31 (a perspective review).

[10] For cobalticenium chemistry, see: a) J. E. Sheats, M. D. Rausch, *J. Org. Chem.* **1970**, *35*, 3245–3249; b) B. Gloaguen, D. Astruc, *J. Am. Chem. Soc.* **1990**, *112*, 4607–4609; c) D. Braga, G. Cojazzi, L. Maini, M. Polito, F. Grepioni, *Chem. Commun.* **1999**, 1949–1950; d) M.-H. Baik, R. A. Fiesner, *J. Phys. Chem. A* **2002**, *106*, 7402–7412.

[11] a) A. S. Abd-El-Aziz, S. Bernardin, *Coord. Chem. Rev.* **2000**, *203*, 219–267; b) C. Moinet, E. Roman, D. Astruc, *J. Electroanal. Chem.* **1981**, *121*, 241–253; c) F. Moulines, D. Astruc, *Angew. Chem.* **1988**, *100*, 1394–1396; *Angew. Chem. Int. Ed. Engl.* **1988**, *27*, 1347–1349; d) M.-H. Desbois, D. Astruc, D. Guillin, *J. Am. Chem. Soc.* **1989**, *111*, 5800–5809.

[12] a) Y. Yan, J. Zhang, Y. Qiao, C. Tang, *Macromol. Rapid Commun.* **2013**, *34*, 254–259.

[13] a) Y. Wang, A. Rapakousiou, C. Latouche, J. C. Daran, A. Singh, I. Ledoux, J. Ruiz, J. Y. Saillard, D. Astruc, *Chem. Commun.* **2013**, *49*, 5862–5864; b) Y. Wang, C. Latouche, A. Rapakousiou, C. Lopez, I. Ledoux-Rak, J. Ruiz, J.-Y. Saillard, D. Astruc, *Chem. Eur. J.* **2014**, *20*, 8086–8098.

[14] M. Wildschek, C. Rieker, P. Jaitner, H. Schottenberger, K. E. Schwarzhans, *J. Organomet. Chem.* **1990**, *396*, 355–361.

[15] J. A. Page, G. Wilkinson, *J. Am. Chem. Soc.* **1952**, *74*, 6149–6150.

[16] a) G. R. Newkome, Z. Yao, G. R. Baker, V. K. Gupta, *J. Org. Chem.* **1985**, *50*, 2003–2004; b) G. R. Newkome, *Pure Appl. Chem.* **1998**, *70*, 2337–2343; c) V. V. Narayanan, G. R. Newkome, *Top. Curr. Chem.* **1998**, *197*, 19–33; d) G. R. Newkome, C. D. Schreiner, *Chem. Rev.* **2010**, *110*, 6338–6442.

[17] a) J. Ruiz, G. Lafuente, S. Marcen, C. Ornelas, S. Lazare, E. Cloutet, J.-C. Blais, D. Astruc, *J. Am. Chem. Soc.* **2003**, *125*, 7250–7257.

[18] M. Zamora, S. Herrero, J. Losada, I. Cuadrado, C. M. Casado, B. Alonso, *Organometallics* **2007**, *26*, 2688–2693.

[19] B. T. Cho, S. K. Kang, *Tetrahedron* **2005**, *61*, 5725–5734.

[20] L. Ren, J. Zhang, C. G. Hardy, D. Doxie, B. Fleming, C. Tang, *Macromolecules* **2012**, *45*, 2267–2275.

[21] H. Lee, T. Ooya, *Chem. Eur. J.* **2012**, *18*, 10624–10629.

[22] a) I. Noviansky, K. N. Brown, D. S. Fleming, P. T. Gulyas, P. A. Lay, A. F. Masters, L. J. Philips, *J. Phys. Chem. B* **1999**, *103*, 6713–6719; b) A. J.

Bard, L. Faulkner, *Electrochemical Methods: Fundamentals and Applications*, Wiley, New York, 2ednd ed**2001**; c) P. Zanello, *Inorganic Electrochemistry: Theory, Practice and Applications*, Royal Society of Chemistry, Cambridge, **2003**.

[23] J. B. Flanagan, S. Margel, A. Bard, *J. Am. Chem. Soc.* **1978**, *100*, 4248–4253.

Received: April 14, 2014
Published online on July 23, 2014

Partie 4

Synthèse et activité rédox de polyélectrolytes de cobalticénium

Partie 4

Synthèse et activité rédox de polyélectrolytes de cobalticénium

La conception de polyélectrolytes contenant des cobalticénium a été réalisé par les deux méthodes 'click' mentionnés à la partie 3. Ces polyélectrolytes présentent l'originalité de devoir leurs charges cationiques à des entités métallocéniques qui, de surcroît, sont extrêmement robustes sur le plan redox. Cette propriété en fait aussi potentiellement des batteries moléculaires de synthèse plus rapide que celle de dendrimères et de potentiel redox remarquablement placé, assez négativement dans l'échelle redox.

Le polymère discuté au chapitre 4.1 a été synthétisé par CuAAC de l'éthynylcobalticénium avec un polystyrène à fonction polyazoture. La synthèse a été réalisée en trois étapes. Le fait que ce polymère soit soluble dans l'eau est remarquable parce que cela peut conduire à des applications comme par exemple la détection redox dans l'eau ou l'encapsulation de molécules hydrophobes et de médicaments dans un milieu aqueux. Par analyse SEC du précurseur polyazoture, nous avons estimé que le nombre d'unités est 31. En utilisant l'équation de Bard par voltammétrie cyclique (VC), avec le décaméthylferrocène comme référence interne, nous avons estimé le nombre n_p d'électrons transférés dans la vague d'oxydation du polymère, n_p = 29 ± 3, résultat qui confirme les résultats de l'analyse SEC. De plus, les études de VC ont montré que tous les deux processus de transfert d'électrons sont réversibles.

.

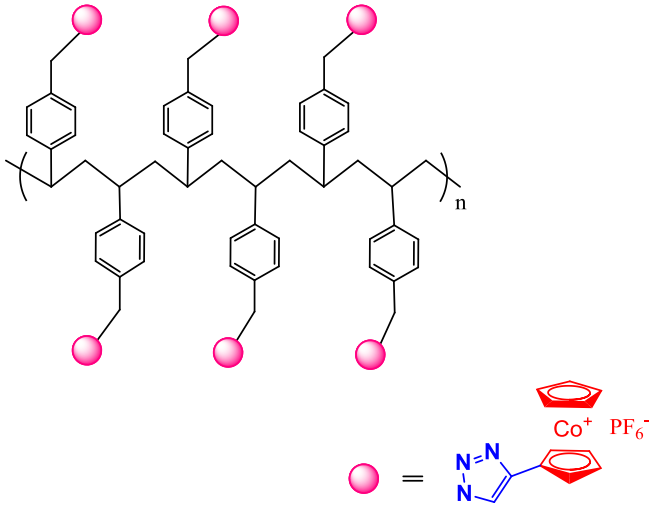

Schéma. Motifs du chapitre 4.1.

Au chapitre 4.2, nous décrivons la conception de polymères de cobalticénium par polymérisation ROMP. La synthèse de ces polymères a été effectuée par Dr. Wang Yanlan et les études rédox par moi-même, avec en particulier la détermination de nombre d'unités à l'aide l'équation de Anson et Bard. La méthode ROMP permet une définition beaucoup plus précise et plus étendue que la polymérisation radicalaire du *p*.chlorométhylstyrène, en particulier grâce à l'utilisation du catalyseur de métathèse de Grubbs de 3ème génération.

J Inorg Organomet Polym (2014) 24:107–113
DOI 10.1007/s10904-013-9958-y

"Click" Synthesis and Redox Activity of a Water-Soluble Triazolylcobalticinium Polyelectrolyte

Amalia Rapakousiou · Yanlan Wang · Jaime Ruiz · Didier Astruc

Received: 30 July 2013 / Accepted: 28 August 2013 / Published online: 17 September 2013

Abstract Ionic macromolecules, i.e. polyelectrolytes are of academic and industrial interest due to their polycharged structures and applications. Here a polyelectrolyte containing redox-active cobalticinium groups is synthesized by Cu^{I}-catalyzed azide alkyne Huisgen-type regioselective 1,3-cycloaddition, which is also-called "click" synthesis between a poly(azidomethylstyrene) polymer and ethynylcobalticinium. Overall, this first triazolylcobalticinium polymer is easily prepared in only three steps, which opens the way for applications such as redox sensing in aqueous media, polymer encapsulation of hydrophobic biomedical molecules in water and stabilization of colloidal suspensions. Cyclic voltammetry shows chemically and electrochemically reversible reductions on the electrochemical time scale, to the neutral 19-electron cobaltocene polymer and to the unstable 20-electron anionic structure. Application of Bard's equation using the decamethylferrocene reference allows estimating that the number of electrons transferred in the first cyclic voltammetry wave is 29 ± 3, close to the number of cobalticinium units, 31 ± 2, determined by size exclusion chromatography.

Dedicated to the memory of our esteemed colleague Professor Dwight A. Sweigart.

Electronic supplementary material The online version of this article (doi:10.1007/s10904-013-9958-y) contains supplementary material, which is available to authorized users.

A. Rapakousiou · Y. Wang · J. Ruiz · D. Astruc (✉)
ISM, UMR CNRS N°5255, Univ. Bordeaux,
33405 Talence Cedex, France
e-mail: d.astruc@ism.u-bordeaux1.fr

Keywords Cobalticinium · Polymer · Click reaction · Redox process · Cyclic voltammetry · Polyelectrolytes

1 Introduction

Cobalticinium derivatives [1–5] are isoelectronic with ferrocenes, but the positive charge of the 18-electron form precludes all the electrophilic functionalization reactions related to ferrocene. Yet cobalticinium salts, as with their ferrocene analogues, have a rich electrochemistry with reversible access to neutral Co^{II}19-electron [6, 7] and anionic 20-electron metallocene species [8, 9] and this positive charge is the potential source of polyelectrolytes upon pairing with an adequate source of anions in cobalticinium polymers [10–22].

When transition metal complexes such as cobalticinium salts are linked to macromolecules, they can undergo transfer of a large number of electrons, and these multiple redox processes are useful for potential nanodevice applications. Indeed, cobalticinium polymers are known [10–22] and have been obtained either by ring-opening cobaltocenophane [10–12] or from cobalticinium carboxylic acid as a derivatizing side group [13–22].

Whereas this functionalization is tedious, ethynylcobalticinium has been known for more than 20 years and is easily synthesized [23] which provided the possibility of easy Cu^{I}-catalyzed "click" reactions [24–27], as demonstrated for ethynylferrocene [28–30] with a variety of alkynes. Indeed, the first "click" reaction between ethynylcobalticinium and alkynes was reported to give triazolylcobalticinium derivatives in 2010 [28], and since then this practical reaction has been systematically used in our group for cobalticinium functionalization [29, 30]. The

triazolyl derivatives are potential ligands that are useful for sensing [31–33] and catalysis [34–36], especially when they are directly linked to a redox-active metallocene unit.

Recently, triazolylcobalticinium dendrimers have been reported [30]. Here we describe the first synthesis of a triazolylcobalticinium polyelectrolyte polymer by Cu^{I}-catalyzed azide-alkyne "click" cycloaddition (CuAAC) of ethynylcobalticinium with an azido-functionalized polymer.

2 Experimental

2.1 Materials

Reagent-grade diethyl ether and tetrahydrofuran (THF) were predried over Na foil and distilled from sodium-benzophenone anion under argon immediately prior to use. All other solvents were used as received. Ethynylcobalticinium **3** was synthesized according to [23]. *p*-Chloromethyl-styrene was purchased from Aldrich. Polymers **1** and **2** were synthesized according to [37] with slight modifications (*vide infra*).

2.2 Physical Measurements

The ^{1}H NMR spectra were recorded at 25 °C with a Bruker AVANCE II 300 MHz spectrometer. The ^{13}C NMR spectra were obtained in the pulsed FT mode at 75.0 MHz with a Bruker AVANCE 300 spectrometer. All chemical shifts are reported in parts per million (δ, ppm) with reference to Me_4Si (TMS). The infrared (IR) spectra were recorded on an ATI Mattson Genesis series FT-IR spectrophotometer. UV–Vis absorption spectra were measured with a Perkin–Elmer Lambda 19 UV–Vis spectrometer. The size exclusion chromatography (SEC) measurements were carried out using the PL-GPC 50 plus Integrated GPC system from Polymer laboratories-Varian equipped with refractometric and UV detectors, column oven and integrated degasser. Columns from TOSOH: TSKgel TOSOH, HXL-L (guard column 6.0 mm ID × 4.0 cm L), G4000HXL (7.8 mm ID × 30.0 cm L), G3000HXL (7.8 mm ID × 30.0 cm L), G2000HXL (7.8 mm ID × 30.0 cm L). Flow Marker: TCB (trichlorobenzene, $C_6H_3Cl_3$), Flow: 1.0 mL/min. Solvent: THF from Aldrich, loop : 100 µL.

2.3 Cyclic Voltammetry (CV) Measurements

All electrochemical measurements were recorded under nitrogen atmosphere. Conditions: solvent: dry DMF; temperature: 20 °C; supporting electrolyte: [*n*-Bu_4N][PF_6] 0.1 M; working and counter electrodes: Pt; reference electrode: Ag; internal reference: $FeCp^*_2$ ($Cp^* = \eta^5$-C_5Me_5) [38]; scan rate: 0.200 V/s^{-1}.

2.4 Synthesis of *p*-Polychloromethylstyrene **1**

p-Chloromethylstyrene (2.17 g, 14.2 mmol) was dissolved in 5 mL dry toluene, then AIBN (0.12 g, 0.7 mmol) was added under nitrogen. The reaction mixture was allowed to stir at 80 °C for 24 h. Then, toluene was removed under vacuum, and the crude product was washed with methanol and precipitated five times in CH_2Cl_2/methanol. The *p*-polychloromethylstyrene 1 was obtained as a white powder in 53.9 % yield. SEC: PDI = 1.40, M_n = 4,758, M_w = 5,297.

2.5 Synthesis of *p*-Polyazidomethylstyrene **2**

In a Schlenk flask, the *p*-polychloromethylstyrene compound **1** (2.5 g, 0.5 mmol) was dissolved in 20 mL DMF, and NaN_3 (1.6 g, 24.6 mmol) was added. The mixture was heated at 80 °C for 24 h, then the suspension was extracted three times with diethyl ether/H_2O, the organic phase was dried over Na_2SO_4, filtered and evaporated. The *p*-polyazidomethylstyrene compound **2** was purified by precipitation in MeOH twice. It was obtained as a white waxy product in 84.6 % yield. IR spectrum: 2,097 cm^{-1} for the azido band. SEC: PDI = 1.24, M_n = 4,901, M_w = 4,938.

2.6 Synthesis of Poly-triazolylcobalticinium Polymer **4**

The ethynylcobalticinium compound **3** (1.5 equiv., 168.7 mg, 0.47 mmol) and the azido polymer **2** (1 equiv., 50 mg, 0.3 mmol) were dissolved in a mixture of degassed THF (15 mL), DMF (20 mL) and H_2O (4 mL), and the reaction mixture was cooled to 0 °C. Then, an aqueous solution of $CuSO_4$ 1 M (1.1 equiv.) was added dropwise, followed by the dropwise addition of a freshly prepared solution of sodium ascorbate (2.2 equiv.) The color of the solution changed from orange to dark red upon addition of sodium ascorbate. The reaction mixture was allowed to stir for 12 h at 50 °C under a nitrogen atmosphere. Then the mixture of solvents was removed under vacuum, and 100 mL of nitromethane was added followed by the addition of an aqueous solution of ammonia. The mixture was allowed to stir for 15 min in order to remove all the copper salt trapped inside the polymer. The organic phase was washed twice with water, dried over sodium sulfate, filtered and the solvent was removed under vacuum. Then the product was washed with THF in order to remove the excess of alkyne and precipitated from an acetone or acetonitrile solution in diethyl ether. Further washing in acetonitrile removed smaller polymer parts. The water-soluble polymer **4** was obtained as an orange-yellow sticky oil in 53 % yield.

^{1}H NMR (1D 1H), (D_2O, 300 MHz): δ_{ppm}: 8.35 (C*H* of trz), 7.0 (C*H* arom.), 6.03 (C*H* of Cp sub.), 5.73 (C*H* of Cp sub.), 5.44 (C*H* of Cp free and CH_2 -trz), 1.56, 1.40 (CH_2 and C*H* of polymeric chain). ^{13}C NMR (D_2O, 75 MHz): 140.43 (*C*q of Ar), 138.68 (*C*q of trz), 128.75 (*C*H of Ar polymer chain), 125.24 (*C*H of trz), 93.22 (*C*q of Cp sub.), 85.83 (*C*H of Cp), 86.74, 85.72, 84.59, 80.55 (*C*H of Cp sub.), 55.34 (CH_2-trz), 53.72 (*C*H, CH_2 of polymeric chain).

3 Results and Discussion

3.1 Synthesis and SEC Characterization of Polymers **1** and **2**

The polychloromethylstyrene polymer **1** was prepared by free-radical polymerization of commercial chloromethylstyrene using AIBN as the initiator (Scheme 1). The reaction took place in toluene, at 80 °C under nitrogen. Azidation reaction gave the azido-polymer **2** in 85 % yield.

SEC (reference: polystyrene) shows the molecular weight distribution curve of **1** with polydispersity index (PDI) = 1.4 and **2** with PDI = 1.2. The polydispersity improved from **1** to **2**, because after the azidation reaction the product was further purified by precipitation in MeOH twice. Molecular weight data using polystyrene as the standard reference show that polymer **2** consists of 31 units (Fig. 1).

3.2 Synthesis of the Cobalticinium Polymer **4**

The polymer **4** was synthesized by CuAAC "click" reaction between ethynylcobalticinium **3** and the azido polymer **2**. Previous studies concerning the click cobalticinium dendrimers showed that as the number of the triazolyl (trz) cobalticinium groups increases in a molecule, its polarity also increases due to charge clustering. Charge clustering favors solubilization in more polar solvents such as water, which is a polyelectrolyte property. Assuming that the polymer **2** consists of a large number of units, a mixture of THF/DMF/H_2O as solvent was chosen for the click reaction in order to achieve the solubility of the final product **4**.

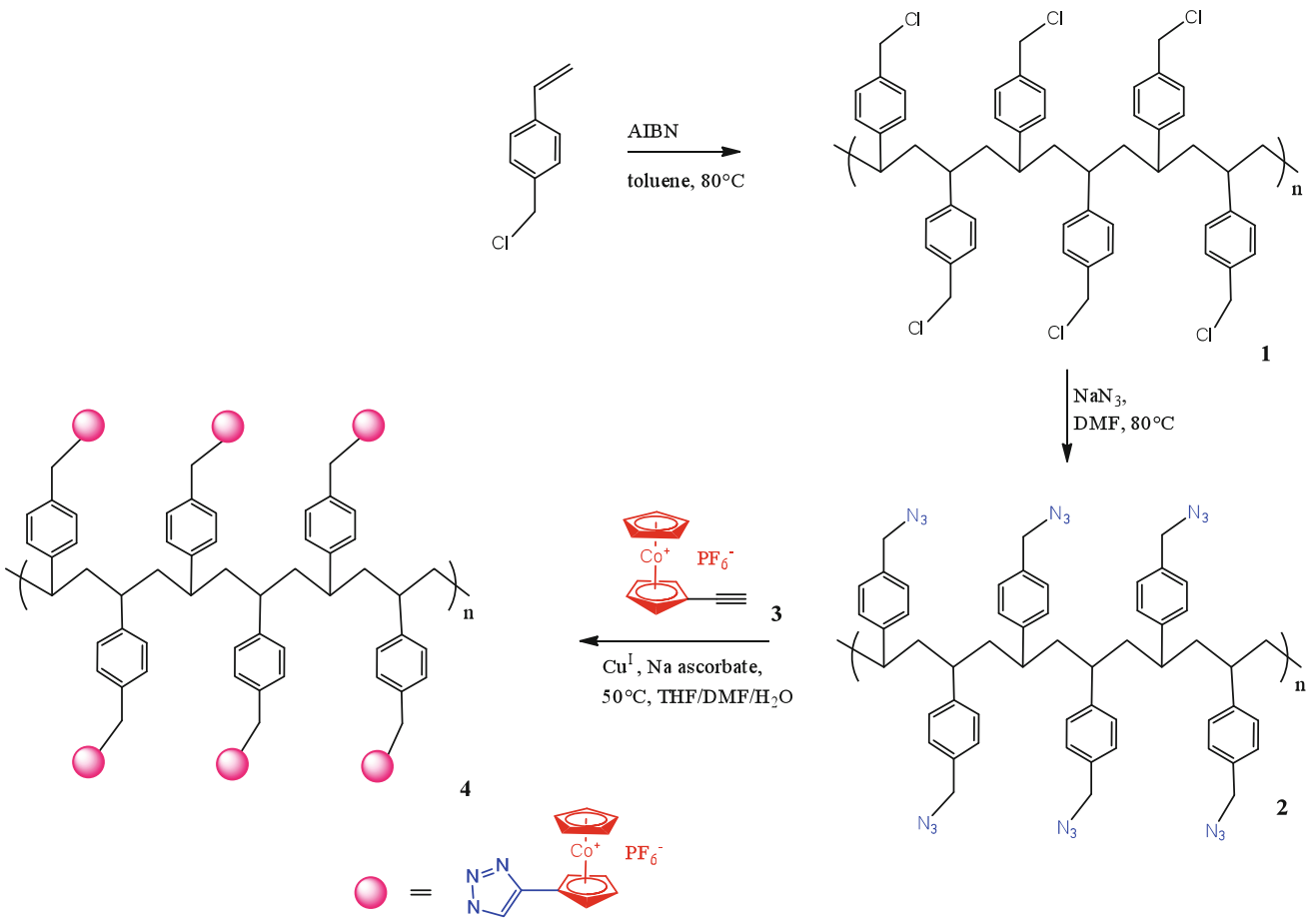

Scheme 1 Synthesis of the water-soluble triazolylcobalticinium polyelectrolyte

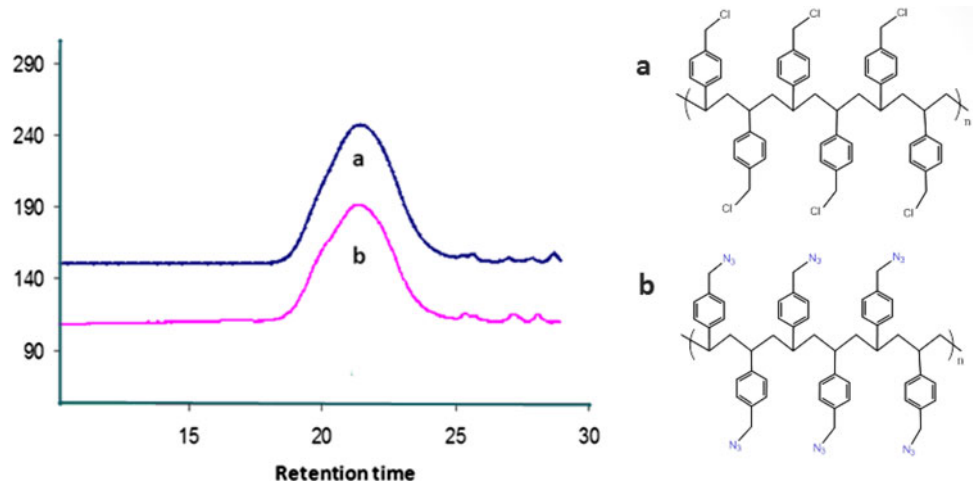

Fig. 1 SEC analysis: **a** *p*-polychloromethylstyrene 1, **b** *p*-polyazidomethylstyrene 2

The reaction lasted 12 h at 50 °C. The copper salt was removed as $[Cu(NH_3)_2(H_2O)_2]$ $[SO_4]$ after adding an aqueous solution of NH_3 to the mixture. The polymer was purified by precipitation in diethyl ether and washed with acetonitrile in order to remove smaller polymeric units that might have formed. The final yellow product was soluble only in very polar solvents such as water (Fig. 2), DMF and DMSO.

3.3 Characterization of the Cobalticinium Polymer **4**

"Click" reactions are easily monitored by infrared spectroscopy (neat), because the azido groups have a characteristic peak at 2,094 cm^{-1} that disappears at the end of the reaction confirming that all the azido groups are replaced by trz groups. A strong band at 838 cm^{-1} is due to the absorption of the PF_6 anion, and the band at 3,118 cm^{-1} is due to the = C–H stretching of the trz and the Cp groups of the cobalticinium units. NMR spectroscopy in D_2O confirms the structure of the water-soluble polymer **4**. ^1H NMR shows the disappearance of the $-CH_2N_3$ peak at 4.25 ppm, the appearance of the trz-C*H* peak at 8.35 ppm as well as the other characteristic peaks of the polymer. The presence of trz group is also confirmed by the appearance of the characteristic peaks of *C*q and *C*H of trz in the ^{13}C NMR spectra. UV–Vis spectroscopy recorded in water shows a strong absorption at 347 nm due to d–d* transitions of cobalticinium and an absorption shoulder at 425 nm (Fig. 2).

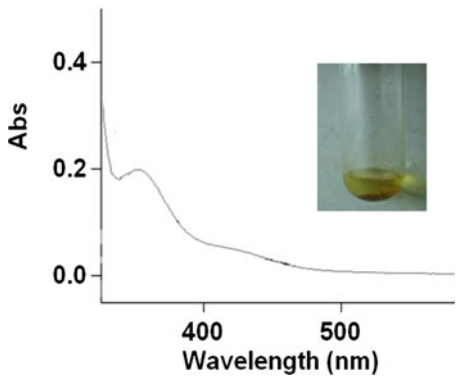

Fig. 2 UV–Vis spectroscopy of the cobalticinium polymer **4** in water (Color figure online)

The MALDI-TOF mass spectrum of the polycationic cobalticinium polymer **4** showed well-defined individual peaks for polymer fragments that are separated by 517 Da, which exactly corresponds to the mass of one methylenestyryltriazolylcobalticinium hexafluorophosphate unit (Fig. 3). The highest molecular peak that could be obtained was that of 5,796 Da corresponding to a polymer fraction of 11 trz-cobalticinium units. Several other fragments are also observed probably due to additions or losses of some PF_6 anions. The intensities of the peaks separated by 517 Da progressively decrease and vanish towards high molecular masses. Thus the molecular peak and higher masses cannot be observed. While this MALDI TOF mass spectrum clearly shows the structure and motifs of the polymer **4**, the SEC analysis of the precursor polymer **2** is a more viable method to determine the total number of units. SEC analysis of the final polycationic cobalticinium itself, polyelectrolyte **4**, is difficult due to the strong electrostatic interactions between the cobalticinium moieties. Therefore CV studies were conducted in order to examine the thermodynamics and kinetics of the heterogeneous electron-transfer processes, the stability of the reduced states and finally to confirm the number of units in the cobalticinium polymer **4**.

3.4 Cyclic Voltammetry Studies and Multi-Electron-Transfer Process

The trz-cobalticinium polymer **4** was studied by cyclic voltammetry using decamethylferrocene as the internal reference [38]. DMF was used as a solvent (Fig. 4). The

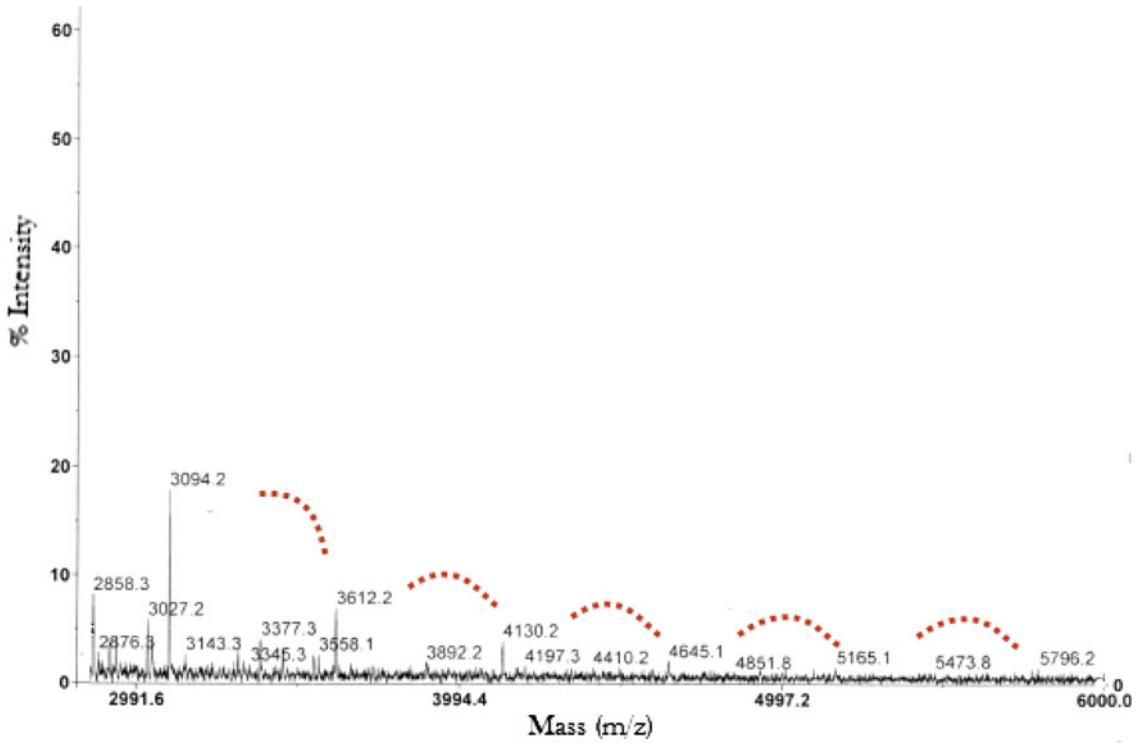

Fig. 3 MALDI-TOF mass spectrum of polymer **4**

first reduction wave corresponding to the reduction of cobalticinium to the 19-electron cobaltocene ($Co^{III/II}$) takes place at −0.8 V [6, 7]. The second wave corresponding to the reduction of cobaltocene to the 20-electron cobaltocenyl anion ($Co^{II/I}$) appears at −1.73 V [8, 9] (Table 1). Although heterogeneous electron transfers from the electrode to the metallocene polymer proceed one by one [39], both waves are single. This can be explained by the weakness of the electrostatic factor between the redox sites which are separated by several bonds [40–43]. Additionally both waves appear to be electrochemically reversible. The electrochemical reversibility is due to very fast rotation within the electrochemical time scale, where all the redox groups come close to the electrode provoking fast electron transfer between all the redox groups and the electrode, [44] and/or the electron-hopping mechanism [45].

Supporting electrolyte: [*n*-Bu_4N][PF_6] 0.1 M; working and counter electrodes: Pt; reference electrode: Ag; internal reference: $FeCp^*_2$ ($Cp^* = \eta^5$-C_5Me_5); scan rate: 0.200 V/s^{-1}. The ΔE value of 0.045 V obtained for the $Co^{III/II}$ wave, slightly lower than the standard 0.059 V value at 25 °C [39], is probably due to partial adsorption of **4** onto the electrode.

The envelope of the first redox wave ($Co^{III/II}$) is slightly broadened compared to a standard single-electron wave shape which is most probably due to electrostatic interactions slightly differentiating the multiple single electron-transfer steps corresponding to the $Co^{III/II}$ redox change. In the second electron-transfer ($Co^{II/I}$) for which the starting polymer does not contain cationic species, this phenomenon does not appear, because it is weaker. The electrostatic interaction for the first electron transfers involve all the cationic charges whereas the last ones involve a neutral or

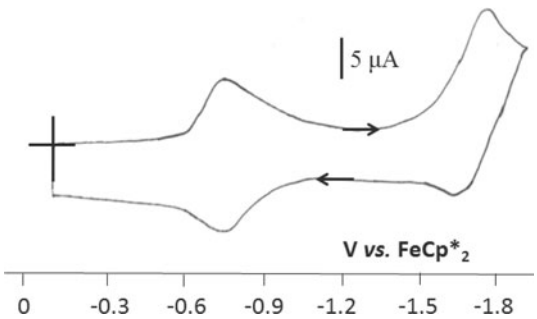

Fig. 4 CV of **4**. Internal reference: $FeCp^*_2$. Solvent: DMF; 298 K; reference electrode: Ag; working and counter electrodes: Pt; scan rate: 0.2 V/s^{-1}; supporting electrolyte: [*n*-Bu_4N][PF_6]

Table 1 Redox potentials, chemical (i_a/i_c) and electrochemical (Ep_a-Ep_c = ΔE) reversibility data for compound **4**

Compound	Solvent	$Co^{III/II}$ [V]			$Co^{II/I}$ [V]		
		$E_{1/2}$	ΔE	i_a/i_c	$E_{1/2}$	ΔE	i_a/i_c
4	DMF	−0.80	0.045	0.8	−1.73	0.060	0.6

anionic polymer. Interactions between the cationic centers, the counter anions and the solvent molecules are responsible for the variation of the electrostatic energy engaged in the heterogeneous electron transfers [43–47].

The second wave ($Co^{II/I}$) is electrochemically reversible, indicating that the 20-electron fully sandwich structure is retained on the electrochemical time scale without significant structural change [8, 9] (only a small increase of the Co–Cp bonds is expected due to the presence of two electrons in slightly anti-bonding e^*_1 orbitals [48, 49]). On the other hand, the chemical reversibility is weaker than that of the first wave (Table 1), signifying that on a longer timescale the anionic metallopolymer structure collapses. Lastly, the number of electrons involved in the first redox change ($Co^{III/II}$) was calculated by cyclic voltammetry analysis in order to confirm the number of trz-cobalticinium units, 31, determined from SEC analysis of the precursor **2**. The total number of electrons transferred in the oxidation wave for the polymer (n_p) can be estimated from the limiting currents and approximate relative values of the diffusion coefficients of the monomer (D_m) and the polymer (D_p):

$$D_p/D_m = \left(M_m/M_p\right)^{0.55}$$

Assuming that the reduction of each redox moiety is an one-electron reaction (Co^{III} Co^{II}), the value of n_p can be estimated by employing Bard's equation previously derived for conventional polarography [39, 40]:

$$n_p = \left(i_{dp}/C_p\right)/\left(i_{dm}/C_m\right)\left(M_p/M_m\right)^{0.275}$$

Consequently comparison with the internal reference [Fe(η^5-$C_5Me_5)_2$] provides a good estimation of the number of electrons n_p involved in the $Co^{III/II}$ redox process as a function of the monomer and polymer intensities (i), concentrations (C) and molecular weights (M) [40]. Measurement of the respective intensities for the decamethylferrocene reference and the first wave led to the data of $n_p = 29 \pm 3$ electrons for the polyelectrolyte **4**, which is in good agreement with the experimental values of 31 ± 2 derived by SEC of the polyazido polystyrene polymer precursor, **2**. The value of 29 is lower than 31, probably due to the lowering of the wave due to the electrostatic factor (vide supra). This factor should indeed result in a lower value than the actual one as found, but the decrease is only modest judging from the comparison with the SEC data.

4 Concluding Remarks

The first triazolylcobalticinium polymer has been synthesized by facile Cu^I-catalyzed azide-alkyne "click" CuAAC of ethynylcobalticinium with an azido-functionalized polymer. The three-step synthesis represents a very practical synthetic method from commercial *p*-chloromethylstyrene. The number of triazolylcobalticinium units in this polymer **4** has been estimated to be 31 using the SEC data of the polyazido polymer and was confirmed (29 ± 3) using Bard's equation by cyclic voltammetry using decamethylferrocene as the internal reference. Remarkably, this polymer is water soluble, which can lead to significant applications in redox sensing in water or polymer encapsulation in aqueous media of hydrophobic biomedical molecules and drugs. Cyclic voltammetry studies showed two reversible electron-transfer processes which make this polymer a very good candidate as a molecular–battery material. Such studies are currently underway in our laboratory.

Acknowledgments Helpful assistance and discussions with Nicolas Guidolin (SEC), Claire Mouche (mass spectrometry) and Jean-Michel Lanier (NMR) from the CESAMO, Université Bordeaux 1, and financial support from the Université Bordeaux 1, the Centre National de la Recherche Scientifique (CNRS), the Agence Nationale de la Recherche (ANR) and the China Scholarship Council (Ph.D. grant to Y. W.) is gratefully acknowledged.

References

1. G. Wilkinson, J. Am. Chem. Soc. **74**, 6148 (1952)
2. G. Wilkinson, P.L. Pauson, F.A. Cotton, J. Am. Chem. Soc. **76**, 1970 (1954)
3. J.E. Sheats, M.D. Rausch, J. Org. Chem. **35**, 3245 (1970)
4. J.E. Sheats, J. Organomet. Chem. Lib **7**, 461 (1979)
5. R.D.W. Kemmit, D.R. Russell, *Comprehensive Organometallic Chemistry* (Pergamon, Oxford, 1982)
6. N.J. Connelly, W.E. Geiger, Chem. Rev. **96**, 877 (1996)
7. W.E. Geiger, Organometallics **26**, 5738 (2007)
8. W.E. Geiger, J. Am. Chem. Soc. **96**, 2632 (1974)
9. W.E. Geiger, W.L. Bowden, N. El Murr, Inorg. Chem. **18**, 2358 (1979)
10. U.F.J. Mayer, J.P.H. Charmant, J. Rae, I. Manners, Organometallics **27**, 1524 (2008)
11. U.F.J. Mayer, J.B. Gilroy, D. O'Hare, I. Manners, J. Am. Chem. Soc. **131**, 10382 (2009)
12. H. Qiu, J.B. Gilry, I. Manners, Chem. Commun. **49**, 42 (2013)
13. T. Ito, T. Kenjo, Bull. Soc. Chem. Jpn. **41**, 614 (1968)
14. C.U. Pittman, O.E. Ayers, S.P. McManus, J.E. Sheats, C.E. Whitten, Macromolecules **4**, 360 (1971)
15. C.M. Casado, F. Lobete, B. Alonso, B. Gonzalez, J. Losada, U. Amadr, Organometallics **18**, 4960 (1999)
16. K. Masakazu, T. Ikuyoshi, Nippon Kagakkai Koen Yokoshu **83**, 805 (2003)
17. M. Kondo, Y. Hayakawa, M. Miyazawa, A. Oyama, K. Unoura, H. Kawaguchi, T. Naito, K. Maeda, F. Uchida, Inorg. Chem. **43**, 5801 (2004)
18. L.X. Ren, C.G. Hardy, C.B. Tang, J. Am. Chem. Soc. **132**, 8874 (2010)
19. L.X. Ren, C.G. Hardy, S.F. Tang, D.B. Doxie, N. Hamidi, C.B. Tang, Macromolecules **43**, 9304 (2010)
20. J.Y. Zhang, L.X. Ren, C.G. Hardy, C.B. Tang, Macromolecules **45**, 6857 (2012)

21. L.X. Ren, J.Y. Zhang, C.G. Hardy, S.G. Ma, C.B. Tang, Macromol. Commun. **33**, 510 (2012)
22. L.X. Ren, J.Y. Zhang, X.L. Bai, C.G. Hardy, K.D. Shimizu, C.B. Tang, Chem. Sci. **3**, 580 (2012)
23. M. Wildschek, C. Rieker, P. Jaitner, H. Schottenberger, K.E. Schwarzhans, J. Organomet. Chem. **396**, 355 (1990)
24. C. Ornelas, J. Ruiz, E. Cloutet, S. Alves, D. Astruc, Angew. Chem. Int. Ed. **46**, 872 (2007)
25. S. Badèche, J.-C. Daran, J. Ruiz, D. Astruc, Inorg. Chem. **47**, 4903 (2008)
26. R. Djeda, A. Rapakousiou, L. Liang, N. Guidolin, J. Ruiz, D. Astruc, Angew. Chem. Int. Ed. **49**, 8152 (2010)
27. D. Astruc, L. Liang, A. Rapakousiou, J. Ruiz, Acc. Chem. Res. **45**, 630 (2012)
28. K. Diallo, S. Menuel, E. Monflier, J. Ruiz, D. Astruc, Tetrahedron Lett. **51**, 4617 (2010)
29. A. Rapakousiou, C. Mouche, M. Duttine, J. Ruiz, D. Astruc, Eur. J. Inorg. Chem **31**, 5071 (2012)
30. A. Rapakousiou, Y. Wang, C. Belin, N. Pinaud, J. Ruiz, D. Astruc, Inorg. Chem **52**(11), 6685 (2013)
31. P.S. Kumar, Pandey. Org. Lett. **10**, 165 (2008)
32. K.M. Mullen, J. Mercurio, C.J. Serpell, P.D. Beer, Angew. Chem. Int. Ed. **48**, 4781 (2009)
33. C. Schulze, M.D. Friebe, W. Hager, U. Gunther, B.O. Kohn, H. Jahn, U.S. Gorls, Schubert. Org. Lett. **12**, 2710 (2010)
34. Y. Li, A.H. Flood, Angew. Chem. Int. Ed. **47**, 2649 (2008)
35. Ornelas, J. Ruiz, L. Salmon, D. Astruc, Adv. Syn. Catal **350**, 837 (2008)
36. Astruc, C. Ornelas, J. Ruiz, Acc. Chem. Res **41**, 841 (2008)
37. L. Liang, A. Rapakousiou, L. Salmon, J. Ruiz, D. Astruc, B.P. Dash, R. Satapathy, N.S. Hosmane, Eur. J. Inorg. Chem. **20**, 3043 (2011)
38. J. Ruiz, D. Astruc, C.R. Acad, Sci. t. 1, Sér. IIc **322**, 21 (1998)
39. J. Bard, L.R. Faulkner, *Electrochemical Methods: fundamentals and Applications*, 2nd edn. (Wiley, New York, 2001)
40. J.B. Flanagan, S. Margel, A. Bard, J. Am. Chem. Soc. **100**, 4248 (1978)
41. J.E. Sutton, P.M. Sutton, H. Taube, Inorg. Chem. **18**, 1017 (1979)
42. E. Richardson, H. Taube, Coord. Chem. Rev. **60**, 107 (1984)
43. W.E. Barrière, Geiger. Acc. Chem. Res. **43**, 1030 (2010)
44. B. Gorman, B.L. Smith, H. Parkhurst, H. Sierputowska-Gracz, C.A. Haney, J. Am. Chem. Soc. **121**, 9958 (1999)
45. C. Amatore, Y. Bouret, E. Maisonhaute, J.I. Goldsmith, H.D. Abruña, Chem-Eur. J **7**, 2206 (2001)
46. K. Diallo, J.C. Daran, F. Varret, J. Ruiz, D. Astruc, Angew. Chem. Int. Ed **48**, 3141 (2009)
47. A.K. Diallo, C. Absalon, J. Ruiz, D. Astruc, J. Am. Chem. Soc. **133**, 629 (2011)
48. J.H. Ammeter, J.D. Swalen, J. Chem. Phys. **57**, 678 (1972)
49. Astruc, *Organometallic Chemistry and Catalysis*. (Springer, Berlin, 2008), pp. 253–254

Macromolecules

Article

pubs.acs.org/Macromolecules

ROMP Synthesis of Cobalticenium−Enamine Polyelectrolytes

Yanlan Wang, Amalia Rapakousiou, and Didier Astruc*

ISM, UMR CNRS No. 5255, Université de Bordeaux, 33405 Talence Cedex, France

Supporting Information

ABSTRACT: The synthesis of redox-robust polyelectrolyte polymers has long been investigated. Two simple methods of synthesis of well-defined cobalticenium-containing polymers are presented using both the norbornene ring-opening-metathesis polymerization (ROMP) method initiated by a third-generation Grubbs catalyst and the mild uncatalyzed hydroamination of the easily available ethynyl cobalticenium hexafluorophosphate salt. In the first strategy, a norbornene monomer functionalized with an enamine-cobalticenium group is polymerized by ROMP, whereas in the second one a norbornene derivative functionalized with a secondary amine group is polymerized by ROMP using the same catalyst followed by hydroamination of ethynyl cobalticenium. The structures of the polymers have been established by ^{1}H, ^{13}C NMR, and DOSY NMR, IR, UV−vis spectroscopy, mass spectrometry, elemental analysis, and cyclic voltammetry. The number of units in the polymers have been determined for various polymer lengths using end-group analysis by ^{1}H NMR using the diffusion coefficient determined by DOSY NMR and by cyclic voltammetry upon comparing the relative intensities of a monomer reference and the cobalticenium polymers.

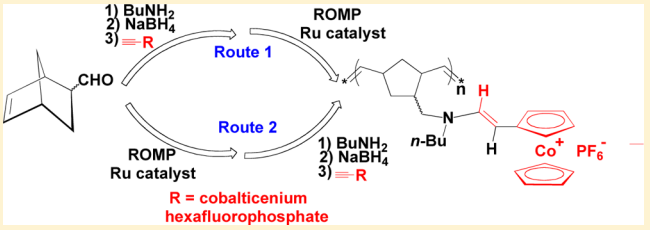

INTRODUCTION

Metallocene polymers[1] have been largely developed as a privileged area of metal-containing polymers,[2] in particular due to their robustness and redox properties.[3] Although by far the most extensively investigated metallocene polymers are ferrocene-containing polymers,[4] cobalticenium containing polymers[5−8] and dendrimers[9,10] have attracted attention for a long time. Cobalticenium salts are monocationic in the robust 18-electron configuration.[11] Cobalticenium polymers and dendrimers are polyelectrolytes, a field of interest in materials chemistry because of specific solubilities, physical properties, and applications, for instance, in batteries.[12]

The most common cobalticenium starting materials for the synthesis of cobalticenium polymers are cobalticenium carboxylic acids that are subjected to amide coupling upon reaction with polymeric[5,6] and dendritic amines.[9] Tang's group has also recently reported several articles on cobalticenium polymers based on such useful coupling reactions.[6] Manners' group[7] very recently published the remarkable, facile, and efficient ring-opening polymerization reaction of a cobaltocenophane monomer as an extension of the rich ferrocenophane ring-opening polymerization chemistry.[13] Another useful starting material is ethynylcobalticenium hexafluorophosphate, **1**,[14] that readily undergoes click reactions with terminal azides yielding 1,2,3-triazolyl cobalticenium derivatives (Scheme 1).[15] This click reaction has indeed been used to synthesize cobalticenium polyelectrolytes[8] and dendritic cobalticenium complexes.[10] Ethynyl cobalticenium hexafluorophosphate has also been reported to react with primary and secondary amines according to a facile uncatalyzed hydroamination reaction yielding *trans*-enamines under ambient or nearly ambient conditions (Scheme 1).[16]

Scheme 1. Two Useful Reactions of Ethynylcobalticenium Hexafluorophosphate, 1[15,16]

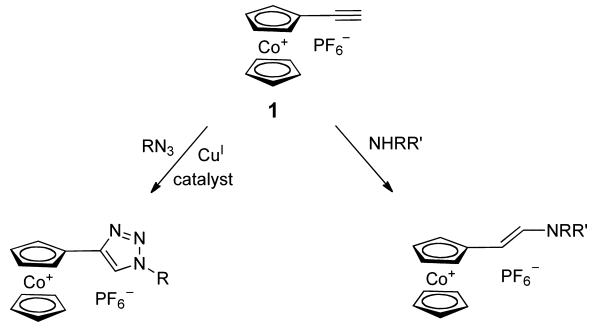

We now report two new mild and efficient routes to cobalticenium polymers using ethynylcobalticenium hydroamination reactions: (i) the functionalization of an amino derivative of a norbornene polymer (obtained by ROMP) with ethynyl cobalticenium and (ii) the ROMP polymerization of a cobalticenium derivative of a norbornene monomer bearing an amino group to which ethynyl cobalticenium has been connected using this hydroamination reaction.

RESULTS AND DISCUSSION

For the preparation of the organic and organometallic polymers, the ring-opening-metathesis polymerization (ROMP) reaction of norbornene derivatives has been selected.[17] This reaction is

Received: April 15, 2014
Revised: May 23, 2014
Published: June 4, 2014

known to be very efficient using the third-generation Grubbs catalyst **3** that is easily prepared using the commercial second-generation Grubbs catalyst **2** (eq 1).[18]

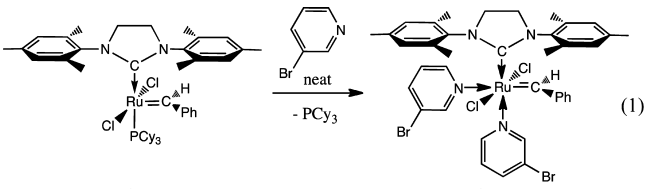

2 **3**

1. Hydroamination of 1 by a Norbornene-Functionalized Secondary Amine. Commercial 5-norbornene-2-carboxaldehyde (endo + exo) monomer was treated with excess butylamine at room temperature under N_2 for 16 h to give the imine product as a light yellow oil quantitatively. The reduction reaction of the imine was carried out in dry THF/CH_3OH (1:1) at 0 °C (Scheme 2) using the mixed powder $NaBH_4$/PhCOOH[19] to give the norbornene-substituted secondary amine as a light yellow oil in 99% yield. This secondary amine reacted stoichiometrically with **1** in CH_3CN at 35 °C for 16h under N_2 to give the cobalticenium−enamine monomer **4** as a deep red solid in 98% yield. This monomer has been fully characterized by ^1H, ^{13}C, ^{31}P NMR, IR, UV−vis, cyclic voltammogram, mass, and elemental analysis (Figures S1−S5, Supporting Information).

2. Ring-Opening-Metathesis Polymerization (ROMP) of Norbornene Functionalized with *trans*-Enamine Cobalticenium Hexafluorophosphate Using Grubbs' Third-Generation Catalyst. The cobalticenium−enamine-substituted norbornene monomer **4** has been polymerized in distilled CH_2Cl_2 in the presence of the catalyst **3** at room temperature in 30 min. Then excess ethyl vinyl ether was added to quench the reaction. After the solvent was removed under vacuum, the remaining deep red solid was washed with THF (3 × 10 mL) to remove the catalyst and the short-chain polymers. The use of different ratio of catalyst (0.01, 0.05, and 0.10 equiv) gives the polymers **5** in 90% yield, **9** in 98% yield, and **10** in 99% yield respectively as deep-red solids, characterized by ^1H, ^{13}C, and DOSY NMR, IR, UV−vis spectroscopy, MALDI−TOF mass spectrometry, cyclic voltammetry (CV), and elemental analysis (Figures S6−S8 and S14−S19).

3. ROMP of Norbornene Functionalized with a Secondary Amine. The cobalticenium−enamine polymer **8** was obtained by the uncatalyzed hydroamination reaction of 1 with the secondary amine-functionalized polymer **7** (Scheme 3). First 5-norbornene-2-carboxaldehyde (*endo* + *exo*) was polymerized in CH_2Cl_2 in the presence of catalyst **3** (0.03 equiv) at room temperature for 30 min. Then excess of ethyl vinyl ether was added to quench the reaction. The mixture was concentrated to 1 mL under vacuum, then excess of MeOH was added to precipitate the polymer **6** as a white solid that was characterized by ^1H and ^{13}C NMR, SEC (size exclusion chromatographie) and elemental analysis (Figures S9 and S10). The SEC of **6** shows a broad-ranged, ill-defined bimodal polymer due to the probably fast aggregation during the measurement (Figure S11). Polymer **6** was treated with excess butylamine at 35 °C to give the imine polymer as a light-yellow oil quantitatively. Then this imine polymer was reduced in THF/CH_3OH (1:1) at 0 °C in the presence of a $NaBH_4$/PhCOOH powdery mixture to give after work-up the secondary amine-substituted polymer **7** as a light yellow oil in 95% yield.[19] Polymer **7** was characterized by ^1H and ^{13}C NMR and elemental analysis (Figures S12 and S13).

4. Hydroamination of 1 with the Secondary Amine-Functionalized Polynorbornene Polymer 7. The secondary amine-functionalized polymer **7** was treated with a slight excess of **1** in CH_2Cl_2:CH_3CN (1:1) providing the cobalticenium−enamine polymer **8** in 2 days in 97% yield, and **8** was fully characterized.

5. Characterization. *^1H NMR Spectra of the Monomer **4** and Polymer **5**.* Figure 1 shows the compared ^1H NMR spectra of the cobalticenium−enamine monomer **4** (Figure 1A) and polymer **5** (Figure 1B) in CD_3COCD_3. For the monomer **4**, the typical two protons on the C═C bond on the norbornene were found in the area of 6.08−6.28 ppm. The splitting of all the peaks is caused by the mixture of *endo* and *exo* structures. The two protons of the C═C bond between the amino and the cobalticenium were found in the area of 4.72−4.78 and 7.16−7.28 ppm, respectively showing the *trans*-enamine−cobalticenium structure. After polymerization in the presence of catalyst **3**, these two protons of the C═C bond on the norbornene structure appeared in the region of 5.37 ppm that was merged with that of the substituted Cp ligand of cobalticenium. All the peaks are broad as reported in the literature for the ROMP polymers and each peak was well assigned for the polymer. The

Scheme 2. ROMP Reaction of the Enamine−Cobalticenium Norbornene Yielding the Homopolymer 5

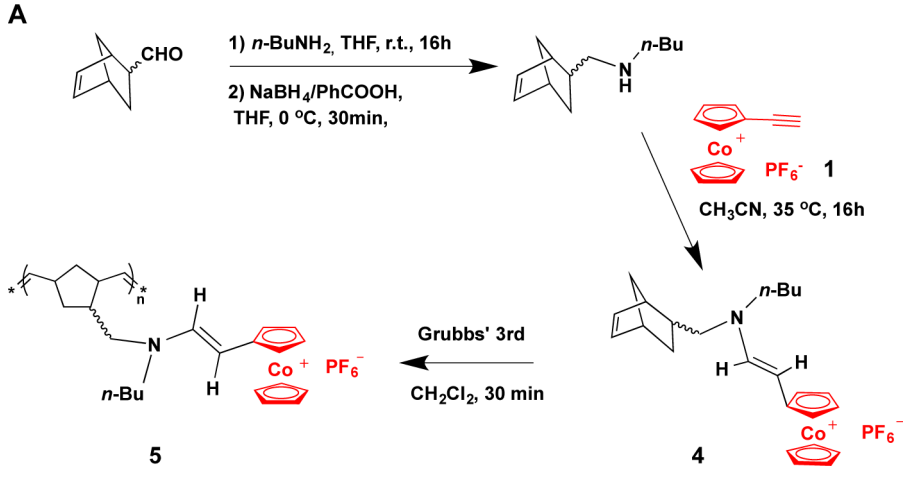

dx.doi.org/10.1021/ma5007864 | *Macromolecules* 2014, 47, 3767−3774

Scheme 3. Hydroamination of 1 by the Secondary Amine-Functionalized Norbornene Polymer 7, Yielding the Cobalticenium–Enamine-Functionalized Norbornene Polymer 8

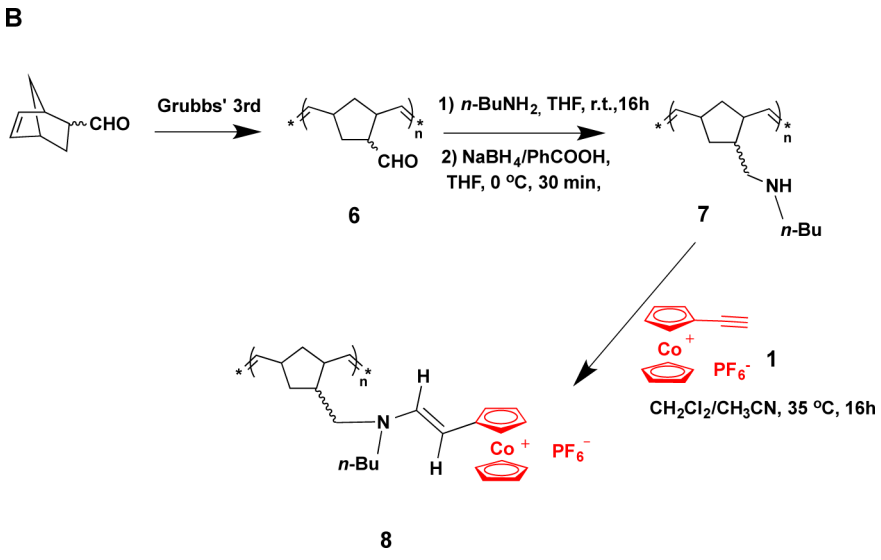

phenyl group of the catalyst is located at the end of the polymer chain after polymerization. This phenyl group in the polymer was found in the area of 7.20–7.40 ppm, which is convenient for the rough estimation of the molecular weight of the polycationic polymers by the end-group analysis (*vide infra*).

MALDI–TOF Mass Spectrometry. The ESI mass spectrum of the cationic monomer **4** ($C_{24}H_{31}CoN^+$) was simulated as 392.44 and found at 392.18 indicating the presence of the molecular ion. The MALDI–TOF spectrum of the polycationic cobalticenium polymer **5** showed well-defined individual peaks for polymer fragments that are separated by exactly 537.1 g/mol corresponding to the mass of one norbornene enamine-cobalticenium hexafluorophosphate unit **4** (Figure 2). The highest molecular peak observed was located at 10303.5 g/mol corresponding to a polymer fraction of 19 monomer units with terminal groups. Several other fragments are also observed due to the additions or losses of PF_6 anions and end groups. Thus, it was not possible to obtain the true molecular weight for the polymer **5** due to the limit of the MALDI–TOF technique, but the MALDI–TOF spectrum clearly shows the structure and motifs of **5**. For the polymers **8**, **9**, and **10**, the MALDI–TOF mass spectra also showed the splitting of each unit in the same area in accord with their structures.

UV–Vis Spectroscopy. The solution of **1** in acetone is yellow (Figure 3, left). On the other hand, all the cobalticenium enamine monomers and polymers are deep red in acetone (Figure 3, right). As shown in Figure 3, compound **1** (blue line) showed adsorptions at 350 and 420 nm in the UV–vis spectrum. The weak peak around 420 nm is assigned to the d–d* transition of cobalticenium.[20] The new absorption around 500 nm seems to be due to d–d* transition mixed with charge transfer from the ligand to the metal in the cobalticenium–enamine monomers and polymers **4**, **5**, and **8**.[16] The weak peak around 420 nm caused by the d–d* transition of cobalticenium is still on the shoulder of the main absorptions around 500 nm for all the cobalticenium–enamine monomers and polymers. The polymers **9** and **10** showed identical adsorptions under the UV–vis with the polymer **5** as expected.

Cyclic Voltammetry (CV) and Multielectron-Transfer Process in the Polymers. The redox processes of cobalticenium salts have been thoroughly studied by cyclic voltammetry and other electrochemical techniques, in particular by Geiger's group.[21] It is well-known that the single-electron reduction of cobalticenium salts gives stable cobaltocene and the second single-electron reduction gives unstable cobaltocene anion. Such studies have been extended to polymers and the cyclic voltammograms have been recorded in this work for all the cobalticenium–enamine monomer and polymers. For example, the cyclic voltammogram of polymer **5** has been recorded at 20 °C with decamethylferrocene, $[Fe(\eta^5\text{-}C_5Me_5)_2]$, $\{(\eta^5\text{-}C_5Me_5) = Cp^*)\}$ as the internal reference in DMF in order to cover the largest possible electroactivity.[22] It shows two redox waves coresponding to the two redox states of the cobalt center. The redox process of cobalticenium does not clearly appear as fully chemically and electrochemically reversible, because it is marred by some adsorption (*vide infra*), but some data have been extracted and gathered in Table 1. For the $Co^{III/II}$ wave $E_{1/2}$ = −1.04 V, and for the $Co^{II/I}$ wave $E_{1/2}$ = −2.02 V vs $FeCp^*_2$ (Figure 4). For the polymer **5**, the first redox wave ($Co^{III/II}$) is slightly broadened compared to a standard single-electron wave. It is probable that some adsorption and electrostatic interactions slightly differentiate the multiple single electron-transfer steps corresponding to the $Co^{III/II}$ redox, whereas in the second electron-transfer ($Co^{II/I}$) for which the starting polymer does not contain cationic species this phenomenon does not appear. The CV of the monomer **4** includes a partly chemically reversible oxidation of the amine group to somewhat unstable aminium at 1.04 V and two reversible waves for the two redox states of cobalt under identical electrode potentials with the polymer **5**. On the other hand, both the monomer **4** and polymer **5** show large differences in electrode potentials compared to the starting complex **1** under identical conditions ($Co^{III/II}$ wave, $E_{1/2}$ = −0.70 V; $Co^{II/I}$ wave, $E_{1/2}$ = −1.63 V vs $FeCp^*_2$) (Table 1).

Molecular Weights. It was challenging to observe a GPC signal for the cobalticenium-containing polymers due to the strong electrostatic interaction between the cationic cobalticenium moieties and the stationary phase of microstyragel columns. It was not possible to determine the precise molecular weight by MALDI–TOF spectrometry due to the limit of this technique, although the splitting of each unit was found for all the cobalticenium polymers in this work (Scheme 1). The end-group analysis by ^1H NMR allows the approximate determination of the

dx.doi.org/10.1021/ma5007864 | *Macromolecules* 2014, 47, 3767–3774

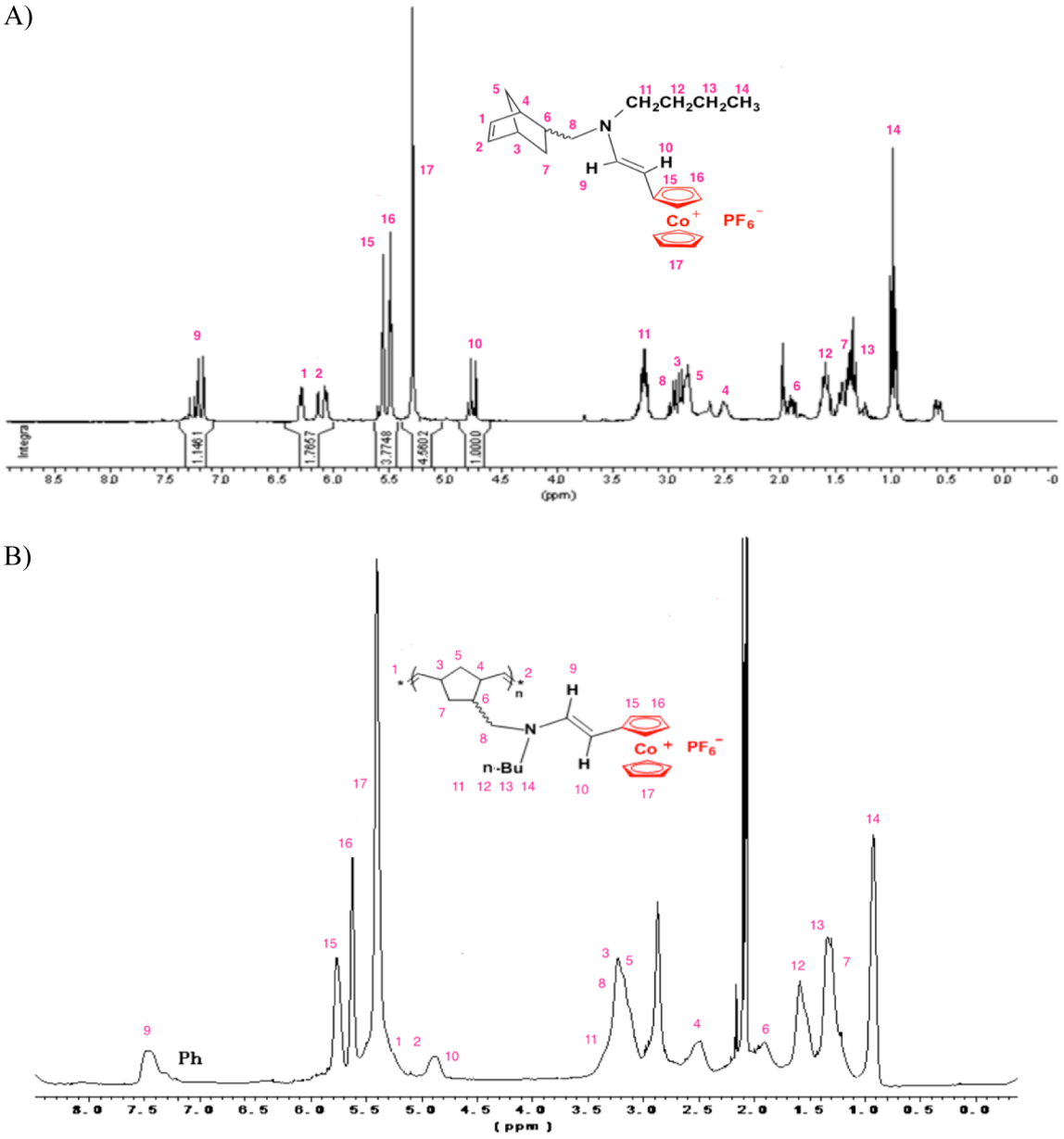

Figure 1. ^{1}H NMR spectra of the cobalticenium−enamine monomer **4** (A) and homopolymer **5** in CD_3COCD_3 (B).

molecular weight of the polymers obtained by ROMP. For example, the molecular weight of polymer **5** determined from end-group analysis is M_n = 44750 g/mol which corresponds to 83 units (Table 2). The objective of DOSY (diffusion-ordered spectroscopy) NMR experiments was thus double: measuring the diffusion coefficients of the molecules in solution and obtaining a DOSY spectrum that reflects the purity of the polymer. The DOSY NMR of the homopolymer **5** obtained in CD_3COCD_3 gives the diffusion coefficient as 9.1 × 10^{-11} m^2/s using eq 2:

$$D_p/D_m = (M_m/M_p)^{0.55} \quad (2)$$

using the known diffusion coefficients of the monomer (D_m) and the polymer (D_p). The molecular weight of **5** is M_n = 47783 g/mol which corresponds to a number of monomer units n_p in the polymer approximatively equal to 89, i.e., slightly higher than the result obtained by end-group analysis using the ^{1}H NMR spectrum. Since the reduction of each redox moiety corresponds to a one-electron process ($Co^{III/II}$), the value of n_p is then estimated by employing the Bard−Anson equation, 3,[23] previously derived for conventional polarography:

$$n_p = (i_{dp}/C_p)/(i_{dm}/C_m)(M_p/M_m)^{0.275} \quad (3)$$

Using this eq 3, comparison between the intensities (i) of the CV wave of the internal reference [$FeCp^*_2$] and the polymer provides a good estimation of the number of electrons n_p involved in the $Co^{III/II}$ redox process of the polymer using the known concentrations (c) and molecular weights (M) obtained from eq 2. Measurement of the ratio between the intensities of the decamethylferrocene reference wave and the first wave of the polymer led to the result n_p = 99 electrons for the polyelectrolyte **5**, which is slightly higher than the experimental values of 83 and 89 derived by the end-group analysis and the DOSY measurements, respectively. It is assumed that some adsorption is responsible for enhancing the n_p value determined with eq 3, thus the actual value is better represented by the average of the two

dx.doi.org/10.1021/ma5007864 | *Macromolecules* 2014, 47, 3767−3774

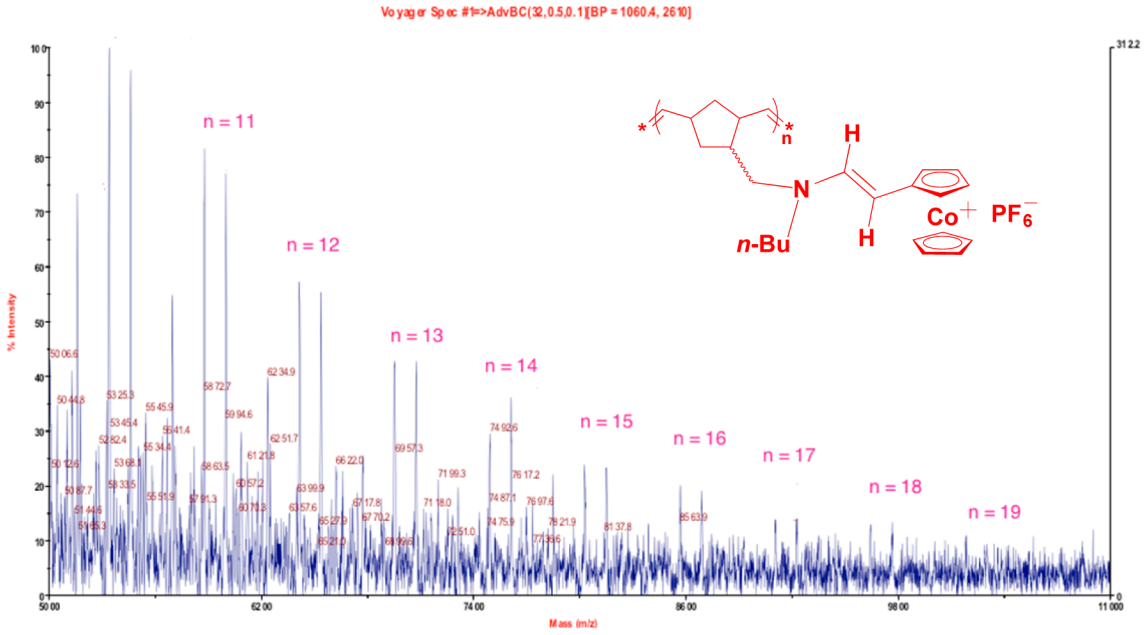

Figure 2. MALDI−TOF spectrum of polymer **5**.

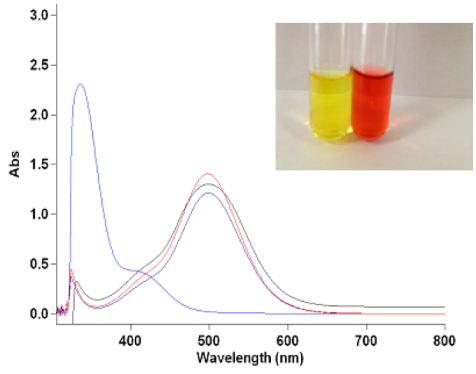

Figure 3. Compared UV−vis spectra of **1** (blue line), cobalticenium−enamine monomer **4** (red line), cobalticenium−enamine polymer **5** (black line) and cobalticenium−enamine polymer **8** (violet line) in acetone. The inset photograph shows the color of **1** (left) and the cobalticenium−enamine norbornene polymers **5** (right) in acetone.

Table 1. Compared $E_{1/2}$ Values for the Cyclic Voltammograms of 1, Monomer 4, and Polymer 5[a]

compound	$E'_{1/2}$ (V)	$\Delta E'$ (mV) ($E'_{pa} - E'_{pc}$)	$E''_{1/2}$ (V)	$\Delta E''$ (mV) ($E''_{pa} - E''_{pc}$)
1	−0.70	70	−1.63	80
4	−1.04	40	−2.02	70
5	−1.04	40	−2.02	40

[a]Cyclic voltammograms (2 mM) were obtained at a Pt electrode at 20 °C in DMF; scan rate = 0.2 V/s; supporting electrolyte = [*n*-Bu_4N][PF_6]; internal reference = $[FeCp^*_2]^{0/+}$ ($Cp^* = \eta^5$-C_5Me_5). The redox potential values for the polymer **8**, **9**, and **10** are identical to those of the polymer **5** under identical conditions.

other methods for the determination of n_p. Identical measurements including the end-group analysis, DOSY NMR for the diffusion coefficient determination and the calculations of the number of electrons heterogeneously transferred in the CV process were also carried out for the polymer **8**, **9** and **10**, and the values obtained are gathered in Table 2.

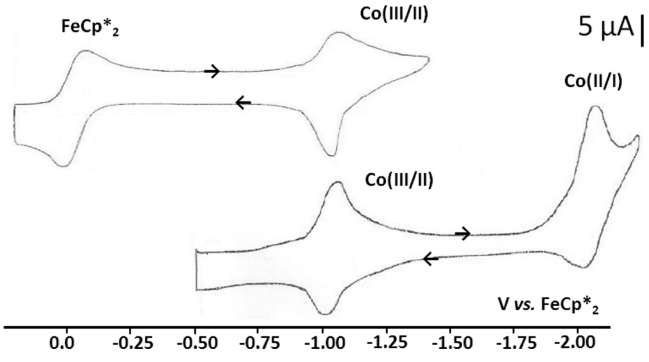

Figure 4. CV of polymer **5** (2 mM) obtained at a Pt electrode at 20 °C in DMF. Supporting electrolyte: [*n*-Bu_4N][PF_6]. Scan rate: 0.2 V/s. Top: Reference and $Co^{III/II}$ wave, $E_{1/2}$ = −1.04 V (ΔE_p = 40 mV) vs $[FeCp^*_2]^{0/+}$ ($Cp^* = \eta^5$-C_5Me_5). Bottom: $Co^{III/II}$ wave, $E_{1/2}$ = −1.04 V (ΔE_p = 40 mV); $Co^{II/I}$ wave, $E_{1/2}$ = −2.02 V (ΔE_p = 40 mV).

Table 2. Sizes of the Polymers (Number of Molecular Units n_p) Obtained from the End-Group Analysis, DOSY NMR Data, and CV Experiments, Respectively

compound	D[a] (diffusion coefficient) (±0.1) m^2/s	n_p (from end group ^1H NMR analysis)[b]	n_p (from eq 2)[c] (DOSY NMR)	n_p (from eq 3)[d] (CV)
5	0.91×10^{-10}	83 ± 10	89 ± 10	99 ± 10
8	1.06×10^{-10}	60 ± 5	67 ± 5	72 ± 5
9	1.28×10^{-10}	44 ± 5	48 ± 5	50 ± 5
10	1.98×10^{-10}	18 ± 3	22 ± 3	25 ± 3

[a]DOSY NMR were measured in CD_3COCD_3 at 25 °C. [b]Values obtained by ^1H NMR in CD_3COCD_3 at 25 °C. [c]Values obtained using eq 2 with the diffusion coefficient obtained from DOSY experiments. [d]Values obtained from eq 3.

CONCLUDING REMARKS

The facile, mild hydroamination of ethynylcobalticenium was shown to easily apply to the syntheses of cobalticenium polymers. It can be used either in the metalation of

dx.doi.org/10.1021/ma5007864 | *Macromolecules* 2014, 47, 3767−3774

polynorbornene polymers containing a secondary amine group and synthesized by ROMP using Grubb's third-generation ROMP catalyst or alternatively in the hydroamination using a secondary amine-functionalized norbornene derivative followed by ROMP using the same ruthenium catalyst. Both methods proceed easily in high yields with various polymer lengths and form facile and readily available routes to redox-robust polycobalticenium polyelectrolytes. It is remarkable that the three methods, end-group analysis, DOSY NMR and cyclic voltammetry give comparable results for the determination of the number of monomeric units in the polymers, although adsorption onto the Pt electrode becomes more significant as the polymer is larger, which provides data in slight excess by the cyclic-voltammetry method for large polymers. This study thus shows the compared reliability of these three methods at least for redox-active metallopolymers of such sizes.

EXPERIMENTAL SECTION

General Information. Reagent-grade THF, diethyl ether, and pentane were dried over Na foil and distilled from sodium benzophenone under nitrogen immediately prior to use. DCM was dried over calcium hydride and distilled under nitrogen prior to use. CH_3CN was dried over P_2O_5 and distilled under nitrogen prior to use. All other solvents and chemicals were used as received. ^1H NMR spectra were recorded at 25 °C with a Bruker AC (200, 300, or 600 MHz) spectrometer. The ^{13}C NMR spectra were obtained in the pulsed FT mode at 75 or 150 MHz with a Bruker AC 300 or 600 spectrometer. All the chemical shifts are reported in parts per million (δ, ppm) with reference to Me_4Si for the ^1H and ^{13}C NMR spectra. ^{31}P stands for ^{31}P (^1H) in the data, with chemical shifts referenced to external H_3PO_4. The mass spectra were recorded using an Applied Biosystems Voyager-DE STR-MALDI−TOF spectrometer. The infrared spectra were recorded on an ATI Mattson Genesis series FT-IR spectrophotometer. UV−vis spectra were measured with PerkinElmer Lambda 19 UV−vis spectrometer. Electrochemical measurements (CV) were recorded on a PAR 273 potentiostat under nitrogen atmosphere. Cyclic voltammograms were obtained at a Pt electrode at 20 °C in DMF; supporting electrolyte, [*n*-Bu_4N][PF_6]; reference, $[FeCp^*_2]^{0/+}$ ($Cp^* = \eta^5$-C_5Me_5). The elemental analyses were performed at the Center of Microanalyses of CNRS at Lyon Solaize (France). DOSY NMR measurements were performed at 25 °C with a Bruker AVANCE II 600 MHz spectrometer. They were performed using ^1H NMR pulsed-gradient experiment: the simulated spin−echo sequence which led to the measurement of the diffusion coefficient *D*. *D* is the slope of the straight line obtained when $\ln(I)$ is displayed against the gradient-pulse power's square according to the following equation: $\ln(I) = -\gamma^2G^2D\delta^2(\Delta - \delta/3)$, I is the relative intensity of a chosen resonance, γ is the proton gyromagnetic ratio, Δ is the intergradient delay (150 ms), δ is the gradient pulse duration (5 ms), and G is the gradient intensity. The diffusion constant of water (2.3×10^{-9} m^2/s) was used to calibrate the instrument. Size exclusion chromatography (SEC) of polymers were performed using a Malvern Viscotek TDA max at 30 °C with THF as eluent and PS standards were used for calibration.

Monomer ***4***. 5-Norbornene-2-carboxaldehyde (1.22 g, 10 mmol, 1 equiv) was dissolved in 10 mL of butylamine. The mixture was stirred at room temperature under N_2 for 16 h, the solvent was removed *in vacuo* to give the imine derivative as a light-yellow oil, dry THF/CH_3OH (1:1), 30 mL, was added, and the solution was stirred at 0 ° C for 10 min. A mixed powder of $NaBH_4$ (1.89 g, 50 mmol, 5 equiv) and PhCOOH (6.10 g, 50 mmol, 5 equiv) was added portionwise into the solution at 0 °C, the mixture was stirred for another 30 min at 0 °C, the solvent was removed *in vacuo*, 30 mL of dry CH_2Cl_2 and 50 mL of saturated $NaHCO_3$ solution were added to the remaining white solid, and the mixture was stirred for 30 min. After separation, the organic phase was washed three times with distilled H_2O and dried with anhydrous Na_2SO_4, and the solvent was removed *in vacuo* to yield the secondary amine-substituted norbornene as a light-yellow oil (1.78 g, 99% yield). Then the norbornene-substituted secondary amine (35.8 mg, 0.2 mmol, 1 equiv) and **1** (71.6 mg, 0.2 mmol, 1 equiv) were dissolved in 10 mL of CH_3CN, the mixture was stirred at 35 °C for 16 h under N_2, the color changed from orange to deep red, and the solvent was removed *in vacuo* to give the enamine monomer **4** as a deep red solid (105.2 mg, yield = 98%). ^1H NMR (300 MHz, $(CD_3)_2CO$), δ_{ppm}: 0.78 (m, 1H), 0.88 (t, 3H, CH_3/Bu), 1.34 (m, 5H), 1.61 (m, 2H), 1.88 (m, 1H), 2.66 (m, 1H), 2.90 (m, 2H), 3.01 (m, 1H), 3.35 (m, 2H, CH_2), 4.91−4.95 (d, 1H), 5.46 (5H/Cp), 5.68 (t, 2H, Cp/sub.), 5.82 (t, 2H, Cp/sub.), 6.08−6.28 (m, 2H/CH═CH), 7.46−7.51 (d, 1H), 2.05 (s, $(CD_3)_2CO$). ^{13}C NMR ($(CD_3)_2CO$, 75 MHz): 147.57 (CH═CH), 137.90 (CH═CH), 131.95 (CH═CH), 117.66 (CH═CH), 84.26 (Cp),84.35 (C/norbornene), 82.67 (sub. Cp), 81.37 (sub. Cp), 73.13 (sub. Cp), 49.33,44.26, 42.25 (C/norbornene), 19.78 (CH_2/Bu), 13.20 (CH_3/Bu), 29.84, 206.26 $(CD_3)_2CO$. ^{31}P NMR (121 MHz, CD_3COCD_3), δ_{ppm}: −144.11 (m, PF_6). UV−vis: λ_{max1} = 320 nm; λ_{max2} = 420 nm; λ_{max3} = 500 nm ($\varepsilon = 1.15 \times 10^4$ L mol^{-1} cm^{-1}). Cyclic voltammogram was obtained at a Pt electrode at 20 °C in DMF: supporting electrolyte, [*n*-Bu_4N][PF_6]. (*i*-Pr)$_2$NR wave: $E_{1/2}$ = 1.04 V (ΔE_p = 80 mV). $Co^{III/II}$ wave: $E_{1/2}$ = −1.04 V (ΔE_p = 40 mV). $Co^{II/I}$ wave: $E_{1/2}$ = −2.02 V (ΔE_p = 70 mV) vs $[FeCp^*_2]^{0/+}$ ($Cp^* = \eta^5$-C_5Me_5). ESI: calcd *m*/*z* for ($C_{24}H_{31}CoN^+$), 392.44; found, 392.18. Anal. Calcd for $C_{24}H_{31}CoNPF_6$: C, 53.64; H, 5.81; N, 2.61. Found: C, 53.76; H, 5.98; N, 2.44.

Polymer ***5***. The cobalticenium enamine-substituted norbornene monomer **4** (40 mg, 0.0745 mmol, 1 equiv) was dissolved in 4 mL of dry CH_2Cl_2, a solution of **3** (0.63 mg, 0.000745 mmol, 0.01 equiv) in 1 mL of CH_2Cl_2 was added to the mixture at room temperature under N_2, and the mixture was stirred at this temperature for 30 min. Then 2 mL of ethyl vinyl ether was added to quench the reaction, the solvent was removed *in vacuo*, and the remaining solid was washed three times with distilled THF. After filtration, the polymer was obtained as a deep red solid. ^1H NMR (300 MHz, $(CD_3)_2CO$), δ_{ppm}: 0.88 (m, 3H, CH_3/Bu), 1.34 (m, 5H), 1.61 (m, 2H), 1.88 (m, 1H), 2.45 (m, 1H), 2.66 (m, 1H), 2.90 (m, 2H), 3.35 (m, 2H, CH_2), 3.61 (m, 1H), 4.89 (m, 1H), 5.38 (5H/Cp), 5.38 (m, 2H/CH═CH), 5.60 (m, 2H, Cp/sub.), 5.73 (m, 2H, Cp/sub.), 7.40 (m, 1H), 2.05 (s, $(CD_3)_2CO$). ^{13}C NMR ($(CD_3)_2CO$, 150 MHz): 147.99 (CH═CH), 130.09−134.99 (CH═CH), 117.71 (CH═CH), 84.32 (Cp), 84.31 (sub. Cp), 81.34 (sub. Cp), 73.12 (sub. Cp), 41.13−37.09 (C/norbornene), 19.80 (CH_2/Bu), 13.36 (CH_3/Bu), 29.84, 206.26 $(CD_3)_2CO$. DOSY (CD_3COCD_3, 600 Hz): the coefficient diffusion $D = 9.1 \times 10^{-11}$ m^2/s. IR (KBr): 1606 cm^{-1} ($\nu_{C=C}$), 835 cm^{-1} (ν_{PF6}). UV−vis: λ_{max1} = 320 nm; λ_{max2} = 420 nm; λ_{max3} = 500 nm (for each nuit, $\varepsilon = 1.15 \times 10^4$ L mol^{-1} cm^{-1}). CV of **5** (2 mM) obtained at a Pt electrode at 20 °C in DMF; supporting electrolyte, [*n*-Bu_4N][PF_6]. $Co^{III/II}$ wave: $E_{1/2}$ = −1.04 V (ΔE_p = 40 mV), $Co^{II/I}$ wave: $E_{1/2}$ = −2.02 V (ΔE_p = 40 mV) vs $[FeCp^*_2]^{0/+}$ ($Cp^* = \eta^5$-C_5Me_5). Anal. Calcd for $(C_{24}H_{31}CoNPF_6)_n$: C, 53.64; H, 5.81; N, 2.61. Found: C, 53.77; H, 5.67; N, 2.49.

Polymer ***6***. 5-Norbornene-2-carboxaldehyde (179 mg, 1.47 mmol, 1equiv) was dissolved in 7.5 mL of dry CH_2Cl_2, a green solution of **3** (12.5 mg, 0.0147 mmol, 0.01 equiv) in 2.5 mL of CH_2Cl_2 was added to the mixture at room temperature under N_2, and the color of the solution instantaneously changed from green to brown, indicating initiation of the polymerization. The mixture was stirred at room temperature for 30 min, 2 mL of ethyl vinyl ether was added to quench the reaction, the solvent was removed *in vacuo* until 0.5 mL of CH_2Cl_2 was left, and 50 mL of MeOH was added to the remaining mixture. The polymer was precipitated as a white solid and washed three times with MeOH. After filtration, the remaining white solid was dried *in vacuo* to give the polymer as a white solid. ^1H NMR (300 MHz, $CDCl_3$), δ_{ppm}: 1.18 (m, 3H, CH_3/Bu), 1.33−1.47 (m, 9H), 1.89 (m, 1H), 2.26−2.34 (m, 2H), 2.58 (m, 3H), 2.81−2.88 (m, 2H), 5.35−5.48 (m, 2H/CH═CH), 9.67 (m, 1H/CHO), 7.26 (s, $CDCl_3$). ^{13}C NMR (150 MHz, $CDCl_3$), δ_{ppm}: 32.36, 37.64, 42.33, 45.52, 54.96 (C/norbornene), 128.53−134.95 (m, CH═CH), 204.02 (broad, CHO), 77.16 ($CDCl_3$). Anal. Calcd for $(C_8H_{10}O)_n$: C, 78.65; H, 8.25. Found: C, 78.77; H, 8.27.

Polymer ***7***. The polymeric aldehyde **6** (122.2 mg, 1 mmol, 1 equiv) was dissolved in 10 mL of a mixed solvent (THF/butylamine: 1/1). The mixture was stirred at room temperature under N_2 overnight, the solvent was removed *in vacuo* to give the polymeric imine as an light-yellow oil, dry THF/CH_3OH (1:1), 30 mL, was added, and the solution was stirred

at 0 °C for 10 min. A mixed powder of $NaBH_4$ (189 mg, 5 mmol, 5 equiv) and PhCOOH (610 mg, 5 mmol, 5 equiv) was added portionwise into the solution under 0 °C, the mixture was stirred for another 30 min at 0 °C, the solvent was removed *in vacuo*, 30 mL of dry CH_2Cl_2, and 50 mL of saturated $NaHCO_3$ solution were added to the remaining white solid. After stirring and separation, the organic phase was washed three times with distilled H_2O and dried over anhydrous Na_2SO_4. The solvent was removed under evaporation to give the polymeric amine as a light-yellow oil in 95% yield. ^{1}H NMR (300 MHz, $CDCl_3$), δ_{ppm}: 1.20 (broad, 3H, CH_3/Bu), 1.85 (broad, 2H), 2.22 (m, 2H), 2.41 (broad, 2H), 2.88 (broad, 2H), 3.68 (broad, 1H), 3.79 (broad, 1H), 3.99 (broad, 1H), 4.28 (broad, 2H), 4.31 (broad, 2H), 5.45 (m, 2H/CH═CH), 7.26 (s, $CDCl_3$), 2.79, 2.89, 7.95 (DMF). ^{13}C NMR (50 MHz, $CDCl_3$), δ_{ppm}: 14.01, 22.18, 25.60, 27.77, 29.28, 31.40, 37.54, 38.62, 42.35, 49.80, 130.21−134.72 (C/polymer), 77.16 ($CDCl_3$). Anal. Calcd for $(C_{12}H_{21}N)_n$: C, 80.38; H, 11.81; N, 7.81. Found: C, 80.77; H, 11.60; N, 7.83.

Polymer ***8***. The norbornene amine polymer **7** (35.8 mg, 0.2 mmol, 1 equiv) and **1** (71.6 mg, 0.2 mmol, 1 equiv) were dissolved in 10 mL of a mixed solvent (CH_2Cl_2/CH_3CN = 1/1). The mixture was stirred for 16h at 35 °C under N_2, the color of the solution changed from orange to deep red, the solvent was removed *in vacuo*, and the remaining solid was washed three times with distilled THF to give the polymeric enamine **8** as a deep red solid (104.2 mg, 90% yield). Anal. Calcd for $(C_{24}H_{31}CoNPF_6)_n$: C, 53.64; H, 5.81; N, 2.61. Found: C, 53.70; H, 5.77; N, 2.60. The characterizations (IR, UV−vis, ^{1}H NMR, ^{13}C NMR, ^{31}P NMR, and cyclic voltammogram) of polymer **8** were identical with those of polymer **5**: except for the diffusion coefficient by DOSY ^{1}H NMR.

Polymers ***9*** *and* ***10***. The use of the ratios of catalyst 0.05 and 0.10 equiv leads to the polymer **9** in 98% yield and polymer **10** in 99% yield, respectively, as deep red solids, giving the same ^{1}H, ^{13}C, NMR, IR, UV−vis spectroscopies, MALDI−TOF mass spectrometry, cyclic voltammetry (CV), and elemental analysis as polymer **5** except for the diffusion coefficient by DOSY ^{1}H NMR.

■ ASSOCIATED CONTENT

Ⓢ Supporting Information

^{1}H NMR, ^{13}C NMR, ^{31}P NMR, IR, UV−vis, and mass spectra, SEC, and CV of monomers and polymers. This material is available free of charge via the Internet at http://pubs.acs.org.

■ AUTHOR INFORMATION

Corresponding Author

*(D.A.) E-mail: d.astruc@ism.u-bordeaux1.fr.

Notes

The authors declare no competing financial interest.

■ ACKNOWLEDGMENTS

Helpful assistance and discussions with Claire Mouche (mass spectrometry) and Jean-Michel Lanier (NMR) from the CESAMO, and Dr Jaime Ruiz, Université Bordeaux 1, and financial support from the University of Bordeaux, the Centre National de la Recherche Scientifique (CNRS), and the China Scholarship Council (Ph.D. grant to Y. W.) is gratefully acknowledged.

■ REFERENCES

(1) Metallocene polymers: (a) MacLachlan, M. J.; Ginzburg, M.; Coombs, N.; T. Coyle, W.; Raju, N. P.; Greedan, J. E.; Ozin, G. A.; Manners, I. *Science* **2000**, *287*, 1460−1463. (b) Kulbaba, K.; Manners, I. *Macromol. Rapid Commun.* **2001**, *22*, 711−724. (c) Ma, Y.; Dong, W.; Hempenius, M. A.; Mohwald, H.; Vancso, G. J. *Nat. Mater.* **2006**, *5*, 724−729.

(2) Metal-containing polymers: (a) Schubert, U. S.; Eschbaumer, C. *Angew. Chem., Int. Ed.* **2002**, *41*, 2892−2926. (b) Shumugam, R.; Gabriel, G. J.; Aamer, K. A.; Tew, G. N. *Macromol. Rapid Commun.* **2010**, *31*, 784−793. (c) Manners, I. *Synthetic Metal-Containing Polymers*; Wiley-VCH: Weinheim, Germany, 2004. (d) Whittell, G. R.; Hager, M. D.; Schubert, U. S.; Manners, I. *Nat. Mater.* **2011**, *10*, 176−188.

(3) Geiger, W. E. *Organometallics* **2007**, *26*, 5738−5765.

(4) Ferrocene-containing macromolecules: (a) Ornelas, C.; Ruiz, J.; Belin, C.; Astruc, D. *J. Am. Chem. Soc.* **2009**, *131*, 590−601. (b) Kim, B. Y.; Ratcliff, E. L.; Armstrong, N. R.; Kowalewski, T.; Pyun, J. *Langmuir* **2010**, *26*, 2083−2092. (c) Hardy, C. G.; Ren, L.; Tamboue, T. C.; Tang, C. *J. Polym. Sci., Part A: Polym. Chem.* **2011**, *49*, 1409−1420.

(5) Pioneering studies of cobalticenium polymers: (a) Ito, T.; Kenjo, T. *Bull. Soc. Chem. Jpn.* **1968**, *41*, 614−619. (b) Pittman, C. U.; Ayers, O. E.; McManus, S. P.; Sheats, J. E.; Whitten, C. E. *Macromolecules* **1971**, *4*, 360−362.

(6) For recent cobalticenium-containing polymers: see ref 7 and the following: (a) Masakazu, K.; Ikuyoshi, T. *Nippon Kagakkai Koen Yokoshu* **2003**, *83*, 805−808. (b) Kondo, M.; Hayakawa, Y.; Miyazawa, M.; Oyama, A.; Unoura, K.; Kawaguchi, H.; Naito, T.; Maeda, K.; Uchida, F. *Inorg. Chem.* **2004**, *43*, 5801−5803. (c) Mayer, U. F. J.; Charmant, J. P. H.; Rae, J.; Manners, I. *Organometallics* **2008**, *27*, 1524−1533. (d) Mayer, U. F. J.; Gilroy, J. B.; O'Hare, D.; Manners, I. *J. Am. Chem. Soc.* **2009**, *131*, 10382−10383. (e) Ren, L. X.; Hardy, C. G.; Tang, C. B. *J. Am. Chem. Soc.* **2010**, *132*, 8874−8875. (f) Ren, L. X.; Hardy, C. G.; Tang, S. F.; Doxie, D. B.; Hamidi, N.; Tang, C. B. *Macromolecules* **2010**, *43*, 9304−9310. (g) Chadha, P.; Ragogna, P. J. *Chem. Commun.* **2011**, *47*, 5301−5303. (h) Zhang, J. Y.; Ren, L. X.; Hardy, C. G.; Tang, C. B. *Macromolecules* **2012**, *45*, 6857−6863. (i) Ren, L. X.; Zhang, J. Y.; Hardy, C. G.; Ma, S. G.; Tang, C. B. *Macromol. Commun.* **2012**, *33*, 510. (j) Ren, L. X.; Zhang, J. Y.; Bai, X. L.; Hardy, C. G.; Shimizu, K. D.; Tang, C. B. *Chem. Sci.* **2012**, *3*, 580−583.

(7) Qiu, H.; Gilroy, J. B.; Manners, I. *Chem. Commun.* **2013**, *49*, 42−44.

(8) Rapakousiou, A.; Wang, Y.; Ruiz, J.; Astruc, D. *J. Inorg. Organomet. Polym. Mater.* **2014**, *24*, 107−113.

(9) Casado, C. M.; Lobete, F.; Alonso, B.; Gonzalez, B.; Losada, J.; Amador, U. *Organometallics* **1999**, *18*, 4960−4969.

(10) Rapakousiou, A.; Wang, Y.; Belin, C.; Pinaud, N.; Ruiz, J.; Astruc, D. *Inorg. Chem.* **2013**, *52*, 6685−6693.

(11) (a) Wilkinson, G. *J. Am. Chem. Soc.* **1952**, *74*, 6148−6149. (b) Wilkinson, G.; Pauson, P. L.; Cotton, F. A. *J. Am. Chem. Soc.* **1954**, *76*, 1970−1974. (c) Sheats, J. E.; Rausch, M. D. *J. Org. Chem.* **1970**, *35*, 3245−3249. (d) Sheats, J. E. *J. Organomet. Chem. Library* **1979**, *7*, 461−521. (e) Kemmit, R. D. W.; Russell, D. R. In *Comprehensive Organometallic Chemistry*; Wilkinson, G., Ed.; Pergamon: Oxford, 1982, *5*, Chapter 34.4.5.1, p 244. (f) Astruc, D. *Organometallic Chemistry and Catalysis*; Springer: Heidelberg, Germany, 2007, Chapter 11.

(12) Tatykhanova, G.; Sadakbayeva, Z.; Berillo, D.; Galaev, I.; Abdullin, K.; Adilov, Z.; Kudaibergenov, S. *Macromol. Symp.* **2012**, *317−318*, 18−27.

(13) Peckham, T. J.; Lough, A. J.; Manners, I. *Organometallics* **1999**, *18*, 1030−1040.

(14) Wildschek, M.; Rieker, C.; Jaitner, P.; Schottenberger, H.; Schwarzhans, K. E. *J. Organomet. Chem.* **1990**, *396*, 355−361.

(15) (a) Diallo, A. K.; Menuel, S.; Monflier, E.; Ruiz, J.; Astruc, D. *Tetrahedron Lett.* **2010**, *51*, 4617−4619. (b) Rapakousiou, A.; Mouche, C.; Duttine, M.; Ruiz, J.; Astruc, D. *Eur. J. Inorg. Chem.* **2012**, 5071−5077.

(16) (a) Wang, Y.; Rapakousiou, A.; Latouche, C.; Daran, J. C.; Singh, A.; Ledoux, I.; Ruiz, J.; Saillard, J. Y.; Astruc, D. *Chem. Commun.* **2013**, *49*, 5862−5864. (b) Wang, Y.; Latouche, C.; Rapakousiou, A.; Lopez, C.; Ledoux-Rak, I.; Ruiz, J.; Saillard, J.-Y.; Astruc, D. *Chem.—Eur. J.* **2014**, DOI: 10.1002/chem.201400373.

(17) (a) *Handbook of Metathesis*, Grubbs, R. H., Ed.; Applications in Polymer Synthesis 3; Wiley-VCH: Weinheim, Germany, 2003. (b) Buchmeiser, M. R. *Chem. Rev.* **2009**, *109*, 303−321. (c) Leitgeb, A.; Wappel, J.; Slugovc, C. *Polymer* **2010**, *51*, 2927−2946.

(18) (a) Choi, T. L.; Grubbs, R. H. *Angew. Chem., Int. Ed.* **2003**, *42*, 1743−1746. (b) Vougioukalakis, G. C.; Grubbs, R. H. *Chem. Rev.* **2010**, *110*, 1746−1787. (c) For a recent review on metathesis reactions, see:

Deraedt, C.; d'Halluin, M.; Astruc, D. *Eur. J. Inorg. Chem.* **2013**, 4881−4908.
(19) Cho, B. T.; Kang, S. K. *Tetrahedron* **2005**, *61*, 5725−5734.
(20) Ren, L.; Zhang, J.; Hardy, C. G.; Doxie, D.; Fleming, B.; Tang, C. *Macromolecules* **2012**, *45*, 2267−2275.
(21) For seminal electrochemical studies of cobalticenium derivatives, see: (a) Geiger, W. E. *J. Am. Chem. Soc.* **1974**, *96*, 2632−2634. (b) Connelly, N. G.; Geiger, W. E. *Adv. Organomet. Chem.* **1984**, *23*, 1−93.
(22) Ruiz, J.; Astruc, D. C. R. *Acad. Sci., Ser. IIc: Chim.* **1998**, *1*, 21−27.
(23) Flanagan, J. B.; Margel, S.; Bard, A. *J. Am. Chem. Soc.* **1978**, *100*, 4248−4253.

Partie 5

Les réservoirs dendritiques d'hydrures (RDH)

Partie 5

Les réservoirs dendritiques d'hydrures (RDH)

La formation et la stabilisation de NPMs de taille contrôlée constitue actuellement un enjeu crucial étant donné l'utilisation de ces NPMs dans différents domaines tels que la catalyse, les capteurs et la nanomédecine. Par exemple les petites NPs d'or sont recherchées en catalyse (< 5 nm) alors que ce sont les grandes NPs d'or qui sont recherchées en imagerie et thérapie médicales (> 20 nm).[1] L'environnement stabilisant moléculaire des NPs joue également un rôle considérable dans leurs applications: force du ligandage, propriétés physico-chimiques et toxicité potentielle. Dans ce contexte, la génération des NPMs dans leur milieu stabilisateur doit se faire simultanément avec la réduction des cations précurseurs en atomes métalliques destinés à s'assembler en NPMs.

Le réducteur habituellement utilisé, $NaBH_4$, conduit à des NPMs données qui ne répondent pas nécessairement aux besoins et laissent des polyboranes plus ou moins définis dont l'existence n'est généralement pas prise en compte dans les publications. D'autres réducteurs, monoélectroniques comme le ferrocène, ont été utilisés avec des succès variables et aboutissent à des résultats particuliers. Nous avons imaginé l'idée de réservoir polyhydrurique dendritique en introduisant à l'intérieur du dendrimère des ligands stabilisant à la fois les ions métalliques précurseurs et les NPMs formées. La nature dendritique du réducteur permet d'assurer un grand nombre d'hydrures en périphérie permettant de réduire un nombre suffisant de cations métalliques. La structure et la topologie dendritique permettent de stabiliser les nanoparticules, ce dernier élément étant connu depuis les travaux de Crooks avec les dendrimères PAMAM.[2] Après transfert, la périphérie du dendrimère devient polycationique, et nous avons anticipé des propriétés protectrices de cette fonction.

Les dendrimères à terminaisons cobalticénium de génération 0 à 2 (G_0-G_2) ont été synthétisés par réactions "click" (cycloaddition d'alcyne terminal avec un dérivé azoturé catalysée par Cu^I)[3] entre les dendrimères G_0-G_2 comportant 9, 27 et 81 terminaisons azido avec l'hexafluorophosphate d'éthynylcobalticénium conduisant à des dendrimères à terminaisons hexafluorophosphate de1,2,3-triazolylcobalticénium. La réduction du cobalticénium (complexe d^6 du Co^{III}, 18e) par $NaBH_4$ conduit à un complexe de cyclopentadiène rouge stable $[Co(\eta^4\text{-}C_5H_6)Cp]$[4] (complexe d^8 du Co^I, 18e).[5] La présence du substituent triazolyl ne perturbe pas la réduction par hydrure du cobalticénium, ce qui est présenté dans le premier mémoire publié de ce chapitre qui concerne cette chimie des monomères. Le second manuscrit concerne les RDHs et la comparaison avec les RDEs (réducteur monoélectroniques de Au^{III} formant de très grosses NPs d'or). Ce manuscrit non publié montre que les RDHs au cobalticénium conduisent systématiquement, par réductions de Au^{III}, Ag^I et Pd^{II} à des capsules très robustes contenant des petites NPs de Pd, Ag et Au, contrairement aux RDEs. La taille énorme des NPs d'or obtenues avec le RDE est attribuée à la lenteur de la réduction monoélectronique devant passer par des intermédiaires radicalaires de haute énergie,

contrairement aux RDHs impliquant probablement seulement des processus énergétiquement faciles tels que des échanges de ligands anioniques suivis d'éliminations réductrices de H_2.

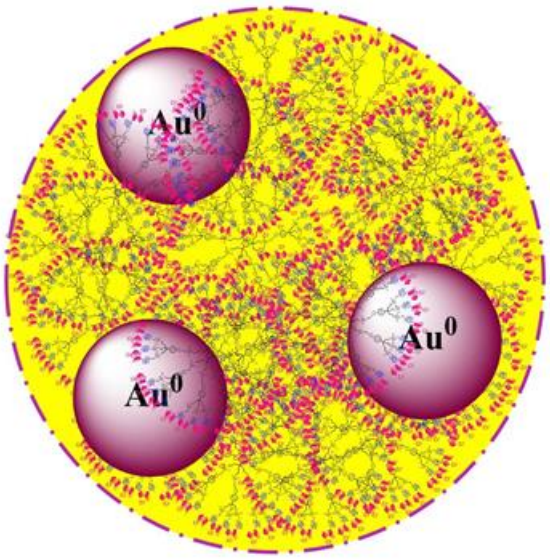

Schéma. Motifs du chapitre 5.2.

Références

1. M-C. Daniel, D. Astruc. Gold Nanoparticles: Assembly, Supramolecular Chemistry, Quantum-size Related Properties, and Applications towards Biology, Catalysis and Nanotechnology. *Chem. Rev* **2004**, 104, 293-346.
2. Myers, V. S. et al. Dendrimer Encapsulated Nanoparticles: New Synthetic and Characterization Methods and Catalytic Applications. *Chem. Sci*. **2011**, *2*, 1632-1646.
3. a) Rostovstev, V. V.; Green, L. G.; Fokin, V. V.; Sharpless, K. B. A. Stepwise Huisgen Cycloaddition Process: Copper(I)-Catalyzed Regioselective Ligation of Azide and Terminal Alkynes. Angew. Chem., Int. Ed. 2002, 41, 2596-2599. b) M. Meldal, C. W. Tornoe, C. Christensen. Peoptidotriazoles on solid phase: [1,2,3]-triazoles by regiospecific copper (I)-catalyzed 1,3-dipolar cycloadditions of terminal alkynes to azides. J. Org. Chem. 2002, 67, 3057-3064.
4. M. L. H. Green, L. Pratt, G. Wilkinson. A New Type of Transition Metal-Cyclopentadiene Compound. *J. Chem. Soc.* **1959**, 3753–3767.
5. a) M. L H. Green, G. Parkin. Application of the Covalent Bond Classification Method for the Teaching of Inorganic Chemistry. J. Chem. Ed. 2014, 91, 807-816. b) D. Astruc. Chimie Organométallique et Catalyse. EDP Science, Les Ullis, 2013, Chapitre 1, pp. 32-35.

EurJIC European Journal of Inorganic Chemistry

FULL PAPER

DOI: 10.1002/ejic.201200755

Click Synthesis and Redox Chemistry of Mono- and Heterobimetallic Triazolyl and Triazolium-Ferrocene and Cobalticinium Complexes

Amalia Rapakousiou,[a] Claire Mouche,[a] Mathieu Duttine,[b] Jaime Ruiz,[a] and Didier Astruc*[a]

Keywords: Metallocenes / Sandwich complexes / Iron / Cobalt / Redox chemistry / Click chemistry / Reduction / Nitrogen heterocycles

Mono- and heterobimetallic triazolylferrocene and cobalticinium complexes and triazolium derivatives were synthesized by click reactions between the ethynylmetallocenes and benzyl azide or (azidomethyl)ferrocene followed by methylation reactions, respectively. Cyclic voltammetry data shed light on the electron-withdrawing character of the 1,2,3-triazolyl and triazolium substituents of the metallocenes, and cathodic reduction of the triazolium group was found to be irreversible even at –50 °C. Chemical reduction of orange triazolylcobalticinium hexafluorophosphate using $NaBH_4$ yielded a mixture of red isomeric triazolyl η^4-cyclopentadiene–cobalt–η^5-cyclopentadienyl complexes, whereas reduction by the single-electron reductant [$Fe^ICp(\eta^6$-$C_6Me_6)$] yielded the brown 19-electron triazolylcobaltocene.

Introduction

The concept of "click" reactions by Sharpless el al. proposes to easily assemble molecular fragments.[1] The Cu^I-catalyzed regioselective azide–alkyne cycloaddition (CuAAC),[2,3] which is presently the most frequent example,[4–22] was reported in 2002 by the research groups of Sharpless et al.[2] and Meldal et al.[3] This synthetic advantage is not the only one, since the resulting 1,2,3-triazolyl derivatives that are selectively produced are also good ligands in a variety of transition-metal complexes that have new luminescent,[23–26] sensor,[27–29] or catalytic properties.[30,31] In this context, one of the key functions of transition-metal complexes is their redox behavior,[32–38] and in particular late transition-metal sandwich complexes are known to withstand stability under two or three oxidation states.[36,39–41] The latter property indeed allows their use as redox reagents,[36] redox catalysts,[42] and redox sensors.[43–47] Therefore, we wish to investigate the redox behavior of simple ferrocene and cobalticinium complexes bound to 1,2,3-triazolyl using click (CuAAC) reactions of the ethynylmetallocene precursors and the related triazolium derivatives subsequently obtained by the methylation of the latter. The investigation of these syntheses and that of the redox properties of the metallocene triazolyl and triazolium derivatives are the subject of this article, and the results are a key step towards potential analytical and synthetic redox chemistry of large nanosystems involving click assemblies.[47]

The alkylation of triazole (trz) to yield the triazolium (trz*) group has been reported as well as the properties of trz and trz* derivatives as molecular sensors.[27–29] The redox chemistry of ferrocene and cobalticinium have been known since Wilkinson's seminal reports on these metallocenes,[48,49] and these properties have been extensively studied by cyclic voltammetry and used in organometallic synthesis, sensing, and catalysis.[32–36,42,50] However, we are not aware of redox or electrochemical studies of trz and trz* derivatives.

Results and Discussion

1. CuAAC Reactions and Syntheses of the Mono- and Heterobimetallic Triazole Compounds

The CuAAC reactions were conducted between benzyl azide and the known ethynylmetallocenes[51,52] to produce the triazolyl derivatives **1** and **3** [Equation (1)], and with ethynylbenzene to produce the reference organic compound **5**.

This CuAAC click reaction is, as is well known, completely selective in the formation of 1,4-disubstituted trz, contrary to the non-catalyzed Huisgen azide–alkyne dipolar cycloaddition that produces both 1,4 and 1,5 isomers.[53] As a Cu^I catalyst, we used a mixture of $CuSO_4 \cdot 5H_2O$ and the reductant sodium ascorbate that is the initial Sharpless catalyst.[2] (Azidomethyl)ferrocene[54] was also used in the CuAAC reaction with ethynylcobalticinium to produce the heterobimetallic triazolyl complex **7**; see Equation (2).

[a] ISM, UMR CNRS N° 5255, Univ. Bordeaux, 33405 Talence Cedex, France
E-mail: d.astruc@ism.u-bordeaux1.fr
Homepage: http://astruc.didier.free.fr/welcome.htm
[b] ICMCB, UPR CNRS N° 9048, Univ. Bordeaux, 33608 Pessac Cedex, France

Supporting information for this article is available on the WWW under http://dx.doi.org/10.1002/ejic.201200755.

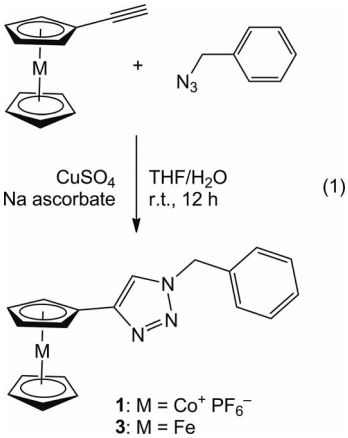

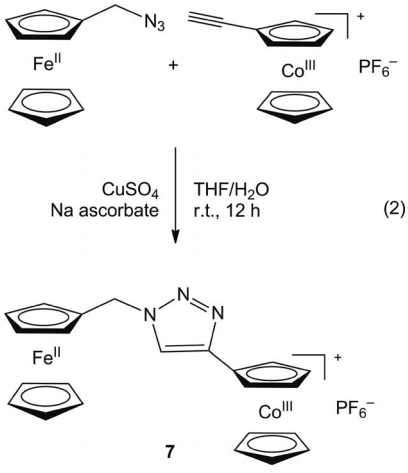

All the triazole derivatives were obtained after precipitation in an overall yield of around 80%. The infrared spectra were a very useful tool in following all these click reactions (compounds **1**, **3**, **5**, and **7**), because the characteristic peak of the azido groups at about 2094 cm^{-1} disappears at the end of each reaction confirming that these azido groups were replaced by the trz. For triazolyl cobalticinium hexafluorophosphate (**1**), which was soluble only in polar solvents such as acetone and acetonitrile, but also in THF, the characteristic band of the PF_6 anion is observed at 837 cm^{-1}. The formation of trz is clearly shown by ^1H NMR spectroscopy by the appearance of the trz CH peak. This is also confirmed in particular by the characteristic peaks of Cq and CH of trz in the ^{13}C NMR spectra. Finally, the structures of all of the new trz compounds were also confirmed by the observation of the molecular peak in the mass spectrum and by elemental analysis (see the Supporting Information).

2. Methylation of the Triazole Compounds to Produce Triazolium Derivatives

Further methylation of the trz rings of the compounds **1**, **3**, and **5**, using Me_3OBF_4 as the methylating agent,[29] resulted in the formation of the trz* compounds **2**, **4**, and **6**, respectively, in yields of about 90% and dimethyl ether that was removed under vacuum; see Equation (3).

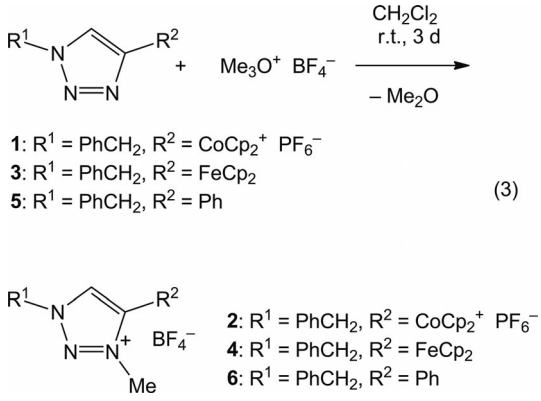

The ^1H and ^{13}C NMR spectra of the trz* compounds **2**, **4**, and **6** show the proton and carbon signals, respectively, of the N–CH_3 methyl group. All the signals in the NMR spectra of these new trz* products were shifted downfield compared to their trz precursors, because of the cationic nature of the trz* species. However, the quaternary carbon of the cobalticinium cation linked to the trz* group was shifted upfield in the ^{13}C NMR spectrum. The infrared spectra of the trz* compounds **2**, **4**, and **6** show the appearance of the characteristic band of BF_4^- at 1070 cm^{-1}, and for trz* cobalticinium hexafluorophosphate (**2**) the characteristic band of the PF_6 anion is observed at 872 cm^{-1}. The structure of the new trz* derivatives was confirmed by the molecular peak in the mass spectra and by elemental analyses (see the Supporting Information).

3. Cyclic Voltammetry Studies

The cyclic voltammograms (CVs) of all the trz and trz* compounds have been recorded in order to investigate the redox properties of the trz and trz* groups and their influence on the redox properties of the neutral and cationic metallocenic groups to which they are directly attached. The results are reported in Table 1.

The new compound **1** shows two chemically and electrochemically reversible reduction waves in THF at the Pt electrode, assigned to the two successive single-electron reductions of cobalticinium[55] (Figure 1). The first (less cathodic) wave corresponds to the reduction of the 18-electron, d^6 Co^{III} complex to the 19-electron, d^7 Co^{II} complex. This wave at –0.85 V vs. $[FeCp_2^*]^{+/0}$ ($Cp^* = \eta^5$-C_5Me_5) in THF is located at a potential that is 40 mV less negative than that of the parent cobalticinium complex, which can be attributed to the electron-withdrawing properties of the 1,2,3-triazolyl group. The second single-electron cathodic wave that is located at –1.90 V vs. $[FeCp_2^*]^{+/0}$ corresponds to the reduction of the 19-electron, d^7 Co^{II} complex to the 20-electron, d^8 Co^{I} species. It is remarkable that this second

Table 1. Redox potentials and chemical (i_a/i_c) and electrochemical ($E_{pa} - E_{pc} = \Delta E$) reversibility data for compounds **1**–**7**. Supporting electrolyte: [nBu$_4$N][PF$_6$] (0.1 M); working and counter electrodes: Pt; reference electrode: Ag; internal reference: FeCp*$_2$ (Cp* = η^5-C$_5$Me$_5$); scan rate: 0.200 V s^{-1}.

	Solvent	$Fe^{II/III}$ [V] ΔE		i	$Co^{III/II}$ [V] ΔE		i	$Co^{II/I}$ [V] ΔE		i	trz*$^{(0/+1)}$	
	–	$E_{1/2}$		$_a/i_c$	$E_{1/2}$		$_a/i_c$	E		$_a/i_c$	E_p	ΔE
1	MeCN	–	–	–	–0.75	0.60	1	E_p = –1.76	0	0	–	–
1	THF	–	–	–	–0.85	0.65	1	$E_{1/2}$ = –1.90	0.90	0.9	–	–
2	MeCN	–	–	–	–0.46	0.50	1	E_p = –1.32	0	0	–2.20	0
3	MeCN	0.55	0.50	1	–	–	–	–	–	–	–	–
3	THF	0.43	0.60	1	–	–	–	–	–	–	–	–
4	MeCN	0.84	0.50	1	–	–	–	–	–	–	–1.64	0
6	MeCN	–	–	–	–	–	–	–	–	–	–1.60	0
6	THF	–	–	–	–	–	–	–	–	–	–1.72	0
7	MeCN	0.62	0.50	1	–0.76	0.50	0.5	E_p = –1.81	0	0	–	–
7	THF	0.48	0.65	1	–0.88	0.65	1	$E_{1/2}$ = –1.92	0.80	0.3	–	–

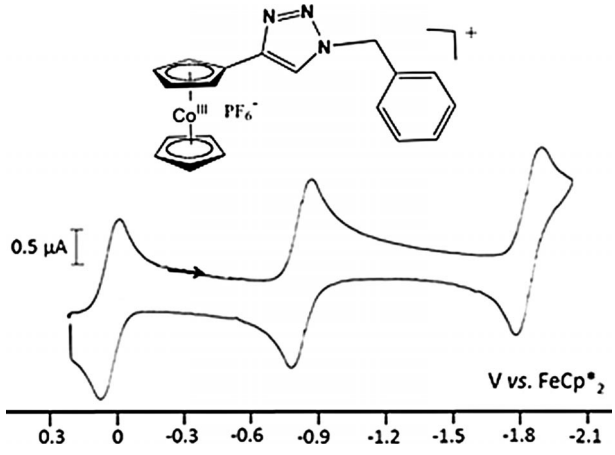

Figure 1. CV of **1** in THF. The wave at 0.0 V corresponds to the internal reference FeCp*$_2$. Solvent: THF; reference electrode: Ag; working and counter electrodes: Pt; scan rate: 0.2 V s^{-1}; supporting electrolyte: [nBu$_4$N][PF$_6$].

cathodic wave is also chemically and electrochemically reversible, which means that both the 19-electron and 20-electron species are stable on the electrochemical time scale, and the trz substituent does not destabilize these oxidation states that are already rendered fragile by the presence of electrons in the antibonding e_1* orbitals. The influence of the electron-withdrawing properties of the trz substituent on the redox potentials appears to be the same for both the first and second reduction wave. In MeCN, the reduction waves are chemically irreversible, which can be attributed to fast ligand substitution by the MeCN ligand in high concentration. Indeed, MeCN is a much stronger ligand than THF, and we know that ligand substitution of π-hydrocarbon ligands in 19-electron late transition-metal complexes by good ligands such as MeCN is of the order of 10^9 faster than the analogous exchange in the 18-electron complexes.[56,57] Thus the 19-electron Co^{II} complexes are kinetically very unstable in MeCN even on the electrochemical time scale, and the 20-electron Co^{I} species even more so. This irreversibility in MeCN (partial for the first wave, total for the second one) is observed for all the compounds containing the cobalticinium group (**1**, **2**, and **7**). For the triazolylferrocene complex **3**, oxidation of the ferrocenyl group is found at a more positive potential than ferrocene itself in MeCN (Table 1), whereas for **7** (Figure 2) the additional influence of the cobalticinium group shifts the oxidation of the ferrocenyl group anodically (Table 1).

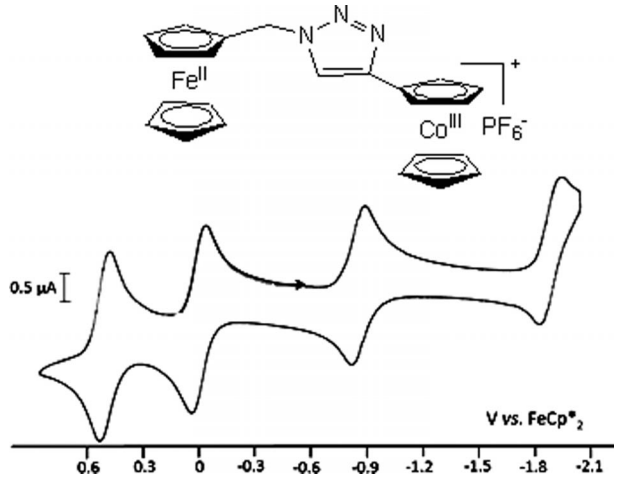

Figure 2. CV of **7** in THF. The wave at 0.0 V corresponds to the internal reference of FeCp*$_2$. Solvent: THF; reference electrode, Ag; working and counter electrodes: Pt; scan rate: 0.2 V s^{-1}; supporting electrolyte: [nBu$_4$N][PF$_6$].

Cathodic reduction of the trz ring in the triazolyl derivatives **1**, **3**, **5**, and **7** was not observed until –2.5 V vs. [FeCp$_2$*]$^{+/0}$. On the other hand, cathodic reduction of the

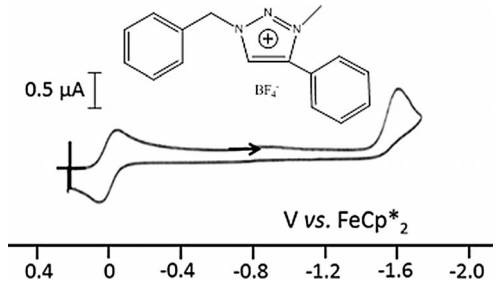

Figure 3. CV of **6** in CH_3CN. The wave at 0.0 V corresponds to the internal reference of FeCp*$_2$. Solvent: CH_3CN; reference electrode: Ag; working and counter electrodes: Pt; scan rate: 0.2 V s^{-1}; supporting electrolyte: [nBu$_4$N][PF$_6$].

trz* derivatives **2**, **4**, and **6** was observed, but it was totally chemically irreversible even at –50 °C. The trz* group in the organic compound **6** (Figure 3) was reduced at a slightly less negative potential (E_p) than the trz* group in the ferrocene derivative **4** because of the electron-releasing property of the ferrocenyl group (compared to the phenyl group), although the comparison between the E_p values does not reflect the exact difference of the E^0 values that are not easily accessible. The trz* group in the cobaltocenyltriazole complex **2** was reduced at a much more negative potential because the 20-electron cobaltocene anionic species that is generated at a less negative potential is strongly electron-releasing. Finally, the trz* group behaves as an even more electron-withdrawing substituent than trz because of the cationic charge of the former. For instance, reversible single-electron anodic oxidation of the ferrocenyl group in MeCN occurs at a potential 220 mV more positive for **4** than for the ferrocenyl group in **7**.

4. Reduction of Triazolylcobalticinium 2 with $NaBH_4$ and Single-Electron Reductants

Reduction of the orange cationic triazolylcobalticinium complex **1** by $NaBH_4$ at 0 °C in THF, in which it was soluble, produced the red, air-sensitive compound **8** that was soluble in diethyl ether enabling its extraction under N_2 [Equation (4)]. Its thermal stability under N_2 is modest under ambient conditions, allowing standard spectroscopic analysis.

The disappearance of the PF_6^- band in the infrared spectrum of **8** is consistent with the formation of a neutral compound in 95% yield, the structure being confirmed by observation of the molecular peak in the mass spectrum. Compound **8** has a rather complex ^1H NMR spectrum showing the formation of a mixture of isomeric triazolyl η^4-cyclopentadiene–cobalt–η^5-cyclopentadienyl complexes.[58] Indeed the hydride reduction of the cationic cobalt sandwich can occur either on the *ipso* 1,2 or 1,3 position of the cyclopentadienyl ligand to which the trz group is attached or to the free cyclopentadienyl ligand. No attempt was made to separate the isomers. The cyclic voltammogram in CH_2Cl_2 shows two totally irreversible oxidation waves at 0.3 V and 0.65 V vs. $[FeCp_2^*]^{+/0}$. It is suggested that these two waves correspond to the oxidation of the triazolylcyclopentadiene–cobalt–Cp and triazolylcyclopentadienyl–cobalt–cyclopentadiene, respectively. The first wave at 0.3 V is more intense than the other, which would be in agreement with the preferential hydride reduction of the substituted ring that is more electron poor than the free ring.

Reduction of **1** by Na/Hg in THF led to decomposition, probably because of the thermal instability of the 20-electron triazolylcobaltocene anion, which is easily formed with reduction by Na/Hg. Therefore we synthesized the known crystalline forest-green 19-electron complex [$Fe^ICp(\eta^5$-$C_6Me_6)$].[59] This complex has a potential E^0 of –1.53 V in THF vs. $[FeCp_2^*]^{+/0}$ [60–61] that is much more cathodic than the first potential of the reduction of **1** but less negative than its second reduction potential. Reduction of **1** by a stoichiometric amount of [$Fe^ICp(\eta^5$-$C_6Me_6)$] in THF instantaneously provoked a color change from orange to brown and formation of a yellow precipitate of [$Fe^{II}Cp(\eta^5$-$C_6Me_6)$][PF_6]; see Equation (5).[58] The reduced brown, air-sensitive compound **9** (the color of cobaltocene) was soluble in diethyl ether and was characterized by UV/Vis and EPR (Figure 4) spectroscopy as well as mass spectrometry. It was also characterized by its re-oxidation in air to the 18-electron complex as shown by ^1H NMR spectroscopy (the shape of the signal of the trz proton therein is broad and different from that of the peak observed in **1**, which may tentatively be assigned to a change of anion for OH^- that forms a hydrogen bond with the trz proton).

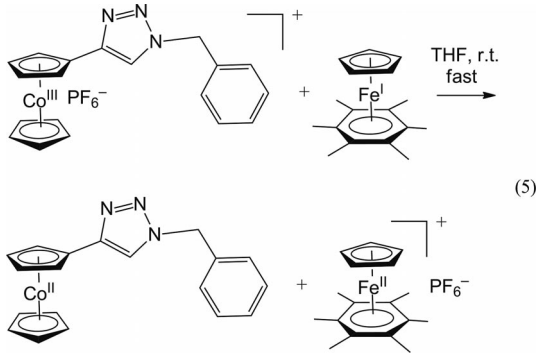

(5)

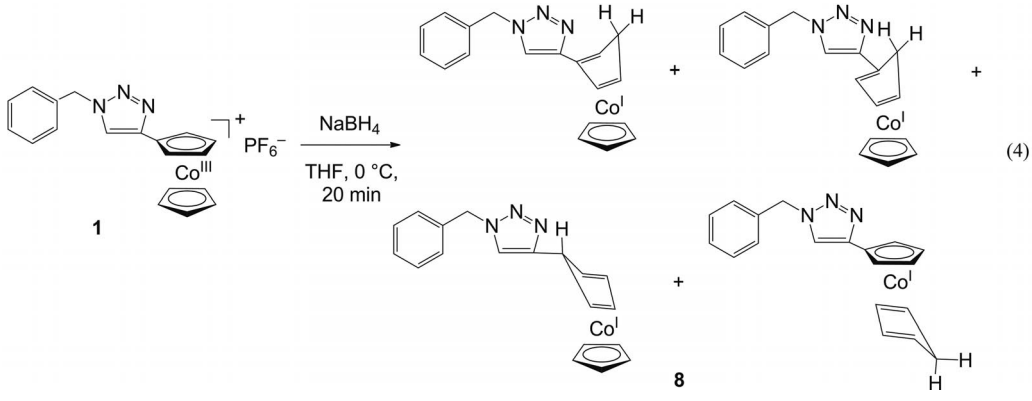

(4)

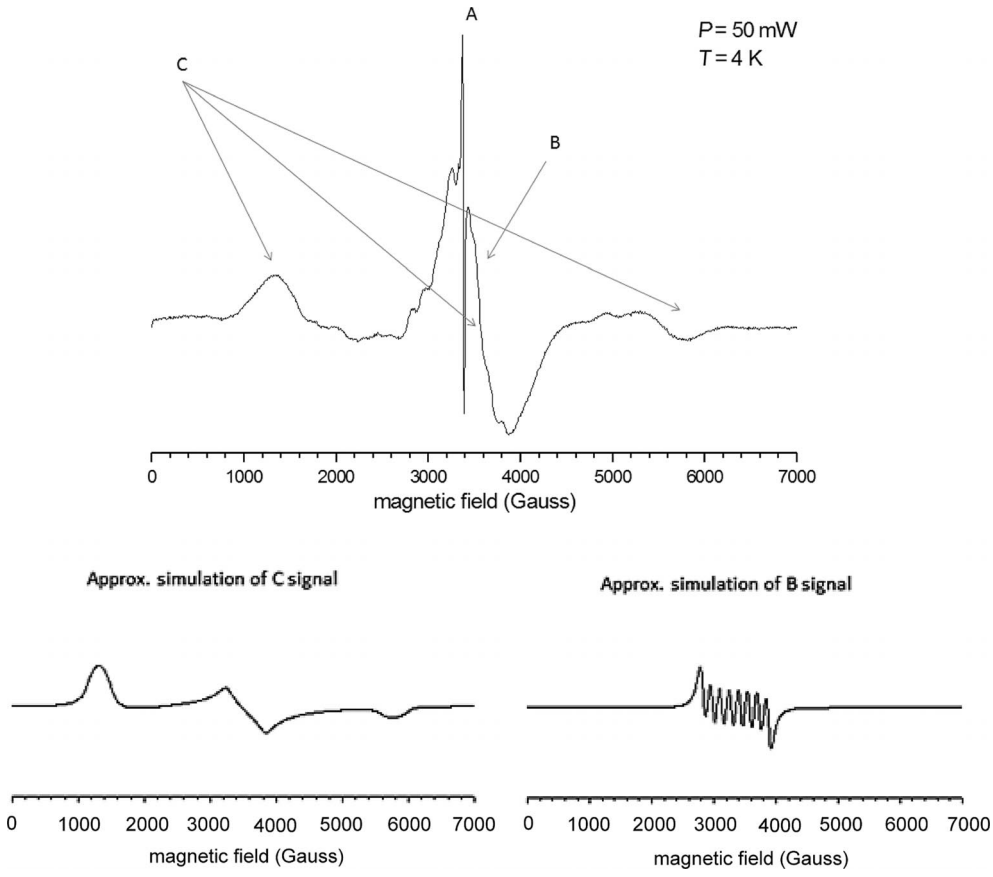

Figure 4. EPR analysis of **9** and approximate simulations of signals B and C[62]. Signal A gives $g_{\|}$ = 2.037 and $g_{\perp}$ = 2.003. Signal B gives g = 2.015 and the hyperfine coupling constant A (Co – I = 7/2) = 150 G. The g values of signal C are g_1 = 1.17, g_2 = 1.9, and g_3 = 5.09.

Conclusions

Three triazolylmetallocenes, including a heterobimetallic complex, have been synthesized by CuAAC click reactions, and their redox chemistry has been investigated including the determination of the oxidation/reduction potentials of the redox-active groups and the nature of the products of reduction by $NaBH_4$ and the electron-reservoir complex [$Fe^{I}Cp(\eta^5\text{-}C_6Me_6)$]. The relatively strong electron-withdrawing nature of trz shifts the redox potentials of the metallocenes anodically. The reduction potential of the trz group itself in the trz-containing compounds was not localized until –2.5 V in THF.

Additionally, trz* tetrafluoroborate derivatives, including those attached to the metallocenes, have been synthesized. The cationic charge of the trz* renders it even more electron-withdrawing than the trz group, which is reflected in the cyclic voltammetry data. The reduction potential of the trz* group is reported here, but the trz* cathodic reduction is totally chemically irreversible, even at –50 °C. In 1-benzyl-3-methyl-4-cobalticinium hexafluorophosphate-1*H*-triazolium (**2**) the addition of the third electron (reduction of trz* group) is hifted cathodically, i.e. reduction is rendered much more difficult (E_p = –2.20 V), because of the negative charge of cobaltocene than in compounds **4** and **6** for which the reduction of the trz* group attached to a neutral ferrocenyl or phenyl takes place around E_p = –1.60 V.

In conclusion, this study has afforded useful information concerning the electronic properties of trz and trz* groups and their effect on the redox potentials of late transition-metal metallocenes. The stability of reduction products synthesized using specific reductants is of the utmost importance if similar procedures are envisaged for large nanosystems such as metallodendrimers and nanoparticles.[47] The satisfying results show that such further steps can be undertaken in the future.

Experimental Section

General: Reagent-grade diethyl ether and tetrahydrofuran (THF) were predried with Na foil and distilled from sodium/benzophenone under argon immediately prior to use. Dichloromethane was distilled from calcium hydride just before use. All other solvents and chemicals were used as received. Ethynylferrocene, styrene, benzyl azide, and Me_3OBF_4 were purchased from Aldrich. ^1H NMR spectra were recorded at 25 °C with a Bruker AC 300 MHz spectrometer. The ^{13}C NMR spectra were obtained in the pulsed FT mode at 75.0 MHz with a Bruker AC 300 spectrometer. The NMR spectra were recorded in d^6 acetone unless noted otherwise. All chemical shifts are reported in parts per million (δ, ppm) with reference to Me_4Si (TMS). The mass spectra were recorded at the CESAMO (Univ. Bordeaux) with a QStar Elite mass spectrometer (Applied Biosystems). The instrument is equipped with an ESI source, and spectra were recorded in the positive mode. The electro-

spray needle was maintained at 5000 V and operated at room temp. Samples were introduced by injection through a 20 μL sample loop into a 4500 μL min^{-1} flow of methanol from the LC pump. Mass spectra of **8** were performed by the CESAMO with an AccuTOF-GcV (JEOL), which is a GC-TOF. The instrument is equipped with a sample introduction system named FD (Field Desorption). The EPR spectrum was recorded with a Bruker EMX X-band spectrometer (microwave frequency 9.46 GHz). Parameters: microwave power: 50 mW; modulation frequency (magnetic field): 100 kHz; modulation amplitude: 8 Gauss; magnetic field sweep width (Gauss): [0; 7000]; T = 4 K. All electrochemical measurements were recorded under nitrogen in dry CH_3CN, THF, or CH_2CH_2 at 20 °C. Supporting electrolyte: [nBu$_4$N][PF_6] (0.1 M); working and counter electrodes: Pt; reference electrode: Ag; internal reference: $FeCp^*_2$; scan rate: 0.200 V s^{-1}.

Click Synthesis of 1: A mixture of 1 equiv. of benzyl azide (70 mg, 0.53 mmol) and 1 equiv. of ethynyl cobalticinium hexafluorophosphate[52] (189.79 mg, 0.53 mmol) were dissolved in 3:2 distilled THF/H_2O. At 0 °C, $CuSO_4$ was added (1 equiv.; 1 M aqueous solution), followed by dropwise addition of a freshly prepared solution of sodium ascorbate (2 equiv.; 1 M aqueous solution). The solution was allowed to stir for 12 h at room temp. under N_2. An aqueous solution of ammonia was added, and the mixture was allowed to stir for 10 min. The organic phase was washed twice with water, dried with sodium sulfate, filtered through paper, and the solvent was removed under vacuum. Complex **1** was purified by precipitation with diethyl ether, and obtained as an orange-red powder; yield 80%. ^{1}H NMR (1D, 1 H): δ = 8.55 (1 H, C*H* of trz), 7.39 (5 H, C*H* of Ar), 6.38 (2 H, C*H* of Cp sub.), 5.97 (2 H, C*H* of Cp sub.), 5.70 (7 H, C*H* of Cp and Ar-CH_2) ppm. ^{13}C NMR (1D 1 H): δ = 138.28 (*Cq* of trz), 135.5 (*Cq* of Ar), 128.98, 128.52, 128.21 (*C*H of Ar), 124.52 (*C*H of trz), 96.04 (*Cq* of Cp sub.), 85.96 (*C*H of Cp), 84.53, 80.92 (*C*H of Cp sub.), 53.82 (Ar-*C*H_2) ppm. MS (*m*/*z*): calcd. for $C_{19}H_{17}N_3Co$ 346.0748; found 346.0746.

Click Synthesis of 7: The compound **7** was synthesized according to the same procedure as for **1** above by the click synthesis between (azidomethyl)ferrocene[53] (80 mg, 0.33 mmol) and ethynylcobalticinium hexafluorophosphate[52] (118.84 mg, 0.33 mmol) and obtained as orange-red needles after precipitation in ether; yield 84%. ^{1}H NMR (1D 1 H): δ = 8.48 (1 H, C*H* of trz), 6.39 (2 H, C*H* of Cp sub. of $CoCp_2^+PF_6^-$), 5.98 (2 H, C*H* of Cp sub. of $CoCp_2^+PF_6^-$), 5.71 (5 H, C*H* of Cp of $CoCp_2^+PF_6^-$), 5.46 (2H of trz-CH_2), 4.42 (2 H, C*H* of Cp sub. of $FeCp_2$), 4.23 (2 H, C*H* of Cp sub. of $FeCp_2$), 4.22 (5 H, C*H* of Cp of $FeCp_2$) ppm. ^{13}C NMR (1D 1 H): δ = 138.75 (*Cq* of trz), 124.81 (*C*H of trz), 97.30 (*Cq* of Cp sub. of $CoCp_2^+PF_6^-$), 86.85 (*C*H of Cp of $CoCp_2^+PF_6^-$), 85.39, 81.85 (*C*H of Cp sub. of $CoCp_2^+PF_6^-$), 82.65 (*Cq* of Cp sub. of $FeCp_2$), 69.98 (*C*H of Cp sub. of $FeCp_2$), 69.80 (*C*H of Cp of $FeCp_2$), 50.89 (trz-*C*H_2) ppm. MS (*m*/*z*): calcd. for $C_{23}H_{21}FeCoN_3$ 454.0429; found 454.0413. $C_{23}H_{21}CoF_6FeN_3P$ (599.18): calcd. C 46.10, H 3.53; found C 45.92, H 3.46.

Synthesis of 2: A mixture of 1 equiv. of **1** (120 mg, 0.24 mmol) with 1 equiv. of Me_3OBF_4 (36.14 mg, 0.24 mmol) in distilled dichloromethane (30 mL) was stirred for 3 d at room temp. under N_2. Then, the organic phase was washed twice with water, dried with sodium sulfate, and the solvent was evaporated under vacuum. Compound **2** was purified upon washing with THF; yield 90%. ^{1}H NMR (1D, 1 H): δ = 9.47 (1 H, CH of trz*), 7.62, 7.46 (5 H, CH of Ar), 6.61 (2 H, CH of Cp sub.), 6.21 (2 H, CH of Cp sub.), 6.03 (5 H, CH of Cp), 5.96 (2 H, CH of Ar-CH_2), 4.53 (3 H, CH of N-CH_3) ppm. ^{13}C NMR (1D, 1 H): δ = 136.15 (Cq of trz*), 132.25 (Cq of Ar), 131.32 (CH of trz*), 129.58, 129.46, 129.22 (CH of Ar), 87.37 (CH of Cp), 86.51, 84.96 (CH of Cp sub.), 85.63 (Cq of Cp sub.), 57.36 (Ar-CH_2), 39.64 (N-CH_3) ppm. MS (*m*/*z*): calcd. for $C_{20}H_{19}N_3Co$ 360.0905; found 360. $C_{20}H_{19}BCoF_{10}N_3P{\cdot}Et_2O$ (426.01): calcd. C 43.19, H 4.71; found C 43.39, H 4.11.

Synthesis of 4: The compound **4** was synthesized from 1 equiv. of **3** (120 mg, 0.35 mmol) and 1 equiv. of Me_3OBF_4 (51.72 mg, 0.35 mmol) according to the same procedure as for **2**. It was purified by precipitation in ether; yield 93%. ^{1}H NMR (1D 1 H): δ = 8.65 (1 H, CH of trz*), 7.52, 7.40 (5 H, CH of Ar), 5.67 (2 H, CH of Ar-CH_2), 4.72 (2 H, CH of Cp sub.), 4.47 (2 H, CH of Cp sub.), 4.22 (5 H, CH of Cp), 4.20 (3 H, CH of N-CH_3) ppm. ^{13}C NMR (1D 1 H): δ = 145.04 (Cq of trz*), 133.64 (Cq of Ar), 130.29, 130.12, 130.01 (CH of Ar), 128.38 (CH of trz*), 72.08 (CH of Cp sub.), 71.16 (CH of Cp), 69.96 (CH of Cp sub.), 66.98 (Cq of Cp sub.), 57.63 (Ar-CH_2), 39.73 (N-CH_3) ppm. MS (*m*/*z*): calcd. for $C_{20}H_{20}N_3Fe$ 358.1001; found 358.1000. $C_{20}H_{20}BF_4FeN_3$ (445.05): calcd. C 53.98, H 4.53; found C 53.63, H 4.44.

Synthesis of 6: The compound **6** was synthesized from 1 equiv. of **5** (120 mg, 0.51 mmol) and 1 equiv. of Me_3OBF_4 (75.49 mg, 0.51 mmol) according to the same procedure as for **2**. It was purified by precipitation in ether; yield 91%. ^{1}H NMR (1D, 1 H) $CDCl_3$: δ_{ppm} = 9.01 (1 H, CH of trz*), 7.79 (2 H, CH of Ph), 7.66 (5 H, 2 CH of Ar and 3 CH of Ph), 7.46 (2 H, CH of Ar), 5.98 (2 H, CH of Ar-CH_2), 4.41 (3 H, CH of N-CH_3) ppm. ^{13}C NMR (1D, 1 H): δ = 144.42 (Cq of trz*), 133.54 (Cq of Ar), 132.51, 130.10 (CH of Ph), 130.47, 130.36, 130.29 (CH of Ar), 129.59 (CH of trz*), 123.75 (Cq of Ph), 57.91 (Ar-CH_2), 39.47 (N-CH_3) ppm. MS (*m*/*z*): calcd. for $C_{16}H_{16}N_3$ 250.1338; found 250.1337. $C_{16}H_{16}BFN_3$ (280.13): calcd. C 57.00, H 4.78; found C 56.75, H 4.56.

Synthesis of 8: A mixture of 1 equiv. of **1** (150 mg, 0.31 mmol) with 1.1 equiv. of $NaBH_4$ (12.71 mg, 0.34 mmol) in distilled THF (20 mL) was stirred for 20 min at 0 °C under N_2. Then, the solvent was evaporated under vacuum, and distilled diethyl ether was added to solubilize the neutral product. After filtration under N_2 and evaporation of the solvent, the product was obtained as a deep red powder; yield 95%. The complex **8** is not air stable and stored under N_2. It is thermally stable under N_2 for a few hours, then degradation appears as indicated by the ^{1}H NMR spectrum and precipitation. ^{1}H NMR (1D, 1 H) $CDCl_3$: δ = 7.41–7.31 (5 H, CH of Ph), 7.13 and 6.66 (1H of trz), 5.51–5.34 (2H of Ph-CH_2 and 2H of diene), 4.88–4.52 (5H of free Cp and 4H of substituted Cp when H$^-$ is added to free Cp), 2.93–2.88 (2H of diene), 2.09–2.04 (2H free) ppm. ^{13}C NMR (1D, 1 H) C_6D_6: δ = 149.59 (*Cq* of triazole), 133.62 (*Cq* of Ar), 129.37, 129.19 (*C*H of Ar), 121.51 (*C*H of triazole), 80.755–80.60 (*C*H of Cp), 78.84–75.16 (*C*H of cyclopentadiene), 55.14 (Ar-*C*H_2), 43.17–39.72 (*C*H_2 of cyclopentadiene) ppm. MS (*m*/*z*): calcd. for $C_{19}H_{18}CoN_3$ 347.08327; found 347.08422.

Synthesis of 9: A solution of **1** (1 equiv., 120 mg, 0.24 mmol) in distilled THF (20 mL) was prepared in a Schlenk flask. Then addition under N_2 of a solution of a stoichiometric amount of the forest-green complex [$Fe^{I}Cp(\eta^5$-$C_6Me_6)$][59] (1 equiv., 0.24 mmol, 67.97 mg) in distilled THF was performed by canula. A color change from orange to brown and a yellow precipitate of [$Fe^{II}Cp(\eta^5$-$C_6Me_6)$][PF_6] appeared immediately. After evaporation of the solvent under vacuum, the neutral brown product **9** was solubilized in distilled diethyl ether and filtered to obtain **9** as a brown powder; yield 97%. The paramagnetic complex **9** is not air stable and was stored under N_2. Oxidation of the product in air yielded **1** after addition of $NaPF_6$. ^{1}H NMR (1D 1 H), ([D_6]acetone, 300 MHz), after oxidation of **9** in air: δ = 8.57 (1 H, C*H* of triazole), 7.41 (5 H, C*H* of Ar), 6.41 (2 H, C*H* of substituted Cp),

6.01 (2 H, C*H* of substituted Cp), 5.74 (5 H, C*H* of Cp), 5.72 (2H of Ar-CH_2) ppm. MS (*m*/*z*): calcd. for $C_{19}H_{17}CoN_3$ 346.0748; found 347.0765.

Supporting Information (see footnote on the first page of this article): General data, ^1H, ^{13}C NMR (including HMBC spectrum of **8**), IR, UV/Vis and mass spectra and cyclic voltammograms.

Acknowledgments

Financial support from the Université Bordeaux, the Centre National de la Recherche Scientifique (CNRS) and the Agence Nationale de la Recherche (ANR) is gratefully acknowledged.

[1] H. C. Kolb, M. G. Finn, K. B. Sharpless, *Angew. Chem.* **2001**, *113*, 2056; *Angew. Chem. Int. Ed.* **2001**, *40*, 2004–2021.
[2] V. V. Rostovtsev, L. G. Green, V. V. Fokin, K. B. Sharpless, *Angew. Chem.* **2002**, *114*, 2708; *Angew. Chem. Int. Ed.* **2002**, *41*, 2596–2599.
[3] C. W. Tornøe, C. Christensen, M. Meldal, *J. Org. Chem.* **2002**, *67*, 3057–3064.
[4] V. D. Bock, H. Hiemstra, J. H. van Maarseveen, *Eur. J. Org. Chem.* **2006**, 51–68.
[5] D. Fournier, R. Hoogenboom, U. S. Schubert, *Chem. Soc. Rev.* **2007**, *36*, 1369–1380.
[6] M. V. Gil, M. J. Arévalo, Ó. López, *Synthesis* **2007**, *11*, 1589–1620.
[7] W. H. Binder, R. Sachsenhofer, *Macromol. Rapid Commun.* **2007**, *28*, 15–54.
[8] M. Meldal, C. W. Tornøe, *Chem. Rev.* **2008**, *108*, 2952–3015.
[9] G. Franc, A. Kakkar, *Chem. Commun.* **2008**, 5267–5276.
[10] J. F. Lutz, Z. Zarafshani, *Adv. Drug Delivery Rev.* **2008**, *60*, 958–970.
[11] J. F. Lutz, H. G. Borner, *Prog. Polym. Sci.* **2008**, *33*, 1–39.
[12] B. Droumaguet, K. Velonia, *Macromol. Rapid Commun.* **2008**, *29*, 1073–1089.
[13] W. H. Binder, R. Zirbs, *Click chemistry in Macromolecular Synthesis*, *Encyclopedia of Polymer Science and Technology*, John Wiley & Sons, New York, **2009**.
[14] H. R. Marsden, A. Kros, *Macromol. Biosci.* **2009**, *9*, 939–951.
[15] P. L. Golas, K. Matyjaszewski, *Chem. Soc. Rev.* **2010**, *39*, 1338–1354.
[16] J. E. Hein, V. V. Fokin, *Chem. Soc. Rev.* **2010**, *39*, 1302–1315.
[17] B. S. Sumerlin, A. P. Vogt, *Macromolecules* **2010**, *43*, 1–13.
[18] H. Struthers, T. L. Mindt, R. Schibli, *Dalton Trans.* **2010**, *39*, 675–696.
[19] U. Mansfeld, C. Pietsch, R. Hoogenboom, C. R. Becer, U. S. Schubert, *Polym. Chem.* **2010**, *1*, 1560–1598.
[20] D. Best, *Biochemistry* **2009**, *48*, 6571–6584.
[21] D. G. Mullen, D. Q. McNerny, A. Desai, X. Cheng, S. C. DiMaggio, A. Kotlyar, Y. Zhong, S. Qin, C. V. Kelly, T. P. Thomas, I. Majoros, B. G. Orr, J. R. Baker, M. M. B. Holl, *Bioconjugate Chem.* **2011**, *22*, 679–689.
[22] L. Liang, D. Astruc, *Coord. Chem. Rev.* **2011**, *255*, 2933–2945.
[23] B. Happ, C. Friebe, A. Winter, M. Hager, R. Hoogenboom, U. S. Schubert, *Chem. Asian J.* **2009**, *4*, 154–163.
[24] Y. Li, A. H. Flood, *Angew. Chem.* **2008**, *120*, 2689; *Angew. Chem. Int. Ed.* **2008**, *47*, 2649–2652.
[25] A. Boulay, A. Seridi, C. Zedde, S. Ladeira, C. Picard, L. Maron, E. Benoist, *Eur. J. Inorg. Chem.* **2010**, 5058–5062.
[26] M. Felici, P. Contreras-Carballada, J. M. M. Smits, R. J. M. Nolte, R. M. Williams, L. De Cola, M. C. Feiters, *Molecules* **2010**, *15*, 2039–2059.
[27] A. Kumar, P. S. Pandey, *Org. Lett.* **2008**, *10*, 165–168.
[28] K. M. Mullen, J. Mercurio, C. J. Serpell, P. D. Beer, *Angew. Chem.* **2009**, *121*, 4875; *Angew. Chem. Int. Ed.* **2009**, *48*, 4781–4784.
[29] B. Schulze, C. Friebe, M. D. Hager, W. Gunther, U. Kohn, B. O. Jahn, H. Gorls, U. S. Schubert, *Org. Lett.* **2010**, *12*, 2710–2713.
[30] C. Ornelas, J. Ruiz, L. Salmon, D. Astruc, *Adv. Synth. Catal.* **2008**, *350*, 837–845.
[31] D. Astruc, L. Liang, A. Rapakousiou, J. Ruiz, *Acc. Chem. Res.* **2012**, *45*, 630–640.
[32] N. G. Connelly, W. E. Geiger, *Adv. Organomet. Chem.* **1984**, *23*, 1–93.
[33] W. E. Geiger, N. G. Connelly, *Adv. Organomet. Chem.* **1985**, *24*, 87–130.
[34] W. E. Geiger, *J. Organomet. Chem. Libr.* **1990**, *23*, 142–172.
[35] N. Connelly, W. E. Geiger, *Chem. Rev.* **1996**, *96*, 877–910.
[36] W. E. Geiger, *Organometallics* **2007**, *26*, 5738–5765: a historial and perspective article.
[37] *Electron Transfer in Chemistry*, vol. 1–4 (Ed.: V. Balzani), Wiley-VCH, Weinheim, Germany, **2001**.
[38] C. M. Casado, I. Cuadrado, M. Moran, B. Alonso, B. Garcia, B. Gonzales, J. Losada, *Coord. Chem. Rev.* **1999**, *185–6*, 53–79.
[39] M. Lacoste, F. Varret, L. Toupet, D. Astruc, *J. Am. Chem. Soc.* **1987**, *109*, 6504–6506.
[40] M. H. Desbois, D. Astruc, J. Guillin, F. Varret, *J. Am. Chem. Soc.* **1989**, *111*, 5800–5809.
[41] J. Ruiz, F. Ogliaro, J.-Y. Saillard, J.-F. Halet, F. Varret, D. Astruc, *J. Am. Chem. Soc.* **1998**, *120*, 11693–11705.
[42] D. Astruc, *Electron Transfer and Radical Processes in Transition Metal Chemistry*, John Wiley & Sons, New York, **1995**, chapter 7.
[43] P. D. Beer, P. A. Gale, *Angew. Chem.* **2001**, *113*, 502; *Angew. Chem. Int. Ed.* **2001**, *40*, 486–416.
[44] O. Reynes, J.-C. Moutet, J. Pecaut, G. Royal, E. Saint-Aman, *New J. Chem.* **2002**, *26*, 9–12.
[45] M. P. G. Armada, J. Losada, M. Zamora, B. Alonso, I. Cuadrado, C. M. Casado, *Bioelectrochemistry* **2006**, *69*, 65–73.
[46] F. J. Martinez, B. Gonzales, B. Alonso, J. Losada, M. P. Garcia-Armada, C. Casado, *J. Inorg. Organomet. Polym. Mater.* **2008**, *18*, 51–58.
[47] D. Astruc, *Nat. Chem.* **2012**, *4*, 255–267.
[48] G. Wilkinson, M. Rosenblum, M. C. Whittig, R. B. Woodward, *J. Am. Chem. Soc.* **1952**, *74*, 2125–2126.
[49] G. Wilkinson, P. L. Pauson, F. A. Cotton, *J. Am. Chem. Soc.* **1954**, *76*, 1970–1974.
[50] J. A. Page, G. Wilkinson, *J. Am. Chem. Soc.* **1952**, *74*, 6149–6150.
[51] J. G. Rodriguez, A. Oñate, R. M. Martin-Villamir, I. Fonseca, *J. Organomet. Chem.* **1996**, *513*, 71–76.
[52] M. Wilschek, C. Rieker, P. Jaitner, H. Schottenberger, K. E. Schwarzhans, *J. Organomet. Chem.* **1990**, *396*, 355–361; R. Huisgen, *Angew. Chem.* **1963**, *75*, 604; *Angew. Chem. Int. Ed. Engl.* **1963**, *2*, 565–598.
[53] J. M. Casas-Slovas, A. Vargas-Berenguel, L. F. Capitan-Vallvey, F. Santoyo-Gonzalez, *Org. Lett.* **2004**, *6*, 3687–3690.
[54] W. E. Geiger, *J. Am. Chem. Soc.* **1974**, *96*, 2632–2634.
[55] J. K. Kochi, *J. Organomet. Chem.* **1986**, *300*, 139–166.
[56] D. Astruc, *Organometallic Chemistry and Catalysis*, Springer, Heidelberg, **2008**, chapter 5.
[57] M. L. H. Green, L. Pratt, G. Wilkinson, *J. Chem. Soc.* **1959**, 3753–3767.
[58] J. R. Hamon, D. Astruc, P. Michaud, *J. Am. Chem. Soc.* **1981**, *103*, 758–766.
[59] C. Moinet, E. Román, D. Astruc, *J. Electroanal. Interfac. Chem.* **1981**, *121*, 241–246.
[60] J. C. Green, M. R. Kelly, M. P. Payne, E. A. Seddon, D. Astruc, J.-R. Hamon, P. Michaud, *Organometallics* **1983**, *2*, 211–218.
[61] J. Ruiz, D. Astruc, *C. R. Acad. Sci. Paris Ser. IIc* **1998**, 21–27.
[62] D. S. Shephard, B. F. G. Johnson, A. Harrison, S. Parsons, S. P. Smidt, L. J. Yellowlees, D. Reed, *J. Organomet. Chem.* **1998**, *563*, 113–136.

Received: July 6, 2012
Published Online: September 11, 2012

Dendritic Organocobalt(I) Hydride Reservoirs as Reductants. Formation of Robust Capsules Containing Pd, Ag or Au Nanoparticles.

Abstract. Three generations of Dendritic Hydride reservoirs (DHR)s are designed based on yellow cobalticenium termini (empty DHRs) and their stable deep-red hydride reduction form (filled DHRs). The filled DHRs reduce various transition metal cations to robust capsules containing transition-metal nanoparticles (NPs). The efficiency of the DHRs is compared to that of Dendritic Electron Reservoirs (DERs) based on ferrocene termini that do not disclose the same properties.

Redox processes are central in Nature and human activities. In biology, key redox processes occur by transfer of electrons such as in cytochromes and iron-sulfur proteins, hydrogen atoms such as in flavin adenine dinucleotide ($FADH_2$ → FAD with $2e^- + 2H^+$) or hydrides such as in nicotimamide adenine dinucleotide (NADH → NAD^+ with $2e^- + H^+$)[1]. Likewise laboratory and industrial redox processes involve single–electron reductants such as alkali metals[2], hydrogen atom transfer agents such as tin hydrides and curcumin[3] and hydride transfer reagents such as borohydrides and aluminohydrides[4]. Multiple-electron transfer is often necessary in redox-catalyzed reactions involved in fuel cells and solar energy storage[5, 6], and electron-reservoir materials are also known as redox catalysts and electrocatalysts[7]. For instance Pt and Au nanoparticles are multi-electron redox catalysts for the reduction side of water photo-splitting to dihydrogen[8, 9, 10]. Hydride transfer processes are presently of general interest in various areas of chemical and technogogical processes including those involving nanoscience[11, 12, 13, 14, 15, 16, 17].
Here we introduce dendritic organocobalt hydride reservoirs including their capacity to selectively reduce Pd^{II}, Ag^{I} and Au^{III} to very robust capsules containing small nanoparticles and compare them with ferrocenyl dendritic electron reservoirs (DERs)[18].

Dendritic hydride reservoirs (DHRs) were synthesized in their empty reservoir form by Cu(I)-catalyzed azide alkyne cycloaddition (CuAAC, "click")[19, 20] between arene-core dendrimers with 1→ 3 connectivity[21] terminated by 9, 27 and 81 azido termini (respectively generations 0, 1 and 2, G_0-G_2) and ethynylcobalticenium hexafluorophosphate leading to yellow 1,2,3-triazolyl-cobalticenium-terminated G_0-G_2 metallodendrimers[22] **1(PF_6^-)**, **2(PF_6^-)** and **3(PF_6^-)** that are soluble as hexafluorophosphates in the polar solvents acetone, acetonitrile and nitromethane (Fig 1). These three generations G_0-G_2, **4**, **5** and **6** of empty DHRs are reduced by $NaBH_4$ in THF to neutral deep-red filled DHRs of 9, 27 and 81 hydrides respectively that are soluble in low-polarity solvents such as THF, dichloromethane and chloroform[23]. These filled DHRs are terminated by 18-electron d^8 [Co(I) Cp(η^4-cyclopentadiene)] groups (Cp = η^5-C_5H_5)[24, 25] that return to the 18-electron d^6 cobalticenium state subsequent to hydride transfer (Figure 2). Both families of deep-red d^8 Co(I) and yellow d^6 Co(III) metallodendrimers are thermally stable, which is indispensible for the reservoir function. These dendrimers were characterized by ^1H, ^{13}C NMR, HSQC 2D NMR, UV-vis., IR and mass spectroscopies.

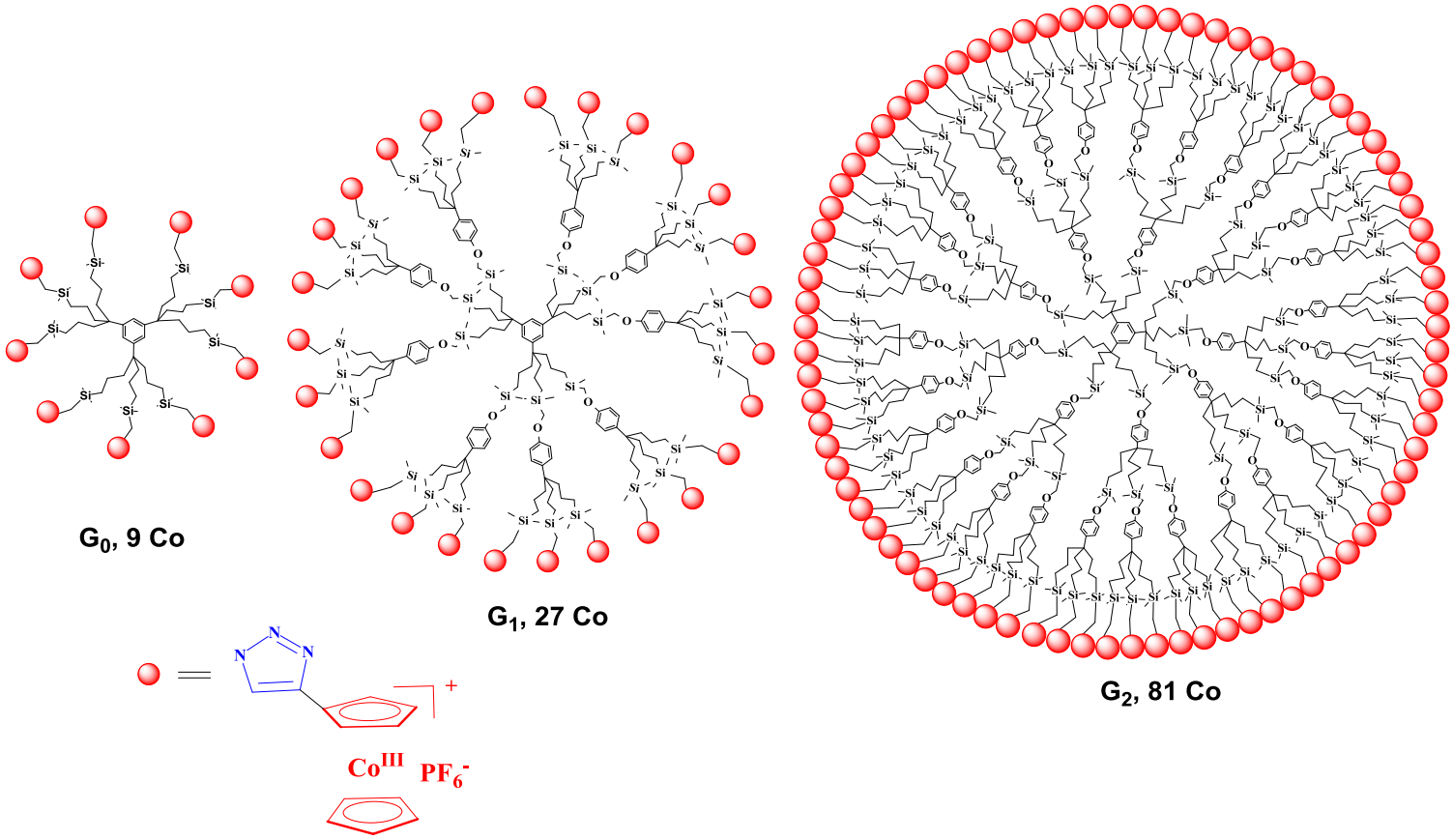

Figure 1. 1,2,3-triazolyl-cobalticenium-terminated dendrimers **1(PF$_6^-$)**, **2(PF$_6^-$)** and **3(PF$_6^-$)**.

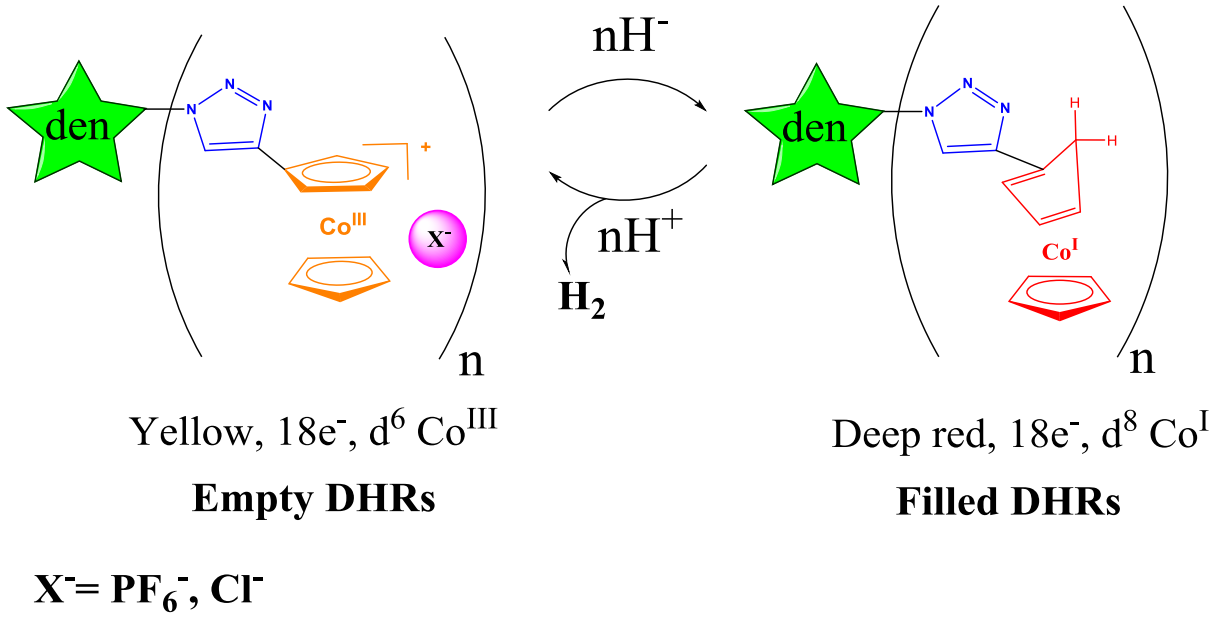

Figure 2. Schematic hydride addition/abstraction reversibility between empty DHRs **1(PF$_6^-$)** (G_0), **2(PF$_6^-$)** (G_1) and **3(PF$_6^-$)** (G_2) and filled DHRs **4** (G_0), **5** (G_1) and **6** (G_2). Addition of HCl to filled DHRs **4**, **5** and **6** also leads to empty DHRs **1(Cl$^-$)**, **2(Cl$^-$)** and **3(Cl$^-$)** respectively**.**

AFM studies of the neutral filled DHRs dendrimers **4**, **5** and **6** allowed the comparison between the three generations G_0-G_2 and with the polycationic empty DHRs **1(PF_6^-)**, **2(PF_6^-)** and **3 (PF_6^-)** (Figure 3).

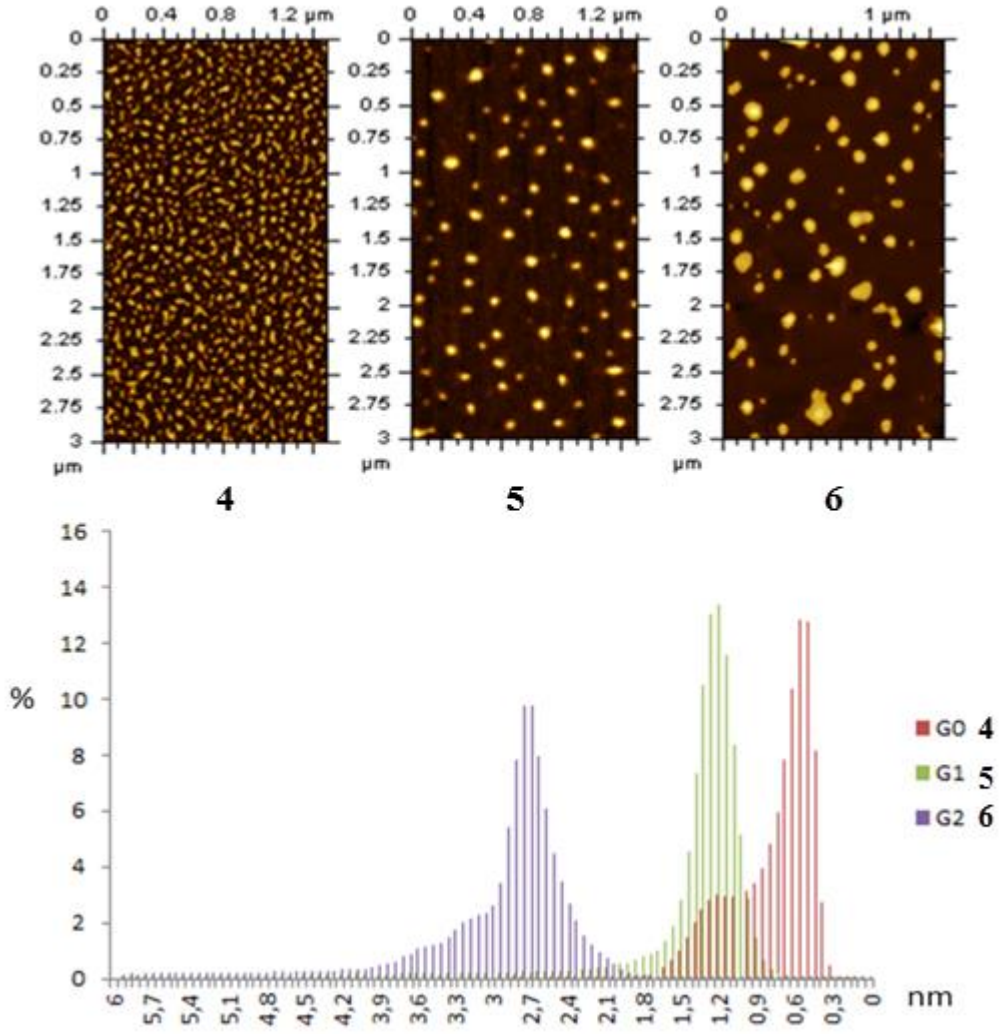

Figure 3. AFM topology images of dendrimers **4**, **5** and **6** and their comparative statistical height distributions.

Evolution of the height with the dendrimer generation is clearly observed, and the height on the mica surface of the neutral dendrimers **4**, **5** or **6** is smaller by 0.3 nm compared to those of the polycationic dendrimers **1(PF_6^-)**, **2(PF_6^-)** and **3 (PF_6^-)** respectively. This was expected due to the electrostatic interactions of the polycationic dendrimers that increases the DHR sizes, i.e. the DHRs "breathe" between their filled and empty forms. The AFM shows that a second layer of the smaller dendrimer **4** is also formed, a tendency that is also noted for the higher generations to a lesser extent.

The d^6 Co(III) metallodendrimers can be isolated with various counter anions X^- upon reaction of the d^8 Co(I) form with acids HX. For instance upon reactions with aqueous HCl, the water-soluble d^6 Co(III) dendrimers **1(Cl^-)**, **2(Cl^-)** and **3 (Cl^-)**, i.e. the empty DHRs, are obtained as chloride salts. H_2, characterized by ^{1}H NMR, is also formed in these reactions as a result of the

protonation of the hydride of the filled DHRs, presumably upon Co(I) protonation followed by diene endo C-H oxidative addition and reductive H_2 elimination (Figure 2).

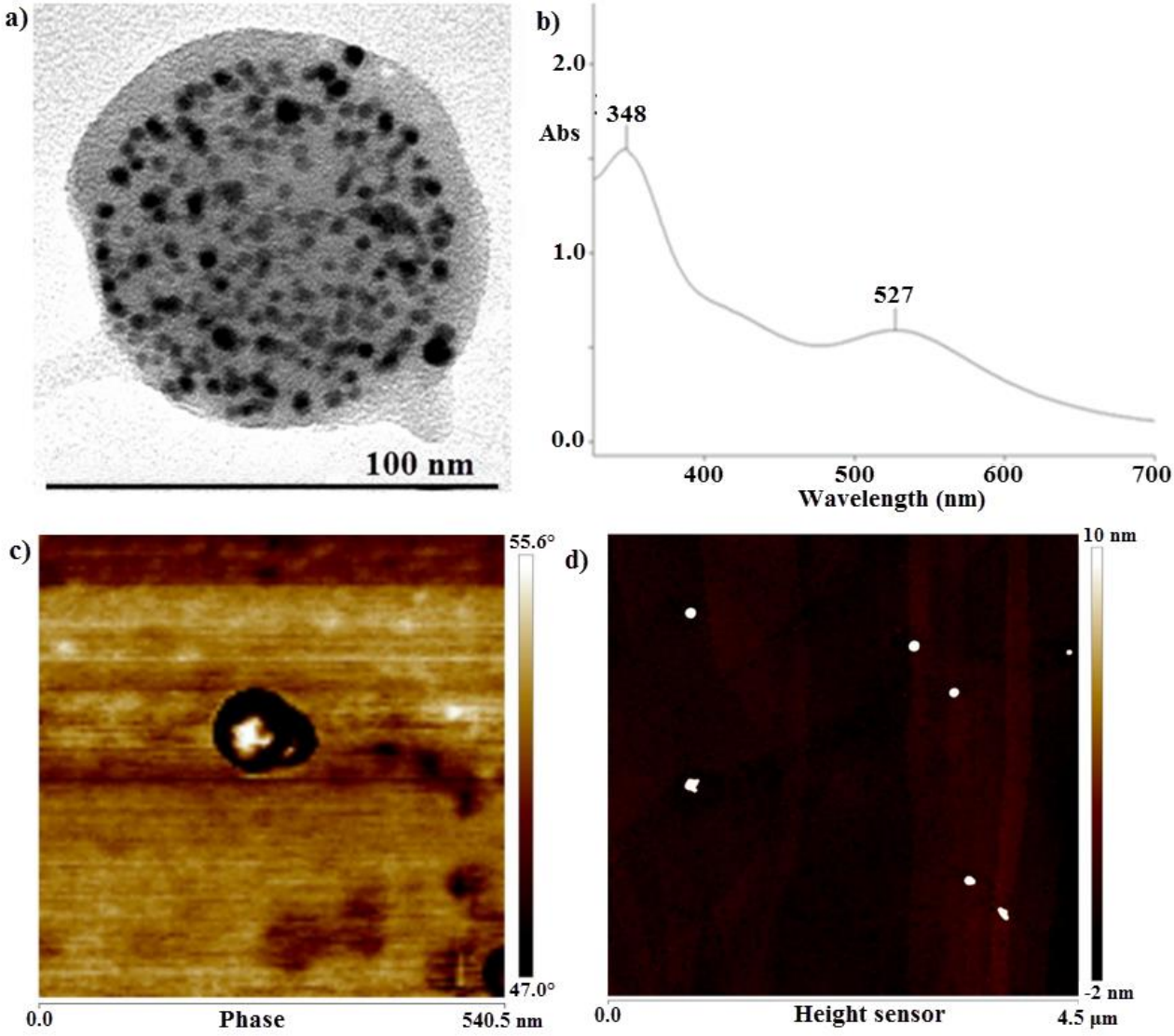

Figure 4. a) TEM image of a capsule with **AuNPs-8**, b) UV-vis. spectrum of **AuNPS-8**, c) AFM phase image of a capsule with **AuNPs-8**, d) AFM topology image (height sensor) of **AuNPs-8**.

The multiple hydride transfer to substrates using DHRs is specifically engineered to reduce within a confined space a number of transition-metal cations to atoms that coalesce to dendrimer-stabilized metal nanoparticles (NPs)[26]. The presence of intradendritic triazole ligands generated by CuAAC reaction during the dendrimer construction[27] is necessary to attract the metal cations in the dendrimer interior by coordination of the triazole ligands before reduction[28]. The metal NPs are also stabilized by the triazole ligands, although less strongly than the metal cations. These NPs have the possibility to remain encapsulated inside the dendrimer if it is large enough or to coalesce with other NPs to be sterically stabilized outside the dendrimer if the dendrimer is too small. The NPs are not only stabilized as usual by a combination of steric and ligand interactions[29, 30, 31], but here the polycationic nature of the empty DHRs also provides

electrostatic stabilization of the NPs. These DHR properties are illustrated with Pd(II), Ag(I) and Au(III) reduction to metal NPs.
Reduction of Au(III) to Au(0) was conducted with the DHRs **4** and **5** in THF using either a THF/water (1/3) solution of $HAuCl_4$ yielding **AuNPs-7** and **AuNPs-8** or a THF solution of $AuCl_3$ yielding **AuNPs-9** according to equations 3 and 4 stoichiometrically considering that each hydride carries two electrons.

$$\text{Den-(Trz-Co}^{I}\text{H)}_n + 2n/3\ HAuCl_4 \rightarrow \text{Den-(Trz-Co}^{III}\text{Cl)}_n,\ 2n/3Au^0 + 5n/3\ HCl\ (aq) \quad (3)$$

$$\text{Den-(Trz-Co}^{I}\text{H)}_n + 2n/3\ AuCl_3 \rightarrow \text{Den-(Trz-Co}^{III}\text{Cl)}_n,\ 2n/3Au^0 + n\ HCl\ (THF) \quad (4)$$

These stoichiometries were verified by the full consumption of both substrates in each case. With $HAuCl_4$ this shows the absence of hydride reduction of protons to H_2 (the solution pH remains acidic, and no H_2 formed). Au(III) reduction to Au(0) is faster than that of protons, which is justified by both thermodynamic (E^0 Au(III/0) > E^0 (H^+/H_2)) and kinetic reasons (structural transformation is more significant for H_2, *vide supra*) . In both cases, the wine-red DHR color instantaneously changed to pink-red upon addition of $HAuCl_4$ or violet in the case of $AuCl_3$. The absorption bands of the cobalticenium (Co^{III}) complexes appeared in the UV-vis. spectra as well as the AuNP plasmon band. The location of this plasmon band[19] was very different, however, depending on the Au(III) source: 530 ± 4 nm for **AuNPs-7** and **AuNPs-8** with $HAuCl_4$ and 571 nm for **AuNPs-9** with $AuCl_3$, characterizing an enormous AuNP size difference (Figures 4 and 5).

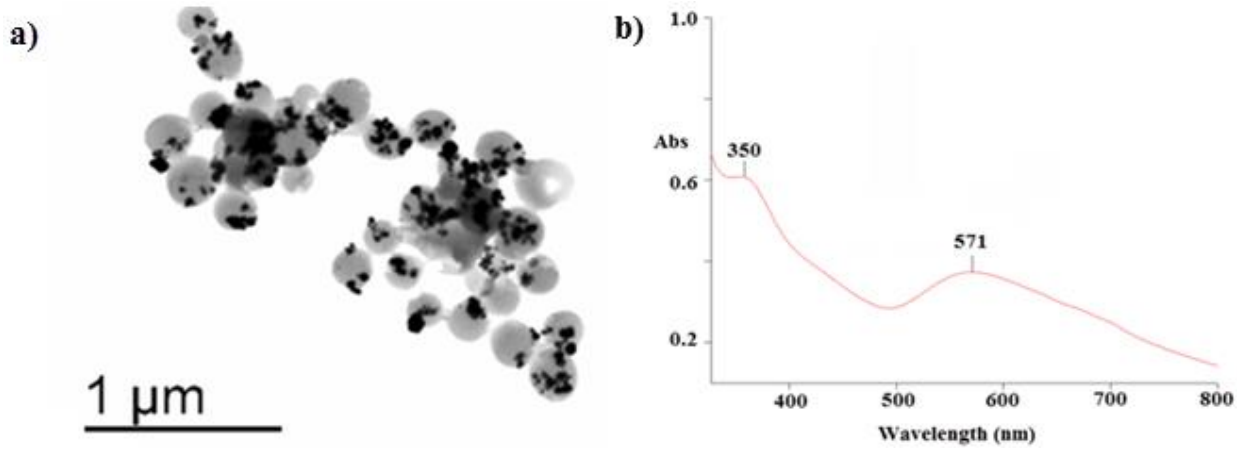

Figure 5. a) TEM image of capsules containing **AuNPs-9** and b) UV-vis. of **AuNPs-9**.

The TEM pictures of these AuNPs show a remarkable and unusual feature. The empty DHRs are assembled in packages forming spherical capsules of 85 ± 20 nm in the case of **AuNPs-8** that incorporate many monodisperse AuNPs of 3± 0.5 nm diameter (Figure 4). With $AuCl_3$, spherical DHR capsules are also formed with diameter around 220 ± 40 nm, but they contain only a few very large **AuNPs-9** of 33 ± 2 nm (Figure 5). The formation of such capsules is taken into account by the major electrostatic forces at the polycationic empty DHR peripheries where multiple ion pairing leads to large assemblies that contain several thousand positive charges and counter anions at the capsule peripheries. Under these conditions the ionic strength of the solvent plays a key role in blocking the NP expansion as observed with the very unusual large size of the **AuNPs-9** formed inside the capsules in the low-polarity THF solvent (Figure 6).
For comparison, a stoichiometric mixture of empty G_1 DHR chloride and $HAuCl_4$ was submitted to reduction by $NaBH_4$ in water and formed polydispersed **AuNPs-10** that were moderately

stabilized by empty G_1 DHR (they flocculate and are reversibly solubilized upon stirring) with an average of 5 nm together with aggregates, but decomposed to aggregates upon heating

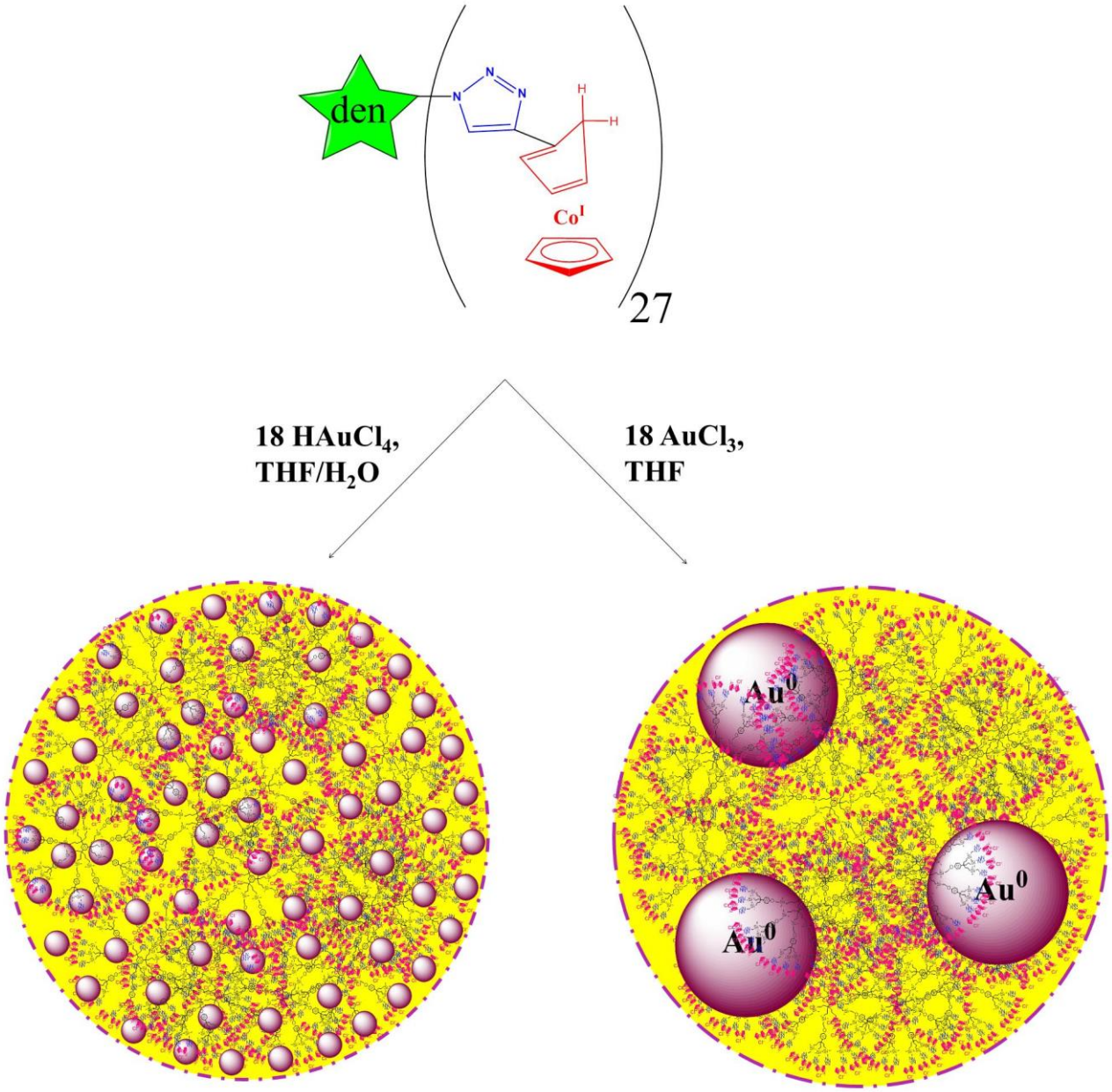

Figure 6. Reaction of DHR **5** with $HAuCl_4$ and $AuCl_3$ yielding capsules containing **AuNPs-8** and **AuNPs-9** respectively**.**

contrary to the capsules that are stable in boiling water and at r.t. in air for several months (Figure 7). The same mixture was also reduced by $NaBH_4$ in THF leading to color change from yellow to purple and subsequently to deep red as the empty DHR was reduced to filled DHR **(AuNPs-11)**.

The **AuNPs-11** formed showed a plasmon band at 519 nm and also flocculated, and TEM analysis showed that capsules were not formed, but these capsules were formed again upon addition of aqueous HPF_6, which confirms the relationship between the polycationic nature of the DHRs and the capsule formation (**AuNPs-12**) (Figure 7).

The principle of robust nanocapsule formation containing metal NPs was extended to Ag and Pd. Reaction of the filled G_1 DHR with $AgBF_4$ was conducted in THF/H_2O and provoked an instantaneous color change from colorless to orange without precipitation (Figure 8).

$$\text{Den-(Trz-Co}^{I}\text{H)}_n + 2n\ \text{Ag}^{I}\text{BF}_4 \rightarrow \text{Den-(Trz-Co}^{III}\ \text{BF}_4)_n,\ 2n\ \text{Ag}^0 + n\ \text{HBF}_4\ (\text{H}_2\text{O/THF}) \qquad (5)$$

The new solution (**AgNPs-13**) presented a plasmon band at 439 nm and was stable for more than a month. The TEM images also show the formation of 85±5 nm capsules containing 5±0.5 nm **AgNPs-13**, a situation analogous to that disclosed with **AuNPs-8**. With $Pd^{II}(OAc)_2$, however reaction of the G1 DHR instantaneously gave a black precipitate indicating agglomeration of instable PdNPs. To circumvent this problem, $Pd(OAc)_2$ was first coordinated with a trz ligand in THF, then reaction of the complex trz-$Pd(OAc)_2$ with the filled G1 DHR provoked a color change from yellow to brown without precipitation (Figure 8).

$$\text{Den-(Trz-Co}^{I}\text{H)}_n + n\ \text{Pd}^{II}\text{trz(OAc)}_2 \rightarrow \text{Den-(Trz-Pd}^{0}\text{trz,OAc)}_n,\ 2n\ \text{Ag}^0 + n\ \text{AcOH (THF)} \qquad (6)$$

This solution is stable, and the TEM picture also showed the formation of capsules of 94±5 nm containing **PdNPs-14** of 2.6±0.2 nm size.

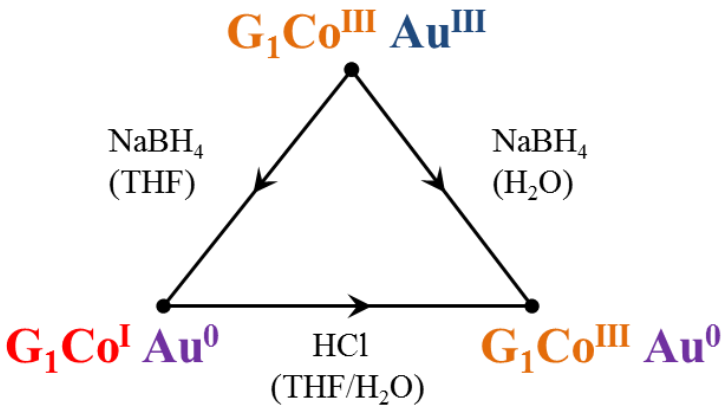

Figure 7. Reduction of $G_1Co^{III}Au^{III}$ by $NaBH_4$ leading to the selective reduction of either Co^{III} (**AuNPs-10**) or Au^{III} (**AuNPs-11**) and selective oxidation of $G_1Co^{I}Au^0$ (**AuNPs-11**) back to $G_1Co^{III}Au^0$ (**AuNPs-12**).

The capsules of **AuNPs-8** and **AgNPs-13** were analyzed by Atomic Force Microscopy (AFM) using tapping mode operation. The topology images of **AuNPs-8** (Figure 4d) revealed the horizontal diameter of the capsules to be 102 ± 25 nm and 80± 20 nm for **AgNPs-13**, data that are close to those of the TEM analysis. The capsules are observed separately or by packages of two or three together. Phase images were also recorded in both cases and qualitative mechanical information was obtained. In Figure 4c a phase image (zoom) at 540.5 nm is obtained showing capsules of **AuNPs-8**. The black-colored part surrounding the capsules indicates an elastic and

flexible material belonging to the dendritic part, whereas the white part in the middle is a stiffer and more rigid material belonging to the AuNPs.

One may compare the DHRs to filled dendritic electron reservoirs (DERs)[32] in which the 18-electron d^6 Fe^{II} ferrocenyl groups located at the dendrimer termini are the reductants. The empty DERs contain the 17-electron d^5 Fe^{III} termini (Figure 9). The new orange filled G_1 DER **15** with the same core frame as the G1 DHR and 27 trz-methylferrocene termini reacts with $HAuCl_4$ in chloroform/methanol to give the blue-purple empty DER that stabilizes **AuNPs-16**.

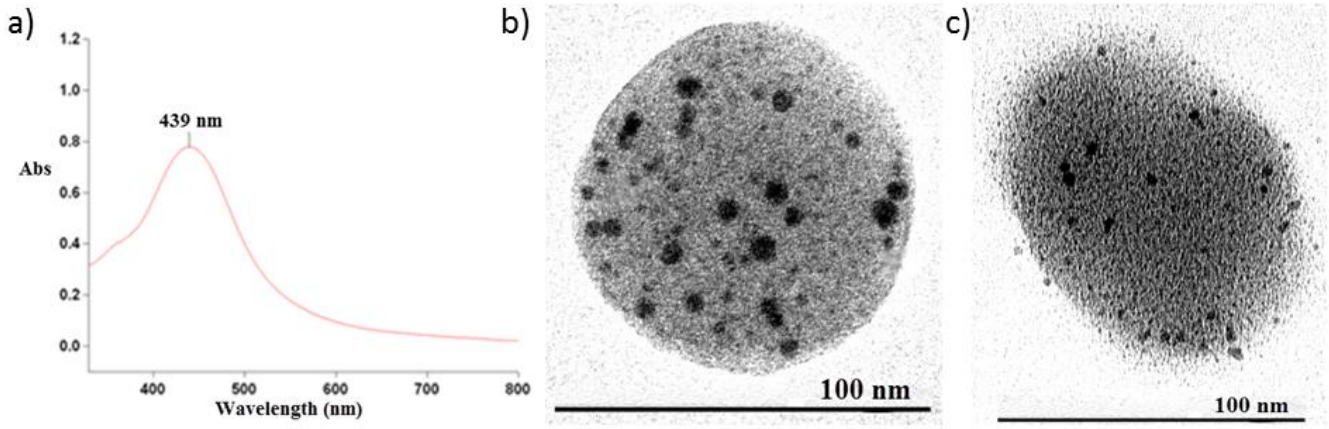

Figure 8. a) UV-vis. of **AgNPs-13**, b) TEM image of **AgNPs-13** and c) TEM image of **PdNPs-14**.

The reaction is very slow, proceeding over several hours at r.t. and giving **AuNPs-16** that are shown by TEM to be extremely large, around 260 nm with a AuNP plasmon band at 590 nm, which confirms the slow rate of the process. No capsule is formed, however (Figure 9). This shows the considerable difference of behavior and reaction rate between the DHR and DER with the same topology and comparable structure.

$$3\ \text{Den-}(\text{TrzCH}_2\text{Fe}^{\text{II}})_n + n\ \text{HAu}^{\text{III}}\text{Cl}_4 \rightarrow 3\ \ \text{Den-}(\text{TrzCH}_2\text{Fe}^{\text{III}},\text{Cl})_n,\ n\ \text{Au}^0 + n\ \text{HCl} \qquad (7)$$

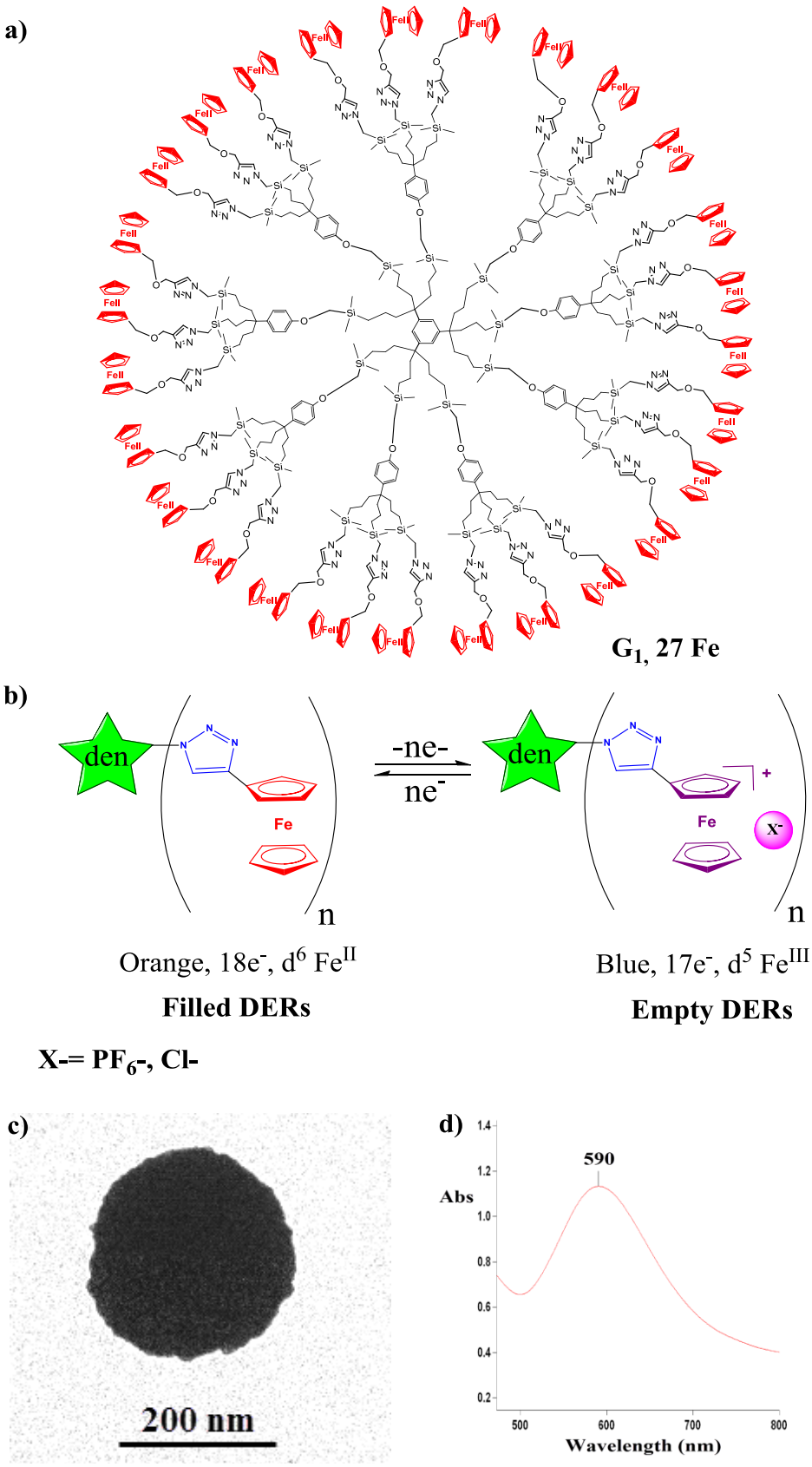

Figure 9. a) Structure of the DER **15**; b) schematic electron addition/abstraction reversibility between empty DERs and filled DERs; c) TEM image of **AuNPs-16** ; d) UV-vis. spectrum of **AuNPs-16**.

Methods

Example of reversible DHRs:
Hydride addition: The empty DHR **2(PF_6)** solid (50 mg, 0.003 mmol) reacted with $NaBH_4$ (4 mg, 0.09 mmol) in distilled THF (15 mL) for 20 min at 0°C under N_2. The color of the solution changed from colorless to deep red. Then, the solution was filtered under nitrogen. The solvent was evaporated *in vacuo*. The deep red solid was washed three times with 10 mL of distilled H_2O. The filled DHR **5** was obtained as a deep red powder in quantitative yield (35 mg). UV-vis.: λ_{max1} = 420 nm, λ_{max2} = 530 nm.
Hydride abstraction: The filled DHR **5** (33 mg, 0.003 mmol) was solubilized in 10 mL of THF. Then a 10 mL aqueous solution of HCl (0.01 M) was added dropwise, and the color gradually changed from deep red to light yellow giving back the empty DHR **2(Cl)** and molecular hydrogen. After stirring for 10 min. the mixture of solvents was evaporated. Product **2(Cl)** was obtained as a yellow waxy product in quantitative yield (36 mg). The empty DHR **2(Cl)** is now water-soluble. ^{1}H NMR (1D 1H), (D_2O, 400 MHz): δ_{ppm}: 8.28 (27H, C*H* of trz), 7.00, 6.66 (39H, C*H* of arom.core), 6.09 (54H, C*H* of Cp sub.), 5.72 (54H, C*H* of Cp sub.), 5.39 (135H, C*H* of Cp), 3.90 (54H, SiCH_2-trz), 3.43 (18H, SiCH_2O), 1.44 (72H, CH_2CH_2CH_2Si), 0.94 (72H, CH$_2$CH_2CH$_2$Si), 0.39 (72H, 18H, CH$_2$CH$_2$CH_2Si), -0.14 (216H, Si(CH_3)$_2$). UV-vis.: λ_{max1} = 355 nm, λ_{max2} = 410 nm (shoulder).

AuNPs-7*:* The filled DHR **5** (10 mg, 0.8 x 10^{-3} mmol, 1 equiv.) was dissolved in 1 mL THF and was added dropwise at 0°C in a solution of $HAuCl_4$ (5.7 mg, 0.014 mmol, 18 equiv.) in 40 mL of H_2O/ THF 3:1, under vigorous stirring. The color instantaneously changed from yellow to pink red, and stirring was continued for another 10 min. The mixture was concentrated *in vacuo* to 30 mL. UV-vis.: λ_{max} = 348 nm, SPR: λ_{max} = 537 nm. TEM: d_{AuNPs} = 3± 0.5 nm, $d_{Capsules}$ = 63 ± 20 nm.

AuNPs-9*:* The filled DHR **5** (10 mg, 0.8 x 10^{-3} mmol, 1 equiv.) was dissolved in 1 mL THF and was added dropwise at 0°C in a solution of $AuCl_3$ (4.4 mg, 0.014 mmol, 18 equiv.) in 30 mL of THF, under vigorous stirring. The color instantaneously changed from yellow to violet, and stirring was continued for another 10 min. The mixture was kept in a closed flask. UV-vis.: λ_{max} = 350 nm, SPR: λ_{max} = 571 nm. TEM: d_{AuNPs} = 33 ± 2 nm, $d_{Capsules}$ = 220 ± 40 nm.

AgNPs-13*:* The filled DHR **5** (10 mg, 0.8 x 10^{-3} mmol, 1 equiv.) was dissolved in 1 mL THF and was added dropwise at 0°C into a solution of $AgBF_4$ (2.1 mg, 0.011 mmol, 13.5 equiv.) in 30 mL of H_2O/ THF 3:1, under vigorous stirring. The color instantaneously changed from colorless to light orange, and stirring was continued for another 10 min. The mixture was concentrated *in vacuo* to 22 mL. UV-vis.: λ_{max} = 350 nm, SPR: λ_{max} = 439 nm. TEM: d_{AgNPs} = 5±0.5 nm, $d_{Capsules}$ = 85±5 nm.

PdNPs-14*:* $Pd(OAc)_2$ (4.8 mg, 0.022 mmol, 27 equiv.) was solubilized in 3 mL of THF. To this solution was added 2 mL of triethylene glycol triazole (4.3 mg, 0.022 mmol, 27 equiv.), and the mixture was stirred vigorously for 20 min. Then, additional 15 mL of THF was added to the solution. Consequently, 1 mL of the filled DHR **5** (10 mg, 0.8 x 10^{-3} mmol, 1 equiv.) was added dropwise at 0°C to the solution under vigorous stirring. The color instantaneously changed from yellow to deep brown, and stirring was continued for another 10 min. The mixture was kept in a closed flask. UV-vis.: λ_{max} = 350 nm. TEM: d_{PdNPs} = 2.6±0.2 nm, $d_{Capsules}$ = 94±5 nm.

AuNPs-16*:* The filled DER **15** (10 mg, 0.8 x 10^{-3} mmol, 1 equiv.) was dissolved in 1 mL DCM and was added dropwise at 0°C into a solution of $HAuCl_4$ (2.9 mg, 0.007 mmol, 9 equiv.) in 30

mL of MeOH/ DCM 2:1, under vigorous stirring. The mixture was stirred for 3h. The color changed gradually from yellow to blue-purple in 1h. The mixture was kept in a closed flask. UV-vis.: SPR: λ_{max} = 590 nm. TEM: d_{AuNPs} = 260 ± 30 nm.

Conclusion

Dendritic Hydride Reservoirs (DHRs) constructed in their empty and filled forms with 9, 27 or 81 stable 18-electron Co(III) and Co(I) complexes at their periphery are very flexible macromolecular materials. They efficiently transform salts of various noble transition metals to stable metal particles that are trapped in large, robust cationic nanocapsules of the order of 100 nm and reversibly disintegrate upon reduction. The polycationic nature of the empty DHRs results in particularly high stability of the DHR capsules involving several thousand peripheral charges. Compared to topologically related Dendritic Electron Reservoirs (DERs) that can be interconverted without breakdown between their 18-electron ferrocenyl and 17-electron ferricenium forms, DHRs are much more efficient, whereas DERs do not form capsules. The considerably slower reduction rates observed with DERs presumably results from the kinetic requirement of high-energy radical intermediates upon electron transfer contrasting with the more straightforward substitution of anionic ligands of transition metal complexes by hydrides followed by reductive elimination of dihydrogen in the case of DHRs.

References

1. Berg, J. M., Tymoczko, J. L., Stryer, L. Biochemistry, 7th ed, Freeman and Co, New York, 2010.
2. Housecroft, C. E. & Sharpe, A. G. "Chapter 14: The group 14 elements". *Inorganic Chemistry, 4th Edition*. Pearson, Cambridge, 2012, p. 386.
3. Jovanovic, S. V., Steenken, S., Boone, C. W. & Simic, M. G. H-atom transfer is a preferred antioxidant mechanism of curcumin. *J. Am. Chem. Soc.* **121**, 9677-9681 (1999).
4. Brown, H. C. & Krishnamurthy, S. 40 Years of Hydride Reductions. *Tetrahedron* **35**, 567-607 (1979).
5. Arico, A. S., Bruce, P., Scrosati, B., Tarascon, J. M. & Van Schalkwijk. W. Nanostructured Materials for Advanced Energy Conversion and Storage Devices. *Nat. Mater.* **4**, 366-377 (2005).
6. Linic, S., Christopher, P. & Ingram, D. B. Plasmonic-metal Nanostructures for Efficient Conversion of Solar to Chemical Energy. *Nat. Mater.* **10**, 911-921 (2011).
7. Astruc, D. Electron-Transfer Processes in Dendrimers and their Implication in Biology, Catalysis, Sensing and Nanotechnology. *Nat. Chem.***4**, 255-267 (2012).
8. Lehn, J. M. & Sauvage, J.-P. Chemical storage of light energy: Catalytic generation of hydrogen by visible light or sunlight irradiation of neutral aqueous solutions. *Nouv. J. Chim.* **1**, 449-451 (1977).
9. Hagfeldt, A. & Grätzel, M. Light-induced Redox Reactions in Nanocristalline Systems. *Chem. Rev.* **95**, 49-68 (1955).
10. Kudo, A. & Miseki, Y. Heterogeneous photocatalyst materials for water splitting". *Chem. Soc. Rev.* **38**, 253-278 (2009) .
11. Ogo, S. et al. A Functional [NiFe] Hydrogenase that Catalyzes Electron and Hydride Transfer from H_2. *Science* **339**, 682-684 (2013).
12. Cheng, F. Y., Liang, J., Tao, Z. L. & Chen, J. Functional Materials for Rechargeable Batteries. *Adv. Mater.* **23**, 1695-1715 (2013).
13. Gunay, A. & Theopold, K. H. C-H Bond Activation by Metal Oxo Compounds. *Chem. Rev.* **110**, 1060-1081 (2010).

14. Bhabha, G.; L et al. A dynamic Knockout Reveals that Conformational Fluctuations Influence the Chemical Step of Enzyme Catalysis. *Science* **332**, 234-238 (2011).
15. Conley, B. L., Pennington-Boggio. M. K., Boz, E. & Williams, T. J. Discovery, Applications and Catalytic Mechanism of Shvo's Catalyst. *Chem. Rev.* **110**, 2294-2312 (2010).
16. Alonso, F., Riente, P. & Yus, M. Nickel Nanoparticles in Hydrogen Transfer Reactions. *Acc. Chem. Res.* **44**, 379-391 (2011).
17. Zheng, C. & You, S.-L. Transfer Hydrogenation with Hantzsch Esters and Related Hydride Donors. *Chem. Soc. Rev.* **41**, 2498-2518 (2012).
18. Ornelas, C., Ruiz, J., Belin, C. & Astruc, D. Giant Dendritic Molecular Electrochrome Batteries with Ferrocenyl and Pentamethylferrocenyl Termini *J. Am. Chem. Soc*. **131**, 590-601 (2009).
19. Rostovstev, V. V., Green, L. G., Fokin, V. V. & Sharpless, K. B. A. Stepwise Huisgen Cycloaddition Process: Copper(I)-Catalyzed Regioselective Ligation of Azide and Terminal Alkynes. *Angew. Chem., Int. Ed.* **41**, 2596-2599 (2002).
20. Meldal, M., Tornoe, C. W. & Christensen, C. Peoptidotriazoles on solid phase: [1,2,3]-triazoles by regiospecific copper (I)-catalyzed 1,3-dipolar cycloadditions of terminal alkynes to azides. *J. Org. Chem.* **67**, 3057-3064 (2002).
21. Newkome, G. R. & Schreiner, C. D. Dendrimers Derived from 1→3 Branching Motifs. *Chem. Rev.* **110**, 6338-6442 (2010).
22. Newkome, G. R., He, E. & Moorefield, C. N. Metallodendrimers: Suprasupermolecules with Novel Properties. *Chem. Rev.* **99**, 1689-1746 (1999).
23. Rapakousiou, A., Wang, Y., Belin, C., Pinaud, N., Ruiz, J. & Astruc, D. Click' Synthesis and Redox Properties of Triazolyl Cobalticinium Dendrimers. *Inorg. Chem*. **52**, 6685-6693 (2013).
24. Green, M. L. H., Pratt, L. & Wilkinson, G. A New Type of Transition Metal-Cyclopentadiene Compound. *J. Chem. Soc.* 3753–3767 (1959).
25. Rapakousiou, A., Mouche, C., Duttine, M., Ruiz, J. & Astruc, D. Click Synthesis and Redox Chemistry of Mono- and Heterobimetallic Triazolyl and Triazolium-Ferrocene and Cobalticinium Complexes. *Eur. J. Inorg. Chem*. **31**, 5071-5077 (2012).
26. Myers, V. S. et al. Dendrimer Encapsulated Nanoparticles: New Synthetic and Characterization Methods and Catalytic Applications. *Chem. Sci.* **2**, 1632-1646 (2011).
27. Wu, P., Feldman, A. K., Nugent, A. K., Hawker, C. J., Scheel, A., Voit, B., Pyun, J., Fréchet, J. M. J., Sharpless, K. B. & Fokin, V. V. Efficiency and Fidelity in a Click Chemistry Route to Dendrimers by the Copper (I)-Catalyzed Ligation of Azides and Alkynes. *New. Chem., Int. Ed.* **43**, 3928-3932 (2004).
28. Ornelas, C., Ruiz, J., Cloutet, E., Alves, S., Astruc, D. Click Assembly of 1,2,3-Triazole-Linked Dendrimers Including Ferrocenyl Dendrimers that Sense Both Oxo-anions and Metal Cations . *Angew. Chem. Int. Ed.* **46**, 872-877 (2007).
29. Rosi, N. L. & Mirkin, C. A. Nanostructures in Biodiagnostics. *Chem. Rev.* **105**, 1547-1562 (2005).
30. Xia, Y. N., Xong, Y. J., Lim, B. & Skrabalak, S. E. Shape-controlled Synthesis of Metal Nanocrystals. *Angew. Chem., Int. Ed.* **48**, 60-103 (2009).
31. Daniel, M. C. & Astruc, D. *Chem. Rev.* **104**, 293-346 (2004).
32. Mulvaney, P. Surface Plasmon Spectroscopy of Nanosized Metal Particles. *Langmuir* **3**, 788-800 (1996).

III) Conclusion générale

Conclusion et perspectives

L'objectif de cette thèse était l'ingéniérie, la synthèse et l'étude des propriétés de nanomatériaux possédant des propriétés redox polyélectroniques et leurs applications. Nous avons effectué un travail de thèse en chimie organométallique macromoléculaire des métaux de transition et nanoscience des nanoparticules d'or. Au cours de ces travaux, nous avons développé des nouveaux nanomatériaux métallopolymèriques et métallodendritiques de type polyélectrolyte et examiné leurs interactions avec les nanoparticules d'or. Outre l'ingéniérie et les synthèses métallomacromoléculaires qui ont été très conséquentes, deux avancées notables ont été réalisées. D'abord la réduction par les macromolécules ferrocéniques et biferrocéniques de Au(III) en nanoparticules d'Au(0) par transfert électronique avec stabilisation concomitante des nanoparticules d'Au(0) et des macromolécules contenant le ferricénium. Ensuite la synthèse de macromolécules contenant les complexes sandwichs cationiques (polyélectrolytes) et neutres du cobalt, avec en particulier la faculté de ces dernier à servir de réservoirs d'hydrures avec, par exemple, formation de capsules de nanoparticules d'Au(0), Ag(0) où Pd(0). Notons ici le parallèle conceptuel entre réservoirs macromoléculaires polyferrocéniques d'électrons et réservoirs cobaltomacromoléculaires d'hydrures et la richesse de la structuration des nanomatériaux à base de nanoparticules d'or qui en a résulté. Les autres applications ont concerné la reconnaissance redox de l'ATP et de cations métalliques, éventuellement simultanément dans le cas des dendrimères à terminaisons biferrocéniques parfois même en milieu aqueux.

Concernant les perspectives ouvertes par cette thèse, dans un avenir proche, on pourra étudier la réduction de ces macromolécules polycationiques en macromolécules neutres comportant 19 électrons de valence, l'encapsulation et le transport des médicaments en milieu macromoléculaire hydrophobe et/ou hydrophile ainsi que le comportement de ce type de polyélectrolytes dans les batteries.

La structuration des réseaux macromoléculaires contenant des nanoparticules métalliques qui constituent l'aspect le plus novateur de la thèse devrait être développée en particulier avec les nanoparticules d'or et les macromolécules biologiques. On peut espérer des applications dans le domaine biomédical, en particulier pour le diagnostic, voire la photothermothérapie (donc la "théranostique").

L'ingénierie de formation des nanoréseaux à partir des macromolécules triazolyl-biferrocényles peut être étendue aux autres complexes de transition et leurs applications peuvent être envisagées dans des domaines tels que l'énergie avec les batteries moléculaires au cobalt et la nanoélectronique avec le branchement de fils moléculaires conducteurs sur les nanoparticules.

IV) Annexes

Annexes

(a) Yanlan Wang, **Amalia Rapakousiou**, Guillaume Chastanet, Lionel Salmon, Jaime Ruiz, Didier Astruc: *Poly(Biferrocenylethynyl)arene and Bis(biferrocenyl)diynyl Complexes and their Redox Chemistry. Organometallics*, **2013**, *32*, 6136-6146. [Contribution de synthèse avec l'éthynylbiferrocène]

(b) N. Li, P. Zhao, M. E. Igartua, **A. Rapakousiou**, L. Salmon, S. Moya, J. Ruiz, D. Astruc: *Stabilization of AuNPs by Monofunctional Triazole Linked to Ferrocene, Ferricenium or Coumarin and Applications to Synthesis, Sensing and Catalysis. Inorg. Chem.* **2014**, *53*, ID: ic-2014-021498.R1. [Contribution avec l'étude électrochimique]

(c) Didier Astruc, Liyuan Liang, **Amalia Rapakousiou**, Jaime Ruiz: *Click dendrimers and triazole-related aspects: catalysts, mechanism, synthesis, and functions. A bridge between dendritic architectures and nanomaterials. Acc. Chem. Res.* **2012**, *45*, 630-640. [Contribution avec la synthèse de l'éthynylcobalticénium, l'éthynylbiferrocène et leurs réactions "click" CuAAC avec les macromolécules]

(d) Haibin Gu, **Amalia Rapakousiou**, Pascal Castel, Nicolas Guidolin, Noel Pinaud, Jaime Ruiz, Didier Astruc: *Living Ring-Opening Metathesis Polymerization and Redox-Sensing Properties of Norbornene Polymers and Copolymers Containing Ferrocenyl and Tetraethylene Glycol Groups.* Organometallics **2014**, *33*, 4323-4335. [Contribution avec l'étude électrochimique et de reconnaissance redox de l'ATP]

ORGANOMETALLICS

Article

pubs.acs.org/Organometallics

Poly(Biferrocenylethynyl)arene and Bis(biferrocenyl)diynyl Complexes and Their Redox Chemistry

Yanlan Wang,[†] Amalia Rapakousiou,[†] Guillaume Chastanet,[‡] Lionel Salmon,[§] Jaime Ruiz,[†] and Didier Astruc*[,†]

[†]ISM, UMR CNRS N°5255, Univ. Bordeaux, 33405 Talence Cedex, France

[‡]CNRS, Université de Bordeaux, ICMCB, UPR 9048, F-33600 Pessac, France

[§]Laboratoire de Chimie de Coordination, CNRS & Université de Toulouse (UPS, INP), 31077 Toulouse, France

Supporting Information

ABSTRACT: Orange linear bis-, star tris-, and dendritic tetra-biferrocenes linked by rigid ethynylaryl and diynyl spacers were synthesized through Sonogashira coupling and homo-coupling reactions and oxidized to robust blue biferrocenium complexes. The proximity of the two ferrocenyl units to each other in the biferrocenyl units introduces electrostatic and electronic effects that are observed by cyclic voltammetry and are responsible for mixed-valence stabilization and localization. The use of the polyfluorinated electrolyte $[n\text{-}Bu_4N][BAr_4^F]$ {Ar^F = 3,5-bis(trifluoromethyl)phenyl} allows observing considerable enhancement of these effects and separation of electrochemical waves representing the two ferrocenyl groups of the biferrocenyl unit. The electrostatic effect is also selectively observed with the latter electrolyte between the two central ferrocenyl units of bis(biferrocenyl)diyne. Oxidation of all of these poly(biferrocenyl) complexes using a ferricinium salt yields blue, robust biferrocenium complexes. Their localized mixed-valent electronic structure was demonstrated at both Mössbauer and infrared time scales even with the counteranion (BAr_4^F) that provokes the maximum electrostatic effect and very much enhances the difference between the two oxidation potentials. Their near-infrared spectra show the intervalent charge transfer and are similar to those previously recorded for biferrocenium and derivatives, confirming the class-II mixed valence. The biferrocene units around the arene linker are completely electronically independent in the neutral and cationic complexes. In conclusion, from a practical standpoint, the easy oxidation of these stiff electrochromic nanosystems and the largely increased robustness of their oxidized form compared to ferricinium make their potential use as electrochromes considerably more attractive than that of simple ferrocene derivatives.

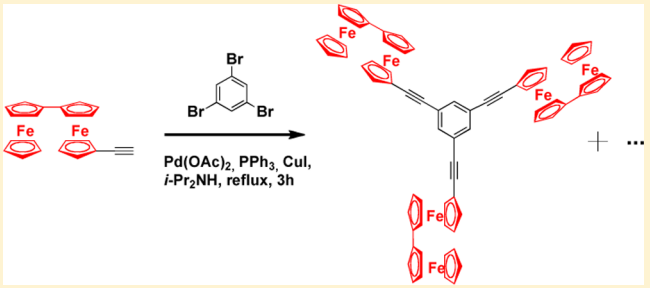

INTRODUCTION

Despite illustrious redox properties,[1] ferrocene undergoes oxidation to ferricinium that is only modestly stable and decomposes in aerobic solutions.[2] On the other hand, among polyferrocene families,[3] biferrocene[4] is the long-known prototype generating organometallic mixed-valence compounds[5] that possess a much richer electro- and electron-transfer chemistry than ferrocene. For instance, biferrocene is more readily oxidized than ferrocene, and its single-electron oxidation product, biferrocenium, is robust. Biferrocene has been used for the molecular electronics properties of nanosystems in gold nanoparticles for electrodeposition,[6] surfaces for molecular printboards,[7] and dendrimers for peripheral redox sensing.[8] It has been shown by Mössbauer, EPR, and near-infrared spectroscopies that the monocationic biferrocenium salts and derivatives belong to the class II of mixed-valent complexes with several anions, the near-infrared spectra showing the intervalent charge-transfer band.[9] The electrochemistry of biferrocene[9,10,11a] and polyferrocene[3e] derivatives has been studied, and in particular, the Geiger group has shown the influence of electrolytes containing a perfluorotetraarylborate anion on the separation of the ferrocenyl waves.[11]

Linking ferrocenyl groups with an aromatic core in the 1-, 3-, and 5-positions has already been achieved.[12] The authors reported 1,3,5-triferrocenyl benzene and its cyclic voltammetry containing a single wave when a standard electrolyte was used. This lack of separation of the electrochemical waves of the three ferrocenyl groups showed that there was no electronic communication through the arene bridge.[12] Later, it was reported that these three waves are well-separated when a perfluorotetraarylborate salt was used, which was selectively attributed to a purely electrostatic effect.[13] Long's group also reported trimetalated 1,3,5-triethynylarene complexes including electronic communication among the three metal centers

Special Issue: Ferrocene - Beauty and Function

Received: August 27, 2013
Published: October 1, 2013

Scheme 1. Sonogashira Coupling Reaction between Ethynylbiferrocene and 1,3,5-Tribromobenzene and Further Coupling Reactions

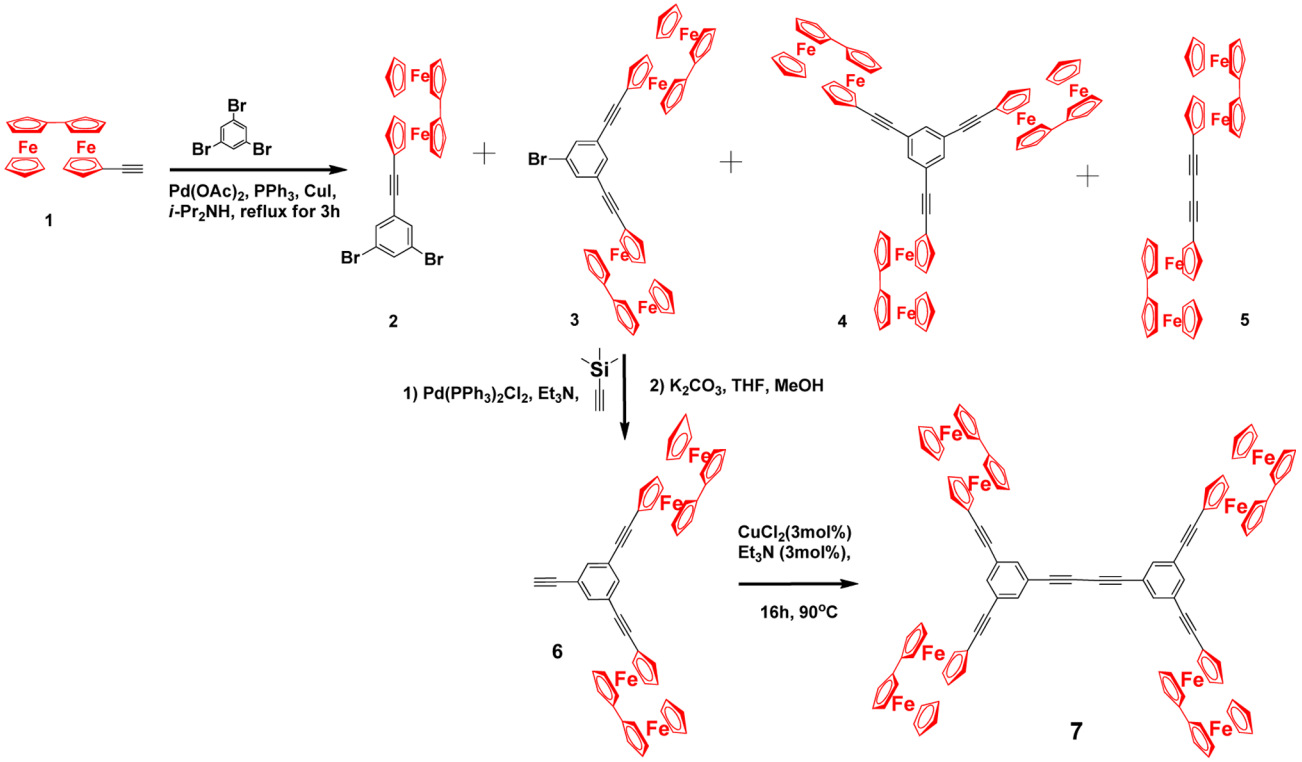

through the core in contrast with the situation of 1,3,5-triferrocenylbenzene.[14]

Since ethynylbiferrocene had already been recently reported,[8] it thus appeared attractive to synthesize poly(biferrocenylethynyl) complexes, because such compounds would yield cations upon oxidation that should be much more stable than polyferricinium compounds and thus behave as robust electrochromes. Then the electronic and electrostatic effects in poly(biferrocenylethynyl)arene derivatives would also be comparable with those of the corresponding poly(ferrocenyl)-arene complexes with various supporting electrolytes.

Bis(alkynyl)biferrocenes have long been known,[12] and the Lang and Lapinte groups have recently reported the use of bis(alkynyl)biferrocene as a bridge between various redox-active group 8 transition-metal fragments.[15] Heinze's group has designed biferrocene amino acids,[16a] oligonuclear ferrocenyl amides,[16b] and organometallic foldamers from ferrocenyl amino acids[16c] that all show stable mixed-valence properties. The construction of dendritic frameworks containing the 1,3,5-triethynylaryl core has been pioneered by Moore,[17a−c] and related cores have been used in particular by Humphrey's group for the synthesis and study of stiff dendrimers containing ruthenium moieties.[17d,e] Biferrocene could also be stored in polyphenylazomethine dendrimers by the Yamamoto and Nishihara groups,[18a] and recently, Hans' group has reported diferrocenyl units bridged by the single-carbon groups CH_2, CO, or CHOH,[18b] Biferrocenylene derivatives are also known to give very stable class-III mixed-valent cations.[19a,b]

Here, we are reporting the results of the synthesis of bis-, tris- and tetra-ethynylbiferrocenes by Sonogashira coupling and homocoupling conditions. We also examine the oxidized complexes deriving from these new systems, whereby the proximity of ferrocenyl units to each other in the biferrocenyl units introduces electronic and electrostatic effects.

RESULTS AND DISCUSSION

Synthesis and Structures of the Bridged Bi(ferrocenyl)ethynyl Complexes 2−7. The Sonogashira coupling[20] between ethynylbiferrocene and 1,3,5-tribromobenzene was carried out with 3 equiv of ethynylbiferrocene **1** and 1 equiv of 1,3,5-tribromobenzene under palladium-catalyzed conditions at reflux for 3 h. After evaporation, the crude orange mixture was separated by column chromatography on silica gel with pentane/CH_2Cl_2 (4:1) to afford the pure compounds: ethynylbiferrocenylarene **2** (34 mg, yield: 9% based on the conversion of ethynylbiferrocene), linear 1,4-bis(biferrocenyl)butadiyne **5** (67 mg, yield: 28%), dendronic 1,3-bis(biferrocenylethynyl)-5-bromo arene **3** (26 mg, yield: 9%), and the main reaction product, star-shaped 1,3,5-tris(biferrocenylethynyl)arene compound **4** (125 mg, yield: 50%) linked by rigid arylethynyl spacers. (Scheme 1).

Overall, the Sonogashira reaction affords rapid access to these biferrocene-containing complexes that are readily separated by standard column chromatography. The formation of **5** corresponds to the Pd-catalyzed coupling alone and is in competition with the Sonogashira reaction. All the complexes obtained in this Sonogashira reaction are of interest for the determination of their redox potential (vide infra) or for further coupling. Because they were readily separated and the yield of the targeted product **3** being reasonable, the reaction was not optimized further toward the formation of any of them. The complexes **2**, **3**, **4**, and **5** were characterized by ^1H NMR, ^{13}C NMR, cyclic voltammetry (CV), IR, UV−vis, ESI, and elemental analyses. The IR spectra showed the characteristic bands around 2211 cm^{-1} corresponding to the alkynyl

dx.doi.org/10.1021/om400864q | Organometallics 2013, 32, 6136−6146

absorption ($\nu_{C\equiv C}$), and the ESI mass spectra showed the correct molecular ion for each compound. The 1,3-di(biferrocenylethynyl)-5-bromobenzene complex **3** was easily synthesized through the Sonogashira reaction shown in Scheme 1; further reaction of **3** with trimethylsilylacetylene under palladium-catalyzed conditions, followed by reaction with K_2CO_3 in a THF/CH_3OH mixture, led to the 1,3-di(biferrocenylethynyl)-5-ethynylbenzene complex **6** (yield: 60%). Then **6** was submitted to Cu^{II}-induced homocoupling to give the tetra(ethynylbiferrocene) complex **7** in 60% isolated yield (Scheme 1). The complexes **6** and **7** were fully characterized by ^1H NMR, ^{13}C NMR, cyclic votammetry, FT-IR, UV−vis, and MALDI-TOF mass spectroscopy and provided correct elemental analyses. The FT-IR (KBr) spectrum of **6** shows the presence of the alkynyl group at 2209 cm^{-1} ($\nu_{C\equiv C}$) and 3292 cm^{-1} ($\nu_{C\equiv CH}$) (see the Supporting Information).

Cyclic Voltammetry of the Bis- and Poly(ethynylbiferrocenyl) Complexes 1−7. The electrochemistry of polyferrocene systems has been thoroughly studied by Geiger's group, including the electrostatic effect induced in the variation of supporting electrolytes.[1,11]

The cyclic voltammograms (CVs) of the bis- and poly(ethynylbiferrocenyl) complexes **1**−**7** compare with those of the known reference compounds **8**−**11** (Chart 1).

Chart 1. Ferrocene, Ethynylferrocene, 1,4-Bis(ferrocenyl)-1,3-butadiyne, and Biferrocene

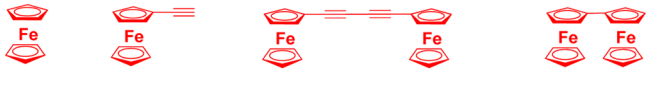

8 9 10 11

Table 1 gathers the electrochemical and thermodynamic data of all the compounds **1**−**11**. It can be easily observed therein that the ethynyl group exerts a quite strong electron-withdrawing effect on ferrocene (**8**). For instance, in CH_2Cl_2 with [*n*-Bu_4N][PF_6] 0.1 M as the supporting electrolyte, the oxidation of ethynylferrocene (**9**) is 165 mV more positive than that of ferrocene; that is, it is more difficult to oxidize than ferrocene. Likewise, under the same conditions, the oxidation of the diyne complex **10** occurs at a potential 280 mV more positive than that of biferrocene. In **1**, the first oxidation is only slightly more difficult (by 40 mV) than in **11**, because it concerns the ferrocenyl site that is not directly bound to the ethynyl group, but the second oxidation, concerning the ferrocenyl site that is attached to the ethynyl group, intervenes at a potential that is 115 mV higher than that of **11**.[8] These basic considerations will be useful to assign the CV waves of the poly(ferrocenylethynyl) complexes studied here.

The large comproportionation constants (K'_{com}) gathered in Table 1 reflect the stability of the mixed-valence Fe^{II}−Fe^{III} biferrocenium complexes. The presence of the ethynyl substituent still increases the large K'_{com} values by an order of magnitude. Another useful experimental tool is the variation of supporting electrolyte from the standard electrolyte [*n*-Bu_4N][PF_6] to [*n*-Bu_4N][BAr_4^F] {Ar^F = 3,5-bis(trifluoromethyl)phenyl} that weakens ion-pairing effects and favors the observation of electrostatic effects in the compounds under study. Geiger highlighted the fact that the use of the polyfluorinated electrolytes such as [*n*-Bu_4N][BAr_4^F] instead of, for instance, [*n*-Bu_4N][PF_6] leads to a much larger wave separation among the various oxidation CV waves of bis- or tetraferrocenyl systems provided the ferrocenyl groups are close to one another.[11] One of the consequences is the larger K'_{com} values leading to easier stabilization of the mixed-valence Fe^{II}−Fe^{III} complexes. This clearly appeared for biferrocene (**11**) for which the wave separation was, in CH_2Cl_2, 375 mV with [*n*-Bu_4N][PF_6] and 590 mV with [*n*-Bu_4N][BAr_4^F]. In the same way, the wave separation in CH_2Cl_2 for **10** increases from 85 mV with [*n*-Bu_4N][PF_6] to 175 mV with [*n*-Bu_4N][BAr_4^F]. It is much attenuated in **10** compared to **11** because of the increased distance and decreased electronic communication and electrostatic effect between the two redox centers. Geiger

Table 1. Compared $E_{1/2}$ and Comproportionation Constant (K'_{com}) Values for a Series of Ferrocenyl and Biferrocenyl Compounds[a]

compound	supporting electrolyte	$E'_{1/2}$ (V)	$E''_{1/2}$ (V)	$\Delta E'_{ox}$ (mV)	K'_{com}
1	[*n*-Bu_4N][PF_6]	0.480	0.930	450	4.04×10^7
2	[*n*-Bu_4N][PF_6]	0.325	0.610	285	6.55×10^4
3	[*n*-Bu_4N][PF_6]	0.473	0.850	377	2.35×10^6
4	[*n*-Bu_4N][BAr_4^F]	0.520	0.980	460	5.94×10^7
	[*n*-Bu_4N][PF_6]	0.465	0.870	405	6.99×10^6
5	[*n*-Bu_4N][BAr_4^F]	0.555	1.230	675	2.56×10^{11}
			$E'''_{1/2}$ (1.430)	$\Delta E''_{ox}$ (200)	K''_{com} (2.4×10^3)
	[*n*-Bu_4N][PF_6]	0.475	0.930	455	4.86×10^7
6	[*n*-Bu_4N][PF_6]	0.395	0.730	335	4.60×10^5
7	[*n*-Bu_4N][PF_6]	0.470	0.837	367	1.59×10^7
8	[*n*-Bu_4N][BAr_4^F]	0.615 (0.40)[b,22]			
9	[*n*-Bu_4N][BAr_4^F]	0.780			
10	[*n*-Bu_4N][BAr_4^F]	0.755	0.930	175	908
	[*n*-Bu_4N][PF_6]	0.700	0.785	85	27
11	[*n*-Bu_4N][BAr_4^F]	0.475 (0.31)[b]	1.065 (0.62)[b]	590	9.39×10^9
	[*n*-Bu_4N][PF_6]	0.440	0.815	375	2.18×10^6

[a]The $E_{1/2}$ values were examined under identical conditions using $FeCp^*_2$ as the internal reference. Solvent: CH_2Cl_2; supporting electrolyte: [*n*-Bu_4N][BAr_4^F] or [*n*-Bu_4N][PF_6] 0.1 M; 293 K; working and counter electrodes: Pt; reference electrode: Ag; scan rate: 0.200 $V{\cdot}s^{-1}$. All the CV measurements were carried out using the following concentrations: **1** (3 mM), **2** (3 mM), **3** (1.5 mM), **4** (0.3 mM), **5** (0.5 mM), **6**, **7**, **8**, **9**, **10**, and **11** (1.5 mM). [b]The $E'_{1/2}$ value of the $Cp^*_2Fe(+/0)$ redox couple vs $Cp_2Fe(+/0)$ is 0.615 V under these conditions with [*n*-Bu_4N][BAr_4^F].[22]

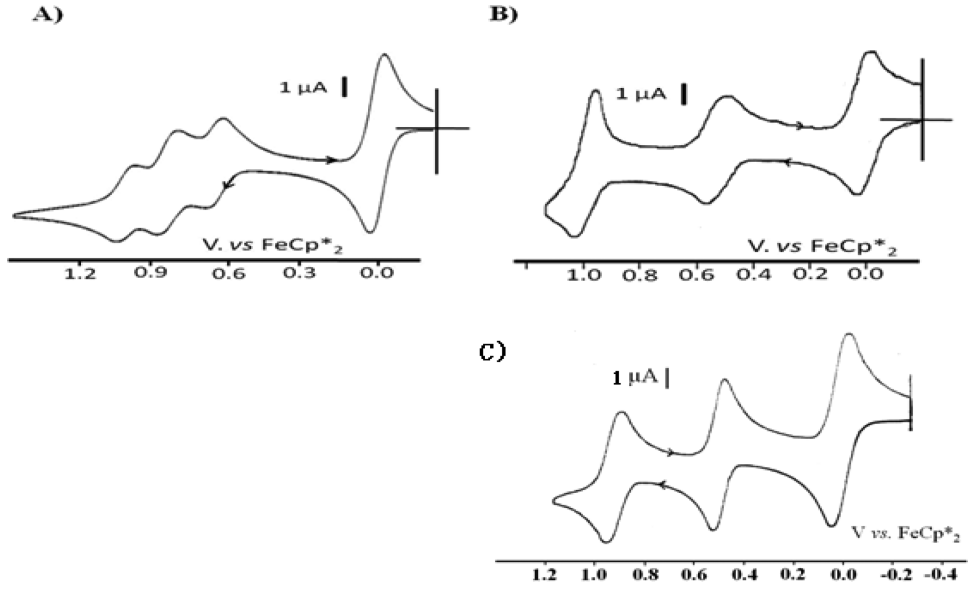

Figure 1. (A) Compared cyclic voltammograms of 1,3,5-tris(ferrocenylethynyl)benzene (0.3 mM), **12**, (B) and 1,3,5-tris(biferrocenylethynyl)-benzene (0.3 mM), **4**, with decamethylferrocene ($FeCp^*_2$) as the internal reference. Solvent: CH_2Cl_2; temperature: 293 K; supporting electrolyte: [*n*-Bu_4N][BAr_4^F] 0.1 M; working and counter electrodes: Pt; reference electrode: Ag; scan rate: 0.200 V·s^{-1}. The three reversible waves for **12** are at $E_{1/2}$ = 0.64, 0.84, and 1.06 V vs $FeCp^*_2$; the two reversible waves for **4** are at $E_{1/2}$ = 0.52 and 0.98 V vs $FeCp^*_2$. (C) Cyclic voltammogram of 1,3,5-tris(biferrocenylethynyl)benzene (0.3 mM), **4**. Solvent: CH_2Cl_2; supporting electrolyte: [*n*-Bu_4N][PF_6]; temperature: 293 K; working and counter electrodes: Pt; reference electrode: Ag; scan rate: 0.200 V·s^{-1}; two reversible waves: $E_{1/2}$ = 0.465 V (ΔE = 30 mV) and 0.870 V (ΔE = 20 mV) vs $FeCp^*_2$.

has pointed out that large changes of $\Delta E_{1/2}$ values raise cautionary notes on the common usage of these values in estimating the degree of electronic communication between different redox sites in a molecule.[11] We believe that this statement perfectly applies to **11** and its derivatives **2**, **3**, **4**, **6**, and **7** that are subject to both electronic communication and electrostatic effects between the very close redox centers of biferrocenyl compounds within each biferrocenyl unit, in particular, when electrolytes with polyfluorinated anions are used, such as in [*n*-Bu_4N][BAr_4^F]. The CVs of the complexes **2**, **3**, **4**, **6**, and **7** all show two fully reversible waves around 0.5 and 1 V vs decamethylferrocene ($FeCp^*_2$),[21] respectively, that are assigned to the two electronically communicated iron centers in the biferrocenyl group.

The electronic communication and proximity resulting in the electrostatic effect induce a mixed-valence system that is very stable, as reflected by the large K'_{com} values that are still increased by an order of magnitude with [*n*-Bu_4N][BAr_4^F] compared to [*n*-Bu_4N][PF_6] (Table 1). Despite these large values, it is not possible to state on the basis of the CV data only whether the mixed-valence Fe^{II}—Fe^{III} are localized or delocalized, and this distinction must await the isolation and spectroscopic characterization. For the CVs, the second wave also shows more or less adsorption due to the precipitation of the polycation salts onto the electrode. Thus, the potential at which this second oxidation occurs that is calculated using the average of the oxidation and reduction potentials (CV maximum) less accurately reflects the standard oxidation potential than in the case of the first oxidation.

For instance, the CV of complex **4** is shown in Figure 1B. This CV compares to that of related tris-1,3,5-(ferrocenyl-ethynyl)benzene, **12**,[13,14] in CH_2Cl_2 with [*n*-Bu_4N][BAr_4^F] as supporting electrolyte that showed three distinct one-electron waves reflecting the pure electrostatic effect between the three ferrocenyl groups in the absence of a through-bond electronic effect (Figure 1A).

With **4**, the electrostatic effect among the three ferrocenyl groups attached to the tris(ethynylferrocenyl) core is almost absent, although the CV was recorded with [*n*-Bu_4N][BAr_4^F] as the electrolyte. Given the electron-withdrawing effect of the alkynyl group that was shown in the reference compound **1**, **9**, and **10**, it could be anticipated that the outer ferrocenyl groups of **2**, **3**, **4**, **5**, and **7** would be oxidized more easily than the inner ones that are attached to the alkynyl groups. Concerning **5**, interestingly, this situation is opposite that disclosed by Heinze's group for a ureylene-bridged bis(biferrocene) complex in which the outer ferrocenyl units bear a strong electron-withdrawing carboxymethyl substituent. Heinze's group has nicely confirmed this by ^{1}HNMR upon partial oxidation of the bi- or oligoferrocenyl derivatives that selectively affects the first-oxidized units, allowing identification of the redox sites.[19b] Thus, in the poly(biferrocenylethynyl) complexes **3**, **4**, **6**, and **7**, the outer ferrocenyl groups are much further from one another than in **12** (Figure 1A). The first oxidation of all the poly(biferrocenylethynyl) compounds is thus found at the same potential in a single CV wave with [*n*-Bu_4N][PF_6]. With [*n*-Bu_4N][BAr_4^F] that brings about the maximum possible electrostatic effect, a somewhat broader CV wave is observed corresponding to three very close potentials, this electrostatic effect remaining very weak due to the large intersite distance (Figure 1B,C). Interestingly, the second oxidation wave of all the poly(biferrocenylethynyl) around 1 V vs $FeCp^*_2$ is unique and not split or broadened even with [*n*-Bu_4N][BAr_4^F], contrary to what was observed for **12** (Figure 1A). Thus, it appears that the three outer ferricinium substituents of **4**, for instance, completely shield and annihilate the purely electrostatic effect observed in their absence in **12**. This shielding is probably due to the positive charge on the outer ferricinium group and is enhanced by the spatial delocalization of these

dx.doi.org/10.1021/om400864q | *Organometallics* 2013, 32, 6136−6146

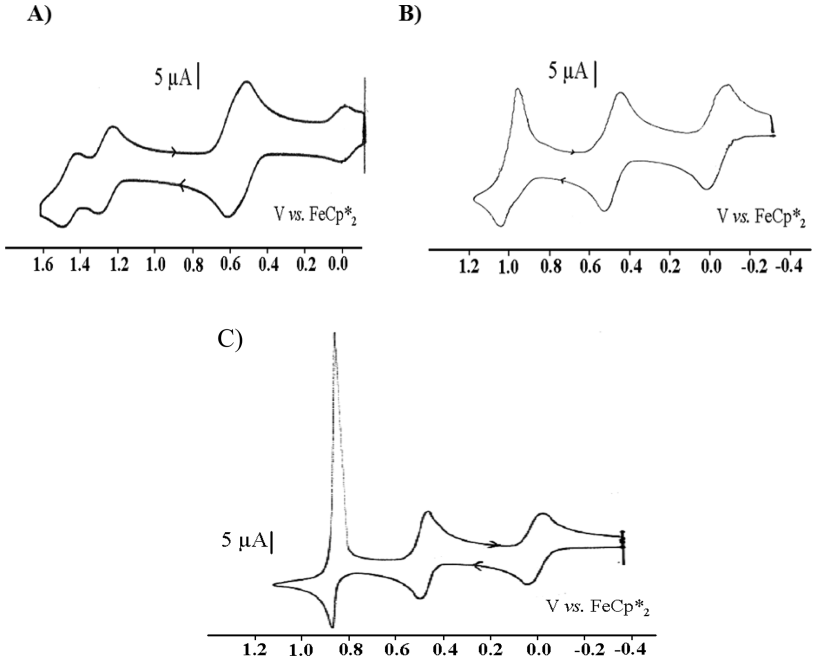

Figure 2. (A) Cyclic voltammogram of 1,4-bis(biferrocenyl)-1,3-butadiyne, **5** (0.5 mM; CH_2Cl_2; supporting electrolyte [*n*-Bu_4N][BAr_4^F]; 293 K): working and counter electrodes: Pt; reference electrode: Ag; scan rate: 0.200 V·s^{-1}; three reversible waves: $E_{1/2}$ = 555 mV (ΔE = 80 mV), 1.230 V (ΔE = 70 mV), and 1.430 V (ΔE = 60 mV) vs $FeCp^*_2$. (B) CV of 1,4-bis(biferrocenyl)-1,3-butadiyne, **5** (0.5 mM; CH_2Cl_2; supporting electrolyte [*n*-Bu_4N][PF_6]; 293 K): working and counter electrodes: Pt; reference electrode: Ag; scan rate: 0.200 V·s^{-1}; two reversible waves: $E_{1/2}$ = 485 mV (ΔE = 40 mV) and 0.930 V (ΔE = 110 mV) vs $FeCp^*_2$. (C) CV of **7** (1.5 mM; CH_2Cl_2; supporting electrolyte [*n*-Bu_4N][PF_6]; 293 K): working and counter electrodes: Pt; reference electrode: Ag; scan rate: 0.200 V·s^{-1}; two reversible waves: $E_{1/2}$ = 470 mV (ΔE = 35 mV) and 0.837 V (ΔE = 10 mV) vs $FeCp^*_2$.

Scheme 2. Oxidation of All the Biferrocenylethynyl Complexes with 1 equiv of Ferricinium Salt [Cp_2Fe][BAr_4^F], 8(BAr_4^F) per Biferrocenylethynyl Group, To Synthesize Bis-, Tris-, and Tetra-Biferroceniumethynyl (Fe^{II}–Fe^{III}) Salts[a]

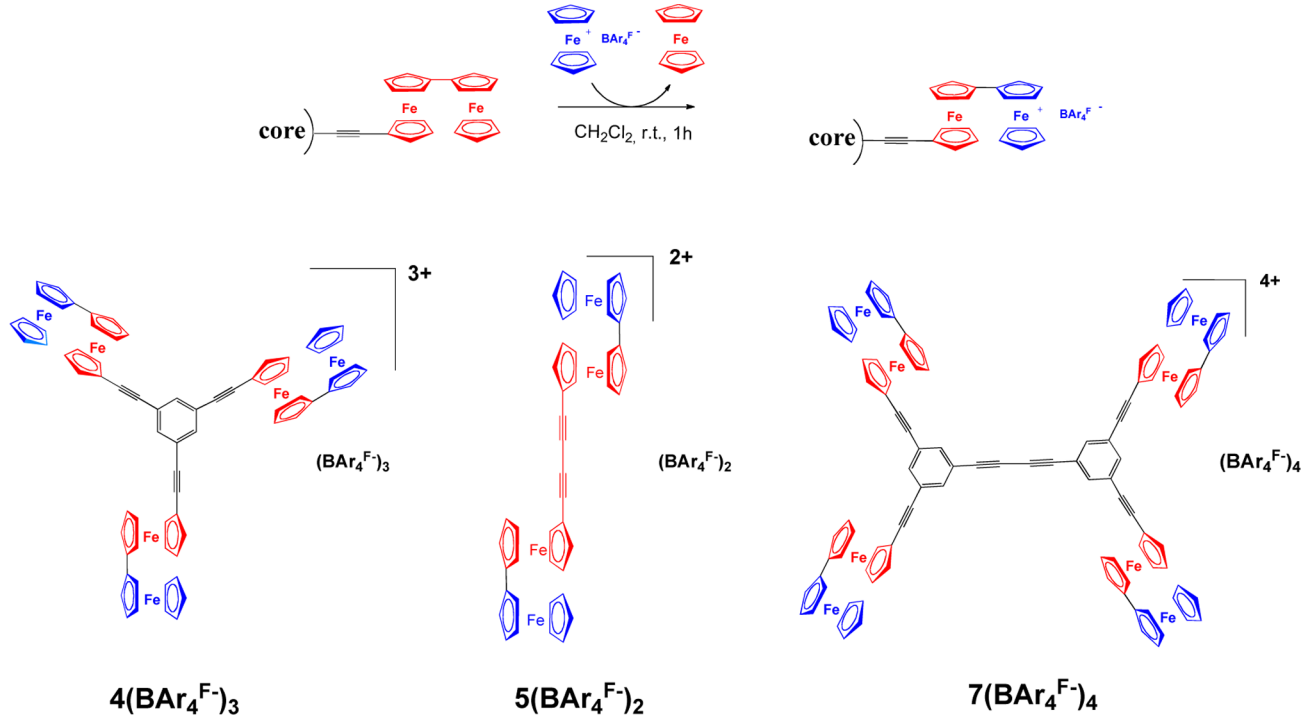

[a]The ferrocenyl groups are red, and the ferricinium groups are blue.

charges given the fast rotation of the ferrocenyl–ferricinium bond at the electrochemical time scale. In all of these poly(biferrocenylethynyl)arene complexes, the biferrocenyl units appear as electronically independent; that is, there is no electronic transmission through the arene core as known in the ferrocenyl analogues.[12,13]

dx.doi.org/10.1021/om400864q | *Organometallics* 2013, 32, 6136–6146

The above analysis also applies to the linear complex **5** concerning the first oxidation near 0.5 V vs $FeCp_2^*$; that is, the single CV wave observed with $[n\text{-}Bu_4N][PF_6]$ broadens to an envelope of a broader wave, reflecting the slight splitting into two close redox potentials with $[n\text{-}Bu_4N][BAr_4^F]$ as the supporting electrolyte, due to the very weak electrostatic effect between the two outer ferrocenyl groups. The situation is very different for the second oxidation wave that is unique (with some adsorption) with $[n\text{-}Bu_4N][PF_6]$, but well-split into two very distinct CV waves with $[n\text{-}Bu_4N][BAr_4^F]$, reflecting a rather strong electrostatic effect. The unicity of the CV wave observed with $[n\text{-}Bu_4N][PF_6]$ indicates that the electronic communication between the two inner ferrocenyl groups of **5**, if any, is negligible. The electrostatic effect is much stronger for **5** than for the poly(biferrocenylethynyl)arene complexes, essentially because the bis(ethynyl) linker in **5** is much shorter than the bis(ethynyl)arene linker in the **3**, **4**, **6**, and **7** (Figure 2). On the basis of Chemdraw simulations, the Fe−Fe distance with the bis(ethynyl) linker is estimated to 6.7 Å,[16a] that is, 3.9 Å shorter than the Fe−Fe distance through the bis(ethynyl)-arene linker (10.6 Å).

Syntheses and Electronic Structures of the Mixed-Valence Biferrocenium Complexes. The electrochemical studies of the preceding section have shown that the first oxidation waves of the neutral biferrocenyl complexes are at potentials 0.1−0.2 more positive than that of ferrocene, which means that ferricinium salts can easily oxidize biferrocenylethynyl derivatives. In terms of redox equilibriums of the oxidation using ferricinium, the reactions are shifted quasi-quantitatively toward the formation of ferrocene and mixed-valent biferrocenium complexes. The oxidant $[Cp_2Fe][BAr_4^F]$ was chosen for the reaction, because (i) strong electrostatic effects are expected, and (ii) an initial attempt with $[Cp_2Fe][PF_6]$ and **4** provided the brown complex $\mathbf{4}(PF_6)_3$ that presented a band of (PF_6^-) inconveniently appearing in the FT-IR spectrum at 840 cm^{-1} near the ferrocene absorption region of interest.

Biferrocene **11**, the poly(biferrocenylethynyl)arene complexes **4** and **7**, and the bis(biferrocenyl)diynyl complex **5** have been oxidized by reactions with 1 equiv of $[Cp_2Fe][BAr_4^F]$ per biferrocenylethynyl unit in CH_2Cl_2, and all of these reactions proceeded virtually quantitatively to produce, respectively, the air and thermally stable salts $\mathbf{11}(BAr_4^F)$, $\mathbf{4}(BAr_4^F)_3$, $\mathbf{7}(BAr_4^F)_4$, and $\mathbf{5}(BAr_4^F)_2$ as brown solids (Scheme 2).

Although the biferrocenium monocation $\mathbf{11}^+$ is known with various anions, the salt $\mathbf{11}(BAr_4^F)$ had not yet been isolated. The biferrocenium salts of $\mathbf{11}^+$ were shown in various reports to be localized class-II mixed-valent complexes, but it is also known that parameters such as the nature of the substituent have an important effect on the intervalent electron-transfer rate.[9,23−26] Therefore, the electronic structure was verified, especially due to the strong electrostatic effect of the (BAr_4^F) anion, although the nature of the anion (BF_4^-, PF_6^-, ClO_4^-) in ligand-bridged Ru^{II}−Ru^{III} complexes was reported to influence electrostatic factors,[11] but not inner-sphere electronic communication between redox sites.[27]

The FT-IR spectrum of **4** (Figure 3A) in KBr pellets showed the absorption of the ferrocenyl group at 814 cm^{-1} (ν_{Fc}). In the FT-IR spectrum of $\mathbf{4}(PF_6)_3$, however, a band of (PF_6^-) inconveniently appears at 840 cm^{-1}. Therefore, the (BAr_4^{F-}) salt was used to investigate this region of the spectrum. Both the ferrocenyl and the ferrocenium groups in the mixed-valence

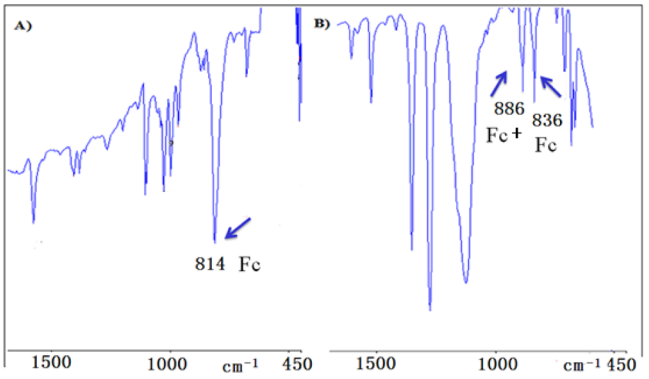

Figure 3. FT-IR spectra in KBr pellets of (A) **4**, 814 cm^{-1} (ν_{Fc}) and (B) $\mathbf{4}(BAr_4^F)_3$, 886 cm^{-1} (ν_{Fc}+), 836 cm^{-1} (ν_{Fc}), where Fc stands for $[Fe(\eta^5\text{-}C_5H_5)(\eta^5\text{-}C_5H_4\text{−})]$.

compound $\mathbf{4}(BAr_4^F)_3$ are detected at 886 cm^{-1} (ν_{Fc}+) and 836 cm^{-1} (ν_{Fc}) (Figure 3B). For the other mixed-valence complexes $\mathbf{11}(BAr_4^F)$, $\mathbf{5}(BAr_4^F)_2$, and $\mathbf{7}(BAr_4^F)_4$, analogous results were obtained, and the data are gathered in Table 2. Indeed, the

Table 2. FT-IR Spectra in KBr Pellets of All the Biferrocenyl Complexes and their Fe^{II}−Fe^{III} Mixed-Valent States Studied in This Work

compound	ν_{Fc} (cm^{-1})	ν_{Fc}+ (cm^{-1})
4	814	
$\mathbf{4}(BAr_4^F)_3$	836	886
5	814	
$\mathbf{5}(BAr_4^F)_2$	838	887
7	815	
$\mathbf{7}(BAr_4^F)_4$	838	886
11	817	
$\mathbf{11}(BAr_4^F)$	836	886

presence of the Fc^+ center close to the Fc group increases the frequencies of the Fc side by 22, 24, 23, and 19 cm^{-1} for $\mathbf{4}(BAr_4^F)_3$, $\mathbf{5}(BAr_4^F)_2$, $\mathbf{7}(BAr_4^F)_4$, and $\mathbf{11}(BAr_4^F)$ in comparison with their neutral analogues **4**, **5**, **7**, and **11**, respectively, as a result of the presence of the electron-withdrawing ferricinium substituent (Table 2).

A large shift in the UV−vis absorption of $\mathbf{4}(PF_6)_3$ and $\mathbf{4}(BAr_4^F)_3$ was recorded compared to **4**. Under identical conditions, λ_{max} of **4** = 454 nm, λ_{max} of $\mathbf{4}(PF_6)_3$ = 555 nm, and λ_{max} of $\mathbf{4}(BAr_4^F)_3$ = 565 nm (Figure 4). For the other mixed-valence complexes $\mathbf{5}(BAr_4^F)_2$, $\mathbf{7}(BAr_4^F)_4$, and $\mathbf{11}(BAr_4^F)$, similar results were obtained, and the data are gathered in Table 3.

A similar large shift in the UV−vis absorption of $\mathbf{5}(BAr_4^F)_2$, $\mathbf{7}(BAr_4^F)_4$, and $\mathbf{11}(BAr_4^F)$ was found (respectively, 106, 109, and 112 nm) in comparison with their neutral analogues **5**, **7**, and **11** (Table 3).

^{57}Fe Mössbauer spectra easily allowed assigning the oxidation states in the mixed-valent compounds $\mathbf{4}(PF_6)_3$, $\mathbf{5}(BAr_4^F)_2$, and $\mathbf{11}(BAr_4^F)$. The spectra were recorded at 78 K at zero field and showed the localized mixed valency with the presence of both the ferrocenyl groups and the ferrocenium groups. This indicates that this property is verified even at a rate of 10^8 s^{-1} that is the Mössbauer frequency. The quadruple splitting (QS) and isomer shift (IS) parameters are gathered in Table 4 and Figure 5. The area ratio is slightly different from the expected 1:1 value, which can be explained by the well-known

dx.doi.org/10.1021/om400864q | Organometallics 2013, 32, 6136−6146

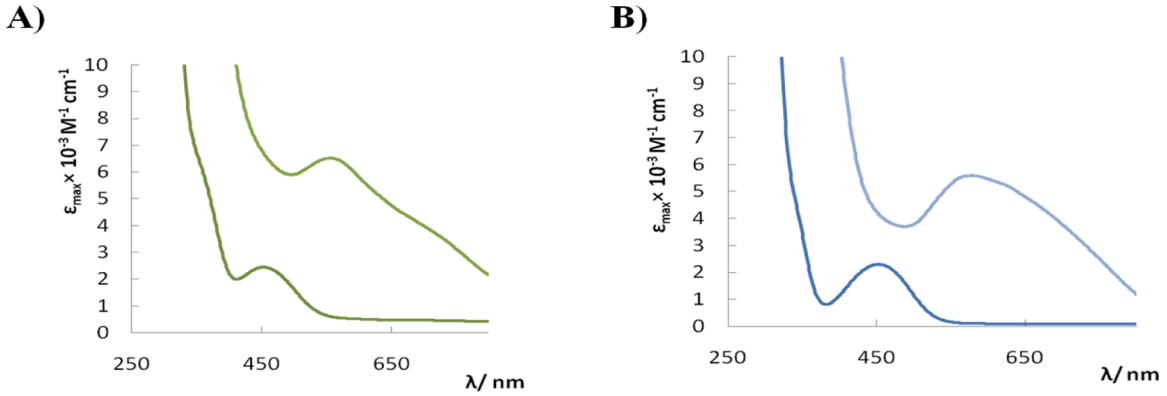

Figure 4. (A) Compared UV−vis spectra of **4** and **4**$(PF_6)_3$: λ_{max} of **4** = 454 nm (deep green); λ_{max} of **4**$(PF_6)_3$ = 555 nm (light green). (B) Compared UV−vis spectra of **4** and **4**$(BAr_4^F)_3$: λ_{max} of **4** = 454 nm (deep blue); λ_{max} of **4**$(BAr_4^F)_3$ = 565 nm (light blue).

Table 3. Wavelengths (in nm) of the UV−vis Transitions for All the Biferrocenyl Complexes and Their Mixed-Valent Fe^{II}−Fe^{III} States

compound	λ_{max} (nm)
4	454
4$(PF_6)_3$	555
4$(BAr_4^F)_3$	565
5	458
5$(BAr_4^F)_2$	564
7	458
7$(BAr_4^F)_4$	567
11	460
11(BAr_4^F)	572

different probabilities of the recoil free absorption of Fe(II) and Fe(III) centers.[28]

In agreement with the infrared spectra results presented above, there is no indication of any electron delocalization between the Fe^{II} and the Fe^{III} ions; thus, the biferrocenium complexes do not belong to the class III of mixed-valent complexes.

To distinguish between class-I and class-II mixed valency, recording near-infrared spectra is necessary in order to search the intervalent charge-transfer band that characterizes the optical transition from the ground state to the intervalence charge-transfer state of the class-II compounds. This band is already known for biferrocenium complexes. Analysis of the band energies, bandwidths, and intensities and the solvent effects on the band characteristics provides Hush[29] parameters that are gathered in Table 5 and the Supporting Information, allowing comparison of these new class-II mixed-valence complexes with known mixed-valence complexes.

Figure 6 shows the absorption spectra as a function of the energy in the near-IR region for the five mixed-valence compounds examined in this work in CD_3COCD_3. Deuterated solvents were used in order to reduce interference from the C−H overtone bands.[29] The observed bandwidth at half-height, $(\Delta\nu_{1/2})_{obs}$, is estimated by doubling the half-bandwidth at half-height on the high-energy side of ν_{max}.[30] The calculated bandwidth, $(\Delta\nu_{1/2})_{calcd}$, is calculated by the equation $\nu_{max} = (\Delta\nu_{1/2})^2/2310$. The values of the ratio $(\Delta\nu_{1/2})_{obs}/(\Delta\nu_{1/2})_{calcd}$ are 1.09−1.33 for **4**$(PF_6)_3$, **4**$(BAr_4^F)_3$, **5**$(BAr_4^F)_2$, **7**$(BAr_4^F)_4$, and **11**(BAr_4^F). For Robin and Day class-II complexes, values of 1.1−1.4 have so far been reported, confirming the class-II mixed valency of the new complexes.[30−32] The intercluster electronic coupling, H_{AB}, was estimated by the equation $H_{AB} = (2.05 \times 10^{-2})(\nu_{max}\varepsilon_{max}\Delta\nu_{1/2})^{1/2}/d$; the calculated values of the electronic coupling H_{AB} of a single biferrocenyl unit are comparable with the reported compounds that contained this unit (d = 5.5 ± 0.5 Å).[16a,33] The IVCT bands were also checked in CD_3CN for all the mixed-valence compounds in this work, and similar results were obtained (see the Supporting Information). The calculated results are in agreement with the infrared and Mössbauer results presented above.

CONCLUDING REMARKS

The synthesis of multiredox systems with biferrocenylethynyl units using Sonogashira and further copper-catalyzed coupling allows forming stable orange solid compounds containing up to eight ferrocenyl groups in compound **7**. The use of the biferrocenyl unit also brings about a large stabilization of mixed-valent biferrocenyl systems with various consequences. Indeed, the tetra(*n*-butyl)ammonium salt of the perfluorinated tetrakis-[(3,5-bistrifluoromethyl)phenyl] borate anion completely changes the cyclic voltammetry of the biferrocenylethynyl complexes in stabilizing mixed-valent compounds (large difference of redox potentials between the first and second cyclovoltammetry waves of the biferrocenyl units yielding large comproportionation constants) due to electrostatic effects that are not observed with the standard electrolyte [*n*-Bu_4N][PF_6]. This is the case of the tetranuclear mixed-valence tricationic salt

Table 4. Mössbauer Parameters for the Mixed-Valent Complexes 4$(PF_6)_3$, 5$(BAr_4^F)_2$, and 11(BAr_4^F)

	Fc		Fc^+		
compound	IS[a] (mm·s^{-1})	QS[a] (mm·s^{-1})	IS[a] (mm·s^{-1})	QS[a] (mm·s^{-1})	% (Fc^+/Fc)[a]
4$(PF_6)_3$	0.514(2)	2.229(3)	0.520(4)	0.495(8)	51/49
5$(BAr_4^F)_2$	0.524(3)	2.046(6)	0.505(9)		61/39
11(BAr_4^F)	0.530(1)	2.042(8)	0.505(9)		42/58

[a]IS = isomer shift vs Fe; QS = quadrupole splitting.

dx.doi.org/10.1021/om400864q | *Organometallics* 2013, 32, 6136−6146

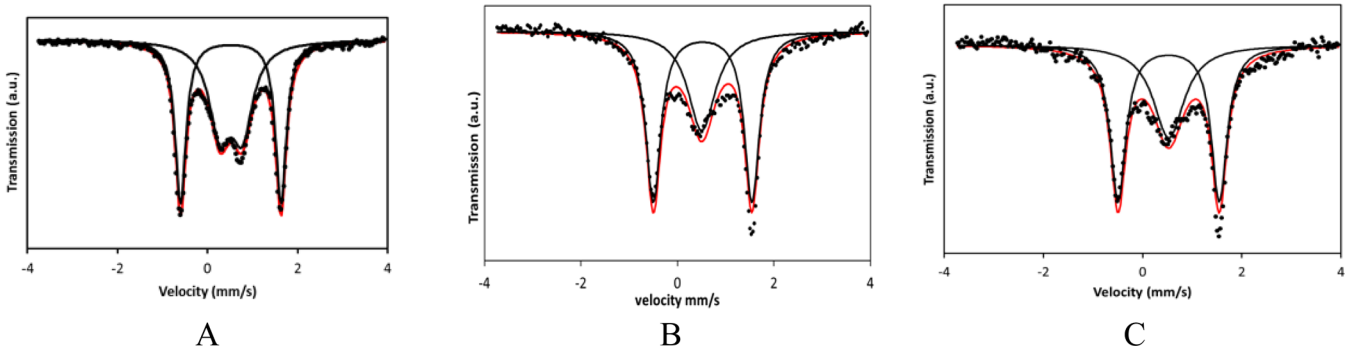

Figure 5. Mössbauer spectra of $4(PF_6)_3$ (A), $5(BAr_4^F)_2$ (B), and $11(BAr_4^F)$ (C) at zero field and 78 K.

Table 5. Properties of the Intervalent Charge-Transfer Band for $7(BAr_4^F)_4$ and $11(BAr_4^F)$[g]

compound	solvent	acetone-d_6
$7(BAr_4^F)_4$	λ_{max} (nm)[a]	1605
	ν_{max} (cm^{-1})[b]	6230
	$(\Delta\nu_{1/2})_{obs}$ (cm^{-1})[c]	4140
	$(\Delta\nu_{1/2})_{calcd}$ (cm^{-1})[d]	3794
	$(\Delta\nu_{1/2})_{obs}/(\Delta\nu_{1/2})_{calcd}$	1.09
	ε_{max} (M^{-1} cm^{-1})[e]	2036
	H_{AB} (cm^{-1})[f]	854
$11(BAr_4^F)$	λ_{max} (nm)[a]	1748
	ν_{max} (cm^{-1})[b]	5720
	$(\Delta\nu_{1/2})_{obs}$ (cm^{-1})[c]	4360
	$(\Delta\nu_{1/2})_{calcd}$ (cm^{-1})[d]	3634
	$(\Delta\nu_{1/2})_{obs}/(\Delta\nu_{1/2})_{calcd}$	1.20
	ε_{max} (M^{-1} cm^{-1})[e]	518
	H_{AB} (cm^{-1})[f]	424

[a] λ_{max}: wavelength of maximum absorbance for the IVCT band. [b] $\nu_{max} = E_{op}$: energy of the band at λ_{max}. [c] $(\Delta\nu_{1/2})_{obs}$: observed bandwidth at half-height. [d] $(\Delta\nu_{1/2})_{calcd}$: calculated bandwidth at half-height. [e] ε_{max}: the molar extinction coefficient at λ_{max}. [f] H_{AB}: the electronic coupling. [g] See the similar data for all mixed-valent complexes in the Supporting Information.

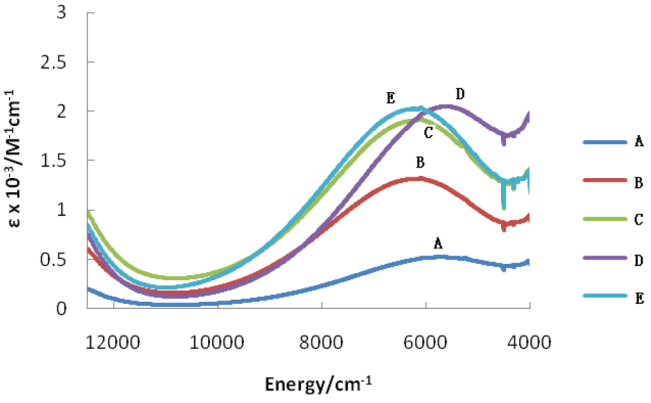

Figure 6. Near-IR spectra of $11(BAr_4^F)$ (A), $4(PF_6)_3$ (B), $4(BAr_4^F)_3$ (C), $5(BAr_4^F)_2$ (D), and $7(BAr_4^F)_4$ (E) in CD_3COCD_3.

5^{3+} and of the most highly charged mixed-valent polynuclear arene complexes. Except in this case of 5^{3+} for which relative stabilization is only provided by the perfluorinated counteranion, resulting in the electrostatic effect between diynyl-linked ferrocenyl units (the inner ones) belonging to two distinct biferrocenyl groups, all the arene-centered poly(biferrocenylethynyl) complexes present biferrocenyl groups that are independent by cyclic voltammetry (no wave separation). They are distinguished neither by electrostatic effect (unlike in 1,3,5-triferrocenyl benzene) nor by arene-mediated electronic communication (as in 1,3,5-triferrocenylbenzene),[12,13] and in contrast with the series of 1,3,5-tris(ethynylmetal)benzene complexes reported by the groups of Long and Zanello that present electronic communication between the three metals through the arene bridge.[14]

The poly(biferrocenylethynyl) systems are easier to oxidize than the parent poly(ferrocenylethynyl) complexes. Then the oxidized mixed-valence systems are very easily synthesized using a ferricinium salt as an oxidant, and the oxidized biferrocenium compounds are much more robust than ferricinium derivatives. The electron-withdrawing effect of the ethynyl and arylethynyl groups on ferrocene shown by the CV data allows easier direct oxidation of the nonethynylated ferrocenyl group than of the ethynylferrocenyl group in the ethynylbiferrocenyl complexes under study. All the oxidized BAr_4^F complexes are, as other previously reported biferrocenes, class-II mixed-valent. This was shown by the observation of both Fe^{II} and Fe^{III} Mössbauer and IR absorption in the mixed-valent compounds and that of the optical intervalence charge-transfer band in the near-IR spectra. Possible applications are the production of electrochrome nanosystems that are commutable at low potentials and robust in both solutions and condensed phases in two oxidation states with distinct colors.

EXPERIMENTAL SECTION

General Data. THF and diethyl ether were dried over Na foil and distilled from sodium-benzophenone anion under nitrogen immediately prior to use. DCM, *i*-Pr_2NH, and Et_3N were distilled from calcium hydride under nitrogen prior to use. All other solvents and chemicals were used as received. ^1H NMR spectra were recorded at 25 °C with a Bruker AC (200, 300 MHz) spectrometer. The ^{13}C NMR spectra were obtained in the pulsed FT mode at 75 MHz with a Bruker AC 300 spectrometer. All the chemical shifts are reported in parts per million (δ, ppm) with reference to Me_4Si for the ^1H and ^{13}C NMR spectra. The mass spectra were recorded using an Applied Biosystems Voyager-DE STR-MALDI-TOF spectrometer. The infrared spectra were recorded on an ATI Mattson Genesis series FT-IR spectrophotometer. The elemental analyses were performed by the Center of Microanalyses of the CNRS at Lyon Villeurbanne, France. UV−vis absorption spectra were measured with a PerkinElmer Lambda 19 UV−vis spectrometer. Electrochemical measurements (CV) were recorded on a PAR 273 potentiostat under a nitrogen atmosphere at 293 K. ^{57}Fe Mössbauer spectra have been recorded using a conventional constant-acceleration type spectrometer equipped with a 50 mCi ^{57}Co source and a flow-type liquid nitrogen cryostat. Least-squares fittings of the Mössbauer spectra have been carried out with

dx.doi.org/10.1021/om400864q | Organometallics 2013, 32, 6136−6146

the assumption of a Lorentzian line shape using the Recoil software package.

General Synthetic Procedure for the Complexes 2−5. The starting material ethynylbiferrocene,**1**, was synthesized according to ref 8. For the Sonogashira reaction, a catalytic amount of CuI (10 mg, 0.05 mmol, 0.25 equiv), $Pd(OAc)_2$ (11 mg, 0.05 mmol, 0.25 equiv), and PPh_3 (30 mg, 0.11 mmol, 0.5 equiv.) in 50 mL of diisopropylamine were stirred at 0 °C for 10 min. The mixture was then treated with ethynylbiferrocene (236.4 mg, 0.6 mmol, 3 equiv) and 1,3,5-tribromobenzene (63 mg, 0.2 mmol, 1 equiv) and stirred at 0 °C for 1 h before warming to r.t. Then the mixture was heated under reflux for 3 h. The solvent was removed under vacuum, the product was extracted with CH_2Cl_2, and diluted aq. HCl was added. The organic phase was washed three times with a saturated aqueous solution of Na_2CO_3 and H_2O, dried over anhydrous Na_2SO_4, and concentrated under vacuum. The crude orange mixture was separated by column chromatography on silica gel with pentane/CH_2Cl_2 (4:1) to provide each pure compound. Complex **2** (R_f = 0.9) was first eluted (34 mg, yield: 9% based on the conversion of ethynylbiferrocene), followed by compound **5** (67 mg, yield: 28%, R_f = 0.7), then compound **3** (26 mg, yield: 9%, R_f = 0.5), and finally compound **4** (125 mg, yield: 50%, R_f = 0.1).

1-Biferrocenylethynyl-3,5-dibromo Benzene 2. ^{1}H NMR (300 MHz, $CDCl_3$), δ ppm: 4.02 (s, 5H, free Cp), 4.13 (t, J = 1.89 Hz, 2H, CH of Cp), 4.20 (m, 2H, CH of Cp), 4.24 (t, J = 1.89 Hz, 2H, CH of Cp), 4.30 (t, J = 1.89 Hz, 2H, CH of Cp), 4.37 (t, J = 1.80 Hz, 2H, CH of Cp), 4.43 (m, 2H, CH of Cp), 7.48 (s, 2H, Ph), 7.58 (s, 1H, Ph), 7.26 (s, $CDCl_3$). ^{13}C NMR (75.0 MHz, $CDCl_3$), δ ppm: 64.8, 66.5, 67.9, 69.3, 69.6, 70.3, 71.3, 72.8, 82.0, 83.3 (C of the Bif.), 86.2, 91.7 (C≡C), 122.5 (Cq of aromatic-Br), 127.6 (Cq of aromatic-C≡C), 132.7, 132.9 (CH of aromatic), 76.6, 77.0, 77.5 ($CDCl_3$). IR (KBr): 2210 cm^{-1} ($\nu_{C\equiv C}$). UV−vis: λ_{max} = 450 nm (ε_{max} = 75 M^{-1} cm^{-1}). Cyclic voltammogram (3 mM, CH_2Cl_2; supporting electrolyte [n-Bu_4N][PF_6]; 293 K): working and counter electrodes: Pt; reference electrode: Ag; scan rate: 0.200 V·s^{-1}; two reversible waves: $E_{1/2}$ = 0.325 V (ΔE = 40 mV), 0.610 V (ΔE = 40 mV) vs $FeCp^*_2$. mp: 144 °C. MALDI-TOF: calcd m/z for M$^+$ ($C_{28}H_{20}Br_2Fe_2$) 627.9; found 627.7. Anal. Calcd for $C_{28}H_{20}Br_2Fe_2$: C, 53.55; H, 3.21. Found: C, 53.45; H, 3.01.

1,3-Bis(biferrocenylethynyl)-5-bromo Benzene 3. ^{1}H NMR (300 MHz, $CDCl_3$), δ ppm: 4.01 (s, 10H, free Cp), 4.14 (m, 4H, CH/sub.Cp), 4.19 (m, 4H, CH/sub.Cp), 4.31 (m, 8H, CH/sub.Cp), 4.41(m, 8H, CH/sub.Cp), 7.41 (s, 1H, Ph), 7.48 (s, 2H, Ph), 7.26 (s, $CDCl_3$). ^{13}C NMR (75.0 MHz, $CDCl_3$), δ ppm: 65.2, 66.6, 67.9, 68.0, 69.3 (free Cp), 69.6, 70.3, 72.7, 82.2, 84.1 (Cp), 86.0, 90.5 (C≡C), 121.6, 125.9, 132.6, 132.8 (Ph), 76.4, 77.0, 77.7 ($CDCl_3$). IR (KBr): 2216 cm^{-1} ($\nu_{C\equiv C}$). UV−vis: λ_{max} = 457 nm (ε_{max} = 155 M^{-1} cm^{-1}). Cyclic voltammogram (1.5 mM; CH_2Cl_2; supporting electrolyte [n-Bu_4N][PF_6]; 293 K): working and counter electrodes: Pt; reference electrode: Ag; scan rate: 0.200 V·s^{-1}; two reversible waves: $E_{1/2}$ = 0.473 V (ΔE = 20 mV), 0.850 V (ΔE = 20 mV) vs $FeCp^*_2$. mp: 177 °C. MALDI-TOF: calcd m/z for M$^+$ ($C_{50}H_{37}BrFe_4$) 941.1; found 939.6. Anal.Calcd for $C_{50}H_{37}BrFe_4$: C, 63.81; H, 3.96. Found: C, 63.66; H, 4.33.

1,3,5-Tris(biferrocenylethynyl) Benzene 4. ^{1}H NMR (300 MHz, $CDCl_3$), δ ppm: 4.05 (s, 15H, free Cp), 4.13 (m, 6H, C/sub.Cp), 4.28 (m, 12H, C/sub.Cp), 4.33 (m, 6H, C/sub.Cp), 4.40 (t, 6H, C/sub.Cp), 4.51(t, 6H, C/sub.Cp), 7.47 (s, 3H, Ph), 7.26 (s, $CDCl_3$), 5.30 (s, CH_2Cl_2). ^{13}C NMR (75.0 MHz, $CDCl_3$), δ ppm: 65.7, 66.6, 68.1, 68.3, 69.6, 69.7, 70.5, 70.6, 71.3 (C/Cp), 72.8 (free Cp), 84.9, 89.3 (C≡C), 124.4, 133.0 (Ph), 76.6, 77.0, 77.5 ($CDCl_3$). The IR (KBr): 2211 cm^{-1} ($\nu_{C\equiv C}$). The CV of **4** (CH_2Cl_2; supporting electrolyte [n-Bu_4N][BAr_4^F]; 293 K): two reversible waves: $E_{1/2}$ = 0.52 and 0.98 V vs $FeCp^*_2$. IR (KBr): 2211 cm^{-1} ($\nu_{C\equiv C}$), 814 cm^{-1} (ν_{Fc}). UV−vis: λ_{max} = 454 nm (ε_{max} = 230 M^{-1} cm^{-1}). Cyclic voltammogram (0.3 mM; CH_2Cl_2; supporting electrolyte [n-Bu_4N][PF_6]; 293 K): working and counter electrodes: Pt; reference electrode: Ag; scan rate: 0.200 V·s^{-1}; two reversible waves: $E_{1/2}$ = 0.465 V (ΔE = 30 mV), 0.870 V (ΔE = 20 mV) vs $FeCp^*_2$. When the supporting electrolyte [n-Bu_4N][BAr_4^F] 0.1 M was used under the identical conditions, the two reversible waves are at $E_{1/2}$ = 0.52 and 0.98 V vs $FeCp^*_2$. mp: 209 °C. MALDI-TOF: calcd m/z for M$^+$ ($C_{72}H_{54}Fe_6$) 1254.2; found 1254.8. Anal. Calcd for $C_{72}H_{54}Fe_6$(1/4CH_2Cl_2): C, 67.58; H, 4.26. Found: C, 67.65; H, 4.38.

Synthesis and Characterizations of 1,3,5-Tris(biferrocenylethynyl) Benzene(PF_6)$_3$, 4(PF_6)$_3$. The compound **4** (62.7 mg, 0.05 mmol, 1 equiv.) and ferricinium PF_6 (49.6 mg, 0.15 mmol, 3 equiv.) was mixed in 30 mL of distilled dichloromethane. The mixture was stirred at r.t. for 10 min under N_2. Then the solvent was removed under vacuum, and the solid that was left was washed three times with distilled pentane to give the **4**(PF_6)$_3$ as a brown solid (80.2 mg, yield: 95%). IR (KBr): 2210 cm^{-1} ($\nu_{C\equiv C}$), 832 cm^{-1} (ν_{PF6-}). UV−vis: λ_{max} = 555 nm (ε_{max} = 680 M^{-1} cm^{-1}). Melting point: decomposition above 200 °C. Anal. Calcd for $C_{72}H_{54}Fe_6P_3F_{18}$: C, 51.20; H, 3.22. Found: C, 51.40; H, 3.17.

Synthesis and Characterizations of 1,3,5-Tris(biferrocenylethynyl) Benzene(BAr_4^F)$_3$, 4(BAr_4^F)$_3$. The compound **4** (12.5 mg, 0.01 mmol, 1 equiv) and ferricinium (BAr_4^{F-}) (31.5 mg, 0.03 mmol, 3 equiv) were mixed in 30 mL of distilled CH_2Cl_2. The mixture was stirred at r.t. for 30 min under N_2. Then the solvent was removed under vacuum, and the solid that was left was washed three times with distilled pentane to give the compound **4**(BAr_4^F)$_3$ (36.5 mg, yield: 94%). IR (KBr): 2210 cm^{-1} ($\nu_{C\equiv C}$), 886 cm^{-1} (ν_{Fc}+), 836 cm^{-1} (ν_{Fc}). UV−vis: λ_{max} = 555 nm (ε_{max} = 600 M^{-1} cm^{-1}). mp: 150 °C. Anal. Calcd for $C_{168}H_{90}Fe_6F_{72}B_3(CH_2Cl_2)$: C, 51.66; H, 2.36. Found: C, 51.35; H, 2.66.

Bis(biferrocenylethynyl) 5. ^{1}H NMR (300 MHz, $CDCl_3$), δ ppm: 4.06 (s, 10H/free Cp), 4.08 (m, 4H/sub.Cp), 4.28 (m, 4H/sub.Cp), 4.32 (m, 8H/sub.Cp), 4.39 (m, 4H/sub.Cp), 4.51 (m, 4H, sub.Cp), 5.30 (s, CH_2Cl_2), 1.53 (H_2O), 7.26 (s, $CDCl_3$). ^{13}C NMR (75.0 MHz, $CDCl_3$), δ ppm: 66.5, 66.6, 68.0, 68.2, 69.3, 69.6, 69.9, 70.2, 70.6, 73.3 (Cp), 78.9 (C≡C), 76.4, 77.0, 77.7 ($CDCl_3$). CV (0.5 mM) in CH_2Cl_2; supporting electrolyte [n-Bu_4N][BAr_4^F]; working and counter electrodes: Pt; reference electrode: Ag; scan rate: 0.200 V·s^{-1}; 293 K; three reversible waves: $E_{1/2}$ = 0.52, 1.20, and 1.40 V vs $FeCp_2$*. CV (0.5 mM) in CH_2Cl_2; supporting electrolyte: [n-Bu_4N][PF_6]; 293 K; working and counter electrodes: Pt; reference electrode: Ag; scan rate: 0.200 V·s^{-1}; two reversible waves: $E_{1/2}$ = 475 mV (ΔE = 40 mV) and 0.930 V (ΔE = 80 mV) vs $FeCp^*_2$. The IR (KBr): 2142 cm^{-1} ($\nu_{C\equiv C}$), 814 cm^{-1}(ν_{Fc}). UV−vis: λ_{max} = 458 nm (ε_{max} = 155 M^{-1} cm^{-1}). mp: 224 °C. MALDI-TOF: calcd m/z for M$^+$ ($C_{44}H_{34}Fe_4$) 786.0; found 785.9. Anal. Calcd for $C_{44}H_{34}Fe_4(H_2O)$: C, 65.72; H, 4.51. Found: C, 65.42; H, 4.54.

Synthesis and Characterizations of [1,4-Bis(biferrocenyl)-butadiyne](BAr_4^F)$_2$, 5(BAr_4^F)$_2$. Compound **5** (39.3 mg, 0.05 mmol, 1 equiv) and [$FeCp_2$][BAr_4^F] (104.9 mg, 0.1 mmol, 2 equiv) were dissolved in 10 mL of distilled CH_2Cl_2. Then the mixture was stirred at r.t. for 30 min under N_2. The solvent was removed under vacuum, and the solid that was left was washed three times with distilled pentane. The mixed-valence compound **5**(BAr_4^{F-})$_2$ was obtained as a brown solid (119.3 mg, yield: 96%). IR (KBr): 2211 cm^{-1} ($\nu_{C\equiv C}$), 887 cm^{-1} (ν_{Fc}^+), 838 cm^{-1} (ν_{Fc}). UV−vis: λ_{max} = 564 nm (ε_{max} = 480 M^{-1} cm^{-1}). mp: 160 °C. Anal. Calcd for $C_{108}H_{58}Fe_4F_{48}B_2$ (CH_2Cl_2): C, 50.40; H, 2.33. Found: C, 50.61; H, 2.52.

Synthesis and Characterizations of 1-Ethynyl-3,5-di(biferrocenylethynyl) Benzene, 6. $Pd(PPh_3)Cl_2$ (7 mg, 0.01 mmol, 0.1 equiv) and CuI (3.8 mg, 0.02 mmol, 0.2 equiv) were dissolved in 5 mL of distilled Et_3N. Then compound **3** (94.2 mg, 0.1 mmol) was added to the mixture. The solution was stirred at 50 °C for 10 min under N_2 before trimethylsilylacetylene (30 μL, 0.2 mmol) was added. Then the mixture was stirred at 50 °C for 2 days. The same amount of $Pd(PPh_3)Cl_2$ (7 mg, 0.01 mmol, 0.1 equiv) and CuI (3.8 mg, 0.02 mmol, 0.2 equiv) was added. Then the mixture was stirred at 50 °C under N_2 for another 5 days. After the solvent was evaporated, the crude reaction mixture was purified by silica gel flash chromatography with dichloromethane/pentane (1/4, R_f = 0.5). After concentration, the intermediate compound was dissolved in THF/CH_3OH (5 mL/5 mL). Then K_2CO_3 (166 mg, 1.2 mmol, 6 equiv) was added. The mixture was stirred at r.t. for 30 min, the reaction mixture was quenched with a saturated ammonium chloride solution, and the

product was extracted three times with dichloromethane. The combined organic layer was dried over anhydrous Na_2SO_4. The solvent was removed under vacuum to give compound **6** (53 mg, yield: 60%). ^{1}H NMR (300 MHz, $CDCl_3$), δ ppm: 3.12 (s, 1H, C≡C−H), 4.02 (s, 10H/free Cp), 4.12 (m, 4H, CH/sub.Cp), 4.21 (m, 4H, CH/sub.Cp), 4.28 (m, 4H, CH/sub.Cp), 4.31 (m, 4H, CH/sub.Cp), 4.40 (m, 4H, CH/sub.Cp), 4.45 (m, 4H, CH/sub.Cp), 5.30 (s, CH_2Cl_2), 7.48 (s, 3H, Ph), 7.26 (s, $CDCl_3$). ^{13}C NMR (75.0 MHz, $CDCl_3$), δ ppm: 65.4, 66.6, 67.9, 68.1, 69.2, 69.6, 70.2, 72.7, (C/sub.Cp), 77.9, 82.4 (C≡C−H), 82.3, 84.5 (CH/sub.Cp), 86.0, 89.7 (C≡C), 122.4 (Cq of aromatic −C≡C−H), 124.7 (Cq of aromatic-C≡C−), 133.5, 134.3 (CH of aromatic), 76.6, 77.0, 77.4 ($CDCl_3$). IR (KBr): 2211 cm^{-1} ($\nu_{C\equiv C}$), 3293 cm^{-1} ($\nu_{\equiv C-H}$). UV−vis: λ_{max} = 454 nm (ε_{max} = 155 M^{-1} cm^{-1}). CV (1.5 mM; CH_2Cl_2; supporting electrolyte [*n*-Bu_4N][PF_6]; 293 K): working and counter electrodes: Pt; reference electrode: Ag; scan rate: 0.200 V·s^{-1}; two reversible waves: $E_{1/2}$ = 395 mV (ΔE = 10 mV), 0.730 V (ΔE = 20 mV) vs $FeCp^*_2$. mp: 177 °C. MALDI-TOF: calcd *m*/*z* for M$^+$ ($C_{52}H_{38}Fe_4$) 886.2; found 885.8. Anal. Calcd for $C_{52}H_{38}Fe_4$: C, 70.47; H, 4.32. Found: C, 70.60; H, 4.22.

Synthesis and Characterizations of Bis{1,3-Di(biferrocenylethynyl)-5-ethynyl Benzene}, 7. Compound **6** (45 mg, 0.05 mmol) was dissolved in 2 mL of distilled Et_3N. Then the catalyst $CuCl_2$ (2 mg, 0.015 mmol, 30% equiv) was added into the solution. The mixture was stirred overnight at 100 °C under N_2, then the solvent was removed under vacuum, and a diluted HCl solution and dichloromethane were added to the solid that was left. After separation, the organic phase was washed three times with distilled H_2O. Then the organic phase was dried over anhydrous Na_2SO_4. The crude product was purified through silica gel flash chromatography with dichloromethane/pentane (1/4, R_f = 0.4). After concentration, compound **7** was obtained (27 mg, yield: 60%). ^{1}H NMR (200 MHz, $CDCl_3$), δ ppm: 4.03 (s, 20H, free Cp), 4.13 (m, 8H, CH/sub.Cp), 4.23 (m, 8H, CH/sub.Cp), 4.28 (m, 8H, CH/sub.Cp), 4.32 (m, 8H, CH/sub.Cp), 4.40 (m, 8H, CH/sub.Cp), 4.46 (m, 8H, CH/sub.Cp), 7.52 (s, 6H, Ph), 7.26 (s, $CDCl_3$). ^{13}C NMR (75.0 MHz, $CDCl_3$), δ ppm: 65.4, 66.6, 68.0, 68.1 (C/sub.Cp), 69.4 (free Cp), 69.6, 70.3, 71.3, 72.8, 74.5 (C/sub.Cp), 82.7, 84.4 (C≡C), 86.2, 90.15 (C≡C), 122.0, 125.0, 133.8, 134.8 (C/Ph), 76.6, 77.0, 77.5 ($CDCl_3$). IR (KBr): 2209 cm^{-1} ($\nu_{C\equiv C}$). UV−vis: λ_{max} = 454 nm (ε_{max} = 335 M^{-1} cm^{-1}). CV (1.5 mM; CH_2Cl_2; supporting electrolyte [*n*-Bu_4N][PF_6]; 293 K): working and counter electrodes: Pt; reference electrode: Ag; scan rate: 0.200 V·s^{-1}; two reversible waves: $E_{1/2}$ = 470 mV (ΔE = 35 mV), 0.837 V (ΔE = 10 mV) vs $FeCp^*_2$. mp: 195 °C. The MALDI-TOF: calcd *m*/*z* for M$^+$ ($C_{104}H_{74}Fe_8$) 1771.1; found 1770.8. Anal. Calcd for $C_{104}H_{78}Fe_8 \cdot (H_2O)_2$: C, 69.15; H, 4.35. Found: C, 69.16; H, 4.44.

Synthesis and Characterizations of [Bis{1,3-di(biferrocenylethynyl)-5-ethynyl Benzene}](BAr$_4^F$)$_4$, 7(BAr$_4^F$)$_4$. Compound **7** (17.7 mg, 0.01 mmol, 1 equiv) and [$FeCp_2$][BAr_4^F] (40.2 mg, 0.04 mmol, 4 equiv) were dissolved in 10 mL of distilled CH_2Cl_2. Then the mixture was stirred at r.t. during 30 min under N_2, the solvent was removed under vacuum, and the solid that was left was washed three times with distilled pentane. Then the compound **7**(BAr_4^F)$_4$ was obtained as a brown solid (49.6 mg, yield: 93%). IR (KBr): 2216 cm^{-1} ($\nu_{C\equiv C}$), 886 cm^{-1} (ν_{Fc^*}), 838 cm^{-1} (ν_{Fc}). UV−vis: λ_{max} = 567 nm (ε_{max} = 850 M^{-1} cm^{-1}). mp: 150 °C. Anal. Calcd for $C_{232}H_{122}Fe_8F_{96}B_4$: C, 53.35; H, 2.35. Found: C, 53.05; H, 2.38.

Synthesis of Biferrocenium(BAr$_4^F$), 11(BAr$_4^F$). Biferrocene (37.0 mg, 0.1 mmol, 1equiv) and [$FeCp_2$](BAr_4^F) (104.9 mg, 0.1 mmol, 1 equiv) were dissolved in 10 mL of distilled CH_2Cl_2. Then the mixture was stirred at r.t. during 30 min under N_2. The solvent was removed under vacuum, and the solid that was left was washed three times with distilled pentane. Then biferrocenium(BAr_4^F) was obtained as a brown solid (117.1 mg; yield: 95%). IR (KBr): 886 cm^{-1} (ν_{Fc}+), 836 cm^{-1} (ν_{Fc}). UV−vis spectrum of **11**(BAr_4^F): λ_{max} = 572 nm (ε_{max} = 235 M^{-1} cm^{-1}). mp: 140 °C. Anal. Calcd for $C_{52}H_{30}Fe_2F_{24}B(1/2CH_2Cl_2)$: C, 49.43; H, 2.45. Found: C, 49.51; H, 2.67.

■ ASSOCIATED CONTENT

Ⓢ Supporting Information

Spectra for all the new complexes and properties of the intervalence charge-transfer band for all the new mixed-valent complexes (43 pages). This material is available free of charge via the Internet at http://pubs.acs.org.

■ AUTHOR INFORMATION

Corresponding Author

*E-mail: d.astruc@ism.u-bordeaux1.fr.

Notes

The authors declare no competing financial interest.

■ ACKNOWLEDGMENTS

Financial support from the China Scholarship Council (CSC) from the People's Republic of China (Ph.D. grant to Y.W.), The Université Bordeaux 1, the Centre National de la Recherche Scientifique (CNRS), and the Agence Nationale de la Recherche (ANR) is gratefully acknowledged.

■ REFERENCES

(1) (a) Cotton, F. A.; Wilkinson, G. *J. Am. Chem. Soc.* **1952**, *74*, 3458. (b) Connelly, N. J.; Geiger, W. E. *Chem. Rev.* **1996**, *96*, 877. (c) Nishihara, H. *Adv. Inorg. Chem.* **2002**, *53*, 41. (d) Geiger, W. E. *Organometallics* **2007**, *26*, 5738.

(2) (a) Abakumova, L. G.; Abakumov, G. A.; Razuvaev, G. A. *Dokl. Akad. Nauk SSSR* **1975**, *220*, 1317. (b) Huang, W. H.; Jwo, J. J. *J. Chin. Chem. Soc.* **1991**, *38*, 343. (c) Zotti, G.; Schiavon, G.; Zecchin, S.; Berlin, A.; Pagani, G. *Langmuir* **1998**, *14*, 1728. (d) Hurvois, J.; Moinet, C. *J. Organomet. Chem.* **2005**, *690*, 1829.

(3) (a) Newkome, G. R.; He, E.; Moorefield, C. N. *Chem. Rev.* **1999**, *99*, 1689. (b) Nguyen, P.; Gomez-Elipe, P.; Manners, I. *Chem. Rev.* **1999**, *99*, 1515. (c) Eloi, J. C.; Chabanne, L.; Whittell, G. R.; Manners, I. *Mater. Today* **2008**, *11*, 28. (d) Martinez, F. J.; Gonzalez, B.; Alonso, B.; Losada, J.; Garcia-Armada, M. P.; Casado, C. M. *J. Inorg. Organomet. Polym. Mater.* **2008**, *18*, 51. (e) For electrochemical studies of multiferrocenyl oligomers and polymers, see: Rulkens, R.; Lough, A.-J.; Manners, I.; Lovelace, S. R.; Grant, C.; Geiger, W. E. *J. Am. Chem. Soc.* **1996**, *118*, 12683.

(4) (a) Cowan, D. O.; Kaufman, F. *J. Am. Chem. Soc.* **1970**, *92*, 219. (b) Cowan, D. O.; Kaufman, F. *J. Am. Chem. Soc.* **1971**, *93*, 3889. (c) Levanda, C.; Cowan, D. O.; Bechgaard, K. *J. Am. Chem. Soc.* **1975**, *97*, 1980.

(5) (a) Robin, M. B.; Melvin, B.; Day, P. *Adv. Inorg. Chem. Radiochem.* **1967**, *10*, 247. (b) Allen, G. C.; Hush, N. S. *Prog. Inorg. Chem.* **1967**, *8*, 357. (c) Richardson, D. E.; Taube, H. *Coord. Chem. Rev.* **1984**, *60*, 107.

(6) (a) Horikoshi, T.; Itoh, M.; Kurihara, M.; Kubo, K.; Nishihara, H. *J. Electroanal. Chem.* **1999**, *473*, 113. (b) Nishihara, H. *Bull. Soc. Chem. Jpn* **2001**, *74*, 19. (c) Yamada, M.; Nishihara, H. *Chem. Commun.* **2002**, 2578. (d) Yamada, M.; Nishihara, H. *Eur. Phys. J. D* **2003**, *24*, 257. (e) Yamada, M.; Nishihara, H. *Langmuir* **2003**, *19*, 8050. (f) Yamada, M.; Nishihara, H. *ChemPhysChem* **2004**, *5*, 555. (g) Yamada, M.; Tadera, T.; Kubo, K.; Nishihara, H. *J. Phys. Chem. B* **2003**, *107*, 3703. (h) Muraa, M.; Nishihara, H. *J. Inorg. Organomet. Polym. Mater.* **2005**, *15*, 147.

(7) Nijhuis, C. A.; Dolatowska, K. A.; Jan Ravoo, B.; Huskens, J.; Reinhoudt, D. N. *Chem.—Eur. J.* **2007**, *13*, 69.

(8) Djeda, R.; Rapakousiou, A.; Liang, L.; Guidolin, N.; Ruiz, J.; Astruc, D. *Angew. Chem., Int. Ed.* **2010**, *49*, 8152.

(9) (a) Morrison, W. H.; Krogsrud, S.; Hendrickson, D. N. *Inorg. Chem.* **1973**, *12*, 1998. (b) Levanda, C.; Cowan, D. O.; Beechgaard, K. *J. Am. Chem. Soc.* **1975**, *97*, 1980. (c) Dong, T. Y.; Hendrickson, D. N.; Iwai, K.; Cohn, M. J.; Geib, S. J.; Rheingold, A. L.; Sano, H.; Motoyama, I.; Nakashima, S. *J. Am. Chem. Soc.* **1985**, *107*, 7996. (d) McManis, G. E.; Gochev, A.; Nielson, R. M.; Weaver, M. J. *J. Phys.*

Chem. **1989**, *93*, 7733. (e) Nakashima, S.; Sano, H. *Hyperfine Interact.* **1990**, *53*, 367. (f) Astruc, D. *Acc. Chem. Res.* **1997**, *30*, 383.
(10) (a) Spescha, M.; Duffy, N. W.; Robinson, B. H.; Simpson, J. *Organometallics* **1994**, *13*, 4895. (b) Colbert, M. C. B.; Hodgson, D.; Lewis, J.; Raithby, P. R.; Long, N. J. *Polyhedron* **1995**, *14*, 2759. (c) Duan, C. Y.; Tian, Y. P.; Liu, Z. H.; You, X. Z.; Mak, T. C. W. *J. Organomet. Chem.* **1998**, *570*, 155. (d) Wang, X. Y.; Deng, Z. X.; Jin, B. K.; Tian, Y. P.; Lin, X. Q. *Electrochim. Acta* **2002**, *47*, 1537. (e) Dong, T. Y.; Shih, H. W.; Chang, L. S. *Langmuir* **2004**, *20*, 9340. (f) Han, L. M.; Hu, Y. Q.; Suo, Q. L.; Luo, M. H.; Weng, L. H. *J. Coord. Chem.* **2010**, *63*, 600.
(11) (a) Camine, N.; Mueller-Westerhoff, U. T.; Geiger, W. E. *J. Organomet. Chem.* **2001**, *637*, 823. (b) Le Suer, R. J.; Geiger, W. E. *Angew. Chem., Int. Ed.* **2000**, *39*, 248. (c) Barrière, F.; Camine, N.; Geiger, W. E. *J. Am. Chem. Soc.* **2002**, *124*, 7262. (d) Barrière, F.; Geiger, W. E. *J. Am. Chem. Soc.* **2006**, *128*, 3980. (e) Barrière, F.; Kirss, R. U.; Geiger, W. E. *Organometallics* **2005**, *24*, 48. (f) Barrière, F.; Geiger, W. E. *Acc. Chem. Res.* **2010**, *43*, 1030.
(12) (a) Fink, H.; Long, N. J.; Martin, A. J.; Opromolla, G.; White, A. J. P.; Williams, D. J.; Zanello, P. *Organometallics* **1997**, *16*, 2646. (b) Jutzi, P.; Kleinebekel, B. *J. Organomet. Chem.* **1997**, *545*−*546*, 573. (c) Li, Y. C.; Tsang, E. M. W.; Chan, A. Y. C.; Yu, H. Z. *Electrochem. Commun.* **2006**, *8*, 951.
(13) (a) Diallo, A. K.; Daran, J.-C.; Varret, F.; Ruiz, J.; Astruc, D. *Angew. Chem., Int. Ed.* **2009**, *48*, 3141. (b) Diallo, A. K.; Absalon, C.; Ruiz, J.; Astruc, D. *J. Am. Chem. Soc.* **2011**, *133*, 629. (c) Astruc, D. *Nat. Chem.* **2012**, *4*, 255.
(14) (a) Long, N. J.; Martin, A. J.; de Biani, F. F.; Zanello, P. *J. Chem. Soc., Dalton Trans.* **1998**, 2017. (b) Long, N. J.; Martin, A. J.; White, A. J. P.; Williams, D. J.; Fontani, M.; Laschi, F.; Zanello, P. *J. Chem. Soc., Dalton Trans.* **2000**, 3387.
(15) (a) Lohan, M.; Justaud, F.; Lang, H.; Lapinte, C. *Organometallics* **2012**, *31*, 3565. (b) Lohan, M.; Justaud, F.; Roisnel, T.; Ecorchard, P.; Lang, H.; Lapinte, C. *Organometallics* **2010**, *29*, 4804. (c) Loban, M.; Ecorchard, P.; Ruffer, T.; Justaud, F.; Lapinte, C.; Lang, H. *Organometallics* **2009**, *28*, 1878.
(16) (a) Siebler, D.; Förster, C.; Gasi, T.; Heinze, K. *Organometallics* **2011**, *30*, 313. (b) Siebler, D.; Linseis, M.; Gasi, T.; Carrella, L. M.; Winter, R. F.; Förster, C.; Heinze, K. *Chem.—Eur. J.* **2011**, *17*, 4540. (c) Siebler, D.; Förster, C.; Heinze, K. *Dalton Trans.* **2011**, *40*, 3558.
(17) (a) Xu, Z.; Moore, J. S. *Angew. Chem., Int. Ed. Engl.* **1993**, *32*, 246. (b) Bhyrappa, P.; Young, J. K.; Moore, J. S.; Suslick, K. S. *J. Am. Chem. Soc.* **1996**, *118*, 5708. (c) Moore, J. S. *Acc. Chem. Res.* **1997**, *30*, 402. (d) Green, K. A.; Cifuentes, M. P.; Samoc, M.; Humphrey, M. G. *Coord. Chem. Rev.* **2011**, *255*, 2025−2530. (e) Green, K. A.; Simpson, P. V.; Corkerey, T. C.; Cifuentes, M. P.; Samoc, M.; Humphrey, M. G. *Macromol. Rapid Commun.* **2012**, *33*, 573.
(18) (a) Ochi, Y.; Suzuki, M.; Imaoka, T.; Murata, M.; Nishihara, H.; Einaga, Y.; Yamamoto, K. *J. Am. Chem. Soc.* **2010**, *132*, 5061. (b) Xie, R. J.; Han, L. M.; Zhu, N.; Hong, H. L.; Suo, Q. L.; Qe, C. L. *Asian J. Chem.* **2013**, *25*, 197.
(19) (a) Breuer, R.; Schmittel, M. *Organometallics* **2012**, *31*, 1870. (b) Breuer, R.; Schmittel, M. *Organometallics* **2013**, DOI: 10.1021/om400502e.
(20) (a) Sonogashira, K.; Tohda, Y.; Hagihara, N. *Tetrahedron* **1975**, *16*, 4467. (b) Chinchilla, R.; Najera, C. *Chem. Rev.* **2007**, *107*, 874.
(21) Ruiz, J.; Astruc, D. *C. R. Acad. Sci., Ser. IIc: Chim.* **1998**, *1*, 21.
(22) Dong, T. Y.; Ke, T. J.; Peng, S. M.; Yeh, S. K. *Inorg. Chem.* **1989**, *28*, 2103.
(23) Kramer, J. A.; Hendrickson, D. N. *Inorg. Chem.* **1980**, *19*, 3330.
(24) Dong, T. Y.; Cohn, M. J.; Hendrickson, D. N.; Pierpont, C. G. *J. Am. Chem. Soc.* **1985**, *107*, 4777.
(25) Dong, T. Y.; Schei, C. C.; Hwang, M. Y.; Lee, T. Y.; Yeh, S. K.; Wen, Y. S. *Organometallics* **1992**, *11*, 573.
(26) Dong, T. Y.; Kambara, T.; Hendrickson, D. N. *J. Am. Chem. Soc.* **1986**, *108*, 4423.
(27) Fellows, E. A.; Keene, F. R. *J. Chem. Phys.* **2007**, *111*, 6667.
(28) (a) Greenwood, N. N.; Gibb, T. C. *Mössbauer Spectroscopy*; Chapmann and Hall: London, 1971. (b) Abraham, M.; Klauß, H. H.; Wagener, W.; Litterst, F. J.; Hofmann, A.; Herberhold, M. *Hyperfine Interact.* **1999**, *120*−*121*, 253.
(29) Hush, N. S. *Prog. Inorg. Chem.* **1967**, *8*, 391.
(30) Powers, M. J.; Meyer, T. J. *J. Am. Chem. Soc.* **1978**, *100*, 4393.
(31) Powers, M. J.; Meyer, T. J. *Inorg. Chem.* **1978**, *17*, 2955.
(32) Colbran, S. B.; Robinson, B. H.; Simpson, J. *Organometallics* **1983**, *2*, 952.
(33) Dong, T. Y.; Lee, T. Y.; Lee, S. H.; Lee, G. H.; Peng, S. M. *Organometallics* **1994**, *13*, 2337.

Inorganic Chemistry

Article

pubs.acs.org/IC

Stabilization of AuNPs by Monofunctional Triazole Linked to Ferrocene, Ferricenium, or Coumarin and Applications to Synthesis, Sensing, and Catalysis

Na Li,[†] Pengxiang Zhao,[†,‡] María E. Igartua,[§] Amalia Rapakousiou,[†] Lionel Salmon,[⊥] Sergio Moya,[§] Jaime Ruiz,[†] and Didier Astruc*[,†]

[†]ISM, Univ. Bordeaux, 351 Cours de la Libération, 33405 Talence Cedex, France

[‡]Science and Technology on Surface Physics and Chemistry Laboratory, P.O. Box 718-35, Mianyang 621907, Sichuan, China

[§]CIC biomaGUNE, Unidad Biosuperficies, Paseo Miramónn 182, Edif. "C", 20009 Donostia-San Sebastián, Spain

[⊥]LCC, CNRS, 205 Route de Narbonne, 31077 Toulouse Cedex, France

Supporting Information

ABSTRACT: Monofunctional triazoles linked to ferrocene, ferricenium, or coumarin (Cou), easily synthesized by copper-catalyzed azide alkyne (CuAAC) "click" reactions between the corresponding functional azides and (trimethylsilyl)acetylene followed by silyl group deprotection, provide a variety of convenient neutral ligands for the stabilization of functional gold nanoparticles (AuNPs) in polar organic solvents. These triazole (trz)-AuNPs are very useful toward a variety of applications to synthesis, sensing, and catalysis. Both ferrocenyl (Fc) and isostructural ferricenium linked triazoles give rise to AuNP stabilization, although by different synthetic routes. Indeed, the first direct synthesis and stabilization of AuNPs by ferricenium are obtained by the reduction of $HAuCl_4$ upon reaction with a ferrocene derivative, AuNP stabilization resulting from a synergy between electrostatic and coordination effects. The ferricenium/ferrocene trz-AuNP redox couple is fully reversible, as shown by cyclic voltammograms that were recorded with both redox forms. These trz-AuNPs are stable for weeks in various polar solvents, but at the same time, the advantage of trz-AuNPs is the easy substitution of neutral trz ligands by thiols and other ligands, giving rise to applications. Indeed, this ligand substitution of trz at the AuNP surface yields a stable Fc-terminated nanogold-cored dendrimer upon reaction with a Fc-terminated thiol dendron, substitution of Cou-linked trz with cysteine, homocysteine, and glutathione provides remarkably efficient biothiol sensing, and a ferricenium-linked trz-AuNP catalyst is effective for $NaBH_4$ reduction of 4-nitrophenol to 4-aminophenol. In this catalytic example, the additional electrostatic AuNP stabilization modulates the reaction rate and induction time.

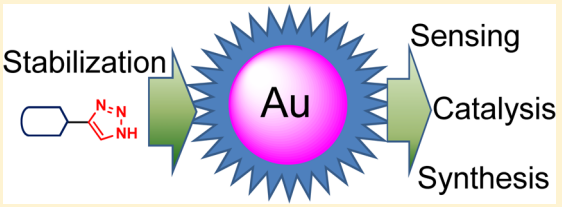

INTRODUCTION

In the past few decades, a variety of ligands[1−9] have been synthesized and used to stabilize gold nanoparticles (AuNPs)[9] either in organic solvents or in water. The surface properties, including the ligand type, binding force of gold with other atoms, as well as ligand coverage of AuNPs, control the solubility, stability, and applications of AuNPs. For example, in thiolate-stabilized AuNPs, covalent bonding between the gold and sulfur atoms contributes to passivation of the surface of thiolate-stabilized AuNPs and makes AuNPs stable in the solid state,[1] whereas citrate-stabilized AuNPs were usually prepared in aqueous solution because of the multipackage of ionic species on the AuNP surface.[2] In addition, the influence of the surface properties of AuNPs was also observed in several examples on the coordination-induced stabilization of AuNPs with nitrogen donors, particularly dendritic supramolecules.[9] Indeed, poly(amidoamine) dendrimers show significant template effects in the formation of nanoparticles in various solvents.[3] Copper-catalyzed azide alkyne (CuAAC) "click" chemistry has generated supermolecules,[4] such as poly(ethylene glycol) (PEG)-terminated dendrimers and polymers,[5] also stabilizing AuNPs in aqueous solution.[6] Besides, other nitrogen ligands, such as imidazoles[7] and pyridines,[8] have also been utilized for the stabilization of AuNPs.[9] The dual property of triazole-AuNPs (trz-AuNPs) that, on the one hand, are stable and, on the other hand, have modest AuNP−N bond strength, allowing facile ligand substitution of triazoles by other ligands for various applications, makes this family of AuNPs particularly attractive. Indeed, upon trz ligand substitution, it is possible to synthesize various other liganded AuNPs, to use the ligand-exchange processes for sensing and to provide catalytically efficient AuNP surfaces.[10] Stabilization and uses of water-soluble PEGylated trz-AuNPs have recently been shown.[11] Here we focus on the stabilization of trz-AuNPs linked to ferrocene,[12,13] ferricenium, and coumarin (Cou) termini using these monofunctional trz-AuNPs that are not synthesized in water and are soluble in organic solvents.

Received: September 3, 2014

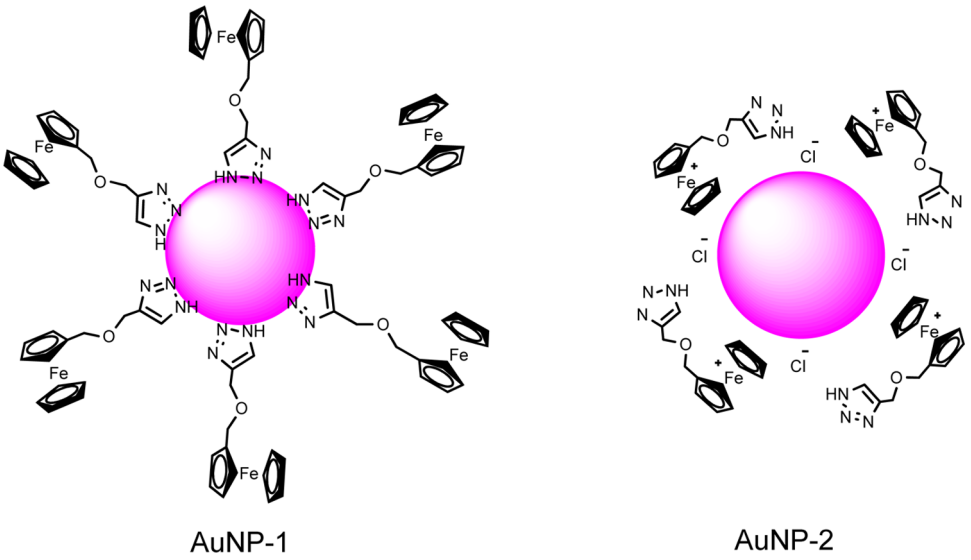

Figure 1. AuNPs stabilized by Fc-trz (**AuNP-1**) or oxidized Fc^{+}-trz-Cl^{-} (**AuNP-2**) in an organic solution.

For applications, ferrocenes have attracted attention because of the sensing and biomedical applications of the ferrocenyl (Fc) derivatives related to their reversible redox properties.[14] Catalytic properties will also be shown to result from fast triazole removal by substrates at the AuNP surface. Indeed, noble-metal nanoparticles,[15] in particular AuNPs, are excellent catalysts for the reduction of 4-nitrophenol (4-NP), which is toxic and inhibitory in nature, in order to produce 4-aminophenol (4-AP), which has properties and applications such as corrosion inhibitor, dying agent, and, in particular, intermediate for the synthesis of paracetamol.[16] Finally, Cou is a well-known fluorescent dye[17] that are linking to triazole-AuNPs for the investigation of fluorescent-sensing properties based on AuNP ligand substitution by biologically relevant thiols. Indeed, the thiols cysteine (Cys), homocysteine (Hcy), and glutathione (GSH) play key roles in the biological systems.[18] Many diseases are relevant to the abnormal contents of Cys or Hcy in the human body. For instance, an abnormal level of Cys may cause skin lesions and liver damage.[19] Furthermore, Hcy is a risk factor for Alzheimer's and cardiovascular diseases.[20] Excess Cys has been associated with neurotoxicity and many other diseases.[21] Accordingly, the development of chemosensors for biological thiol derivatives (biothiols) is of great importance, as recently indicated.[22] Sensing biological thiols using the fluorescence "turn-on" method on the surface of AuNPs results from either the formation of new fluorescent species or the release of dye adsorbed on the AuNPs, as recently reported.[23]

RESULTS AND DISCUSSION

In order to easily incorporate the redox complex and other functionalities into AuNPs in an organic solution, two kinds of small monosubstituted triazole molecules, Fc-trz and Cou-trz, were synthesized, taking into account their electrochemical or photochemical properties. Each functional unit was linked to the trz ring by an ether group that increased the flexibility of the trz ligand to make sure that the triazoles smoothly arrange on the surface of AuNPs.

Ferrocene- and Ferricenium-Triazole-Stabilized AuNPs. Late-transition-metal sandwich complexes are known for their stability in several oxidation states and their ability to effect efficient stoichiometric and catalytic electron-transfer processes[24] for multiple applications.[25,26] They are also rather easy to functionalize on the ligands,[25] and thus the introduction of alkynyl or azido groups has been reported in view of further CuAAC "click" functionalizing chemistry.[27] The Fc-linked 1,2,3-triazole (Fc-trz; see Figure 1) was synthesized using the CuAAC "click" reaction between (trimethylsilyl)azide and propargyloxymethylferrocene in a *N*,*N*-dimethylformamide (DMF)/methanol (MeOH) solution at 100 °C with CuI as the catalyst (Experimental Section). Fc-trz was characterized by ^{1}H and ^{13}C NMR and IR spectroscopies, electrospray ionization mass spectrometry (ESI-MS), elemental analysis, and cyclic voltammetry (see the Supporting Information, SI). Coumarin triazole (Cou-trz) was synthesized according to the literature,[28] but its photochemical property and applications were not reported.

A one-step process to functionalize AuNPs with Fc-trz was carried out in an organic solution. Compared to the above-mentioned ligand-substitution method, Fc-trz was used as the stabilizer instead of ferrocene thiolate ligands.[12a] The preparation of AuNPs stabilized by Fc-trz was performed using two pathways. In the first method, Fc-trz and $NaBH_4$ were dissolved in ethanol (EtOH), and a $HAuCl_4$/EtOH solution was slowly injected into this solution under a nitrogen atmosphere with stirring. After being further stirred for 2 h, **AuNP-1** was purified by dialysis against a large volume of EtOH. In this process, gold(III) was reduced by $NaBH_4$, while Fc-trz played the role of stabilizer. No oxidation of Fc was found according to UV−vis spectroscopy analysis of **AuNP-1**, which is well taken into account by the fact that $NaBH_4$ is a much stronger and faster reducing reagent than ferrocene. Indeed, as shown in Figure 2a, two bands at 321 and 430 nm belong to the ferrocene unit.

On the other hand, during the preparation of **AuNP-2**, no external reductant was involved. The Fc group works not only as the capping agent in its oxidized form but also as the reductant. In this reaction, the Fc group was oxidized to ferricenium chloride, with gold(III) being reduced to gold(0) atoms that form AuNPs. **AuNP-2** is stabilized by the ferricenium chloride triazole ligand, with stabilization resulting from the positive synergy between the electrostatic factor and

dx.doi.org/10.1021/ic5021498 | *Inorg. Chem.* XXXX, XXX, XXX−XXX

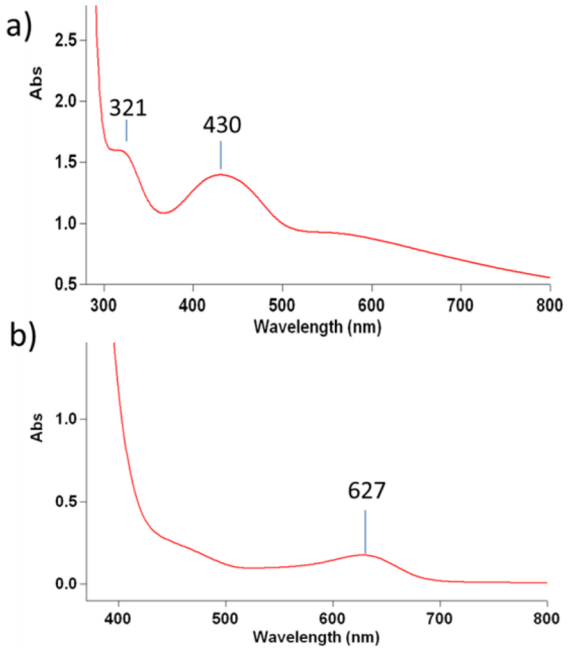

Figure 2. UV−vis spectra revealing the characteristic bands of (a) the Fc group in **AuNP-1** (321 and 430 nm) and (b) the ferricenium group in **AuNP-2** (627 nm) (both were recorded in an EtOH solution).

the trz ligand coordination to the AuNP surface (Figure 1). The oxidation of ferrocene to ferricenium was successfully recorded by UV−vis spectroscopy, with the band at 627 nm in Figure 2b corresponding to the ferricenium unit. In Figure 2a, a very weak shoulder band (because of the large ferrocene absorption) around 530−580 nm corresponds to the surface plasmon band (SPB) of **AuNP-1**. The SPB of **AuNP-2** overlaps with the ferricenium band, which is deduced from a comparison with the SPB band of **AuNP-3**. Both MeOH and tetrahydrofuran (THF) were suitable solvents in the one-step preparation of **AuNPs-1** and **AuNPs-2**.

The transmission electron microscopy (TEM) images shown in Figure 3 revealed the sizes of the Fc-trz-capped AuNPs that were prepared with or without $NaBH_4$, indicating that **AuNP-1** (5 nm) was slightly larger than **AuNP-2** (4.4 nm). The size difference between **AuNP-1** and **AuNP-2** in core size may arise from the difference of the reduction and stabilization rates in each case. Indeed, the stabilization in **AuNP-2** is stronger compared to **AuNP-1** because of the additional electrostatic stabilization of **AuNP-2**. Both **AuNP-1** and **AuNP-2** are monodispersed in an EtOH solution, as disclosed by TEM and dynamic light scattering (DLS) analyses. The multiionic layers of **AuNP-2** led to the formation of small clusters (9.8 nm) in solution compared to **AuNP-1**, which formed relatively larger clusters (12 nm). The electrochemical characterization of **AuNP-1** and **AuNP-2** was conducted by cyclic voltammetry. As shown in Figure S7 in the SI on the cyclic voltammogram of **AuNP-1**, the expected chemically and electrochemically reversible waves of the ferricenium/Fc redox system were observed. The difference between the anodic and cathodic peak potentials (ΔE) is 0.06 V, and the intensity ratio i_a/i_c is 1.0, showing the chemical reversibility of the iron(III/II) system without being marred by adsorption. The measured redox potential value of this multiferrocenyl redox system, i.e., the average of the anodic and cathodic wave potentials [$E_{1/2} = (E_{pa} + E_{pc})/2$], is 0.44 V versus decamethylferrocene.[24c] Both **AuNPs-1** and **AuNPs-2** are qualified for redox-sensing applications.

4-NP Reduction. **AuNP-2** was selected because it was the only AuNP in this series that was water-soluble, which facilitated the catalytic experiments. The lability of the AuNP−trz and AuNP−Cl^- connections on the surface of **AuNP-2** was employed to catalyze 4-NP reduction in water/EtOH (95:5) in the presence of $NaBH_4$[29] with catalyst amounts of 0.5% or 1%. This reaction was carried out in a standard quartz cuvette (path length: 1 cm) and monitored by UV−vis spectroscopy every 40 s (Figure S11 in the SI). The plots of the decrease rate of 4-NP [$-\ln(C/C_0)$] versus the reaction times (Figure 4) were collected (with C and C_0 being the 4-NP concentrations at times t and $t = 0$, respectively). The rate constant k of the catalytic reduction of 4-NP was found to be

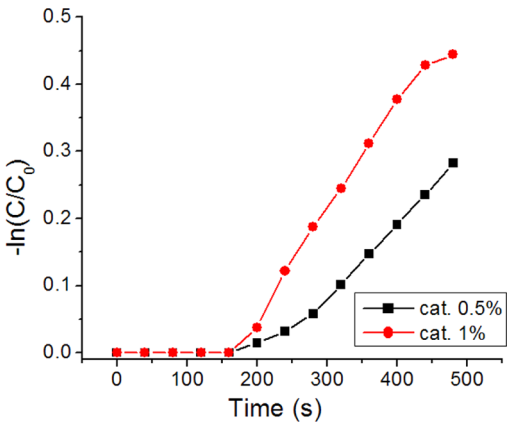

Figure 4. Plots of the decreasing rate of 4-NP [$-\ln(C/C_0)$] versus the reaction times using two distinct amounts of catalyst **AuNP-2** (0.5% catalyst in the black curve and 1% catalyst in the red curve).

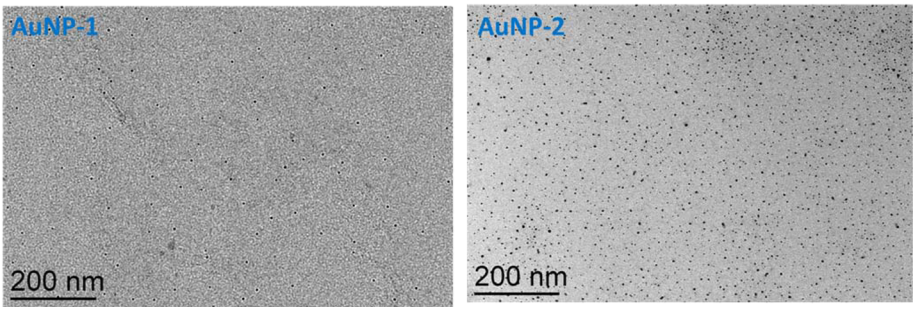

Figure 3. TEM images of **AuNP-1** (d = 5 nm) and **AuNP-2** (d = 4.4 nm) prepared using two distinct methods.

dx.doi.org/10.1021/ic5021498 | Inorg. Chem. XXXX, XXX, XXX−XXX

1.1×10^{-3} s^{-1} with 0.5% **AuNP-2** as the catalyst, and the k value increased to 1.6×10^{-3} s^{-1} with an increase of the catalyst amount to 1%. Moreover, an induction period (200 s) was required because of the AuNP surface organization of the substrates in the mixed solvent.[30] Compared to the catalysis of 4-NP reduction with bulky water-soluble PEG-trz ligands, which provided $k = 5.2 \times 10^{-3}$ s^{-1} (0.5% catalyst),[13a] the catalytic efficiency of **AuNP-2** that was stabilized by the present triazole ligands was relatively lower (1.1×10^{-3} s^{-1}), although the core of **AuNP-2** was slightly smaller than that of AuNPs with PEG-trz ligands. However, **AuNPs-2** remained superior for 4-NP reduction to triazole-stabilized AuNPs of close size stabilized by other ligands such as thiolate and citrate because of the labile character of the AuNP−trz bonds.

Cou-trz-Stabilized AuNPs. Cou-trz-stabilized AuNPs (**AuNP-3**) were prepared in EtOH with sodium borohydride as the reductant to reduce Au^{III} to Au^0. Thus, $HAuCl_4$ and Cou-trz were dissolved together in an EtOH solution, and an EtOH solution of $NaBH_4$ was added dropwise to the mixture under a nitrogen atmosphere. The yielded solution was further stirred for 2 h. These AuNPs precipitated in EtOH in 24 h, and they were redissolved in dimethyl sulfoxide (DMSO). After precipitation−redissolution three times, excess Cou-trz was easily removed with the supernatant. The size of the **AuNP-3** core shown by TEM is 6.3 nm, i.e., slightly larger than those of **AuNP-1** and **AuNP-2**. TEM and DLS (average diameter size: d = 16 nm) analyses showed that **AuNP-3** has lower dispersion than **AuNP-1** and **AuNP-2**, presumably because of the precipitation−redissolution purification process.

According to the fluorescence quenching effect of the AuNP core of **AuNP-3**, the very high molar extinction coefficients and broad energy bandwidths of AuNPs result in emission−extinction of a fluorescent dye that is relatively close to the surface of **AuNP-3**. As shown in Figure 5, in which the fluorescence emission spectra of Cou-trz and **AuNP-3** are presented, the emission band (λ_{max}) of Cou-trz at 537 nm is of high intensity (λ_{ex} = 405 nm in a DMSO/water solution). On the other hand, a dramatic decrease was observed after capping AuNPs with Cou-trz ligands (see the red curve in Figure 5); that is, the emission of Cou-trz was quenched by the AuNP core of **AuNP-3**.

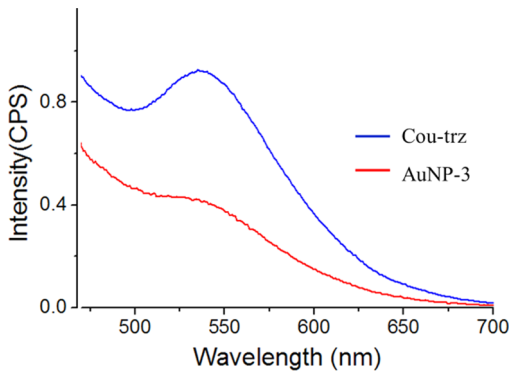

Figure 5. Fluorescent emission spectra of Cou-trz (0.2 mM) and Cou-trz-capped **AuNP-3** (both in a DMSO/water solution; λ_{ex} = 405 nm, recorded at 22 °C).

Given the combination of the fluorescence quenching effect of AuNPs and the flexible bonding of AuNPs to trz rings facilitating trz substitution at the AuNP surface, it was reasoned that sensing by a dramatic change of the fluorescence intensity upon ligand substitution should be efficient. It was indeed possible to easily detect the presence in solution of thiol or sulfide compounds in this way. Three biological thiols that are known to cause illness in the human body were taken as models to verify the sensing property of **AuNP-3**. As illustrated in Scheme 1, an aqueous solution of biothiol (Hcy, Cys, or GSH) was progressively titrated upon an increase in the concentration in a DMSO/water solution of **AuNP-3** in a standard quartz cuvette (path length = 1 cm). Along with the progress of ligand substitution, Cou-trz−**AuNP-3** was removed from the solution and replaced by AuNPs bound to biothiols. The recovery of photochemical emission of Cou-trz was consequently observed. The emission intensity of **AuNP-3** increased distinctly with an increase of the biothiols (up to 10 equiv) after being mixed for 10 min after titration (Figure 6; see full-scale fluorescence emission spectra in Figure S12 in the SI). The same phenomena were observed in sensing Cys and GSH (Figures S13 and S14 in the SI), demonstrating the photochemical application of **AuNP-3** in the sensing of biothiols.

Synthesis of a Nanogold-Cored Fc-Terminated Dendrimer. Another way to utilize the lability of trz in monosubstituted trz-stabilized AuNPs for the synthesis of Fc-containing AuNPs was achieved by the facile reaction of trz-AuNPs with Fc-terminated dendrons containing a thiol focal point as the potential AuNP thiolate ligand. Thus, the nonabranched Fc-terminated thiol dendron **6** was synthesized and utilized to substitute for the trz ligand from the surface of AuNPs. This method allows the formation of very stable AuNP thiolates containing a bulky Fc-loaded surface.[13a]

The nonaferrocene dendron **6** with 1 → 3 directionalities[31] was synthesized via the CuAAC "click" reaction of azidomethylferrocenyl with a nonaalkyne dendron.[13a] This dendron was easily grafted onto the surface of AuNPs by fast and quantitative trz ligand substitution to give **AuNP-5** (Scheme 2). In order to limit the Fc bulk at the dendrimer periphery, the dendron **6** was introduced together with linear dodecanethiol, which were found in 70% of the total of 540 ± 80[32] thiol per **AuNP-5**. **AuNP-5** retained its core size and monodispersity during the reaction in an organic solvent, which resulted in a AuNP-cored dendrimer containing about 140 ± 25 thiol dendrons, i.e., 1260 ± 180 Fc termini, and displayed chemical and electrochemical reversibility together with significant adsorption in its cyclic voltammogram (see the SI).[33]

CONCLUSION

In this work, the first trz-AuNPs that are soluble in organic media have been synthesized in a size range of 4.4−6.3 nm with narrow dispersities in EtOH with ferrocene, ferricenium, and Cou groups linked to the trz ligands. The first ferricenium-stabilized AuNPs have been synthesized by direct redox reaction between the trz-linked Fc and $HAuCl_4$ without any other reductant. The excellent stabilization of these AuNPs results from synergistic stabilization by both the electrostatic effect and trz coordination. This excellence of stabilization is confirmed by the slower catalysis of 4-NP reduction by $NaBH_4$ than with other trz-AuNP catalysts. In addition, the retention time characterized here was not found with other trz-AuNPs, indicating a higher reorganization energy at the AuNP surface than with neutral trz ligands. The two Fe^{II} and Fe^{III} redox forms of the trz-AuNPs with closely related AuNP core sizes were independently synthesized and shown to reversibly interconvert by cyclic voltammetry. Easy trz ligand substitution has been shown to usefully apply to dendrimer synthesis, biothiol

dx.doi.org/10.1021/ic5021498 | Inorg. Chem. XXXX, XXX, XXX−XXX

Scheme 1. General Illustration of Fluorescent Sensing of Biothiols (Cys, Hcy, and GSH) with AuNP-3 via Ligand Substitution on the Surface of AuNPs Inducing Fluorescence "Turn-On" Phenomenon[a]

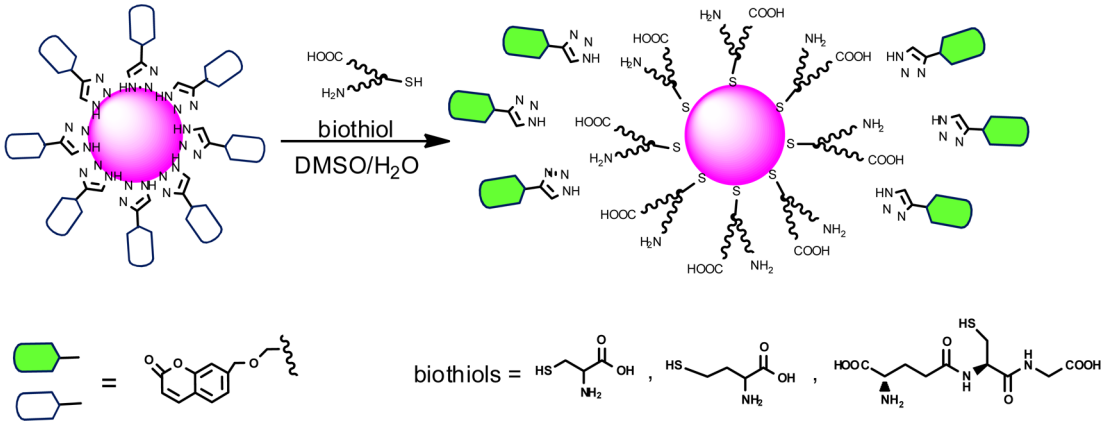

[a]The green color represents the recovery of the Cou fluorescence property.

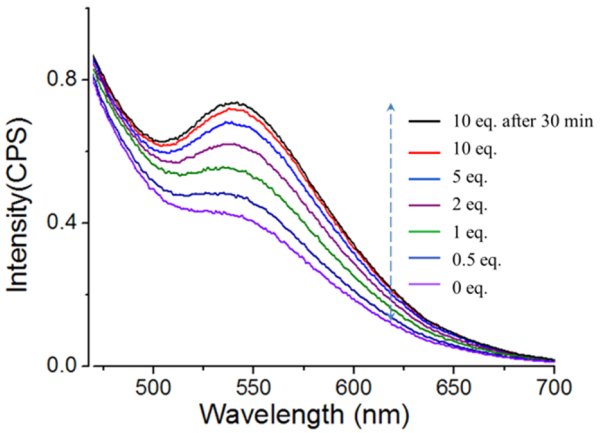

Figure 6. Fluorescent emission spectra of **AuNP-3** mixed with various amounts of Hcy (1 equiv of analyte = 0.05 mM in the solution; λ_{ex} = 405 nm; standard quartz cuvette; path length = 1 cm, recorded at 25 °C; see full-scale spectra in Figure S12 in the SI).

fluorescence "turn-on" sensing assay, and nitrophenol reduction by $NaBH_4$. Finally, concerning the synthetic aspect, facile AuNP-cored dendrimer construction is demonstrated upon triazole substitution by a thiol dendron. These remarkable applications show the versatility and applicability of trz-AuNP in organic media. The strategy that consists of stabilizing stable AuNPs by easily synthesized 1,2,3-triazoles is conclusively powerful because of the complementarity between the stability of these AuNPs and the multiple applications resulting from facile triazole substitution at the AuNP surfaces.

EXPERIMENTAL SECTION

General Data. All solvents and chemicals were used as purchased. Dialysis was performed with a Spectra/Por 6 dialysis membrane. NMR spectra were recorded at 25 °C with a Bruker 300 (300 MHz) spectrometer. All of the chemical shifts are reported in parts per million (δ, ppm) with reference to Me_4Si for the ^1H and ^{13}C NMR spectra. IR spectra were recorded on an ATI Mattson Genesis series Fourier transform infrared spectrophotometer. UV–vis absorption spectra were measured with a PerkinElmer Lambda 19 UV–vis spectrometer. DLS measurements were made using a Malvern Zetasizer 3000 HSA instrument at 25 °C at an angle of 90°. Fluorescence emission spectra were recorded by a Spex FluoroLog 2 spectrofluorimeter. Cyclic voltammetry measurements: All electrochemical measurements were recorded under a nitrogen atmosphere at 25 °C.

Synthesis of the 1,2,3-Triazoles. Synthesis of Fc-trz: trimethylsilyl azide (0.23 mL, 1.8 mmol) was added to a DMF and MeOH solution (3 mL, 9:1) of CuI (7.5 mg, 0.04 mmol) and propargyloxymethylferrocene (300 mg, 1.18 mmol) under nitrogen atmosphere in a pressure vial. The reaction mixture was stirred at 100 °C for 12 h. The mixture was cooled to room temperature, then filtered, and concentrated. The residue was purified by silica gel column chromatography (*n*-hexane/EtOAc, 5:1 to 2:1) to afford Fc-trz in 60% yield (210 mg). ^1H NMR (300 MHz, $CDCl_3$): δ 7.66 (1H, CH_{trz}), 4.65 (2H, CH_2-trz), 4.35 (2H, CH_2-Fc), 4.24 (2H, CH_{Cp}), 4.15 (2H, CH_{Cp}), 4.13 (5H, CH_{Cp}). ^{13}C NMR (75 MHz, $CDCl_3$): δ 145, 122.2, 82.7, 69.1, 68.9, 62.4, 50.2. IR: ν_{Cp} at 819 cm^{-1}, disappearance of the $\sigma_{C\equiv C}$ band at 2100 cm^{-1}. ESI-MS. Calcd for $C_{14}H_{15}FeN_3O$ [M + Na^+]: m/z 320.12. Found m/z 320.0. Anal. (calcd, found for $C_{14}H_{15}FeN_3O$): C (56.59, 56.70), H (5.09, 5.34), N (14.14, 13.87) .

Coumarin triazole (Cou-trz) was synthesized according to the literature.[28]

Synthesis of the AuNPs. ***AuNP-1***. Fc-trz (19 mg, 0.06 mmol) and $NaBH_4$ (2.5 mg, 0.06 mmol) were dissolved in 20 mL of EtOH in a Schlenk flask, and a $HAuCl_4$ (4.3 mg, 0.012 mmol)/EtOH (10 mL) solution was then injected dropwise into the flask in a nitrogen atmosphere with vigorous stirring. The solution was further stirred for 1 h and purified by dialysis against a large volume of EtOH before analysis. AuNPs were prepared in MeOH or THF with the same procedure.

AuNP-2. Fc-trz (11.5 mg, 0.04 mmol) was dissolved in 20 mL of EtOH in a Schlenk flask, and a $HAuCl_4$ (4.3 mg, 0.012 mmol)/EtOH (10 mL) solution was then injected into the flask under a nitrogen atmosphere with stirring. The solution was further stirred for 1 h and purified by dialysis against a large volume of EtOH before analysis. AuNPs were prepared in MeOH or THF with the same procedure.

AuNP-3. Cou-trz (30 mg, 0.06 mmol) and $HAuCl_4$ (4.3 mg, 0.012 mmol) were dissolved in 20 mL of EtOH in a Schlenk flask that is refilled with nitrogen. A $NaBH_4$ (2.5 mg, 0.06 mmol)/EtOH (10 mL) solutionwas then added dropwise into the flask under a nitrogen atmosphere with stirring. The solution was further stirred for 1 h. **AuNP-3** was purified by precipitation in EtOH and redissolution in DMSO three times.

Catalytic Reduction of 4-Nitrophenol (4-NP). A typical procedure is as follows: An aqueous solution (2.5 mL) containing $NaBH_4$ (7.2 μmol) and 4-NP (0.09 μmol) was prepared in a 3 mL standard quartz cuvette (path length: 1 cm). **AuNP-2** (0.5%, 0.45 × 10^{-3} μmol; 1%, 0.9 × 10^{-3} μmol) in EtOH was injected into the cuvette. The reaction progress was detected by UV–vis spectroscopy every 40 s.

dx.doi.org/10.1021/ic5021498 | *Inorg. Chem.* XXXX, XXX, XXX–XXX

Scheme 2. Ligand Substitution of the trz-Capped AuNP-4 by a Nonaferrocenylthiol Dendron on the AuNP Surface, Yielding the AuNP Thiolate Poly-Fc-Terminated Dendrimer (AuNP-5)

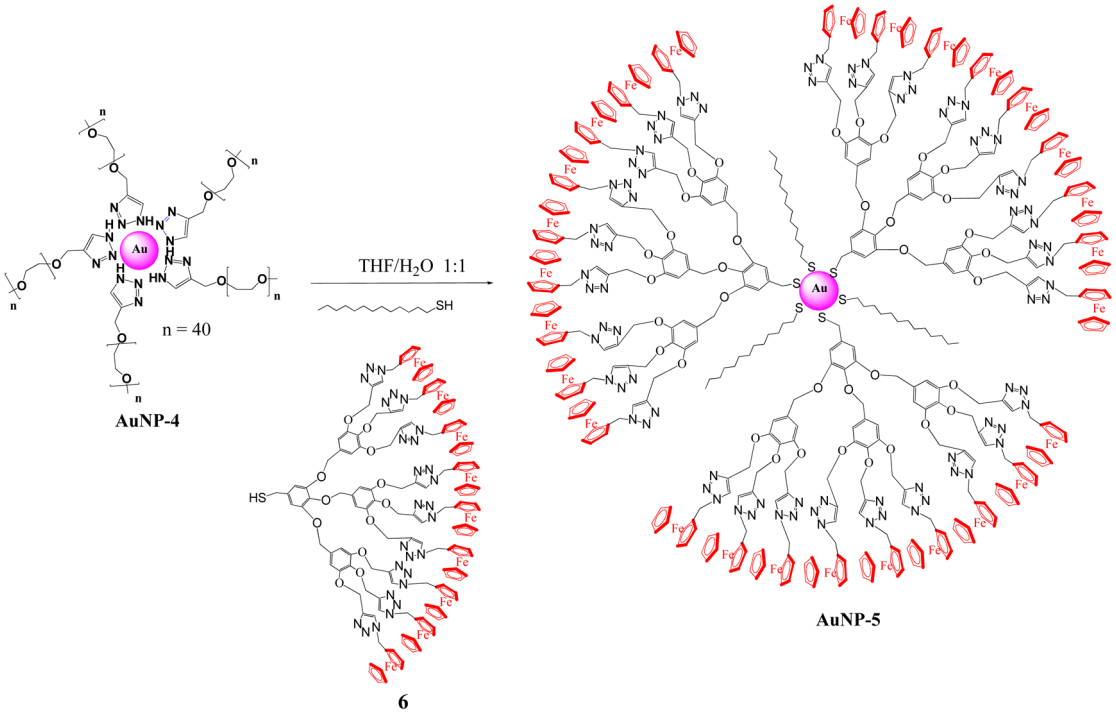

Sensing of Homocysteine (Hcy), Cysteine (Cys), and Glutathione (GSH). A gradually increasing amount of Hcy (40 mM, 0.5, 1, 2, 5, and 10 equiv) in water was added to a 2.5 mL solution of **AuNP-3** (0.05 mM; 3:7 water/DMSO) in a standard quartz cuvette (path length: 1 cm). The solution was monitored using a fluorimeter 10 min after mixing. Titration of Cys and GSH was conducted according to the same process.

Ligand-Substitution Reaction of AuNP-4 by a Mixture of Nonaferrocenyl Thiolate Dendron 6 and Dodecanethiol To Synthesize AuNP-5. A total of 3 mL of a THF solution of the nonaferrocenylthiol dendron[13a] (150 mg, 0.25 mmol) and dodecanethiol (10 mg, 0.05 mmol, 12 μL) was added into 3 mL (1 mM) of a mPEG-trz-stabilized AuNP (**AuNP-4**)[13a] and stirred for 10 min. Then 10 mL of dichloromethane was added to the mixed solution, and the organic phase was then separated and dried over Na_2SO_4. After evaporation of the solvent, AuNPs were washed with acetone and then EtOH followed by precipitation in dichloromethane/MeOH. ^{1}H NMR ($CDCl_3$, 200 MHz): δ 7.61 (9H, C*H* in triazole), 6.71 (8H, H_{Ar}), 5.28, 5.16 (24 H, ArOCH_2−), 4.91 (18H, −CH_2Cp), 4.24−4.12 (81H, CH_{Cp}), 1.83, 1.59. 1.24 (22H, CH_2− in the alkyl chain), 0.86 (3H, CH_3CH$_2$−). UV−vis spectroscopy: plasmon band at 535 nm. DLS: 16.3 ± 3 nm.

Using Leff's method,[32] the number of AuNP atoms in **AuNP-5** and the number of ligands, 540 thiol ligands on the surface of **AuNP-5**, were determined. From the integration of H-1 (CH_3 in dodecanethiolate) and H-2 (C*H* in Cp) in the ^{1}H NMR spectrum (Figure S14 in the SI) of **AuNP-5**, the ratio of the numbers of the two ligands (Fc-dendron/dodecanethiolate) was calculated to be about 1:2.8; that is, 70% of the thiolates on the surface of **AuNP-5** are dodecanethiolate ligands (about 400 ± 70 dodecanethiolates per AuNP). Meanwhile, approximately 140 ± 25 Fc dendrons on average are located on each AuNP surface. The calculations indicate that there are on average about 1260 ± 180 Fc units surrounding every **AuNP-5** (see the SI).

■ ASSOCIATED CONTENT

Ⓢ Supporting Information

Characterization and data of compounds and AuNPs. This material is available free of charge via the Internet at http://pubs.acs.org.

■ AUTHOR INFORMATION

Corresponding Author

*E-mail: d.astruc@ism.u-bordeaux1.fr.

Notes

The authors declare no competing financial interest.

■ ACKNOWLEDGMENTS

Financial support from the China Scholarship Council (Ph.D. grants to N.L.), the Univ. Bordeaux, the CNRS, and L'Oréal is gratefully acknowledged.

■ REFERENCES

(1) (a) Giersig, M.; Mulvaney, P. *Langmuir* **1993**, *9*, 3408−3413. (b) Brust, M.; Walker, M.; Bethell, D.; Schiffrin, D. J.; Whyman, R. J. *J. Chem. Soc., Chem. Commun.* **1994**, 801−802. (c) Rongchao, J. *Nanoscale* **2010**, *2*, 343−362.

(2) (a) Turkevitch, J.; Stevenson, P. C. *Discuss. Faraday Soc.* **1951**, *11*, 55−75. (b) Frens, G. *Nature (London), Phys. Sci.* **1973**, *132*, 20−22. (c) Connor, E. E.; Mwamuka, J.; Gole, A.; Murphy, C. J.; Wyatt, M. D. *Small* **2005**, *1*, 325−327. (d) Kimling, J.; Maier, M.; Okenve, B.; Kotaidis, V.; Ballot, H.; Plech, A. *J. Phys. Chem. B* **2006**, *110*, 15700−15707.

(3) Scott, R. W. J.; Wilson, O. M.; Oh, S.-K.; Kenik, E. A.; Crooks, R. M. *J. Am. Chem. Soc.* **2004**, *126*, 15583−15591.

(4) (a) Boisselier, E.; Diallo, A. K.; Salmon, L.; Ornelas, C.; Astruc, D. *J. Am. Chem. Soc.* **2010**, *132*, 2729−2742. (b) Astruc, D. *Nat. Chem.* **2012**, *4*, 255−267.

(5) Deraedt, C.; Rapakousiou, A.; Wang, Y.; Salmon, L.; Bousquet, M.; Astruc, D. *Angew. Chem., Int. Ed.* **2014**, *53*, 8445−8449.

(6) Li, N.; Echeverría, M.; Moya, S.; Ruiz, J.; Astruc, D. *Inorg. Chem.* **2014**, *53*, 6954−6961.
(7) (a) Serpell, C. J.; Cookson, J.; Ozkaya, D.; Beer, P. D. *Nat. Chem.* **2011**, *3*, 478−483. (b) Knighton, R. C.; Sambrook, M. R.; Vincent, J. C.; Smith, S. A.; Serpell, C. J.; Cookson, J.; Vichers, M. S.; Beer, P. D. *Chem. Commun.* **2013**, *49*, 2293−2295.
(8) (a) Yu, A.; Liang, Z.; Cho, J.; Caruso, F. *Nano Lett.* **2003**, *3*, 1203−1207. (b) Devadoss, A.; Spehar-Délèze, A.-M.; Tanner, D. A.; Bertoncello, P.; Marthi, R.; Keyes, T. E.; Forster, R. J. *Langmuir* **2010**, *26*, 2130−2135.
(9) (a) Chen, X.; Mao, S. S. *Chem. Rev.* **2007**, *107*, 2891−2959. (b) Xia, Y.; Xiong, Y.; Lim, B.; Skrabalak, S. E. *Angew. Chem., Int. Ed.* **2009**, *48*, 60−103. (c) Louis, C.; Pluchery, O. *Gold Nanoparticles for Physics, Chemistry, Biology*; Imperial College Press: London, 2012.
(10) Astruc, D.; Liang, L.; Rapakousiou, A.; Ruiz, J. *Acc. Chem. Res.* **2012**, *45*, 630−640.
(11) (a) Zhao, P.; Li, N.; Salmon, L.; Liu, N.; Ruiz, J.; Astruc, D. *Chem. Commun.* **2013**, *49*, 3218−3220. (b) Li, N.; Zhao, P.; Liu, N.; Echeverría, M.; Moya, S.; Salmon, L.; Ruiz, J.; Astruc, D. *Chem.—Eur. J.* **2014**, *20*, 8363−8369.
(12) (a) Labande, A.; Ruiz, J.; Astruc, D. *J. Am. Chem. Soc.* **2002**, *124*, 1782−1789. (b) Daniel, M.-C.; Ruiz, J.; Nlate, S.; Blais, J. C.; Astruc, D. *J. Am. Chem. Soc.* **2003**, *125*, 2617−2628. (c) Otón, F.; Espinosa, A.; Tárraga, A.; de Arellano, C. R.; Molina, P. *Chem.—Eur. J.* **2007**, *13*, 5742−5725. (d) Wang, Y.; Salmon, L.; Ruiz, J.; Astruc, D. *Nat. Commun.* **2014**, *5*, 3489, doi: 10.1038/ncomms4489.
(13) (a) Sardar, R.; Beasley, C. A.; Murray, R. W. *J. Am. Chem. Soc.* **2010**, *132*, 2058−2063. (b) Mars, A.; Parolo, C.; Raouafi, N.; Boujlel, K.; Merkoçi, A. *J. Mater. Chem. B* **2013**, *1*, 2951−2955.
(14) (a) Ornelas, C. *New J. Chem.* **2011**, *35*, 1973−1985. (b) Gasser, G.; Ott, I.; Metzler-Nolte, N. *J. Med. Chem.* **2011**, *54*, 3−25. (c) Hillard, E. A.; Jaouen, G. *Organometallics* **2011**, *30*, 20−27. (d) Hartinger, C. G.; Metzler-Nolte, N.; Dyson, P. J. *Organometallics* **2012**, *31*, 5677−5685.
(15) (a) Herves, P.; Perez-Lorenzo, M.; Liz-Marzán, L. M.; Dzubiella, J.; Lu, Y.; Ballauff, M. *Chem. Soc. Rev.* **2012**, *41*, 5577−5587. (b) Shivhare, A.; Ambrose, S. J.; Zhang, H.; Purves, R. W.; Scott, R. W. J. *Chem. Commun.* **2013**, *49*, 276−278. (c) Pachfule, P.; Kandambeth, S.; Díaz, D.; Banerjee, R. *Chem. Commun.* **2014**, *50*, 3169−3172. (d) Zhang, Y.; Cui, X.; Shi, F.; Deng, Y. *Chem. Rev.* **2012**, *112*, 2467−2505.
(16) (a) Woo, Y.-T.; Lai, D. Y. *Aromatic Amino and Nitro−Amino Compounds and Their Halogenated Derivatives. Patty's Toxicology*; Wiley-VCH: New York, 2001; pp 1−96. (b) Mitchell, S. C.; Waring, R. H. Aminophenols. In *Ullmann's Encyclopedia of Industrial Chemistry*; Wiley-VCH: New York, 2002.
(17) (a) Mizukami, S.; Nagano, T.; Urano, Y.; Odani, A.; Kikuchi, K. *J. Am. Chem. Soc.* **2002**, *124*, 3920−3925. (b) Xu, Z.; Liu, X.; Pan, J.; Spring, D. R. *Chem. Commun.* **2012**, *48*, 4764−4766.
(18) Zhang, S. Y.; Ong, C.-N.; Shen, H.-M. *Cancer Lett.* **2004**, *208*, 143−153.
(19) Shahrokhian, S. *Anal. Chem.* **2001**, *73*, 5972−5978.
(20) Seshadri, S.; Beiser, A.; Selhub, J.; Jacques, P. F.; Rosenberg, I. H.; D'Agostino, R. B.; Wilson, P. W. F.; Wolf, P. A. *N. Engl. J. Med.* **2002**, *346*, 476−483.
(21) Kleinman, W. A.; Richie, J. P. *Biochem. Pharmacol.* **2000**, *60*, 19−29.
(22) (a) Li, Y.; Li, Z.; Gao, Y.; Gong, A.; Zhang, Y.; Hosmane, N. S.; Shen, Z.; Wu, A. *Nanoscale* **2014**, *6*, 10631−10637. (b) Long, L.; Zhou, L.; Wang, L.; Meng, S.; Gong, A.; Du, F. *Org. Biomol. Chem.* **2013**, *11*, 8214−8220.
(23) (a) Jung, H. S.; Chen, X.; Kim, J. S.; Yoon, J. *Chem. Soc. Rev.* **2013**, *42*, 6019−6031. (b) Lin, J.-H.; Chang, C.-W.; Tseng, W.-L. *Analyst* **2010**, *135*, 104−110.
(24) (a) Madonik, A.; Astruc, D. *J. Am. Chem. Soc.* **1984**, *106*, 2437−2439. (b) Desbois, M.-H.; Astruc, D.; Guillin, J.; Varret, F.; Trautwein, A. X.; Villeneuve, G. *J. Am. Chem. Soc.* **1989**, *111*, 5800−5809. (c) Ruiz, J.; Astruc, D. *C. R. Seances Acad. Sci., Sér.* Пc **1998**, 21−27.
(25) (a) Moinet, C.; Román, E.; Astruc, D. *J. Electroanal. Chem. Interfacial Chem.* **1981**, *121*, 241−246. (b) Green, J. C.; Kelly, M. R.; Payne, M. P.; Seddon, E. A.; Astruc, D.; Hamon, J.-R.; Michaud, P. *Organometallics* **1983**, *2*, 211−218.
(26) (a) Abd-El-Aziz, A.; Bernardin, S. *Coord. Chem. Rev.* **2000**, *203*, 219−267. (b) Manners, I. *Science* **2001**, *294*, 1664−1666. (c) Abd-El-Aziz, A. S. *Coord. Chem. Rev.* **2002**, *233−234*, 177−191. (d) Geiger, W. E. *Organometallics* **2007**, *26*, 5738−5765. (e) Abd-El-Aziz, A. S.; Winram, D. J.; Shipman, P. O.; Bichler, L. *Macromol. Rapid Commun.* **2010**, *31*, 1992−1997.
(27) (a) Tornøe, C. W.; Christensen, C.; Meldal, M. *J. Org. Chem.* **2002**, *67*, 3057−3064. (b) Devadoss, A.; Chidsay, C. E. D. *J. Am. Chem. Soc.* **2007**, *129*, 5370−5371. (c) Rapakousio, A.; Wang, Y.; Belin, C.; Pinaud, N.; Ruiz, J.; Astruc, D. *Inorg. Chem.* **2013**, *52*, 6685−6693.
(28) Robilotto, T. J.; Deligonul, N.; Updegraff, J. B.; Gray, T. G. *Inorg. Chem.* **2013**, *52*, 9659−9668.
(29) (a) Wunder, S.; Lu, Y.; Albrecht, M.; Ballauff, M. *ACS Catal.* **2011**, *1*, 908−916. (b) Pradhan, N.; Pal, A.; Pal, T. *Colloids Surf. A* **2002**, *196*, 247−257. (c) Esumi, K.; Isono, R.; Yoshimura, T. *Langmuir* **2004**, *20*, 237−243.
(30) Mei, Y.; Sharma, G.; Lu, Y.; Drechsler, M.; Irgang, T.; Kempe, R.; Ballauff, M. *Langmuir* **2005**, *21*, 12229−12234.
(31) (a) Newkome, G. R.; Yao, Z.; Baker, G. R.; Gupta, G. K. *J. Org. Chem.* **1985**, *50*, 2003−2004. (b) Newkome, G. R.; Shreiner, C. *Chem. Rev.* **2010**, *110*, 6338−6442.
(32) Leff, D. V.; Ohara, P. C.; Geath, J. R.; Gelbart, W. M. *J. Phys. Chem.* **1995**, *99*, 7036−7041.
(33) For reviews on Fc-terminated dendrimers, see: (a) Casado, C. M.; Cuadrado, I.; Moran, M.; Alonso, B.; Garcia, B.; Gonzales, B.; Losada, J. *Coord. Chem. Rev.* **1999**, *185−186*, 53−79. (b) Casado, C. M.; Alonso, B.; Losada, J.; Garcia-Armada, M. P. In *Designing Dendrimers*; Campagna, S., Ceroni, P., Puntoriero, F., Eds.; John Wiley & Sons: Hoboken, NJ, 2012; pp 219−262.

ACCOUNTS
of chemical research

Click Dendrimers and Triazole-Related Aspects: Catalysts, Mechanism, Synthesis, and Functions. A Bridge between Dendritic Architectures and Nanomaterials

DIDIER ASTRUC,* LIYUAN LIANG, AMALIA RAPAKOUSIOU, AND JAIME RUIZ

Institut des Sciences Moléculaires, UMR CNRS No. 5255, Université Bordeaux 1, 33405 Talence Cedex, France

RECEIVED ON SEPTEMBER 9, 2011

CONSPECTUS

One of the primary recent improvements in molecular chemistry is the now decade-old concept of click chemistry. Typically performed as copper-catalyzed azide–alkyne (CuAAC) Huisgen-type 1,3-cycloadditions, this reaction has many applications in biomedicine and materials science. The application of this chemistry in dendrimer synthesis beyond the zeroth generation and in nanoparticle functionalization requires stoichiometric use of the most common click catalyst, $CuSO_4 \cdot 5H_2O$ with sodium ascorbate.

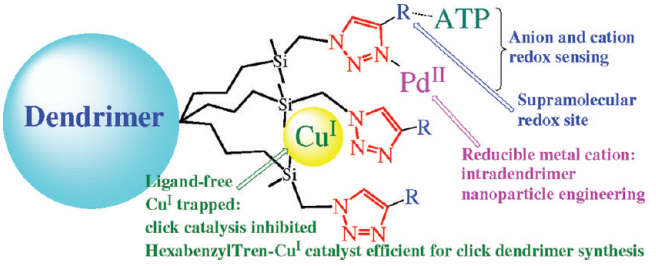

Efforts to develop milder reaction conditions for these substrates have led to the design of polydentate nitrogen ligands. Along these lines, we have described a new, efficient, practical, and easy-to-synthesize catalytic complex, [Cu^I(hexabenzyltren)]Br, **1** [tren = tris(2-aminoethyl)amine], for the synthesis of relatively large dendrimers and functional gold nanoparticles (AuNPs). This efficient catalyst can be used alone in 0.1% mol amounts for nondendritic click reactions or with the sodium-ascorbate additive, which inhibits aerobic catalyst oxidation. Alternatively, catalytic quantities of the air-stable compounds hexabenzyltren and CuBr added to the click reaction medium can provide analogously satisfactory results. Based on this catalyst as a core, we have also designed and synthesized analogous Cu^I-centered dendritic catalysts that are much less air-sensitive than **1** and are soluble in organic solvents or in water (depending on the nature of the terminal groups). These multivalent catalysts facilitate efficient click chemistry and exert positive dendritic effects that mimic enzyme activity. We propose a monometallic CuAAC click mechanism for this process.

Although the primary use of click chemistry with dendrimers has been to decorate dendrimers with a large number of molecules for medicinal or materials purposes, we are specifically interested in the formation of intradendritic [1,2,3]-triazole heterocycles that coordinate to transition-metal ions via their nitrogen atoms. We describe applications including molecular recognition of anions and cations and the stabilization of transition metal nanoparticles according to a principle pioneered by Crooks with poly(amido amine) (PAMAM) dendrimers, and in particular, the control of structural and reactivity parameters in which the intradendritic [1,2,3]-triazoles and peripheral tripodal tri(ethylene glycol) termini play key roles in the click-dendrimer mediated synthesis and stabilization of gold nanoparticles (AuNPs). By varying these parameters, we have stabilized water-soluble, weakly liganded AuNPs between 1.8 and 50 nm in size and have shown large differences in behavior between AuNPs and PdNPs. Overall, the new catalyst design and the possibilities of click dendrimer chemistry introduce a bridge between dendritic architectures and the world of nanomaterials for multiple applications.

Introduction

The study of dendrimers[1−21] is now a broad and crucial supramolecular research field[8−11] that has applications *inter alia* in catalysis,[11−14] materials science,[11,15,16] and nanomedicine.[17−21] Click dendrimers have evolved in 2004[22] subsequently to Sharpless' concept of easy and practical

Published on the Web 12/08/2011 www.pubs.acs.org/accounts
10.1021/ar200235m

SCHEME 1. Comparison of Noncatalyzed and Cu^{I}-Catalyzed Alkyne–Azide Cycloadditions[a]

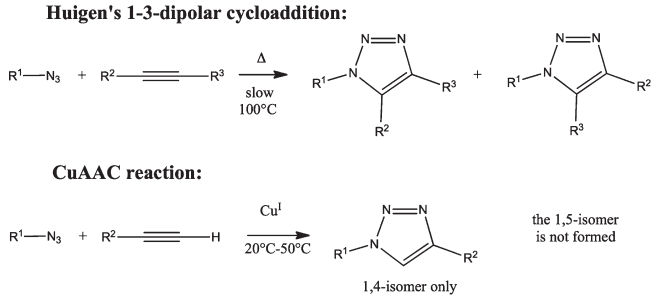

[a]The noncatalyzed Huisgen reaction is faster with electron-withdrawing alkyne substituent(s) than with electron-rich alkynes.

assembly of molecular fragments.[23] Among the various click reactions,[23] the copper-catalyzed azide–alkyne cycloaddition (CuAAC)[24−28] rapidly appeared as the most useful one and will be examined here (Scheme 1). There are indeed myriad ways to synthesize dendrimers,[1−11] but the CuAAC click reaction has recently appeared as one of the most efficient and productive.[29−32]

Since our initial interest in iterative reactions[33] on the way to dendrimers, we have developed dendrimer synthetic pathways that involve the Williamson reaction,[34,35] cross olefin metathesis,[36] and finally the CuAAC click reaction. The latter was used by either introducing the azido groups at the periphery and the ethynyl group at the focal point of incoming dendrons[37] or the converse.[38] We will first delineate here the specific problems encountered for the click synthesis of nanosystems that led us to disclose new efficient catalysts including dendritic ones. Then, whereas in the rich click literature the purpose was to assemble useful functional groups, our goal has also been to utilize the inorganic properties of the coordination and supramolecular interactions of the intradendritic [1,2,3]-triazole link. Designed applications are toward control of transition-metal nanoparticle growth and molecular recognition and will also be the subject of this Account.

CuAAC Click Synthesis in Nanoscience: A New, Efficient, and Easily Available Catalyst

The CuAAC click reaction is catalyzed by a large variety of Cu^{I} species that can be either generated *in situ* or directly introduced into the reaction medium.[23−32] One of the most important properties of the Sharpless catalyst, $CuSO_4$ + sodium ascorbate, is its simplicity and easy use including in aqueous solvents. Another key property, shared by all the Cu^{I} catalysts, is that it yields a single triazole isomer, the 1,4-substituted one, whereas the noncatalyzed Huisgen

SCHEME 2. Synthesis of the Dendrimer **5** Catalyzed by $[Cu^{I}$(hexabenzyltren)]Br, **1**, Compared with the Use of $CuSO_4$ + Sodium Ascorbate and the Catalyst $Cu^{I}[tren(C_{18}H_{37})_6]Br$, **2**

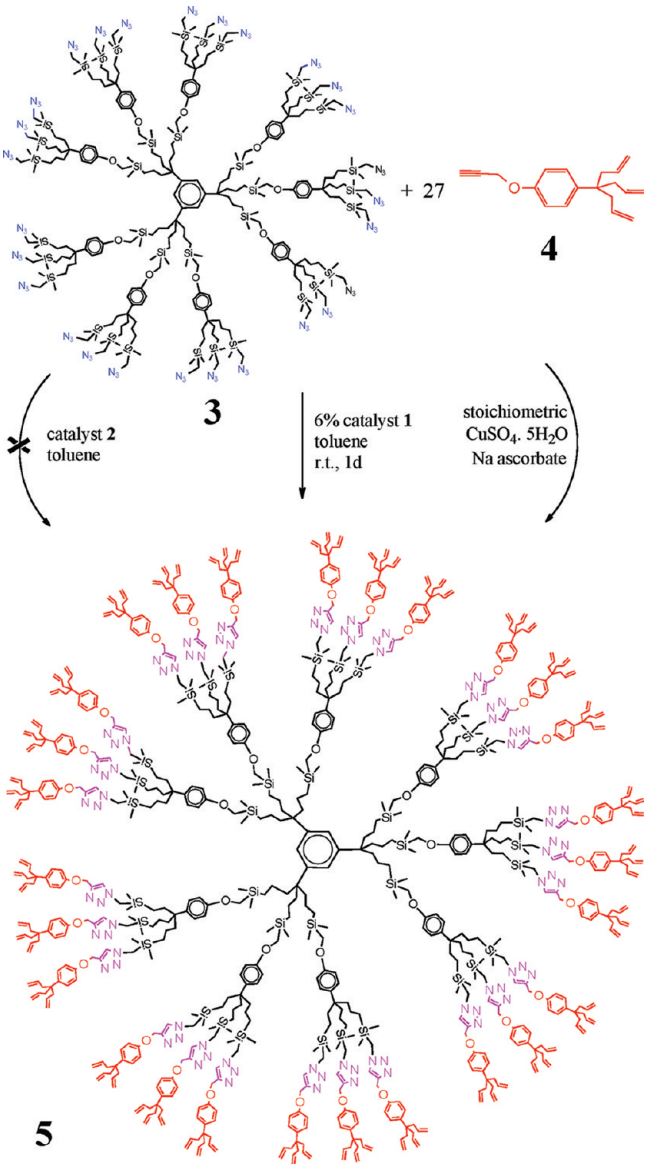

cycloaddition produces a mixture of 1,4- and 1,5-disubstituted triazoles (Scheme 1).

Finally, catalysis allows one to conduct the reactions under much milder conditions (20–60 °C) than the uncatalyzed reactions, which require temperatures above 100 °C, especially if the alkyne substituent is electron-rich. Indeed this catalyst presently is by far the most used CuAAC catalyst.[24] Several research groups have synthesized click dendrimers using this catalyst.[29,30] We have found, however, that catalytic amounts of this Sharpless catalyst probed in several solvents and under various temperatures could not lead to completion of the click reaction in the dendrimers

SCHEME 3. Synthesis of the Catalyst Cu^{I}(hexabenzyltren), **1**, of the CuAAC Reaction

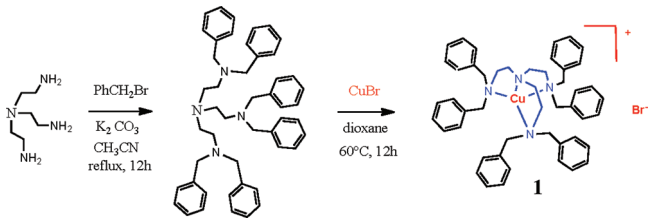

SCHEME 4. Synthesis of the Dendritic Cu^{I} Catalysts **6** and **7** of the CuAAC Reaction

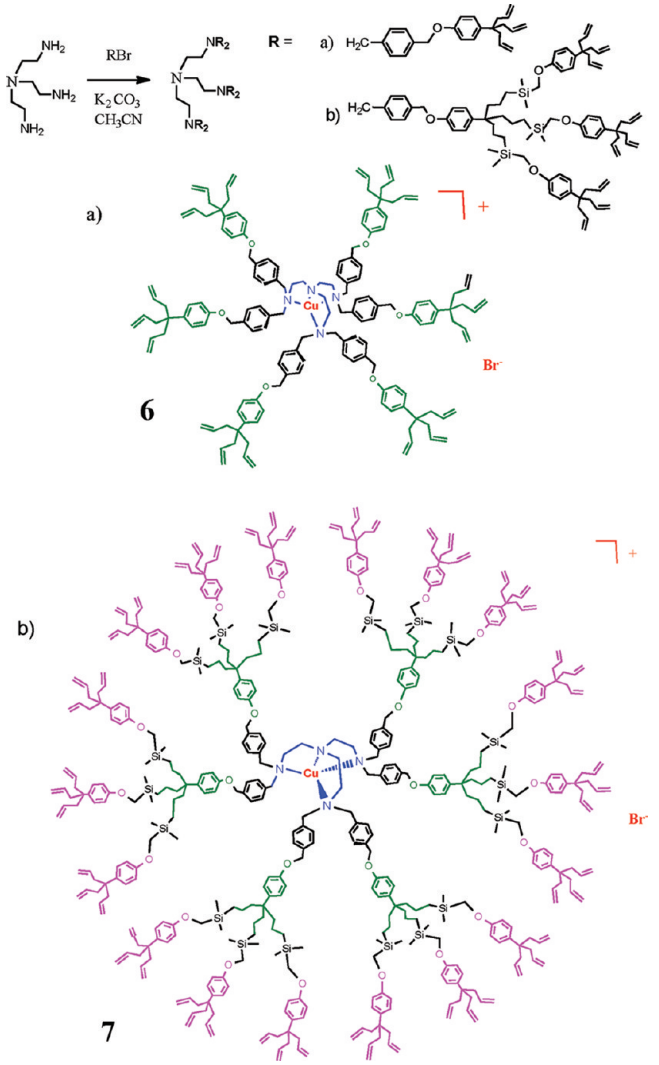

and that a stoichiometric amount of catalyst was required to obtain a satisfactory result beyond the zeroth dendritic generation.[37,38] The use of large quantities of toxic copper reagent is not compatible with green conditions required for biomedical use; thus improvements are needed. This problem in dendrimers and other branched nanosystems results

SCHEME 5. Monometallic Mechanism for the Click Reaction, Based on the Fokin–Finn Mechanism and Extended to Cu^{I}tren[a]

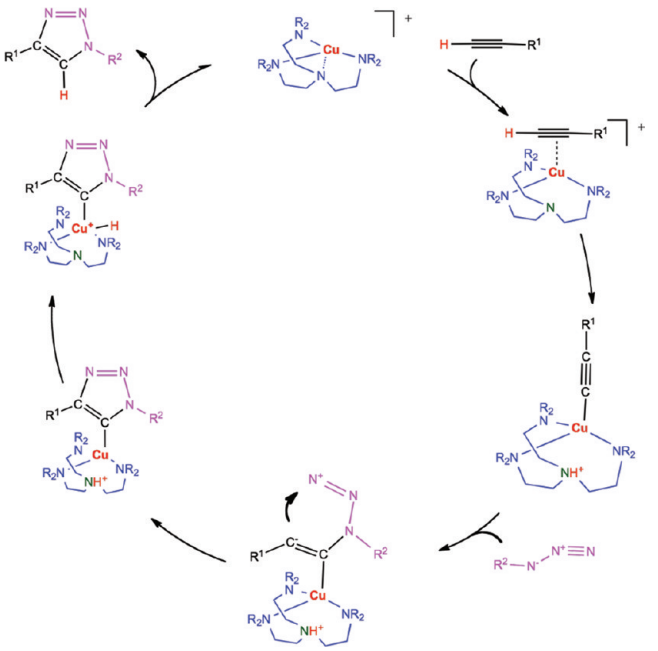

[a]Th Fokin–Finn mechanism involves azide attack on the metal before migration to the alkynyl ligand and a σ,π-bimetallic Cu^{I} intermediate that does not appear to be possible with the Cu^{I}-centered dendritic catalysts **6**, **7**, and **8**.

from the coordination of the Cu^{I} species to two or several intradendritic triazoles formed in the reactions, blocking further catalysis. The dendrimer topology facilitates this entropy-favored interbranch chelation of Cu^{I} in dendrimers, a problem that is not encountered in nondendritic click syntheses. We also noticed that the click CuAAC functionalization of gold nanoparticles (AuNPs) that were reported in the literature had involved very low reaction yields.[39] We could improve the click CuAAC functionalization of AuNPs with a variety of alkynes by carrying out the reaction under inert atmosphere, but again a stoichiometric amount of Sharpless catalyst[40] or even more[41] was required. Matyjaszewski's group showed that the Me_6tren [tren = tris(2-aminoethyl)-amine] ligand accelerates the Cu^{I} click catalysis by a factor of 50 compared with CuBr.[42] Subsequently, the pentane-soluble complex Cu[tren($C_{18}H_{37}$)$_6$]Br, **2**, was shown to catalyze the click functionalization of a zeroth-generation dendrimer bearing nine azido termini,[43] but this catalyst was inefficient for the click synthesis of the corresponding first-generation dendrimer because of its bulk.[44] On the other hand, the new toluene-soluble complex Cu[tren(CH_2Ph)$_6$]Br, **1**, was an efficient catalyst for the CuAAC click reaction of the first-generation (G1) dendrimer **3** containing 27 azido termini with a dendron **4** functionalized at the focal point with a propargyl group, cleanly yielding dendrimer **5** with 81 allyl termini (Scheme 2).[44]

SCHEME 6. Synthesis of the Water-Soluble Catalyst **8** Including Click Ligand Synthesis Catalyzed by **1**

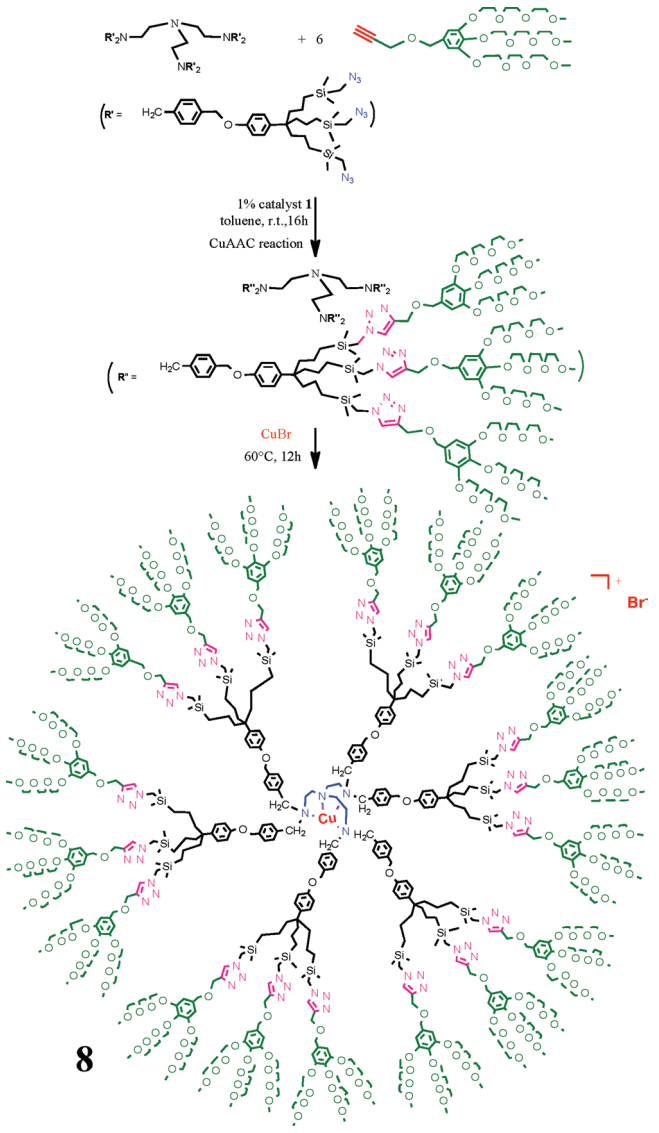

This complex was also an efficient catalyst in 10 mol % for the click functionalization of AuNPs. The complex **1** was synthesized by reaction of commercial tren with benzylbromide followed by heating hexabenzyltren with CuBr in dioxane (Scheme 3).

Although the medium is air-sensitive, the click reactions using this catalyst work well under air in the additional presence of sodium ascorbate. Alternatively, catalysis can be carried out as well if equal molar amounts of the air stable compound hexabenzyltren and CuBr are added together to the reaction medium in catalytic quantities. The catalytic use of **1** in click dendrimer synthesis and AuNP functionalization shows that the hexabenzyltren ligand of **1** resists full decoordination that would trap Cu^{I} stoichiometrically as in the

SCHEME 7. Click Synthesis of the Triazolylbiferrocenyl Dendrimers **9**–**13** from Five Generations of Azido-Terminated Dendrimers and Ethynylbiferrocene

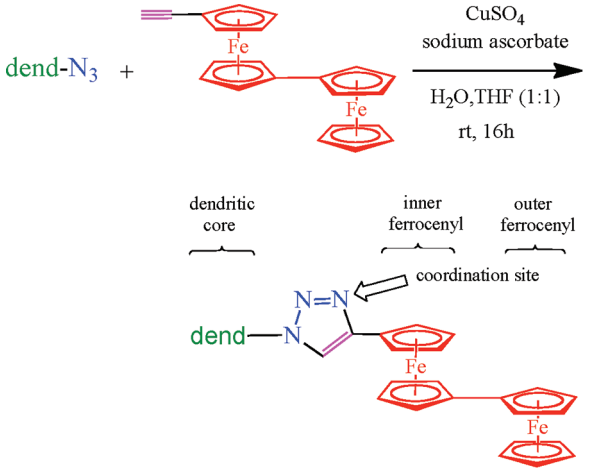

9: G0-9 biferrocenyltriazolyl termini (BiFc)
10: G1-27 BiFc
11: G2-81 BiFc
12: G3-243 -BiFc
13: G4-729 BiFc

case of the Sharpless Cu^{I} catalyst. This is also in favor of the monometallic mechanism shown in Scheme 2 for the series of Cu^{I} tren catalysts.

Reactions using the catalyst **1** or its above components are best conducted in toluene in which **1** is soluble, because the triazole reaction products are insoluble in this solvent and thus easily separated.[44]

Positive Dendritic Effects in CuAAC Click Catalysis and Catalysis "on" Water

$Cu[tren(CH_2Ph)_6]Br$-centered dendritic catalysts of zeroth and first generations, **6** and **7**, have been synthesized by covalently attaching dendrons in the para position of the phenyl groups of **1**,[44] according to a 1 → 3 connectivitity (Scheme 4).[45–47] Aerobic Cu^{I} oxidation to μ-oxo-bridged dicopper species is sterically prevented in these Cu^{I}-centered dendrimers. These dendritic catalysts are consequently much less air-sensitive than the parent complex **1**, due to the absence of possible inner-sphere oxidation pathways. Catalytic click reactions in toluene were also shown to proceed faster with **6** and **7** than with the parent catalyst **1**. Some click reactions such as that of phenyl acetylene with benzylazide are even faster with the G1 catalyst **7** than with the G0 catalyst **6**, indicating that intradendritic Cu^{I}–substrate supramolecular interactions are reminiscent of enzymatic catalysis. Thus for small substrates, the dendritic effect[48] is positive. This also shows that a monometallic mechanism is efficient for the click reaction (Scheme 5), because the

SCHEME 8. Selective Oxidation of the Outer Ferrocenyl Groups of the Triazolylbiferrocenyl Dendrimer **10** Using Ferrocenium Hexafluorophosphate Producing the Mixed-Valence Dendrimer **14**

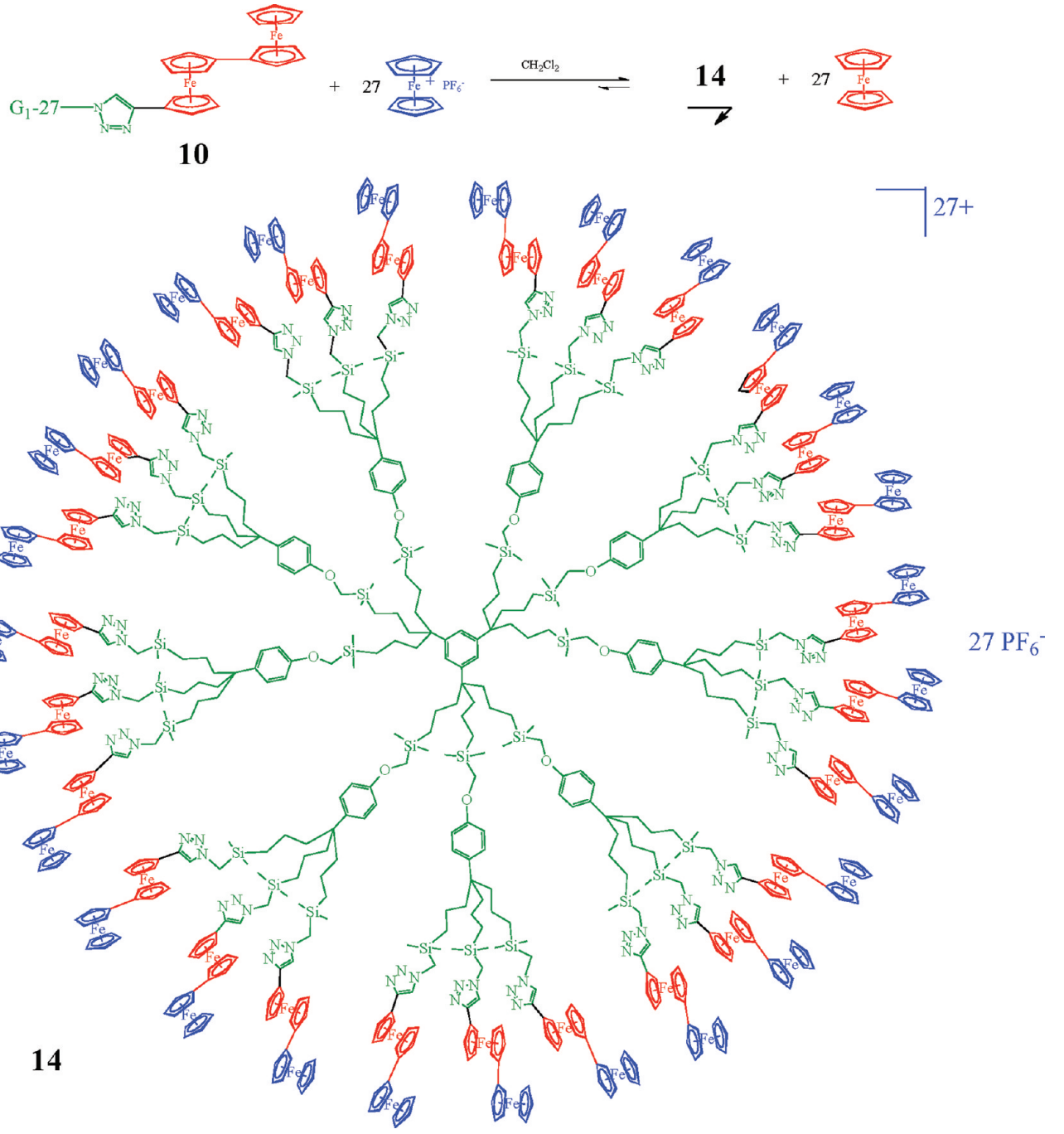

dendritic frame inhibits the approach of a second Cu^{I}-centered dendrimer.

Following detailed kinetic studies, Fokin and Finn pointed out the possibility of a σ,π-bimetallic Cu^{I} intermediate.[28,49−51] Indeed, in the absence of bulky (dendritic) polydentate accelerating ligands, a bimetallic mechanism is favored, because the $\pi-$Cu^{I} coordination of the σ-alkynyl ligand decreases the electronic density on this ligand, which facilitates the azide attack. If the tridentate ligand is not bulky, partial decoordination (even in the case of **1**) can eventually also give rise to this bimetallic mechanism. This was shown by the Scripps group using very efficient click catalysts of the type Cu^{I}{tris-(triazolylmethyl)amine} and related catalysts.[28,51]

Finally, a water-soluble Cu[tren(CH_2Ph)$_6$]$^{+}$-centered click catalyst **8** was synthesized by CuAAC click reaction between the Cu[tren(CH_2Ar)$_6$]Br core functionalized in the *para* aryl

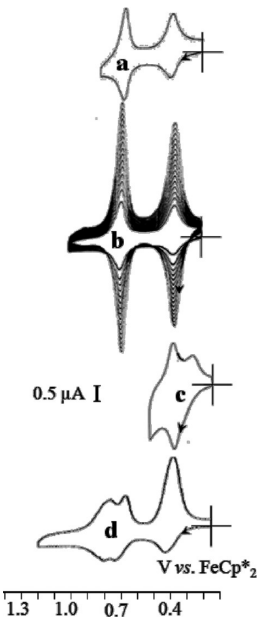

FIGURE 1. Selective roles of the inner and outer ferrocenyl groups of the 81-biferrocenyl dendrimer in the redox recognition of ATP^{2-} and Pd^{2+}. Cyclic voltammograms of the G2-81-biferrocenyl dendrimer **11** (a) in CH_2Cl_2, $[n\text{-}Bu_4N][PF_6]$ 0.1 M, (b) progressive adsorption upon scanning around the potential of the biferrocenyl potential area, (c) splitting of the outer-ferrocenyl CV wave upon addition of ATP, and (d) addition of $Pd(OAc)_2$ provoking the splitting of the inner ferrocenyl CV wave at 0.7 V.

position with azido groups and a tri(ethylene glycol)-terminated dendron bearing a propargyl group at the focal point. The click synthesis of the dendritic tren ligand of **8** was also catalyzed by the parent click catalyst **1** (Scheme 6). This complex catalyzed the CuAAC click reactions of water-insoluble substrates "on" water under air at ambient temperature and was recyclable several times without loss of activity. Catalysis of reactions "on" water is a broad research field that has recently been reviewed.[52]

Recognition of Transition-Metal Cations and Oxo-Anions Using the Coordination of Intradendritic [1,2,3]-Triazolyl Groups

Click dendrimer syntheses were designed not only as a very practical way to decorate dendrimers with useful organometallic groups,[53,54] water-solubilizing sugars,[55] and thermally robust carboranes (which advantageously bring a large number of such groups within a single molecular assembly)[56] but also specifically in order to benefit from the intradendritic generation of [1,2,3]-triazolyl ligands for coordination to transition-metal ions.[37,38] For instance, with $PdCl_2(PhCN)_2$, an X-ray crystal structure determination allowed the location of the [1,2,3]-triazole coordination site of $PdCl_2$ on the terminal N atom next to the substituent of the alkyne precursor of the triazole.[57] Such a coordination allowed the recognition of Cu^{I}, Cu^{II}, Pd^{II}, and Pt^{II}.[37] In the case of Pd^{II}, titration could indicate a 1:1 triazole/Pd^{II} stoichiometry and predict the number of Pd^{0} atoms, confirmed by transmission electron microscopy, in intradendritic PdNPs formed by reduction of these Pd^{II} ions in large dendrimers. This strategy generated with precise PdNP catalytic studies[58−60] was inspired by Crooks' pioneering studies of the poly(amido amine) (PAMAM)-dendrimer encapsulated PdNP catalysts.[61,62] Extremely efficient ("homeopathic") PdNP catalysts were disclosed in this way,[58] including some that were very efficient in aqueous media.[60] Along this line, note Yamamoto's approach who also conducted dendrimer encapsulation of transition-metal species using intradendritic phenylazomethine ligands for catalysis and materials science purposes.[63,64]

A recent remarkable use of triazole-containing dendrimers was achieved with biferrocenyl triazole dendrimers **9**−**13**, which were synthesized by click reactions between five generations of azido-terminated dendrimers, constructed with 1 → 3 connectivity, and ethynylbiferrocene (Scheme 7).[65]

Biferrocenyl-containing nanomaterials have been extensively studied by Nishihara's group and present unique mixed-valence properties.[66] Mixed-valence biferrocenium triazole dendrimers such as **14** were synthesized by oxidation of the neutral metallodendrimers with ferricinium hexafluorophosphate (Scheme 8).

These polycationic dendrimers result from selective oxidation of the outer ferrocenyl groups (*vide infra*), because the inner ferrocenyl groups are more difficult to oxidize due to the presence of the nearby electron-withdrawing triazolyl group. The Mössbauer spectrum at zero field of the mixed-valence dendrimer **14** with 27 biferrocenium termini showed a doublet for the ferrocenium groups and another one for the ferrocenyl groups indicating the localization of the mixed valence.[67] The cyclic voltammograms (CVs) of these dendrimers showed two chemically and electrochemically reversible waves at 0.4 and 0.7 V vs the internal reference decamethylferrocene,[68] although adsorption characterized by the decrease of the difference of potential between the anodic and cathodic waves decreased as the dendrimer generation increased (Figure 1). Addition of $[Pd(MeCN)_4][PF_6]_2$ to a CH_2Cl_2 solution of the dendrimer **11** containing 81 biferrocenyl triazole termini led to selective recognition by the second oxidation wave at 0.7 V, whereas addition of the oxo anion $[n\text{-}Bu_4N]_2[ATP]$ to the same solution of **11** led to selective recognition by the first oxidation wave at 0.4 V. This confirms that the inner ferrocenyl groups that are located near the triazole rings are more difficult to oxidize than the

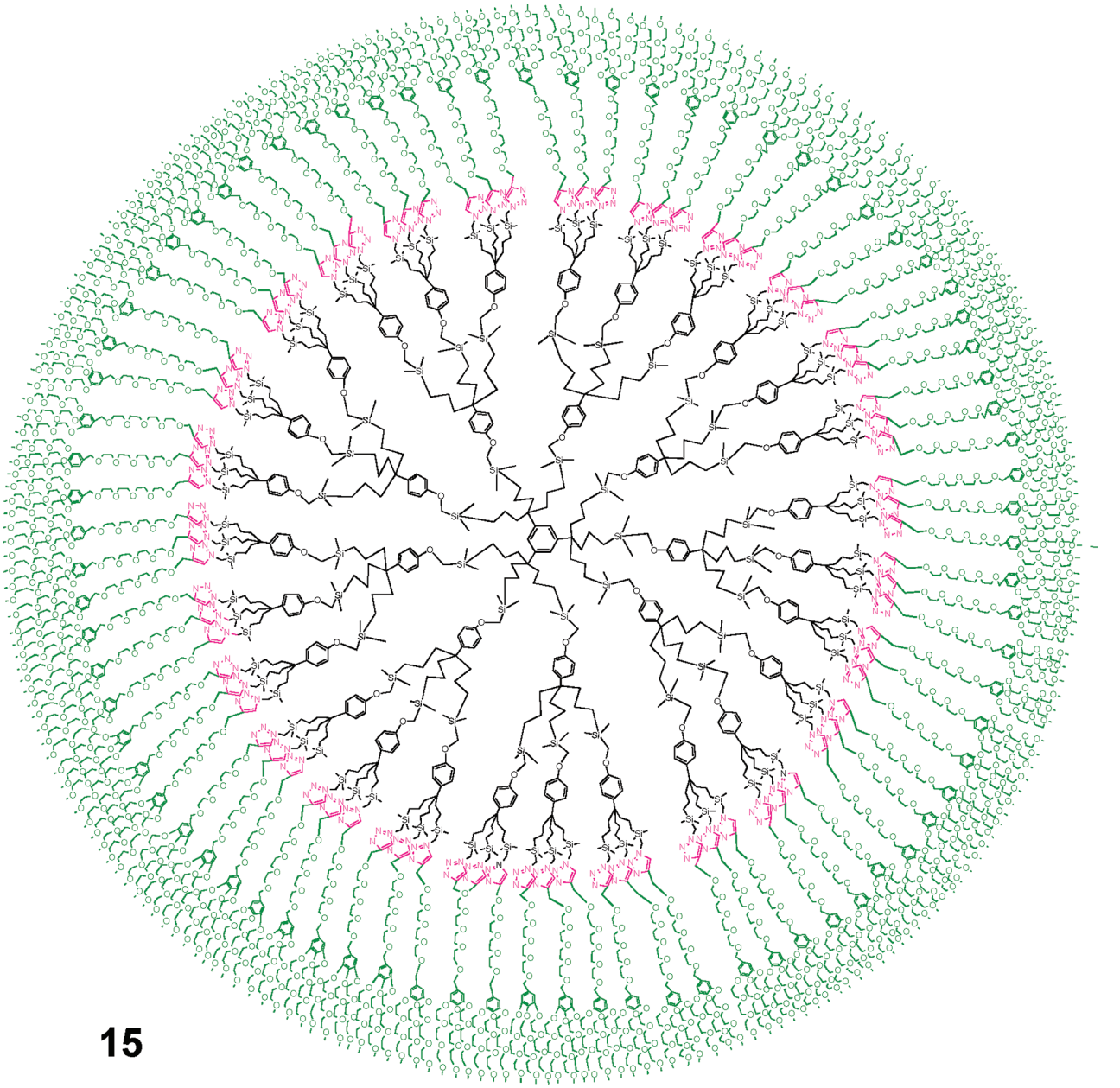

FIGURE 2. Generation-2 click dendrimer **15** terminated by 243 tri(ethylene glycol) groups (81 Percec-type dendrons) and constructed with 1 → 3 connectivity.

outer ones. The easier oxidation of the outer ferrocenes to ferricinium selectively creates positive charges at the dendrimer periphery that form ion pairing with the [ATP] anions just by setting the potential between 0.4 and 0.7 V (Figure 1).

Use and Role of the Intradendritic [1,2,3]-Triazolyl Groups in the Formation of Water-Soluble Dendrimer-Stabilized Gold Nanoparticles (AuNPs)

Initial work on click dendrimer-mediated stabilization of nanoparticles involved catalytically active PdNPs as mentioned above. We have recently been interested in click-dendrimer stabilization of water-soluble AuNPs because of the roles of AuNPs in catalysis (small AuNPs, in the range 1−3 nm)[69−73] and nanomedicine (large AuNPs, in the range 3−50 nm giving rise to plasmonic absorptions that are useful for both diagnostics and therapy).[41,74−77] Seminal work on PAMAM-dendrimer stabilization of AuNPs and other transition-metal NPs was carried out in the late 1990s,[78,79] in particular by the Crooks group, and has been reviewed including catalytic properties.[61,62,80,81]

In order to stabilize AuNPs in water, a variety of new dendrimers were synthesized from poly-azido-terminated

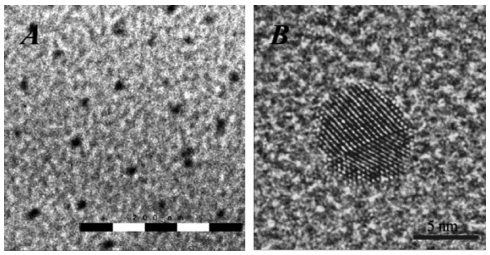

FIGURE 3. (a) TEM of the dendrimer **15** + 1 equiv of $HAuCl_4$ reduced by $[Fe^{I}Cp(\eta^6\text{-}C_6Me_6)]$ and (b) HRTEM of the dendrimer **15** + 1 equiv of $HAuCl_4$ reduced by $[Fe^{I}Cp(\eta^6\text{-}C_6Me_6)]$.

TABLE 1. Size Variation of AuNPs Stabilized by the Generation-2 Click Dendrimer **15** Terminated by 243 Tri(ethylene glycol) Groups (see Figure 3) in Methanol upon Reduction Using $NaBH_4$ in Methanol as a Function of the Addition of $HAuCl_4$

equiv. number of $HAu^{III}Cl_4$ per triazole	AuNP diameter (nm)
1	1.9 ± 0.2
3	3.8 ± 0.4
5	5.3 ± 0.5
7	6.8 ± 0.7
10	11.0 ± 1
20	11.3 ± 1

dendritic precursors (with 9, 27, and 81 azido groups) by CuAAC click reactions using 1 → 3 connectivity[44−46] with a Percec-type dendron[10] containing three tri(ethylene glycol) (TEG) termini and a tetra(ethylene glycol) functionalized with a propargyl group at the focal point (See the example of dendrimer **15** shown in Figure 2)

These dendrimers were compared with other structurally related dendrimers built using Williamson coupling[34,35] instead of CuAAC click coupling, in order to investigate the influence of the intradendritic triazolyl motifs. The TEG termini provided ideal conditions for AuNP formation from $HAuCl_4$ either using $NaBH_4$ as the reductant or without external reductant.[82] With $NaBH_4$, however, it was also indispensable to use click dendrimers terminated by Percec-type TEG dendrons in order to introduce Au^{III} inside the dendrimer by coordination to the triazole rings, which adequately modulated the nucleation. With the smallest dendrimer of the series that was terminated by only 27 TEGs, the AuNPs formed were larger (4.1 ± 0.5 nm) than the dendrimers and thus were stabilized by several dendrimers and showed a plasmon band at 540 nm. The larger dendrimers containing 81 (Figure 2) and 243 terminal TEGs (Figure 3) encapsulated AuNPs that were too small (1.9 ± 0.4 nm) to present a plasmon band. For comparison, when the dendrimer structure contained only TEG termini but no [1,2,3]-triazole or [1,2,3]-triazoles but no TEG-terminated dendrons, $NaBH_4$ reduction led to unstable AuNPs that precipitated after a few minutes. This was in contrast with PdNPs that were fully stabilized by such dendrimers and catalytically active in olefin hydrogenation and Suzuki−Miyaura reactions under ambient conditions.[58] On the other hand, in the absence of external reductant, Au^{III}−triazole coordination slowed Au^{III} reduction in dendrimers terminated by TEG dendrons, because the distal Percec-type dendron itself was the reductant. The semicavitand effect of the three TEGs of the dendron was then crucial, as shown by the failure of Au^{III} reduction using a click dendrimer terminated by a linear tetra(ethylene glycol) instead of a Percec-type TEG dendron. Dendrimer-stabilized AuNPs were formed with the click as well as nonclick dendrimers from $HAuCl_4$ in this way in the absence of additional reductant. Then AuNPs had a 23−42 nm size depending on the generation.[83] Choosing the $AuCl_4$/dendrimer stoichiometry also oriented the size of the AuNPs formed (Table 1).

Monoelectronic reductants such as ferrocene, ethynylferrocene, decamethylferrocene, and the electron-reservoir sandwich complex $[Fe^{I}(\eta^5\text{-}C_5H_5)(\eta^6\text{-}C_6Me_6)]$, which has 19 valence electrons on the iron valence shell,[33,84] have also been used for the first time for the reduction of $HAuCl_4$ to AuNPs (Figure 3). Their outer-sphere reduction mechanism[67] implied a much slower reduction than that involving the inner-sphere reductant $NaBH_4$, and the size of the dendrimer-stabilized AuNPs formed (between 7 and 38 nm) was directly related to the standard oxidation potentials of the Fe^{I} and Fe^{II} reductants. This provided the possibility to finely tune the size of the AuNPs.[83]

All these water-soluble dendrimer-stabilized PEGylated AuNPs were only weakly stabilized and are thus potentially useful for catalytic (small size) and biomedical applications (large size).

Conclusion and Prospects

The CuAAC click synthesis is a superb synthetic tool that has been usefully and successfully applied by the pioneers of this chemistry to the biological and biomedical field.[22−28] Concerning the synthesis of relatively large dendrimers and click functionalized transition-metal nanoparticles the design of new liganded catalysts was required as illustrated here by the efficient, practical, and easily made complex Cu[tren-$(CH_2Ph)_6$]Br. Very efficient dendritic analogue catalysts showed that a mononuclear Cu^{I} catalysis is involved, and the positive dendritic effect recalls enzymatic catalysis.[85] Even if the copper catalyst is not desired in green processes, it can be removed from the click reaction medium when these catalysts are used.

Alternatively, copper-free solutions are known either with electron-deficient alkyne substrates (the Huisgen cycloadditions are then possible in water under mild conditions)[86] or using strain-promoted alkyne−azide cycloaddition.[87] The synthesis of click dendrimers not only allows decoration of dendrimers with a large number of substrates of interest but also the introduction of the intradendritic [1,2,3]-triazoles to allow their use to coordinate transition-metal ions. Applications have been illustrated here in molecular recognition and for the fine-tuning of the formation of small catalytically active PdNPs as well as AuNPs of various sizes ranging from 1.8 to 42 nm. The difference of influence of the multiple structural and reactivity parameters on the stabilization and size of the NPs of these two metals is thus impressive. The intradendritic [1,2,3]-triazole ligands are also a key to redox recognition that is helpful for the control of the size of potentially useful, weakly liganded transition-metal nanoparticles.

In summary, CuAAC click chemistry plays a pivotal role in the interplay between dendritic architectures and nanoparticles, that is, between molecular nanoscience and nanomaterials, and this concept is clearly called for many further developments and applications.

Excellent contributions by the colleagues and students cited in the references and financial support from the Université Bordeaux 1, the Centre National de la Recherche Scientifique, and the Agence Nationale pour la Recherche (ANR project 07-CPD-05-01)) are gratefully acknowledged.

BIOGRAPHICAL INFORMATION

Didier Astruc is Professor at the Université Bordeaux 1 and Member of the Institut Universitaire de France. He did his doctorates in Rennes, and a postdoctoral term with Richard R. Schrock at MIT. His interests are in inorganic chemistry and applications of nanosystems to catalysis, sensors, energy-related problems, and nanomedicine.

Liyuan Liang presented her Ph.D. thesis with Didier Astruc on dendritic nanoreactors and molecular recognition in 2011. She is now pursuing postdoctoral studies in Toronto with Doug Stephan. Her interests are in nanosciences.

Following undergraduate studies in Athens, **Amalia Rapakousiou**, is a graduate student in Didier Astruc's group. Her present research project is related to giant biferrocenyl dendrimers and nanosystems.

After undergraduate studies in Santiago de Chile, **Jaime Ruiz** passed his Ph.D. and Habilitation in Bordeaux on the reactivity 19-electron Fe(I) complexes. He has been a CNRS Engineer in Didier Astruc's group in Bordeaux for more than a decade, and his interests are in organometallic synthesis, electrochemistry, dendrimers, and nanoparticles.

FOOTNOTES

*E-mail: d.astruc@ism.u-bordeaux1.fr.

REFERENCES

1 Newkome, G. R.; Moorefield, C. N.; Vögtle, F. *Dendrimers and Dendrons. Concepts, Syntheses, Applications*; Wiley-VCH: Weinheim, Germany, 2001.
2 *Dendrimers and Other Dendritic Polymers*; Tomalia, D. A., Fréchet, J. M. J., Eds; Wiley: Amsterdam, 2001.
3 Vögtle, F.; Richardt, G.; Werner, N. *Dendrimer Chemistry: Concepts, Syntheses, Properties, Applications*; Wiley: Weinheim, Germany, 2009.
4 Tomalia, D. A.; Naylor, A. M.; Goddard, W., III Starburst Dendrimers. Molecular Level Control of Size, Shape, Surface Chemistry, Topology and Flexibility from Atoms to Macroscopic Matter. *Angew. Chem., Int. Ed.* **1990**, *29*, 138–175.
5 *Advances in Dendritic Macromolecules*; Newkome, G. R., Ed., JAI Press: Greenwich, CT, 1994, 1995, 1996, 1999, and 2002; respectively, Vols 1, 2, 3, 4, and 5.
6 *New. J. Chem.* 2007, *31*, 1025−1380. Special issue on Dendrimers, Majoral, J.-P. Ed.
7 Dendrimers and Nanosciences. *C. R. Chim.* 2003, *6*, 709−1208; Astruc, D., Ed., Elsevier, Paris.
8 Bosman, A. W.; Janssen, H. M.; Meijer, E. W. About Dendrimers: Structure, Physical Properties, and Applications. *Chem. Rev.* **1999**, *99*, 1665–1688.
9 Zeng, F.; Zimmermann, S. C. Dendrimers in Supramolecular Chemistry: From Molecular Recognition to Self-Assembly. *Chem. Rev.* **1997**, *97*, 1681–1712.
10 Rosen B., M.; Wilson, C. J.; Wilson, D. A.; Peterca, M.; Imam, M. R.; Percec, V. Dendron-Mediated Self-Assembly, Disassembly, and Self-Organization of Complex Systems. *Chem. Rev.* **2009**, *109*, 6275–6340.
11 Astruc, D.; Boisselier, E.; Ornelas, C. Dendrimers Designed for Functions: From Physical, Photophysical and Supramolecular Properties to Applications in Sensing, Catalysis, Molecular Electronics, Photonics and Nanomedicine. *Chem. Rev.* **2010**, *110*, 1857–1959.
12 Chase, P. A.; Gebbink, R. J. M. K.; van Koten, G. Where Organometallics and Dendrimer Merge: The Incorporation of Organometallic Species into Dendritic Molecules. *J. Organomet. Chem.* **2004**, *689*, 4016–4054.
13 Oosterom, G. E.; Reek, J. N. H.; Kamer, P. C. J.; van Leeuwen, P. W. N. M. Transition Metal Catalysis Using Functionalized Dendrimers. *Angew. Chem., Int. Ed.* **2001**, *40*, 1828–1849.
14 *Dendrimer Catalysis*; Gade, L., Ed.; Springer: Heidelberg, Germany, 2006.
15 Balzani, V.; Ceroni, P.; Juris, A.; Venturi, M.; Campagna, S.; Puntoriero, F.; Serroni, S. Dendrimers Based on Photoactive Metal Complexes. Recent Advances. *Coord. Chem. Rev.* **2001**, *219−221*, 545–572.
16 Andronov, A.; Fréchet, J. M. J. Light-Harvesting Dendrimers. *Chem. Commun.* **2000**, 1701–1710.
17 Svenson, S.; Tomalia, D. A. Commentary. Dendrimers in Biochemical Applications. Reflexions on the Field. *Adv. Drug Delivery Rev.* **2005**, *57*, 2106–2129.
18 Gillies, E. R.; Fréchet, J. M. J. Dendrimers and Dendritic Polymers in Drug Delivery. *Drug Discovery Today* **2005**, *10*, 35–43.
19 Boas, U.; Christensen, J. B. *Dendrimers in Medicine and Biotechnology*; Royal Chemical Society Publishing: Cambridge, U.K., 2006.
20 *Dendrimer-Based Nanomedicine*; Majoros, I. J., Baker, J. R., Jr., Eds., Pan Stanford Publishing: Stanford, CA, 2008.
21 Astruc, D. Research Avenues on Dendrimers Towards Molecular Biology from Biomimetism to Medicinal Engineering. *C. R. Acad. Sci.* **1996**, *322* (Ser. IIb), 757–766.
22 Kolb, H. C.; Finn, M. G.; Sharpless, K. B. Click Chemistry: Diverse Chemical Functions from a Few Good Reactions. *Angew. Chem., Int. Ed.* **2001**, *40*, 2004–2021.
23 Wu, P.; Feldman, A. K.; Nugent, A. K.; Hawker, C. J.; Scheel, A.; Voit, B.; Pyun, J.; Fréchet, J. M. J.; Sharpless, K. B.; Fokin, V. V. Efficiency and Fidelity in a Click Chemistry Route to Dendrimers by the Copper(I)-Catalyzed Ligation of Azides and Alkynes. *Angew. Chem., Int. Ed.* **2004**, *43*, 3928–3932.
24 Rostovtsev, V. V.; Green, L. G.; Fokin, V. V.; Sharpless, K. B. A Stepwise Huisgen Cycloaddition Process: Copper(I)-Catalyzed Regioselective Ligation of Azides and Terminal Alkynes. *Angew. Chem., Int. Ed.* **2002**, *41*, 2596–2599.
25 Tornøe, C. W.; Christensen, C.; Meldal, M. Peptidotriazoles on Solid Support: [1,2,3]-Triazoles by Regiospecific Copper (I)-Catalyzed 1,3-Dipolar Cycloaddition of Terminal Alkynes to Azides. *J. Org. Chem.* **2002**, *67*, 3057–3064.
26 Bock, V. D.; Hiemstra, H.; van Maarseveen, J. H. Cu(I)-Catalyzed Azide-Alkyne Click Cycloaddition from a Mechanistic and Synthetic Perspective. *Eur. J. Org. Chem.* **2005**, 51–68.
27 Meldal, M.; Tornøe, C. W. Cu-Catalyzed Azide-Alkyne Cycloaddition. *Chem. Rev.* **2008**, *108*, 2952–3015.

28 Hein, J. E.; Fokin, V. V. Copper-Catalyzed Azide-Alkyne Cycloaddition (CuAAC) and Beyond: New Reactivity of Copper(I) Acetylides. *Chem. Soc. Rev.* **2010**, *39*, 1302–1315.

29 Voit, B. The Potential of Cycloaddition Reactions in the Synthesis of Dendritic Polymers. *New J. Chem.* **2007**, *31*, 1139–1151.

30 Franc, G.; Kakkar, A. Dendrimer Design Using Cu(I)-Catalyzed Alkyne-Azide Click Chemistry. *Chem. Commun.* **2008**, 5267–5276.

31 Fournier, D.; Hoogenboom, R.; Schubert., U. S. Clicking Polymers: A Straightforward Approach to Novel Macromolecular Architectures. *Chem. Soc. Rev.* **2007**, *36*, 1369–1380.

32 Liang, L.; Astruc, D. The Copper(I)-Catalyzed Alkyne-Azide Cycloaddition (CuAAC) Click Reaction and its Applications. An Overview. *Coord. Chem. Rev.* **2011**, *255*, 2933–2945.

33 Astruc, D.; Hamon, J.-R.; Althoff, G.; Román, E.; Batail, P.; Michaud, P.; Mariot, J.-P.; Varret, F.; Cozak, D. Design, Stabilization and Efficiency of Organometallic "Electron Reservoirs". 19-Electron Sandwichs η^5-$C_5R_5Fe^I$ η^6-$C_6R'_6$, a Key Class Active in Redox Catalysis. *J. Am. Chem. Soc.* **1979**, *101*, 5445–5447.

34 Sartor, V.; Djakovitch, L.; Fillaut, J.-L.; Moulines, F.; Neveu, F.; Marvaud, V; Guittard, J.; Blais, J.-C.; Astruc, D. Organoiron Routes to a New Dendron for Fast Dendritic Syntheses Using Divergent and Convergent Methods. *J. Am. Chem. Soc.* **1999**, *121*, 2929–2930.

35 Ruiz, J.; Lafuente, G.; Marcen, S.; Ornelas, C.; Lazare, S.; Cloutet, E.; Blais, J.-C.; Astruc, D. Construction of Giant Dendrimers Using a Tripodal Buiding Block. *J. Am. Chem. Soc.* **2003**, *125*, 7250–7257.

36 Ornelas, C.; Méry, D.; Cloutet, E.; Ruiz, J.; Astruc, D. Cross Olefin Metathesis for the Selective Functionalization, Ferrocenylation, and Solubilization in Water of Olefin-Terminated Dendrimers, Polymers and Gold Nanoparticles and for a Divergent Dendrimer Construction. *J. Am. Chem. Soc.* **2008**, *130*, 1495–1506.

37 Ornelas, C.; Ruiz, J.; Cloutet, E.; Alves, S.; Astruc, D. Click Assembly of [1,2,3]-Triazole-Linked Dendrimers Including Ferrocenyl Dendrimers that Sense Both Oxo-Anions and Metal Cations. *Angew. Chem., Int. Ed.* **2007**, *46*, 872–877.

38 Camponovo, J.; Ruiz, J.; Cloutet, E.; Astruc, D. New Polyalkynyl Dendrons and Dendrimers, Click Chemistry with Azidomethylferrocene and Anion and Cation Redox Sensing Properties of the [1,2,3]-Triazole-Containing Dendrimers. *Chem.—Eur. J.* **2009**, *15*, 2990–3002.

39 Thode, C. J.; Williams, M. E. Kinetics of 1,3-Dipolar Cycloaddition on the Surface of Au Nanoparticles. *J. Colloid Interface Sci.* **2008**, *320*, 346–352.

40 Boisselier, E.; Salmon, L.; Ruiz, J.; Astruc, D. How to Very Efficiently Functionalize Gold Nanoparticles by Click Chemistry. *Chem. Commun.* **2008**, 5788–5790.

41 François, A.; Laroche, Pinaud, N.; Salmon, L.; Ruiz, J.; Robert, J.; Astruc, D. Encapsulation of Docetaxel into PEGylated Gold Nanoparticles for Vectorization to Cancer Cells and in vitro Results. *ChemMedChem* **2011**, *6*, 2003–2008.

42 Golas, P. L.; Tsarevsky, N. V.; Sumerlin, B. S.; Matyjaszewski, K. Catalyst Performances in Click Coupling Reactions of Polymers Prepared by ATRP: Ligand and Metal Effects. *Macromolecules* **2006**, *39*, 6451–6457.

43 Candelon, N.; Lastécouère, D.; Diallo, A. K.; Ruiz, J.; Astruc, D.; Vincent, J.-M. A Highly Active and Reusable Copper(I)-Tren Catalyst for the Click 1,3-Dipolar Cycloaddition of Azides and Alkynes. *Chem. Commun.* **2008**, 741–743.

44 Liang, L.; Ruiz, J.; Astruc, D. The Efficient Copper(I) (hexabenzyl)tren Catalyst and Dendritic Analogues for Green Click Reactions between Azides and Alkynes in Organic Solvent and in Water. Positive Dendritic Effects and Monometallic Mechanism. *Adv. Synth. Catal.* **2011**, *in press*.

45 Newkome, G. R.; Yao, Z.; Baker, G. R.; Gupta, V. K. Micelles 1. Cascade Molecules: A New Approach to Micelles. A 27-Arborol. *J. Org. Chem.* **1985**, *50*, 2003–2004.

46 Newkome, G. R.; Shreiner, C. D. Dendrimers Derived from 1→3 Branching Motifs. *Chem. Rev.* **2010**, *110*, 6338–6442.

47 Astruc, D.; Ruiz, J. Organoiron-Mediated Dendrimer Syntheses with 1→3 Connectivity. *Tetrahedron* **2010**, *66*, 1769–1785.

48 Astruc, D.; Chardac, F. Dendritic Catalysts and Dendrimers in Catalysis. *Chem. Rev.* **2001**, *101*, 2991–3031.

49 Chan, T. R.; Hilgraf, R.; Sharpless, K. B.; Fokin, V. V. *Org. Lett.* **2004**, *6*, 2853–2855.

50 Rodionov, V. O.; Presolski, V. I.; Gardiner, S.; Lim, Y. H.; Finn, M. G. Benzimidazole and Related Ligands for Cu-Catalyzed Cycloaddition. *J. Am. Chem. Soc.* **2007**, *129*, 12696–12704.

51 Rodionov, V. O.; Presolski, V. I.; Diaz, D. D.; Fokin, V. V.; Finn, M. G. Ligand-Accelerated Cu-Catalyzed Azide-Alkyne Cycloaddition: A Mechanistic Report. *J. Am. Chem. Soc.* **2007**, *129*, 12705–12712.

52 Chanda, A.; Fokin, V. V. Organic Synthesis "on" Water. *Chem. Rev.* **2009**, *109*, 725–748.

53 Astruc, D.; Ornelas, C.; Ruiz, J. Click Synthesis of Organosilicon Dendrimers. *Main Group Chem.* **2010**, *9*, 87–100.

54 Djeda, R.; Ornelas, C.; Ruiz, J.; Astruc, D. Branching the Electron-Reservoir Complex [Fe(η^5-C_5H_5)(η^6-C_6Me_6)][PF_6] onto Large Dendrimers: Click, Amide and Ionic Bonds. *Inorg. Chem.* **2010**, *49*, 6085–6101.

55 Gatard, S.; Liang, L.; Salmon, L.; Ruiz, J.; Astruc, D.; Bouquillon, S. Water-Soluble Glycodendrimers: Synthesis and Stabilization of Catalytically Active Pd and Pt Nanoparticles. *Tetrahedron Lett.* **2011**, *52*, 1842–1846.

56 Djeda, R.; Ruiz, J.; Astruc, D.; Satapathy, R.; Prasanna Dash, B.; Hosmane, N. S. Click Synthesis and Properties of Carborane-Appended Large Dendrimers. *Inorg. Chem.* **2010**, *49*, 10702–10709.

57 Badèche, S.; Daran, J.-C.; Ruiz, J.; Astruc., D. Synthesis and Coordination Chemistry of Ferrocenyl-[1,2,3]-Triazolyl Ligands. *Inorg. Chem.* **2008**, *47*, 4903–4908.

58 Diallo, A. K.; Ornelas, C.; Salmon, L.; Ruiz, J.; Astruc, D. Homeopathic Catalytic Activity and Atom-Leaching Mechanism in the Miyaura-Suzuki Reactions under Ambient Conditions Using Precise Click Dendrimer-Stabilized Pd Nanoparticles. *Angew. Chem., Int. Ed.* **2007**, *46*, 8644–8648.

59 Ornelas, C.; Salmon, L.; Ruiz, J.; Astruc., D. Click Dendrimers: Synthesis, Redox Sensing of $Pd(OAc)_2$, and Remarkable Catalytic Hydrogenation Activity of Precise Pd Nanoparticles Stabilized by [1,2,3]-Triazole-Containing Dendrimers. *Chem.—Eur. J.* **2008**, *14*, 50–64.

60 Ornelas, C.; Ruiz, J.; Salmon, L.; Astruc, D. Sulfonated Click Dendrimer-Stabilized Palladium Nanoparticles as Highly Efficient Catalysts for Olefin Hydrogenation and Suzuki Coupling Reactions Under Ambient Conditions in Aqueous Media. *Adv. Synth. Catal.* **2008**, *350*, 837–845.

61 Crooks, R. M.; Zhao, M.; Sun, L.; Chechik, V.; Yeung, L. K. Dendrimer-Encapsulated Metal Nanoparticles: Synthesis, Characterization, and Applications to Catalysis. *Acc. Chem. Res.* **2001**, *34*, 181–190.

62 Scott, R. W. J.; Wilson, O. M.; Crooks, R. M. Synthesis, Characterization and Applications of Dendrimer-Encapsulated Nanoparticles. *J. Phys. Chem. B* **2005**, *109*, 692–718.

63 Nakajima, R.; Tsuruta, M.; Higuchi, M; Yamamoto, K. Fine Control and Encapsulation of Fe Ions in Dendrimers through Ferritin-Like Redox Switching. *J. Am. Chem. Soc.* **2004**, *126*, 1630–1631.

64 Yamamoto, K.; Higuchi, M. Dendritic Polyphenylazomethines: Synthesis, Structure, and Metal-Assembling Function. *Pure Appl. Chem.* **2004**, *76*, 1399–1408.

65 Djeda, R.; Rapakousiou, A.; Liang, L.; Guidolin, N.; Ruiz, J.; Astruc, D. Click Syntheses of Large [1,2,3]-Triazolylbiferrocenyl Dendrimers and Selective Roles of the Inner and Outer Ferrocenyl Groups in the Redox Recognition of the ATP^{2-} Anion and Pd^{II} Cation. *Angew. Chem., Int. Ed.* **2010**, *49*, 8152–8156.

66 Yamada, M.; Nishihara, H. Electrodeposition of Biferrocene Derivative-Attached Gold Nanoparticles: Solvent Effects and Lithography Assembly. *Langmuir* **2003**, *19*, 8050–8056.

67 Astruc, D. *Electron-Transfer and Radical Processes in Transition-Metal Chemistry*; VCH: New York, 1995; Chapters 1 and 4.

68 Ruiz, J.; Astruc, D. Permethylated Electron-Reservoir Sandwich Complexes as References for the determination of Redox Potentials. Suggestion of a New Redox Scale. *C. R. Acad. Sci. Paris* **1998** (Ser. II c), 21–27.

69 Haruta, M. Size and Support Dependency of the Catalysis of Gold. *Catal. Today* **1997**, *36*, 153–166.

70 Hashmi, A. S. K.; Hutchings, G. J. Gold Catalysis. *Angew. Chem., Int. Ed.* **2006**, *45*, 7896–7936.

71 Corma, A.; Leyva-Perez, A.; Sabater, M. J. Gold-Catalyzed Carbon-Heteroatom Bond-Forming Reactions. *Chem. Rev.* **2011**, *111*, 1657–1712.

72 Della Pina, C.; Faletta, M.; Prati, L.; Rossi, M. Selective Oxidation Using Gold. *Chem. Soc. Rev.* **2008**, *37*, 2077–2095.

73 Louis, C. In *Nanoparticles and Catalysis*; Astruc, D., Ed.; Wiley-VCH: Weinheim, Germany, 2007; Chapter 15 (see also AuNP catalysis in Chapters 1 and 12—14).

74 Hirsch, L. R.; Stafford, R. J.; Halas, N. J.; Bakson, J. A.; Shershen, S. R.; Rivera, B.; Price, R. E.; Hazle, J. D.; West, J. L. Nanoshell-Mediated Near-Infrared Therapy of Tumors under Magnetic Resonance Guidance. *Proc. Natl. Acad. Sci. U.S.A.* **2003**, *100*, 13549–13554.

75 Murphy, C. J.; Gole, A. M.; Hunyadi, S. E.; Stone, J. W.; Sisco, P. N.; Alkilany, A.; Kinard, B. E.; Hankins, P. Chemical Sensing and Imaging with Metallic Nanorods. *Chem. Commun.* **2008**, 544–557.

76 Jain, P. K.; Huang, X. H.; El Sayed, I. H.; El Sayed, M. A. Noble Metals on the Nanoscale: Optical and Photothermal Properties and Some Applications in Sensing, Biology and Nanomedicine. *Acc. Chem. Res.* **2008**, *41*, 1578–1586.

77 Boisselier, E.; Astruc, D. Gold Nanoparticles in Nanomedicine: Preparations, Diagnostic, Therapy and Toxicity. *Chem. Soc. Rev.* **2009**, *38*, 1759–1782.

78 Zhao, M.; Sun, L.; Crooks, R. M. Preparation of Cu Nanoclusters within Dendrimer Templates. *J. Am. Chem. Soc.* **1998**, *120*, 4877–4878.

79 Balogh, L.; Tomalia, D. A. Poly(amidoamine) Dendrimer Composites 1. Synthesis of Zerovalent Copper Nanoclusters. *J. Am. Chem. Soc.* **1998**, *120*, 7355–7356.

80 Zhao, M. Q.; Crooks, R. M. Homogeneous Hydrogenation Catalysis with Monodisperse Dendrimer-Encapsulated Nanoparticles. *Angew. Chem., Int. Ed.* **1999**, *38*, 364–366.

81 Yancey, D. F.; Carino, E. V.; Crooks, R. M. Electrochemical Synthesis and Electrocatalytic Properties of Au@Pt Dendrimer-Encapsulated Nanoparticles. *J. Am. Chem. Soc.* **2010**, *132*, 2942–2950.

82 Boisselier, E.; Diallo, A. K.; Salmon, L.; Ruiz, J.; Astruc, D. Gold Nanoparticles Synthesis and Stabilization via New Clicked Polyethyleneglycol Dendrimers. *Chem. Commun.* **2008**, 4819–4821.

83 Boisselier, E.; Diallo, A. K.; Salmon, L.; Ornelas, C.; Ruiz, J.; Astruc, D. Encapsulation and Stabilization of Gold Nanoparticles with Click Polyethyleneglycol Dendrimers. *J. Am. Chem. Soc.* **2010**, *132*, 2729–2742.

84 Desbois, M.-H.; Astruc, D.; Guillin, J.; Varret, F.; Trautwein, A. X.; Villeneuve, G. *J. Am. Chem. Soc.* **1989**, *111*, 5800–5809.

85 Liu, L.; Breslow, R. Dendrimeric Pyridoamine Enzyme Mimics. *J. Am. Chem. Soc.* **2003**, *125*, 12110–12111.

86 Li, Z. M.; Seo, T. S.; Ju, J. Y. 1,3-Dipolar Cycloaddition of Azides with Electron-Deficit Alkynes under Mild Conditions in Water. *Tetrahedron Lett.* **2004**, *45*, 3143–3146.

87 Ornelas, C.; Broichhagen, J.; Weck, M. Strain-Promoted Alkyne Azide Cycloaddition for the Functionalization of Poly(amide)-Based Dendrons and Dendrimers. *J. Am. Chem. Soc.* **2010**, *132*, 3923–3931.

ORGANOMETALLICS

Article

pubs.acs.org/Organometallics

Living Ring-Opening Metathesis–Polymerization Synthesis and Redox-Sensing Properties of Norbornene Polymers and Copolymers Containing Ferrocenyl and Tetraethylene Glycol Groups

Haibin Gu,[†,§] Amalia Rapakousiou,[†] Patricia Castel,[†] Nicolas Guidolin,[‡] Nöel Pinaud,[†] Jaime Ruiz,[†] and Didier Astruc*[,†]

[†]ISM, UMR CNRS No. 5255, University of Bordeaux, 33405 Talence Cedex, France

[‡]LCPO, UMR CNRS No. 5629, University of Bordeaux, 33607 Pessac Cedex, France

Supporting Information

ABSTRACT: The controlled synthesis of monodisperse, redox-active metallopolymers and their redox properties and functions, including robust electrode derivatization and sensing, remains a challenge. Here a series of polynorbornene homopolymers and block copolymers containing side-chain amidoferrocenyl groups and tetraethylene glycol linkers were prepared via living ring-opening metathesis polymerization initiated by Grubbs' third-generation catalyst (**1**). Their molecular weights were determined using MALDI-TOF mass spectra, size exclusion chromatography (SEC), end-group analysis, and the empirical Bard–Anson electrochemical equation. All polymerizations followed a living and controlled manner, and the number of amidoferrocenyl units varied from 5 to 332. These homopolymers and block copolymers were successfully used to prepare modified Pt electrodes that showed excellent stability. The modified Pt electrodes show excellent qualitative sensing of ATP^{2-} anions, in particular those prepared with the block copolymers. The quantitative recognition and titration of $[n\text{-}Bu_4N]_2[ATP]$ was carried out using the CH_2Cl_2 solution of the homopolymers, showing that two amidoferrocenyl groups of the homopolymers interacted with each ATP^{2-} molecule. This stoichiometry led us to propose the H-bonding modes in the supramolecular polymeric network.

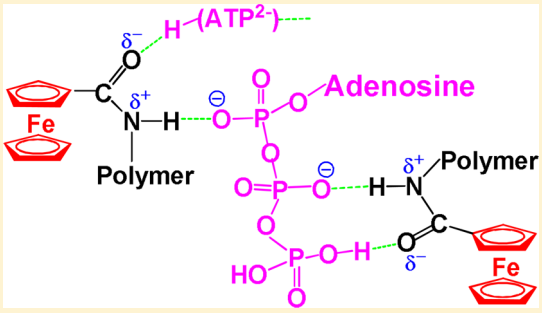

1. INTRODUCTION

The past several decades have witnessed the rapid development of metallocene-containing macromolecules, especially with ferrocenyl groups,[1−23] owing to their multielectron redox properties and wide applications such as catalysts,[24] biosensors,[25] virus-like receptors,[26] models of molecular batteries,[27] colorimetric sensors,[28] etc. Among the polymers, there are two major classes of materials: (i) main chain ferrocene containing polymers in which the ferrocenyl group is an integral part of the polymer backbone[29] and (ii) side chain ferrocene containing polymers in which the ferrocenyl moiety is a pendant group.[12,13] For the side chain ferrocene containing polymers, early studies focused mainly on vinylferrocene and ferrocene containing acrylate and methacrylate that were polymerized by conventional techniques such as free radical, cationic, and anionic polymerization. The polymers that were prepared using these methods often had low molecular weight (<10000) and lacked control of the molecular weight and molecular weight distribution.[30−38] Therefore, the synthetic challenges have halted further interest in the exploration of side chain ferrocene containing polymers prepared by such conventional polymerization techniques.

Recently, significant attention has been paid again to the first originally developed side chain ferrocene containing polymers, especially well-defined polymers and block copolymers synthesized by controlled and living polymerization such as living anionic polymerization (LAP)[39] and ring-opening metathesis polymerization (ROMP),[40] as well as controlled and living radical polymerization (CRP) techniques[41,42] including atom transfer radical polymerization (ATRP),[43−45] reversible addition–fragmentation chain transfer polymerization (RAFT),[46] and nitroxide-mediated polymerization (NMP).[47] These techniques allow the preparation of polymers with predetermined molecular weight, low polydispersity, high functionality, and diverse architectures.[12,13]

Ring-opening metathesis polymerization (ROMP), a variation of the olefin metathesis reaction, has emerged as a particularly powerful method for synthesizing polymers with tunable sizes, shapes, and functions.[48] It has found a tremendous utility for the synthesis of materials having specific biological, electronic, and mechanical properties. In 1992, the living ROMP was first applied to prepare well-defined side chain ferrocene containing polymers and block copolymers by Schrock and co-workers, who used the molybdenum-based metathesis catalyst [Mo(CH-*t*-Bu)(NAr)(O-*t*-Bu)$_2$] (Figure

Received: July 1, 2014
Published: August 5, 2014

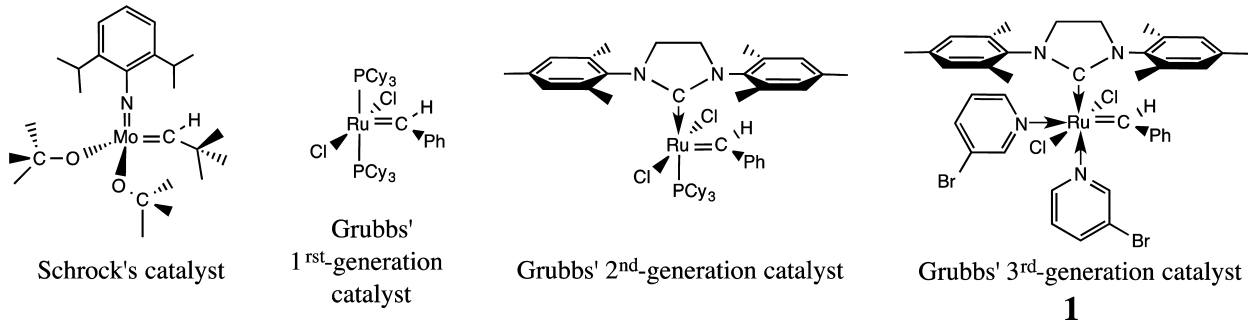

Figure 1. Catalysts successively used for ROMP syntheses of ferrocenyl-containing polymers since 1992 (from left to right).

Scheme 1. Synthesis of Amidoferrocenyl-Containing Homopolymers 6 by ROMP

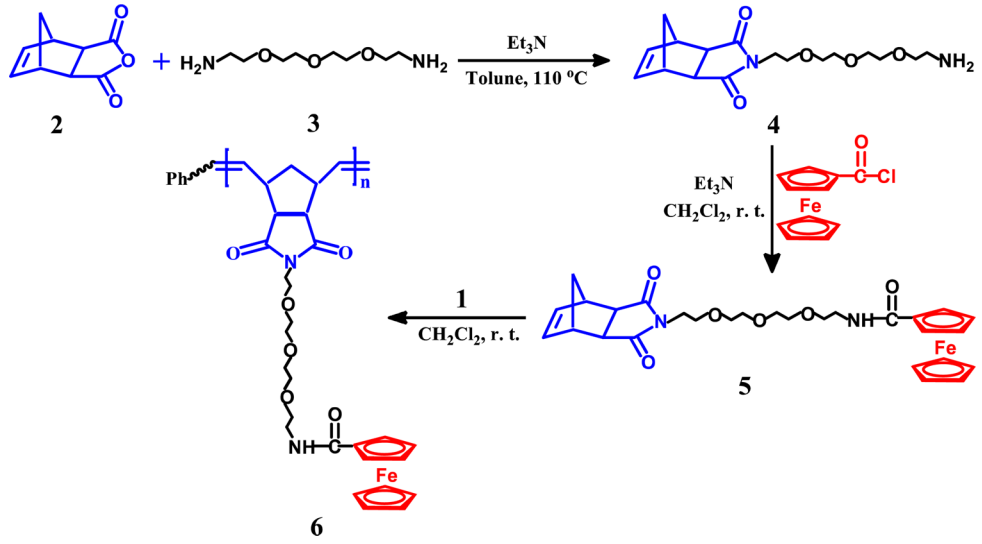

Scheme 2. Synthesis of Amidoferrocenyl-Containing Block Copolymers 10 by ROMP

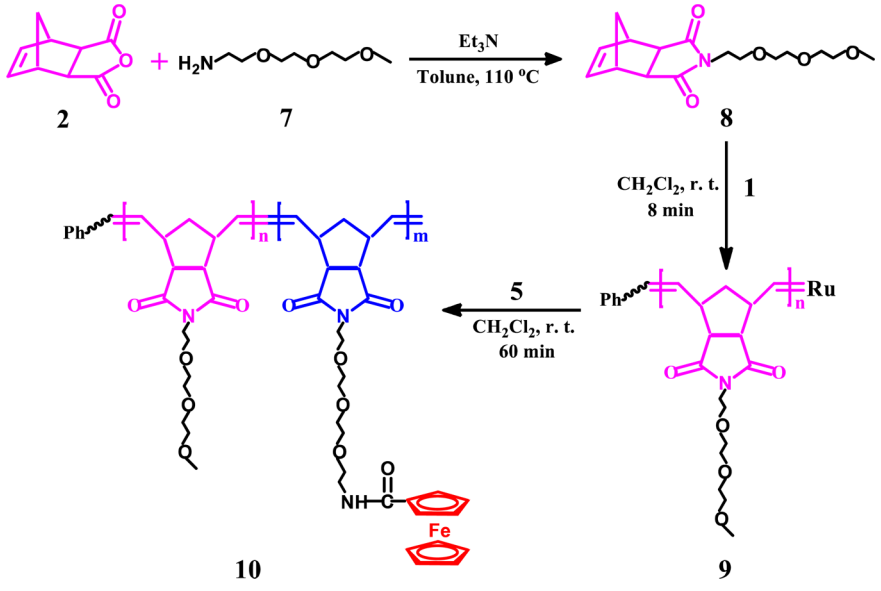

1).[49−51] Since then, the groups of Mirkin,[52−57] Abd-El-Aziz,[58−66] and Luh[67−76] prepared a series of side chain ferrocene containing polynorbornene homopolymers and block copolymers by ROMP. The most frequently used catalysts were ruthenium-based Grubbs first- and second-generation catalysts (Figure 1).[77] Furthermore, although most of the obtained polymers showed low polydispersity, they are often oligomers or polymers with a relatively small number of pendant ferrocenyl units (no more than 30). Up to now, only Tew and co-workers[78] used Grubbs' third-generation catalyst (**1**), shown in Figure 1, a very active catalyst that has a much faster initiation (by at least 3 orders of magnitude) than

dx.doi.org/10.1021/om5006897 | *Organometallics* 2014, 33, 4323−4335

Grubbs' first- and second-generation catalysts.[79,80] Tew's group prepared a series of metal-containing block−random copolymers composed of an alkyl-functionalized homo block (C_{16}) and a random block of cobalt carbonyl (alkyne) units (Co) and ferrocenyl-functionalized (Fe) units via ROMP. These copolymers showed excellent monodispersities (PDI < 1.1) and had the largest theoretical number of ferrocene units of 75. Therefore, these successful results obtained with alkylferrocenyl units opened the route to more work involving *functional* ferrocenyl units and large polymers and the exploration of their properties and applications.

In this work, the very active Grubbs' third-generation ROMP catalyst **1** is used as the initiator (Figure 1).

We present the syntheses and some applications of side chain amidoferrocenyl containing homopolymers (Scheme 1) and block copolymers (Scheme 2) by controlled and living ROMP. Tetraethylene glycol (TEG) was chosen as the linker between the norbornene moiety and amidoferrocenyl units to improve the solubility of macromolecules[81,82] and their biocompatibility that also involves enhanced permeation and retention effects.[82,83] The molecular weights of these new polymers have been well characterized by end-group analysis, MALDI-TOF mass spectra, size exclusion chromatography (SEC), and the Bard−Anson electrochemical method.[84,85] These homopolymers and block copolymers showed an excellent potential in electrode modification resulting from the large polymer sizes and in electrochemical sensing of the ATP^{2-} anion provided by the presence of the amido group on the ferrocenyl moiety that forms efficient hydrogen bonding with oxoanions.[86−88]

2. EXPERIMENTAL SECTION

2.1. General Data. For general data including solvents, apparatuses, compounds, reactions, spectroscopy, CV, and SEC, see the Supporting Information.

2.2. *N*-[11′-Amine-3′,6′,9′-trioxahendecyl]-*cis*-5-norbornene-*exo*-2,3-dicarboximide (4). To a solution of freshly prepared **3** (2.49 g, 12.97 mmol, 5.3 equiv) in toluene (25 mL) was added a solution of **2** (0.4 g, 2.44 mmol, 1 equiv) in toluene (25 mL) dropwise at room temperature over 0.5 h with vigorous stirring. Then, triethylamine (0.2 mL, 1.43 mmol, 0.59 equiv) was added dropwise. The obtained mixture was refluxed for 12 h with a Dean−Stark apparatus before the solvent as well as residual triethylamine were removed via distillation in vacuo. Purification was achieved by column chromatography with dichloromethane (DCM)/methanol (1% → 60%) as eluent, and the product was obtained as a pale yellow oil. Yield: 0.56 g, 68%. ^{1}H NMR of **4** (300 MHz, $CDCl_3$): δ_{ppm} 1.35 (d, J = 10.1 Hz, 1H, CH_2 bridge), 1.48 (d, J = 10.1 Hz, 1H, CH_2-bridge), 1.89 (s, br, 3H, $-NH_2 + H_2O$), 2.68 (d, J = 1.1 Hz, 2H, CO-CH), 2.85 (t, J = 10.6 Hz, 2H, CH_2-NH_2), 3.26 (t, J = 3.4 Hz, 2H, =CH-C*H*), 3.49 (t, J = 10.3 Hz, 2H, $CH_2CH_2NH_2$), 3.57−3.71 (m, 12H, 6 × CH_2), 6.28 (t, J = 3.6 Hz, 2H, CH=CH). ^{13}C NMR of **4** (75 MHz, $CDCl_3$): δ_{ppm} 178.01 (CO-N), 137.79 (C=C), 73.07 ($-CH_2CH_2NH_2$), 70.53, 70.47, 70.205, 69.86 ($-OCH_2CH_2OCH_2CH_2O-$), 66.88 ($-CH_2NH_2$), 47.78 (CO-CH), 45.235 (=CH-CH), 42.675 (CH_2-bridge), 41.45 (CH_2-N-CO), 37.74 (-CH_2CH_2-N-CO). MS (ESI, m/z): calcd for $C_{17}H_{26}N_2O_5$, 338; found, 339.19 (M + H^+).

2.3. *N*-[11′-Ferroceneformamido-3′,6′,9′-trioxahendecyl]-*cis*-5-norbornene-*exo*-2,3-dicarboximide Monomer (5). To a suspension of ferrocenecarboxylic acid (0.5 g, 2.17 mmol) in dry DCM (40 mL) was added dropwise triethylamine (0.1 mL, 0.72 mmol) at room temperature under a nitrogen atmosphere. Then, oxalyl chloride (0.7 mL, 8.2 mmol) was added dropwise at 0 °C. The obtained mixture was stirred overnight at room temperature and dried in vacuo. The residual red solid of crude chlorocarbonyl ferrocene (FcCOCl) was dissolved in dry DCM (20 mL) and added dropwise to a DCM solution (20 mL) of **4** (0.2 g, 0.59 mmol) and triethylamine (1.5 mL, 10.7 mmol). The mixture was stirred overnight under a nitrogen atmosphere at room temperature and then washed with saturated $NaHCO_3$ solution (1 × 100 mL) and distilled water (3 × 100 mL). The organic solution was dried over anhydrous sodium sulfate and filtered, and the solvent was removed in vacuo. The product was purified by column chromatography with DCM/methanol (1% → 20%) as the eluent and obtained as a brown sticky oil. Yield: 0.234 g, 71.8%. ^{1}H NMR of **5** (300 MHz, $CDCl_3$): δ_{ppm} 1.20 (d, J = 9.9 Hz, 1H, CH_2-bridge), 1.32 (d, J = 9.9 Hz, 1H, CH_2-bridge), 2.52 (d, J = 0.9 Hz, 2H, CO-CH), 3.09 (t, J = 3.1 Hz, 2H, =CH-C*H*), 3.41−3.55 (m, 16H, 4 × CH_2CH_2), 4.05 (s, 5H, free Cp), 4.18 (t, J = 3.4 Hz, 2H, sub. Cp), 4.61 (t, J = 3.8 Hz, 2H, sub. Cp), 6.12 (t, J = 3.6 Hz, 2H, CH=CH), 6.59 (t, J = 9.9 Hz, 1H, NHCO). ^{13}C NMR of **5** (50 MHz, $CDCl_3$): δ_{ppm} 177.841 (CON), 170.25 (CONH), 137.71 (CH=CH), 70.375, 70.24, 70.11, 69.975, 69.745, 69.65, 68.20 ($-OCH_2CH_2OCH_2CH_2OCH_2-$, sub. Cp and free Cp), 66.76 (-CH_2NH), 47.68 (CO-CH), 45.14 (=CH-CH), 42.615 (CH_2-bridge), 39.20 (CH_2−NCO), 37.665 ($-CH_2CH_2$-NCO). MS (ESI, m/z): calcd for $C_{28}H_{34}N_2O_6Fe$, 550; found, 573.2 (M + Na^+).

2.4. General Procedure for the Synthesis of Polymeric *N*-[3-(3′,6′,9′-Trioxaundecyl-11′-ferroceneformamido)]-*cis*-5-norbornene-*exo*-2,3-dicarboximide (6) via ROMP. The desired amount of **1** was placed in a small Schlenk flask, flushed with nitrogen, and dissolved in a minimum amount of dry DCM. A known amount of monomer **5** in dry DCM (1 mL per 100 mg of monomer **5**) was added to the catalyst solution under a nitrogen atmosphere with vigorous stirring. The reaction mixture was stirred vigorously for 1 h and then quenched with 0.2 mL of ethyl vinyl ether (EVE). The yellow solid polymers **6** were purified by precipitating in methanol five times and dried in vacuo until constant weight. ^{1}H NMR of **6** (300 MHz, $CDCl_3$): δ_{ppm} 7.23−7.44 (m, phenyl and $CDCl_3$), 6.65 (broad, 1H, NHCO), 5.75 and 5.53 (double broad, 2H, CH=CH), 4.76 (s, 2H, sub. Cp), 4.35 (s, 2H, sub. Cp) (Cp = η^5-C_5H_5), 4.22(s, 5H, free Cp), 3.51−3.67 (broad, 16H, $-CH_2(CH_2OCH_2)_3CH_2-$), 3.26 (broad, =CH-C*H*), 2.71 (broad, CH=CHCHCH_2), 2.13 (broad, CO−CH), 1.61 (broad, CH=CHCHCH_2).

2.5. *N*-[3-(3′,6′,9′-Trioxadecyl)]-*cis*-5-norbornene-*exo*-2,3-dicarboximide Monomer (8). To a solution of freshly prepared 2-(2-(2-methoxyethoxy)ethoxy) ethylamine (7; 1.99 g, 12.21 mmol, 5.0 equiv) in toluene (20 mL) was added dropwise a solution of **2** (0.4 g, 2.44 mmol, 1 equiv) in toluene (25 mL) at room temperature in 0.5 h with vigorous stirring. Then, triethylamine (0.2 mL, 1.43 mmol, 0.59 equiv) was added dropwise. The obtained mixture was refluxed for 12 h with a Dean−Stark apparatus before the solvent as well as residual triethylamine were removed via vacuum distillation. Purification was achieved by column chromatography with DCM/methanol (1% → 50%) as eluent, and the product was obtained as a colorless oil. Yield: 0.65 g, 86.3%. ^{1}H NMR of **8** (300 MHz, $CDCl_3$): δ_{ppm} 1.37 (d, J = 9.6 Hz, 1H, CH_2-bridge), 1.49 (d, J = 9.6 Hz, 1H, CH_2-bridge), 2.69 (d, J = 3.6 Hz, 2H, CO-CH), 3.27 (d, J = 1.8 Hz, 2H, =CH-C*H*), 3.38 (s, J = 4.3 Hz, 3H, CH_3), 3.536−3.683 (m, 12H, 6 × CH_2), 6.23 (t, J = 3.8 Hz, 2H, CH=CH). ^{13}C NMR of **8** (75 MHz, $CDCl_3$): δ_{ppm} 177.45 (CO-N), 137.60 (C=C), 71.657, 70.223, 69.612, 66.53 ($-OCH_2CH_2OCH_2CH_2O-$), 58.64 ($-CH_3$), 47.49 (CO-CH), 45.00 (=CH-CH), 42.464 (CH_2-bridge), 37.47 (N-CH_2CH_2). MS (ESI, m/z): calcd for $C_{16}H_{23}NO_5$, 309; found, 332.2 (M + Na^+).

2.6. General Procedure for the Synthesis of the Block Copolymers 10 by ROMP. The desired amount of **1** was placed in a small Schlenk flask, flushed with nitrogen, and dissolved in a minimum amount of dry DCM. Known amounts of monomers **8** and **5** were placed in two small glass tubes, respectively, and dissolved in dry DCM (1 mL per 100 mg of monomers). First, the monomer **8** was transferred to the flask containing **1** via a syringe. The reaction mixture was stirred vigorously for 8 min, and a known amount of the reaction solution was taken out and quenched with 0.1 mL of ethyl vinyl ether (EVE) for ^{1}H NMR analysis. Then, the solution containing monomer **5** was transferred to the reaction flask via a syringe. The polymerization was allowed to continue for 60 min and quenched with 0.2 mL of ethyl EVE. The copolymers **10** were purified by precipitation in diethyl ether five times and dried in vacuo to constant

dx.doi.org/10.1021/om5006897 | *Organometallics* 2014, 33, 4323−4335

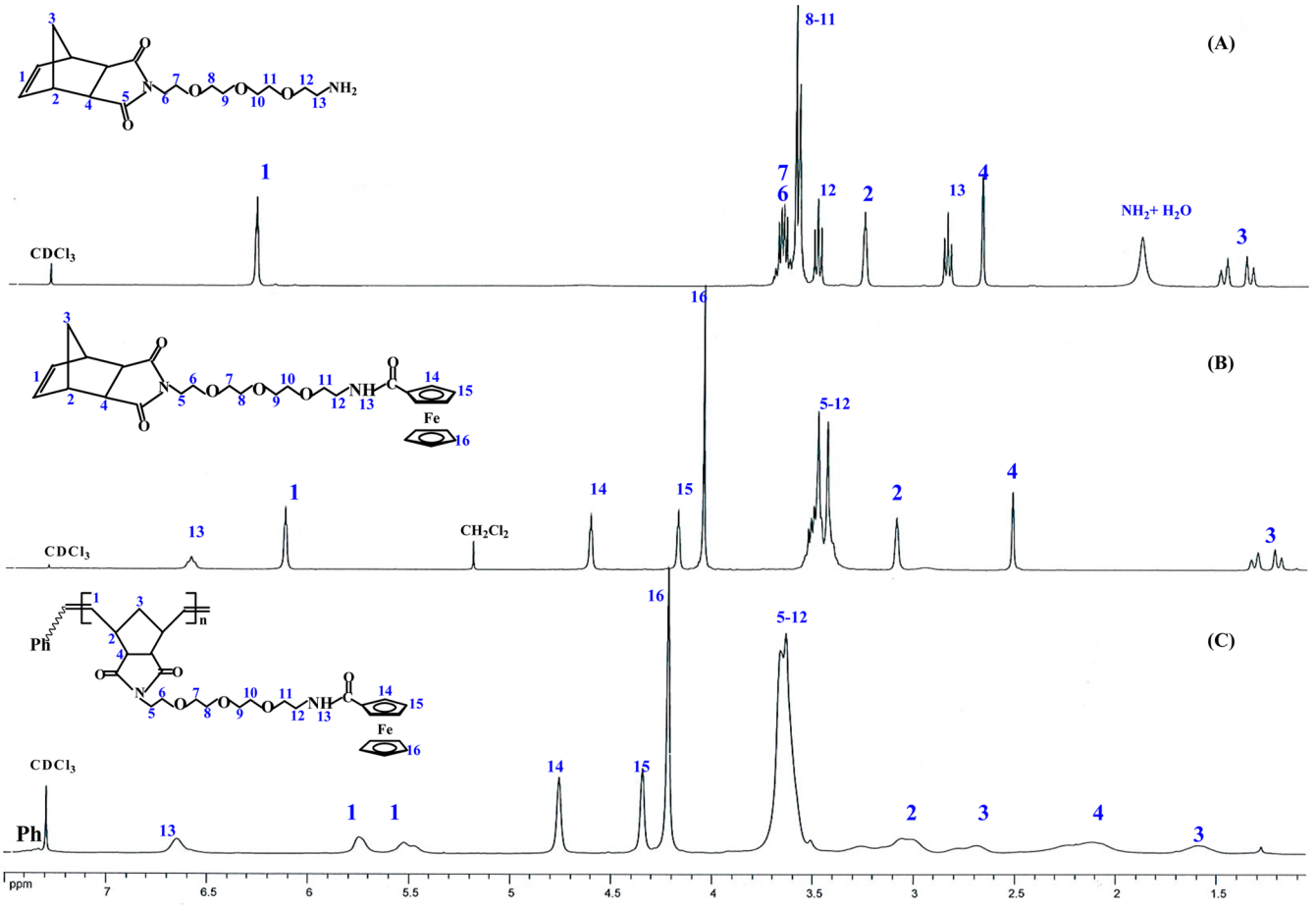

Figure 2. ^{1}H NMR spectra of **4** (A), monomer **5** (B), and polymer **6** (C) in $CDCl_3$.

weight. ^{1}H NMR of polymers **9** (300 MHz, $CDCl_3$): δ_{ppm} 7.190−7.354 (m, phenyl and $CDCl_3$), 5.751 and 5.508 (broad doublet, 2H, CH═CH), 3.521−3.595 (broad, 12H, $-CH_2(CH_2OCH_2)_2CH_2-$), 3.355 (s, 3H, OCH_3), 3.043 (broad, ═CH-C*H*), 2.683 (broad, CH═CHCHCH_2), 2.070 (broad, CO-CH), 1.578 (broad, CH═CHCHCH_2). ^{1}H NMR of copolymers **10** (300 MHz, $CDCl_3$): δ_{ppm} 7.26−7.36 (m, phenyl and $CDCl_3$), 6.47 (broad, NHCO), 5.75 and 5.50 (broad doublet, CH═CH), 4.71 (s, sub. Cp), 4.32 (s, sub. Cp), 4.19 (s, free Cp), 3.52−3.60 (broad, $-CH_2(CH_2OCH_2)_2CH_2-$ and $-CH_2(CH_2OCH_2)_3CH_2-$), 3.355 (s, OCH_3), 3.04 (broad, ═CH-C*H*), 2.68 (broad, CH═CHCHCH_2), 2.08 (broad, CO-CH), 1.575 (broad, CH═CHCHCH_2).

2.7. Electrochemistry, Modified Electrodes, and Redox Sensing. All electrochemical measurements were recorded under a nitrogen atmosphere. Conditions: solvent, dry dichloromethane; temperature, 20 °C; supporting electrolyte, [nBu$_4$N][PF$_6$] 0.1 M; working and counter electrodes, Pt; reference electrode, Ag; internal reference, FeCp*$_2$ (Cp* = η^5-C$_5$Me$_5$); scan rate, 0.200 V s^{-1}. The number of electrons involved in the oxidation wave of ferrocenyl polymers was calculated by the Bard−Anson equation: $n_p = (i_{dp}/C_p)/(i_{dm}/C_m)(M_p/M_m)^{0.775}$ (see text and the Supporting Information). The experiments were conducted by adding a known amount of polymer (see the Supporting Information) in 3 mL of dry DCM, and then a known amount of [FeCp*$_2$] (see the Supporting Information) in 2 mL of DCM was added to the solution. After the CVs were recorded, the intensities of the oxidation waves of the polymers and of the internal reference [FeCp*$_2$] were measured. The values were introduced in the above equation, giving the final number of electrons (n_p). The modified electrodes were prepared after approximately 25 adsorption cycles around the ferrocenyl potential on Pt electrodes. Their electrochemical behavior was checked in 5 mL of a DCM solution containing only [nBu$_4$N][PF$_6$] 0.1 M at various scan rates: 25, 50, 100, 200, 300, 400, 500, and 600 mV s^{-1}. Redox recognition was conducted in two different ways. (a) In solution via titration: the CVs were recorded upon addition of 0, 0.25, and 0.5 equiv of [n-Bu$_4$N]$_2$[ATP]. The potentials of the new wave were measured using [FeCp*$_2$] as an internal reference. (b) With modified electrodes: the CVs were recorded upon addition of [n-Bu$_4$N]$_2$[ATP] to an electrochemical cell containing a Pt-modified electrode.

3. RESULTS AND DISCUSSION

3.1. Synthesis and ROMP of the Amidoferrocenyl-Containing Monomer 5. As shown in Scheme 1, the new amidoferrocenyl-containing monomer **5** was prepared by an amidation reaction between ferrocenylcarbonyl chloride and the key intermediate *N*-[11′-amine-3′,6′,9′-trioxahendecyl]-*cis*-5-norbornene-*exo*-2,3-dicarboximide (**4**). This compound **4** was prepared from *cis*-5-norbornene-*exo*-2,3-dicarboxylic anhydride (**2**) in the presence of 1,11-diamine-3,6,9-trioxaundecane (**3**), whose method of synthesis is well described in the Supporting Information. Figure 2A shows the ^{1}H NMR spectrum of the intermediate **4**. The peak at 6.28 ppm corresponds to the olefinic protons, while the two double peaks at 1.36−1.37 and 1.46−1.50 ppm originate from the characteristic bridge-methylene protons of the *cis*-norbornene structure. As shown in the ^{1}H NMR spectrum of monomer **5** (Figure 2B), the appearance of the amido proton at 6.59 ppm and the three characteristic cyclopentadienyl (Cp) protons at 4.61, 4.18, and 4.05 ppm, respectively, demonstrate the success of the amidation reaction. The methylene protons of the TEG linker are concentrated at 3.41−3.53 ppm, which is different from the

dx.doi.org/10.1021/om5006897 | *Organometallics* 2014, 33, 4323−4335

Table 1. Molecular Weight Data for the Amidoferrocenyl-Containing Polymer 6

	$[M_5]:[C]^a$				
	5:1	16:1	50:1	100:1	400:1
conversn (%)[b]	>99	>99	>99	>99	83
n_{p1}[c]	5 ± 1	16 ± 2	50 ± 5	95 ± 5	332
n_{p2}[d]	4.2 ± 0.4	14 ± 1	34 ± 2	51 ± 3	64 ± 3
n_{p3}[e]	4 ± 0.1	15 ± 1	47 ± 3	94 ± 5	336 ± 8
M_n[f]	2854	8904	27604	55104	182704
M_n[g]	2878.7	8930.2			
M_n[h]	1417	4239	5508		
PDI[h]	1.09	1.08	1.03		

[a] $[M_5]:[C]$ is the molar feed ratio of monomer **5** and **1**. [b] Monomer conversion determined by ^{1}H NMR. [c] Degree of polymerization obtained from ^{1}H NMR using conversion of monomer **5**. [d] Degree of polymerization determined via end-group analysis by ^{1}H NMR spectroscopy in CD_2Cl_2. [e] Degree of polymerization determined by the Bard–Anson electrochemical method. [f] MWs obtained by ^{1}H NMR using conversion of monomer **5**. [g] MWs ($+Na^+$) determined via MALDI-TOF mass spectroscopy. [h] Obtained from SEC using polystyrenes as standards.

dispersed distribution in intermediate **4**. All of the other peaks are clearly assigned. ^{13}C NMR and mass spectroscopy (Figures S6 and S7, Supporting Information) further confirm the structure of the monomer **5**.

The preparation of amidoferrocenyl-containing polymers **6** by ROMP was carried out in dry DCM at room temperature using catalyst **1**. As shown in Figure 2C, the disappearance of the peak at 6.13 ppm corresponding to the olefinic protons of monomer **5** and the appearance of new two broad peaks at 5.53 and 5.75 ppm that arise from the olefinic protons of polymers **6** indicate the successful polymerization of the monomer **5**. Furthermore, the other peaks of the *cis*-norbornene backbone in polymers **6** change into broad signals that are very different from the sharp signals of the monomers.

In this study, a series of amidoferrocenyl-containing homopolymers **6** were synthesized with molar feed ratios of monomer to catalyst from 5:1 to 400:1. In situ ^{1}H NMR analysis of the crude reaction mixture indicated that the monomer conversions, which were calculated by comparing the ^{1}H NMR signals of the olefinic protons between monomer **5** (6.13 ppm) and the polymers **6** (5.53 and 5.75 ppm), were nearly 100% within 60 min when the molar feed ratio was less than 50. It was necessary to extend the polymerization time in order to obtain the larger polymers. For instance, when the molar feed ratio was 100:1, the monomer conversion was only 50% after 60 min but improved to nearly 100% after overnight stirring. For the largest molar feed ratio of 400:1, the monomer conversion only reached 83% even after 4 days. The amidoferrocenyl-containing homopolymers **6** are not soluble in organic solvents such as acetone, acetonitrile, methanol, and diethyl ether, unlike the monomer **5**, but they are soluble in dichloromethane, chloroform, tetrahydrofuran (THF), and strongly polar solvents such as DMF and dimethyl sulfoxide (DMSO). The smaller polymers have better solubilities than the larger polymers. For instance, the polymer **6** with a molar feed ratio of 50:1 is partially soluble in THF, but when the

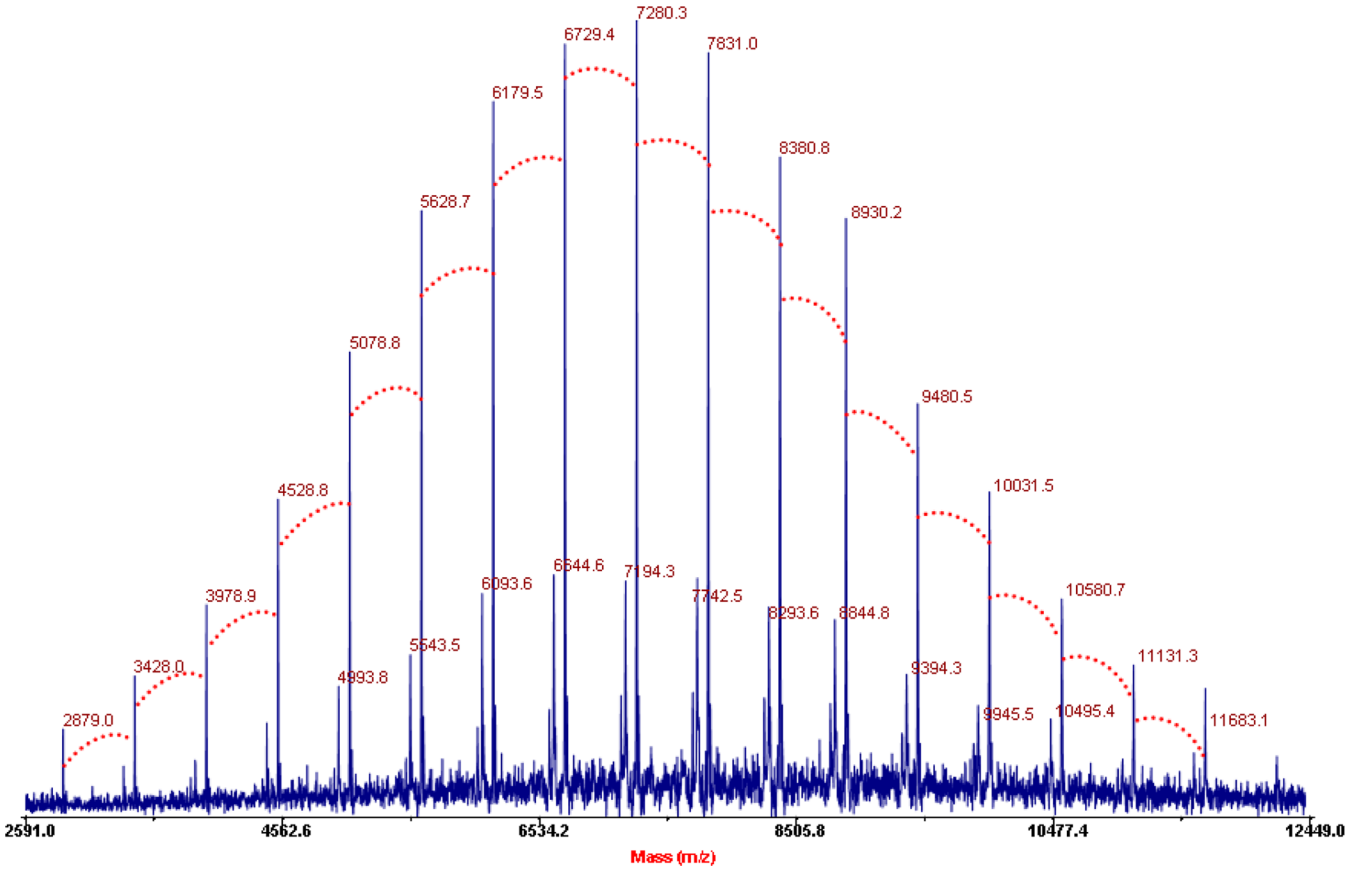

Figure 3. MALDI-TOF MS spectrum of polymer **6**[16]. The molar feed ratio of monomer **5** to **1** is 16:1. The red dotted lines correspond to the difference between molecular peaks of a value of 550 ± 1 Da (MW of **5**).

dx.doi.org/10.1021/om5006897 | *Organometallics* 2014, 33, 4323–4335

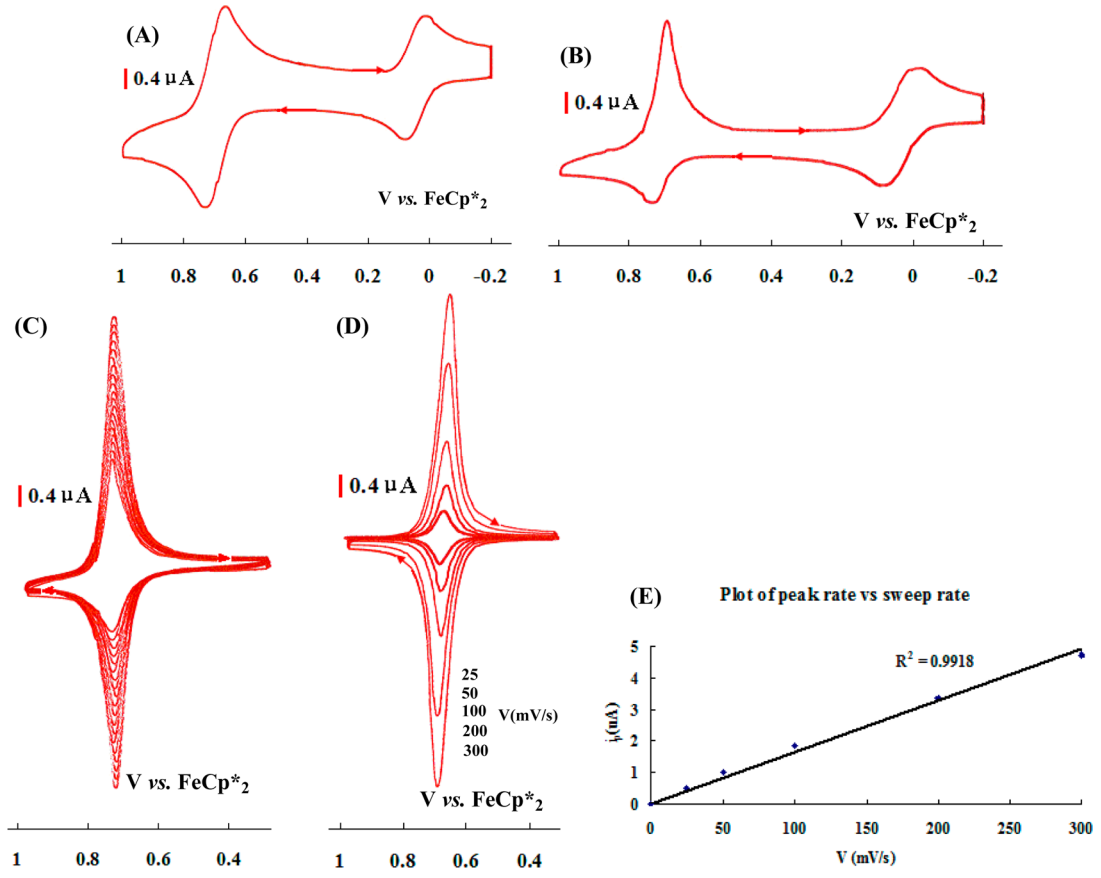

Figure 4. Electrochemical properties of monomer **5** and polymer $\mathbf{6}^{50}$. The molar feed ratio of monomer **5** to **1** is 50:1. (A) CV of monomer **5** in CH_2Cl_2: internal reference, $FeCp^*_2$; reference electrode, Ag; working and counter electrodes, Pt; scan rate, 0.4 mV/s; supporting electrolyte, [*n*-Bu_4N][PF_6]. The wave at 0.0 V is that of the reference [$FeCp^*_2$]. (B) CV of the polymer $\mathbf{6}^{50}$ in CH_2Cl_2: internal reference, [$FeCp^*_2$]; reference electrode, Ag; working and counter electrodes, Pt; scan rate, 0.2 mV/s; supporting electrolyte, [*n*-Bu_4N][PF_6]. The wave at 0.0 V is that of the reference [$FeCp^*_2$]. (C) Progressive adsorption of the polymer $\mathbf{6}^{50}$ upon scanning around the ferrocenyl area. (D) Pt electrode modified with the polymer $\mathbf{6}^{50}$ at various scan rates in CH_2Cl_2 solution (containing only the supporting electrolyte). (E) Intensity as a function of scan rate (linearity shows the expected behavior of the absorbed polymer).

Table 2. Redox Potentials and Chemical (i_c/i_a) and Electrochemical ($E_{pa} - E_{pc} = \Delta E$) Reversibilities for Monomer 5, Polymers 6, and Corresponding Modified Electrodes

			modified electrode		
compd	$E_{1/2}$ (ΔE) (mV)	i_c/i_a	$E_{1/2}$ (ΔE) (mV)	Γ (mol/cm^2)[a]	Γ (mol/cm^2)[a] (ferrocenyl sites)
monomer **5**	680 (70)	1.0			
polymer $\mathbf{6}^{16}$	680 (30)	2.2	660 (0)	5.52×10^{-11}	8.27×10^{-10}
polymer $\mathbf{6}^{50}$	680 (40)	3.1	660 (0)	4.53×10^{-11}	2.13×10^{-9}
polymer $\mathbf{6}^{100}$	680 (30)	2.2	660 (0)	3.11×10^{-11}	2.92×10^{-9}
polymer $\mathbf{6}^{400}$	680 (40)	2.5	660 (0)	1.30×10^{-11}	4.40×10^{-9}

[a]Surface coverage on the modified Pt electrode obtained after approximately 25 adsorption cycles.

molar feed ratio is increased to 100:1, the polymer **6** is insoluble in THF.

3.2. Molecular Weight Analysis of the Polymers 6. Molecular weights (MWs) can be measured via a variety of techniques, including gel permeation chromatography (GPC), osmometry, static light scattering, matrix-assisted laser desorption-ionization time-of-flight mass spectrometry (MALDI-TOF MS), viscometry, small-angle X-ray scattering, small-angle neutron scattering, ultracentrifugation, cryoscopy, ebulliometry, and end-group analysis.[86] Each method has its respective advantages and disadvantages, and the most suitable methods also depend on the polymer type. In this study, size exclusion chromatography (SEC), MALDI-TOF MS, end-group analysis, and the Bard–Anson electrochemical method[84,85] were used to investigate the MWs of the amidoferrocenyl-containing polymers **6**.

As shown in Table 1, the theoretical MWs and polymerization degrees of the polymers **6** were calculated according to the molar feed ratios and the corresponding monomer conversions from ^{1}H NMR. End-group analysis by ^{1}H NMR of the polymers **6** in CD_2Cl_2 (see Figure S10, Supporting Information) was conducted by comparing the five protons of end-group phenyls (7.20–7.43 ppm) with amido protons (6.59 ppm), olefinic protons (5.56 and 5.77 ppm), Cp protons (4.23, 4.37, and 4.74 ppm), and linker protons (3.55–3.65 ppm), respectively. For the small polymers in which theoretical MWs

dx.doi.org/10.1021/om5006897 | *Organometallics* 2014, 33, 4323–4335

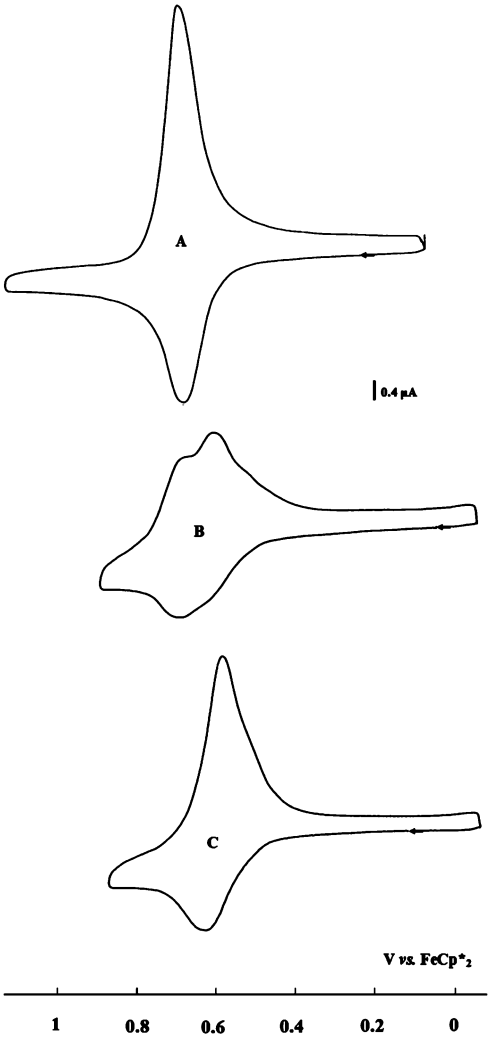

Figure 5. CVs for the titration of $[n\text{-}Bu_4N]_2[ATP]$ with polymer **6**[50] in CH_2Cl_2 at 20 °C by adding the salt of the anion to the polymer solution: (A) before addition of $[n\text{-}Bu_4N]_2[ATP]$; (B) during the titration with 0.25 equiv of $[n\text{-}Bu_4N]_2[ATP]$; (C) with 0.5 equiv of $[n\text{-}Bu_4N]_2[ATP]$.

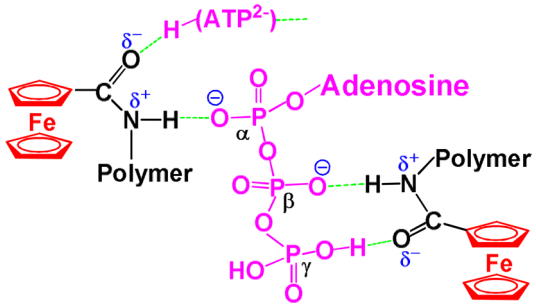

Figure 6. Hydrogen-bonding interactions between ATP^{2-} and two amidoferrocenyl groups of polymers **6**.

were less than 10000 Da, the MWs by NMR conversion and end-group analysis were in good agreement, which was further confirmed by MALDI-TOF MS results (Figure 3 and Figure S13 (Supporting Information)). As shown in Figure 3, the MALDI-TOF mass spectrum of polymer **6**[16] showed well-defined individual peaks for polymer fragments that are separated by 550 ± 1 Da corresponding to the mass of one

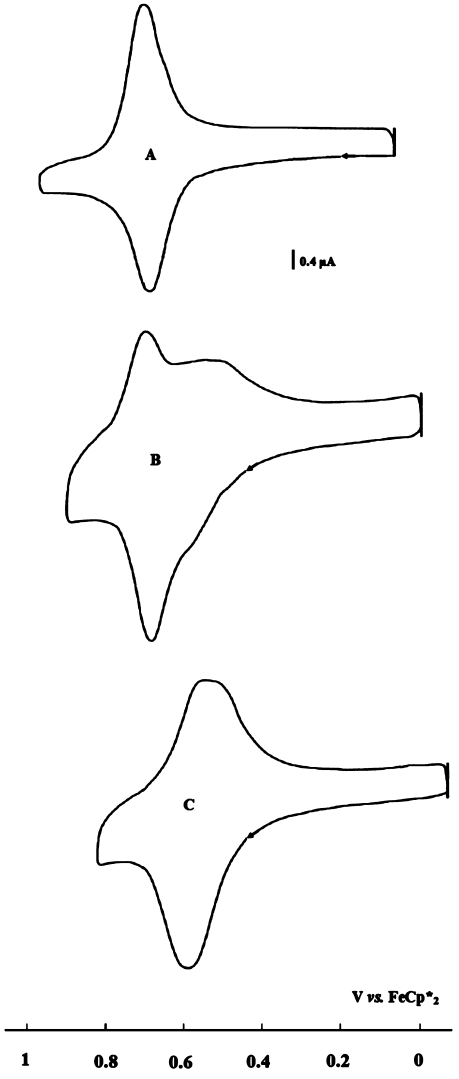

Figure 7. CVs for the titration of $[n\text{-}Bu_4N]_2[ATP]$ by the modified Pt electrode with polymer **6**[50] in CH_2Cl_2 at 20 °C: (A) before addition of $[n\text{-}Bu_4N]_2[ATP]$; (B) during titration of $[n\text{-}Bu_4N]_2[ATP]$; (C) after addition of excess $[n\text{-}Bu_4N]_2[ATP]$.

monomer **5** unit. There is a peak at 8930.2 Da that corresponds to the molecular weight of $(C_6H_6)(C_{28}H_{34}N_2O_6Fe)_{16}(C_2H_2)$-Na. On the other hand, the MWs obtained by SEC were always smaller than the theoretical values, which may result from the obvious structural difference between the polystyrene standards and the amidoferrocenyl-containing polymers **6**. However, none the polydispersity indexes (PDI) obtained by SEC traces were larger than 1.1, which demonstrated a controlled polymerization.

End-group analysis and MALDI-TOF MS are not reliable for the large polymers, however. The SEC traces of the large polymers **6** could not be obtained in THF because of solubility problems. SEC measurements were also attempted in $CHCl_3$, but no signal was observed, probably because of the strong adsorption of the large polymers **6** on the column stationary phase. From the DOSY ^1H NMR spectra of the polymers **6** (Figure S14–S16, Supporting Information), the hydrodynamic diameters of polymers **6** can be calculated using the Stokes–Einstein equation (see Supporting Information). A progressive increase of the hydrodynamic diameters was observed upon increasing the molar feed ratio of monomer **5** to **1** from 50:1 to

dx.doi.org/10.1021/om5006897 | *Organometallics* 2014, 33, 4323–4335

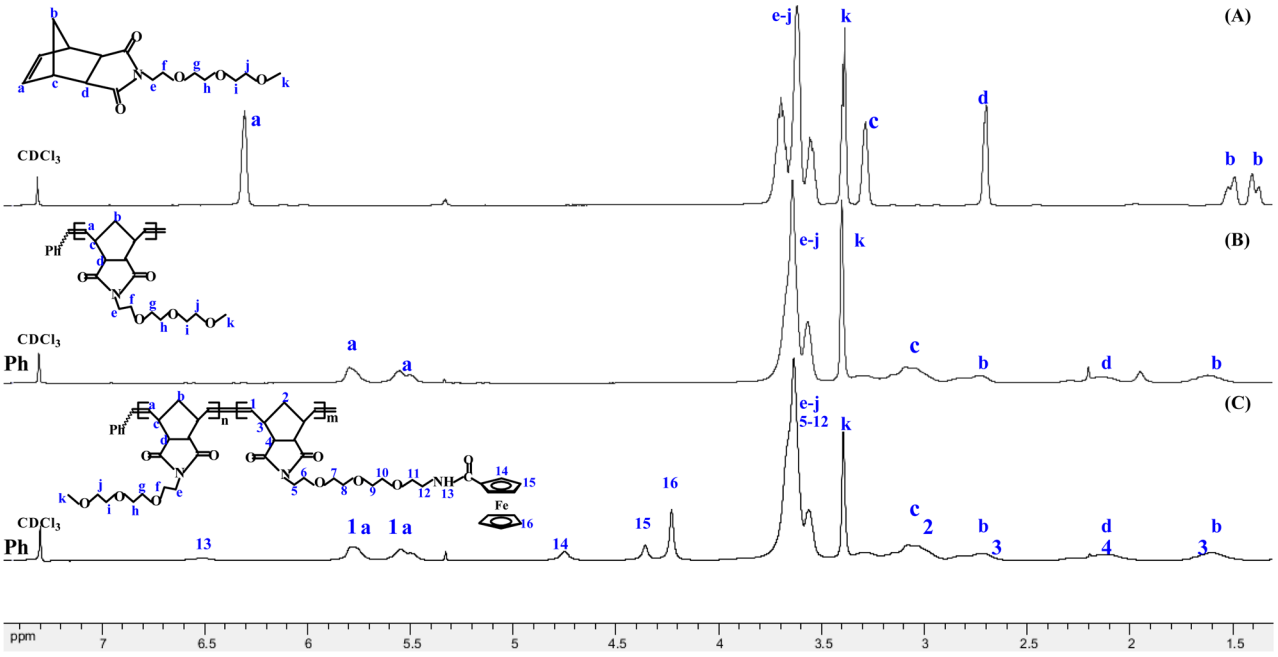

Figure 8. ^{1}H NMR spectra of monomer **8** (A), polymer **9** (B), and copolymer **10** (C) in $CDCl_3$.

Table 3. Molecular Weight Data of the Amidoferrocenyl-Containing Block Copolymers 10

	$[M_8]$:$[M_5]$:$[C]^a$			
	6:3:1	20:10:1	100:50:1	100:100:1
conversn (%)^b	>99	>99	>99	>99
$n_{p1}{}^c$	3	10	50	100
$n_{p2}{}^d$	3 ± 0.3	10 ± 1	44 ± 3	82 ± 5
$n_{p3}{}^e$	2.7 ± 0.3	9 ± 1	44 ± 3	98 ± 3
$M_n{}^f$	3608	11784	58504	86004
$M_n{}^g$	3633.9			
$M_n{}^h$	2585	7139	25454	22325
PDI^h	1.10	1.06	1.14	1.11

^{a}[M_8]:[M_5]:[C]: molar feed ratio of monomer **8**, monomer **5**, and **1**. ^{b}Monomer conversion of monomer **5** determined by ^{1}H NMR. ^{c}Degree of polymerization obtained from ^{1}H NMR using conversion of the amidoferrocenyl-containing monomer **5**. ^{d}Degree of polymerization for the amidoferrocenyl-containing block determined via end-group analysis by ^{1}H NMR spectroscopy. ^{e}Degree of polymerization for the amidoferrocenyl-containing monomer **5** determined by the Bard–Anson electrochemical method. ^{f}MWs obtained for copolymers **10** by ^{1}H NMR using conversion of monomers **8** and **5**. ^{g}MWs (+Na^+) determined by MALDI-TOF mass spectroscopy. ^{h}Obtained from SEC using polystyrenes as standards.

400:1, which indicates a concomitant increase of MWs. Although the DOSY results cannot quantitatively characterize the polydispersity of polymers, the low deviation values of the diffusion coefficient (D) from different DOSY ^{1}H NMR peaks show that these polymers should have a narrow molecular weight distribution.

In order to further characterize the polymers **6**, especially the large ones, we have used the Bard–Anson electrochemical method,[84,85] in which the compared intensities in the cyclic voltammograms (CVs) of the polymers and monomer were used. The total number of electrons transferred in the oxidation wave for the polymer (n_p) is the same as that of monomer units in the polymer, because only one electron from Fe^{II} (ferrocene) to Fe^{III} (ferrocenium) is transferred from each monomer unit to the anode during the electrochemical experiment. This number n_p is estimated by employing the Bard–Anson empirical equation[84,85] previously derived for conventional polarography, where i_d, M, and C are the CV wave intensity of the diffusion current, molecular weight, and concentration of the monomer (m) and polymer (p), respectively:

$$n_p = \frac{(i_{dp}/C_p)}{(i_{dm}/C_m)}\left(\frac{M_p}{M_m}\right)^{0.275}$$

As shown in Table 1, the estimated values of electrons (n_{p3}) for all of the polymers **6** showed excellent consistency with the polymerization degree (n_{p1}) obtained from ^{1}H NMR, which further demonstrated the controlled characteristic for the ROMP of the amidoferrocenyl-containing monomer **5**. For example, for the polymer $\mathbf{6}^{400}$, the largest polymer prepared in this study, the calculated polymerization degree (n_{p1}) from the conversion rate is 332, and the value of n_{p2} from end-group analysis is 64 ± 3, but the n_{p3} value from the above formula is 336 ± 8, which is very close to the theoretical result. Thus, the Bard–Anson electrochemical method is a valuable tool to check the n_p and MW values of amidoferrocenyl containing polymers **6**.

3.3. Redox Properties of Polymers 6 and Electrochemical Sensing of ATP^{2-}. The new ferrocenyl monomer **5** and the side chain amidoferrocenyl containing homopolymers **6** have been studied by CV[87–90] using decamethylferrocene [$FeCp^*_2$] as the internal reference.[90] The CVs have been recorded in DCM (Figure 4 and Figures S20 and S21 (Supporting Information)), and the $E_{1/2}$ data (measured vs [$FeCp^*_2$]) are gathered in Table 2. For monomer **5** and all of the polymers **6**, a single oxidation wave is observed for all the ferrocenyl groups, and this single wave is marred by adsorption of the polymer onto the electrode. For the monomer **5**, the $Fe^{III/II}$ oxidation potential of the ferrocenyl redox center is around 680 mV, whereas for polymers **6** the potentials are also around 680 mV, although the precise value is to a certain extent not as precise due to the adsorption (Figure 4B).

dx.doi.org/10.1021/om5006897 | Organometallics 2014, 33, 4323–4335

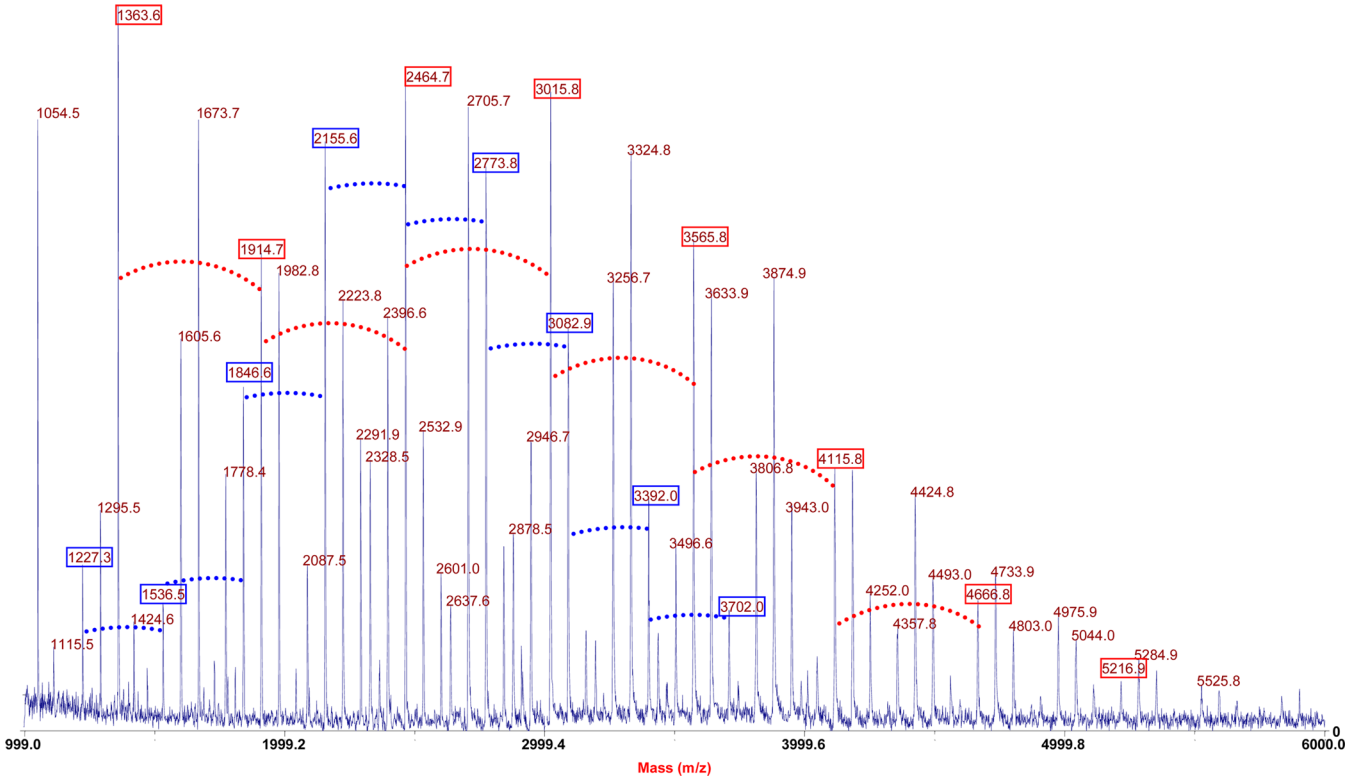

Figure 9. MALDI-TOF MS spectrum of the copolymer $\mathbf{10}^{6/3}$. The molar feed ratio of monomers **8** and **5** to **1** is 6:3:1. The dotted red and blue lines correspond to the difference between molecular peaks of 550 ± 1 (MW of **5**) and 309 ± 1 Da (MW of **8**), respectively.

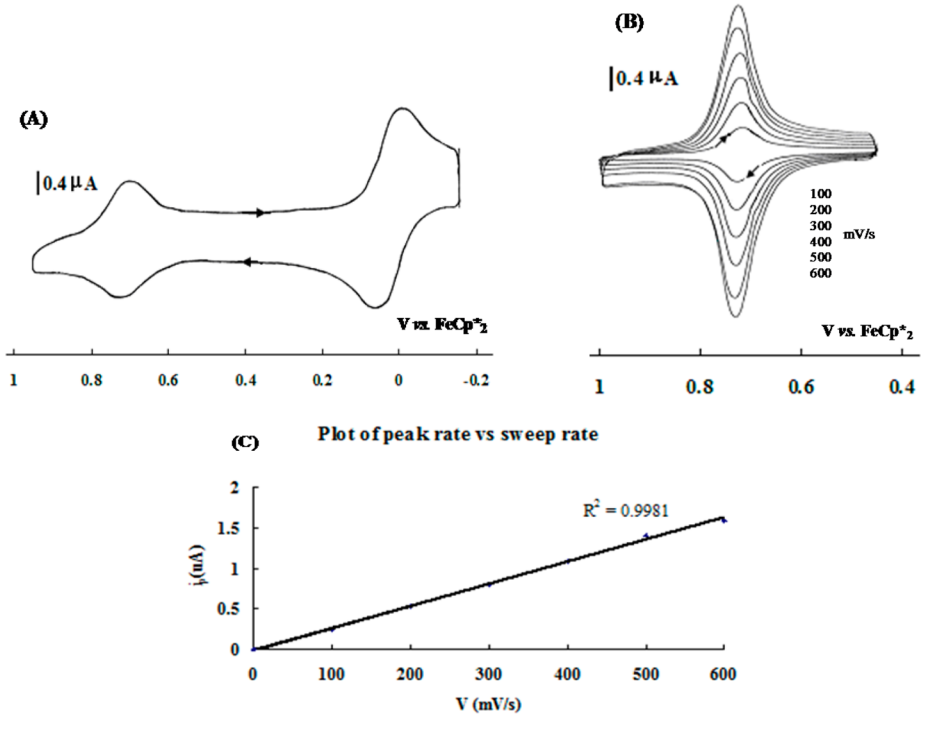

Figure 10. Electrochemical properties of the copolymer $\mathbf{10}^{100/50}$. The molar feed ratio of monomers **8** and **5** to **1** is 100:50:1. (A) CV of the copolymer in DCM: internal reference, [$FeCp^*_2$]; reference electrode, Ag; working and counter electrodes, Pt; scan rate, 0.4 mV/s; supporting electrolyte, [n-Bu_4N][PF_6]. (B) Pt electrode modified by the copolymer at various scan rates in DCM solution containing only the supporting electrolyte. (C) Intensity as a function of scan rate (the linearity shows the expected behavior of the adsorbed polymer).

There was no adsorption phenomenon during CV for monomer **5**, but for all the polymers **6** obvious and strong adsorption onto electrodes was observed, as shown in Figure 4C, upon scanning around the oxidation potential of the amidoferrocenyl group. The progressive adsorption onto electrodes is an advantage for the facile formation of robust

dx.doi.org/10.1021/om5006897 | *Organometallics* 2014, 33, 4323−4335

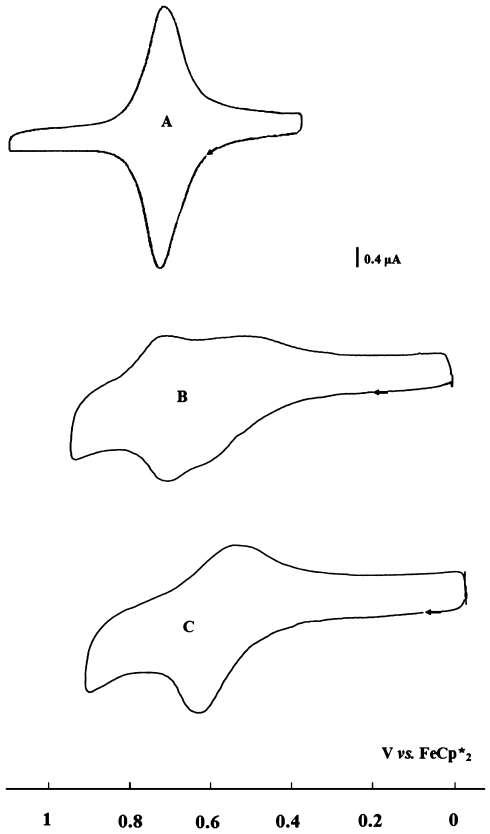

Figure 11. CVs for the titration of $[n\text{-}Bu_4N]_2[ATP]$ by the Pt electrode modified with the copolymer $\mathbf{10}^{100/50}$ in DCM at 20 °C: (A) before addition of $[n\text{-}Bu_4N]_2[ATP]$; (B) during addition of $[n\text{-}Bu_4N]_2[ATP]$; (C) after addition of excess $[n\text{-}Bu_4N]_2[ATP]$.

metallopolymer-modified electrodes upon scanning around the amidoferrocenyl potential zone.[87−90] Modification of electrodes using polymers **6** with various MWs has been successful, resulting in detectable electroactive materials. The electrochemical behavior of the modified electrodes was studied in DCM containing only the supporting electrolyte (Figure 4D). A well-defined symmetrical redox wave is observed that is characteristic of a surface-confined redox couple, with the expected linear relationship of peak current with potential sweep rate (Figure 4E).[87] The modified electrode is stable, as repeated scanning does not modify the CVs. Furthermore, no splitting between oxidation and reduction peaks is observed (ΔE = 0 mV), which suggests that no structural change takes place within the electrochemical redox process.[85,87] These Pt electrodes modified by polymers **6** are durable and reproducible, as no loss of electroactivity is observed after scanning several times or after standing in air for several days. The surface coverages of the electroactive amidoferrocenyl sites of the modified electrodes for all the polymers are given in Table 2.

Oxoanion sensing is a key field of molecular recognition,[91−93] in particular because DNA fragments include adenosine triphosphate anion (ATP^{2-}), an important coenzyme that transports chemical energy to cells for metabolism. Here electrochemical recognition of ATP^{2-} by the redox-active polymers was studied first in dichloromethane (DCM) solution using the *n*-butylammonium salt $[n\text{-}Bu_4N]_2[ATP]$ and then using a modified electrode that was derivatized by adsorption of the polymers. Let us first examine the redox recognition in solution. Addition of $[n\text{-}Bu_4N]_2[ATP]$ to an electrochemical cell containing a solution of polymer $\mathbf{6}^{50}$ in DCM led to the appearance of a new wave at a potential less positive than the initial wave, the intensity of which decreased while that of the new wave increased (Figure 5). Indeed, the interaction of the anions with redox groups releases electron density, rendering oxidation of the amidoferrocenyl group easier. The difference in amidoferrocenyl redox potential between the initial wave and the new wave (ΔE) is 70 mV. The equivalence point is reached when 0.5 equiv of $[n\text{Bu}_4N]_2[ATP]$ has been added (Figure 5C), which is in accord with the double negative charge of this anion and signifies that the ATP^{2-} anion is quantitatively recognized by the polymer $\mathbf{6}^{50}$ in DCM solution and that two amidoferrocenyl groups are interacting with each ATP^{2-}.

The α and β phosphates near the ribose are those that were found by the group of Hampe and Kappes using infrared multiple photon dissociation and photoelectron spectroscopy to bear the two negative charges of ATP^{2-}.[94] Accordingly, the stoichiometry of the titration that corresponds to two amidoferrocenyl units per ATP^{2-} is dictated by the interactions of these two negatively charged α and β phosphates with the NH groups of amidoferrocenyl units. In the oxidized ferrocenium form generated at the anode, the interaction of the oxygen anions involves an NH group of considerably increased acidity due to the positive charge that is delocalized over the amidoferrocenium moiety. The H bond is then strengthened, and the synergy between this H bond and the electrostatic bond between the cation and the anion is sufficiently strong to significantly modify the ferrocenyl redox potential. The two negatively charged phosphates are very different from each other (Figure 6): the β and γ phosphates form a favorable chelating double H bond with an amidoferrocenyl group of polymers **6** ("intramolecular H bonding"), whereas the α phosphate can only form a single H bond with another amidoferrocenyl group. This group also forms another H bond between its carbonyl group and another ATP^{2-} molecule ("intermolecular" H bonding), as shown in Figure 6.

The Pt electrode modified with the polymer $\mathbf{6}^{50}$ was also used for its recognition in DCM solution containing only $[n\text{-}Bu_4N][PF_6]$ as the supporting electrolyte, and a similar trend was observed. As shown in Figure 7, the addition of $[n\text{-}Bu_4N]_2[ATP]$ to an electrochemical cell containing the modified Pt electrode in DCM caused the appearance of a new wave at a potential less positive than that for the initial wave. The intensity of the initial wave decreased, while that of the new wave increased. The difference in ferrocenyl redox potential between the initial wave and the new wave (ΔE) is 130 mV: i.e., 60 mV larger than that observed with polymer $\mathbf{6}^{50}$ in solution. The larger ΔE value signifies a rather strong interaction of the amidoferrocenium group on the modified Pt electrode with the ATP^{2-} anions. Consequently, the modified Pt electrode with polymer $\mathbf{6}^{50}$ is a good candidate for the qualitative recognition of ATP^{2-} anions.[91−93]

3.4. Synthesis of the Amidoferrocenyl Block Copolymers 10. As shown in Scheme 2, first the new monomer *N*-[3-(3′,6′,9′-trioxadecyl)]-*cis*-5-norbornene-*exo*-2,3-dicarboximide (**8**) was synthesized by reaction between **2** and 2-(2-(2-methoxyethoxy)ethoxy)ethylamine (**7**). Figure 8A shows the ^{1}H NMR spectrum of the monomer **8**. The peak at 6.30 ppm corresponds to the olefinic protons, and two doublet peaks at 1.36−1.39 and 1.47−1.51 ppm originate from the bridge-methylene protons of the *cis*-norbornene structure. Further-

more, the protons of the methyl group of the side chain are found at 3.37 ppm.

The block copolymers **10** were synthesized by chain extension of monomer **8** to the second amidoferrocenyl-containing monomer **5** via a one-pot two-step sequential ROMP. The preparation of the first block, polymer **9**, was accomplished with nearly 100% monomer conversion in 8 min, which was demonstrated by the disappearance of the peak at 6.30 ppm corresponding to the olefinic protons of monomer **8** and the appearance of new two broad peaks at 5.51 and 5.75 ppm corresponding to the olefinic protons of polymers (Figure 8B). The SEC results (Figures S32−S34, Supporting Information) show the good monodispersity (PDI < 1.1) of polymers **9** and demonstrate the controlled polymerization of monomer **8**. Full characterization of polymers **9** is detailed in the Supporting Information. Figure 8C shows the ^{1}H NMR spectrum of the block copolymer **10**. The protons of the Cp of the ferrocenyl groups are located at 4.71, 4.32, and 4.19 ppm, respectively. The peak at 6.47 ppm corresponds to the proton of the amido group in the amidoferrocenyl block. The presence of the above new peaks indicates the successful preparation of the block copolymers **10**.

Similarly, a series of amidoferrocenyl-containing copolymers **10** were synthesized with various molar feed ratios of monomer **8** and **5** to catalyst **1**. The polymerization of monomer **8** is finished at nearly 100% conversion within 8 min, even when the molar feed ratio of monomer **8** to **1** was increased to 200:1. However, for the second block, reaction times longer than 60 min (48 h in this study) were necessary when the feed ratio of monomer **5** to **1** was increased to 100:1. The most obvious difference in structure between monomers **5** and **8** is the presence of the amidoferrocenyl moiety in **5**. Thus, it is believed that the polymerization is slowed down by the presence of the amidoferrocenyl moiety due to steric constraint of the linked ferrocenyl bulk.[95] Furthermore, the block copolymers **10** show a better solubility than the homopolymers **6**. All of the prepared copolymers are soluble in DCM, $CHCl_3$, THF, DMF, and DMSO, and the small copolymers are even soluble in acetone, acetonitrile, and ethyl acetate.

3.5. Molecular Weight Analysis of Block Copolymers 10. The MWs of polymers **9** and block copolymers **10** were characterized by end-group analysis, MALDI-TOF MS, and SEC, respectively. The polymerization degrees of the first, polymers **9**, were first obtained by end-group analysis using the ^{1}H NMR spectra of polymers **9** in CD_3CN (Figure S27, Supporting Information). Then, the polymerization degrees of the second block, polymers **10**, were calculated by comparing the integration of the methyl proton (3.355 ppm) with that of the protons of the amido group (6.472 ppm) and Cp rings (4.710, 4.318, and 4.189 ppm), respectively. As shown in Table 3, the polymerization degrees from end-group analysis (n_{p2}) are very close to that obtained using the ^{1}H NMR conversion (n_{p1}). The number of amidoferrocenyl units in the copolymers **10** was also determined using the Bard−Anson electrochemical method. The estimated values of electrons (n_{p3}) for all of the copolymers showed a good consistency with the value of n_{p1}, as well. As shown in Figure 9, the MALDI-TOF MS of the small copolymer $\mathbf{10}^{6/3}$, in which the molar feed ratio of monomer **8** and **5** to **1** is 6:3:1, shows well-defined individual peaks for polymer fragments that are separated by 550 Da (MW of monomer **5**) and 309 Da (MW of monomer **8**), respectively. The MW found for $(C_6H_6)(C_{16}H_{23}NO_5)_6(C_{28}H_{34}N_2O_6Fe)_3(C_2H_2)Na$ is 3633.9 Da, which is very close to the calculated value of 3633.4 Da. For polymers **9**, the MW from SEC analysis (Figures S32−S34, Supporting Information) is also close to the theoretical values obtained by ^{1}H NMR conversion. For the corresponding copolymers **10**, as for the homopolymers **6**, the MWs obtained by SEC are always smaller than the calculated values. Fortunately, the PDI values for all the copolymers **10** are less than 1.15, which shows the good monodispersity of the copolymers.

3.6. Redox Properties and Electrochemical Sensing of ATP^{2-} for the Block Copolymers 10. The side chain amidoferrocenyl containing block copolymers **10** were studied by CV using $[FeCp^*_2]$ as the internal reference. The CVs were recorded in DCM (Figure 10 and Figures S44−S46 (Supporting Information)), and the $E_{1/2}$ data (measured vs $[FeCp^*_2]$) are gathered in Table S3 (Supporting Information). As shown in Figure 10A, a single oxidation wave is observed for the ferrocenyl groups of the copolymer $\mathbf{10}^{100/50}$, and this single wave shows better reversibility and less adsorption than that of **6**, which is taken into account by the solubilizing property of the TEG chains in **10**. Some adsorption is still observable, however, as characterized by an intensity ratio i_a/i_c (0.9) that is lower than 1 and a ΔE value that is lower (0.020 V) that the Nernstian value of 0.059 V at 25 °C. The anodic and cathodic CV waves are also slightly broader than those of the monomer **5**, which is probably due to the nonequivalence of all the ferrocenyl groups in the polymer chain. The $Fe^{III/II}$ oxidation potential of the ferrocenyl redox center is found around 680 mV as well.

The accessibility of modified electrodes[85−90] has also been explored. Indeed, upon scanning around the oxidation potential of the amidoferrocenyl group, the copolymers are adsorbed onto electrodes (see Figure S46B). Thus, modification of electrodes using the copolymers **10** has been successful. Figure 10B and Figure S46C show the electrochemical behavior of modified electrodes in DCM containing only the supporting electrolyte. A well-defined symmetrical redox wave that is characteristic of a surface-confined redox couple is observed, including the expected linear relationship of peak current with potential sweep rate. Furthermore, repeated scanning does not change the CVs, which indicates that the modified electrode is stable. There is no structural change during the electrochemical redox process, as no splitting between the oxidation and reduction peaks is observed (ΔE = 0 mV).

Finally, electrochemical recognition of $[n\text{-}Bu_4N]_2[ATP]$ by the copolymer **10** was also found to be possible. As shown in Figure 11, the addition of $[n\text{-}Bu_4N]_2[ATP]$ to an electrochemical cell containing the Pt electrode modified with copolymer $\mathbf{10}^{100/50}$ in DCM provoked the appearance of a new wave at a potential less positive than the initial wave. The intensity of the initial wave decreased, while that of the new wave increased. The difference in amidoferrocenyl redox potential between the initial wave and the new wave (ΔE) is 150 mV: i.e., 20 mV larger than that obtained using the modified Pt electrode with polymer $\mathbf{6}^{50}$. This might possibly be the consequence of encapsulation by the triethylene glycol branch network of the amidoferrocene−ATP interaction. Consequently for the qualitative recognition of ATP^{2-} anions the Pt electrode modified with the copolymer **10** shows a better effect in comparison to that modified with the homopolymer **6**.

dx.doi.org/10.1021/om5006897 | *Organometallics* 2014, 33, 4323−4335

4. CONCLUSION

These series of side chain amidoferrocenyl containing homopolymers and block copolymers that were successfully synthesized by controlled and living ROMP catalyzed by Grubbs' third-generation catalyst (**1**) are monodisperse and can reach up to 332 units, with the solubility decreasing as the number of monomer units increases. Given the relatively good solubility of up to large sizes, they could be easily used. They very efficiently modified Pt electrodes with excellent stability and robustness, and the modified Pt electrodes recognized ATP^{2-} anions. The Pt electrodes modified with block copolymers show a slightly better qualitative sensing of ATP^{2-} anion in comparison to those modified with the corresponding homopolymers, possibly because the triethylene glycol branch network favors the amidoferrocene−ATP interaction by encapsulation. Quantitative recognition (titration) of ATP^{2-} is obtained, with the DCM solutions of the homopolymers showing the interaction of two amidoferrocenyl groups with each ATP^{2-}. This leads us to conclude that a chelating intramolecular H bond occurs with the β and γ phosphate groups of ATP^{2-} and a single H bond between the α phosphate and another amidoferrocenyl group involves intermolecular H bonding: i.e., a polymeric network of H bonds.

■ ASSOCIATED CONTENT

Supporting Information

Text, figures, and tables giving general data, including solvents, apparatuses, reagents, syntheses of intermediates, ^{1}H, ^{13}C, and DOSY NMR, IR, and MALDI-TOF mass spectra, cyclic voltammograms, and SEC of the polymers. This material is available free of charge via the Internet at http://pubs.acs.org.

■ AUTHOR INFORMATION

Present Address

[§]On sabbatical leave from the Key Laboratory of Leather Chemistry and Engineering of Ministry of Education, Sichuan University, Chengdu 610065, People's Republic of China.

Notes

The authors declare no competing financial interest.

■ ACKNOWLEDGMENTS

Financial support from the National Science Foundation of China (21106088), the Ph.D. Program Foundation of the Ministry of Education of China (20110181120079), the University of Bordeaux, the Centre National de la Recherche Scientifique, and L'Oréal are gratefully acknowledged.

■ REFERENCES

(1) Abd-El-Aziz, A. S.; Manners, I. *Frontiers in Transition-Metal-Containing Polymers*; Wiley: Hoboken, NJ, 2007.
(2) Manners, I. *Science* **2001**, *294*, 1664−1666.
(3) Wang, X.; Guerin, G.; Wang, H.; Wang, Y.; Manners, I.; Winnik, M. A. *Science* **2007**, *317*, 644−647.
(4) Abd-El-Aziz, A. S. *Coord. Chem. Rev.* **2002**, *233*−*234*, 177−191.
(5) Jakle, F. *Chem. Rev.* **2010**, *110*, 3985−4022.
(6) Whittell, G. R.; Hager, M. D.; Schubert, U. S.; Manners, I. *Nat. Mater.* **2011**, *10*, 176−188.
(7) Qiu, H.; Cambridge, G.; Winnik, M. A.; Manners, I. *J. Am. Chem. Soc.* **2013**, *135*, 12180−12183.
(8) Qiu, H.; Du, V. A.; Winnik, M. A.; Manners, I. *J. Am. Chem. Soc.* **2013**, *135*, 17739−17742.
(9) McGrath, N.; Schacher, F. H.; Qiu, H.; Mann, S.; Winnik, M. A.; Manners, I. *Polym. Chem.* **2014**, *5*, 1923−1929.
(10) Burnworth, M.; Tang, L.; Kumpfer, J. R.; Duncan, A. J.; Beyer, F. L.; Fiore, G. L.; Rowan, S. J.; Weder, C. *Nature* **2011**, *472*, 334−337.
(11) Holliday, B. J.; Swager, T. M. *Chem. Commun.* **2005**, 23−36.
(12) Hardy, C. G.; Ren, L.; Zhang, J.; Tang, C. *Isr. J. Chem.* **2012**, *52*, 230−245.
(13) Hardy, C. G.; Ren, L.; Tamboue, T. C.; Tang, C. *J. Polym. Sci., Part A* **2011**, *49*, 1409−1420.
(14) Astruc, D. *Nat. Chem.* **2012**, *4*, 255−267.
(15) Ornelas, C.; Ruiz, J.; Belin, C.; Astruc, D. *J. Am. Chem. Soc.* **2009**, *131*, 590−601.
(16) Duan, Q.; Cao, Y.; Li, Y.; Hu, X.; Xiao, T.; Lin, C.; Pan, Y.; Wang, L. *J. Am. Chem. Soc.* **2013**, *135*, 10542−10549.
(17) Feng, C.; Lu, G.; Li, Y.; Huang, X. *Langmuir* **2013**, *29*, 10922−10931.
(18) Dong, Z.; Cao, Y.; Yuan, Q.; Wang, Y.; Li, J.; Li, B.; Zhang, S. *Macromol. Rapid Commun.* **2013**, *34*, 867−872.
(19) Yan, Q.; Yuan, J.; Cai, Z.; Xin, Y.; Kang, Y.; Yin, Y. *J. Am. Chem. Soc.* **2010**, *132*, 9268−9270.
(20) Tonhauser, C.; Alkan, A.; Schömer, M.; Dingels, C.; Ritz, S.; Mailänder, V.; Frey, H.; Wurm, F. R. *Macromolecules* **2013**, *46*, 647−655.
(21) Elbert, J.; Gallei, M.; Rüttiger, C.; Brunsen, A.; Didzoleit, H.; Stühn, B.; Rehahn, M. *Organometallics* **2013**, *32*, 5873−5878.
(22) Nakahata, M.; Takashima, Y.; Yamaguchi, H.; Harada, A. *Nat. Commun.* **2011**, *2*, No. 511, DOI: 10.1038/ncomms1521.
(23) Xia, W.; Hu, X.; Chen, Y.; Lin, C.; Wang, L. *Chem. Commun.* **2013**, *49*, 5085−5087.
(24) Rider, D. A.; Manners, I. *Polym. Rev.* **2007**, *47*, 165−195.
(25) Kaifer, A. E. *Eur. J. Inorg. Chem.* **2007**, 5015−5027.
(26) Daniel, M. C.; Ruiz, J.; Astruc, D. *J. Am. Chem. Soc.* **2003**, *125*, 1150−1151.
(27) Ornelas, C.; Méry, D.; Cloutet, E.; Ruiz, J.; Astruc, D. *J. Am. Chem. Soc.* **2008**, *130*, 1495−1506.
(28) Eloi, J. C.; Chabanne, L.; Whittell, G. R.; Manners, I. *Mater. Today* **2008**, *11*, 28−36.
(29) (a) Nguyen, P.; Gómez-Elipe, P.; Manners, I. *Chem. Rev.* **1999**, *99*, 1515−1548. (b) Ahmed, R.; Patra, S. K.; Hamley, I. W.; Manners, I.; Faul, C. F. J. *J. Am. Chem. Soc.* **2013**, *135*, 2455−2458. (c) Deraedt, C.; Rapakousiou, A.; Wang, Y.; Salmon, L.; Bousquet, M.; Astruc, D. *Angew. Chem., Int. Ed.* **2014**, DOI: 10.1002/chem.201403085.
(30) Pittman, C. U.; Lai, J. C.; Vanderpool, D. P.; Good, M.; Prado, R. *Macromolecules* **1970**, *3*, 746−754.
(31) Pittman, C. U.; Voges, R. L.; Jones, W. B. *Macromolecules* **1971**, *4*, 298−302.
(32) Pittman, C. U.; Voges, R. L.; Jones, W. B. *Macromolecules* **1971**, *4*, 291−297.
(33) Pittman, C. U.; Ayers, O. E.; McManus, S. P.; Sheats, J. E.; Whitten, C. E. *Macromolecules* **1971**, *4*, 360−362.
(34) Pittman, C. U.; Hirao, A. *J. Polym. Sci., Polym. Chem.* **1977**, *15*, 1677−1686.
(35) Pittman, C. U.; Hirao, A. *J. Polym. Sci., Polym. Chem.* **1978**, *16*, 1197−1209.
(36) Pittman, C. U.; Lin, C. C. *J. Polym. Sci., Polym. Chem.* **1979**, *17*, 271−275.
(37) Wright, M. E. *Organometallics* **1990**, *9*, 853−856.
(38) Deschenaux, R.; Izvolensk, V.; Turpin, F.; Guillon, D.; Heinrich, B. *Chem. Commun.* **1996**, 439−440.
(39) Hadjichristidis, N.; Pitsikalis, M.; Pispas, S.; Iatrou, H. *Chem. Rev.* **2001**, *101*, 3747−3792.
(40) Buchmeiser, M. R. *Chem. Rev.* **2000**, *100*, 1565−1604.
(41) Matyjaszewski, K.; Xia, J. *Chem. Rev.* **2001**, *101*, 2921−2990.
(42) Kamigaito, M.; Ando, T.; Sawamoto, M. *Chem. Rev.* **2001**, *101*, 3689−3745.
(43) Wang, J.-S.; Matyjaszewski, K. *J. Am. Chem. Soc.* **1995**, *117*, 5614−5615.
(44) Percec, V.; Barboiu, B. *Macromolecules* **1995**, *28*, 7970−7972.

(45) Kato, M.; Kamigaito, M.; Sawamoto, M.; Higashihara, T. *Macromolecules* **1995**, *28*, 1721−1723.
(46) Zhang, J.; Ren, L.; Hardy, C. G.; Tang, C. *Macromolecules* **2012**, *45*, 6857−6863.
(47) Hawker, C. J.; Bosman, A. W.; Harth, E. *Chem. Rev.* **2001**, *101*, 3661−3688.
(48) (a) Bielawskia, C. W.; Grubbs, R. H. *Prog. Polym. Sci.* **2007**, *32*, 1−29. (b) Grubbs, R. H. Living ring-opening olefin metathesis polymerization. In *Polymer Science: A Comprehensive Reference*; Elsevier: Amsterdam, 2012; Vol. *4*, pp 21−29. (c) Deraedt, C.; d'Halluin, M.; Astruc, D. *Eur. J. Inorg. Chem.* **2013**, 4881−4908. (d) Knall, A.-C.; Slugovc, C. In *Olefin Metathesis. Theory and Practice*; Grela, K., Ed.; Wiley: Hoboken, NJ, 2014; pp 269−284.
(49) Albagli, D.; Bazan, G. C.; Wrighton, M. S.; Schrock, R. R. *J. Am. Chem. Soc.* **1992**, *114*, 4150−4158.
(50) Albagli, D.; Bazan, G. C.; Schrock, R. R.; Wrighton, M. S. *J. Phys. Chem.* **1993**, *97*, 10211−10216.
(51) Albagli, D.; Bazan, G. C.; Schrock, R. R.; Wrighton, M. S. *J. Am. Chem. Soc.* **1993**, *115*, 7328−7334.
(52) Watson, K. J.; Zhu, J.; Nguyen, S. T.; Mirkin, C. A. *J. Am. Chem. Soc.* **1999**, *121*, 462−463.
(53) Watson, K. J.; Zhu, J.; Nguyen, S. T.; Mirkin, C. A. *Pure Appl. Chem.* **2000**, *72*, 67−72.
(54) Watson, K. J.; Nguyen, S. T.; Mirkin, C. A. *J. Organomet. Chem.* **2000**, *606*, 79−83.
(55) Watson, K. J.; Park, S.; Im, J.; Nguyen, S. T.; Mirkin, C. A. *J. Am. Chem. Soc.* **2001**, *123*, 5592−5593.
(56) Liu, X.; Guo, S.; Mirkin, C. A. *Angew. Chem., Int. Ed.* **2003**, *42*, 4785−4789.
(57) Gibbs, J. M.; Park, S.; Anderson, D. R.; Watson, K. J.; Mirkin, C. A.; Nguyen, S. T. *J. Am. Chem. Soc.* **2005**, *127*, 1170−1178.
(58) Abd-El-Aziz, A. S.; Todd, E. K.; Ma, G. Z. *J. Polym. Sci., Part A* **2001**, *39*, 1216−1231.
(59) Abd-El-Aziz, A. S.; May, L. J.; Hurd, J. A.; Okasha, R. M. *J. Polym. Sci., Part A* **2001**, *39*, 2716−2722.
(60) Abd-El-Aziz, A. S. *Macromol. Rapid Commun.* **2002**, *23*, 995−1031.
(61) Abd-El-Aziz, A. S.; Todd, E. K.; Okasha, R. M.; Wood, T. E. *Macromol. Rapid Commun.* **2002**, *23*, 743−748.
(62) Abd-El-Aziz, A. S.; Okasha, R. M.; Afifi, T. H.; Todd, E. K. *Macromol. Chem. Phys.* **2003**, *204*, 555−563.
(63) Abd-El-Aziz, A. S.; Okasha, R. M.; Afifi, T. H. *J. Inorg. Organomet. Polym.* **2004**, *14*, 269−278.
(64) Abd-El-Aziz, A. S.; Todd, E. K.; Okasha, R. M.; Shipman, P. O.; Wood, T. E. *Macromolecules* **2005**, *38*, 9411−9419.
(65) Abd-El-Aziz, A. S.; Okasha, R. M.; May, L. J.; Hurd, J. *J. Polym. Sci., Part A* **2006**, *44*, 3053−3070.
(66) Abd-El-Aziz, A. S.; Winram, D. J.; Shipman, P. O.; Bichler, L. *Macromol. Rapid Commun.* **2010**, *31*, 1992−1997.
(67) Yang, H.; Lin, S.; Yang, H.; Lin, C.; Tsai, L.; Huang, S.; Chen, I. W.; Chen, C.; Jin, B.; Luh, T. *Angew. Chem., Int. Ed.* **2006**, *45*, 726−730.
(68) Yang, H.; Lin, S.; Liu, Y.; Wang, Y.; Chen, M.; Sheu, H.; Tsou, D.; Lin, C.; Luh, T. *J. Organomet. Chem.* **2006**, *691*, 3196−3200.
(69) Lin, C.; Yang, H.; Lin, N.; Hsu, I.; Wang, Y.; Luh, T. *Chem. Commun.* **2008**, 4484−4486.
(70) Luh, T.; Yang, H.; Lin, N.; Lin, S.; Lee, S.; Chen, C. *Pure Appl. Chem.* **2008**, *80*, 819−829.
(71) Yang, H.; Lee, S.; Chen, C.; Lin, N.; Yang, H.; Jina, B.; Luh, T. *Chem. Commun.* **2008**, 6158−6160.
(72) Lin, N.; Lee, S.; Yu, J.; Chen, C.; Huang, S.; Luh, T. *Macromolecules* **2009**, *42*, 6986−6991.
(73) Chou, C.; Lee, S.; Chen, C.; Biju, A. T.; Wang, H.; Wu, Y.; Zhang, G.; Yang, K.; Lim, T.; Huang, M.; Tsai, P.; Lin, K.; Huang, S.; Chen, C.; Luh, T. *J. Am. Chem. Soc.* **2009**, *131*, 12579−12585.
(74) Luh, T. *Acc. Chem. Res.* **2013**, *46*, 378−389.
(75) Zhu, L.; Flook, M. M.; Lee, S.; Chan, L.; Huang, S.; Chiu, C.; Chen, C.; Schrock, R. R.; Luh, T. *Macromolecules* **2012**, *45*, 8166−8171.
(76) Yeh, N.; Chen, C.; Lee, S.; Wu, H.; Chen, C.; Luh, T. *Macromolecules* **2012**, *45*, 2662−2667.
(77) Dragutan, I.; Dragutan, V.; Fischer, H. *J. Inorg. Organomet. Polym.* **2008**, *18*, 311−324.
(78) Zha, Y.; Thaker, H. D.; Maddikeri, R. R.; Gido, S. P.; Tuominen, M. T.; Tew, G. N. *J. Am. Chem. Soc.* **2012**, *134*, 14534−14541.
(79) Sanford, M. S.; Love, J. A.; Grubbs, R. H. *Organometallics* **2001**, *20*, 5314−5318.
(80) Camm, K. D.; Castro, N. M.; Liu, Y.; Czechura, P.; Snelgrove, J. L.; Fogg, D. E. *J. Am. Chem. Soc.* **2007**, *129*, 4168−4169.
(81) Boisselier, E.; Diallo, A. K.; Salmon, L.; Ornelas, C.; Ruiz, J.; Astruc, D. *J. Am. Chem. Soc.* **2010**, *132*, 2729−2742.
(82) Llevot, A.; Astruc, D. *Chem. Soc. Rev.* **2012**, *41*, 242−257.
(83) Iyer, A. K.; Khaled, G.; Fang, J.; Maeda, H. *Drug Discovery Today* **2006**, *11*, 813−818.
(84) Flanagan, J. B.; Margel, S.; Bard, A. J.; Anson, F. C. *J. Am. Chem. Soc.* **1978**, *100*, 4248−4253.
(85) Murray, R. W. *Electroanal. Chem.* **1984**, *13*, 191−368.
(86) Li, W.; Chung, H.; Daeffler, C.; Johnson, J. A.; Grubbs, R. H. *Macromolecules* **2012**, *45*, 9595−9603.
(87) Abruña, H. D. *Coord. Chem. Rev.* **1988**, *86*, 135−189.
(88) Bard, A. J.; Faulkner, L. R. *Electrochemical Methods: Fundamentals and Applications*, 2nd ed.; Wiley: New York, 2001.
(89) Zanello, P. *Inorganic Electrochemistry. Theory, Practice and Application*; RSC Publishing: Cambridge, U.K., 2003.
(90) (a) Ruiz, J.; Astruc, D. *C. R. Acad. Sci., Ser. IIc: Chim.* **1998**, *1*, 21−27. (b) Geiger, W. E. *Organometallics* **2007**, *26*, 5738−5765.
(91) Beer, P. D. *Acc. Chem. Res.* **1998**, *31*, 71−80.
(92) Beer, P. D.; Gale, P. A. *Angew. Chem., Int. Ed.* **2001**, *40*, 486−516.
(93) Astruc, D.; Daniel, M.-C.; Ruiz, J. *Chem. Commun.* **2004**, 2637−2649.
(94) Schinle, F.; Crider, P. E.; Vonderach, M.; Weis, P.; Hampe, O.; Kappes, M. M. *Phys. Chem. Chem. Phys.* **2013**, *15*, 6640−50.
(95) For a kinetic approach to ROMP synthesis of precision functional poly(norbornene) polymers, see: Moatsou, D.; Hansell, C. F.; O'Reilly, R. K. *Chem. Sci.* **2014**, *5*, 2246−2250.

List of PhD publications

1) **Amalia Rapakousiou** Rodrigue Djeda, Maxime Grillaud, Na Li, Jaime Ruiz and Didier Astruc: *'Click' Assemblies and Redox Propertiesof Arene- and Gold-nanoparticles-cored Triazolylbiferrocene-terminated Dendrimers*. Organometallics **2014**, ASAP.

2) N. Li, P. Zhao, M. E. Igartua, **A. Rapakousiou**, L. Salmon, S. Moya, J. Ruiz, D. Astruc: *Stabilization of AuNPs by Monofunctional Triazole Linked to Ferrocene, Ferricenium or Coumarin and Applications to Synthesis, Sensing and Catalysis.* Inorg. Chem. **2014**, 53, 11802-11808.

3) **Amalia Rapakousiou**, Christophe Dedaedt, Haibin Gu, Lionel Salmon, Colette Belin, Jaime Ruiz, Didier Astruc: *Mixed-Valent Intertwinned Polymer Units Containg Biferrocenium Chloride Side Chains Form Nanosnakes that Encapsulate Gold Nanoparticles. J. Am. Chem. Soc*. **2014**, 13995-13998.

4) Haibin Gu, **Amalia Rapakousiou**, Pascal Castel, Nicolas Guidolin, Noel Pinaud, Jaime Ruiz, Didier Astruc: *Living Ring-Opening Metathesis Polymerization and Redox-Sensing Properties of Norbornene Polymers and Copolymers Containing Ferrocenyl and Tetraethylene Glycol Groups.* Organometallics, **2014**, *33*, 4323-4335.

5) **Amalia Rapakousiou**, Yanlan Wang, Roberto Ciganda, Jean-Michel Lasnier, Didier Astruc: *Click Chemistry of an Ethynylarene Iron Complex. Syntheses, Properties and Redox Chemistry of Cationic Bimetallic and Dendritic Iron-Sandwich Complexes.* Organometallics **2014**, *33*, 3583-3590.

6) Yanlan Wang, **Amalia Rapakousiou**, Didier Astruc: *ROMP Synthesis of Cobalticenium-Enamine Polyelectrolytes.* Macromolecules **2014**, *47*, 3767-3774.

7) Didier Astruc, **Amalia Rapakousiou**, Yanlan Wang, Rodrigue Djeda, Abdou Diallo, Jaime Ruiz, Catia Ornelas: *Mixed-valent metallodendrimers: design and functions.* J. Coord. Chem. **2014**, *67*, 3809-3821. (Juan Costamagna issue).

8) Yanlan Wang, **Amalia Rapakousiou**, Jaime Ruiz, Didier Astruc: *Metallation of Polyamine Dendrimers with Ethynylcobalticenium for the Construction of Mono- and Heterobimetallic Polycationic Metallodendrimers.* Chem. Eur. J. **2014**, *20*. 11176-1186.

9) Christophe Deraedt, **Amalia Rapakousiou**, Yanlan Wang, Lionel Salmon, Melanie Bousquet, Didier Astruc: *Multi-function Redox Polymers: Electrochrome, Polyelectrolyte, Sensor, Electrode Modifier, Nanoparticle Stabilizer and Catalyst Template.* Angew. Chem., Int. Ed. **2014**, *53*, 8445-8449.

10) Didier Astruc, Yanlan Wang, **Amalia Rapakousiou**, Abdou Diallo, Rodrigue Djeda, Jaime Ruiz, Catia Ornelas: *Organoiron-mediated synthesis and redox activity of organoiron-containing dendrimers.* Polyhedron **2014,** doi.org/10.1016/j.poly.2014.04.002 (C. Lapinte issue).

11) Yanlan Wang, Camille Latouche, **Amalia Rapakousiou**, Colin Lopez, Isabelle Ledoux-Rak, Jaime Ruiz, Jean-Yves Saillard, Didier Astruc: *Uncatalyzed Hydroamination of Electrophilic Organometallic Alkynes: Fundamental, Theoretical and Applied Aspects*. Chem. Eur. J. **2014**, *20*. 8076-8088.

12) **Amalia Rapakousiou**, Lucia Herrer Jimenez, Yanlan Wang, Claire Mouche, Didier Astruc: *Rhodocenium Salts: From Basic Chemistry to Polyelectrolyte and dendritic Macromolecules.* Organometallics, **2014**, 33, 1259-1265.

13) **Amalia Rapakousiou**, Yanlan Wang, Jaime Ruiz, Didier Astruc: *''Click'' Synthesis and Redox Activity of a Water-Soluble Triazolylcobalticinium Polyelectrolyte*. J. Inorg. Organomet. Polym. Mater. **2014**, *24*, 107-113 (Dwight Sweigart issue)**.**

14) Yanlan Wang, **Amalia Rapakousiou**, Guillaume Chastanet, Lionel Salmon, Jaime Ruiz, Didier Astruc: *Poly(Biferrocenylethynyl)arene and Bis(biferrocenyl)diynyl Complexes and their Redox Chemistry* .Organometallics, **2013**, *32*, 6136-6146.
15) **Amalia Rapakousiou**, Yanlan Wang, Frida Nzulu, Rodrigue Djeda, Noël Pinaud, Jaime Ruiz, Didier Astruc: *Ferrocenyl Dendrimers with Ionic Tethers and Dendrons*. Organometallics **2013**, *32*, 6079-6090 (Ferrocene: Beauty and function issue)**.**
16) Yanlan Wang, **Amalia Rapakousiou**, Camille Latouche, Jean-Claude Daran, Anu Singh, Isabelle Ledoux-Rak, Jaime Ruiz, Jean-Yves Saillard, Didier Astruc: *Mild uncatalyzed hydroamination of an electrophilic alkyne, ethynylcobalticinium.*. Chem. Commun., **2013**, *49*, 5862-5864.
17) **Amalia Rapakousiou**, Yanlan Wang, Colette Belin, Noël Pinaud, Jaime Ruiz, Didier Astruc: *'Click' Synthesis and Redox Properties of Triazolyl Cobalticinium Dendrimers.* Inorg. Chem., **2013**, 52, 6685-6693.
18) **Amalia Rapakousiou,** Claire Mouche, Mathieu Duttine, Jaime Ruiz, Didier Astruc: *Click Synthesis and Redox Chemistry of Mono- and Heterobimetallic Triazolyl and Triazolium-Ferrocene and Cobalticinium Complexes*. Eur. J. Inorg. Chem., **2012,** *31*, 5071–5077.
19) Didier Astruc, Pengxiang Zhao, Liyuan Liang, **Amalia Rapakousiou**, Rodrigue Djeda, Abdou Diallo, Tetsuro Kusamoto, Jaime Ruiz, Catia Ornelas: *Dendritic Molecular Nanobatteries and the Contribution of Click Chemistry*. J. Inorg. Organomet.Polym. Mater, **2012**, *23*, 41-49.
20) Didier Astruc, Liyuan Liang, **Amalia Rapakousiou**, Jaime Ruiz: *Click dendrimers and triazole-related aspects: catalysts, mechanism, synthesis, and functions. A bridge between dendritic architectures and nanomaterials.*. Acc. Chem. Res. **2012**, *45*, 630-640.
21) Didier Astruc, Cátia Ornelas, **Amalia Rapakousiou**, Liyuan Liang, Rodrigue Djeda, Jaime Ruiz: *Redox recognition using "click" chemistry*. Inorg. Chim. Acta, **2011**, *374*, 51–58.

Titre : Ingéniérie des nanomatériaux redox métallocéniques

Résumé :

Les dendrimères et polymères contenant des métaux de transition comme le fer, le cobalt et le rhodium peuvent servir à la fabrication des nanomatériaux utiles à la catalyse, la reconnaissance moléculaire et l'électronique moléculaire. Pour leur construction, des liaisons ioniques, de la chimie click : CuAAC et hydroamination, la polymérisation ROMP et la polymérisation radicalaire ont été utilisés et ont permis la formation de nouveaux types de polyélectrolytes metallocéniques. La synthèse de nouvelles nanoparticules d'or, d'argent et de palladium à partir de ces métallopolymères et métallodendrimères ont été mises au point, conduisant à des réseaux à architecture spécifique bien définie. Ces assemblages supramoléculaires et ingénierie moléculaire ouvrent la voie vers l'application de la chimie organométallique dans la conception de nouveaux nanomatériaux nanoparticulaires structurés à l'aide des propriétés rédox des métallomacromolécules.

Mots clés : polyélectrolytes, dendrimères, rédox, nanoparticules, métallocènes

---

Title : Engineering of redox metallocenic nanomaterials

Abstract :

Dendrimers and polymers containing transition metals such as iron, cobalt and rhodium can serve in the fabrication of useful nanomaterials for catalysis, molecular recognition and molecular electronics. For their construction, ionic bonds, click chemistry: CuAAC and hydroamination, ROMP and radical polymerization were used and allowed the formation of new types of metallocenyl polyélectrolytes. The synthesis of new gold, silver and palladium nanoparticles from these metallopolymers and metallodendrimers has been developed, leading to specific and well-defined architectures. These supramolecular assemblies and molecular engineering opens the way towards the application of organometallic chemistry in the design of new structured nanoparticle-containing nanomaterials using the redox properties of metallomacromolecules.

Keywords : polyelectrolytes, dendrimers, redox, nanoparticles, metallocenes

Unité de recherche

Institut des Sciences Moléculaires (ISM, UMR CNRS 5255), Université de Bordeaux, 351 Cours de la Libération, 33405 Talence Cedex